Improving the Engraftment Activities of Cryopreserved Human Umbilical Cord Blood Through the Development of Novel Glyco(peptide)-Based Aryl Ice Recrystallization Inhibitors

Madeleine Katrina Adam

B.Sc. Honours Medicinal Chemistry – University of New Brunswick, 2014

Thesis submitted to the University of Ottawa
in partial fulfillment of the requirements for the
Doctorate in Philosophy degree in Chemistry

Department of Chemistry and Biomolecular Sciences
Faculty of Science
University of Ottawa

Candidate	Supervisor
Madeleine K. Adam	Robert N. Ben

ABSTRACT

The ability to preserve samples (e.g. biological substances) for extended periods has enabled many medical and industrial advancements including the development of blood banks and improvements to food storage. Cryopreservation, a biopreservation technique where samples are stored between -80 °C to -196 °C, allows for increased storage times of weeks to years for various cell types such as hematopoietic stem and progenitor cells (HSPCs). Cryopreserved HSPCs from human umbilical cord blood (UCB) can be used for hematopoietic stem cell transplantation used to treat over 80 diseases. Cryoprotectants like dimethyl sulfoxide are implemented to protect cells from cryoinjuries during cold storage; however, they fail to address phenomena that result in considerable loss of viable and functional cells after thawing. For instance, ice recrystallization occurring during cryopreservation involves the growth of larger ice crystals from smaller ones and this process is a substantial contributor to cellular damage. Along with the inability to mitigate ice recrystallization, numerous conventional cryoprotectants are toxic and lead to adverse outcomes to the cellular products undergoing preservation and to the recipients of the corresponding treatments. There is, therefore, tremendous interest in the development of novel non-toxic cryoprotectants able to reduce ice recrystallization during the storage of cellular products. That being said, the design and analysis of these ice recrystallization inhibitors (IRIs) are paramount for future innovations in regenerative and transfusion medicines.

Over the past two decades, the Ben laboratory has designed a collection of IRIs originally inspired by the naturally occurring biological antifreezes (e.g. antifreeze glycoproteins, AFGPs) found in a variety of cold-tolerating animals (e.g. fish and insects). From the development of these IRI-active AFGP analogues came a series of carbohydrate-based small molecules found to

improve the post-thaw properties of cells *in vitro* when used as cryosupplements during cryopreservation. The class of *N*-aryl-D-gluconamide IRIs, for example, has been shown to increase the post-thaw viability and function of HSPCs from UCB in small scale experiments. Notably, the impact of these cryoadditives on the post-thaw *in vivo* activities of cryopreserved cells had yet to be determined and this analysis would offer true insight into the clinical relevance of IRIs as cryoprotectants.

Consequently, the research described herein marks the first time the *in vivo* significance of using IRIs during cryopreservation has been investigated. Specifically, this thesis reports both the *in vitro* impact (viability and functionality of cells post-thaw) as well as the *in vivo* impact (the engraftment activity of grafts in a xenotransplantation model) of using *N*-aryl-D-gluconamides for the cryopreservation of HSPCs from UCB. Moreover, through structure-activity relationship (SAR) studies of the *N*-aryl-D-gluconamides, a series of novel analogues were developed including derivatives with modified aryl and carbohydrate components. These analogues were analyzed for their IRI activity and cytotoxicity, and the promising candidates were assessed for their cryoprotectant abilities. Finally, an innovative approach to the development of IRI-active glyco(peptides) is achieved through the design of macromolecular AFGP analogues possessing unique physicochemical properties. This included the development of IRI-active materials able to self-assemble in solution as well as the production of carbohydrate-based surfactants with tuneable IRI activity using an external trigger. Collectively, these studies provide substantial insight into the structural features required for the IRI activity of glyco(peptide) and gluconamide IRIs as well as their corresponding impacts on cryopreserved biological samples.

ACKNOWLEDGEMENTS

I am grateful for the tremendous support I have received from so many individuals throughout my studies. First, thank you to my supervisor, Prof. Robert Ben, for all the support and guidance over the years. From providing research advice to suggesting the best food and hiking places to explore during downtime at the GlycoNet symposiums in Banff, I appreciate it all. Thank you to my TAC members, Prof. André Beauchemin and Prof. Christopher Boddy, for their guidance and insightful conversations during my comprehensive examination, research proposal, and seminar. Thank you to my thesis examiners, Prof. Christopher Boddy, Prof. Dayong Gao, Prof. John Pezacki, and Prof. Adam Shuhendler, for evaluating my thesis and for providing invaluable comments. I would like to acknowledge my collaborators for the support and opportunities to publish truly interdisciplinary work. Thanks to Prof. Nicolas Pineault for the opportunity to explore the field of stem cell biology. It was a pleasure to collaborate with Pineault group members including Dr. Suria Jahan, Dr. Javed Manesia, Richa Kausal, Roya Pasha, and Emily Doxtator. Thank you to Prof. Brendan Wilkinson and colleagues for such an innovative collaboration and especially one that involved a 14-hour time difference. Additionally, thank you to Prof. Kyle Biggar, Prof. Ravin Narain, and their colleagues. I would also like to acknowledge the organizations that provided funding and support for my research: the University of Ottawa, the Natural Sciences and Engineering Research Council of Canada (NSERC; for my CGS-M and CGS-D), and the GlycoNet community for welcoming me as a Highly Qualified Personnel (HQP).

Next, I would like to thank all the members of the Ben lab including Dr. Kyle McClymont, Stephanie Abraham, Dr. Malay Doshi, Dr. Jennie Briard, Vanessa Musca, Dr.

Jessica Poisson, Thomas Charlton, Julia Meyer, Anna Ampaw, Salma Alasmar, Karishma Chopra, Jatinder Singh, Leah McMunn, Marcus Diamante, all the undergraduate students, and the Durst lab members. I appreciate all the research-related discussions as well as those about football, games, etc. We've made some great memories like those at the GlycoNet symposium and the Canadian Chemistry Conference and Exhibitions. Thank you to Anna Ampaw for her helpful thesis edits. I would especially like to acknowledge all my honour's, summer, and UROP students for all their hard work and dedication: thank you to Odile Pressoir, Geneviève O'Keefe, Emiliyan Staykov, Sierra Dowling, Angelo Caruso, and numerous volunteers! To the other graduate students in the Dept. including the CBGSA exec.: thank you for the memorable volleyball games, coffee breaks, and all the day-to-day hallway conversations.

Finally, I must acknowledge the tremendous support of my family and friends throughout my studies. *My thesis is dedicated to you*. To Zarah, Tara, Mike, Jeremy, Hamza, members of the Book Club, and the ski crew: thanks for always being there… whether "there" meant exploring Ottawa, meeting in Cuba, camping at Joeperry or in Algonquin, toasting champagne in the D. R., skiing the Quebec slopes, or participating in Book Clubs throughout the pandemic. To Mary, Michel, Monique, Justin, Brielle, and Catherine: thank you for all the support. A HUGE thank you to my parents, Rita and Allan, and my sisters, Jennifer and Kristen, for all the love and encouragement. The visits in Freddy and Ott, Henry, group chats featuring lots of laughs and advice, and everything that "New Phone Who Dis" encompasses were absolutely vital to the success of my degree. And finally, thank you to Étienne (featuring Juno and Athena), for all the inspiration, laughter, encouragement, adventures, bean burritos, and so much more. We've made so many memories exploring this city together. I am so grateful to have such an amazing partner and I am excited to see where our adventure takes us next!

TABLE OF CONTENTS

LIST OF FIGURES

Chapter 2

Chapter 3

Chapter 4

LIST OF TABLES

LIST OF SCHEMES

LIST OF ABBREVIATIONS

1D	One-dimensional
Ac	Acetyl
Ac_2O	Acetic anhydride
AcOH	Acetic acid
AFGP	Antifreeze glycoprotein
AFGP-8	Antifreeze glycoprotein fraction 8
AFM	Atomic force microscopy
AFP	Antifreeze protein
Ala	Alanine
ANOVA	Analysis of variance
APC	Allophycocyanin
Ar	Aryl
Azo	Azobenzene
BA	Biological antifreeze
BFU-E	Burst-forming unit-erythroid
BM	Bone marrow
Boc	*tert*-Butyloxycarbonyl
Boc_2O	Boc anhydride
br	broad
C-AFGP	*C*-linked antifreeze glycoprotein
C-linked	*Carbon*-linked (and *C6*-functionality = functionality linked to *Carbon* 6)
CB	Cord blood
Cbz	Carboxybenzyl
CD	Circular dichroism
CD (CD34)	Cluster of differentiation
$CDCl_3$	Deuterated chloroform
Cel	Cellobiose
CFC	Colony-forming cell
CFU	Colony-forming unit

CFU-GEMM	Colony-forming-granulocyte, erythrocyte, monocyte, and megakaryocyte
CFU-GM	Colony-forming unit-granulocyte, monocyte
CMC	Critical micelle concentration
CPA	Cryoprotective agent
CuAAC	Copper(I)-catalyzed Azide-Alkyne Cycloaddition
d	doublet
DCM	dichloromethane
dd	doublet of doublets
ddd	doublet of doublet of doublets
dddd	doublet of doublet of doublet of doublets
dH_2O	distilled water
ddH_2O	double-distilled water
DIS	Dynamic ice shaping
DMAP	4-Dimethylaminopyridine
DMF	Dimethylformamide
DMSO	Dimethyl sulfoxide
DMSO-d_6	Deuterated dimethyl sulfoxide
DPBS	Dulbecco's phosphate-buffered saline
ESI	Electrospray ionization mode
Et_2O	Diethyl ether
EtOAc	Ethyl acetate
EtOH	Ethanol
FACS	Fluorescence-activated cell sorting
FBS	Fetal bovine serum
FITC	Fluorescein isothiocyanate
Gal	Galactose
Glc	Glucose
GVHD	Graft-versus-host disease
HBSS	Hanks’ Balanced Salt solution
HepG2	Human hepatocellular carcinoma cell line
HES	Hydroxyethyl starch

HI	Hydration index
HLA	Human leukocyte antigen
HLB	Hydrophilic-lipophilic balance
HPLC	High-performance liquid chromatography
hPLT	Human platelet
HSA	Human serum albumin
HSC	Hematopoietic stem cell
HSCT	Hematopoietic stem cell transplant(ation)
HSPC	Hematopoietic stem and progenitor cell
I_c	Cubic ice
I_h	Hexagonal ice
I_{sd}	Stacking-disordered ice
IIF	Intracellular ice formation
IR resin	Amberlite ion exchange resin
IRI	Ice recrystallization inhibitor
LRMS	Low resolution mass spectrometry
LTC-IC	Long-term culture-initiating cell
m	multiplet
M+	Molecular ion (e.g. for LRMS cacluations)
Man	Mannose
MEM	Minimum essential media
MeOD	Deuterated methanol
MeOH	methanol
% MGS	Percent mean grain size
MTT	3-[4,5-Dimethylthiazol-2-yl]-2,5-diphenyl tetrazolium bromide
NAD (H)	Nicotinamide adenine dinucleotide (+ hydrogen)
NK	Natural killer
NMR	Nuclear magnetic resonance
NSERC	Natural Sciences and Engineering Research Council of Canada
NSG	NOD scid gamma
pA	*p*-anisaldehyde

PBI	Perylene bisimide
PBS	Phosphate-buffered saline
PE	Phycoerythrin
pet. ether	Petroleum ether
PEG	Polyethylene glycol
RPMI	Roswell Park Memorial Institute (media)
PSA/MSA	Polar surface area to molecular surface area
PVA	Polyvinyl alcohol
PVP	Polyvinyl pyrrolidone
q	quartet
Q-TOF	Quadrupole time-of-flight
QLL	Quasi-liquid layer
QSAR	Quantitative Structure-Activity Relationship
RBC	Red blood cells
Rf	Retention factor
rt (RT)	room temperature
s	singlet
SAR	Structure-activity relationship
sat.	saturated
SD	Standard deviation
SDS	Sodium dodecyl sulfate
% SEM	Percent standard error of the mean
t	triplet
TBAF	Tetrabutylammonium fluoride
TEM	Transmission electron microscopy
TF-1α	Human bone marrow erythroblasts
T_g	Glass transition
TH	Thermal hysteresis
THF	Tetrahydrofuran
Thr	Threonine
TIPS	Triisopropylsilyl

TIPS	Triisopropylsilyl chloride
TLC	Thin-layer chromatography
TNC	Total nucleated cell
TsCl	4-Toluenesulfonyl chloride
tt	triplet of triplets
UCB	Umbilical cord blood
USRA	Undergraduate student research award
UV	Ultraviolet
UV-vis	Ultraviolet-visible

1 Advancements to Cryopreservation using Ice Recrystallization Inhibitors

Cryopreservation of biological substances, or the use of low temperatures for the preservation and storage of various cell types, tissues, organs, and other substances, has allowed for significant advancements in the field of medicine and cryobiology, among numerous other applications. From a historical perspective, research in the field of cryobiology can be divided based on the date of the discovery that glycerol could be used to improve the preservation of cells at low temperatures in 1949 (pre- and post- glycerol discovery).[1,2] Glycerol as a cryoprotective agent (CPA) could permeate the cell and displace water due to the osmotic pressure differential; thereby reducing the intracellular ice growth.[3,4] In 1950, Smith *et al*. successfully cryopreserved red blood cells (RBC) with glycerol.[5] In 1959, Lovelock and Bishop identified dimethyl sulfoxide (DMSO) as a CPA that was more cell permeating than glycerol.[6] Notably, in 1971-1972, reports described the successful use of DMSO as a water-displacing cryoprotective agent (CPA) for various cell types and mouse embryos.[1,7–9] A key finding from these studies was the realization that an optimal cooling rate existed for each cell type.[4] Collectively, these fundamental discoveries advanced the field of cryobiology and facilitated the development of other techniques such as a non-equilibrium ice-free, ultra-rapid freezing technique and vitrification.[10–15] For example, the first hematopoietic stem cell transplant (HSCT) from cryopreserved umbilical cord blood was conducted in 1988 and to this day, the transplant recipient is still healthy thus showcasing the applications for cryopreserved umbilical cord blood.[16] Beginning in the late 1990s, researchers began to study the phenomenon of delayed-onset cell death post-cryopreservation and its link to disruption of the proteome or genome

resulting in a lower cell survival.[17–20] As new cellular therapies emerged over the past decades and continue to emerge today, there is a drastic need for better cryopreservation techniques. To this end, research in the optimization of cooling and warming rates, automation of cryopreservation, and biological substance banking worldwide have been reported. One emerging field of cryobiology involves the development of CPAs able to mitigate the cellular damage associated with ice crystal growth in biological substances. The continued research on these molecules, ice recrystallization inhibitors (IRIs), is the focus of this thesis.

1.1 Cryopreservation and its current issues

1.1.1 Cryopreservation

The three common techniques for biopreservation are hypothermic storage, vitrification, and cryopreservation. Hypothermic storage involves the preservation of substances with a cryoprotectant at temperatures such as between 4 °C and 10 °C, but above the sample's freezing temperature. These low temperatures allow for a reduction in the cell's consumption of important cellular metabolites, and therefore, significant cellular injuries are avoided.[21–23] This "metabolic suppression" technique offers a means of achieving short-term storage (several days to weeks); however, it induces a loss of viable and functional cells due to chilling injuries including necrosis and apoptosis.[17–19,24,25] Cell rupture may occur immediately upon exposure to cold storage while some other cells may eventually (multiple hours after cold exposure) experience severe membrane damage resulting in necrosis. Research focusing on how specific cell/tissue types respond to stress are resulting in improved solutions for hypothermic storage.[26–28] Vitrification is the preservation of samples in an ice-free glass-like state. This involves the introduction of a

CPA into the biological sample as the substance is quickly cooled thereby creating a more viscous cryomedium.[15,29,30] As viscosity increases, a phase transition to a glass-solid state is observed. The difficulties of using this method include achieving an ultra-rapid cooling rate on large samples, which is required to produce the glass-solid state, as well as having to use high concentrations of CPAs. Further, cryoinjuries can arise as a result of ice formation and growth when devitrification occurs as a result of too slow a warming rate. Recent techniques aimed at overcoming such cryoinjuries are continually being developed including the concepts of isochoric (constant volume) vitrification or the use of nano-warming after vitrification (where nanoparticles from glass are used to prevent ice formation).[31–33] The third common preservation technique is cryopreservation. Cryopreservation stores samples at sub-zero temperatures (-80 °C to -196 °C) whereby biological processes are essentially halted. This biopreservation method allows for the long-term storage of various cell types such as for more than 10 years. However, cryopreservation requires attention to various factors such as cell concentration and sample volume, cooling and warming rates, storage temperature, and choice of cryoprotective agent(s).[21,23,34–36] Significant loss of viability is associated with the formation of intra- and extracellular ice during the freezing and thawing processes of cryopreservation as well as due to osmotic shock on the cell. While CPAs can mitigate these issues, they are often cytotoxic and therefore must be removed after thawing. Numerous approaches to improve cryopreservation include the concepts of ice recrystallization inhibitors to decrease the amount of CPA required, implementation of isochoric cryopreservation (resulting in storage between -5 °C to -30 °C instead of -196 °C), among others.[32]

1.1.2 Mechanisms of cryoinjury

Cell injury associated with cryopreservation (rupturing of cells, necrosis, and apoptosis) usually occurs as the result of the freezing and thawing processes.[3,37] Thermal and osmotic shock, reactive oxygen species, ischemia, exposure to toxic cryoadditives, and mechanical damage due to ice formation and growth result in either immediate or delayed non-repairable membrane damage.[38] If cells experience immediate severe damage to their membranes, this results in cell rupture. However, cells may respond differently to cold exposure during freezing and thawing; in fact, some cells may rupture multiple hours after exposure (e.g. during thawing of cell substances) as a result of necrotic cell death.[20,25,39] Mazur's Two-Factor Hypothesis informs us there are optimal freezing and thawing rates for each cell type based on the permeability of the cellular membrane as well as the cryoprotectant used during the process.[4] As the temperature of a system is reduced to -5 °C, supercooling occurs (**Figure 1.1a**). As the sample cools further, ice begins to spontaneously nucleate in the extracellular medium. Finally, as the ice grows, solutes become concentrated in the non-frozen extracellular medium. Due to increased osmotic pressure of the partially frozen extracellular medium, the unfrozen intracellular water now has a higher chemical potential, and this osmotic difference leads to water efflux out of the cell. When using a fast cooling rate, cells may not dehydrate fast enough to achieve osmotic equilibrium, resulting in intracellular ice formation (IIF) which is a significant contributor to cryoinjury (**Figure 1.1a**). While there are various mechanisms proposed for the formation of intracellular ice based on cooling rate, temperature, and the specific cell type, it is widely accepted that IIF leads to substantial cell death specifically as a result of ice recrystallization during the thawing period.[3,4,40–46] In contrast, if the cooling rate is slow (sub-optimal), water efflux will occur leading to a severe decrease in cell volume. This

results in a toxic environment for the cell due to high intracellular solute concentration, and both this cell shrinkage and the high intracellular electrolyte concentration can lead to significant cellular injury.[4] For instance, the weakening of the lipid-protein composition of the cell membrane has been proposed as a result of these electrolyte and osmotic imbalances ultimately leading to cell rupture.[47] An optimal cooling rate (which is cell-specific) mitigates the issues that arise due to the "solution effects" and also prevents IIF, as cells have time for sufficient dehydration.[4] In a graph of cooling rates versus cell survival, cell survival follows an inverted "U shape" based on the cooling rate, the water permeability of the cell, and the solution effects (**Figure 1.1b**).

(a)

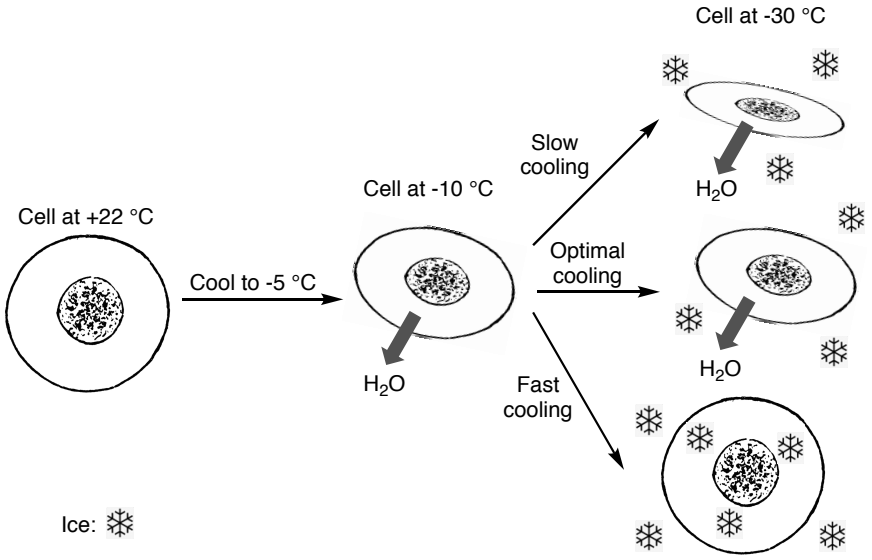

b)

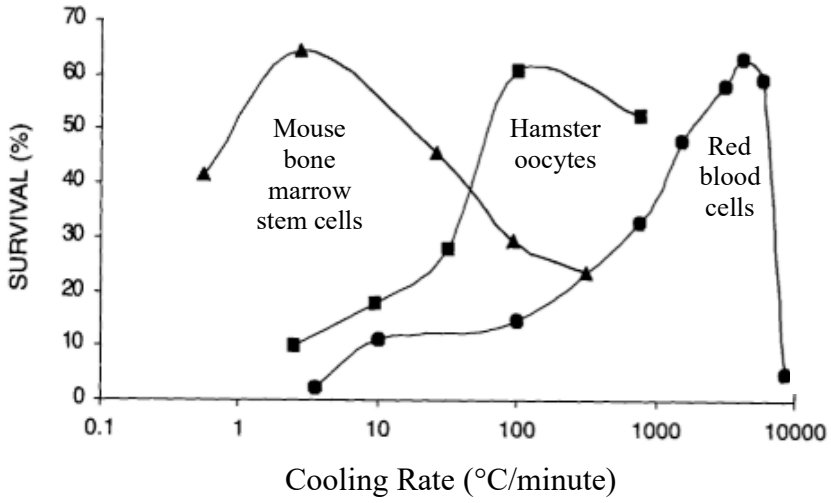

Figure 1.1. **(a)** A depiction of the processes occurring during the freezing procedure,[4,46,48,49] and **(b)** survival of cell types as a function of cooling rate adapted from Elsevier (Cryobiology) and Oxford University Press.[49,50] Figure adapted from Cryobiology, 14(*3*), P. Mazur, The Role of Intracellular Freezing in the Death of Cells Cooled at Supraoptimal Rates, 251-272, 1977, with permission from Elsevier (Cryobiology).

In addition to using an optimal freezing rate, the thawing rate is also paramount to cell survival and this is due to the process of ice recrystallization, whereby ice crystals grow larger

and lead to mechanical damage to the cell. In addition to the physical and mechanical injuries associated with cryopreservation, there are also biochemical cellular injuries resulting from the freezing/thawing methods due to reduced energy and metabolic abilities, uncoupling of biochemical pathways, as well as activation of stress response pathways.[38] Until the cell reaches the glass transition of water (T_g, below -140 °C), biochemical processes are slowed but not entirely halted thereby often leading to incomplete and unregulated reactions. In addition to alterations to cell membrane integrity, ionic and osmotic imbalances, the formation and accumulation of toxic intermediates (free radicals, anaerobic metabolites, and waste products) leads to further damage either immediately or by activating stress responses upon warming the sample. Often, the accumulation of these stressors leads to programmed cell death as well as necrosis.[19,20,27,36,51] Even the exposure to potentially toxic but otherwise beneficial cryoadditives can lead to damage, highlighting the necessity of developing new and improved cryoprotectants.

1.1.3 Cryoprotective Agents

Even while adhering to optimal cooling and warming rates for cryopreservation, biological samples still require further protection to avoid cryoinjuries; therefore, supplementation of the cryomedium with a cryoprotective agent (CPA), such as glycerol or dimethyl sulfoxide (DMSO), can result in increased cell survival. A typical cryopreservation protocol involves the addition of a cryoprotectant to the sample before the freezing process, cooling the sample to a low temperature, followed by thawing of the sample, and potential removal of the CPA post-thaw. The chosen cryoprotectant can either be a permeating CPA, non-permeating CPA, or a cryoprotectant mixture containing both components and this is based on the cell type and biological sample.[52–58] By remaining outside of the cell during the

cryopreservation process, non-permeating cryoprotectants mitigate cryoinjury associated with insufficient cell dehydration by increasing the concentration of solutes in the extracellular medium.[48,52,54] This class of CPAs offer protection to cells during rapid cooling rates by reducing the possibility of IIF and includes various polymers, starches, and carbohydrates, ranging from large molecules including like dextran 40, polyethylene glycol (PEG), polyvinyl pyrrolidone (PVP), hydroxyethyl starch (HES) to lower molecular weight compounds such as trehalose and sucrose.[59–66] In addition to their osmotic effects, non-permeating CPAs also stabilize the cell membrane through oncotic forces of the high molecular weight compounds as well as their alterations to the unfrozen water.[67–69] Non-permeating CPAs are typically less toxic than other CPAs and therefore do not always need to be washed out after cryopreservation.[53] However, reduced cell recovery is usually observed with these CPAs compared to permeating CPAs. Permeating cryoprotectants, meanwhile, cross the cell membrane and are effective at protecting intracellular compartments during slow cooling rates by replacing the intracellular water thereby maintaining appropriate cell volumes.[70,71] Common permeating CPAs, such as glycerol and dimethyl sulfoxide (DMSO), also prevent cryoinjuries associated with high electrolyte concentrations through "salt buffering" where neutral solutes depress the freezing point of the solution thereby avoiding the exposure of the cell to lethal salt concentrations.[6,49,55,72,73] During thawing, care must be taken to follow appropriate re-hydration techniques since water can cross into the cell more quickly than dimethyl sulfoxide which would result in cell swelling.

The addition and removal of cryoprotectants, as well as the toxicity of the CPA, can lead to significant cellular injury. While more research into CPA toxicity is required, permeating CPAs are known to disrupt cellular signalling and other cellular activities including various protein functions.[53,72,74] For example, dimethyl sulfoxide, a cryoprotectant commonly used for

numerous cell types and tissues including hematopoietic stem cells (HSC) has a significant toxicity profile associated with its properties.[74–81] Further, molecular dynamic simulations have shown that cell membranes become less thick in the presence of dimethyl sulfoxide followed by the formation of pores at a critical CPA concentration, and a reduction of membrane stability at higher concentrations.[82] Due to the toxicity of these CPAs, there has been considerable research identifying biophysical factors required to successfully cryopreserve biological samples including investigations into the effective concentration of these cytotoxic CPAs.[53] Numerous studies have shown that reduction of the concentration of DMSO for cryopreservation from 10% DMSO to 7.5% or 5% DMSO results in comparable post-thaw viabilities.[83] Exploring methods of reducing CPA concentrations while still observing cryoprotective effects is of great importance due to the relatively high concentration of CPAs used and their impacts on a multitude of targets. Despite these efforts, there remains significant injury associated with cryopreservation; specifically, with the formation and subsequent growth of ice crystals in both the intracellular and extracellular space. Notably, there is a significant need to mitigate injuries associated with ice formation and the subsequent increase in the size of ice crystals at the expense of smaller crystals in order to implement more effective CPAs and to improve the cryopreservation protocols.

1.1.4 Cryopreservation of hematopoietic stem and progenitor cells

Hematopoietic stem and progenitor cells (HSPCs) are a heterogeneous pool of cells that maintain an organism's blood system through the HSPCs' abilities of quiescence, self-renewal, and differentiation. Hematopoietic stem cell transplantation (HSCT) from a cryopreserved umbilical cord blood (UCB) source has emerged as a life-saving treatment in which HSPCs are

used to reintroduce stem cells into an organism after disease or malignancy. HSCTs are often used as a last resort to treat various malignant and non-malignant hematologic disorders including acute and chronic leukemias, and anemias. The benefit of using UCB for HSCT applications as opposed to HSPCs from other sources is that there are less stringent HLA matching criteria due to the lower rates of graft-versus-host disease (GVHD) associated with HSCT from UCB, UCB is a readily available source of HSPC, as well as the fact that the collection of UCB is non-invasive and low risk for the donor. However, one major disadvantage to the use of UCB is the relatively lower number of HSPC available from the one-time collection and cryopreservation of the cells in comparison to other HSPC sources, such as from bone marrow (BM). To account for this reduced cell dose, research has been aimed at increasing the number of viable and functional HSPCs that are isolated from UCB. Toward this end, one such approach is to improve the cryopreservation of HSPCs.[59,77,84] Current conventional cryoprotectants and protocols result in a loss of post-thaw viability and functional capacity of HSPCs.[85–87] As a result of cryopreservation, higher levels of apoptotic HSPCs leads to reduced activities of the cells post-thaw, and ultimately these apoptotic cells may negatively influence engraftment success.[59,77,84,87–89] Dimethyl sulfoxide (DMSO), the standard cryoprotectant used for the cryopreservation of HSPCs, fails to mitigate uncontrolled ice growth which ultimately leads to a loss of cell number and potency after cryopreservation.[90–95] Further, residual DMSO in thawed stem cell grafts has been linked to negative outcomes in the transplant recipient associated with the gastrointestinal, cardiovascular, respiratory, renal, hepatic, and central nervous systems.[79,93,96–98] While several other additives for HSPC preservation have been explored including ethylene glycol, propylene glycol, and various carbohydrates, these CPAs have yet to be implemented clinically.[59–63,94] Taken together, these indicate a strong need for

cryoprotective agents able to inhibit ice recrystallization (IRIs) for improving the cryopreservation methods of HSPCs from human UCB.[90,99]

1.2 The nature of ice and strategies to control ice

1.2.1 Ice recrystallization

Ice recrystallization, or the growth of larger ice crystals from smaller ones, is a thermodynamically driven phenomenon that results in a gradual increase of the mean ice crystal size present in frozen samples.[100] As discussed in detail in the previous section, the process of ice recrystallization results in significant cryoinjury. This is especially observed during the thawing process of cryopreservation of biological samples including hematopoietic stem cells and red blood cells. This thermodynamic process is also apparent in numerous other scientific applications and technologies including ice formation in aviation fuel as well as the frozen food industry.[101–104] Therefore, mitigating the damage of ice recrystallization has tremendous implications for a wide range of technologies, including the improvement of cryopreservation protocols for biological samples. The understanding of ice formation and growth is thus required prior to the rational development of inhibitors of ice recrystallization.

1.2.1.1 Structure of Ice and Ice Nucleation

The phase transition of water to ice is ubiquitous. Ice crystals in a sample can exist in many different polymorphic forms due to the arrangement of water molecules in the crystals at various temperatures and pressures. Conventionally, ice has been viewed as displaying the distinctive stable hexagonal (I_h) and metastable cubic crystal structures (I_c) depending on the

conditions.[105–108] However, recent reports indicate that ice is a complex material that often exhibits a stacking disorder structure depending on how it was formed and whether it was subjected to temperature changes.[105,109,110] Further, experimental results and molecular simulations suggest that at ambient pressure, supercooled water nucleates to form the meta-stable stacking-disordered ice (I_{sd}) which contains cubic ice mixed with hexagonal sequences.[109,111–114] Notably, this stacking-disordered form of ice can then transform through recrystallization mechanisms to the highly-ordered hexagonal ice (I_h) which is the most thermodynamically stable and common sub-zero polymorph at atmospheric pressure.[106,109,115] As depicted in **Figure 1.2**,[116] the I_h lattice is comprised of four axes (a_1, a_2, a_3, c) that form eight faces.[106,115,117,118] This polymorph contains the basal plane, the primary and secondary prism planes, and the pyramidal plane.[116] In this highly ordered state, the water molecules are arranged through intermolecular hydrogen bonds in which a molecule's oxygen atom forms hydrogen bonds with two adjacent hydrogen atoms. This formation leads to the characteristics observed for hexagonal ice including rapid growth along the *a*-axis of the growing sheets (prism planes) and slower growth along the *c*-axis (basal plane) leading to hexagonal-shaped crystals.[106,115,117,119]

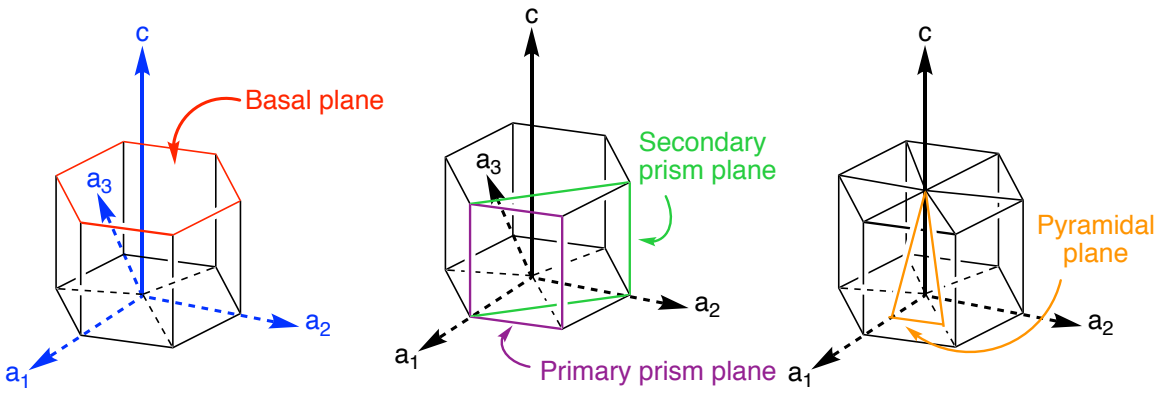

Figure 1.2. Representation of the axes and planes that give rise to hexagonal-shaped ice crystals (I_h).[116]

The freezing process includes the movement of water molecules, hydrogen bond formation at the ice surfaces, and the final phase change that includes the release of heat.[120] In a partly frozen sample, there is a transitional layer between the disordered bulk water phase and the ice crystal lattices, and this layer is termed the quasi-liquid layer (QLL). The QLL's structure and dynamics have tremendous implications for the adsorption of molecules onto the surface of ice as well as the kinetics and thermodynamics of reactions at this interface.[118,121–125] Notably, light scattering techniques have revealed that ice crystal growth occurs in this semi-ordered layer.[126,127] There is considerable variation observed in reports of the other QLL properties such as the layer's structure and thickness, its ice-like or water-like characteristics, as well as its density and diffusion constants.[100,128,129] Interfacial force microscopy data describe the quasi-liquid layer as exhibiting both viscous and elastic behaviours, while other studies report the QLL displaying more water-like properties or others suggesting more ice-like characteristics.[123,124,130–135] Computational results suggest that ice formation occurs in a region with low liquid movement, where water molecule mobility continues to decrease before arranging into ice-like crystals, and these molecules further slow the motion of neighbouring water molecules.[136–139] The thickness of this QLL is dependent on the temperature: the QLL layer is reported as being roughly one monolayer of water (<0.3 nm) thick when the temperature is below -10 °C compared to approximately 15 nm in thickness at temperatures near the melting point of the ice.[122,134,140–142] These results also differ based on the face and plane of the ice in question. While research supports the existence of the quasi-liquid layer initially proposed by Faraday in 1859, further investigation into the QLL is undoubtedly required.

1.2.1.2 Mechanism of ice recrystallization

Ice growth in a frozen sample (recrystallization) has been described to occur through two possible mechanisms: grain boundary migration and Ostwald ripening. Grain boundary migration involves the net increase in crystal sizes of certain ice grains at the expense of smaller crystals through migration of the interfaces between the differently oriented ice grains.[143,144] The majority of the ice grains are initially of differing sizes and tend to display differing curvature: small grains exhibit a more convex shape which results in increased surface energy in comparison to the larger ice grains which display less convex curvature than the smaller grains (**Figure 1.3a**). To reduce the overall free energy of the system (by lowering the amount of grain boundary area per unit volume), the boundaries of the smaller ice grains will migrate toward their centres of curvature as to reduce the radius of curvature. As a result, boundaries of crystals with a more convex shape migrate inward as their grains grow smaller and eventually disappear.[143,145,146] Conversely, large ice grains displaying a less convex shape grow outward toward their centre of curvature thereby growing in size. Notably, grain boundary migration describes the direct movement of water molecules in systems below -10 °C, and as a result, this theory does not account for the presence of a bulk-water layer and a QLL observed in ice at ambient pressure.[145]

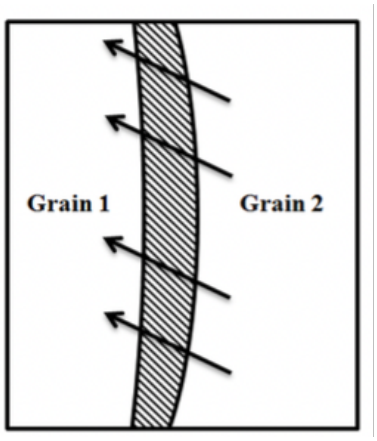

Figure 1.3. A schematic representation of grain-boundary migration adapted from the literature.[147] The arrows indicate the movement of a grain boundary (the shaded liquid-layer) as the larger ice grain (Grain 2) becomes larger while the smaller Grain 1 decreases in size to reduce its degree of boundary curvature.

Ostwald ripening, however, takes this entire system into consideration. This mechanism describes the thermodynamic growth of larger ice crystals at the expense of smaller ice crystals leading to a reduction in the crystal surface/water interface energy of the system.[148–152] At a constant ice volume, the decrease in the number of ice crystals as a result of the increase of average ice crystal sizes occurs by accretion in materials containing high-ice fractions, whereby two crystals fuse to form one larger crystal.[148] Alternatively, if the ice fraction is of a lower volume, ice recrystallization occurs by water molecule diffusion whereby water molecules may diffuse from smaller crystals to larger ones through the QLL. The rate of crystallization is dependent on the diffusion rate of molecules between crystals as well as the activation energy required for alterations of the crystal surface. Since smaller crystals have a higher surface-area-to-volume ratio compared to larger ice crystals, the process of recrystallization leads to a reduction of free energy of the system. This drive to equilibrium whereby larger ice crystals grow as smaller crystals disappear leads to a coarser matrix and this physical process leads to a

reduction in product quality of biological samples; for example, the formation of intracellular ice in cellular products results in reduced viability.[151] Furthermore, ice recrystallization also occurs in a system subjected to temperature fluctuations, such as the improper handling of frozen samples.[153] Thus, there is a clear rationale for the development of materials able to inhibit these processes. As described in **Section 1.2.2**, many living organisms have methods of controlling ice and are often the inspiration for the development of synthetic ice growth inhibitors.

1.2.2 Strategies to control ice

Many living organisms, such as plants, fish, amphibians, and insects use various strategies to reduce injuries incurring from ice recrystallization.[154–156] Species that are "freeze-avoiding" prevent the formation of ice by increasing the concentration of solutes (e.g. polyols like carbohydrates) in their bodily fluids thereby lowering the freezing point of water and/or by eliminating species that nucleate ice thereby preventing ice nucleation.[148,154] On the other hand, freeze-tolerating species survive exposure to sub-zero temperatures by producing antifreeze proteins (AFPs) and antifreeze glycoproteins (AFGPs) which enable ice formation but inhibit ice growth. These AF(G)Ps are termed biological antifreezes (BAs) and inhibit ice growth by adsorbing to various faces of hexagonal ice (I_h).[115,117,118,157–159] AF(G)Ps have attracted attention due to their ability to act as ice recrystallization inhibitors (IRIs); however, due to the proteins' abilities to irreversibly bind to ice, they also exhibit a property termed thermal hysteresis (TH). While biological antifreezes (BAs) have diverse structures and sizes, all AF(G)Ps exhibit ice-binding behaviours. The affinity the AF(G)P has for a specific plane of ice dictates the antifreeze activity observed and this is proposed to have to do with the ice-binding sites present on the proteins.[160–167] Further, several structure-activity relationship studies on the amino acids

comprising the ice-binding sites of AF(G)Ps have revealed that there are a variety of important features for activity including a balance between hydrogen bonding,[163] the ordering of water molecules,[164,168,169] van der Waals interactions,[170] hydrophobic forces,[170–172] among other contributors.[173–175] Nevertheless, this ice-binding activity leads to two of the common mechanisms by which AF(G)Ps offer protection to freeze-avoidant and freeze-tolerant organisms which are thermal hysteresis (TH) activity and ice recrystallization inhibition (IRI) activity.

Thermal hysteresis (TH) activity describes the process of reducing the freezing point of a solution below the melting point.[176,177] This phenomenon leads to a thermal hysteresis gap where intracellular ice present is inhibited from growing or melting.[178] TH activity is commonly assessed using nanolitre osmometry where solutions are frozen and thawed slowly to observe the behaviour of a single ice crystal (**Figure 1.5a**).[179–181] Studies have shown that the TH activity is a non-colligative property produced by adsorption of AFGPs to the non-basal planes of ice crystals.[116,163,177,182] The Adsorption-Inhibition model describes the irreversible and preferential binding of an AF(G)P to a specific plane of the ice crystal thereby preventing growth along this axis.[177] As a result of the adsorption, the ice must grow along a different axis leading to a bipyramidal crystal shape (dynamic ice shaping or DIS) and ultimately, an increase in ice surface curvature.[177] Higher energy is required to add further water molecules to the curved crystal surface and therefore, the freezing point is lowered. This process, as described by the Gibbs-Thomson (Kelvin) Effect, occurs for the freezing point; however, not for the melting point.[116,176] Within this resulting TH gap, AF(G)Ps inhibit further ice growth either through a step-pinning mechanism whereby bound AF(G)Ps force further growth to occur at sites along the same plane but where the proteins are not bound, or through the mattress mechanism whereby the growth would have to occur perpendicular to the specific ice plane.[163,177]

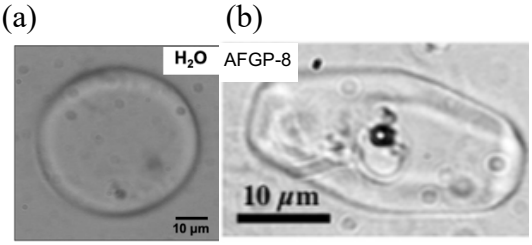

Figure 1.5. **(a)** Image of ice crystal in the absence of AF(G)P and therefore no thermal hysteresis,[183] and **(b)** image of an ice crystal undergoing dynamic ice shaping (1 mg/mL AFGP-8 in water) reprinted from Crybiology, 70, C. J. Capicciotti, J. S. Poisson, C. N. Boddy, R. N. Ben, Modulation of Antifreeze Activity and the Effect Upon Post-Thaw HepG2 Cell Viability After Cryopreservation, 79-89, 2015, with permission from Elsevier (Cryobiology).[184]

In addition to TH activity, AFGPs also inhibit ice recrystallization thereby preventing the growth of larger ice crystals from smaller ones as previously described in **Section 1.2.1.2**.[116,185–188] The ability of AFGPs to inhibit ice recrystallization can be modulated depending on the presence of ions and hydrocolloids. This IRI activity, along with TH activity resulting from AF(G)Ps binding to ice surfaces, offers promising properties for technologies aimed at preserving substances at low temperatures; however, TH activity is considered detrimental to the cryopreservation process.[194–197] In the laboratory, ice recrystallization inhibition activity (IRI) can be assessed using a variety of methods[189–192] including the sandwich assay;[148] however, the activity is often investigated by polarized optical microscopy using the splat-cooling assay (**Figure 1.6**).[193] Briefly, the splat-cooling assay (performed in triplicate) involves the freezing of a test sample dissolved in phosphate-buffered saline (PBS) followed by an annealing period of 5- or 30-minutes at -6.4 °C. After this time, images of ice crystals are taken using a microscope-fitted camera and the areas of ice crystals are analyzed. There are two variations of ice crystal analysis using the splat-cooling assay: the first of which offers a snapshot of IRI activity at a single concentration while the second option offers a truly quantifiable method of IRI

determination albeit through a more time-consuming process. The first analysis involves implementing the splat-cooling assay with a 30-minute incubation period followed by determination of the percent mean grain size (% MGS) of ice crystals compared to ice crystals in the control condition. The % MGS is determined by measuring the cross-sectional areas of 12 random ice crystals in an image (three images are analyzed per run of the assay). Ice recrystallization inhibitors can be identified by comparing the resulting % MGS obtained for a test compound, as smaller ice crystals indicate the presence of an inhibitor compared to the larger ice crystals indicating no IRI is present (**Figure 1.6**). Previously, the Ben laboratory has arbitrarily deemed a % MGS above 80% to be negligible or weak IRI activity, a % MGS between 30-80% to be moderate IRI activity, and a % MGS below 30% to be potent IRI activity. This protocol involving a 30-minute annealing period followed by determination of the percent mean grain size of ice crystals offers a way to screen a set of compounds for potential activity at a single concentration (and time point). Altogether, the % MGS analysis provides a general overview of the activity of a compound(s) at a specific concentration using a relatively rapid analysis.

However, the 30-minute IRI analysis protocol does not provide information on the IRI kinetics, it does not address the heterogeneous nature of ice crystal sizes observed, nor does it address the concentration or time dependence of crystal growth. Instead, the second analysis is used in conjunction with a modified splat-cooling assay involving a 5-minute annealing period. This second approach is implemented as a tool to obtain the additional kinetic parameters surrounding the IRI activity of promising compounds, and for overcoming the drawbacks of the original splat-cooling assay. In this modified technique, multiple concentrations of a compound are analyzed, and the initial rates of ice recrystallization are obtained for each condition.

Accordingly, dose-response curves for the IRI activity are generated as well as determination of the concentration at which 50% inhibition is achieved (IC_{50} value). An annealing period of 5-minutes and the associated initial rates of inhibition provide accurate kinetic data, and as a result, this modified approach is a reliable and quantifiable analysis of promising IRI candidates.

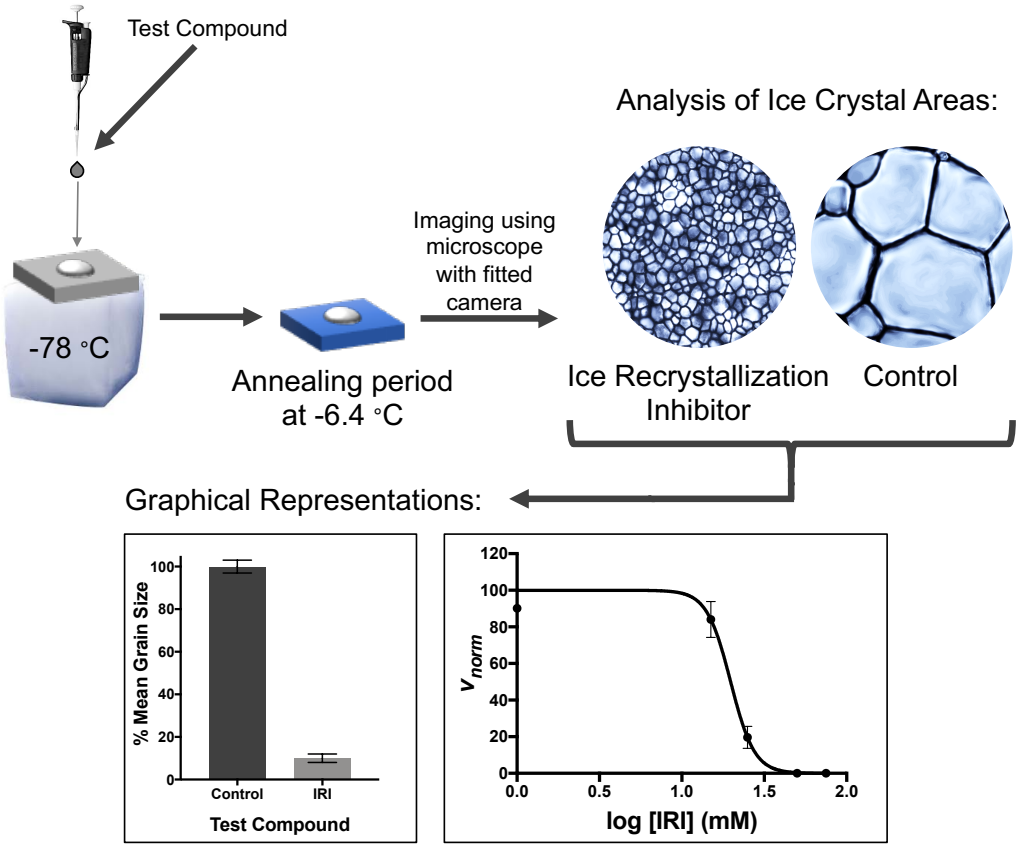

Figure 1.6. The splat-cooling assay used for the determination of ice recrystallization inhibition activity. Ice crystals in the absence of an inhibitor are larger than those in the presence of an inhibitor. IRI activity is represented either as the percent mean grain size (% MGS) of ice crystals obtained after a 30-minute annealing period or as dose-response curves generated by normalized rates after 5-minute annealing periods.[193,198,199]

1.3 Ice recrystallization inhibitors

AF(G)Ps can be potent ice recrystallization inhibitors (IRIs) at low micromolar concentrations; however, they exhibit thermal hysteresis (TH) which is detrimental to biological samples. Further, the high cost of synthesis or expression of AF(G)Ps as well as their low stability reduces their potential for large-scale use in industrial applications. Small-molecular weight ice recrystallization inhibitors (IRIs), on the other hand, offer the advantage of lower production costs with higher-yielding syntheses, more long-term stabilities, as well as the potential for scientists to tailor the properties of the IRIs to the specific needs of the technology. Owing to several structure-function studies, various moieties of AF(G)Ps can now be incorporated into synthetic analogues to "custom-tailor" these molecules to display IRI activity but not TH activity.

1.3.1 Key structural features for antifreeze activity

As mentioned in the previous section, studies on the structure-activity relationship of AF(G)Ps and analogues have indicated a variety of important structural features for ice-binding activity and thermal hysteresis activity. These include a balance between hydrogen bonding of the ice molecules and protein residues,[163] the ordering of water molecules,[164,168,169] van der Waals interactions[170] and hydrophobic interactions[170–172] at ice-binding sites of the proteins, as well as other factors.[173–175] Further, studies have revealed that hydroxyl groups of the carbohydrates in AFGPs and their glyco-analogues play an important role due to their hydrogen bonding abilities with the ice crystal lattice,[182,200] as well as the glycoprotein's size and secondary shape.[201,202] Over the past decade, there has been tremendous research toward the

identification of the structural features required for ice recrystallization inhibition (IRI) activity. This investigation began with synthetic AFGP analogues with varying TH and/or IRI activity,[201,203–209] and then progressed to small-molecule IRIs that are IRI-active yet do not display TH activity.[184,199,200,210–216] Further, there have been numerous studies on polymeric analogues possessing these antifreeze activities.[188,217–222] Small-molecule IRIs that exhibit ice recrystallization inhibition but do not bind to ice are promising cryoprotectants for a variety of cellular products and are subject to further investigation toward the development of more promising cryoprotectants.

1.3.2 Synthetic macromolecules as ice recrystallization inhibitors and AFGP analogues

Antifreeze glycoproteins (AFGPs) have drawn significant interest within the field of materials sciences including in the development of synthetic materials that mimic the activity of naturally occurring antifreezes (BAs). The first instance of a synthetic polymer exhibiting ice recrystallization inhibition was in 1995 when polyvinyl alcohol (PVA) was reported to display potent IRI activity,[188] and higher molecular weight polymers of PVA have since then been found to be more IRI-active than PVA polymers with lower molecular weights.[221] Polymers are advantageous in that they are more easily synthesized and are therefore more amenable to large scale production than the naturally occurring BAs. Unfortunately, the spacing of hydroxyl groups in PVA polymers may result in ice binding activities and would explain the dynamic ice shaping and a small TH gap observed as part of PVA's antifreeze activities.[217,218] Since the discovery of PVA, there have been many studies toward the development of other structurally diverse, synthetic (glyco)polymers as ice recrystallization inhibitors.[219–229] For example, polyethylene glycol (PEG), poly-L-lysine, poly-L-glutamic acid, among others are weak inhibitors of ice

recrystallization.[222,230] Poly-L-hydroxyproline was found to display IRI activity similar to PVA.[222] Various dyes have been investigated, such as Safranin-O (an aromatic and planar organic dye) which assembles into facially amphipathic fibres in solution and was found to be highly IRI active.[231] Additionally, amphipathic metallohelices have also displayed IRI activity.[232] Recently, the development of biopolymeric mimetics of AFGPs has been investigated as materials that self-assemble into structures able to inhibit ice growth. For example, recent studies have shown that IRI activity of synthetic macromolecules may be controlled by exploiting their unique spatiotemporal properties: Nisin A is an antimicrobial peptide that exhibits switchable IRI activity based on its pH-sensitive amphiphilicity.[233] Evidently, the development of synthetic macromolecular IRIs as AFGP-analogues would offer many intriguing properties for a variety of industrial and clinical applications.

1.3.3 The rational design of IRI-active glycopeptides as AFGP analogues

1.3.3.1 The tripeptide unit of glycopeptides and its role in IRI activity

Research in the Ben laboratory on glycopeptide analogues of naturally occurring AFGPs began by exploring changes to the glycosidic bond, the linker length between the peptide and the carbohydrate moiety, the peptide backbone structure, and the carbohydrate itself. To prevent hydrolysis of an *O*-glycoside under acidic or basic conditions, glycopeptide analogues bearing a carbon linker, termed *C*-linked AFGPs, were initially synthesized.[234] These analogues also included substitution of the disaccharide with a-D-galactose, the substitution of L-threonine in the peptide unit with L-lysine, and replacement of L-alanine with L-glycine to avoid complications arising due to racemization during solid-phase synthesis (**Figure 1.7**).[234,235]

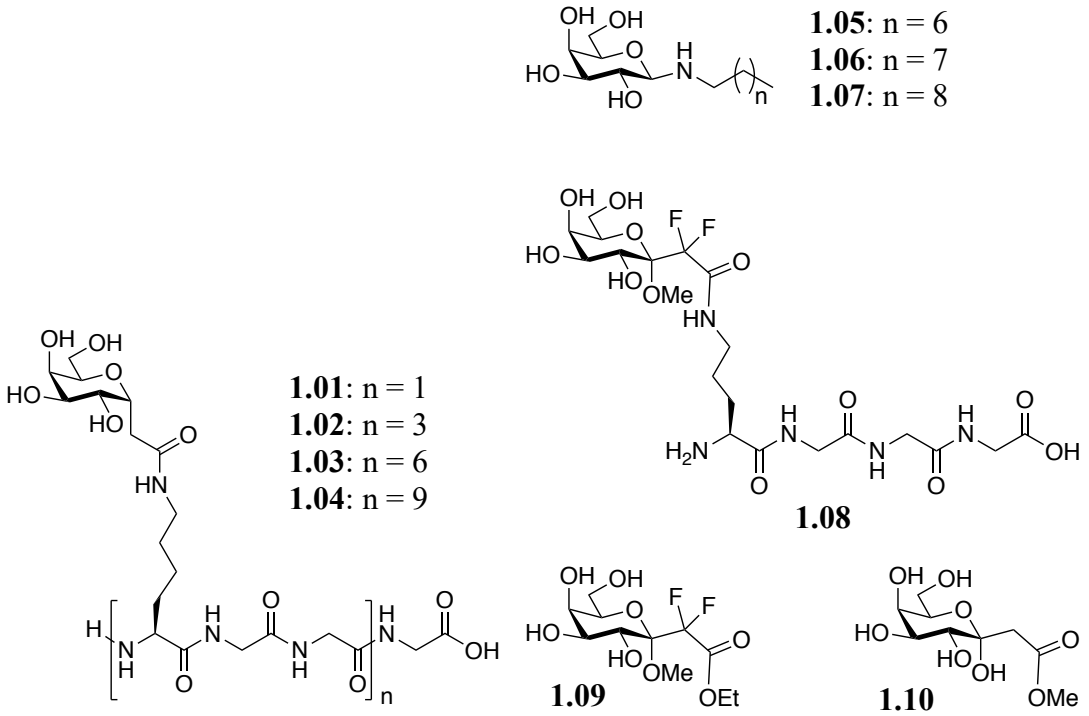

Figure 1.7. The general structure of *C*-linked AFGPs **1.01-1.04**, and the structures of *C*-linked AFGP analogues bearing alkyl chains (**1.05-1.07**) or fluorine moieties (**1.08-1.09**; a non-fluorinated analogue **1.10** is also depicted for reference).

When the analogue's peptide contained one tripeptide repeat (**1.01**, where n = 1) or 3 repeats (**1.02**, n = 3), the IRI activity was minimal at 5.5 μM (the concentration where AFGP-8 is a potent IRI). However, as the tripeptide repeat increased to n = 6 (**1.03**) or n = 9 (**1.04**), there was an increasing trend of IRI activity, and these compounds exhibited only minimal TH activity. While the n = 3 tripeptide analogue displayed weak IRI activity at 5.5 μM, further investigation revealed that this repeat length is the minimum length required for IRI activity at 22 mM.[236] IRI activity was found to depend on the number of tripeptide repeats of these *C*-linked AFGP analogues. Interestingly, this trend was also noted in a structure-activity relationship study examining the effect of replacing the peptide unit altogether with an alkyl chain in small molecule derivatives of the *C*-linked AFGP analogues. As the length of the alkyl chain increased,

so did the IRI activity (**Figure 1.7**) up until the addition of more hydrophobic moieties resulted in a drastic decrease in solubility.[236] Octyl- (**1.05**), nonyl- (**1.06**), and decyl-chain (**1.07**) derivatives were IRI active at 5.5 mM. This dependence of IRI activity on hydrophobic functionalities is consistent with other investigations, and these results clearly showed the ability of small molecule IRIs to exhibit potent inhibitory activity like the AFGP analogues.[219,224,237,238] Interestingly, octyl-β-D-galactose (**1.05**) was more active than D-galactose (**1.20**, see **Figure 1.9**) at 22 mM further confirming the notion that hydrophobic components are required for the more significant disruption of ice recrystallization mechanisms.[238] Additionally, a series of fluorine-containing *C*-linked AFGP analogues exemplified that IRI activity is more dependent on the amphipathic nature of AFGPs and their analogues than previously postulated (**Figure 1.7**).[239] In fact, fluorine analogues **1.08** and **1.09** displayed reduced IRI activity. The incorporation of a fluorine in this linker-like position (derivative **1.09**) did not affect IRI activity compared to its non-fluorine counterpart (derivative **1.10**).

1.3.3.2 The linker component of glycopeptides and its role in IRI activity

The linker length between the carbohydrate moiety and the peptide unit was examined by incorporating a *C*-serine in the peptide functionality. Generally, IRI activity decreased as the linker length increased (**Figure 1.8**) with a linker length containing six atoms displaying the most activity.[210,211] Interestingly, in derivatives with four tripeptide repeats (n = 4), a *C*-serine (**1.11**) and an ornithine analogue (**1.14**) exhibited similar potent IRI activity to that of AFGP-8 at the same concentration of 5.5 μM (**Figure 1.8**) but without the TH activity (the ornithine analogue **1.14** exhibited minimal dynamic ice shaping activity).[200] Notably, this marked the first time that analogues displayed IRI activity without the accompanying TH activity. The results

suggested that these AFGP analogues do not bind to ice to enact their antifreeze activities. Through further exploration into the role of the linker component of AFGP analogues, the presence of an amide-bond was found to be important for IRI activity and therefore derivatives with a triazole ring instead of the amide-bond resulted in reduced IRI activity.[205]

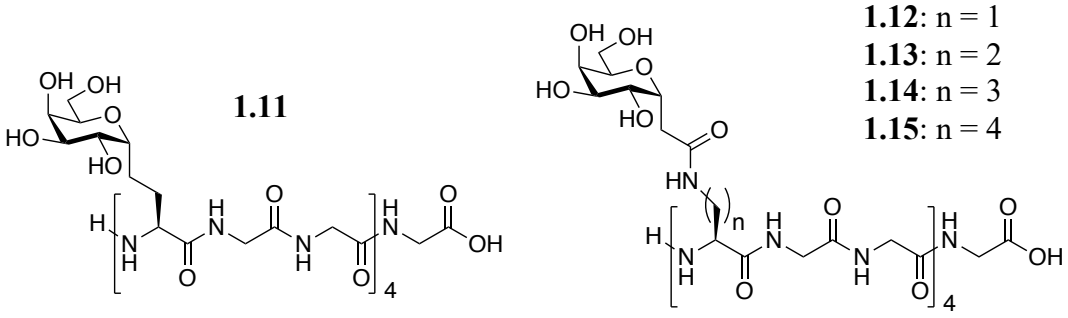

Figure 1.8. The structures of *C*-serine (**1.11**) or ornithine-based AFGP analogues (**1.12-1.15**).

1.3.3.3 The importance of the carbohydrate moiety for IRI activity of AFGP-analogues

The carbohydrate moiety's ability to impact IRI activity was investigated through the development of a series of ornithine analogue derivatives **1.16-1.19**.[200] This structure-activity relationship study revealed that substituting D-galactose (**1.16**) with D-glucose (**1.17**), D-mannose (**1.18**), and D-talose (**1.19**) led to a substantial decrease in IRI activity (**Figure 1.9**). Evidently, the stereochemistry of the monosaccharide moiety, in this case specifically at the C-2 and C-4 positions, was important for IRI activity presumably due to the effect on the ordering of the bulk-water layer surrounding the carbohydrate.[200,240,241] Carbohydrate hydration in an aqueous solution, or the amount of bound water molecules surrounding the sugar, is thought to be related to several factors including the carbohydrate's stereochemistry (specifically, the number of axial and equatorial hydroxyl groups),[242–244] the anomeric effect,[245] hydration number,[246–249] hydrophilic volume,[250] hydrophobic index,[251] and how the carbohydrate affects the neighbouring

bulk-water (its compatibility with bulk-water).[252,253] Once hydrated in an aqueous solution, a carbohydrate's size and volume affect the three-dimensional arrangement of the hydrogen-bonding of water surrounding the sugar. The number of water molecules presumed to be hydrogen-bonded to the sugar is calculated to determine the parameter termed "hydration number." Therefore, the increased IRI activity observed for the galactose derivative suggested that more disorder to the hydrogen-bonding network of water between the quasi-liquid layer and the ordered ice crystal lattice reduced the favourability of water molecules adding to the ice crystal lattice and thereby inhibiting ice recrystallization.[200] IRI activity, therefore, appeared to increase for more hydrated molecules.

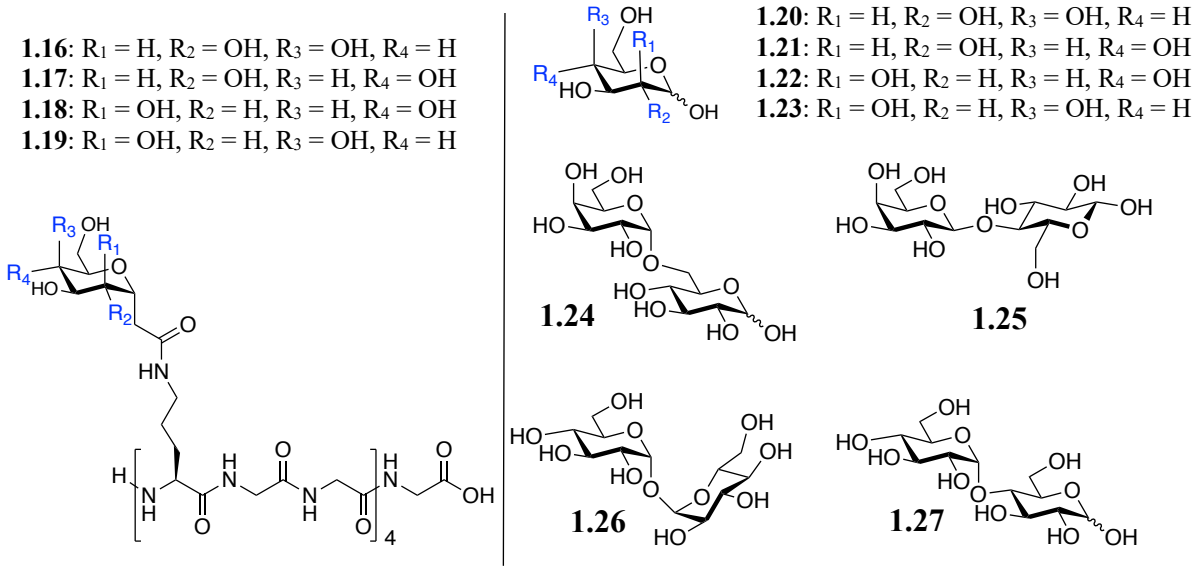

Figure 1.9. Structures of ornithine-derived AFGP analogues **1.16-1.19**, and the structure of some mono- and disaccharides tested for IRI activity.

To further elucidate the importance of carbohydrate hydration on IRI activity, a series of simple, commercially-available carbohydrates were examined for inhibitory activity (**Figure 1.9**).[240] Monosaccharides with established hydration parameters, such as D-galactose (**1.20**), D-

glucose (**1.21**), D-mannose (**1.22**), and D-talose (**1.23**), as well as various disaccharides including melibiose (**1.24**), lactose (**1.25**), trehalose (**1.26**), maltose (**1.27**), and sucrose were investigated.[241,254,255] A parameter termed "hydration index" was defined as the amount of hydration per molar volume, and accordingly, IRI activity at a low-millimolar concentration (22mM) was found to be positively correlated with the hydration index of carbohydrates.[200,240] As expected, monosaccharides with increased hydration indexes (e.g. D-galactose > D-glucose > D-mannose > D-talose) were more IRI active (exhibiting moderate-to-weak activity at 22 mM). Further, moderate-to-weak IRI activity was observed for D-melibiose, D-lactose, and D-trehalose and the activity was once again correlated with the hydration indexes of the disaccharides (e.g. D-melibiose > D-lactose > D-trehalose > D-maltose > D-sucrose). As these carbohydrates did not display thermal hysteresis nor dynamic ice shaping abilities, this antifreeze activity was not a result of direct interaction of the carbohydrates to the ice crystal lattice. The mechanism by which these carbohydrates enacted their ice recrystallization inhibition was suggested to be due to their presence at the bulk-water and quasi-liquid layer (QLL) interface. Disturbing the hydrogen-bonding arrangement of bulk-water at this interface would increase the amount of energy required for a water molecule to transfer from the bulk-water layer to the QLL, and finally to become part of the ordered ice crystal lattice.[240] This study exemplified the presence of IRI activity in molecules smaller and less complex than AFGP analogues and further, suggested a plausible mechanism by which these molecules enact their inhibitory activity. This discovery offered a new foundational point for the development of novel carbohydrate-based IRI-active small molecules that are more easily synthesized and at a lower cost than the synthesis of AF(G)P analogues. Further, these new IRIs would not lead to the detrimental effects resulting

from TH and DIS activities, and therefore, would be amenable toward the needs of the medical and commercial industries.

1.3.4 Small molecules as ice recrystallization inhibitors: Pyranose- and aldonamide-based aryl IRIs

Using the foundations discussed in **Section 1.3.3**, the Ben laboratory began developing a series of low molecular weight carbohydrate-based ice recrystallization inhibitors including a number of pyranose-based derivatives. These studies began through the exploration of surfactants and hydrogelators. These amphiphilic molecules possessed both a hydrophilic carbohydrate head and hydrophobic anomeric component (see **Figure 1.7**).[237] As expected from their surfactant-like properties, these early pyranose-based IRIs reduced cell viabilities when used as cryoprotectants, presumably due to the solubilization of cell membranes resulting from the surfactant-like structure. To avoid this detrimental property whilst maintaining important hydrophobic features, an aromatic ring was explored in place of an alkyl group at the anomeric position (**Figure 1.10**). Many pyranose-based aryl glycosides bearing *o*-, *m*-, and *p*-substituents have since been synthesized and investigated for their IRI and cryoprotective abilities.[184,199,212,215,216,256] Interestingly, the *p*-substituted derivatives, 4-methoxyphenyl-β-D-glucoside (**1.28**) and 4-bromophenyl-β-D-glucoside (**1.29**), displayed potent IRI activity and were more active than their galactose counterparts. Further investigation into the hydration of these molecules may explain this result. These studies also highlighted the importance of regioselectivity within the aryl component of the IRI as well as at the anomeric position of the carbohydrate. For example, IRI activity was reduced when the *para*-methoxy substituent in **1.28** was moved to the *meta*-position (derivative **1.30**). IRI activity was further reduced when 4-

methoxyphenyl-β-D-glucoside was compared to its alpha derivative. Nevertheless, this class of IRI possesses promising cryoprotectant candidates amenable for a variety of cells especially for red blood cell products.[212,215,256]

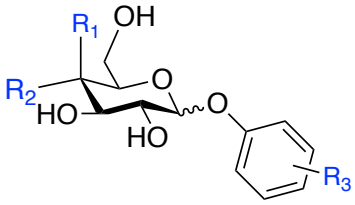

Select examples:
1.28: R_1 = H, R_2 = OH, R_3 = 4-OCH_3
1.29: R_1 = H, R_2 = OH, R_3 = Br
1.30: R_1 = OH, R_2 = H, R_3 = 3-OCH_3

Figure 1.10. The general structures of aryl glycosides developed in the Ben laboratory.

Another class of promising IRIs being developed in the Ben laboratory includes the aldonamide-based derivatives (**Figure 1.11**) and these also resulted from the investigation of surfactant and hydrogelator IRIs.[237] Specifically, the synthesized *N*-alkyl-D-gluconamides (e.g. **1.31** and **1.32**) were open-chain carbohydrates with similarities to their pyranose counterparts: they displayed a hydrophilic head group (carbohydrate component) connected a hydrophobic alkyl chain through an amide bond. Interestingly, *N*-hexyl- (**1.31**) and *N*-octyl (**1.32**) derivatives in this class displayed potent IRI activity while this activity was diminished as the length of the alkyl chain was reduced. This reduction in IRI activity was presumably due to the decreased ability of shorter alkyl chains to disrupt the hydrogen bonding at the interface of the bulk water and QLL.[237] The erythronamide series of IRIs (e.g. erythronamide **1.33**) possessed reduced IRI in comparison to the gluconamides and the alkyl tail length did not drastically influence the IRI activity; however, this shortening of the hydrophilic component was clearly detrimental to activity. The balance between hydrophobic and hydrophilic moieties is evidently very important for IRI activity as was also observed earlier with the AFGP analogues. Similar to the aryl pyranose-based IRIs, a series of aryl aldonamide-based IRIs were developed to mitigate issues

arising in a cellular setting due to the compounds' surfactant-like properties. As depicted in **Figure 1.11**, aryl derivatives with varying aryl regiochemistry have been assessed for IRI activity.[214] Derivatives such as the *N*-(2-fluorophenyl)-D-gluconamide (**1.34**) and *N*-(4-methoxyphenyl)-D-gluconamide (**1.35**) displayed promising IRI results without the cytotoxic properties observed with their alkyl-chain parent molecules.[214,237]

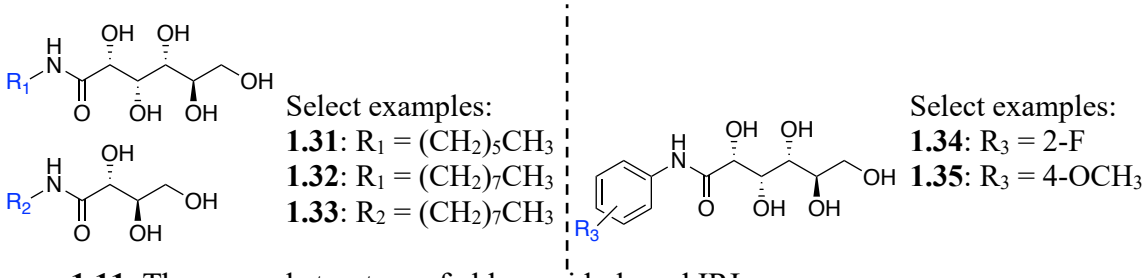

Figure 1.11. The general structure of aldonamide-based IRIs.

Evidently, the design of small molecule ice recrystallization inhibitors is not only possible, but it can lead to the development of promising cryoprotective agents. These small molecule CPAs have tremendous potential for reducing the use of toxic conventional cryoprotectants used in the cryopreservation of various biological substances. The elucidation of key structural features required for IRI activity, therefore, is crucial toward the design of IRIs and ultimately for improving the long-term storage of biological samples.

1.4 References

(1) Sztein, J. M.; Takeo, T.; Nakagata, N. History of Cryobiology, with Special Emphasis in Evolution of Mouse Sperm Cryopreservation. *Cryobiology* **2018**, *82*, 57–63. https://doi.org/10.1016/J.CRYOBIOL.2018.04.008.

(2) Polge, C.; Smith, A. U.; Parkes, A. S. Revival of Spermatozoa after Vitrification and Dehydration at Low Temperatures. *Nature* **1949**, *164* (4172), 666–666. https://doi.org/10.1038/164666a0.

(3) Mazur, P. Kinetics of Water Loss from Cells at Subzero Temperatures and the Likelihood of Intracellular Freezing. *J. Gen. Physiol.* **1963**, *47* (2), 347–369. https://doi.org/10.1085/JGP.47.2.347.

(4) Mazur, P.; Leibo, S. P.; Chu, E. H. Y. A Two-Factor Hypothesis of Freezing Injury: Evidence from Chinese Hamster Tissue-Culture Cells. *Exp. Cell Res.* **1972**, *71* (2), 345–355. https://doi.org/10.1016/0014-4827(72)90303-5.

(5) Smith, A. U. Prevention of Haemolysis during Freezing and Thawing of Red Blood-Cells. *Lancet* **1950**, *256* (6644), 910–911. https://doi.org/10.1016/S0140-6736(50)91861-7.

(6) Lovelock, J. E.; Bishop, M. W. H. Prevention of Freezing Damage to Living Cells by Dimethyl Sulphoxide. *Nature* **1959**, *183* (4672), 1394–1395. https://doi.org/10.1038/1831394a0.

(7) Whittingham, D. G.; Leibo, S. P.; Mazur, P. Survival of Mouse Embryos Frozen to -196 ° and -269 ° C. *Science (80-.).* **1972**, *178* (4059), 411–414.

(8) Whittingham, D. G. Survival of Mouse Embryos after Freezing and Thawing. *Nature* **1971**, *233* (5315), 125–126. https://doi.org/10.1038/233125a0.

(9) Wilmut, I. The Effect of Cooling Rate, Warming Rate, Cryoprotective Agent and Stage of Development of Survival of Mouse Embryos during Freezing and Thawing. *Life Sci.* **1972**, *11* (22), 1071–1079. https://doi.org/10.1016/0024-3205(72)90215-9.

(10) Rall, W. F.; Fahy, G. M. Ice-Free Cryopreservation of Mouse Embryos at −196 °C by Vitrification. *Nature* **1985**, *313* (6003), 573–575. https://doi.org/10.1038/313573a0.

(11) Nakagata, N. Survival of 4-Cell Mouse Embryos Derived from in Vitro Fertilization after Ultrarapid Freezing and Thawing. *Jikken Dobutsu* **1989**, *38* (3), 279–282.

(12) Nakagata, N. Cryopreservation of Unfertilized Mouse Oocytes from Inbred Strains by

Ultrarapid Freezing. *Jikken Dobutsu* **1990**, *39* (2), 303–305.

(13) Nakagata, N. Cryopreservation of Mouse Strains by Ultrarapid Freezing. *Jikken Dobutsu* **1990**, *39* (2), 299–301.

(14) Nakao, K.; Nakagata, N.; Katsuki, M. Simple and Efficient Procedure for Cryopreservation of Mouse Embryos by Simple Vitrification. *Exp. Anim.* **1997**, *46* (3), 231-234.

(15) Fahy, G. M.; MacFarlane, D. R.; Angell, C. A.; Meryman, H. T. Vitrification as an Approach to Cryopreservation. *Cryobiology* **1984**, *21* (4), 407–426. https://doi.org/10.1016/0011-2240(84)90079-8.

(16) Broxmeyer, H. E. Enhancing the Efficacy of Engraftment of Cord Blood for Hematopoietic Cell Transplantation. *Transfus. Apher. Sci.* **2016**, *54* (3), 364–372. https://doi.org/10.1016/J.TRANSCI.2016.05.013.

(17) Baust, J. M.; Vogel, M. J.; Buskirk, R. Van; Baust, J. G. *A Molecular Basis of Cryopreservation Failure and Its Modulation to Improve Cell Survival*; 2001; Vol. 10.

(18) Baust, J. M.; Van Buskirk, R.; Baust, J. G. Modulation of the Cryopreservation Cap: Elevated Survival with Reduced Dimethyl Sulfoxide Concentration. *Cryobiology* **2002**, *45* (2), 97–108. https://doi.org/10.1016/S0011-2240(02)00100-1.

(19) Baust, J. M.; Van Buskirk, R.; Baust, J. G. *Gene Activation of the Apoptotic Caspase Cascade Following Cryogenic Storage*; 2002; Vol. 1.

(20) Baust, J. M.; Buskirk, R. Van; Baust, J. G. *Cell Viability Improves Following Inhibition of Cryopreservation-Induced Apoptosis*; 2000; Vol. 36.

(21) Baust, J. G.; Gao, D.; Baust, J. M. Cryopreservation: An Emerging Paradigm Change. *Organogenesis* **2009**, *5* (3), 90–96.

(22) Kanias, T.; Acker, J. P. Biopreservation of Red Blood Cells - the Struggle with Hemoglobin Oxidation. *FEBS J.* **2010**, *277* (2), 343–356. https://doi.org/10.1111/j.1742-4658.2009.07472.x.

(23) Scott, K. L.; Lecak, J.; Acker, J. P. Biopreservation of Red Blood Cells: Past, Present, and Future From the Canadian Blood Services. *Transfus. Med. Rev.* **2005**, *19* (2), 127. https://doi.org/10.1016/j.tmrv.2004.11.004.

(24) Villalba, R.; Pea, J.; Luque, E.; Gómez Villagrán, J. L. Characterization of Ultrastructural Damage of Valves Cryopreserved under Standard Conditions. *Cryobiology* **2001**, *43* (1),

81–84. https://doi.org/10.1006/cryo.2001.2336.

(25) Fowke, K. R.; Behnke, J.; Hanson, C.; Shea, K.; Cosentino, L. M. Apoptosis: A Method for Evaluating the Cryopreservation of Whole Blood and Peripheral Blood Mononuclear Cells. *J. Immunol. Methods* **2000**, *244* (1–2), 139–144. https://doi.org/10.1016/S0022-1759(00)00263-5.

(26) Baust, J. Concepts in Biopreservation. In *Advances in Biopreservation*; Baust, J., Baust, J., Eds.; CRC Press: Boca Raton, FL, 2007; pp 1–14.

(27) Baust, J. M. *Molecular Mechanisms of Cellular Demise Associated with Cryopreservation Failure*; 2002; Vol. 1.

(28) Taylor, M. J. Biology of Cell Survival in the Cold: The Basis for Biopreservation of Tissues and Organs. In *Advances in Biopreservation*; Baust, J. G., Baust, J. M., Eds.; CRC Press: Boca Raton, FL, 2007; pp 15–62.

(29) Fahy, G. M.; Levy, D. I.; Ali, S. E. Some Emerging Principles Underlying the Physical Properties, Biological Actions, and Utility of Vitrification Solutions. *Cryobiology* **1987**, *24* (3), 196–213. https://doi.org/10.1016/0011-2240(87)90023-X.

(30) MacFarlane, D. R. Physical Aspects of Vitrification in Aqueous Solutions. *Cryobiology* **1987**, *24* (3), 181–195. https://doi.org/10.1016/0011-2240(87)90022-8.

(31) Fahy, G. M.; Wowk, B. Principles of Cryopreservation by Vitrification. *Methods Mol. Biol.* **2015**, *1257*, 21–82. https://doi.org/10.1007/978-1-4939-2193-5_2.

(32) Taylor, M. J.; Weegman, B. P.; Baicu, S. C.; Giwa, S. E. New Approaches to Cryopreservation of Cells, Tissues, and Organs. *Transfus. Med. Hemotherapy* **2019**, *46* (3), 197–215. https://doi.org/10.1159/000499453.

(33) Zhang, Y.; Ukpai, G.; Grigoropoulos, A.; Powell-Palm, M. J.; Weegman, B. P.; Taylor, M. J.; Rubinsky, B. Isochoric Vitrification: An Experimental Study to Establish Proof of Concept. *Cryobiology* **2018**, *83*, 48–55. https://doi.org/10.1016/j.cryobiol.2018.06.005.

(34) Bakhach, J. The Cryopreservation of Composite Tissues: Principles and Recent Advancement on Cryopreservation of Different Type of Tissues. *Organogenesis* **2009**, *5* (3), 119–126.

(35) Meryman, H. T. Cryopreservation of Living Cells: Principles and Practice. *Transfusion* **2007**, *47* (5), 935–945.

(36) Baust, J. M.; Campbell, L. H.; Harbell, J. W. Best Practices for Cryopreserving, Thawing,

Recovering, and Assessing Cells. *Vitr. Cell. Dev. Biol. - Anim.* **2017**, *53*, 855–871. https://doi.org/10.1007/s11626-017-0201-y.

(37) Bissoyi, A.; Nayak, B.; Pramanik, K.; Sarangi, S. K. Targeting Cryopreservation-Induced Cell Death: A Review. *Biopreserv. Biobank.* **2014**, *12* (1), 23–34. https://doi.org/10.1089/bio.2013.0032.

(38) Baust, J. M.; Corwin, W. L.; VanBuskirk, R.; Baust, J. G. Biobanking: The Future of Cell Preservation Strategies; Springer, Cham, 2015; pp 37–53. https://doi.org/10.1007/978-3-319-20579-3_4.

(39) Martin, H.; Bournique, B.; Sarsat, J. P.; Albaladejo, V.; Lerche-Langrand, C. Cryopreserved Rat Liver Slices: A Critical Evaluation of Cell Viability, Histological Integrity, and Drug-Metabolizing Enzymes. *Cryobiology* **2000**, *41* (2), 135–144. https://doi.org/10.1006/cryo.2000.2275.

(40) Mazur, P. Equilibrium, Quasi-Equilibrium, and Nonequilibrium Freezing of Mammalian Embryos. *Cell Biophys.* **1990**, *17* (1), 53–92. https://doi.org/10.1007/BF02989804.

(41) Toner, M.; Cravalho, E. G.; Karel, M. Thermodynamics and Kinetics of Intracellular Ice Formation during Freezing of Biological Cells. *J. Appl. Phys.* **1990**, *67* (3), 1582. https://doi.org/10.1063/1.345670.

(42) Muldrew, K.; McGann, L. E. The Osmotic Rupture Hypothesis of Intracellular Freezing Injury. *Biophys. J.* **1994**, *66* (2), 532–541. https://doi.org/10.1016/S0006-3495(94)80806-9.

(43) Mazur, P. *Life in the Frozen State - Principles of Cryobiology*, 1st ed.; Fuller BJ, Lane N, B. E., Ed.; CRC Press LLC: Boca Raton, FL, 2004. https://doi.org/10.1201/9780203647073-10.

(44) Acker, J. P.; Mcgann, L. E. *Innocuous Intracellular Ice Improves Survival of Frozen Cells*; 2002; Vol. 11.

(45) Farrant, J. Water Transport and Cell Survival in Cryobiological Procedures [and Discussion]. *Philos. Trans. R. Soc. B Biol. Sci.* **1977**, *278* (959), 191–205. https://doi.org/10.1098/rstb.1977.0037.

(46) Mazur, P. The Role of Intracellular Freezing in the Death of Cells Cooled at Supraoptimal Rates. *Cryobiology* **1977**, *14* (3), 251–272. https://doi.org/10.1016/0011-2240(77)90175-4.

(47) Lovelock, J. E. The Denaturation of Lipid-Protein Complexes as a Cause of Damage by Freezing. *Proc. R. Soc. London. Ser. B - Biol. Sci.* **1957**, *147* (929), 427–433. https://doi.org/10.1098/rspb.1957.0062.

(48) Mazur, P. Freezing of Living Cells: Mechanisms and Implications. *Am. J. Physiol.* **1984**, *247* (3 Pt 1), C125-42. https://doi.org/10.1152/ajpcell.1984.247.3.C125.

(49) Gao, D.; Critser, A. K. *Mechanisms of Cryoinjury in Living Cells*. ILAR Journal. **2000**, 41(4), 187-196.

(50) Mazur, P. Freezing and Low Temperature Storage of Living Cells. In *Proceedings of the 1974 Workshop on Basic Aspects of Freeze Preservation of Mouse Strains*; Muhlbock, O., Ed.; Stuttgart: Gustav Fisher Verlag.: Bar Habor, ME, 1976; pp 1–12.

(51) Jurisicova, A.; Varmuza, S.; Casper, R. F. *Involvement of Programmed Cell Death in Preimplantation Embryo Demise*; 1995; Vol. 1.

(52) McGann, L. E. Differing Actions of Penetrating and Nonpenetrating Cryoprotective Agents. *Cryobiology* **1978**, *15* (4), 382–390. https://doi.org/10.1016/0011-2240(78)90056-1.

(53) Elliott, G. D.; Wang, S.; Fuller, B. J. Cryoprotectants: A Review of the Actions and Applications of Cryoprotective Solutes That Modulate Cell Recovery from Ultra-Low Temperatures. *Cryobiology* **2017**, *76*, 74–91. https://doi.org/10.1016/J.CRYOBIOL.2017.04.004.

(54) Meryman, H. T. Cryoprotective Agents. *Cryobiology* **1971**, *8*, 173–183.

(55) Lovelock, J. E. The Protective Action of Neutral Solutes against Haemolysis by Freezing and Thawing. *Biochem. J.* **1954**, *56* (2), 265–270. https://doi.org/10.1042/bj0560265.

(56) Karlsson, J. O. M.; Toner, M. Long-Term Storage of Tissues by Cryopreservation: Critical Issues. *Biomaterials* **1996**, *17* (3), 243–256.

(57) Karow Jr., A. M. Biological Effects of Cryoprotectants as Related to Cardiac Cryopreservation. *Cryobiology* **1969**, *5* (6), 429–443. https://doi.org/10.1016/S0011-2240(69)80109-4.

(58) Karow Jr., A. M. Cryoprotectants-a New Class of Drugs. *J. Pharm. Pharmacol.* **1969**, *21* (4), 209–223. https://doi.org/10.1111/j.2042-7158.1969.tb08235.x.

(59) Sasnoor, L. M.; Kale, V. P.; Limaye, L. S. Supplementation of Conventional Freezing Medium with a Combination of Catalase and Trehalose Results in Better Protection of

Surface Molecules and Functionality of Hematopoietic Cells. *J. Hematother. Stem Cell Res.* **2003**, *12* (5), 553–564. https://doi.org/10.1089/152581603322448268.

(60) Svalgaard, J. D.; Haastrup, E. K.; Reckzeh, K.; Holst, B.; Glovinski, P. V.; Gørløv, J. S.; Hansen, M. B.; Moench, K. T.; Clausen, C.; Fischer-Nielsen, A. Low-Molecular-Weight Carbohydrate Pentaisomaltose May Replace Dimethyl Sulfoxide as a Safer Cryoprotectant for Cryopreservation of Peripheral Blood Stem Cells. *Transfusion* **2016**, *56* (5), 1088–1095. https://doi.org/10.1111/trf.13543.

(61) Svalgaard, J. D.; Talkhoncheh, M. S.; Haastrup, E. K.; Munthe-Fog, L.; Clausen, C.; Hansen, M. B.; Andersen, P.; Gørløv, J. S.; Larsson, J.; Fischer-Nielsen, A. Pentaisomaltose, an Alternative to DMSO. Engraftment of Cryopreserved Human CD34+ Cells in Immunodeficient NSG Mice. *Cell Transplant.* **2018**, *27* (9), 1407–1412. https://doi.org/10.1177/0963689718786226.

(62) Xian, M.; Fatima, Z.; Zhang, W.; Fang, J.; Li, H.; Pei, D.; Loo, J.; Stevenson, T.; Wang, P. Identification of α-Galactosyl Epitope Mimetics through Rapid Generation and Screening of C-Linked Glycopeptide Library. *J. Comb. Chem.* **2004**, *6* (1), 126–134. https://doi.org/10.1021/CC030042U.

(63) Motta, J. P. R.; Paraguassú-Braga, F. H.; Bouzas, L. F.; Porto, L. C. Evaluation of Intracellular and Extracellular Trehalose as a Cryoprotectant of Stem Cells Obtained from Umbilical Cord Blood. *Cryobiology* **2014**, *68* (3), 343–348. https://doi.org/10.1016/j.cryobiol.2014.04.007.

(64) Poisson, J. S.; Briard, J. G.; Turner, T. R.; Acker, J. P.; Ben R. N. Hydroxyethyl Starch Supplemented with Ice Recrystallization Inhibitors Greatly Improves Cryopreservation of Human Red Blood Cells. *Bioprocess. J.* **2017**, *15* (4), 16–21. https://doi.org/10.12665/J154.Ben.

(65) Arakawa, T.; Carpenter, J. F.; Kita, Y. A.; Crowe, J. H. The Basis for Toxicity of Certain Cryoprotectants: A Hypothesis. *Cryobiology* **1990**, *27* (4), 401–415. https://doi.org/10.1016/0011-2240(90)90017-X.

(66) Ohboshi, S.; Fujihara, N.; Yoshida, T.; Tomogane, H. Usefulness of Polyethylene Glycol for Cryopreservation by Vitrification of in Vitro-Derived Bovine Blastocysts. *Anim. Reprod. Sci.* **1997**, *48* (1), 27–36. https://doi.org/10.1016/S0378-4320(97)00034-1.

(67) Anchordoguy, T. J.; Rudolph, A. S.; Carpenter, J. F.; Crowe, J. H. Modes of Interaction of

Cryoprotectants with Membrane Phospholipids during Freezing. *Cryobiology* **1987**, *24* (4), 324–331. https://doi.org/10.1016/0011-2240(87)90036-8.

(68) Crowe, J. H.; Crowe, L. M.; Carpenter, J. F.; Rudolph, A. S.; Wistrom, C. A.; Spargo, B. J.; Anchordoguy, T. J. Interactions of Sugars with Membranes. *Biochim. Biophys. Acta - Rev. Biomembr.* **1988**, *947* (2), 367–384. https://doi.org/10.1016/0304-4157(88)90015-9.

(69) Rudolph, A. S.; Crowe, J. H. Membrane Stabilization during Freezing: The Role of Two Natural Cryoprotectants, Trehalose and Proline. *Cryobiology* **1985**, *22* (4), 367–377. https://doi.org/10.1016/0011-2240(85)90184-1.

(70) Carpenter, J. F.; Crowe, J. H. The Mechanism of Cryoprotection of Proteins by Solutes. *Cryobiology* **1988**, *25*, 244–255.

(71) Clegg, J. S.; Seitz, P.; Seitz, W.; Hazlewood, C. F. Cellular Responses to Extreme Water Loss: The Water-Replacement Hypothesis. *Cryobiology* **1982**, *19* (3), 306–316. https://doi.org/10.1016/0011-2240(82)90159-6.

(72) Best, B. P. Cryoprotectant Toxicity: Facts, Issues, and Questions. *Rejuvenation Res.* **2015**, *18* (5), 422–436. https://doi.org/10.1089/rej.2014.1656.

(73) Lovelock, J. E. The Mechanism of the Protective Action of Glycerol against Haemolysis by Freezing and Thawing. *Biochim. Biophys. Acta* **1953**, *11*, 28–36. https://doi.org/10.1016/0006-3002(53)90005-5.

(74) Hallare, A. V.; Kohler, H. R.; Triebskorn, R. Developmental Toxicity and Stress Protein Responses in Zebrafish Embryos after Exposure to Diclofenac and Its Solvent, DMSO. *Chemosphere* **2004**, *56* (7), 659–666. https://doi.org/10.1016/J.CHEMOSPHERE.2004.04.007.

(75) Shu, Z.; Heimfeld, S.; Gao, D. Hematopoietic SCT with Cryopreserved Grafts: Adverse Reactions after Transplantation and Cryoprotectant Removal before Infusion. *Bone Marrow Transplant.* **2014**, *49*, 469–476.

(76) Rowley, S. D.; Anderson, G. L. Effect of DMSO Exposure without Cryopreservation on Hematopoietic Progenitor Cells. *Bone Marrow Transplant.* **1993**, *11* (5), 389–393.

(77) Yang, H.; Zhao, H.; Acker, J. P.; Liu, J. Z.; Akabutu, J.; McGann, L. E. Effect of Dimethyl Sulfoxide on Post-Thaw Viability Assessment of CD45+ and CD34+ Cells of Umbilical Cord Blood and Mobilized Peripheral Blood. *Cryobiology* **2005**, *51* (2), 165–175. https://doi.org/10.1016/j.cryobiol.2005.06.003.

(78) Windrum, P.; Morris, T. C. M.; Drake, M. B.; Niederwieser, D.; Ruutu, T. Variation in Dimethyl Sulfoxide Use in Stem Cell Transplantation: A Survey of EBMT Centres. *Bone Marrow Transplant.* **2005**, *36* (7), 601–603. https://doi.org/10.1038/sj.bmt.1705100.

(79) Zambelli, A.; Poggi, G.; Da Prada, G.; Pedrazzoli, P.; Cuomo, A.; Miotti, D.; Perotti, C.; Preti, P.; Robustelli della Cuna, G. Clinical Toxicity of Cryopreserved Circulating Progenitor Cells Infusion. *Anticancer Res. 18* (6B), 4705–4708.

(80) Kollerup Madsen, B.; Hilscher, M.; Zetner, D.; Rosenberg, J. Adverse Reactions of Dimethyl Sulfoxide in Humans: A Systematic Review. *F1000Research* **2018**, *7* (1746), 1–17. https://doi.org/10.12688/f1000research.16642.1.

(81) Stroncek, D.; Fautsch, S.; Lasky, L.; Hurd, D.; Ramsay, N.; McCullough, J. Adverse Reactions in Patients Transfused with Cryopreserved Marrow. *Transfusion* **1991**, *31* (6), 521–526. https://doi.org/10.1046/j.1537-2995.1991.31691306250.x.

(82) Hughes, Z. E.; Mark, A. E.; Mancera, R. L. Molecular Dynamics Simulations of the Interactions of DMSO with DPPC and DOPC Phospholipid Membranes. *J. Phys. Chem. B* **2012**, *116* (39), 11911–11923. https://doi.org/10.1021/jp3035538.

(83) Mitrus, I.; Smagur, A.; Fidyk, W.; Czech, M.; Prokop, M.; Chwieduk, A.; Glowala-Kosinska, M.; Czerw, T.; Sobczyk-Kruszelnicka, M.; Mendrek, W.; Michalak, K.; Sadus-Wojciechowska, M.; Najda, J.; Holowiecki, J.; Giebel, S. Reduction of DMSO Concentration in Cryopreservation Mixture from 10% to 7.5% and 5% Has No Impact on Engraftment after Autologous Peripheral Blood Stem Cell Transplantation: Results of a Prospective, Randomized Study. *Bone Marrow Transplant.* **2018**, *53* (3), 274–280. https://doi.org/10.1038/s41409-017-0056-6.

(84) Shim, J. S.; Cho, B.; Kim, M.; Park, G. S.; Shin, J. C.; Hwang, H. K.; Kim, T. G.; Oh, I. H. Early Apoptosis in CD34+ Cells as a Potential Heterogeneity in Quality of Cryopreserved Umbilical Cord Blood. *Br. J. Haematol.* **2006**, *135* (2), 210–213. https://doi.org/10.1111/j.1365-2141.2006.06270.x.

(85) Hunt, C. J.; Armitage, S. E.; Pegg, D. E. Cryopreservation of Umbilical Cord Blood: 1. Osmotically Inactive Volume, Hydraulic Conductivity and Permeability of CD34(+) Cells to Dimethyl Sulphoxide. *Cryobiology* **2003**, *46* (1), 61–75. https://doi.org/10.1016/s0011-2240(02)00180-3.

(86) Hunt, C. J.; Pegg, D. E.; Armitage, S. E. Optimising Cryopreservation Protocols for

Haematopoietic Progenitor Cells: A Methodological Approach for Umbilical Cord Blood. *Cryo Letters 27* (2), 73–86.

(87) Duggleby, R. C.; Querol, S.; Davy, R. C.; Fry, L. J.; Gibson, D. A.; Horton, R. B. V.; Mahmood, S. N.; Gomez, S. G.; Madrigal, J. A. Flow Cytometry Assessment of Apoptotic CD34+ Cells by Annexin v Labeling May Improve Prediction of Cord Blood Potency for Engraftment. *Transfusion* **2012**, *52* (3), 549–559. https://doi.org/10.1111/j.1537-2995.2011.03305.x.

(88) Sasnoor, L. M.; Kale, V. P.; Limaye, L. S. A Combination of Catalase and Trehalose as Additives to Conventional Freezing Medium Results in Improved Cryoprotection of Human Hematopoietic Cells with Reference to in Vitro Migration and Adhesion Properties. *Transfusion* **2005**, *45* (4), 622–633. https://doi.org/10.1111/j.0041-1132.2005.04288.x.

(89) Wu, L.; Al-Hejazi, A.; Filion, L.; Ben, R.; Halpenny, M.; Yang, L.; Giulivi, A.; Allan, D. S. Increased Apoptosis in Cryopreserved Autologous Hematopoietic Progenitor Cells Collected by Apheresis and Delayed Neutrophil Recovery after Transplantation: A Nested Case-Control Study. *Cytotherapy* **2012**, *14* (2), 205–214. https://doi.org/10.3109/14653249.2011.610302.

(90) Chaytor, J. L.; Tokarew, J. M.; Wu, L. K.; Leclre, M.; Tam, R. Y.; Capicciotti, C. J.; Guolla, L.; Von Moos, E.; Findlay, C. S.; Allan, D. S.; Ben, R. N. Inhibiting Ice Recrystallization and Optimization of Cell Viability after Cryopreservation. *Glycobiology* **2012**, *22* (1), 123–133. https://doi.org/10.1093/glycob/cwr115.

(91) Deller, R. C.; Vatish, M.; Mitchell, D. A.; Gibson, M. I. Glycerol-Free Cryopreservation of Red Blood Cells Enabled by Ice-Recrystallization-Inhibiting Polymers. *ACS Biomater. Sci. Eng.* **2015**, *1* (9), 789–794. https://doi.org/10.1021/acsbiomaterials.5b00162.

(92) Bevilacqua, A. E.; Zaritzky, N. E. Ice Recrystallization in Frozen Beef. *J. Food Sci.* **1982**, *47* (5), 1410–1414. https://doi.org/10.1111/j.1365-2621.1982.tb04950.x.

(93) Berz, D.; McCormack, E. M.; Winer, E. S.; Colvin, G. A.; Quesenberry, P. J. Cryopreservation of Hematopoietic Stem Cells. *Am. J. Hematol.* **2007**, *82* (6), 463–472. https://doi.org/10.1002/ajh.20707.

(94) Rodrigues, C. A.; Sanz, G.; Brunstein, C. G.; Sanz, J.; Wagner, J. E.; Renaud, M.; de Lima, M.; Cairo, M. S.; Fürst, S.; Rio, B.; Dalley, C.; Carreras, E.; Harousseau, J.-L.;

Mohty, M.; Taveira, D.; Dreger, P.; Sureda, A.; Gluckman, E.; Rocha, V. Analysis of Risk Factors for Outcomes After Unrelated Cord Blood Transplantation in Adults With Lymphoid Malignancies: A Study by the Eurocord-Netcord and Lymphoma Working Party of the European Group for Blood and Marrow Transplantation. *J. Clin. Oncol.* **2009**, *27* (2), 256–263. https://doi.org/10.1200/JCO.2007.15.8865.

(95) Rubinstein, P.; Dobrila, L.; Rosenfield, R. E.; Adamson, J. W.; Migliaccio, G.; Migliaccio, A. R.; Taylor, P. E.; Stevens, C. E. Processing and Cryopreservation of Placental/Umbilical Cord Blood for Unrelated Bone Marrow Reconstitution. *Proc. Natl. Acad. Sci. U. S. A.* **1995**, *92* (22), 10119–10122. https://doi.org/10.1073/pnas.92.22.10119.

(96) Davis, J. M.; Rowley, S. D.; Braine, H. G.; Piantadosi, S.; Santos, G. W. Clinical Toxicity of Cryopreserved Bone Marrow Graft Infusion. *Blood* **1990**, *75* (3), 781–786. https://doi.org/10.1182/blood.v75.3.781.bloodjournal753781.

(97) Davis, J.; Rowley, S. D.; Santos, G. W. Toxicity of Autologous Bone Marrow Graft Infusion. *Prog. Clin. Biol. Res.* **1990**, *333*, 531–540.

(98) Alessandrino, E. P.; Bernasconi, P.; Caldera, D.; Colombo, A.; Bonfichi, M.; Malcovati, L.; Klersy, C.; Martinelli, G.; Maiocchi, M.; Pagnucco, G.; Varettoni, M.; Perotti, C.; Bernasconi, C. Adverse Events Occurring during Bone Marrow or Peripheral Blood Progenitor Cell Infusion: Analysis of 126 Cases. *Bone Marrow Transplant.* **1999**, *23* (6), 533–537. https://doi.org/10.1038/sj.bmt.1701609.

(99) Wu, L. K.; Tokarew, J. M.; Chaytor, J. L.; Von Moos, E.; Li, Y.; Palii, C.; Ben, R. N.; Allan, D. S. Carbohydrate-Mediated Inhibition of Ice Recrystallization in Cryopreserved Human Umbilical Cord Blood. *Carbohydr. Res.* **2011**, *346* (1), 86–93. https://doi.org/10.1016/j.carres.2010.10.016.

(100) Capicciotti, C. J.; Doshi, M.; Ben, R. N. Ice Recrystallization Inhibitors: From Biological Antifreezes to Small Molecules. In *Recent Developments in the Study of Recrystallization*; Wilson, P., Ed.; InTech Open, Ltd.: London, UK, 2013; pp 177–224. https://doi.org/10.5772/54992.

(101) Pham, Q. T.; Mawson, R. F. Moisture Migration and Ice Recrystallization in Frozen Foods. In *Quality in Frozen Food*; Erickson, M. C., Hung, Y.-C., Eds.; Springer US: Boston, MA, 1997; pp 67–91. https://doi.org/10.1007/978-1-4615-5975-7_5.

(102) Zhu, Z.; Zhou, Q.; Sun, D.-W. Measuring and Controlling Ice Crystallization in Frozen

Foods: A Review of Recent Developments. *Trends Food Sci. Technol.* **2019**, *90*, 13–25. https://doi.org/10.1016/J.TIFS.2019.05.012.

(103) Murray, B. J.; Broadley, S. L.; Morris, G. J. Supercooling of Water Droplets in Jet Aviation Fuel. *Fuel* **2011**, *90* (1), 433–435. https://doi.org/10.1016/J.FUEL.2010.08.018.

(104) Lam, J. K.-W.; Hetherington, J. I.; Carpenter, M. D. Ice Growth in Aviation Jet Fuel. *Fuel* **2013**, *113*, 402–406. https://doi.org/10.1016/J.FUEL.2013.05.048.

(105) Thürmer, K.; Nie, S. Formation of Hexagonal and Cubic Ice during Low-Temperature Growth. *Proc. Natl. Acad. Sci. U. S. A.* **2013**, *110* (29), 11757–11762. https://doi.org/10.1073/pnas.1303001110.

(106) Fletcher, N. H. *The Chemical Physics of Ice*; Cambridge University Press, 1970.

(107) Hobbs, P. V. *Ice Physics*; Clarendon Press: Oxford, 1974.

(108) Petrenko, V. F.; Whitworth, R. W. *Physics of Ice*; Oxford University Press: Oxford, 1999.

(109) Malkin, T. L.; Murray, B. J.; Salzmann, C. G.; Molinero, V.; Pickering, S. J.; Whale, T. F. Stacking Disorder in Ice I. *Phys. Chem. Chem. Phys.* **2015**, *17* (1), 60–76. https://doi.org/10.1039/C4CP02893G.

(110) Malkin, T. L.; Murray, B. J.; Brukhno, A. V; Anwar, J.; Salzmann, C. G. Structure of Ice Crystallized from Supercooled Water. *Proc. Natl. Acad. Sci. U. S. A.* **2012**, *109* (4), 1041–1045. https://doi.org/10.1073/pnas.1113059109.

(111) Li, T.; Donadio, D.; Russo, G.; Galli, G. Homogeneous Ice Nucleation from Supercooled Water. *Phys. Chem. Chem. Phys.* **2011**, *13* (44), 19807. https://doi.org/10.1039/c1cp22167a.

(112) Haji-Akbari, A.; Debenedetti, P. G. Direct Calculation of Ice Homogeneous Nucleation Rate for a Molecular Model of Water. *Proc. Natl. Acad. Sci. U. S. A.* **2015**, *112* (34), 10582–10588. https://doi.org/10.1073/pnas.1509267112.

(113) Lupi, L.; Hudait, A.; Peters, B.; Grünwald, M.; Gotchy Mullen, R.; Nguyen, A. H.; Molinero, V. Role of Stacking Disorder in Ice Nucleation. *Nature* **2017**, *551* (7679), 218–222. https://doi.org/10.1038/nature24279.

(114) Moore, E. B.; Molinero, V. Is It Cubic? Ice Crystallization from Deeply Supercooled Water. *Phys. Chem. Chem. Phys.* **2011**, *13* (44), 20008. https://doi.org/10.1039/c1cp22022e.

(115) Devries, A. L.; Lin, Y. Structure of a Peptide Antifreeze and Mechanism of Adsorption to

Ice. *Biochim. Biophys. Acta - Protein Struct.* **1977**, *495* (2), 388–392. https://doi.org/10.1016/0005-2795(77)90395-6.

(116) Olijve, L. L. C.; Meister, K.; DeVries, A. L.; Duman, J. G.; Guo, S.; Bakker, H. J.; Voetsa, I. K. Blocking Rapid Ice Crystal Growth through Nonbasal Plane Adsorption of Antifreeze Proteins. *Proc. Natl. Acad. Sci. U. S. A.* **2016**, *113* (14), 3740–3745. https://doi.org/10.1073/pnas.1524109113.

(117) Harding, M. M.; Ward, L. G.; Haymet, A. D. J. Type I "antifreeze" Proteins. Structure-Activity Studies and Mechanisms of Ice Growth Inhibition. *Eur. J. Biochem.* **1999**, *264* (3), 653–665. https://doi.org/10.1046/j.1432-1327.1999.00617.x.

(118) Hayward, J. A.; Haymet, A. D. J. The Ice/Water Interface: Molecular Dynamics Simulations of the Basal, Prism, {20$\bar{2}$1}, and {21$\bar{1}$0} Interfaces of Ice Ih. *J. Chem. Phys.* **2001**, *114* (8), 3713–3726. https://doi.org/10.1063/1.1333680.

(119) Harding, M. M.; Anderberg, P. I.; Haymet, A. D. J. "Antifreeze" Glycoproteins from Polar Fish. *Eur. J. Biochem.* **2003**, *270* (7), 1381–1392. https://doi.org/10.1046/j.1432-1033.2003.03488.x.

(120) Zhu, Z.; Liu, J. Modeling Ice Crystal Formation of Water in Biological System. In *Advanced Topics on Crystal Growth*; InTech, 2013. https://doi.org/10.5772/54098.

(121) Fletcher, N. H. Surface Structure of Water and Ice. *Philos. Mag.* **1968**, *18* (156), 1287–1300. https://doi.org/10.1080/14786436808227758.

(122) Karim, O. A.; Haymet, A. D. J. The Ice/Water Interface: A Molecular Dynamics Simulation Study. *J. Chem. Phys.* **1988**, *89* (11), 6889–6896. https://doi.org/10.1063/1.455363.

(123) Furukawa, Y.; Ishikawa, I. Direct Evidence for Melting Transition at Interface between Ice Crystal and Glass Substrate. *J. Cryst. Growth* **1993**, *128* (1–4), 1137–1142. https://doi.org/10.1016/S0022-0248(07)80112-6.

(124) Beaglehole, D.; Nason, D. Transition Layer on the Surface on Ice. *Surf. Sci.* **1980**, *96* (1–3), 357–363. https://doi.org/10.1016/0039-6028(80)90313-1.

(125) Faraday, P. XXIV. On Regelation, and on the Conservation of Force. *London, Edinburgh, Dublin Philos. Mag. J. Sci.* **1859**, *17* (113), 162–169. https://doi.org/10.1080/14786445908642645.

(126) Bilgram, J. H. The Structure and Properties of Melt and Concentrated Solutions. *Prog.*

Cryst. Growth Charact. Mater. **1993**, *26*, 99–119. https://doi.org/10.1016/0960-8974(93)90012-S.

(127) Halter, P. U.; Bilgram, J. H.; Känzig, W. Properties of the Solid–Liquid Interface Layer of Growing Ice Crystals: A Raman and Rayleigh Scattering Study. *J. Chem. Phys.* **1988**, *89* (5), 2622–2629. https://doi.org/10.1063/1.455011.

(128) Björneholm, O.; Hansen, M. H.; Hodgson, A.; Liu, L.-M.; Limmer, D. T.; Michaelides, A.; Pedevilla, P.; Rossmeisl, J.; Shen, H.; Tocci, G.; Tyrode, E.; Walz, M.-M.; Werner, J.; Bluhm, H. Water at Interfaces. *Chem. Rev.* **2016**, *116* (13), 7698–7726. https://doi.org/10.1021/acs.chemrev.6b00045.

(129) Shultz, M. J. Ice Surfaces. *Annu. Rev. Phys. Chem.* **2017**, *68* (1), 285–304. https://doi.org/10.1146/annurev-physchem-052516-044813.

(130) Goertz, M. P.; Zhu, X.-Y.; Houston, J. E. Exploring the Liquid-like Layer on the Ice Surface. *Langmuir* **2009**, *25* (12), 6905–6908. https://doi.org/10.1021/la9001994.

(131) Henson, B. F.; Voss, L. F.; Wilson, K. R.; Robinson, J. M. Thermodynamic Model of Quasiliquid Formation on H2O Ice: Comparison with Experiment. *J. Chem. Phys.* **2005**, *123* (14), 144707. https://doi.org/10.1063/1.2056541.

(132) Furukawa, Y.; Yamamoto, M.; Kuroda, T. Ellipsometric Study of the Transition Layer on the Surface of an Ice Crystal. *J. Cryst. Growth* **1987**, *82* (4), 665–677. https://doi.org/10.1016/S0022-0248(87)80012-X.

(133) Döppenschmidt, A.; Kappl, M.; Butt, H.-J. Surface Properties of Ice Studied by Atomic Force Microscopy. *J. Phys. Chem. B* **1998**, *102* (40), 7813–7819. https://doi.org/10.1021/JP981396S.

(134) Bluhm, H.; Ogletree, D. F.; Fadley, C. S.; Hussain, Z.; Salmeron, M. The Premelting of Ice Studied with Photoelectron Spectroscopy. *J. Phys. Condens. Matter* **2002**, *14* (8), L227–L233. https://doi.org/10.1088/0953-8984/14/8/108.

(135) Beaglehole, D.; Wilson, P. Thickness and Anisotropy of the Ice-Water Interface. *J. Phys. Chem.* **1993**, *97* (42), 11053–11055. https://doi.org/10.1021/j100144a025.

(136) Fitzner, M.; Sosso, G. C.; Cox, S. J.; Michaelides, A. Ice Is Born in Low-Mobility Regions of Supercooled Liquid Water. *Proc. Natl. Acad. Sci. U. S. A.* **2019**, *116* (6), 2009–2014. https://doi.org/10.1073/pnas.1817135116.

(137) Elbaum, M.; Lipson, S. G.; Dash, J. G. Optical Study of Surface Melting on Ice. *J. Cryst.*

Growth **1993**, *129* (3–4), 491–505. https://doi.org/10.1016/0022-0248(93)90483-D.

(138) Dosch, H.; Lied, A.; Bilgram, J. H. Disruption of the Hydrogen-Bonding Network at the Surface of Ih Ice near Surface Premelting. *Surf. Sci.* **1996**, *366* (1), 43–50. https://doi.org/10.1016/0039-6028(96)00805-9.

(139) Golecki, I.; Jaccard, C. Intrinsic Surface Disorder in Ice near the Melting Point. *J. Phys. C Solid State Phys.* **1978**, *11*, 4229–4237.

(140) Sadtchenko, V.; Ewing, G. E.; Sadtchenko, V.; Ewing, G. E. Interfacial Melting of Thin Ice Films: An Infrared Study. *J. Chem. Phys.* **2002**, *116* (11), 4686–4697. https://doi.org/10.1063/1.1449947.

(141) Kaverin, A.; Tsionsky, V.; Zagidulin, D.; Daikhin, L.; Alengoz, E.; Gileadi, E. A Novel Approach for Direct Measurement of the Thickness of the Liquid-like Layer at the Ice/Solid Interface. *J. Phys. Chem. B* **2004**, *108* (26), 8759–8762. https://doi.org/10.1021/JP031299L.

(142) Karim, O. A.; Kay, P. A.; Haymet, A. D. J. The Ice/Water Interface: A Molecular Dynamics Simulation Using the Simple Point Charge Model. *J. Chem. Phys.* **1990**, *92* (7), 4634–4635. https://doi.org/10.1063/1.457730.

(143) Knight, C. A.; Wen, D.; Laursen, R. A. Nonequilibrium Antifreeze Peptides and the Recrystallization of Ice. *Cryobiology* **1995**, *32* (1), 23–34. https://doi.org/10.1006/CRYO.1995.1002.

(144) Knight, C. A. Grain Boundary Migration and Other Processes in the Formation of Ice Sheets on Water. *J. Appl. Phys.* **1966**, *37* (2), 568–574. https://doi.org/10.1063/1.1708217.

(145) Alley, R. B.; Perepezko, J. H.; Bentley, C. R. Grain Growth in Polar Ice: I. Theory. *J. Glaciol.* **1986**, *32* (112), 415–424. https://doi.org/10.3189/S0022143000012120.

(146) Alley, R. B.; Perepezko, J. H.; Bentley, C. R. Grain Growth in Polar Ice: II. Application. *J. Glaciol.* **1986**, *32* (112), 425–433. https://doi.org/10.3189/S0022143000012132.

(147) J., C.; Doshi, M.; N., R. Ice Recrystallization Inhibitors: From Biological Antifreezes to Small Molecules. *Recent Dev. Study Recryst.* **2013**. https://doi.org/10.5772/54992.

(148) Budke, C.; Heggemann, C.; Koch, M.; Sewald, N.; Koop, T. Ice Recrystallization Kinetics in the Presence of Synthetic Antifreeze Glycoprotein Analogues Using the Framework of LSW Theory. *J. Phys. Chem. B* **2009**, *113* (9), 2865–2873. https://doi.org/10.1021/jp805726e.

(149) Sutton, R. L.; Lips, A.; Piccirillo, G.; Sztehlo, A. Kinetics of Ice Recrystallization in Aqueous Fructose Solutions. *J. Food Sci.* **1996**, *61* (4), 741–745. https://doi.org/10.1111/j.1365-2621.1996.tb12194.x.

(150) Cook, K. L. K.; Hartel, R. W. Mechanisms of Ice Crystallization in Ice Cream Production. *Compr. Rev. Food Sci. Food Saf.* **2010**, *9*, 213–222.

(151) van Westen, T.; Groot, R. D. Predicting the Kinetics of Ice Recrystallization in Aqueous Sugar Solutions. *Cryst. Growth Des.* **2018**, *18*, 2405–2416.

(152) Dalvi-Isfahan, M.; Jha, P. K.; Tavakoi, J.; Daraei-Garmakhany, A.; Xanthakis, E.; Le-Bail, A. Review on Identification, Underlying Mechanisms and Evaluation of Freezing Damage. *J. Food Eng.* **2019**, *255*, 50–60. https://doi.org/10.1016/J.JFOODENG.2019.03.011.

(153) van Westen, T.; Groot, R. D. Effect of Temperature Cycling on Ostwald Ripening. *Cryst. Growth Des.* **2018**, *18* (9), 4952–4962. https://doi.org/10.1021/acs.cgd.8b00267.

(154) Zachariassen, K. E.; Kristiansen, E. Ice Nucleation and Antinucleation in Nature. *Cryobiology* **2000**, *41* (4), 257–279. https://doi.org/10.1006/cryo.2000.2289.

(155) Franks, F.; Mathias, S. F.; Hatley, R. H. M.; Baust, J. G.; Hvidt, A.; Chapman, D.; Jaenicke, R. Water, Temperature and Life. *Philos. Trans. R. Soc. B Biol. Sci.* **1990**, *326* (1237), 517–533. https://doi.org/10.1098/rstb.1990.0029.

(156) Smallwood, M.; Bowles, D. J. Plants in a Cold Climate. *Philos. Trans. R. Soc. London. Ser. B Biol. Sci.* **2002**, *357* (1423), 831–847. https://doi.org/10.1098/rstb.2002.1073.

(157) Knight, C. A.; De Vries, A. L.; Oolman, L. D. Fish Antifreeze Protein and the Freezing and Recrystallization of Ice. *Nature* **1984**, *308* (5956), 295–296. https://doi.org/10.1038/308295a0.

(158) Yeh, Y.; Feeney, R. E. Antifreeze Proteins: Structures and Mechanisms of Function. *Chem. Rev.* **1996**, *96* (2), 601–618. https://doi.org/10.1021/cr950260c.

(159) Davies, P. L.; Baardsnes, J.; Kuiper, M. J.; Walker, V. K. Structure and Function of Antifreeze Proteins. *Philos. Trans. R. Soc. London. Ser. B Biol. Sci.* **2002**, *357* (1423), 927–935. https://doi.org/10.1098/rstb.2002.1081.

(160) Wathen, B.; Kuiper, M.; Walker, V.; Jia, Z. A New Model for Simulating 3-D Crystal Growth and Its Application to the Study of Antifreeze Proteins. *J. Am. Chem. Soc.* **2003**, *125* (3), 729–737. https://doi.org/10.1021/ja0267932.

(161) Strom, C. S.; Liu, X. Y.; Jia, Z. Antifreeze Protein-Induced Morphological Modification Mechanisms Linked to Ice Binding Surface. *J. Biol. Chem.* **2004**, *279* (31), 32407–32417. https://doi.org/10.1074/jbc.M401712200.

(162) Budke, C.; Dreyer, A.; Jaeger, J.; Gimpel, K.; Berkemeier, T.; Bonin, A. S.; Nagel, L.; Plattner, C.; Devries, A. L.; Sewald, N.; Koop, T. Quantitative Efficacy Classification of Ice Recrystallization Inhibition Agents. *Cryst. Growth Des.* **2014**, *14* (9), 4285–4294. https://doi.org/10.1021/cg5003308.

(163) Knight, C. A.; Cheng, C. C.; DeVries, A. L. Adsorption of Alpha-Helical Antifreeze Peptides on Specific Ice Crystal Surface Planes. *Biophys. J.* **1991**, *59* (2), 409–418. https://doi.org/10.1016/S0006-3495(91)82234-2.

(164) Sun, T.; Lin, F.-H.; Campbell, R. L.; Allingham, J. S.; Davies, P. L. An Antifreeze Protein Folds with an Interior Network of More than 400 Semi-Clathrate Waters. *Science* **2014**, *343* (6172), 795–798. https://doi.org/10.1126/science.1247407.

(165) Scott, G. K.; Davies, P. L.; Shears, M. A.; Fletcher, G. L. Structural Variations in the Alanine-Rich Antifreeze Proteins of the Pleuronectinae. *Eur. J. Biochem.* **1987**, *168* (3), 629–633. https://doi.org/10.1111/j.1432-1033.1987.tb13462.x.

(166) Liu, Y.; Li, Z.; Lin, Q.; Kosinski, J.; Seetharaman, J.; Bujnicki, J. M.; Sivaraman, J.; Hew, C.-L. Structure and Evolutionary Origin of Ca(2+)-Dependent Herring Type II Antifreeze Protein. *PLoS One* **2007**, *2* (6), e548. https://doi.org/10.1371/journal.pone.0000548.

(167) Garnham, C. P.; Natarajan, A.; Middleton, A. J.; Kuiper, M. J.; Braslavsky, I.; Davies, P. L. Compound Ice-Binding Site of an Antifreeze Protein Revealed by Mutagenesis and Fluorescent Tagging. *Biochemistry* **2010**, *49* (42), 9063–9071. https://doi.org/10.1021/bi100516e.

(168) Meister, K.; Strazdaite, S.; DeVries, A. L.; Lotze, S.; Olijve, L. L. C.; Voets, I. K.; Bakker, H. J. Observation of Ice-like Water Layers at an Aqueous Protein Surface. *Proc. Natl. Acad. Sci. U. S. A.* **2014**, *111* (50), 17732–17736. https://doi.org/10.1073/pnas.1414188111.

(169) Garnham, C. P.; Campbell, R. L.; Davies, P. L. Anchored Clathrate Waters Bind Antifreeze Proteins to Ice. *Proc. Natl. Acad. Sci. U. S. A.* **2011**, *108* (18), 7363–7367. https://doi.org/10.1073/pnas.1100429108.

(170) Howard, E. I.; Blakeley, M. P.; Haertlein, M.; Petit-Haertlein, I.; Mitschler, A.; Fisher, S.

J.; Cousido-Siah, A.; Salvay, A. G.; Popov, A.; Muller-Dieckmann, C.; Petrova, T.; Podjarny, A. Neutron Structure of Type-III Antifreeze Protein Allows the Reconstruction of AFP-Ice Interface. *J. Mol. Recognit.* **2011**, *24* (4), 724–732. https://doi.org/10.1002/jmr.1130.

(171) Fairley, K.; Westman, B. J.; Pham, L. H.; Haymet, A. D. J.; Harding, M. M.; Mackay, J. P. Type I Shorthorn Sculpin Antifreeze Protein: Recombinant Synthesis, Solution Conformation, and Ice Growth Inhibition Studies. *J. Biol. Chem.* **2002**, *277* (27), 24073–24080. https://doi.org/10.1074/jbc.M200307200.

(172) Haymet, A. D. J.; Ward, L. G.; Harding, M. M. Winter Flounder "Antifreeze" Proteins: Synthesis and Ice Growth Inhibition of Analogues That Probe the Relative Importance of Hydrophobic and Hydrogen-Bonding Interactions. *J. Am. Chem. Soc.* **1999**, *121* (5), 941–948. https://doi.org/10.1021/JA9801341.

(173) Davies, P. L. Ice-Binding Proteins: A Remarkable Diversity of Structures for Stopping and Starting Ice Growth. *Trends Biochem. Sci.* **2014**, *39* (11), 548–555. https://doi.org/10.1016/j.tibs.2014.09.005.

(174) Gwak, Y.; Jung, W.; Lee, Y.; Kim, J. S.; Kim, C. G.; Ju, J.-H.; Song, C.; Hyun, J.-K.; Jin, E. An Intracellular Antifreeze Protein from an Antarctic Microalga That Responds to Various Environmental Stresses. *FASEB J.* **2014**, *28* (11), 4924–4935. https://doi.org/10.1096/fj.14-256388.

(175) Yang, D. S. C.; Hon, W. C.; Bubanko, S.; Xue, Y.; Seetharaman, J.; Hew, C. L.; Sicheri, F. Identification of the Ice-Binding Surface on a Type III Antifreeze Protein with a "flatness Function" Algorithm. *Biophys. J.* **1998**, *74* (5), 2142–2151. https://doi.org/10.1016/S0006-3495(98)77923-8.

(176) Kristiansen, E.; Zachariassen, K. E. The Mechanism by Which Fish Antifreeze Proteins Cause Thermal Hysteresis. *Cryobiology* **2005**, *51* (3), 262–280. https://doi.org/10.1016/j.cryobiol.2005.07.007.

(177) Raymond, J. A.; DeVries, A. L. Adsorption Inhibition as a Mechanism of Freezing Resistance in Polar Fishes. *Proc. Natl. Acad. Sci. U. S. A.* **1977**, *74* (6), 2589–2593. https://doi.org/10.1073/pnas.74.6.2589.

(178) Cziko, P. A.; DeVries, A. L.; Evans, C. W.; Christina Cheng, C. H. Antifreeze Protein-Induced Superheating of Ice inside Antarctic Notothenioid Fishes Inhibits Melting during

Summer Warming. *Proc. Natl. Acad. Sci. U. S. A.* **2014**, *111* (40), 14583–14588. https://doi.org/10.1073/pnas.1410256111.

(179) DeVries, A. L.; Komatsu, S. K.; Feeney, R. E. Chemical and Physical Properties of Freezing Point-Depressing Glycoproteins from Antarctic Fishes. *J. Biol. Chem.* **1970**, *245* (11), 2901–2908.

(180) Devries, A. L. Glycoproteins as Biological Antifreeze Agents in Antarctic Fishes. *Science (80-.).* **1971**, *172* (3988), 1152–1155. https://doi.org/10.1126/science.172.3988.1152.

(181) Chakrabartty, A.; Hew, C. L. The Effect of Enhanced A-Helicity on the Activity of a Winter Flounder Antifreeze Polypeptide. *Eur. J. Biochem.* **1991**, *202*, 1057–1063.

(182) Knight, C. A.; Driggers, E.; DeVries, A. L. Adsorption to Ice of Fish Antifreeze Glycopeptides 7 and 8. *Biophys. J.* **1993**, *64* (1), 252–259. https://doi.org/10.1016/S0006-3495(93)81361-4.

(183) Adam, M. K.; Jarrett-Wilkins, C.; Beards, M.; Staykov, E.; MacFarlane, L. R.; Bell, T. D. M.; Matthews, J. M.; Manners, I.; Faul, C. F. J.; Moens, P. D. J.; Ben, R. N.; Wilkinson, B. L. 1D Self-Assembly and Ice Recrystallization Inhibition Activity of Antifreeze Glycopeptide-Functionalized Perylene Bisimides. *Chem. - A Eur. J.* **2018**, *24* (31), 7834–7839. https://doi.org/10.1002/chem.201800857.

(184) Capicciotti, C. J.; Poisson, J. S.; Boddy, C. N.; Ben, R. N. Modulation of Antifreeze Activity and the Effect upon Post-Thaw HepG2 Cell Viability after Cryopreservation. *Cryobiology* **2015**, *70* (2), 79–89. https://doi.org/10.1016/j.cryobiol.2015.01.002.

(185) Hassas-Roudsari, M.; Goff, H. D. Ice Structuring Proteins from Plants: Mechanism of Action and Food Application. *Food Research International*. April 2012, pp 425–436. https://doi.org/10.1016/j.foodres.2011.12.018.

(186) Leiter, A.; Rau, S.; Winger, S.; Muhle-Goll, C.; Luy, B.; Gaukel, V. Influence of Heating Temperature, Pressure and PH on Recrystallization Inhibition Activity of Antifreeze Protein Type III. *J. Food Eng.* **2016**, *187*, 53–61. https://doi.org/10.1016/j.jfoodeng.2016.04.019.

(187) Gaukel, V.; Leiter, A.; Spieß, W. E. L. Synergism of Different Fish Antifreeze Proteins and Hydrocolloids on Recrystallization Inhibition of Ice in Sucrose Solutions. *J. Food Eng.* **2014**, *141*, 44–50. https://doi.org/10.1016/j.jfoodeng.2014.05.016.

(188) Knight, C. A.; Wen, D.; Laursen, R. A. Nonequilibrium Antifreeze Peptides and the

Recrystallization of Ice. *Cryobiology*. 1995, pp 23–34. https://doi.org/10.1006/cryo.1995.1002.

(189) Tomczak, M. M.; Marshall, C. B.; Gilbert, J. A.; Davies, P. L. A Facile Method for Determining Ice Recrystallization Inhibition by Antifreeze Proteins. *Biochem. Biophys. Res. Commun.* **2003**, *311* (4), 1041–1046. https://doi.org/10.1016/j.bbrc.2003.10.106.

(190) Yu, S. O.; Brown, A.; Middleton, A. J.; Tomczak, M. M.; Walker, V. K.; Davies, P. L. Ice Restructuring Inhibition Activities in Antifreeze Proteins with Distinct Differences in Thermal Hysteresis. *Cryobiology* **2010**, *61* (3), 327–334. https://doi.org/10.1016/j.cryobiol.2010.10.158.

(191) Yagci, Y. E.; Antonietti, M.; Börner, H. G. Synthesis of Poly(Tartar Amides) as Bio-Inspired Antifreeze Additives. *Macromol. Rapid Commun.* **2006**, *27* (19), 1660–1664. https://doi.org/10.1002/marc.200600451.

(192) Mastai, Y.; Rudloff, J.; Cölfen, H.; Antonietti, M. Control over the Structure of Ice and Water by Block Copolymer Additives. *ChemPhysChem* **2002**, *3* (1), 119–123. https://doi.org/10.1002/1439-7641(20020118)3:1<119::AID-CPHC119>3.0.CO;2-R.

(193) Knight, C. A.; Hallett, J.; DeVries, A. L. Solute Effects on Ice Recrystallization: An Assessment Technique. *Cryobiology* **1988**, *25* (1), 55–60. https://doi.org/10.1016/0011-2240(88)90020-X.

(194) Carpenter, J. F.; Hansen, T. N. Antifreeze Protein Modulates Cell Survival during Cryopreservation: Mediation through Influence on Ice Crystal Growth. *Proc. Natl. Acad. Sci. U. S. A.* **1992**, *89* (19), 8953–8957. https://doi.org/10.1073/pnas.89.19.8953.

(195) Chao, H.; Davies, P. L.; Carpenter, J. F. Effects of Antifreeze Proteins on Red Blood Cell Survival during Cryopreservation. *J. Exp. Biol.* **1996**, *199* (Pt 9), 2071–2076.

(196) Wang, T.; Zhu, Q.; Yang, X.; Layne, J. R.; Devries, A. L. Antifreeze Glycoproteins from Antarctic Notothenioid Fishes Fail to Protect the Rat Cardiac Explant during Hypothermic and Freezing Preservation. *Cryobiology* **1994**, *31* (2), 185–192. https://doi.org/10.1006/cryo.1994.1022.

(197) Rubinsky, B.; Arav, A.; Devries, A. L. The Cryoprotective Effect of Antifreeze Glycopeptides from Antarctic Fishes. *Cryobiology* **1992**, *29* (1), 69–79. https://doi.org/10.1016/0011-2240(92)90006-n.

(198) Jackman, J.; Noestheden, M.; Moffat, D.; Pezacki, J. P.; Findlay, S.; Ben, R. N. Assessing

Antifreeze Activity of AFGP 8 Using Domain Recognition Software. *Biochem. Biophys. Res. Commun.* **2007**, *354* (2), 340–344. https://doi.org/10.1016/j.bbrc.2006.12.225.

(199) Abraham, S.; Keillor, K.; Capicciotti, C. J.; Perley-Robertson, G. E.; Keillor, J. W.; Ben, R. N. Quantitative Analysis of the Efficacy and Potency of Novel Small Molecule Ice Recrystallization Inhibitors. *Cryst. Growth Des.* **2015**, *15* (10), 5034–5039. https://doi.org/10.1021/acs.cgd.5b00995.

(200) Czechura, P.; Tam, R. Y.; Dimitrijevic, E.; Murphy, A. V.; Ben, R. N. The Importance of Hydration for Inhibiting Ice Recrystallization with C-Linked Antifreeze Glycoproteins. *J. Am. Chem. Soc.* **2008**, *130* (10), 2928–2929. https://doi.org/10.1021/ja7103262.

(201) Tachibana, Y.; Fletcher, G. L.; Fujitani, N.; Tsuda, S.; Monde, K.; Nishimura, S.-I. Antifreeze Glycoproteins: Elucidation of the Structural Motifs That Are Essential for Antifreeze Activity. *Angew. Chemie* **2004**, *116* (7), 874–880. https://doi.org/10.1002/ange.200353110.

(202) Wilkinson, B. L.; Stone, R. S.; Capicciotti, C. J.; Thaysen-Andersen, M.; Matthews, J. M.; Packer, N. H.; Ben, R. N.; Payne, R. J. Total Synthesis of Homogeneous Antifreeze Glycopeptides and Glycoproteins. *Angew. Chemie - Int. Ed.* **2012**, *51* (15), 3606–3610. https://doi.org/10.1002/anie.201108682.

(203) Garner, J.; Harding, M. M. Design and Synthesis of Antifreeze Glycoproteins and Mimics. *Chembiochem* **2010**, *11* (18), 2489–2498. https://doi.org/10.1002/cbic.201000509.

(204) Peltier, R.; Brimble, M. A.; Wojnar, J. M.; Williams, D. E.; Evans, C. W.; DeVries, A. L. Synthesis and Antifreeze Activity of Fish Antifreeze Glycoproteins and Their Analogues. *Chem. Sci.* **2010**, *1* (5), 538. https://doi.org/10.1039/c0sc00194e.

(205) Capicciotti, C. J.; Trant, J. F.; Leclère, M.; Ben, R. N. Synthesis of C -Linked Triazole-Containing Afgp Analogues and Their Ability to Inhibit Ice Recrystallization. *Bioconjug. Chem.* **2011**, *22* (4), 605–616. https://doi.org/10.1021/bc100394k.

(206) Miller, N.; Williams, G. M.; Brimble, M. A. Synthesis of Fish Antifreeze Neoglycopeptides Using Microwave-Assisted "Click Chemistry." *Org. Lett.* **2009**, *11* (11), 2409–2412. https://doi.org/10.1021/ol9005536.

(207) Peltier, R.; Evans, C. W.; Devries, A. L.; Brimble, M. A.; Dingley, A. J.; Williams, D. E. Growth Habit Modification of Ice Crystals Using Antifreeze Glycoprotein (AFGP) Analogues. *Cryst. Growth Des.* **2010**, *10* (12), 5066–5077.

https://doi.org/10.1021/cg1005083.

(208) Heggemann, C.; Budke, C.; Schomburg, B.; Majer, Z.; Wissbrock, M.; Koop, T.; Sewald, N. Antifreeze Glycopeptide Analogues: Microwave-Enhanced Synthesis and Functional Studies. *Amino Acids* **2010**, *38* (1), 213–222. https://doi.org/10.1007/s00726-008-0229-0.

(209) Norgren, A. S.; Budke, C.; Majer, Z.; Heggemann, C.; Koop, T.; Sewald, N. On-Resin Click-Glycoconjugation of Peptoids. In *Synthesis*; 2009; pp 488–494. https://doi.org/10.1055/s-0028-1083302.

(210) Liu, S.; Ben, R. N. C-Linked Galactosyl Serine AFGP Analogues as Potent Recrystallization Inhibitors. *Org. Lett.* **2005**, *7* (12), 2385–2388. https://doi.org/10.1021/ol050677x.

(211) Tam, R. Y.; Rowley, C. N.; Petrov, I.; Zhang, T.; Afagh, N. A.; Woo, T. K.; Ben, R. N. Solution Conformation of C-Linked Antifreeze Glycoprotein Analogues and Modulation of Ice Recrystallization. *J. Am. Chem. Soc.* **2009**, *131* (43), 15745–15753. https://doi.org/10.1021/ja904169a.

(212) Capicciotti, C. J.; Kurach, J. D. R.; Turner, T. R.; Mancini, R. S.; Acker, J. P.; Ben, R. N. Small Molecule Ice Recrystallization Inhibitors Enable Freezing of Human Red Blood Cells with Reduced Glycerol Concentrations. *Sci. Rep.* **2015**, *5*, 1–10. https://doi.org/10.1038/srep09692.

(213) Ghobadloo, S. M.; Balcerzak, A. K.; Gargaun, A.; Muharemagic, D.; Mironov, G. G.; Capicciotti, C. J.; Briard, J. G.; Ben, R. N.; Berezovski, M. V. Carbohydrate-Based Ice Recrystallization Inhibitors Increase Infectivity and Thermostability of Viral Vectors. *Sci. Rep.* **2014**, *4*, 1–6. https://doi.org/10.1038/srep05903.

(214) Briard, J. G.; Jahan, S.; Chandran, P.; Allan, D.; Pineault, N.; Ben, R. N. Small-Molecule Ice Recrystallization Inhibitors Improve the Post-Thaw Function of Hematopoietic Stem and Progenitor Cells. *ACS Omega* **2016**, *1* (5), 1010–1018. https://doi.org/10.1021/acsomega.6b00178.

(215) Capicciotti, C. J.; Mancini, R. S.; Turner, T. R.; Koyama, T.; Alteen, M. G.; Doshi, M.; Inada, T.; Acker, J. P.; Ben, R. N. O-Aryl-Glycoside Ice Recrystallization Inhibitors as Novel Cryoprotectants: A Structure-Function Study. *ACS Omega* **2016**, *1* (4), 656–662. https://doi.org/10.1021/acsomega.6b00163.

(216) Balcerzak, A. K.; Capicciotti, C. J.; Briard, J. G.; Ben, R. N. Designing Ice

Recrystallization Inhibitors: From Antifreeze (Glyco)Proteins to Small Molecules. *RSC Adv.* **2014**, *4* (80), 42682–42696. https://doi.org/10.1039/c4ra06893a.

(217) Inada, T.; Lu, S. S. Thermal Hysteresis Caused by Non-Equilibrium Antifreeze Activity of Poly(Vinyl Alcohol). *Chem. Phys. Lett.* **2004**, *394* (4–6), 361–365. https://doi.org/10.1016/j.cplett.2004.07.021.

(218) Budke, C.; Koop, T. Ice Recrystallization Inhibition and Molecular Recognition of Ice Faces by Poly(Vinyl Alcohol). *ChemPhysChem* **2006**, *7* (12), 2601–2606. https://doi.org/10.1002/cphc.200600533.

(219) Congdon, T.; Notman, R.; Gibson, M. I. Antifreeze (Glyco)Protein Mimetic Behavior of Poly(Vinyl Alcohol): Detailed Structure Ice Recrystallization Inhibition Activity Study. *Biomacromolecules* **2013**, *14* (5), 1578–1586. https://doi.org/10.1021/bm400217j.

(220) Olijve, L. L. C.; Hendrix, M. M. R. M.; Voets, I. K. Influence of Polymer Chain Architecture of Poly(Vinyl Alcohol) on the Inhibition of Ice Recrystallization. *Macromol. Chem. Phys.* **2016**, *217* (8), 951–958. https://doi.org/10.1002/macp.201500497.

(221) Inada, T.; Lu, S. S. Inhibition of Recrystallization of Ice Grains by Adsorption of Poly(Vinyl Alcohol) onto Ice Surfaces. *Cryst. Growth Des.* **2003**, *3* (5), 747–752. https://doi.org/10.1021/cg0340300.

(222) Gibson, M. I.; Barker, C. A.; Spain, S. G.; Albertin, L.; Cameron, N. R. Inhibition of Ice Crystal Growth by Synthetic Glycopolymers: Implications for the Rational Design of Antifreeze Glycoprotein Mimics. *Biomacromolecules* **2009**, *10* (2), 328–333. https://doi.org/10.1021/bm801069x.

(223) Stubbs, C.; Lipecki, J.; Gibson, M. I. Regioregular Alternating Polyampholytes Have Enhanced Biomimetic Ice Recrystallization Activity Compared to Random Copolymers and the Role of Side Chain versus Main Chain Hydrophobicity. *Biomacromolecules* **2017**, *18* (1), 295–302. https://doi.org/10.1021/acs.biomac.6b01691.

(224) Deller, R. C.; Congdon, T.; Sahid, M. A.; Morgan, M.; Vatish, M.; Mitchell, D. A.; Notman, R.; Gibson, M. I. Ice Recrystallisation Inhibition by Polyols: Comparison of Molecular and Macromolecular Inhibitors and Role of Hydrophobic Units. *Biomater. Sci.* **2013**, *1* (5), 478–485. https://doi.org/10.1039/c3bm00194f.

(225) Matsumura, K.; Hyon, S. H. Polyampholytes as Low Toxic Efficient Cryoprotective Agents with Antifreeze Protein Properties. *Biomaterials* **2009**, *30* (27), 4842–4849.

https://doi.org/10.1016/j.biomaterials.2009.05.025.

(226) Mitchell, D. E.; Lilliman, M.; Spain, S. G.; Gibson, M. I. Quantitative Study on the Antifreeze Protein Mimetic Ice Growth Inhibition Properties of Poly(Ampholytes) Derived from Vinyl-Based Polymers. *Biomater. Sci.* **2014**, *2* (12), 1787–1795. https://doi.org/10.1039/c4bm00153b.

(227) Jain, M.; Rajan, R.; Hyon, S. H.; Matsumura, K. Hydrogelation of Dextran-Based Polyampholytes with Cryoprotective Properties via Click Chemistry. *Biomater. Sci.* **2014**, *2* (3), 308–317. https://doi.org/10.1039/c3bm60261c.

(228) Rajan, R.; Jain, M.; Matsumura, K. Cryoprotective Properties of Completely Synthetic Polyampholytes via Reversible Addition-Fragmentation Chain Transfer (RAFT) Polymerization and the Effects of Hydrophobicity. *J. Biomater. Sci. Polym. Ed.* **2013**, *24* (15), 1767–1780. https://doi.org/10.1080/09205063.2013.801703.

(229) Mitchell, D. E.; Cameron, N. R.; Gibson, M. I. Rational, yet Simple, Design and Synthesis of an Antifreeze-Protein Inspired Polymer for Cellular Cryopreservation. *Chem. Commun.* **2015**, *51* (65), 12977–12980. https://doi.org/10.1039/c5cc04647e.

(230) Gibson, M. I. Slowing the Growth of Ice with Synthetic Macromolecules: Beyond Antifreeze(Glyco) Proteins. *Polym. Chem.* **2010**, *1* (8), 1141. https://doi.org/10.1039/c0py00089b.

(231) Drori, R.; Li, C.; Hu, C.; Raiteri, P.; Rohl, A. L.; Ward, M. D.; Kahr, B. A Supramolecular Ice Growth Inhibitor. *J. Am. Chem. Soc.* **2016**, *138* (40), 13396–13401. https://doi.org/10.1021/jacs.6b08267.

(232) Mitchell, D. E.; Clarkson, G.; Fox, D. J.; Vipond, R. A.; Scott, P.; Gibson, M. I. Antifreeze Protein Mimetic Metallohelices with Potent Ice Recrystallization Inhibition Activity. *J. Am. Chem. Soc.* **2017**, *139* (29), 9835–9838. https://doi.org/10.1021/jacs.7b05822.

(233) Mitchell, D. E.; Gibson, M. I. Latent Ice Recrystallization Inhibition Activity in Nonantifreeze Proteins: Ca2+-Activated Plant Lectins and Cation-Activated Antimicrobial Peptides. *Biomacromolecules* **2015**, *16* (10), 3411–3416. https://doi.org/10.1021/acs.biomac.5b01118.

(234) Eniade, A.; Purushotham, M.; Ben, R. N.; Wang, J. B.; Horwath, K. A Serendipitous Discovery of Antifreeze Protein-Specific Activity in C-Linked Antifreeze Glycoprotein

Analogs. *Cell Biochem. Biophys.* **2003**, *38* (2), 115–124. https://doi.org/10.1385/CBB:38:2:115.

(235) Robert N. Ben, *; Adewale A. Eniade, and; Hauer, L. Synthesis of a C-Linked Antifreeze Glycoprotein (AFGP) Mimic: Probes for Investigating the Mechanism of Action. **1999**. https://doi.org/10.1021/OL991025+.

(236) Trant, J. F.; Biggs, R. A.; Capicciotti, C. J.; Ben, R. N. Developing Highly Active Small Molecule Ice Recrystallization Inhibitors Based upon C-Linked Antifreeze Glycoprotein Analogues. *RSC Adv.* **2013**, *3* (48), 26005–26009. https://doi.org/10.1039/c3ra43835j.

(237) Capicciotti, C. J.; Leclère, M.; Perras, F. A.; Bryce, D. L.; Paulin, H.; Harden, J.; Liu, Y.; Ben, R. N. Potent Inhibition of Ice Recrystallization by Low Molecular Weight Carbohydrate-Based Surfactants and Hydrogelators. *Chem. Sci.* **2012**, *3* (5), 1408–1416. https://doi.org/10.1039/c2sc00885h.

(238) Balcerzak, A. K.; Febbraro, M.; Ben, R. N. The Importance of Hydrophobic Moieties in Ice Recrystallization Inhibitors. *RSC Adv.* **2013**, *3* (10), 3232–3236. https://doi.org/10.1039/c3ra23220d.

(239) Chaytor, J. L.; Ben, R. N. Assessing the Ability of a Short Fluorinated Antifreeze Glycopeptide and a Fluorinated Carbohydrate Derivative to Inhibit Ice Recrystallization. *Bioorg. Med. Chem. Lett.* **2010**, *20* (17), 5251–5254. https://doi.org/10.1016/j.bmcl.2010.06.148.

(240) Tam, R. Y.; Ferreira, S. S.; Czechura, P.; Chaytor, J. L.; Ben, R. N. Hydration Index - A Better Parameter for Explaining Small Molecule Hydration in Inhibition of Ice Recrystallization. *J. Am. Chem. Soc.* **2008**, *130* (8), 17494–17501.

(241) Galema, S. A.; Howard, E.; Engberts, J. B. F. N.; Grigera, J. R. The Effect of Stereochemistry upon Carbohydrate Hydration. A Molecular Dynamics Simulation of β-d-Galactopyranose and (α,β)-d-Talopyranose. *Carbohydr. Res.* **1994**, *265* (2), 215–225. https://doi.org/10.1016/0008-6215(94)00241-X.

(242) Suggett, A. Molecular Motion and Interactions in Aqueous Carbohydrate Solutions. III. A Combined Nuclear Magnetic and Dielectric-Relaxation Strategy. *J. Solution Chem.* **1976**, *5* (1), 33–46. https://doi.org/10.1007/BF00647179.

(243) Franks, F. Solute-Water Interactions: Do Polyhydroxy Compounds Alter the Properties of Water? *Cryobiology* **1983**, *20* (3), 335–345. https://doi.org/10.1016/0011-2240(83)90022-

6.

(244) Painter, T. J. Effect of Axial Hydroxyl Groups upon the Hydration of Glycopyranosides: Evidence from Mechanistic Studies of Acid Hydrolysis. *Carbohydr. Res.* **1980**, *82* (2), 362–365. https://doi.org/10.1016/S0008-6215(00)85711-0.

(245) Kabayama, M. A.; Patterson, D.; Piche, L. THE THERMODYNAMICS OF MUTAROTATION OF SOME SUGARS: I. MEASUREMENT OF THE HEAT OF MUTAROTATION BY MICROCALORIMETRY. *Can. J. Chem.* **1958**, *36* (3), 557–562. https://doi.org/10.1139/v58-078.

(246) Stokes, R. H.; Robinson, R. A. Interactions in Aqueous Nonelectrolyte Solutions. I. Solute-Solvent Equilibria. *J. Phys. Chem.* **1966**, *70* (7), 2126–2131. https://doi.org/10.1021/j100879a010.

(247) Tait, M. J.; Suggett, A.; Franks, F.; Ablett, S.; Quickenden, P. A. Hydration of Monosaccharides: A Study by Dielectric and Nuclear Magnetic Relaxation. *J. Solution Chem.* **1972**, *1* (2), 131–151. https://doi.org/10.1007/BF01028450.

(248) Suggett, A.; Ablett, S.; Lillford, P. J. Molecular Motion and Interactions in Aqueous Carbohydrate Solutions. II. Nuclear-Magnetic-Relaxation Studies. *J. Solution Chem.* **1976**, *5* (1), 17–31. https://doi.org/10.1007/BF00647178.

(249) Uedaira, H.; Uedaira, H. Sugar-Water Interaction from Diffusion Measurements. *J. Solution Chem.* **1985**, *14* (1), 27–34. https://doi.org/10.1007/BF00646727.

(250) Walkinshaw, M. D. Variation in the Hydrophilicity of Hexapyranose Sugars Explains Features of the Anomeric Effect. *J. Chem. Soc. Perkin Trans. 2* **1987**, No. 12, 1903–1906. https://doi.org/10.1039/p29870001903.

(251) Miyajima, K.; Machida, K.; Nakagaki, M. Hydrophobic Indexes for Various Monosaccharides. *Bull. Chem. Soc. Jpn.* **1985**, *58* (9), 2595–2599. https://doi.org/10.1246/bcsj.58.2595.

(252) Danford, M. D.; Levy, H. A. The Structure of Water at Room Temperature. *Journal of the American Chemical Society*. 1962, pp 3965–3966. https://doi.org/10.1021/ja00879a035.

(253) Warner, D. T. Some Possible Relationships of Carbohydrates and Other Biological Components with the Water Structure at 37°. *Nature* **1962**, *196* (4859), 1055–1058. https://doi.org/10.1038/1961055a0.

(254) Galema, S. A.; Høiland, H. Stereochemical Aspects of Hydration of Carbohydrates in

Aqueous Solutions. 3. Density and Ultrasound Measurements. *J. Phys. Chem.* **1991**, *95* (13), 5321–5326. https://doi.org/10.1021/j100166a073.

(255) Galema, S. A.; Engberts, J. B. F. N.; Høiland, H.; Førland, G. M. Informative Thermodynamic Properties of the Effect of Stereochemistry on Carbohydrate Hydration. *J. Phys. Chem.* **1993**, *97* (26), 6885–6889. https://doi.org/10.1021/j100128a023.

(256) Briard, J. G.; Poisson, J. S.; Turner, T. R.; Capicciotti, C. J.; Acker, J. P.; Ben, R. N. Small Molecule Ice Recrystallization Inhibitors Mitigate Red Blood Cell Lysis during Freezing, Transient Warming and Thawing. *Sci. Rep.* **2016**, *6* (March), 2–11. https://doi.org/10.1038/srep23619.

2. Goals and Objectives

2.1 Thesis goal

The ability to preserve biological substances at ultra-low temperatures has allowed for significant medical and cryobiological advancements. One of such advancements include the discovery that cryopreserved hematopoietic stem and progenitor cells (HSPCs) isolated from umbilical cord blood can be transplanted into patients and that these hematopoietic stem cell transplants (HSCTs) can be used as a treatment of over 80 diseases and disorders.[1–4] As new cellular therapies continue to emerge, there is a significant need to optimize the biopreservation techniques of cellular products. Cryopreservation is currently the only preservation technique that allows the long-term storage of a variety of cellular products including HSPCs from umbilical cord blood (UCB).[5,6,15,7–14] The development of novel cryoprotectants (CPAs) able to address issues that arise during cryopreservation, therefore, continues to warrant extensive investigation.[8,10] Presently, the use of penetrating CPAs, such as dimethyl sulfoxide (DMSO), typically results in acceptable cell numbers and functionality after cryopreservation of different cell types. Notably, however, there is significant toxicity associated with the current CPAs, and this often results in the requirement of removing the additive from the cellular product before use in regenerative and transfusion medicines.[10,16–23] This additional CPA-removal process is expensive and time-consuming resulting in prolonged wait times for patients prior to treatments and is associated with cellular injury resulting in less functional cells for therapies.[12,24–27] Additionally, current CPAs also fail to address other cell injuries associated with cryopreservation.

One such method for improving cryoprotectants includes developing novel non-toxic additives that can reduce the amount of toxic CPA required and address additional sources of cell injuries during cryopreservation. An additional source of cryoinjury during cryopreservation involves the phenomenon of ice recrystallization.[5,13,28] Thus, the development of non-toxic CPAs able to mitigate cryoinjury associated with ice crystal growth in biological samples would significantly improve the current cryopreservation techniques. Compounds able to inhibit ice recrystallization, termed ice recrystallization inhibitors (IRIs), therefore have tremendous potential. Previous research from the Ben laboratory involved the development of a variety of novel, small molecule carbohydrate-based IRIs stemming from structural studies of antifreeze glycoproteins (AFGPs).[29,30,39–41,31–38] These compounds have significant potential as cryoprotectants owing to their ability to inhibit ice recrystallization without additional thermal hysteresis activity, a property known to be detrimental to cells for use in clinical applications.[42,43] In examining the structural features required for IRI activity, the Ben laboratory has developed an aldonamide-based class of IRIs.[30,33] Through structure-activity relationship (SAR) work, the aldonamide IRIs bearing an aryl-head group joined to a glucose-tail group through an amide bond linkage (termed "*N*-aryl-D-gluconamides", see **Figure 2.2.1**) have been shown to exhibit promising cryoprotectant abilities for HSPCs isolated from human UCB.[33] Owing to these promising *in vitro* results, further SAR work on the *N*-aryl-D-gluconamides is warranted in addition to the development of other of novel classes of IRIs. Continued development of ice recrystallization inhibitors through synthetic modifications of the *N*-aryl-D-gluconamide class of IRIs will provide a better understanding of how certain structural features affect the abilities of these IRIs to improve the cryopreservation of various cellular products. Therefore, the first goal of this thesis is the continued development of IRIs able to improve the functionality and viability

of cellular products *in vitro*. Specifically, novel modifications to both the hydrophobic head and hydrophilic tail groups of the aldonamides are investigated. Furthermore, to date, there have been no reports examining the impact of these small molecule carbohydrate-based IRIs on the *in vivo* use of cryopreserved cellular products. Therefore, the second thesis goal involves exploring the effect of IRIs on the activities of cryopreserved cellular products both *in vitro* and *in vivo*. These *in vivo* results are essential for the translation of IRI-cryoprotectants into numerous clinical applications, including in preserving HSPCs for regenerative and transfusion medicine applications.

Finally, the continued development of novel glyco(peptide)-based macromolecules will further elucidate the features necessary for ice recrystallization inhibition of this class of compounds, and therefore, this is the third thesis goal. While considerable research has been conducted on polymers as IRIs,[44–48] this thesis includes the exploration of novel photocontrollable glyco(peptide)-based surfactants as IRIs in addition to unique glycopeptide-based perylene bisimides as IRI-active self-assembled materials. The following three objectives clearly outline the research included in this thesis.

2.2 Objective 1 – Development of *N*-aryl-D-gluconamide derivatives as ice recrystallization inhibitors

The *N*-aryl-D-gluconamides are a class of ice recrystallization inhibitor structurally comprised of a hydrophobic aryl group connected to a hydrophilic carbohydrate component (e.g. the open-chain form of glucose) through an amide bond (**Figure 2.2.1**). Previous structure-activity relationship (SAR) studies have indicated that IRI-active aldonamides possess a distinct hydrophobic-hydrophilic balance.[30,31,33,49–52] Investigating aryl group regiochemistry

requirements among the aryl-D-gluconamides led to the discovery that *N*-(2-fluorophenyl)-D-gluconamide (**2.01**), *N*-(4-methoxyphenyl)-D-gluconamide (**2.02**), *N*-(2,6-difluorobenzyl)-D-gluconamide (**2.03**), and *N*-(4-chlorophenyl)-D-gluconamide (**2.04**) are active ice recrystallization inhibitors (**Figure 2.2.1**).[49,50] Further, *in vitro* results suggest that *N*-(2-fluorophenyl)-D-gluconamide (**2.01**) and other select gluconamides improve the post-thaw function and viability of cryopreserved hematopoietic stem and progenitor cells (HSPCs) from umbilical cord blood.[33,50] While numerous IRI candidates have now been developed for cryopreservation purposes, there is significant SAR work remaining. For example, there is no clear trend relating an aldonamide's aryl substituent composition to IRI activity.[38,49,50] The rational design of novel aldonamide-based IRIs, therefore, continues to be challenging. Objective 1 (**Chapter 3**) focuses on continuing the SAR studies of *N*-aryl-D-gluconamides toward determining the key structural features required for IRI activity. This objective focuses on two separate aspects of the aldonamides: 1) the study of the hydrophobic aryl component of *N*-aryl-D-gluconamides and 2) the exploration of modifications to the carbohydrate component of the gluconamide structure.

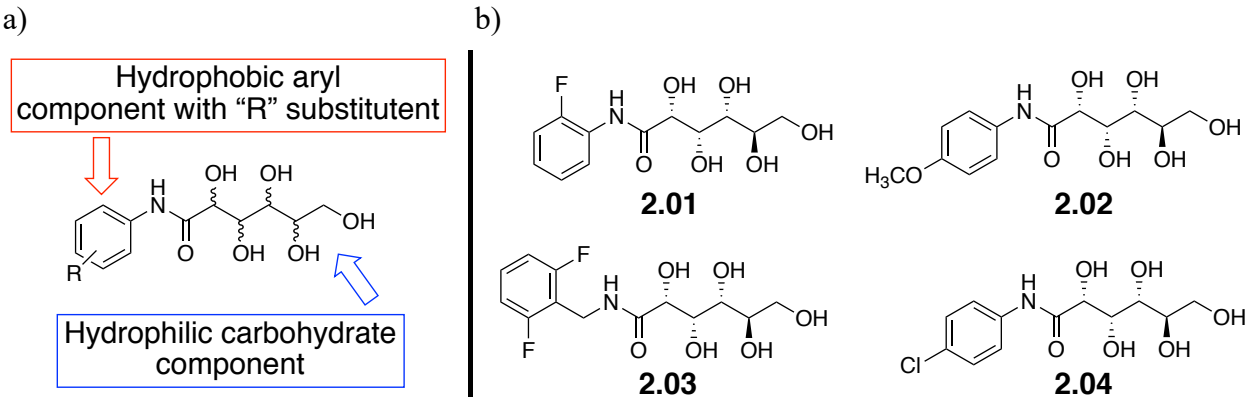

Figure 2.2.1. a) Components of the *N*-aryl-D-gluconamides studied in Objective 1, and **b)** and the structures of select *N*-aryl-D-gluconamides (**2.01-2.04**).[33,50]

The first aspect focuses on the study of the hydrophobic aryl component of *N*-aryl-D-gluconamides (gluconamides **2.01-2.04**). A 2-fluoro-4-methoxyphenyl derivative (e.g. where R = 2-F-4-OCH_3) is designed to analyze the impact of combining the two respective substituents of 2-fluorophenyl gluconamide (**2.01**, R = 2-F) and 4-methoxyphenyl gluconamide (**2.02**, R = 4-OCH_3) into one structure. Next, electron-donating substituents as R groups are considered (e.g. R = amine) and compared to other gluconamides with electron-rich aryl groups.

The second aspect investigates how modifications to the carbohydrate component of the *N*-aryl-D-gluconamides affect IRI activity. Derivatives with alterations to the stereochemistry or to the oxidation state and functionality of the terminal hydroxyl group (e.g. carboxylic acid and azide groups) group are compared to their parent gluconamides (namely gluconamides **2.01-2.04**). Inspired by previous work in which the length of the aldonamide's carbohydrate-tail group was altered,[51,52] derivatives with shortened and modified poly-hydroxylated chains are investigated in order to determine the importance of the polyol chain. Altogether, these structural and stereochemical changes explore the potential for the respective requirements of this carbohydrate component.

The IRI activities of the aforementioned gluconamide derivatives are explored using a multi-step approach involving the initial synthesis of targets, a general IRI screening for activity, followed by the further assessment (e.g. analysis of IRI kinetics) of the more promising candidates (**Figure 2.2.2**). The strategy utilizes the robust splat-cooling assay for initial IRI determination whereby a series of compounds (tested at a single concentration) are annealed for 30-minutes at -6.4 °C prior to determination of the potential IRI activities. A modified splat-cooling assay is implemented for more in-depth and quantitative analysis (e.g. "IRI kinetics") of the promising compounds. This involves assessment of multiple concentrations of compounds

after 5-minute annealing periods at -6.4 °C in order to obtain rate constants for the inhibition activity.[53–55] These kinetic IRI data, including the concentration of inhibitor resulting in 50% inhibition (IC_{50} value), offer a way to further compare the effectiveness of IRI candidates that may be considered for further testing (presented in subsequent chapters) such as analysis of cytotoxicity, additional antifreeze activities (thermal hysteresis), and cryoprotectant abilities (*in vitro* and *in vivo*).

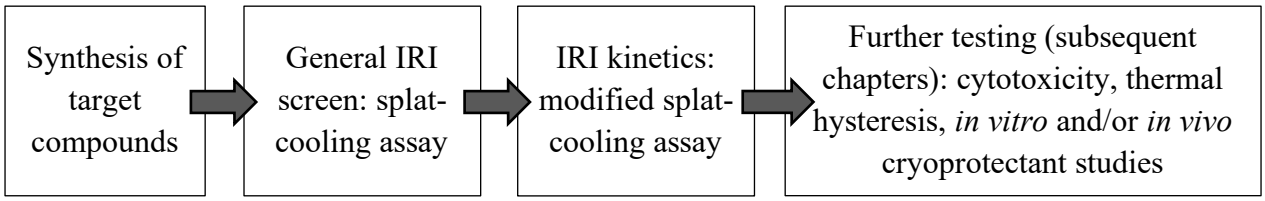

Figure 2.2.2. The assessment of gluconamide derivatives includes initial synthesis followed by IRI analysis using splat-cooling assays.[54,55]

2.3 Objective 2 – The impact of *N*-aryl-D-gluconamides on the activities of cryopreserved human umbilical cord blood

The class *N*-aryl-D-gluconamide IRIs has shown compelling potential toward the improvement of post-thaw activities of cryopreserved hematopoietic stem and progenitor cells (HSPCs).[33] Specifically, the *in vitro* post-thaw functions and viabilities of HSPCs isolated from human umbilical cord blood have been improved when select gluconamides were used as supplements to the standard cryoprotectant solution involving dimethyl sulfoxide (DMSO). Complementation of the cryomedium with *N*-2-fluorophenyl-D-gluconamide **2.01**, for example, resulted in a two-fold increase in the recovery of progenitors after cryopreservation.[33] Other IRI-active gluconamides (e.g. **2.02-2.04** in **Figure 2.2.1**) also resulted in compelling preliminary

data. These promising small-scale results may translate into future significant advancements in the treatment of over 80 life-threatening diseases and disorders. Indeed, HSPCs are a diverse pool of stem cells that give rise to many different blood and immune cell types. Through myelopoiesis, the differentiation and proliferation of HSPCs lead to many different blood cells including erythrocytes (red blood cells), megakaryocytes, platelets, granulocytes, monocytes, and macrophages.[56] It, therefore, follows that HSPCs can be administered (e.g. through hematopoietic stem cell transplants) to repopulate cells in a body after disease, intensive chemotherapy and/or radiation therapy.[57,58] The many uses of umbilical cord blood (UCB) as a source for hematopoietic stem cell transplantation (HSCT) is not yet fully realized owing to the relatively small number of stem cells obtained from one UCB unit compared to other sources like the bone marrow or adult peripheral blood.[59–63] Strategies to improve the number and quality of the stem cells isolated from UCB are therefore paramount to improving HSCT.[60,64–66] Consequently, Objective 2 of this thesis consists of investigating the potential for gluconamide IRIs to positively impact the *in vitro* and *in vivo* properties of cryopreserved HSPCs from human UCB. This objective begins by assessing the cytotoxicity of promising gluconamide derivatives from Objective 1 followed by the analysis of the cryoprotectant abilities of non-toxic and promising candidates (**Figure 2.3.1**). The cytotoxicity of compounds is indirectly assessed using a fluorescent-based assay that determines the metabolic activity of human hepatic cells exposed to IRIs.[67,68] In collaboration with the Pineault laboratory at the Canadian Blood Services, the *in vitro* impact of cryopreserving cord blood in the presence of gluconamides is assessed by determining the post-thaw viabilities (flow cytometry-based assays) and clonogenic potentials (using colony-forming cell assay) of the HSPCs.[33,62,69–71] The *in vivo* impact of using an IRI as a supplement for stem cell graft cryopreservation is assessed by studying the engraftment activities

of stem cell grafts using serial transplantation experiments in a murine model.[72–74] This serial xenotransplantation assay is considered the 'gold-standard' method for determining the activities of cryopreserved HSPCs and therefore offers true insight into the impact of IRIs in mitigating the cellular injuries experienced by HSPCs during conventional cryopreservation. This marks the first *in vivo* analysis of cells cryopreserved in the presence of IRI cryoprotectants.

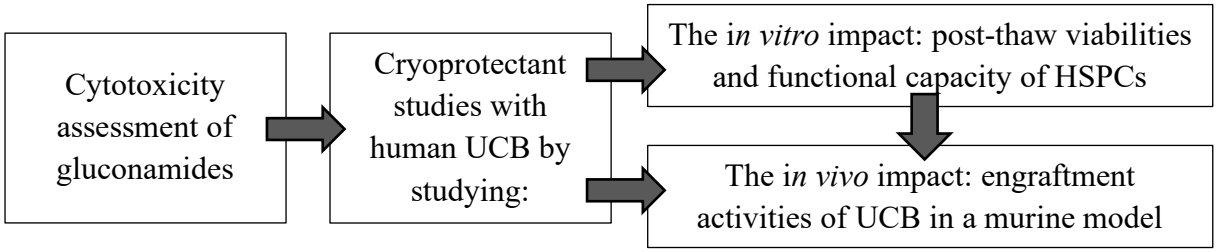

Figure 2.3.1. The approach to assessing the cytotoxicity and cryoprotectant abilities of *N*-aryl-D-gluconamides.

2.4 Objective 3 – Development of photocontrollable glyco(peptide)-functionalized ice recrystallization inhibitors

Chapter 5 focuses on Objective 3 and investigates glyco(peptide) macromolecules for their ability to act as ice recrystallization inhibitors. Using a similar SAR approach described for Objective 1, the IRI activity, potential thermal hysteresis activity, and the cytotoxicity of antifreeze glycoprotein (AFGP) analogues are studied. More specifically, this objective is broken down into three sub-components: 1) the development of glyco(peptide)-functionalized lipopeptides and perylene bisimides as IRIs, 2) the production of glyco(peptide)-based azobenzene compounds for the novel potential of photocontrollable inhibition of ice recrystallization, and 3) the study of carbohydrate-based azobenzene fluorosurfactants for their

use as photoswitchable IRIs. These studies were conducted in collaboration with Dr. Brendan Wilkinson's laboratory in Australia (University of New England).

First, a series of lipopeptides comprised of the AFGP glycotripeptide (Ala-Thr-Ala)$_4$ tethered to a phenol ether through a triethylene glycolate spacer was developed and assessed for IRI activity (**Figure 2.4.1**). From there, the continued development of AFGP analogues involved the study of self-assembled IRI materials incorporating a perylene bisimide core connected to two of the glycopeptide fragments (**Figure 2.4.1**).[75] Molecules able to self-assemble in solution would be able to counteract the drawbacks of using large biopolymers for industrial antifreeze purposes (e.g. difficulty obtaining adequate amounts and purity of AFGP analogues). Perylene bisimides (PBIs) are compelling structures for the development of self-assembled materials since PBIs are planar structures that undergo intermolecular pi-pi stacking interactions in solution. In an effort to design IRIs that self-assemble, the IRI activity and other properties of the AFGP-PBIs are analyzed.

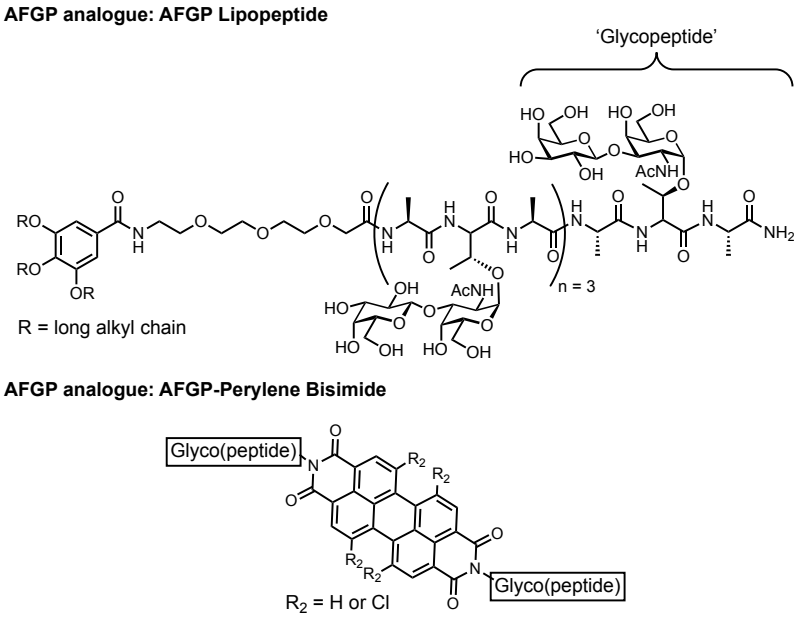

Figure 2.4.1. General structures of lipopeptides and glyco(peptide)-functionalized perylene bisimides studied for their potential as AFGP analogues.

The next sub-section discusses the development of glyco(peptides) possessing tuneable ice recrystallization inhibition using an external stimulus (**Figure 2.4.2**).[76] Specifically, the incorporation of an azobenzene moiety into the glyco(peptide) structure was studied for the ability to control the molecule's physicochemical properties using UV-vis light. An azobenzene "switch" involves the conversion of the *trans*-photostationary state of the molecule to its *cis*-isomer upon photoirradiation (361 nm) which then reverses under visible light (450 nm). This conversion instills physicochemical changes including modifications to a compound's hydrophobicity/hydrophilicity, planarity, critical micelle concentrations (CMC), among others. We hypothesized that we could use this structural change to control the resulting IRI activity of the glyco(peptide)-based compounds. Similarly, the last sub-section involves the analysis of a series of carbohydrate-based fluorosurfactants for their potential for photocontrollable IRI activity (**Figure 2.4.2**). Once again, we expected that structural changes resulting from the photoisomerization of the fluorosurfactants would allow for controllable IRI activity.

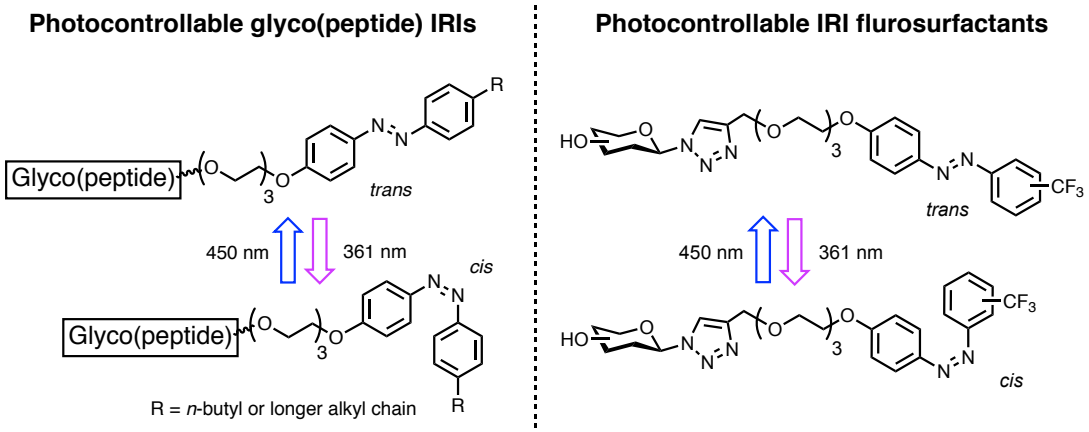

Figure 2.4.2. The general structure of photocontrollable glyco(peptides).

2.5 Summary of goals and objectives

The overall goal of this thesis is the development of novel ice recrystallization inhibitors (IRIs) for the improvement of the cryopreservation of cellular products (e.g. hematopoietic stem and progenitor cells). Exploration involves the following objectives:

1. Assessment of the important features of *N*-aryl-D-aldonamide IRIs through synthetic modifications to the promising parent aldonamides. (**Chapter 3**)
2. Determination of the impact of *N*-aryl-D-gluconamide cryoprotectants on the *in vitro* activities of hematopoietic stem and progenitor cells (HSPCs) as well as on the *in vivo* engraftment of cryopreserved HSPCs from umbilical cord blood (UCB). (**Chapter 4**)
3. Development of glyco(peptide)-based macromolecules as ice recrystallization inhibitors. This includes materials that self-assemble in solution to act as biomimetics of antifreeze glycoproteins (AFGPs) as well as photocontrollable carbohydrate-based surfactants as IRIs. (**Chapter 5**)

2.6 References

(1) Hunt, C. J. Cryopreservation of Human Stem Cells for Clinical Application: A Review. *Transfusion Medicine and Hemotherapy*. April 2011, pp 107–123. https://doi.org/10.1159/000326623.

(2) Harris, D. T. Non-Haematological Uses of Cord Blood Stem Cells. *British Journal of Haematology*. October 2009, pp 177–184. https://doi.org/10.1111/j.1365-2141.2009.07767.x.

(3) Harris, D. T. Cord Blood Stem Cells: Current Uses and Future Challenges. *AIMS Cell Tissue Eng.* **2017**, *1* (2), 158–164. https://doi.org/10.3934/celltissue.2017.2.158.

(4) Broxmeyer, H. E. Enhancing the Efficacy of Engraftment of Cord Blood for Hematopoietic Cell Transplantation. *Transfus. Apher. Sci.* **2016**, *54* (3), 364–372. https://doi.org/10.1016/J.TRANSCI.2016.05.013.

(5) Mazur, P. *Life in the Frozen State - Principles of Cryobiology*, 1st ed.; Fuller BJ, Lane N, B. E., Ed.; CRC Press LLC: Boca Raton, FL, 2004. https://doi.org/10.1201/9780203647073-10.

(6) Kanias, T.; Acker, J. P. Biopreservation of Red Blood Cells - the Struggle with Hemoglobin Oxidation. *FEBS J.* **2010**, *277* (2), 343–356. https://doi.org/10.1111/j.1742-4658.2009.07472.x.

(7) Meryman, H. T. Cryopreservation of Living Cells: Principles and Practice. *Transfusion* **2007**, *47* (5), 935–945.

(8) Baust, J. M.; Corwin, W. L.; VanBuskirk, R.; Baust, J. G. Biobanking: The Future of Cell Preservation Strategies; Springer, Cham, 2015; pp 37–53. https://doi.org/10.1007/978-3-319-20579-3_4.

(9) Baust, J. G.; Gao, D.; Baust, J. M. Cryopreservation: An Emerging Paradigm Change. *Organogenesis* **2009**, *5* (3), 90–96.

(10) Baust, J. M.; Campbell, L. H.; Harbell, J. W. Best Practices for Cryopreserving, Thawing, Recovering, and Assessing Cells. *Vitr. Cell. Dev. Biol. - Anim.* **2017**, *53*, 855–871. https://doi.org/10.1007/s11626-017-0201-y.

(11) Bakhach, J. The Cryopreservation of Composite Tissues: Principles and Recent Advancement on Cryopreservation of Different Type of Tissues. *Organogenesis* **2009**, *5*

(3), 119–126.

(12) Scott, K. L.; Lecak, J.; Acker, J. P. Biopreservation of Red Blood Cells: Past, Present, and Future From the Canadian Blood Services. *Transfus. Med. Rev.* **2005**, *19* (2), 127. https://doi.org/10.1016/j.tmrv.2004.11.004.

(13) Fowler, A.; Toner, M. Cryo-Injury and Biopreservation. *Annals of the New York Academy of Sciences*. March 1, 2005, pp 119–135. https://doi.org/10.1196/annals.1363.010.

(14) Valeri, C. R.; Ragno, G. Cryopreservation of Human Blood Products. *Transfus. Apher. Sci.* **2006**, *34* (3), 271–287. https://doi.org/10.1016/j.transci.2005.11.010.

(15) Holovati, J. L.; Hannon, J. L.; Gyongyossy-Issa, M. I. C.; Acker, J. P. Blood Preservation Workshop: New and Emerging Trends in Research and Clinical Practice. *Transfus. Med. Rev.* **2009**, *23* (1), 25–41. https://doi.org/10.1016/j.tmrv.2008.09.003.

(16) Best, B. P. Cryoprotectant Toxicity: Facts, Issues, and Questions. *Rejuvenation Res.* **2015**, *18* (5), 422–436. https://doi.org/10.1089/rej.2014.1656.

(17) Hallare, A. V.; Kohler, H. R.; Triebskorn, R. Developmental Toxicity and Stress Protein Responses in Zebrafish Embryos after Exposure to Diclofenac and Its Solvent, DMSO. *Chemosphere* **2004**, *56* (7), 659–666. https://doi.org/10.1016/J.CHEMOSPHERE.2004.04.007.

(18) Shu, Z.; Heimfeld, S.; Gao, D. Hematopoietic SCT with Cryopreserved Grafts: Adverse Reactions after Transplantation and Cryoprotectant Removal before Infusion. *Bone Marrow Transplant.* **2014**, *49*, 469–476.

(19) Gao, D.; Critser, A. K. *Mechanisms of Cryoinjury in Living Cells*.

(20) Rowley, S. D.; Anderson, G. L. Effect of DMSO Exposure without Cryopreservation on Hematopoietic Progenitor Cells. *Bone Marrow Transplant.* **1993**, *11* (5), 389–393.

(21) Yang, H.; Zhao, H.; Acker, J. P.; Liu, J. Z.; Akabutu, J.; McGann, L. E. Effect of Dimethyl Sulfoxide on Post-Thaw Viability Assessment of CD45+ and CD34+ Cells of Umbilical Cord Blood and Mobilized Peripheral Blood. *Cryobiology* **2005**, *51* (2), 165–175. https://doi.org/10.1016/j.cryobiol.2005.06.003.

(22) Zambelli, A.; Poggi, G.; Da Prada, G.; Pedrazzoli, P.; Cuomo, A.; Miotti, D.; Perotti, C.; Preti, P.; Robustelli della Cuna, G. Clinical Toxicity of Cryopreserved Circulating Progenitor Cells Infusion. *Anticancer Res. 18* (6B), 4705–4708.

(23) Kollerup Madsen, B.; Hilscher, M.; Zetner, D.; Rosenberg, J. Adverse Reactions of

Dimethyl Sulfoxide in Humans: A Systematic Review. *F1000Research* **2018**, *7* (1746), 1–17. https://doi.org/10.12688/f1000research.16642.1.

(24) Robert Valeri, C.; Ragno, G.; Pivacek, L.; Mary O'Neill, E. In Vivo Survival of Apheresis RBCs, Frozen with 40-Percent (Wt/Vol) Glycerol, Deglycerolized in the ACP 215, and Stored at 4°C in AS-3 for up to 21 Days. *Transfusion* **2001**, *41* (7), 928–932. https://doi.org/10.1046/j.1537-2995.2001.41070928.x.

(25) Hess, J. R. Red Cell Freezing and Its Impact on the Supply Chain. *Transfus. Med.* **2004**, *14* (1), 1–8. https://doi.org/10.1111/j.0958-7578.2004.00472.x.

(26) Meryman, H. T.; Hornblower, M. A Method for Freezing and Washing Red Blood Cells Using a High Glycerol Concentration. *Transfusion* **1972**, *12* (3), 145–156. https://doi.org/10.1111/j.1537-2995.1972.tb00001.x.

(27) Chang, A.; Kim, Y.; Hoehn, R.; Jernigan, P.; Pritts, T. Cryopreserved Packed Red Blood Cells in Surgical Patients: Past, Present, and Future. *Blood Transfusion*. SIMTI Servizi Sri 2017, pp 341–347. https://doi.org/10.2450/2016.0083-16.

(28) Acker, J. P.; Mcgann, L. E. *Innocuous Intracellular Ice Improves Survival of Frozen Cells*; 2002; Vol. 11.

(29) J., C.; Doshi, M.; N., R. Ice Recrystallization Inhibitors: From Biological Antifreezes to Small Molecules. *Recent Dev. Study Recryst.* **2013**. https://doi.org/10.5772/54992.

(30) Capicciotti, C. J.; Leclère, M.; Perras, F. A.; Bryce, D. L.; Paulin, H.; Harden, J.; Liu, Y.; Ben, R. N. Potent Inhibition of Ice Recrystallization by Low Molecular Weight Carbohydrate-Based Surfactants and Hydrogelators. *Chem. Sci.* **2012**, *3* (5), 1408–1416. https://doi.org/10.1039/c2sc00885h.

(31) Balcerzak, A. K.; Capicciotti, C. J.; Briard, J. G.; Ben, R. N. Designing Ice Recrystallization Inhibitors: From Antifreeze (Glyco)Proteins to Small Molecules. *RSC Adv.* **2014**, *4* (80), 42682–42696. https://doi.org/10.1039/c4ra06893a.

(32) Eniade, A.; Purushotham, M.; Ben, R. N.; Wang, J. B.; Horwath, K. A Serendipitous Discovery of Antifreeze Protein-Specific Activity in C-Linked Antifreeze Glycoprotein Analogs. *Cell Biochem. Biophys.* **2003**, *38* (2), 115–124. https://doi.org/10.1385/CBB:38:2:115.

(33) Briard, J. G.; Jahan, S.; Chandran, P.; Allan, D.; Pineault, N.; Ben, R. N. Small-Molecule Ice Recrystallization Inhibitors Improve the Post-Thaw Function of Hematopoietic Stem

and Progenitor Cells. *ACS Omega* **2016**, *1* (5), 1010–1018. https://doi.org/10.1021/acsomega.6b00178.

(34) Chaytor, J. L.; Tokarew, J. M.; Wu, L. K.; Leclre, M.; Tam, R. Y.; Capicciotti, C. J.; Guolla, L.; Von Moos, E.; Findlay, C. S.; Allan, D. S.; Ben, R. N. Inhibiting Ice Recrystallization and Optimization of Cell Viability after Cryopreservation. *Glycobiology* **2012**, *22* (1), 123–133. https://doi.org/10.1093/glycob/cwr115.

(35) Trant, J. F.; Biggs, R. A.; Capicciotti, C. J.; Ben, R. N. Developing Highly Active Small Molecule Ice Recrystallization Inhibitors Based upon C-Linked Antifreeze Glycoprotein Analogues. *RSC Adv.* **2013**, *3* (48), 26005–26009. https://doi.org/10.1039/c3ra43835j.

(36) Balcerzak, A. K.; Febbraro, M.; Ben, R. N. The Importance of Hydrophobic Moieties in Ice Recrystallization Inhibitors. *RSC Adv.* **2013**, *3* (10), 3232–3236. https://doi.org/10.1039/c3ra23220d.

(37) Czechura, P.; Tam, R. Y.; Dimitrijevic, E.; Murphy, A. V.; Ben, R. N. The Importance of Hydration for Inhibiting Ice Recrystallization with C-Linked Antifreeze Glycoproteins. *J. Am. Chem. Soc.* **2008**, *130* (10), 2928–2929. https://doi.org/10.1021/ja7103262.

(38) Ampaw, A.; Charlton, T. A.; Briard, J. G.; Ben, R. N. Designing the next Generation of Cryoprotectants - From Proteins to Small Molecules. *Pept. Sci.* **2018**, No. May, e24086. https://doi.org/10.1002/pep2.24086.

(39) Chaytor, J. L.; Ben, R. N. Assessing the Ability of a Short Fluorinated Antifreeze Glycopeptide and a Fluorinated Carbohydrate Derivative to Inhibit Ice Recrystallization. *Bioorg. Med. Chem. Lett.* **2010**, *20* (17), 5251–5254. https://doi.org/10.1016/j.bmcl.2010.06.148.

(40) Liu, S.; Ben, R. N. C-Linked Galactosyl Serine AFGP Analogues as Potent Recrystallization Inhibitors. *Org. Lett.* **2005**, *7* (12), 2385–2388. https://doi.org/10.1021/ol050677x.

(41) Capicciotti, C. J.; Mancini, R. S.; Turner, T. R.; Koyama, T.; Alteen, M. G.; Doshi, M.; Inada, T.; Acker, J. P.; Ben, R. N. O-Aryl-Glycoside Ice Recrystallization Inhibitors as Novel Cryoprotectants: A Structure-Function Study. *ACS Omega* **2016**, *1* (4), 656–662. https://doi.org/10.1021/acsomega.6b00163.

(42) Carpenter, J. F.; Hansen, T. N. Antifreeze Protein Modulates Cell Survival during Cryopreservation: Mediation through Influence on Ice Crystal Growth. *Proc. Natl. Acad.*

Sci. U. S. A. **1992**, *89* (19), 8953–8957. https://doi.org/10.1073/pnas.89.19.8953.

(43) Chao, H.; Davies, P. L.; Carpenter, J. F. Effects of Antifreeze Proteins on Red Blood Cell Survival during Cryopreservation. *J. Exp. Biol.* **1996**, *199* (Pt 9), 2071–2076.

(44) Knight, C. A.; Wen, D.; Laursen, R. A. Nonequilibrium Antifreeze Peptides and the Recrystallization of Ice. *Cryobiology*. 1995, pp 23–34. https://doi.org/10.1006/cryo.1995.1002.

(45) Gibson, M. I.; Barker, C. A.; Spain, S. G.; Albertin, L.; Cameron, N. R. Inhibition of Ice Crystal Growth by Synthetic Glycopolymers: Implications for the Rational Design of Antifreeze Glycoprotein Mimics. *Biomacromolecules* **2009**, *10* (2), 328–333. https://doi.org/10.1021/bm801069x.

(46) Gibson, M. I. Slowing the Growth of Ice with Synthetic Macromolecules: Beyond Antifreeze(Glyco) Proteins. *Polym. Chem.* **2010**, *1* (8), 1141. https://doi.org/10.1039/c0py00089b.

(47) Biggs, C. I.; Bailey, T. L.; Ben Graham, B.; Stubbs, C.; Fayter, A.; Gibson, M. I. Polymer Mimics of Biomacromolecular Antifreezes. *Nat. Commun.* **2017**, *8* (1), 1546. https://doi.org/10.1038/s41467-017-01421-7.

(48) Biggs, C. I.; Stubbs, C.; Graham, B.; Fayter, A. E. R.; Hasan, M.; Gibson, M. I. Mimicking the Ice Recrystallization Activity of Biological Antifreezes. When Is a New Polymer "Active"? *Macromol. Biosci.* **2019**, 1900082. https://doi.org/10.1002/mabi.201900082.

(49) Briard, J. G.; Fernandez, M.; De Luna, P.; Woo, T. K.; Ben, R. N. QSAR Accelerated Discovery of Potent Ice Recrystallization Inhibitors. *Sci. Rep.* **2016**, *6* (October 2015), 1–8. https://doi.org/10.1038/srep26403.

(50) Briard, J. G. The Rational Design and Use of Novel Small-Molecule Ice Recrystallization Inhibitors for the Cryopreservation of Hematopoietic Stem Cells and Red Blood Cells (Doctoral Dissertation, Université d'Ottawa/University of Ottawa), Université d'Ottawa/University of Ottawa, 2016.

(51) Capicciotti, C. The Rational Design of Potent Ice Recrystallization Inhibitors for Use as Novel Cryoprotectants (Doctoral Dissertation, Université d'Ottawa/University of Ottawa), Université d'Ottawa/University of Ottawa, 2014.

(52) Doshi, M. Synthesis of Nitrogen-Containing Carbohydrate Derivatives and Their Use

Toward Inhibiting Ice Recrystallization and Gas Hydrate Formation (Doctoral Dissertation, Université d'Ottawa/University of Ottawa), Université d'Ottawa/University of Ottawa, 2016.

(53) Knight, C. A.; Hallett, J.; DeVries, A. L. Solute Effects on Ice Recrystallization: An Assessment Technique. *Cryobiology* **1988**, *25* (1), 55–60. https://doi.org/10.1016/0011-2240(88)90020-X.

(54) Jackman, J.; Noestheden, M.; Moffat, D.; Pezacki, J. P.; Findlay, S.; Ben, R. N. Assessing Antifreeze Activity of AFGP 8 Using Domain Recognition Software. *Biochem. Biophys. Res. Commun.* **2007**, *354* (2), 340–344. https://doi.org/10.1016/j.bbrc.2006.12.225.

(55) Abraham, S.; Keillor, K.; Capicciotti, C. J.; Perley-Robertson, G. E.; Keillor, J. W.; Ben, R. N. Quantitative Analysis of the Efficacy and Potency of Novel Small Molecule Ice Recrystallization Inhibitors. *Cryst. Growth Des.* **2015**, *15* (10), 5034–5039. https://doi.org/10.1021/acs.cgd.5b00995.

(56) Akashi, K.; Traver, D.; Miyamoto, T.; Weissman, I. L. A Clonogenic Common Myeloid Progenitor That Gives Rise to All Myeloid Lineages. *Nature* **2000**, *404* (6774), 193–197. https://doi.org/10.1038/35004599.

(57) WHO | Haematopoietic Stem Cell Transplantation HSCtx. *WHO* **2013**.

(58) Niederwieser, D.; Baldomero, H.; Szer, J.; Gratwohl, M.; Aljurf, M.; Atsuta, Y.; Bouzas, L. F.; Confer, D.; Greinix, H.; Horowitz, M.; Iida, M.; Lipton, J.; Mohty, M.; Novitzky, N.; Nunez, J.; Passweg, J.; Pasquini, M. C.; Kodera, Y.; Apperley, J.; Seber, A.; Gratwohl, A. Hematopoietic Stem Cell Transplantation Activity Worldwide in 2012 and a SWOT Analysis of the Worldwide Network for Blood and Marrow Transplantation Group Including the Global Survey. *Bone Marrow Transplant.* **2016**, *51* (6), 778–785. https://doi.org/10.1038/bmt.2016.18.

(59) Keating, A. K.; Langenhorst, J.; Wagner, J. E.; Page, K. M.; Veys, P.; Wynn, R. F.; Stefanski, H.; Elfeky, R.; Giller, R.; Mitchell, R.; Milano, F.; O'Brien, T. A.; Dahlberg, A.; Delaney, C.; Kurtzberg, J.; Verneris, M. R.; Boelens, J. J. The Influence of Stem Cell Source on Transplant Outcomes for Pediatric Patients with Acute Myeloid Leukemia. *Blood Adv.* **2019**, *3* (7), 1118–1128. https://doi.org/10.1182/bloodadvances.2018025908.

(60) Allan, D. S.; Keeney, M.; Howson-Jan, K.; Popma, J.; Weir, K.; Bhatia, M.; Sutherland, D. R.; Chin-Yee, I. H. Number of Viable CD34+ Cells Reinfused Predicts Engraftment in

Autologous Hematopoietic Stem Cell Transplantation. *Bone Marrow Transplant.* **2002**, *29* (12), 967–972. https://doi.org/10.1038/sj.bmt.1703575.

(61) Abrahamsen, J. F.; Rusten, L.; Bakken, A. M.; Bruserud, Ø. Better Preservation of Early Hematopoietic Progenitor Cells When Human Peripheral Blood Progenitor Cells Are Cryopreserved with 5 Percent Dimethylsulfoxide Instead of 10 Percent Dimethylsulfoxide. *Transfusion* **2004**, *44* (5), 785–789. https://doi.org/10.1111/j.1537-2995.2004.03336.x.

(62) Page, K. M.; Zhang, L.; Mendizabal, A.; Wease, S.; Carter, S.; Gentry, T.; Balber, A. E.; Kurtzberg, J. Total Colony-Forming Units Are a Strong, Independent Predictor of Neutrophil and Platelet Engraftment after Unrelated Umbilical Cord Blood Transplantation: A Single-Center Analysis of 435 Cord Blood Transplants. *Biol. Blood Marrow Transplant.* **2011**, *17* (9), 1362–1374. https://doi.org/10.1016/j.bbmt.2011.01.011.

(63) Yoder, M. C. Cord Blood Banking and Transplantation: Advances and Controversies. *Curr. Opin. Pediatr.* **2014**, *26* (2), 163–168. https://doi.org/10.1097/MOP.0000000000000065.

(64) Zaucha, J. M.; Gooley, T.; Bensinger, W. I.; Heimfeld, S.; Chauncey, T. R.; Zaucha, R.; Martin, P. J.; Flowers, M. E.; Storek, J.; Georges, G.; Storb, R.; Torok-Storb, B. CD34 Cell Dose in Granulocyte Colony-Stimulating Factor-Mobilized Peripheral Blood Mononuclear Cell Grafts Affects Engraftment Kinetics and Development of Extensive Chronic Graft-versus-Host Disease after Human Leukocyte Antigen-Identical Sibling Transpla. *Blood* **2001**, *98* (12), 3221–3227. https://doi.org/10.1182/blood.v98.12.3221.

(65) Theilgaard-Mönch, K.; Raaschou-Jensen, K.; Heilmann, C.; Andersen, H.; Bock, J.; Russel, C. A.; Vindeløv, L.; Jacobsen, N.; Dickmeiss, E. A Comparative Study of CD34+ Cells, CD34+ Subsets, Colony Forming Cells and Cobblestone Area Forming Cells in Cord Blood and Bone Marrow Allografts. *Eur. J. Haematol.* **2009**, *62* (3), 174–183. https://doi.org/10.1111/j.1600-0609.1999.tb01741.x.

(66) Carral, A.; de la Rubia, J.; Martín, G.; Mollá, S.; Martínez, J.; Sanz, G. F.; Soler, M. A.; Jarque, I.; Jiménez, C.; Sanz, M. A. Factors Influencing the Collection of Peripheral Blood Stem Cells in Patients with Acute Myeloblastic Leukemia and Non-Myeloid Malignancies. *Leuk. Res.* **2003**, *27* (1), 5–12. https://doi.org/10.1016/s0145-

2126(02)00068-1.

(67) Gerets, H. H. J.; Tilmant, K.; Gerin, B.; Chanteux, H.; Depelchin, B. O.; Dhalluin, S.; Atienzar, F. A. Characterization of Primary Human Hepatocytes, HepG2 Cells, and HepaRG Cells at the MRNA Level and CYP Activity in Response to Inducers and Their Predictivity for the Detection of Human Hepatotoxins. *Cell Biol. Toxicol.* **2012**, *28* (2), 69–87. https://doi.org/10.1007/s10565-011-9208-4.

(68) Anoopkumar-Dukie, S.; Carey, J. B.; Conere, T.; O'Sullivan, E.; van Pelt, F. N.; Allshire, A. Resazurin Assay of Radiation Response in Cultured Cells. *Br. J. Radiol.* **2005**, *78* (934), 945–947. https://doi.org/10.1259/bjr/54004230.

(69) Wu, L. K.; Tokarew, J. M.; Chaytor, J. L.; Von Moos, E.; Li, Y.; Palii, C.; Ben, R. N.; Allan, D. S. Carbohydrate-Mediated Inhibition of Ice Recrystallization in Cryopreserved Human Umbilical Cord Blood. *Carbohydr. Res.* **2011**, *346* (1), 86–93. https://doi.org/10.1016/j.carres.2010.10.016.

(70) Pasha, R.; Elmoazzen, H.; Pineault, N. Development and Testing of a Stepwise Thaw and Dilute Protocol for Cryopreserved Umbilical Cord Blood Units. *Transfusion* **2017**, *57* (7), 1744–1754. https://doi.org/10.1111/trf.14136.

(71) Migliaccio, A. R.; Adamson, J. W.; Stevens, C. E.; Dobrila, N. L.; Carrier, C. M.; Rubinstein, P. Cell Dose and Speed of Engraftment in Placental/Umbilical Cord Blood Transplantation: Graft Progenitor Cell Content Is a Better Predictor than Nucleated Cell Quantity. *Blood* **2000**, *96* (8), 2717–2722.

(72) Purton, L. E.; Scadden, D. T. Limiting Factors in Murine Hematopoietic Stem Cell Assays. *Cell Stem Cell*. September 13, 2007, pp 263–270. https://doi.org/10.1016/j.stem.2007.08.016.

(73) Harrison, D. Competitive Repopulation: A New Assay for Long-Term Stem Cell Functional Capacity. *Blood* **1980**, *55* (1), 77–81. https://doi.org/10.1182/blood.V55.1.77.77.

(74) Jahan, S.; Adam, M. K.; Manesia, J. K.; Doxtator, E.; Ben, R. N.; Pineault, N. Inhibition of Ice Recrystallization during Cryopreservation of Cord Blood Grafts Improves Platelet Engraftment. *Transfusion* **2020**, *60* (4), 769–778. https://doi.org/10.1111/trf.15759.

(75) Adam, M. K.; Jarrett-Wilkins, C.; Beards, M.; Staykov, E.; MacFarlane, L. R.; Bell, T. D. M.; Matthews, J. M.; Manners, I.; Faul, C. F. J.; Moens, P. D. J.; Ben, R. N.; Wilkinson,

B. L. 1D Self-Assembly and Ice Recrystallization Inhibition Activity of Antifreeze Glycopeptide-Functionalized Perylene Bisimides. *Chem. - A Eur. J.* **2018**, *24* (31), 7834–7839. https://doi.org/10.1002/chem.201800857.

(76) Adam, M. K.; Poisson, J. S.; Hu, Y.; Prasannakumar, G.; Pottage, M. J.; Ben, R. N.; Wilkinson, B. L. Carbohydrate-Based Surfactants as Photocontrollable Inhibitors of Ice Recrystallization. *RSC Adv.* **2016**, *6* (45), 39240–39244. https://doi.org/10.1039/c6ra07030b. - Reproduced by permission of The Royal Society of Chemistry

3. *N*-Aryl-D-Gluconamide Derivatives as Ice Recrystallization Inhibitors

3.1 The *N*-aryl-D-gluconamide class of ice recrystallization inhibitors

The class of *N*-aryl-D-gluconamides (**Figure 3.1.1.1a**) was previously investigated by former Ph.D. student Dr. Jennie Briard, and contains a number of carbohydrate-based small molecules able to effectively prevent the growth of ice crystals and thereby mitigate cryoinjury for various cellular systems.[1] This ice recrystallization inhibitor (IRI) class is comprised of molecules with common structural features including a D-gluconamide linked to an aryl group bearing various substituents. *N*-(4-methoxyphenyl)-D-gluconamide (**3.01**) contains an electron-donating *para*-methoxy group on the phenyl ring of the phenyl-D-gluconamide, *N*-(2-fluorophenyl)-D-gluconamide (**3.02**) includes an *ortho*-fluoro group on its phenyl ring, *N*-(4-chlorophenyl)-D-gluconamide (**3.03**) includes a *para*-chloro group on its phenyl ring, and *N*-(2,6-difluorobenzyl)-D-gluconamide (**3.04**) is comprised of a D-gluconamide linked to a 2,6-difluorobenzyl unit.[1] The development of this class of ice recrystallization inhibitor stemmed from studies on the ice recrystallization inhibition (IRI) activity of the *N*-(cyclo)alkyl-aldonamides conducted by former students including by Dr. Capicciotti and Dr. Doshi (**Figure 3.1.1.1b**).[2,3] Several trends between the IRI activity of the *N*-(cyclo)alkyl-aldonamides **3.05-3.23** and their structural features were found through structure-activity relationship (SAR) studies. *N*-(cyclo)alkyl-aldonamides **3.05-3.23** were found to possess varying degrees of IRI activity depending on the length of the hydrophobic alkyl chains attached to the amide's nitrogen and the length of the hydrophilic polyol component (the carbohydrate component). The percent mean

grain size (% MGS) of ice crystals is used to describe IRI activity in **Figure 3.1.1.1b**, where a smaller % MGS is indicative of ice crystals in the presence of an inhibitor with stronger activity. Note that these data were obtained using the splat-cooling assay with a 30-minute annealing period at -6.4 °C followed by analysis of the cross-sectional areas of ice crystals present in test conditions. Generally, as the length of the amide alkyl chain increased, the IRI activity increased as well (gluconamides **3.05-3.09** and aldonamides **3.10-3.13** in **Figure 3.1.1.1).** The trend was more modest within the *N*-cycloalkyl-aldonamide class, where increasing IRI activity was also correlated with the increasing size of the cycloalkyl group (aldonamides **3.14-3.18** and **3.19-3.23**). As such, it became apparent that the addition of hydrophobic moieties on the amide of the aldonamide tended to improve the IRI activity. Further, the structure-activity relationship (SAR) studies revealed that the length of the hydrophilic polyol also played a role in the observed IRI activity. Generally, the IRI activity increased with increasing length of the carbohydrate group, as is observed by comparing *N*-hexyl-gluconamide (**3.08**) with *N*-hexyl-erythronamide (**3.12**) which differ by two CH_2-OH group units, or by comparing *N*-cycloheptyl-gluconamide (**3.17**) with *N*-cycloheptyl-arabonamide (**3.22**) which differ by one CH_2-OH group unit, for example.

a)

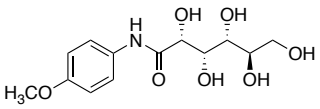

3.01

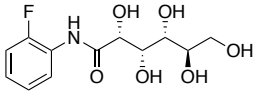

3.02

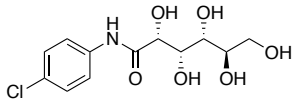

3.03

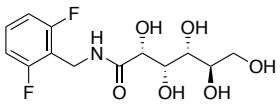

3.04

b)

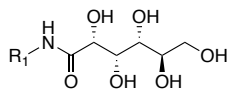

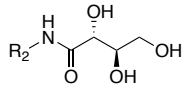

3.05 $R_1 = CH_2CH_3$ % MGS = 100%
3.06 $R_1 = (CH_2)_2CH_3$ % MGS = 82%
3.07 $R_1 = (CH_2)_3CH_3$ % MGS = 95%
3.08 $R_1 = (CH_2)_5CH_3$ % MGS = 3%
3.09 $R_1 = (CH_2)_7CH_3$ % MGS = 82% (5.5 mM)

3.10 $R_2 = (CH_2)_3CH_3$ % MGS = 71%
3.11 $R_2 = (CH_2)_4CH_3$ % MGS = 74%
3.12 $R_2 = (CH_2)_5CH_3$ % MGS = 69%
3.13 $R_2 = (CH_2)_7CH_3$ % MGS = 56%

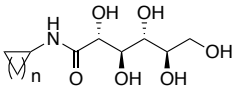

3.14 n = 1 % MGS = 63%
3.15 n = 3 % MGS = 57%
3.16 n = 4 % MGS = 54%
3.17 n = 5 % MGS = 48%
3.18 n = 6 % MGS = 45%

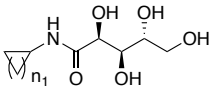

3.19 $n_1 = 1$ % MGS = 64%
3.20 $n_1 = 3$ % MGS = 65%
3.21 $n_1 = 4$ % MGS = 70%
3.22 $n_1 = 5$ % MGS = 71%
3.23 $n_1 = 6$ % MGS = 59%

Figure 3.1.1.1. The structures and IRI activities of **a)** select *N*-aryl-D-gluconamides, and **b)** *N*-(cyclo)alkyl-aldonamides.[1–3] IRI activity is displayed as percent Mean Grain Size (% MGS) where a lower percentage is indicative of stronger IRI activity. Aldonamides were tested at 22 mM in phosphate-buffered saline (PBS) using the standard splat-cooling assay,[5] unless otherwise indicated.

These data indicated that a clear balance between hydrophobicity and hydrophilicity is required for effective IRI activity and that this IRI activity was not correlated with micelle formation.[6,7] Additional studies were initiated to further explore this balance since the rational design of new IRI-active small molecules is dependent on understanding the structural features required for ice recrystallization inhibition activity. One study was conducted to determine a potential correlation between IRI activity and the amphiphilicity of the small molecules, described as the ratio of polar surface area to molecular surface area (PSA/MSA).[1,8] Additionally, a CH_n/OH ratio was another metric investigated, which represented the ratio of the number of carbons present in the hydrophobic alkyl chain to the number of hydroxyl groups

present in the carbohydrate component of the aldonamide. In both cases, these metrics were plotted as a function of the IRI activity of numerous aldonamides (**Figure 3.1.1.2**), and linear correlations were observed (apart for the IRI activity of gluconamide **3.08** which may be the result of transient aggregation or formation of other conformations in solution).[1,8] As the net polarity of the aldonamide increased, the IRI activity was shown to decrease. Further, aldonamides with lower CH_n/OH ratios, or lower hydrophobic components, also displayed decreased IRI activity. Taken together, these results verified that there is an important balance between hydrophobicity and hydrophilicity and that this balance is required for IRI activity.[1]

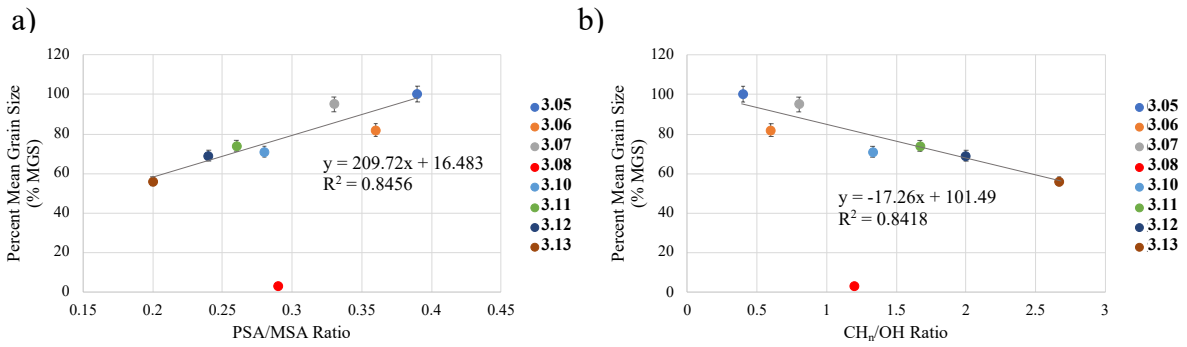

Figure 3.1.1.2. The correlation between IRI activity of the *N*-alkyl-aldonamides (depicted as the percent Mean Grain Size, % MGS) and their amphiphilicity metrics: a) PSA/MSA ratio and b) CH_n/OH ratio.[1,8] Graphs are adapted from the literature with permission (John Wiley & Sons).[1,8]

Despite these new-found correlations, the *N*-alkyl-aldonamides were unfortunately not amenable for use in cryopreservation applications due to their long alkyl chains and the corresponding cytotoxicity resulting from their surfactant properties, such as their propensities to interact with and solubilize cell membranes.[9,10] Nevertheless, the *N*-alkyl-aldonamides (along with the promising aryl-glycoside class of IRIs[11] discussed previously in **Chapter 1**) inspired a new set of carbohydrate-based small molecules, where a hydrophobic aromatic group was used in place of the long alkyl chain of the *N*-alkyl-aldonamides (**Figure 3.1.1.3**). This substitution

minimized the potential for a compound to display cell cytotoxicity whilst maintaining the amphiphilic nature required for IRI activity. The *N*-aryl-D-gluconamides possessed differing substituent(s) on the aromatic group, and the identity of the substituent(s), as well as the resulting regiochemistry, had a significant impact on the IRI activity observed.[1] Further, the addition of carbon linkers between the aryl- and carbohydrate-components also affected IRI activity. Interestingly, a Quantitative Structure-Activity Relationship (QSAR) approach was implemented to help screen for new gluconamide IRIs and this model did reasonably well at predicting experimentally-active *N*-aryl-D-gluconamides.[12]

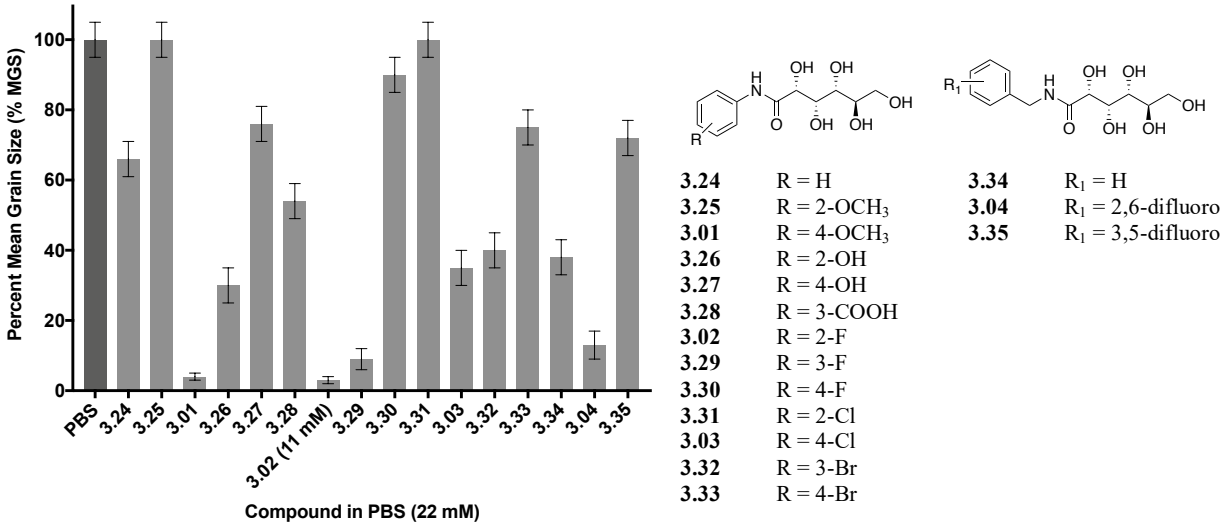

Figure 3.1.1.3. The IRI activity (% MGS) of select *N*-aryl-D-gluconamides where error bars represent the percent standard error of the mean (% SEM).[1] The gluconamides were tested at 22 mM in phosphate-buffered saline (PBS) using the standard splat-cooling assay,[5] unless otherwise indicated.

The outcome of the previous SAR studies included the development of IRI-active gluconamides **3.01**, **3.02**, **3.03**, and **3.04**.[1] In each of these cases, the position of the substituent around the aromatic ring significantly affected the resulting IRI activity.[4] As depicted in **Figure**

3.1.1.3, a gluconamide bearing a 2-methoxy group (**3.25**) did not possess any IRI activity yet *N*-(4-methoxyphenyl)-D-gluconamide (**3.01**) was effective at inhibiting ice recrystallization. The opposite trend was observed when a fluoro group was placed in the *ortho*- (**3.02**) or *meta*-position (**3.29**); the gluconamide was very active as opposed to the compound containing the 4-fluorophenyl functionality (**3.30**). Unfortunately, a clear trend relating all the substituents to IRI activity has yet to be determined. While the trend observed with the fluorophenyl analogues was the same as that observed when the phenyl substituent was a bromine (**3.32** and **3.33**), the opposite was observed when the substituent was a chlorine (**3.31** and **3.03**).[1,4] Meanwhile, while 4-methoxy derivative (**3.01**) was more IRI-active than its 2-methoxy counterpart (**3.25**), the opposite was observed for *N*-(4-hydroxyphenyl)-D-gluconamide (**3.27**) and the 2-hydroxy derivative (**3.26**).[1] Overall, due to the inability to hone in on the specific features required for IRI activity, the rational design of new IRI-active aldonamides continues to be the result of a laborious trial-and-error process. Additional SAR work is certainly warranted in order to discover trends relating the features of aldonamides with their IRI activities.

3.1.1 Improving the IRI activity of *N*-aryl-D-gluconamide ice recrystallization inhibitors and their potential use as cryoprotectants

Despite the lack of clear trends relating the structural features to an aldonamide's IRI activity, a large number of IRI-active *N*-aryl-D-gluconamides have now been developed.[1,4] Generally, these aldonamides have straightforward synthetic routes, including some with one-step syntheses. Further, a number of these *N*-aryl-D-gluconamides have shown promising cryoprotective properties for a variety of cell lines, such as for hematopoietic stem and progenitors cells (HSPCs), the details of which are discussed in detail in **Chapter 4**.[4] Owing to

the promising nature of the *N*-aryl-D-gluconamide class of IRI, this thesis chapter further explores the structural features of the gluconamides in order to progress the development of novel *N*-aryl-aldonamides for their use in cellular cryopreservation applications. Structural-activity relationships were studied for the following modifications:

- Alterations to the hydrophobic component of *N*-(phenyl)-D-gluconamides. Structural changes included the development of an analogue bearing both 2-fluoro- and 4-methoxy-aryl moieties to compare to its two parent compounds (**3.01** and **3.02**). Further, amino-aryl-D-gluconamides and their derivatives are compared to other gluconamides bearing electron-donating substituents on their phenyl ring (**Figure 3.1.1.4**).
- Modifications to the carbohydrate component of the aldonamide structure. Structural changes involved stereochemical alterations, changes to the polyhydroxylated chain, and *C*6-oxidation state modifications (as well as *C6*-composition) to examine IRI activity relative to the parent compounds (**Figure 3.1.1.4**).

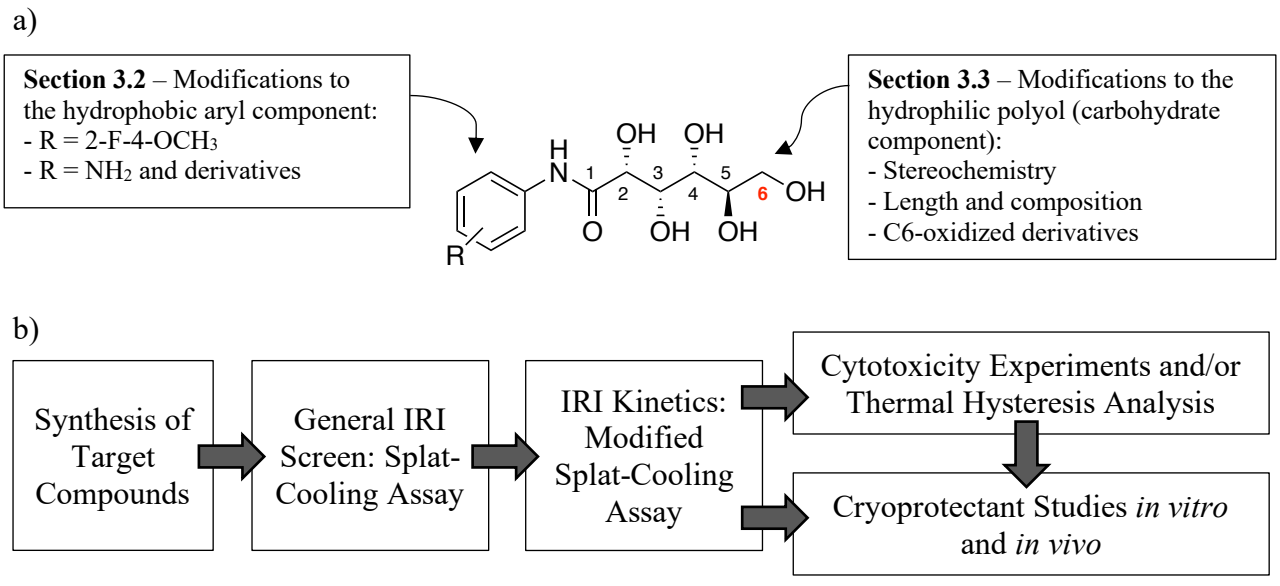

Figure 3.1.1.4. **a)** The general modifications for SAR studies of *N*-aryl-D-aldonamide analogues, and **b)** the overall approach to IRI and cryoprotectant development.

Following the synthesis of the *N*-aryl-D-aldonamide analogues required in the SAR studies, their potential ice recrystallization inhibition activity was screened (**Figure 3.1.1.4b**). Analogues that displayed promising results were further analyzed in order to obtain detailed kinetic data surrounding the IRI activity, and finally, the potential for promising IRIs to act as cryoprotectants was analyzed. Results from the IRI analysis and cryoprotectant studies offered new insights into the continued development of novel synthetic targets. This general approach to cryoprotectant development ensured that novel compound development through SAR studies was ongoing whilst further resources were focused on the most promising candidates. The splat-cooling assay for IRI activity determination was implemented for the SAR studies since the assay is a common and robust method for the screening of compounds' IRI activities.[5,13] This assay involves the freezing of a 10 μL droplet of a compound dissolved in phosphate-buffered saline (PBS) followed by an annealing period at -6.4 °C (**Figure 3.1.1.5**). After this time period (30 or 5 minutes), the areas of ice crystals in the presence of the compound are measured, and the results are compared relative to the ice crystal sizes present in the PBS control sample. The calculated percent mean grain size (% MGS) offered a way to compare a large number of compounds for potential activity and was, therefore, a good tool for obtaining a general overview of the activity of new compounds at select concentrations (**Figure 3.1.1.5**). A smaller % MGS obtained for a compound was indicative of ice recrystallization inhibition compared to a larger % MGS.

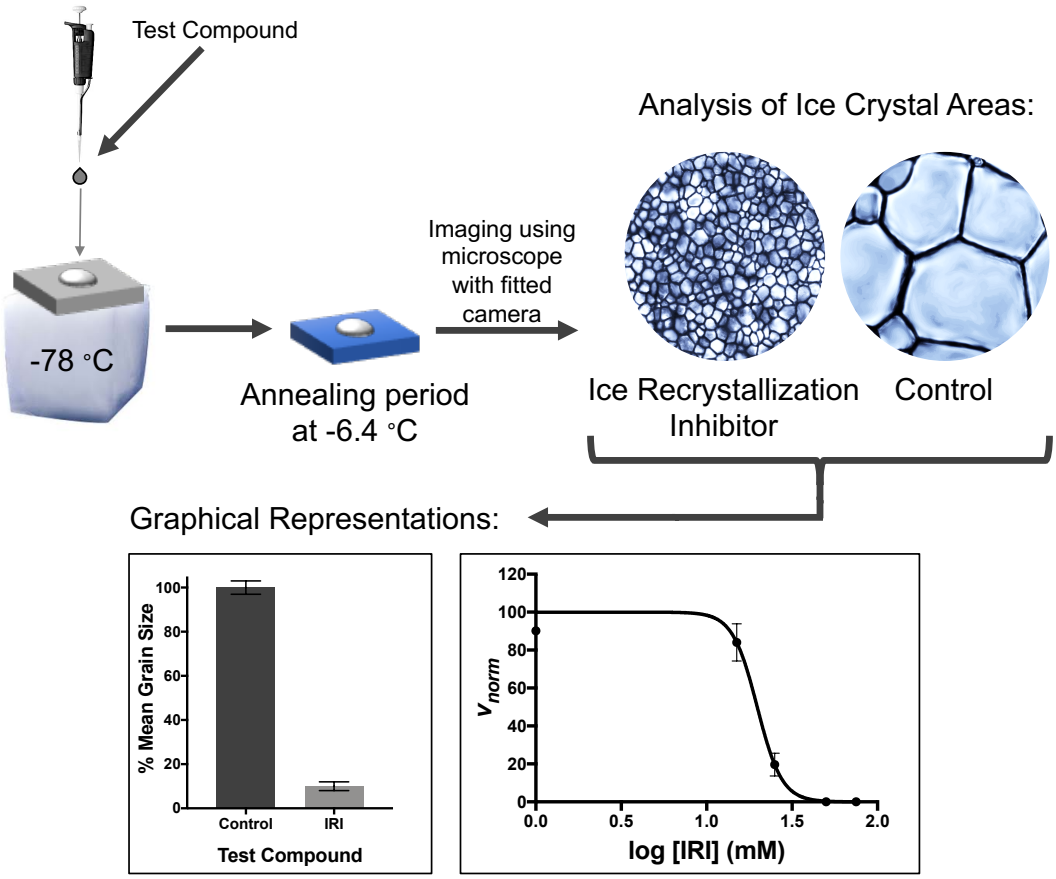

Figure 3.1.1.5. The splat-cooling assay used for the determination of ice recrystallization inhibition activity. Depending on the assay and analysis conducted, the IRI activity is represented either as the percent mean grain size (% MGS) of ice crystals or as dose-response curves generated by normalized rates.[5,13,14]

The traditional splat-cooling assay, however, does not provide detailed kinetic data nor does it address the heterogeneous nature of the crystal sizes observed during ice recrystallization or the concentration and time dependence of crystal growth.[5,14] Fortunately, a modified splat-cooling assay, developed by the Ben and Keillor laboratories, can be implemented to address these shortfalls as well as to obtain kinetic parameters like the concentration of IRI at which 50% inhibition is achieved (IC_{50}).[5,14,15] For this reason, the original splat-cooling assay is often used to determine whether a series of compounds may exhibit activity at specific concentrations while

the modified splat-cooling assay can be implemented to further characterize the activity of promising candidates including to better compare the effectiveness of different IRIs. In this modified assay, a binning approach is implemented where ice crystal areas are sorted based on their size into discrete bins. If the ice crystals are small, as they are at time = 0 (after freezing of the test droplet) or in the presence of an effective inhibitor after time = 5 mins, the crystal areas are placed in "Bin 1". As ice recrystallization occurs, ice crystals grow larger and their areas are placed into bins corresponding to larger sizes (bin size increases in 0.001 mm^2 increments). The proportion of ice crystals in the bins is then analyzed for each compound in order to obtain an initial rate (v) of ice recrystallization which can then be normalized to the phosphate-buffered saline (PBS) control thereby leading to normalized rates, v_{norm}.[14,15] Dose-response curves can then be generated and IC_{50} values can be obtained from the two-parameter sigmoidal curve fit to the data (**Figure 3.1.1.5**).

3.2 The development of ice recrystallization inhibitors through modifications to the hydrophobic aryl component of *N*-aryl-D-gluconamides

Section 3.2 contains two discrete sub-sections based on two studied modifications to the hydrophobic aryl component of *N*-aryl-D-gluconamides: the development of a di-substituted aryl gluconamide based on the structural moieties of the parent gluconamides and the production of amino-aryl-D-gluconamides. **Sub-section 3.2.1** begins by detailing additional studies of the IRI activities of the previously developed *N*-aryl-D-gluconamides **3.01-3.04** (**Figure 3.2.1.1** shows how the compounds differ from each other at their aryl functionality). Once the IRI activity of the parent compounds was fully explored, an analogue that combined the electronic features of the aryl groups of both gluconamides **3.01** (whose aryl group is substituted with a 4-methoxy

group) and **3.02** (aryl group is substituted with a 2-fluoro moiety) was developed. The IRI activity of the analogue was compared to the parent compounds' inhibitory activities. In contrast, **sub-section 3.2.2** discusses the development of analogues bearing an amino- or amido- group present on the aryl component of the *N*-aryl-D-gluconamides in place of the original aryl moieties. Specifically, these structural modifications were designed in order to compare the IRI activities of the derivatives to that of 4-methoxyphenyl gluconamide (**3.01**) owing to the similarities in aryl group electronics.

3.2.1 Development of a (2-fluoro-4-methoxy)phenyl analogue of the original *N*-aryl-D-gluconamide ice recrystallization inhibitors

Progress toward the development of structurally modified *N*-aryl-D-gluconamides first involved the optimization and further characterization of the parent gluconamides. For this reason, the synthesis of *N*-(4-methoxyphenyl)-D-gluconamide (**3.01**), *N*-(2-fluorophenyl)-D-gluconamide (**3.02**), *N*-(4-chlorophenyl)-D-gluconamide (**3.03**), and *N*-(2,6-difluorobenzyl)-D-gluconamide (**3.04**) was adapted from that previously described in the literature (**Scheme 3.2.1.1**).[1,4,12] Modifications of the reaction procedures leading to increased overall yields relative to those previously reported include the use of an ethanol and water recrystallization sequence of the final gluconamide crude products after the reaction.[16] Route A) in **Scheme 3.2.1.1** was the acid-catalyzed reaction condition with heat, and this route was generally required for the synthesis of gluconamides where the aniline precursor bore electron-withdrawing substituents (e.g. the syntheses of **3.02** and **3.03**). Alternatively, when the aniline starting material was more nucleophilic, such as anilines bearing a *p*-methoxy group, route B) conditions could be

implemented. This was the case for **3.01** and **3.04** (where the starting material was a benzylamine).

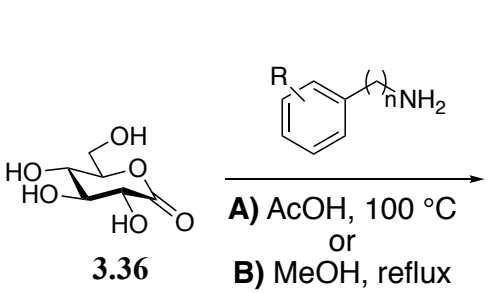

Product	R	n	Conditions	Yield (%)
3.01	4-OCH_3	0	B) 12 h	59
3.02	2-F	0	A) 2.5 h	47
3.03	4-Cl	0	A) 2 h	50
3.04	2,6-F,F	1	B) 24 h[1]	89[1]

Scheme 3.2.1.1. One-step synthesis of *N*-aryl-D-gluconamides.

With an optimized synthetic route amenable to the multi-gram syntheses of the gluconamides (the yield of **3.01** was enhanced by 2.2 times while the yield of **3.02** was increased by 1.8 times; n = 2 for both calculations of yield comparisons), the next step was to fully assess their IRI activities. Since the general screening for this original class of gluconamide had been previously generated using the splat-cooling assay, these IRIs were analyzed directly using the modified splat-cooling assay (recall that this analysis involves a 5-minute annealing period at -6.4 °C followed by determination of the initial rates of ice recrystallization occurring in the presence of differing concentrations of a sample).[1,4] The dose-response curves generated via the modified splat-cooling assay for gluconamides **3.01** and **3.02** are displayed in **Figure 3.2.1.1**, which also includes Dr. Briard's IRI data for **3.03** and **3.04**.[1] With IC_{50} values of 5 ± 1 mM (**3.01)** and 3 ± 0.1 mM (**3.02**), the gluconamides bearing a 4-methoxyphenyl group or a 2-fluorophenyl group are the most active ice recrystallization inhibitors of the four. By considering the 95% confidence intervals associated with the IC_{50} values, gluconamide **3.02** is the most active inhibitor followed by **3.01**, and finally, gluconamides **3.03** and **3.04** are the least active of

the set. As previously reported in Dr. Briard's doctoral thesis, gluconamide **3.03** has an IC_{50} value of 12 ± 3 mM while **3.04** has a value of 11 ± 3 mM.[1]

a)

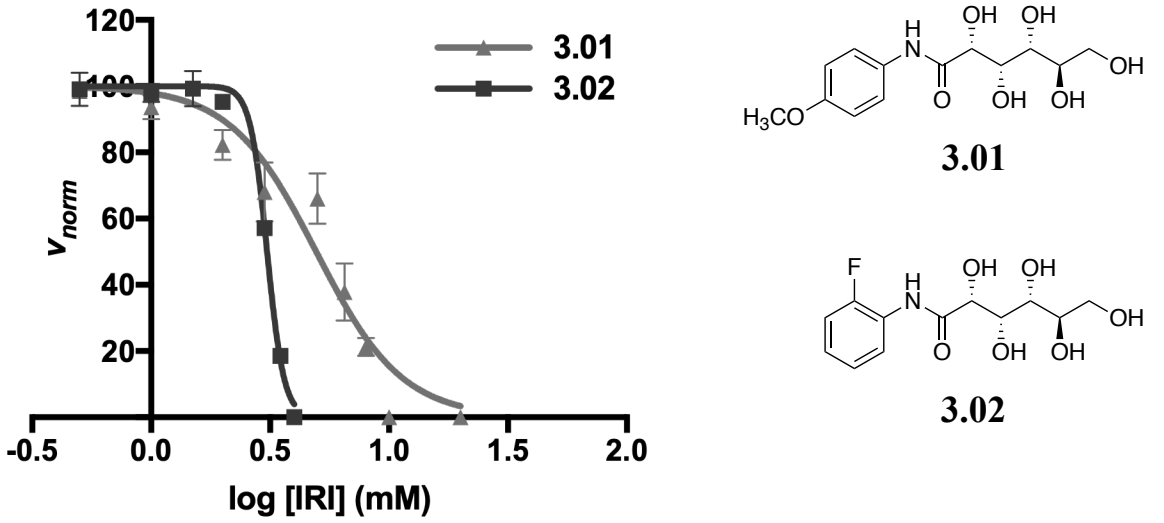

b)

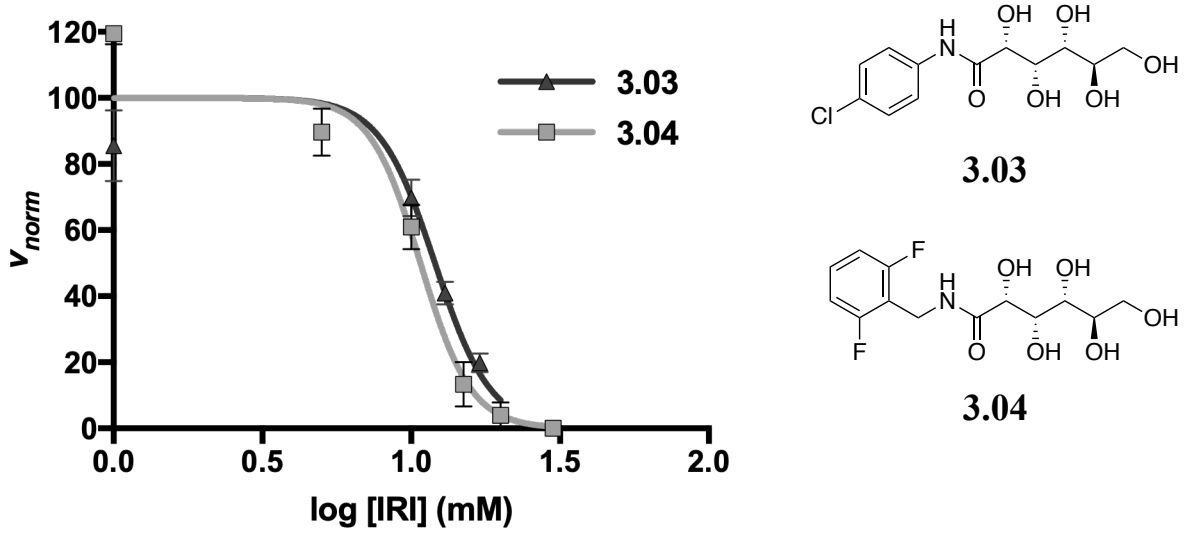

Figure 3.2.1.1. Dose-response curves for the IRI activities of **a) 3.01** (IC_{50} = 5 ± 1 mM, R^2 = 0.94) and **3.02** (IC_{50} = 3 ± 0.1 mM, R^2 = 0.99), and **b) 3.03** (IC_{50} = 12 ± 3 mM, R^2 = 0.95) and **3.04** (IC_{50} = 11 ± 3 mM, R^2 = 0.96). IC_{50} values are reported with 95% confidence intervals. Data for **3.03** and **3.04** are adapted from Dr. Briard's doctoral dissertation.[1] Error bars represent the standard error of the mean (SEM) and experiment was replicated in triplicate (n = 3).

Gluconamides **3.01** and **3.02** both display promising IRI activity and cryoprotectant abilities for cell lines such as human hematopoietic stem and progenitor cells.[17] Notably, however, there are some limitations to their applicability in cellular systems. For example, higher millimolar concentrations of 4-methoxyphenyl derivative **3.01** reduced metabolic activity observed from human hepatic cells incubated *in vitro* with the IRI. While the 2-fluorophenyl derivative **3.02** displayed no cytotoxicity up to its maximum solubility in media (25 mM), its use is limited in aqueous media due to its poor solubility profile (derivative **3.02** is half as soluble as gluconamide **3.01**). Thus, in an effort to overcome the limitations observed with either **3.01** and **3.02**, an analogue bearing both the 2-fluoro and 4-methoxy functionalities combined on the same aryl ring was sought (gluconamide **3.38**, **Figure 3.2.1.2**). 2-Fluoro-4-methoxyphenyl analogue **3.38** was hypothesized to have a more straightforward synthesis than the 2-fluorophenyl parent compound **3.02** owing to its slightly more nucleophilic aniline starting material (as well as being more soluble than **3.02** in aqueous media), and **3.38** may also display more promising results in cellular studies than the 4-methoxyphenyl derivative **3.01** owing to the additional 2-fluorophenyl component (no cytotoxicity was observed in multiple cell lines incubated *in vitro* with **3.02**).

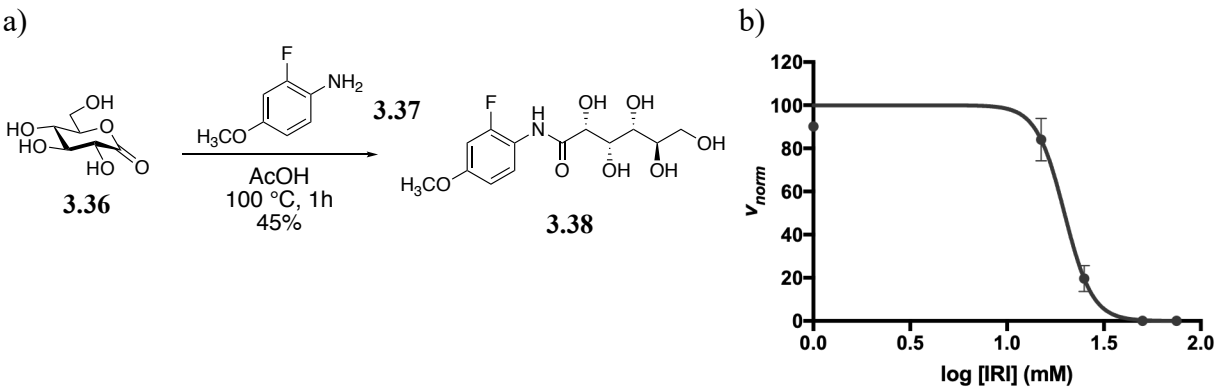

Figure 3.2.1.2. The synthesis **(a)** and IRI activity **(b)** of *N*-(2-fluoro-4-methoxyphenyl)-D-gluconamide **3.38**. The IC_{50} value for **3.38** generated from the dose-response curve is 20 ± 3 mM (95% confidence interval, $R^2 = 0.99$). Error bars indicate SEM (n = 3).

The one-step synthesis of *N*-(2-fluoro-4-methoxyphenyl)-D-gluconamide **3.38** involved a condensation reaction between 2-fluoro-4-methoxyaniline **3.37** and D-(+)-gluconic acid δ-lactone **3.36** in acetic acid at 100 °C. Despite the moderate yield (45%), **3.38** was produced in gram quantities for IRI analysis and cellular studies. **Figure 3.2.1.2b** displays the dose-response curve generated via the modified splat-cooling assay for the IRI activity of **3.38**, the first gluconamide generated bearing two different aryl group substitutions. With an IC_{50} value of 20 ± 3 mM (95% confidence interval), the analogue is significantly less effective at inhibiting ice recrystallization than either of its parent compounds. The parent compound with solely a 4-methoxy substituent present on its aryl component (gluconamide **3.01**) displayed an IC_{50} value of 5 mM for its IRI activity while that of the 2-fluorophenyl compound (gluconamide **3.02**) was 3 mM. In the end, the significant reduction in IRI activity observed with the disubstituted gluconamide **3.38** may not be all that surprising since gluconamide **3.38** bears a 2,4-disubstituted pattern, which may diminish the inhibition. This was indeed observed in a QSAR model of the IRI activity of gluconamides, where an *N*-(2,4-dichlorophenyl)-D-gluconamide was predicted to be inactive (>70% MGS in the study) while its *N*-(chlorophenyl)-D-gluconamide counterpart **3.03** was shown to be an effective ice recrystallization inhibitor.[12] On the other hand, perhaps the electron density of a gluconamide's aromatic ring plays a significant role in the unknown mechanism of ice recrystallization inhibition and that this may be directly related to the nature of the aromatic substituents. Evidently, more SAR work is required moving forward in order to fully elucidate the IRI trends observed. Regardless of di-substituted derivative **3.38**'s diminished IRI activity, its solubility in aqueous solutions was found to be similar to that of the 4-methoxyphenyl compound **3.01** thereby offering more concentrations for cryopreservation applications, and therefore, **3.38** was further assessed for its cytotoxicity and cryoprotective abilities (**Chapter 4**).

3.2.2 Development of amino-phenyl and gluconamido-phenyl derivatives of the *N*-aryl-D-gluconamides

3.2.2.1 Synthesis of amino-phenyl and gluconamido-phenyl derivatives

Recent research stemming from the Ben laboratory includes a significant interest in the production of IRI-active small molecules bearing amino group functionality.[3,18] Previously, IRI activity has been linked to the hydration of the small molecule: the more hydrated a carbohydrate was, the better it 'fit' into the three-dimensional network of hydrogen bonds in the bulk water layer, and therefore, the more IRI activity the molecule exhibited.[19] With this in mind, a number of pyranose-based carbohydrates bearing amino groups in place of hydroxyl groups have been previously prepared, and a number of the derivatives exhibited effective IRI activity.[3,18] Importantly, previous SAR work on the *N*-aryl-D-gluconamides has explored the presence of a variety of substituents on the aryl ring; however, the aryl-amine class of *N*-aryl-D-gluconamide has not yet been explored. The protonated aryl amine has a pka of approximately 4.6 in water, and therefore, gluconamides bearing an aminophenyl group exist mainly as their neutral species at the pH of phosphate-buffered saline (PBS) solution used in the assay for IRI activity (pH of 7.4). Accordingly, when considering the electron density of the corresponding aryl ring, an aryl amino group would act primarily as an electron-donating group. Therefore, amino-aryl-D-gluconamides and their derivatives (gluconamides **3.39-3.47**, **Figure 3.2.2.1**) were envisioned to be compared to methoxyphenyl gluconamides. Derivatives of **3.42-3.44** would possess electron-withdrawing groups and were intermediates in the synthesis of the amino-aryl gluconamides (described below). The presence of two gluconamide moieties in one structure was explored with analogues **3.45-3.47**. I acknowledge Ms. O'Keefe (undergraduate summer research student) and

Ms. Pressoir (honour's student) for their assistance in synthesizing and assessing the aminophenyl-gluconamides.

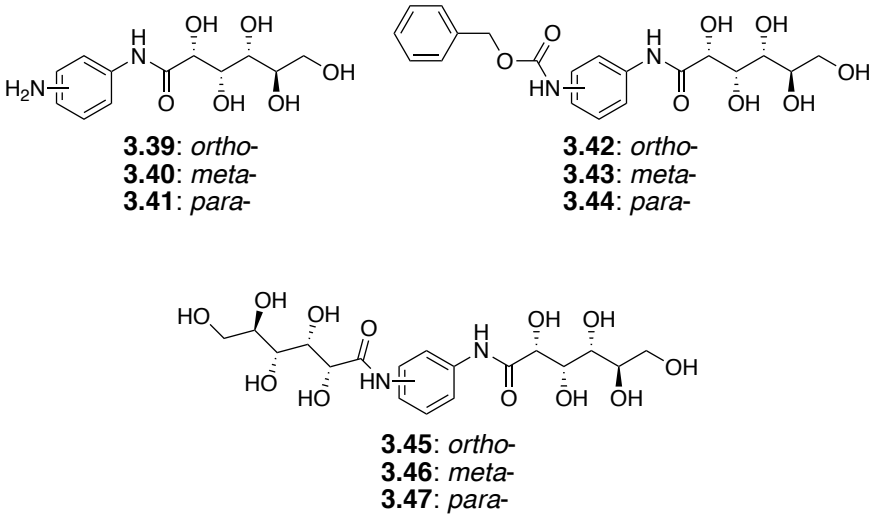

Figure 3.2.2.1. The structures of the envisioned *N*-(amino-phenyl)-D-gluconamides **3.39-3.41** and their derivatives **3.42-3.47**.

Initial efforts to synthesize the aminophenyl-gluconamides (**3.39-3.41**) by directly combining a phenylenediamine with D-gluconolactone **3.36** proved low yielding owing to the production of a mixture of products which included gluconamido-phenyl targets **3.45-3.47** (**Scheme 3.2.2.1a**). Further, efforts toward the aryl-amines **3.39-3.41** through the initial preparation of an *N*-(nitro-phenyl)-D-gluconamide precursors **3.49** followed by reduction to the corresponding aryl-amines **3.39-3.41** also proved unsuccessful (**Scheme 3.2.2.1a**). Although harsh conditions for the condensation of nitroaniline **3.48** with D-gluconolactone **3.36** were used, no product was observed; presumably due to the electron-withdrawing nature of the nitro group leading to an extremely poor nucleophile for the condensation reaction. Next, another simple premise was envisioned for the synthesis of the *N*-(amino-phenyl)-D-gluconamides: condensation of a monoprotected phenylenediamine **3.50-3.52** with D-gluconolactone **3.36**

followed by deprotection of the amino-aryl group to yield the final amino-aryl-gluconamides (**Scheme 3.2.2.1b**). The choice of the protecting group used in the protection of phenylenediamine proved to be important. Initially, the use of a *tert*-butyloxycarbonyl (Boc) protecting group was implemented, and the corresponding monoprotection of the diamine with boc anhydride was efficient (86% - 96% yield based on regiochemistry of aniline). The proceeding condensation of the resulting monoprotected aniline **3.52** with gluconolactone **3.36** also proved successful in moderate yield (41% yield). However, removal of the Boc group on gluconamide **3.53** was attempted under a variety of acidic (hydrochloric acid or trifluoroacetic acid) or neutral conditions (heating in water). Unfortunately, the product was not observed, and it appeared that the aryl gluconamide may have degraded since the nuclear magnetic resonance (NMR) spectra obtained no longer contained aryl components.

a)

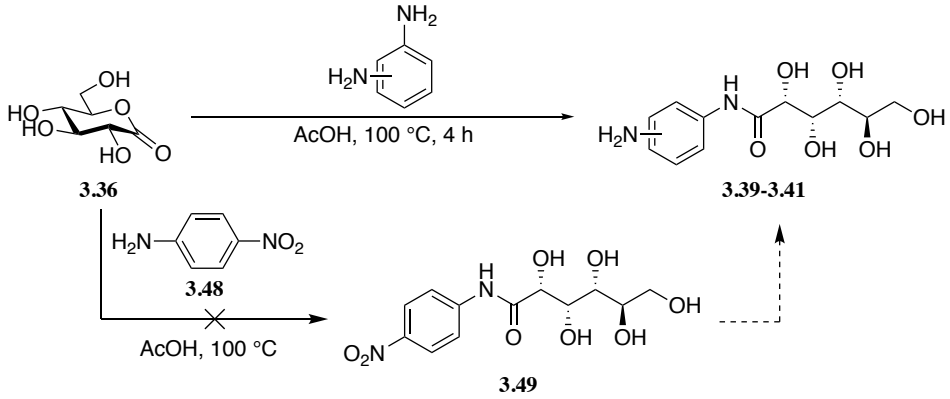

b)

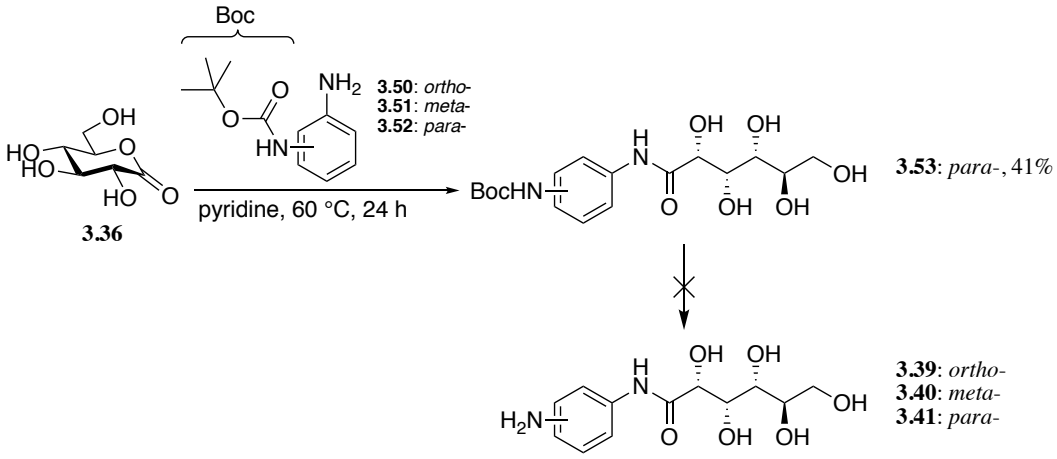

Scheme 3.2.2.1. Synthetic attempts toward the production of *N*-(amino-phenyl)-D-gluconamides including **a)** direct condensation between **3.36** and phenylenediamine or the synthetic route through *N*-(nitro-phenyl)-D-gluconamide precursors **3.48**, and **b)** approach using a boc group.

To avoid the potential for gluconamide degradation in future syntheses, efforts were set on finding more mild conditions for the final deprotection step. As outlined in **Scheme 3.2.2.2**, the carboxybenzyl (Cbz) protecting group was implemented for the monoprotection of the phenylenediamines which ultimately offered an appealing final deprotection step: hydrogenolysis of the protecting group via an *in situ* prepared Pd^0/C catalyst.[20] Using this route, the corresponding phenylenediamine starting material **3.54-3.56** was monoprotected in the presence of benzyl chloroformate in an aqueous solution of acetic acid in dioxane, thereby resulting in 15%-53% yields of the monoamines **3.57-3.59**.[21] The lower yields were the result of

the production of fully-protected anilines or an intramolecular product in the case of *ortho*-phenylenediamine **3.57**. After isolating the monoprotected aniline from the mixture of protected products, the desired aniline **3.57-3.59** was combined with D-gluconolactone **3.36** under basic conditions and heat to yield the corresponding gluconamides **3.42-3.44** in moderate yields. The presence of a bulky *ortho*-carbamate substituent could have led to the decreased yield of the *ortho*-Cbz gluconamide **3.42** (7%) compared to the other two regioisomers (41% yield for *meta*-Cbz **3.43** and 55% yield for *para*-Cbz **3.44**). Finally, removal of the carboxybenzyl group was performed by hydrogenolysis: in methanol, the gluconamides **3.42-3.44** were subjected to an *in situ* Pd^0/C catalyst prepared from $Pd(OAc)_2$ and charcoal under a hydrogen atmosphere. These mild conditions, adapted from the literature, led to the production of the desired *N*-(amino-phenyl)-D-gluconamides **3.39-3.41** in nearly quantitative yields (92% - 97% yields).[20] In summary, using this short three-step synthesis afforded the target gluconamides in 1% (**3.39**), 15% (**3.40**), and 28% (**3.41**) overall yields.

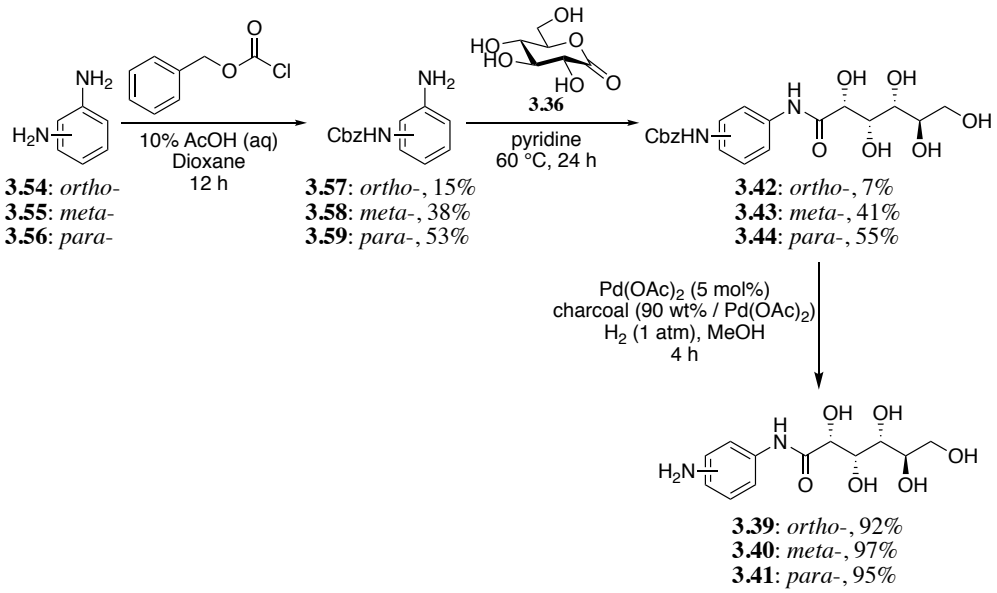

Scheme 3.2.2.2. Synthesis of *N*-(amino-phenyl)-D-gluconamides **3.39-3.41**.

With the *N*-(amino-phenyl)-D-gluconamides **3.39-3.41** in hand, the focus was then turned toward the synthesis of their derivatives, the *N*-(gluconamido-phenyl)-D-gluconamides **3.45-3.47**. Initial attempts at producing these derivatives were based on preliminary work performed by Dr. Briard whereby *para*-phenylenediamine was directly combined with D-gluconic acid δ-lactone under acidic conditions and then purified to yield the desired derivative (**3.47**).[1] However, this route yielded crude products that proved difficult to purify and for this reason, a modified route was implemented (**Scheme 3.2.2.3**) based off literature procedures.[12,22] This synthesis began by directly coupling the appropriate phenylenediamine **3.54-3.56** with four equivalents of D-gluconic acid δ-lactone **3.36** under acidic conditions at 100 °C for four hours. After acetylation of the crude mixture, the resulting *meta*-gluconamido **3.61** and *para*-gluconamido **3.62** intermediates could be easily isolated by flash chromatography to yield a 4:1 bis:monogluconamide product mixture (62% and 17% yields for the desired *meta* and *para* intermediates after two steps, respectively). The desired *ortho* intermediate **3.60** was not achieved in adequate yield (13% crude yield but could not be purified) presumably due to the unfavourable amount of steric hindrance present in the product. With purified products **3.61** and **3.62** in hand, the final step in the synthesis involved deacetylation of these intermediates under Zemplén conditions[23] to furnish the desired *meta*- **3.46** and *para*- **3.47** targets in 28% and 98% yields, respectively. Overall, both the *meta*- and *para*-gluconamido-phenyl-D-gluconamides **3.46** and **3.47** were produced with 17% overall yields.

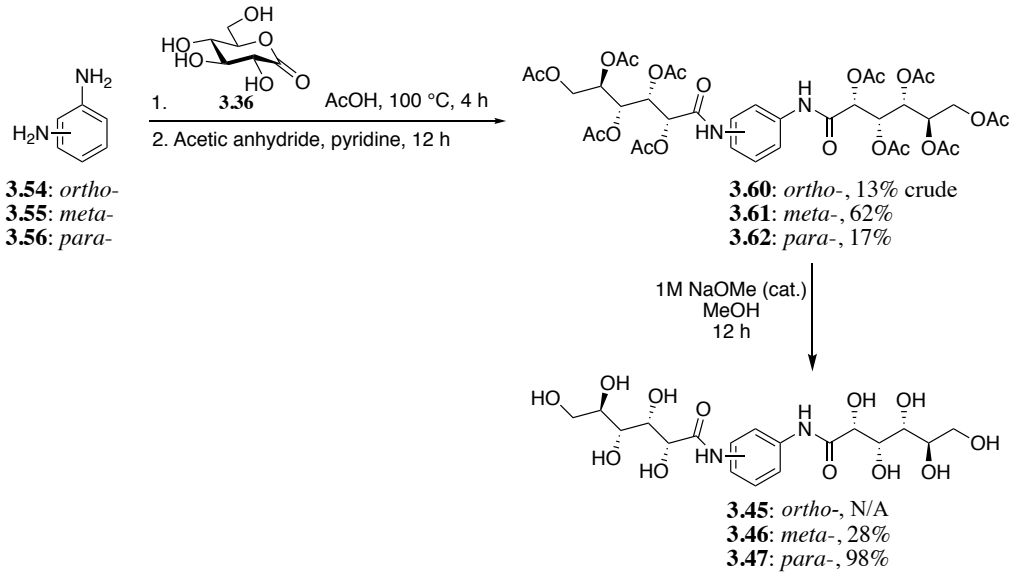

Scheme 3.2.2.3. Synthesis of *N*-(gluconamido-phenyl)-D-gluconamides using a three-step synthesis including a condensation reaction between D-gluconolactone **3.36** and the appropriate phenylenediamine **3.54-3.56**, acetylation of the intermediate gluconamides, and finally, deacetylation to yield *N*-(gluconamido-phenyl)-D-gluconamides **3.46** and **3.47**.

3.2.2.2 The ice recrystallization inhibition (IRI) activity of amino- and gluconamido-phenyl derivatives

With the desired *N*-(amino-phenyl)-D-gluconamides **3.39-3.41**, intermediate gluconamides **3.42-3.44**, and *N*-(gluconamido-phenyl)-D-gluconamides **3.46** and **3.47** in hand, attention was turned toward their potential abilities to inhibit ice recrystallization. The IRI activity of the small molecules was first determined using the splat-cooling assay, and owing to the resulting activities, the modified splat-cooling assay was implemented to generate the corresponding dose-response curves displayed in **Figure 3.2.2.2**.[14] The derivatives all displayed some level of IRI activity including four of the six analogues exhibiting IRI activities with IC_{50} values between 4-12 mM. These fall into the range of the previously reported promising *N*-aryl-D-gluconamides **3.01-3.04** discussed earlier in **Section 3.2** (notably, the 4-methoxyphenyl-D-gluconamide **3.01** possesses an IC_{50} value of 5 ± 1 mM).

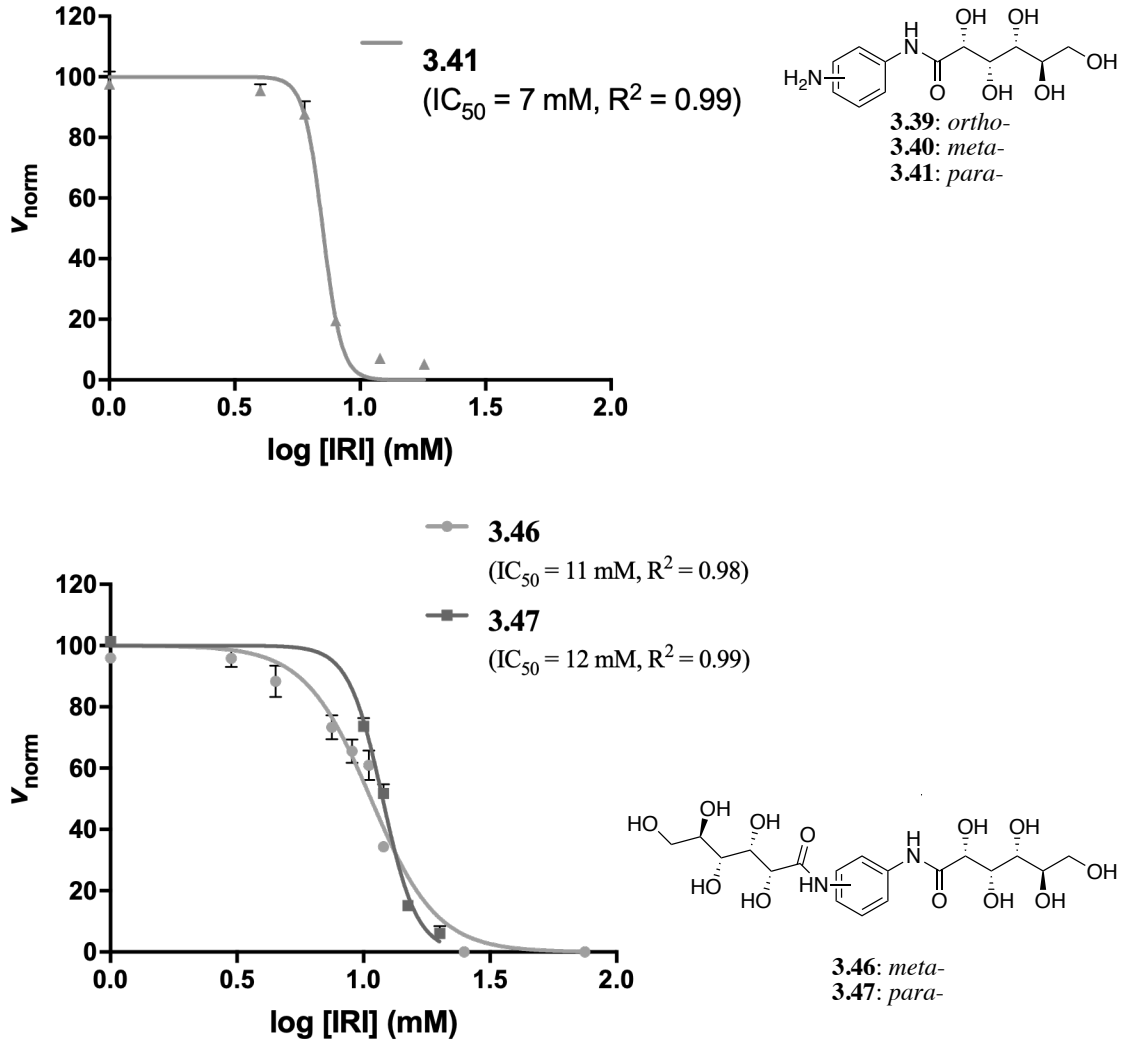

Figure 3.2.2.2. Dose-response curves for the IRI activity of *N*-(amino-phenyl)-D-gluconamides **3.39-3.41**, and *N*-(gluconamido-phenyl)-D-gluconamides **3.46** and **3.47**. The experiments were performed in triplicate (n = 3) and the error bars indicate SEM.

The *N*-(4-amino-phenyl)-D-gluconamide **3.41** displayed the most effective IRI activity out of the three amino-gluconamides tested (**3.39-3.41**) with an IC_{50} value of 7 ± 0.4 mM (IC_{50} value reported with 95% confidence interval). Notably, both **3.39** and **3.40** also exhibited IRI activity, albeit less so than **3.41**. However, full dose-response curves and the corresponding IC_{50} values could not be obtained due to their poor solubilities in the phosphate-buffered solution

(PBS) used in the IRI assay. This poor solubility observed in aqueous solutions is also observed with the general *N*-aryl-D-gluconamide class of small molecules and a table in the **Experimental Section** (**Table A1** in **Appendix III**) lists the maximum solubilities for IRIs in PBS. At a pH of 7.4, the pH of PBS, the amino groups of **3.39-3.41** are mainly in their neutral form and this may explain the poor solubility of these compounds. Using the original splat-cooling assay (% mean grain size determination, % MGS), the IRI activity of the aminophenyl-D-gluconamides **3.39-3.41** appear similar to one another despite a change in regiochemistry of the aminoaryl group (**Figure 3.2.2.3**): the % MGS of ice crystals in the presence of the 2-aminoaryl gluconamide **3.39** at 10 mM was 59%, the % MGS in the presence of 10 mM of the *meta*-substituted **3.40** was 77%, and finally, the % MGS in the presence of 12 mM *para*-substituted **3.41** was 44%. As discussed in **Section 3.1**, significant differences have been observed when the regiochemistry of the aryl group is altered such as a *para*-methoxy derivative (**3.01**, IC_{50} value of 5 mM) being more active than its *ortho*-analogue (**3.25**).[1] After considering statistical analysis, the IRI activity of a derivative where the *ortho*-amino group was functionalized with a carboxybenzyl group (**3.42**) was similar relative to its *ortho*-amino counterpart (**3.39**) suggesting that this structural change doesn't impact the mechanism by which these molecules exert their IRI activity. Nevertheless, this highlights the necessity for continued SAR work in order to fully elucidate the features of *N*-aryl-D-gluconamides required for effective IRI activity.

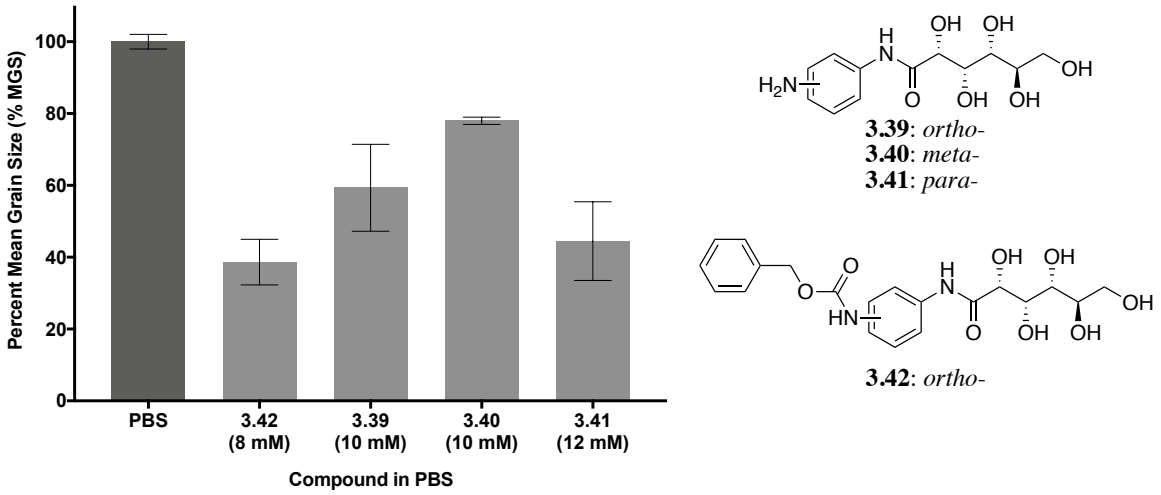

Figure 3.2.2.3. The IRI activity of *N*-(aminophenyl)-D-gluconamides **3.39-3.41,** as well as **3.42,** presented as percent mean grain size (% MGS) of ice crystals when in the presence of the compounds at 8-12 mM. The experiment was performed in triplicate (n = 3) and error bars indicate percent standard error of the mean (% SEM). Using one-way ANOVA with Tukey's multiple comparisons test, compounds **3.39** (*), **3.41** (**), and **3.42** (**) were statistically significant from the PBS control (* $p < 0.05$, ** $p < 0.01$), and compounds **3.42** and **3.40** were significantly different ($p < 0.05$).

As observed in **Figure 3.2.2.2**, both the *meta*- (**3.46**) and the *para*- (**3.47**) isomers of *N*-(gluconamido-phenyl)-D-gluconamide exhibited similar IRI activity with IC_{50} values of 11 ± 1 mM and 12 ± 1 mM, respectively. These were not found to be significantly different values owing to the overlap of their 95% confidence intervals. Preliminary work conducted by Dr. Briard found that ice crystals in the presence of 22 mM *para*-isomer **3.47** had a % MGS of 67% using the standard splat-cooling assay.[1] This differs from the current results for **3.47** which suggest that at 20 mM (the maximum solubility of **3.47** in PBS) the ice crystals in the IRI assay had a % MGS of 34%. While these two results differ, they both describe a compound with moderate IRI activity (recall that 30-80% MGS is deemed moderate IRI activity). Finally, by comparing the two *para*-substituted gluconamides **3.41** and **3.47** (**Figure 3.2.2.2**), it is clear that

the *N*-(4-amino-phenyl)-D-gluconamide (**3.41**) is more IRI-active than its *N*-(4-gluconamido-phenyl)-D-gluconamide counterpart with **3.41** possessing an IC_{50} value of 7 ± 0.4 mM while that of **3.47** is 12 ± 1 mM (IC_{50} values are reported with 95% confidence intervals). The important balance between hydrophobic and hydrophilic components of an IRI may explain the difference in the inhibitory activity of the two compounds. The presence of an additional gluconamide moiety (**3.47**) decreased the hydrophobicity of the aryl component of the gluconamide and this resulted in decreased IRI activity. Evidently, further studies that can explain the delicate balance between the hydrophobicity and hydrophilicity of a carbohydrate-based IRI are warranted.

3.3 The development of *N*-aryl-D-gluconamide analogues through modifications to the carbohydrate component

3.3.1 *N*-(4-methoxyphenyl)-D-gluconamide analogues with modified carbohydrate stereochemistry and C6-oxidation states

N-(4-methoxyphenyl)-D-gluconamide **3.01** was used as a model substrate for SAR studies discussed in **Section 3.3.1** since the gluconamide had been found to exhibit effective IRI activity (**Section 3.2.1**) as well as promising results in a number of cellular studies.[1,4] Additionally, owing to the nucleophilic *p*-anisidine starting material (**Scheme 3.2.1.1**), the synthesis of **3.01** is straightforward which would enable easier syntheses of many of the derivatives. Therefore, a series of derivatives bearing modifications to the carbohydrate component of the parent compound were sought. Specifically, a series of analogues of the parent gluconamide (*N*-(4-methoxyphenyl)-D-gluconamide **3.01**) were designed with differing stereochemistry **3.63** and **3.64**, oxidized components such as analogues bearing a *C6*-carboxylate

moiety **3.65-3.67** (or the *C6*-azide moiety discussed in **Section 3.3.2**), or aldonamide mimics with reduced amounts of hydroxyl groups in the polyol chain **3.68-3.74** (**Figure 3.3.1.1**).

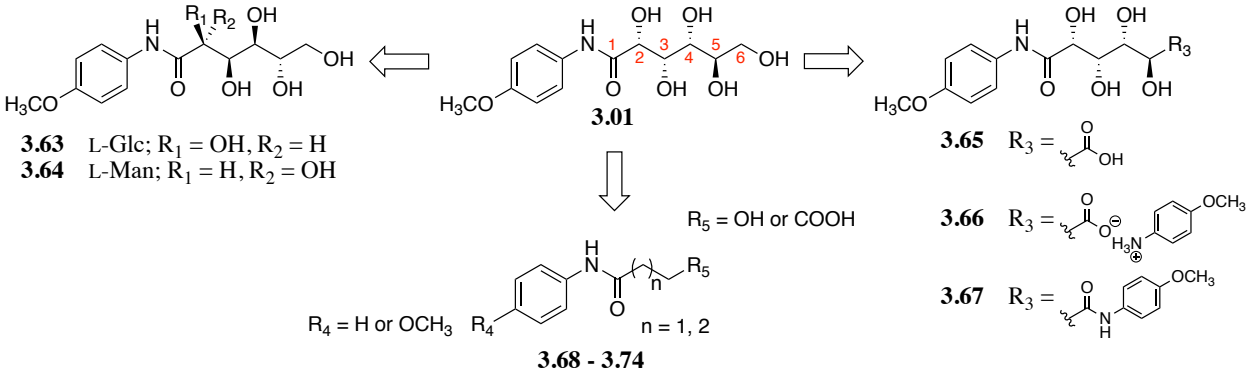

Figure 3.3.1.1. Derivatives of *N*-(4-methoxyphenyl)-D-gluconamide **3.01** in **Section 3.3.1**.

Studies began by synthesizing stereoisomers of *N*-(4-methoxyphenyl)-D-gluconamide **3.01** (aldonamides **3.63** and **3.64** in **Scheme 3.3.1.1**) to determine the influence of a gluconamide's stereochemistry on the resulting IRI activity. The syntheses of the L-glucono and L-mannono-analogues of *N*-(4-methoxyphenyl)-D-gluconamide, **3.63** and **3.64** respectively, were proposed to be conducted similarly to that of the parent compound: a condensation reaction between the purified *p*-anisidine and the corresponding lactone (**Scheme 3.3.1.1**).[16] While the synthetic approach was successful for both aldonamides, the condensation reaction between *p*-anisidine and L-glucono-1,5-lactone **3.75** led to the L-gluconamide **3.63** in a moderate yield (46%) while the reaction with L-Mannono-1,4-lactone **3.76** led to mannonamide **3.64** in a meager 6% yield. This poor yield is presumably due to the less reactive nature of the starting 1,4-lactone and may be improved by optimizing the conditions. Notably, performing the ring-opening reaction under acidic conditions did not improve the yield of the product.

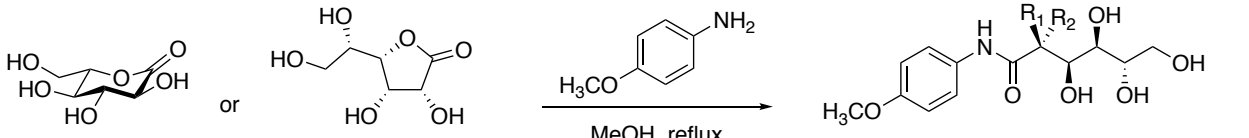

3.75 **3.76**

3.63 L-Glc; R_1 = OH, R_2 = H, 46%
3.64 L-Man; R_1 = H, R_2 = OH, 6%

Scheme 3.3.1.1. Synthesis of **3.63** and **3.64**, the L-glucono- and L-mannono-stereoisomers of D-gluconamide **3.01**.

The IRI activities of the stereoisomers were then determined using a modified splat-cooling assay whereby dose-response curves and IC_{50} values for the inhibitory activity could be generated (**Figure 3.3.1.2**).[14,15] The IC_{50} value for L-gluconamide **3.63** was found to be similar to that of D-gluconamide **3.01** (5 mM) while L-mannonamide **3.64** was slightly more active (based on 95% confidence intervals). Changing the stereochemistry of the carbohydrate component from a glucose to a mannose derivative, therefore, influenced the IRI activity of the molecule. Additionally, L-mannonamide **3.64** is significantly less soluble than the gluconamides **3.01** and **3.63**. The resulting IRI activity is contrary to a previous result from the Ben laboratory: the IRI activity of *N*-(octyl)-L-mannonamide (22% MGS at 0.5 mM using 30-min. annealing splat-cooling assay) was slightly reduced to that of the D-gluconamide derivative (12% MGS at 0.5 mM using 30-min. annealing splat-cooling assay).[2,5] The stereochemistry of the acyclic carbohydrate in other amphiphilic small molecules has been shown to impact the conformation that the amphiphiles adopted in crystals.[24–30] Acyclic carbohydrates possessing stereochemistry with 'all-trans' configurations would result in more energetically favourable linear conformations (e.g. rod-like structures). However, acyclic carbohydrates that possessed a "1,3-*syn* interaction" between the *C2* and *C4* hydroxyl groups in such a linear conformation (see **Figure 3.3.1.2**) would therefore adopt more of a "bent" conformation in order to reduce the energetically unfavourable interaction. In the case of the aldonamide IRIs **3.01**, **3.63**, and **3.64**,

both D-gluconamide **3.01** and L-gluconamide **3.63** possess this "1,3-*syn* interaction" if their polyol chain adopted linear rod-like conformations. Accordingly, their polyol chains may adopt more of a bent conformation. The L-mannonamide derivative **3.64**, on the other hand, may adopt more of a linear conformation owing to the lack of syn interactions. However, when in solution, these aldonamides may adopt multiple different conformations including as a result of interactions with solvent molecules.[31] Interestingly, mannitol has been shown to have a lower degree of free rotation in solution than glucitol, and it is therefore plausible that the different conformations observed have an influence on the resulting IRI activity observed with the related mannono- and gluconamides.[31,32] Further, mannitol has a slightly increased hydration number (e.g. the average number of water molecules within 1.2 molecular diameters of the polyol) than glucitol (13.23 and 11.45, respectively) which would align with the trend that more hydrated small molecules display increased IRI activity.[31,33] Notably, at this point, further studies (e.g. the hydration of the specific aldonamide IRIs **3.01**, **3.63**, and **3.64**) are warranted in order to explain how exactly these conformational differences influence the IRI activity (the mechanism of which is still not fully understood).

Aldonamide	IC_{50} value (± 95% confidence interval)
3.01	5 ± 1 mM
3.63	4 ± 1 mM
3.64	2 ± 0.4 mM

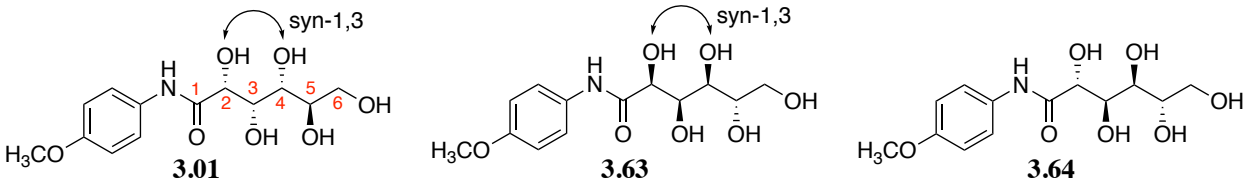

Figure 3.3.1.2. The IC_{50} values obtained for the IRI activity of L-gluconamide **3.63** and L-mannonamide **3.64** isomers of D-gluconamide **3.01**. The IRI assay was performed in triplicate (n = 3). Depiction of the "1,3-*syn* interaction" present in the gluconamides also shown.

After having investigated the IRI activity observed with changes to the stereochemistry of a gluconamide's carbohydrate component, attention was focused on modifying the oxidation state of this carbohydrate portion. From a SAR standpoint, a carboxyl group at the terminal end of the gluconamide's carbohydrate component in place of a terminal hydroxyl group could influence the resulting IRI activity. Therefore, synthetic approaches for the *C6*-carboxylic acid analogues **3.65-3.67** were envisioned (**Scheme 3.3.1.2**). Initial approaches toward the derivatives involved the use of selective protecting group chemistry. For example, the installation of a *C6*-silyl ether (triisopropyl silyl ether or TIPS group) followed by global acetylation for the remaining hydroxyl groups would afford silyl ether **3.78**. Removal of the TIPS group to afford the free *C6*-alcohol **3.79** using tetrabutylammonium fluoride (TBAF), however, was unsuccessful. Migration of acetyl groups may have occurred under these conditions, leading to an inseparable mixture of products. Despite this initial setback, the *C6*-carboxylic acid analogues **3.65-3.67** could be produced using a one-step procedure whereby the nucleophilic *p*-anisidine reacts with the electrophilic D-saccharic acid-1,4-lactone. All three derivatives **3.65-3.67** were produced using this approach in addition to slightly modified work up conditions (e.g. acidic workup to yield **3.65**, or organic extraction to yield **3.67**).

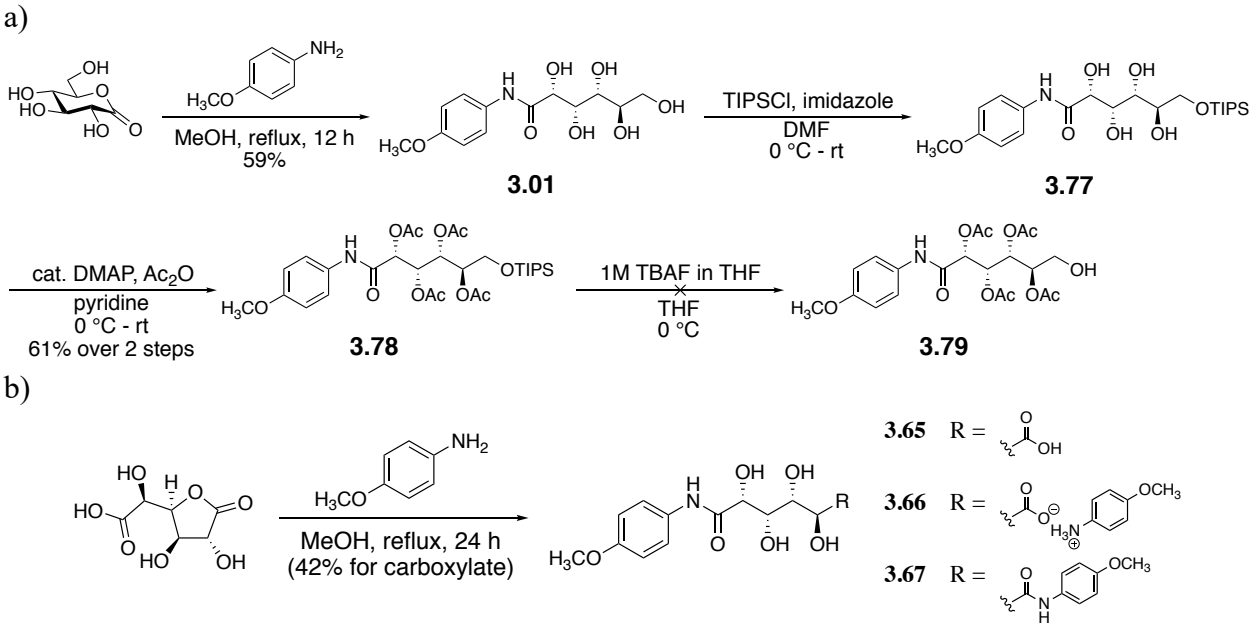

Scheme 3.3.1.2. Synthesis of *C6*-carboxylic acid derivatives **3.65-3.67**.

In order to elucidate the result of replacing a terminal hydroxyl group of a gluconamide with the respective oxidized species, the IRI activity of gluconamides **3.65-3.67** was probed at their maximum solubilities in phosphate-buffered saline (PBS) using the splat-cooling assay. The IRI activity of these *C6*-carboxylic acid derivatives is depicted as the % MGS of ice crystals in the presence of the derivatives compared to ice crystals in the presence of the PBS control (**Figure 3.3.1.3**). Interestingly, these derivatives were still poorly soluble in aqueous media with reduced or similar solubility to their parent gluconamide compound (**3.01**). In fact, the IRI activity of **3.67** could not be determined owing to its insolubility (<1 mM). Up to their maximum solubilities, **3.65** (5 mM) and **3.66** (20 mM) were not effective inhibitors of ice recrystallization with % MGS of 81% and 69%, respectively. This is in contrast to the % MGS obtained for ice crystals in the presence of **3.01** at 5 mM (20 % MGS). As expected, no difference was observed between the IRI of the carboxylic acid **3.65** and the corresponding carboxylate **3.66** at 5 mM. Interestingly, 20 mM *p*-anisidine on its own displayed moderate IRI activity which was then

reduced when it was used as the counterion of the gluconamide carboxylate (**3.66**). Taken together, these results conclude that the installation of a carboxylic acid at the *C6*-position of *N*-(aryl)-D-gluconamides, especially that of gluconamide **3.01**, leads to a drastic reduction of IRI activity. When considering this result in terms of a CH_n/OH ratio (**Section 3.1**), the modification of a hydroxyl group to carboxylic acid would lower the ratio of carbon to oxygens which has been correlated to a decrease in IRI activity.[1,8] Alternatively, perhaps the carboxylate functionality results in the intermolecular dimerization of gluconamides in solution thereby reducing the IRI activity. This dimerization may reduce the carbohydrate's ability to negatively impact water adding to the ice lattice (by reducing the carbohydrate's ability to disrupt the hydrogen-bonding network of water between the quasi-liquid layer and the ordered ice lattice).

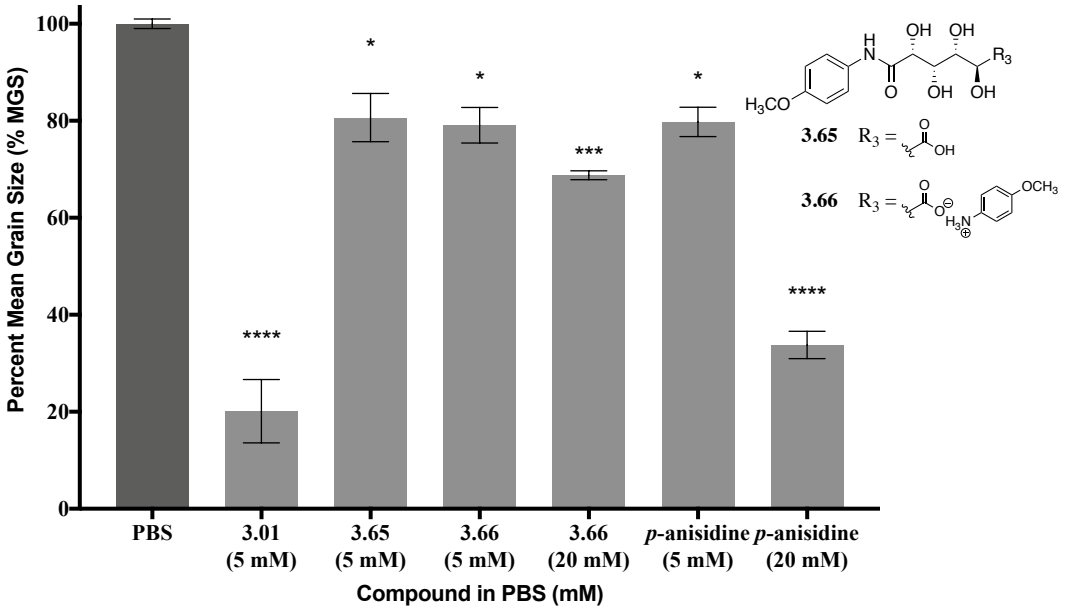

Figure 3.3.1.3. The IRI activity of **3.65-3.66** compared to *N*-(4-methoxyphenyl)-D-gluconamide **3.01** as depicted as the percent mean grain size (% MGS) of ice crystals in the presence of a compound compared to PBS.[14] Error bars indicate % SEM (n = 3). Asterisks indicate significant differences between PBS and each condition (* $p < 0.05$, *** $p < 0.001$, **** $p < 0.0001$) determined using one-way ANOVA with Tukey's multiple comparisons test. The IRI activities of **3.65** and **3.66** were also found to be significant from that of gluconamide **3.01** ($p < 0.0001$).

In an effort to further expose how altering the polyol chain (D-gluconamide's carbohydrate component) influences the corresponding IRI activity, a series of aldonamide mimetics were then envisioned (**Scheme 3.3.1.3**). These derivatives possessed no hydroxyl groups within the polyol chain apart from either a terminal hydroxyl group or carboxylate in order to offer additional evidence regarding the impact of carboxylates on IRI activity. The syntheses of derivatives **3.68-3.74** were straightforward and moderate- to high-yielding using adapted literature procedures. This included the implementation of an organocatalytic ring-opening aminolysis of lactones as well as a chemoselective acylation of amines in aqueous solutions to produce the appropriate *N*-phenyl amides.[34,35] Briefly, synthesis of derivatives bearing a terminal hydroxyl group (for comparison to the corresponding carboxylic acids) were produced by performing a ring-opening aminolysis of lactones of varying sizes in the presence of the catalyst 1,5,7-triazabicyclo[4.4.0]dec-5-ene. Derivatives bearing a terminal carboxylic acid were generally produced through the ring-opening of the appropriate anhydride in aqueous solutions.

a)

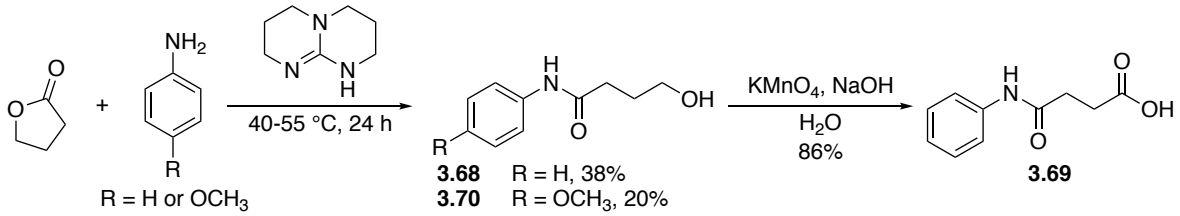

b)

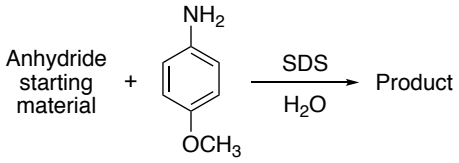

Starting material	Product (% yield)	Starting material	Product (% yield)
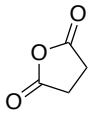	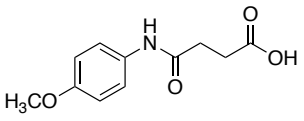 **3.71** (43%)	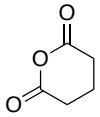	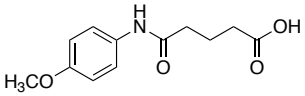 **3.73** (54%)
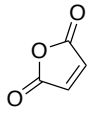	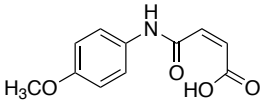 **3.72** (79%)	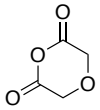	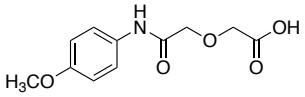 **3.74** (31%)

Scheme 3.3.1.3. **a)** Synthesis of aldonamide mimics **3.68-3.70**, and **b)** synthesis of mimics **3.71-3.74**.

The series of derivatives **3.68-3.74** were developed to probe the effect of chain length and terminal-carbon oxidation state on IRI activity. **3.68-3.74** were tested for their ability to inhibit ice recrystallization at their maximum solubilities in aqueous solutions using the splat-cooling assay. As observed in **Figure 3.3.1.4** and as hypothesized, the removal of polar groups from the carbohydrate-component of gluconamides resulted in a drastic reduction in IRI activity. The oxidation state of the terminal carbon of the "polyol" chain did not change the resulting IRI activity, as observed when comparing alcohol **3.68** to its carboxylic acid derivative (**3.69**). Changing the chain length did not alter the IRI activity either, as observed when comparing homologues **3.71** and **3.73**. However, by incorporating an oxygen into the carbon chain, as is the

case for derivative **3.74**, the solubility was improved and the IRI activity increased with respect to increasing concentration. Evidently, the delicate balance of hydrophobicity and hydrophilicity of gluconamides required for effective IRI activity is destroyed upon drastically altering the carbohydrate-component of the gluconamides. Further SAR work should maintain the carbohydrate component of the gluconamides whilst performing smaller structural modifications to the structure. For example, the next section (**Section 3.3.2**) details another modification of the terminal hydroxyl group (*C6*-position) of *N*-(4-methoxyphenyl)-D-gluconamide to a *C6*-azido group. This modification is much less drastic than the changes occurring with the aforementioned aldonamide mimics **3.68-3.74**.

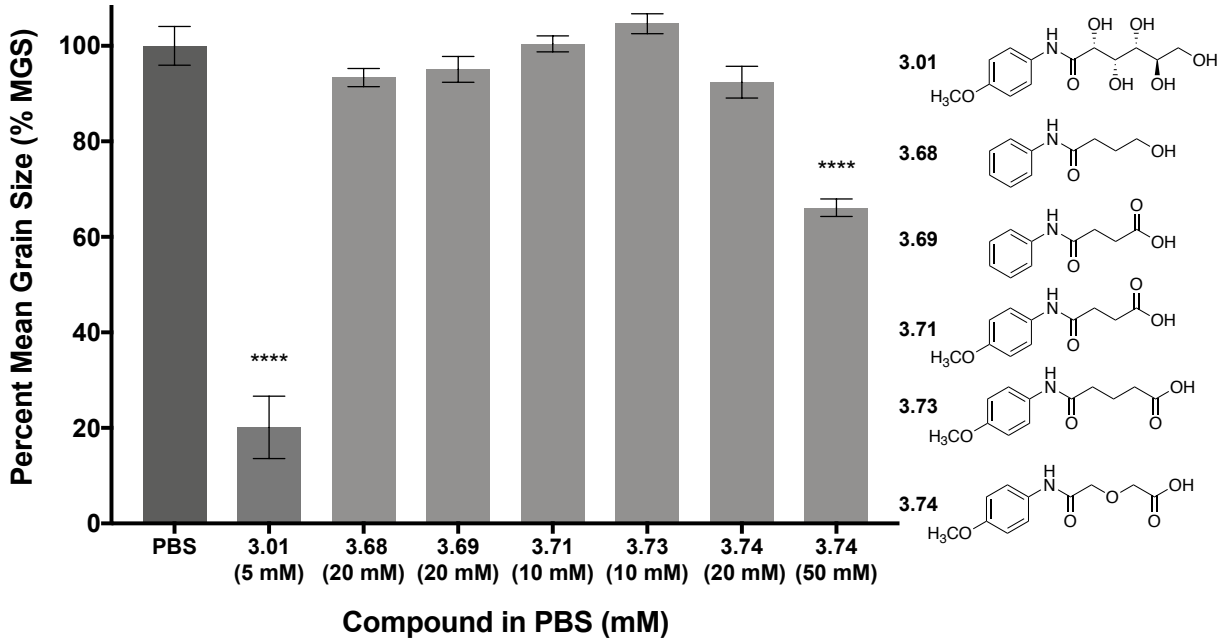

Figure 3.3.1.4. The IRI activity of compounds **3.68-3.74** depicted as the percent mean grain size (% MGS) of ice crystals in the presence of these small molecules. Error bars indicate % SEM (n = 3). Asterisks indicate significant differences between PBS and test condition (**** $p < 0.0001$) determined using one-way ANOVA with Tukey's multiple comparisons test. The IRI activities of all compounds were also found to be significant from that of gluconamide **3.01** ($p < 0.0001$) and 50 mM **3.74** ($p < 0.001$ or 0.0001).

3.3.2 Development of 6-azido-*N*-(aryl)-D-gluconamides as *C6*-analogues of the *N*-aryl-D-gluconamides

After having explored a number of gluconamide derivatives developed by altering the polyol chain (**Section 3.3.1**) and in noticing how drastic these changes influence IRI activity, the focus was turned toward the development of gluconamides bearing an azido group attached to the polyol chain. Previously in the Ben laboratory, there have been numerous studies set on the development of azide derivatives owing to the zwitterionic nature of the functional group which alters the hydrophobicity/hydrophilicity balance required for IRI activity.[18] Interestingly, Dr. Poisson has recently determined that the incorporation of a *C3*-azido group to pyranose-based IRIs resulted in the development of effective inhibitors of ice recrystallization whilst installation of the azide group elsewhere around the pyranose ring resulted in less efficacious IRIs.[18] The IRI-active derivatives were well tolerated in cell lines and showed promising results for the cryopreservation of red blood cells. With the promising nature of the *C3*-azide pyranose-based IRIs in mind, we hypothesized that incorporating an azido group into the carbohydrate component of gluconamides may also be beneficial for their IRI activity. That said, we expected to achieve gluconamides with an azido group installed at the *C6*-position through a relatively straightforward synthesis (**Scheme 3.3.2.1**). Interestingly, the derivatives described in **Section 3.3.2** (and previously in **Section 3.3.1**) mark the first time that different functional groups have been added to the carbohydrate component of gluconamides, and thus this offers important insight into the structural and electronic features required in the carbohydrate component of aldonamides for effective IRI activity. I would like to thank Mr. Staykov (undergraduate summer student researcher) for his help with the synthesis and IRI analysis of these derivatives.

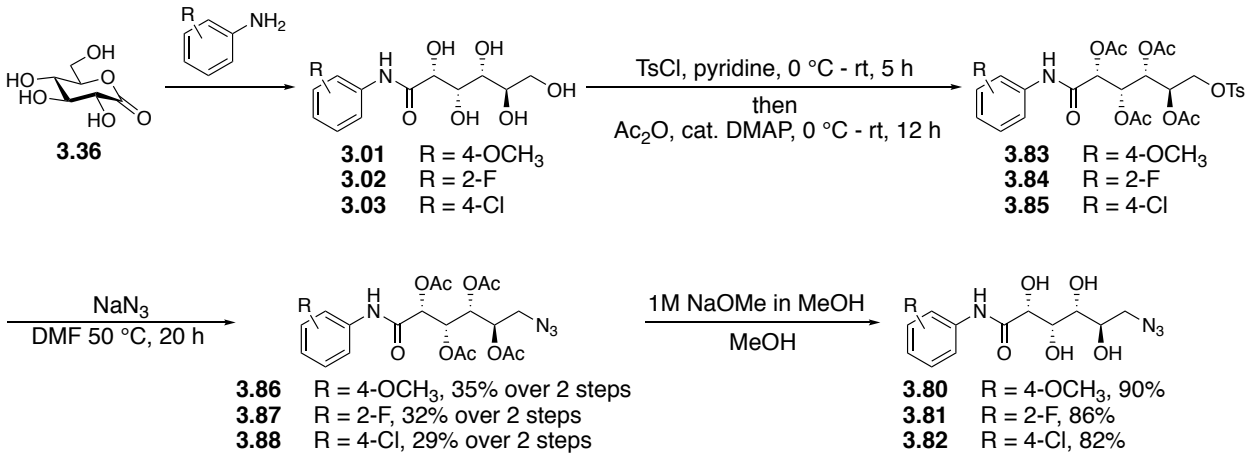

Scheme 3.3.2.1. Synthesis of *C6*-azido-*N*-(aryl)-D-gluconamides **3.80-3.82**.

The *C6*-azido gluconamides **3.80-3.82** were hypothesized to be achieved through a late-stage nucleophilic displacement of an appropriate leaving group at the *O6*-position of the gluconamide using a good nucleophile (azide) (**Scheme 3.3.2.1**). In using this late stage nucleophilic displacement, this synthetic approach could be tailored for a variety of future synthetic targets by reacting diverse nucleophiles with the corresponding electrophilic gluconamides **3.83-3.85**. The intermediate gluconamides **3.83-3.85** could be prepared from the corresponding parent gluconamide **3.01-3.03** by selectively installing a leaving group on the *O6*-position followed by global protection of the remaining carbohydrate hydroxyl groups. Finally, the parent gluconamide could be obtained as previously reported (**Section 3.2.1**) by the direct condensation reaction between D-gluconolactone **3.36** and the appropriate aniline. The first leaving group considered for this multi-step synthesis was a toluenesulfonyl group (Ts) which could be introduced under mild basic conditions using toluenesulfonyl chloride and a proton scavenger. Based on this, the protecting groups selected for the synthesis were acetyl groups (Ac) which could be installed immediately after the installation of the *C6*-leaving group and would be stable during the future nucleophilic attack by the azide. **Scheme 3.3.2.1** outlines the corresponding synthesis for the C6-azide derivatives. The beginning of the synthesis involved

the condensation of the appropriate aniline with D-gluconolactone **3.36** to afford gluconamides **3.01-3.03** in moderate yields (**Section 3.2**). Upon purification of the gluconamides **3.01-3.03**, these carbohydrate-based molecules were dissolved in pyridine in the presence of toluenesulfonyl chloride. Once TLC analysis indicated the conversion of starting material gluconamides **3.01-3.03** into the corresponding *O6*-tosyl intermediates, acetic anhydride was added directly to the reaction to yield the acetylated *O6*-tosyl gluconamides **3.83-3.85**. This one-pot approach was implemented after initial attempts at producing *O6*-tosyl gluconamides **3.83-3.85** via two separate steps led to poor yields of the intended products presumably due to degradation of the non-acetylated *O6*-tosyl gluconamides. Gluconamides **3.83-3.85** were then subjected to sodium azide under anhydrous conditions to yield the acetylated *C6*-azido gluconamides **3.86-3.88** in approximately 30% yield over the previous two steps. The final step in the synthesis involved deacetylation of the gluconamides using Zemplén conditions,[23] leading to the desired *C6*-azido-*N*-(aryl)-D-gluconamides **3.80-3.82** in 82%-90% yields after recrystallizations.

With the derivatives **3.80-3.82** in hand, attention was turned toward determining their abilities to inhibit ice recrystallization (**Figure 3.3.2.1**). Unfortunately, the *C6*-azide derivatives **3.80-3.82** were poorly soluble in aqueous solutions, and full dose-response curves could not be obtained using the modified splat-cooling assay (e.g., the normalized initial rates of recrystallization obtained for the maximum solubilities of the compounds were not 0). Therefore, the splat-cooling assay was used to test the IRI activities at low-millimolar concentrations and resulted in obtaining the percent mean grain size (% MGS) of ice crystals in the presence of select concentrations of the derivatives (up to their maximum solubilities). **Figure 3.3.2.1** depicts

the % MGS of ice crystals in the presence of **3.80-3.82** normalized to the % MGS of crystals in the presence of the control, phosphate-buffered saline (PBS).

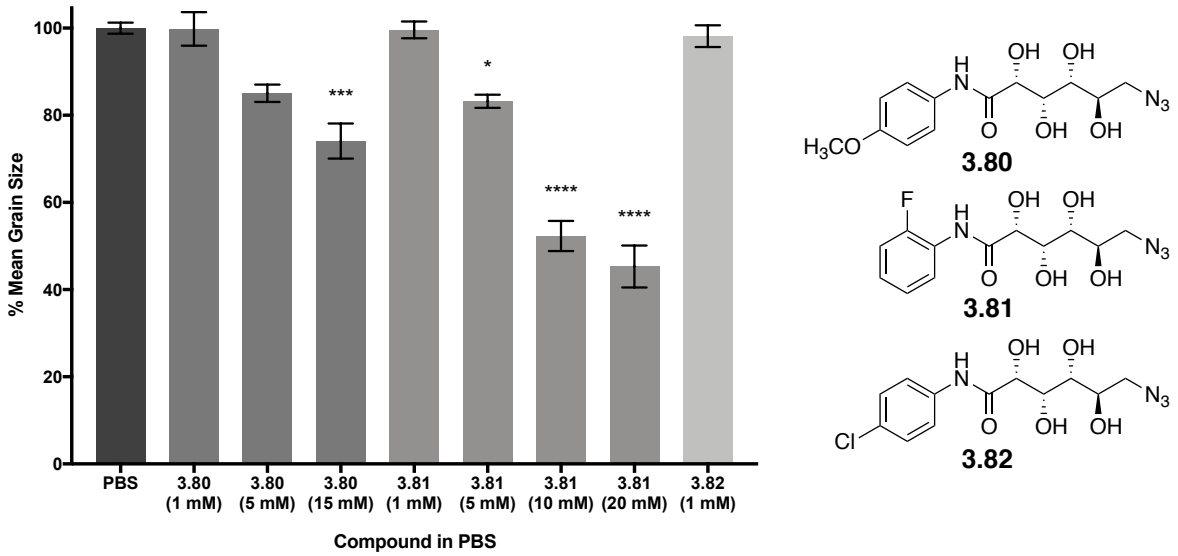

Figure 3.3.2.1. The IRI activity of *C6*-azido-*N*-(aryl)-D-gluconamides **3.80-3.82** up to the maximum solubilities of the molecules. Activity is depicted as percent mean grain size (% MGS) with error bars indicating percent standard error of the mean (% SEM) compared to the PBS control. The assay was performed in triplicate (n = 3). Asterisks indicate significant differences between PBS and test condition (* $p < 0.05$, *** $p < 0.001$, **** $p < 0.0001$) determined using one-way ANOVA with Tukey's multiple comparisons test.

Remarkably, the replacement of a *C6*-hydroxyl group with an azido group on gluconamides **3.01-3.03** led to drastically reduced IRI activity and solubility. Up to the maximum solubility of 4-methoxy derivative **3.80** (15 mM) the % MGS was 74%, that of the 2-fluoro derivative **3.81** was 45% at 20 mM, and finally, at 1 mM the 4-chloro derivative **3.82** displayed a % MGS of 98%. Recall that using the % MGS approach, an inhibitor with a % MGS between 30-80% was deemed to be moderately IRI-active while those with a <30% MGS were considered potent inhibitors. In using this classification of activity, these azide derivatives were

found to be moderate-to-weak inhibitors of ice recrystallization. By way of contrast (and discussed in **Section 3.1**), the parent gluconamides of the azide analogues are considered potent or moderate inhibitors (4-methoxy derivative **3.01** has a 4% MGS at 22 mM, 2-fluoro derivative **3.02** has a 3% MGS at 11 mM, and 4-chloro derivative **3.03** has a 35% MGS at 22 mM). Nevertheless, the trend observed with the IRI activity of the parent gluconamides (**3.01** and **3.02**) is also consistent within the *C6*-azido derivatives **3.80-3.82** where the derivative bearing a 2-fluorophenyl functionality (**3.81**) appears more IRI-active than the derivative bearing a 4-methoxyphenyl compound (**3.80**). Statistical analysis confirmed this conclusion: 15 mM of azide **3.80** was found to be significantly less active than azide **3.81** at 10 mM ($p < 0.01$) and 15 mM ($p < 0.0001$). Further, the installation of the zwitterionic azide at the *C6*-position also drastically reduced the solubility of the gluconamides in aqueous solutions: the solubility of *N*-(4-chlorophenyl)-D-gluconamide **3.03** was reduced to low millimolar concentrations (1 mM) upon installation of the azide functionality (whereas the parent 4-chlorophenyl gluconamide **3.03** was previously tested for IRI activity at 22 mM). This diminished solubility is not unexpected as the incorporation of an azide in place of a hydroxyl group may reduce the hydrophilicity of the molecule. Interestingly, this reduced solubility and reduced hydrophilicity may partly explain the diminished IRI activity of the azide derivatives (and may also be the case for the azide-functionalized pyranose IRIs).[18] Clearly, the delicate hydrophobic-hydrophilic balance required for the IRI activity of the gluconamides was adversely impacted upon installation of an azide group. Despite the poor IRI activities and solubilities of these azido derivatives **3.80-3.82**, their potential cytotoxic and cryoprotectant properties would give insight for the design of future IRI-active cryoprotectants, and therefore, these derivatives are further assessed in **Chapter 4**.

3.4 Summary

Sections 3.2 and **3.3** discuss the development of novel *N*-aryl-D-aldonamides to further elucidate the features required in this class of carbohydrate-based small molecule IRIs. Ultimately, the rational design of new molecules able to preserve cellular substances at low temperatures (e.g. cryopreservation) is made possible by having fully characterized the structural features necessary for IRI activity. **Section 3.2** began by optimizing the synthesis of the promising IRIs **3.01-3.04** as well as further characterizing their ice recrystallization inhibition activity. The IRI activity was consistent with the trends previously discovered,[1] **3.02** was found to be the most active of the four gluconamides with **3.01** exhibiting similarly effective IRI activity. *N*-(2-fluoro-4-methoxyphenyl)-D-gluconamide **3.38** was designed to determine the influence of having both aryl substituents (4-methoxy group from **3.01** and a 2-fluoro group from **3.02**) on the same small molecule. Gluconamide **3.38**, however, was found to have significantly decreased IRI activity to that of the parent gluconamides. The classes of amino-phenyl **3.39-3.41** and gluconamido-phenyl derivatives **3.45-3.47** were then developed in order to probe the IRI activity of these structural features. Notably, the *p*-aminophenyl analogue **3.41** displayed effective IRI activity while its *m*- (**3.40**) and *o*- (**3.39**) counterparts had reduced activity owing to their poor solubilities in solution. Both gluconamido-phenyl analogues **3.46** (*m*-substituted) and **3.47** (*p*-substituted) displayed an effective ability to inhibit ice recrystallization as well; albeit with reduced activity compared to the amino-phenyl analogues. Next, stereoisomers of the parent *N*-(4-methoxyphenyl)-D-gluconamide **3.01** were synthesized, and as a result, derivative **3.64** (L-mannonamide) was found to exhibit increased IRI activity to that of the D-gluconamide **3.01**. This suggested that stereochemical change significantly influences the IRI activity of aldonamides. Next, installation of a *C*6-carboxylic acid moiety as a replacement of the *C6*-

hydroxyl group present in *N*-(4-methoxyphenyl)-D-gluconamide also significantly impacted the resulting IRI activity. *C6*-carboxylic acid derivatives **3.65** and **3.66** both displayed reduced IRI activity to their parent gluconamide **3.01**. Other changes to the carbohydrate component of the gluconamides that were investigated with aldonamide-mimetics **3.68-3.74** also possessing reduced IRI activity. Finally, gluconamides bearing a *C6*-azido functionality (**3.80-3.82**) resulted in less active IRIs compared to their parent gluconamides; although as previously observed with their corresponding parent IRIs, an IRI with a 2-fluorophenyl component was more active than one with a 4-methoxyphenyl component.

Overall, the carbohydrate-based small molecules discussed in **Chapter 3** mark the first time that the IRI activity has been assessed for gluconamide analogues with altered functional groups in the carbohydrate-component. Therefore, these small molecules offer substantial insight moving forward for the rational design of gluconamide-IRIs. Even more information can be drawn from the promising derivatives presented in **Chapter 3** in terms of their effects in cellular systems. Notably, the cytotoxicities of promising molecules will be discussed in the following chapter as well as their ability to aid in the cryopreservation of various cellular substances (using both *in vitro* and *in vivo* experiments).

3.5 References

(1) Briard, J. G. The Rational Design and Use of Novel Small-Molecule Ice Recrystallization Inhibitors for the Cryopreservation of Hematopoietic Stem Cells and Red Blood Cells (Doctoral Dissertation), Université d'Ottawa/University of Ottawa, 2016.

(2) Capicciotti, C. The Rational Design of Potent Ice Recrystallization Inhibitors for Use as Novel Cryoprotectants (Doctoral Dissertation), University of Ottawa, 2014.

(3) Doshi, M. Synthesis of Nitrogen-Containing Carbohydrate Derivatives and Their Use Toward Inhibiting Ice Recrystallization and Gas Hydrate Formation (Doctoral Dissertation), Université d'Ottawa/University of Ottawa, 2016.

(4) Briard, J. G.; Jahan, S.; Chandran, P.; Allan, D.; Pineault, N.; Ben, R. N. Small-Molecule Ice Recrystallization Inhibitors Improve the Post-Thaw Function of Hematopoietic Stem and Progenitor Cells. *ACS Omega* **2016**, *1* (5), 1010–1018. https://doi.org/10.1021/acsomega.6b00178.

(5) Jackman, J.; Noestheden, M.; Moffat, D.; Pezacki, J. P.; Findlay, S.; Ben, R. N. Assessing Antifreeze Activity of AFGP 8 Using Domain Recognition Software. *Biochem. Biophys. Res. Commun.* **2007**, *354* (2), 340–344. https://doi.org/10.1016/j.bbrc.2006.12.225.

(6) Capicciotti, C. J.; Leclère, M.; Perras, F. A.; Bryce, D. L.; Paulin, H.; Harden, J.; Liu, Y.; Ben, R. N. Potent Inhibition of Ice Recrystallization by Low Molecular Weight Carbohydrate-Based Surfactants and Hydrogelators. *Chem. Sci.* **2012**, *3* (5), 1408–1416. https://doi.org/10.1039/c2sc00885h.

(7) Balcerzak, A. K.; Febbraro, M.; Ben, R. N. The Importance of Hydrophobic Moieties in Ice Recrystallization Inhibitors. *RSC Adv.* **2013**, *3* (10), 3232–3236. https://doi.org/10.1039/c3ra23220d.

(8) Ampaw, A.; Charlton, T. A.; Briard, J. G.; Ben, R. N. Designing the next Generation of Cryoprotectants - From Proteins to Small Molecules. *Pept. Sci.* **2018**, No. May, e24086. https://doi.org/10.1002/pep2.24086.

(9) Lorber, B.; Bishop, J. B.; DeLucas, L. J. Purification of Octyl Beta-D-Glucopyranoside and Re-Estimation of Its Micellar Size. *Biochim. Biophys. Acta* **1990**, *1023* (2), 254–265. https://doi.org/10.1016/0005-2736(90)90421-j.

(10) Michel, H.; Oesterhelt, D. Three-Dimensional Crystals of Membrane Proteins: Bacteriorhodopsin. *Proc. Natl. Acad. Sci. U. S. A.* **1980**, *77* (3), 1283–1285.

https://doi.org/10.1073/pnas.77.3.1283.

(11) Capicciotti, C. J.; Kurach, J. D. R.; Turner, T. R.; Mancini, R. S.; Acker, J. P.; Ben, R. N. Small Molecule Ice Recrystallization Inhibitors Enable Freezing of Human Red Blood Cells with Reduced Glycerol Concentrations. *Sci. Rep.* **2015**, *5*, 1–10. https://doi.org/10.1038/srep09692.

(12) Briard, J. G.; Fernandez, M.; De Luna, P.; Woo, T. K.; Ben, R. N. QSAR Accelerated Discovery of Potent Ice Recrystallization Inhibitors. *Sci. Rep.* **2016**, *6* (October 2015), 1–8. https://doi.org/10.1038/srep26403.

(13) Knight, C. A.; Hallett, J.; DeVries, A. L. Solute Effects on Ice Recrystallization: An Assessment Technique. *Cryobiology* **1988**, *25* (1), 55–60. https://doi.org/10.1016/0011-2240(88)90020-X.

(14) Abraham, S.; Keillor, K.; Capicciotti, C. J.; Perley-Robertson, G. E.; Keillor, J. W.; Ben, R. N. Quantitative Analysis of the Efficacy and Potency of Novel Small Molecule Ice Recrystallization Inhibitors. *Cryst. Growth Des.* **2015**, *15* (10), 5034–5039. https://doi.org/10.1021/acs.cgd.5b00995.

(15) Abraham, S. Development and Implementation of a Kinetic Quantitative Analysis of Novel Small Molecule Ice Recrystallization Inhibitors (MSc Thesis), Université d'Ottawa/University of Ottawa, 2015.

(16) Armarego, Wilfred L. F., Chai, C. L. L. *Purification of Laboratory Chemicals*, 6th ed.; Elsevier Inc., 2009. https://doi.org/https://doi.org/10.1016/C2009-0-26589-5.

(17) Jahan, S.; Adam, M. K.; Manesia, J. K.; Doxtator, E.; Ben, R. N.; Pineault, N. Inhibition of Ice Recrystallization during Cryopreservation of Cord Blood Grafts Improves Platelet Engraftment. *Transfusion* **2020**, *60* (4), 769–778. https://doi.org/10.1111/trf.15759.

(18) Poisson, J. S. Synthesis and In Vitro Applications of Ice Recrystallization Inhibitors (Doctoral Dissertation, Université d'Ottawa/University of Ottawa), Université d'Ottawa/University of Ottawa, 2019.

(19) Tam, R. Y.; Ferreira, S. S.; Czechura, P.; Chaytor, J. L.; Ben, R. N. Hydration Index - A Better Parameter for Explaining Small Molecule Hydration in Inhibition of Ice Recrystallization. *J. Am. Chem. Soc.* **2008**, *130* (8), 17494–17501.

(20) Felpin, F. X.; Fouquet, E. A Useful, Reliable and Safer Protocol for Hydrogenation and the Hydrogenolysis of o-Benzyl Groups: The in Situ Preparation of an Active Pd 0/C

Catalyst with Well-Defined Properties. *Chem. - A Eur. J.* **2010**, *16* (41), 12440–12445. https://doi.org/10.1002/chem.201001377.

(21) Perron, V.; Abbott, S.; Moreau, N.; Lee, D.; Penney, C.; Zacharie, B. A Method for the Selective Protection of Aromatic Amines in the Presence of Aliphatic Amines. *Synthesis (Stuttg).* **2009**, No. 2, 283–289. https://doi.org/10.1055/s-0028-1083290.

(22) Arévalo, M. J.; Avalos, M.; Babiano, R.; Cabanillas, A.; Cintas, P.; Jiménez, J. L.; Palacios, J. C. Optically Active Sugar Thioamides from δ-Gluconolactone. *Tetrahedron Asymmetry* **2000**, *11* (9), 1985–1995. https://doi.org/10.1016/S0957-4166(00)00140-3.

(23) Zemplén, G.; Kunz, A. Über Die Natriumverbindungen Der Glucose Und Die Verseifung Der Acylierten Zucker. *Berichte der Dtsch. Chem. Gesellschaft* **1923**, *56B*, 1705–1710.

(24) Svenson, S.; Schäfer, A.; Fuhrhop, J. H. Conformational Effects of 1,3-Syn-Diaxial Repulsion and 1,2-Gauche Attraction between Hydroxy Groups in Monomolecular N-Octyl-D-Hexonamide Solutions. Δ 13C and 1H NMR Spectroscopic Study. *J. Chem. Soc. Perkin Trans. 2* **1994**, No. 5, 1023–1028. https://doi.org/10.1039/p29940001023.

(25) Fuhrhop, J. H.; Boettcher, C. Stereochemistry and Curvature Effects in Supramolecular Organization and Separation Processes of Micellar N-Alkylaldonamide Mixtures. *J. Am. Chem. Soc.* **1990**, *112* (5), 1768–1776. https://doi.org/10.1021/ja00161a018.

(26) Fuhrhop, J. H.; Schnieder, P.; Boekema, E.; Helfrich, W. Lipid Bilayer Fibers from Diastereomeric and Enantiomeric N-Octylaldonamides. *J. Am. Chem. Soc.* **1988**, *110* (9), 2861–2867. https://doi.org/10.1021/ja00217a028.

(27) Fuhrhop, J. H.; Svenson, S.; Boettcher, C.; Roessler, E.; Vieth, H. M. Long-Lived Micellar N-Alkylaldonamide Fiber Gels. Solid-State NMR and Electron Microscopic Studies. *J. Am. Chem. Soc.* **1990**, *112* (11), 4307–4312. https://doi.org/10.1021/ja00167a029.

(28) Van Doren, H. A. *4 Tailor-Made Carbohydrate Surfactants? Systematic Investigations into Structure-Property Relationships of N-Acyl N-Alkyl 1-Amino-1-Deoxy-D-Glucitols*.

(29) Gaudin, T.; Lu, H.; Fayet, G.; Berthauld-Drelich, A.; Rotureau, P.; Pourceau, G.; Wadouachi, A.; Van Hecke, E.; Nesterenko, A.; Pezron, I. Impact of the Chemical Structure on Amphiphilic Properties of Sugar-Based Surfactants: A Literature Overview. *Advances in Colloid and Interface Science*. Elsevier B.V. August 1, 2019, pp 87–100. https://doi.org/10.1016/j.cis.2019.06.003.

(30) Pfannemüller, B.; Welte, W. Amphiphilic Properties of Synthetic Glycolipids Based on amid Linkages I. Electron Microscopic Studies on Aqueous Gels. *Chem. Phys. Lipids* **1985**, *37*, 227–240.

(31) Franks, F.; Dadok, J.; Ying, S.; Kay, R. L.; Grigera, J. R. High-Field Nuclear Magnetic Resonance and Molecular Dynamics Investigations of Alditol Conformations in Aqueous and Non-Aqueous Solvents. *J. Chem. Soc. Faraday Trans.* **1991**, *87* (4), 579–585. https://doi.org/10.1039/FT9918700579.

(32) Bastos, M.; Volkova, N. N.; Wadsö, I. Heat Capacities of D-Mannitol and D-Sorbitol in Water, Dimethyl Sulfoxide and Formamide. *J. Chem. Soc. Faraday Trans.* **1993**, *89* (9), 1351–1352. https://doi.org/10.1039/FT9938901351.

(33) *Water Science Reviews 5: Volume 5: The Molecules of Life*; Franks, F., Ed.; Cambridge University Press, 1990; Vol. 5.

(34) Guo, W.; Gómez, J. E.; Martínez-Rodríguez, L.; Bandeira, N. A. G.; Bo, C.; Kleij, A. W. Metal-Free Synthesis of N-Aryl Amides Using Organocatalytic Ring-Opening Aminolysis of Lactones. *ChemSusChem* **2017**, *10* (9), 1969–1975. https://doi.org/10.1002/cssc.201700415.

(35) Naik, S.; Bhattacharjya, G.; Talukdar, B.; Patel, B. K. Chemoselective Acylation of Amines in Aqueous Media. *European J. Org. Chem.* **2004**, No. 6, 1254–1260. https://doi.org/10.1002/ejoc.200300620.

4. The Impact of *N*-Aryl-D-Gluconamides on the Activities of Cryopreserved Human Umbilical Cord Blood

4.1 Human umbilical cord blood as a promising source of stem cells for hematopoietic stem cell transplantation

Hematopoietic stem and progenitor cells (HSPCs) are a heterogeneous pool of cells that are paramount to the maintenance of an organism's blood system throughout their lifetime by giving rise to diverse blood and immune cells (**Figure 4.1.1.1**). The unique abilities of HSPCs including quiescence, self-renewal, and differentiation are controlled through intrinsic and extrinsic factors and are advantageous in the treatment of many diseases and disorders. Specifically, hematopoietic stem cell transplantation (HSCT) is a routine clinical procedure generally used to reintroduce stem cells in a body system after disease, intensive chemotherapy and/or radiation therapy. HSCT is beneficial for the treatment of over 80 life-threatening diseases and disorders, such as hematologic cancers, bone marrow deficiencies, aplastic anemias, in addition to immune system and metabolic disorders.[1,2]

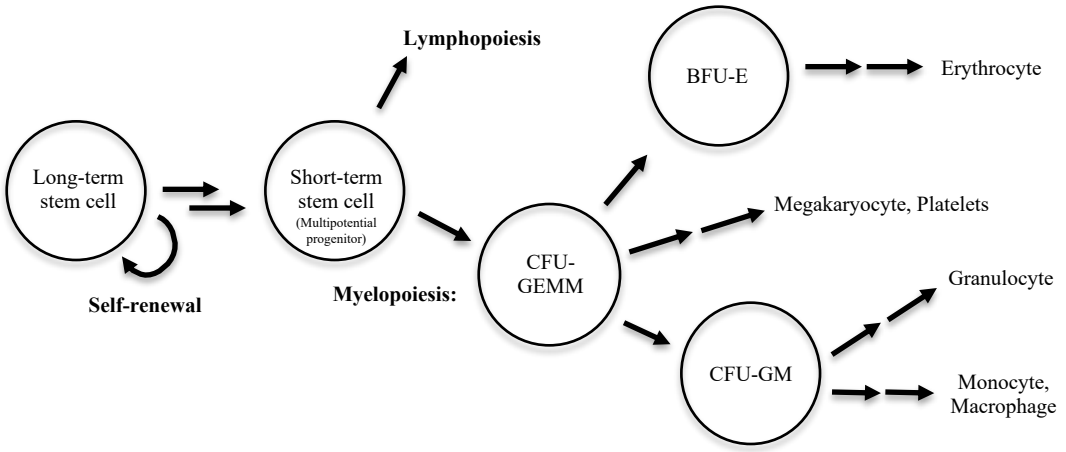

Figure 4.1.1. A simplified representation of hematopoietic stem cell myelopoiesis, where differentiation and proliferation of stem cells give rise to diverse blood cells. Select cell sub-populations include the Colony-Forming Unit-Granulocyte, Monocyte (CFU-GM) population, the Colony-Forming Unit-Granulocyte, Erythrocyte, Monocyte, and Megakaryocyte (CFU-GEMM) population, and the Burst-Forming Unit-Erythroid (BFU-E) population.

Further, the number of HSCTs performed continues to grow annually with more than 50,000 transplants worldwide each year.[2,3] According to data obtained by the Centre for International Blood and Marrow Transplant Research, the number of both autologous and allogenic transplants performed are rising in the US.[4] Autologous transplantation, the most common HSCT in the clinic, involves the use of a patient's own stem cells removed from the patient prior to the transplant. By contrast, allogenic HSCT involves the use of a stem cell donor other than the patient (e.g. someone with a similar genetic makeup to the patient or other sources). While autologous HSCTs are generally associated with fewer side effects than allogenic transplants, autologous HSCTs are potentially less effective in treating some diseases.[5] The Graft-versus-Tumor effect, which describes the immune response of donor cells against malignancy, may result in lower rates of relapse after allogenic HSCT but is not observed after autologous transplants.[5] Notably, Graft-versus-Host disease (GVHD) is a major concern after allogenic HSCTs owing to the donor's immune cells attacking the recipient's tissues.

In both transplant cases, the non-embryonic multipotent stem cells constituting the engraftment are usually harvested from the bone marrow, adult peripheral blood, or umbilical cord blood (UCB). Bone marrow is a rich source of HSPCs; however, the stem cell harvesting procedure is invasive for the donor. Adult peripheral blood stem cell collection is more common than bone marrow harvest; however, the donor still requires treatment (e.g. the injection of granulocyte colony-stimulating factor as a mobilizing agent for multiple days prior to collection) in order for this apheresis collection to be successful. The third option is human umbilical cord blood (UCB) collection at the time of delivery of a healthy newborn. While cord blood grafts typically contain only 5-10% of the cell doses relative to grafts from the marrow or adult peripheral blood sources, UCB offers unique clinical and logistical advantages to the other sources and has been an alternative option for grafts for allogenic transplants ever since the first successful one was performed in 1988.[6,7] The collection from this readily available and rich source of HSPCs is non-invasive for the donor, there are less stringent Human Leukocyte Antigen (HLA) matching criteria, and HSCTs from UCB are associated with lower rates and severity of Graft-versus-Host (GVHD) disease in recipients.[6,8–11] Further, HSPCs from UCB are more primitive than HSPCs harvested from other sources which can lead to higher stem cell proliferation.[8] Notably, there are now over 2,000 cord blood HSCTs performed globally each year.[2] Despite the overwhelming advantages of UCB as an HSPC source, it is still the least common source for HSCTs. A major reason for this is the reduced quality and number of stem cells isolated from cord blood units where selection of a unit for transplant is determined by the amount of total nucleated cells (TNCs) and/or hematopoietic stem and progenitor cells (HSPCs) in the transplant product.[12] Lower cell doses as a function of recipient weight is correlated with higher incidences of engraftment failure as well as delayed hematopoietic and immune recovery.[13–22] In one study,

myeloid engraftment had occurred in 74% of recipients (42 days after HSCT from UCB) where the pre-cryopreservation TNC dose was 7-24 million TNC/kg and the engraftment success increased to 91% when the pre-cryopreservation TNC dose was above 100 million TNC/kg.[16] Moreover, delayed hematopoietic recovery in recipients after cord blood transplantation, specifically that of neutrophil and platelet recoveries, leads to prolonged hospital stays and early transplantation-related mortality due to infection, and this slower graft recovery is associated with the lower cell doses obtained from one single cord blood unit.[9,23–26] Notably, maintaining an appropriate level of platelets after procedures (not to mention before surgeries and other clinical procedures) is essential to hemostasis. Clearly, approaches aimed at increasing the number and quality of HSPCs isolated from UCB is essential to improving HSCTs.[23,24,27–30] Additionally, as new uses of HSCT continue to emerge, including within the field of regenerative medicine, reducing the incidence of adverse outcomes as well as reducing the barrier of procedure costs associated with engraftment failure and prolonged hospital stays due to adverse events is crucial to the treatment's potential application. In the US, for example, the median cost of umbilical cord blood transplants for non-malignant conditions in pediatric patients is over $450,000.[31,32]

4.1.1 Improving the cryopreservation of human umbilical cord blood using ice recrystallization inhibitors

One approach aimed at increasing the number of viable and functional HSPCs isolated from UCB is to improve the cryopreservation of such cells.[33–35] Despite current efforts to minimize cell loss during the processing and cryopreservation of UCB units, the post-thaw viability and functionality of cryopreserved HSPCs is negatively affected by the current

conventional protocols and cryoprotectants.[36–38] More specifically, the higher levels of apoptotic $CD45^+CD34^+$ cells (where the CD34 glycoprotein is a marker for hematopoietic cells that are in the primitive stages of differentiation and the $CD45^+$ marks the leukocyte lineage) associated with cryopreservation of HSPCs may reduce the proliferation and differentiation ability of the cells post-thaw.[33,34,38,39] Moreover, these apoptotic cells may negatively influence engraftment success.[33–35,38–40] Conventional cryoprotectants, such as dimethyl sulfoxide (DMSO), fail to reduce the amount of uncontrolled ice growth that occurs during the preservation process which can lead to significant cryoinjury resulting in decreased cell number and potency post-cryopreservation.[41–46] Additionally, residual DMSO present in thawed stem cell grafts has been associated with negative effects in the transplant recipient including outcomes to the gastrointestinal, cardiovascular, respiratory, renal, hepatic, and central nervous systems.[44,47–50] Removing DMSO prior to transfusion may reduce the side effects due to DMSO toxicity, an appealing option for patients with pre-existing conditions; however, washings to remove this cryoprotective additive results in unwanted loss of HSPCs.[51–55] Alternative cryoprotective agents for HSPCs such as ethylene glycol, propylene glycol, and various carbohydrates have been explored; however, these additives have yet to be implemented in the clinic.[35,45,56–59] For this reason, molecules able to inhibit ice recrystallization (IRIs) are of great interest for the improvement of the cryopreservation methods of HSPCs from human UCB.[41,60]

In fact, a recent collaboration involving the Ben laboratory has demonstrated through small-scale cryopreservation experimentation that the use of ice recrystallization inhibitors in addition to dimethyl sulfoxide during cryopreservation of HSPCs can improve both the *in vitro* function and number of cells post-thaw.[61] From this collaboration, a number of gluconamides have shown promising results for improving the cryopreservation outcomes for HSPCs isolated

from UCB, including *N*-(2-fluorophenyl)-D-gluconamide (**4.01**), *N*-(4-methoxyphenyl)-D-gluconamide (**4.02**), *N*-(2,6-difluorobenzyl)-D-gluconamide (**4.03**), and *N*-(4-chlorophenyl)-D-gluconamide (**4.04**), among others (**Figure 4.1.2.1a**).[61]

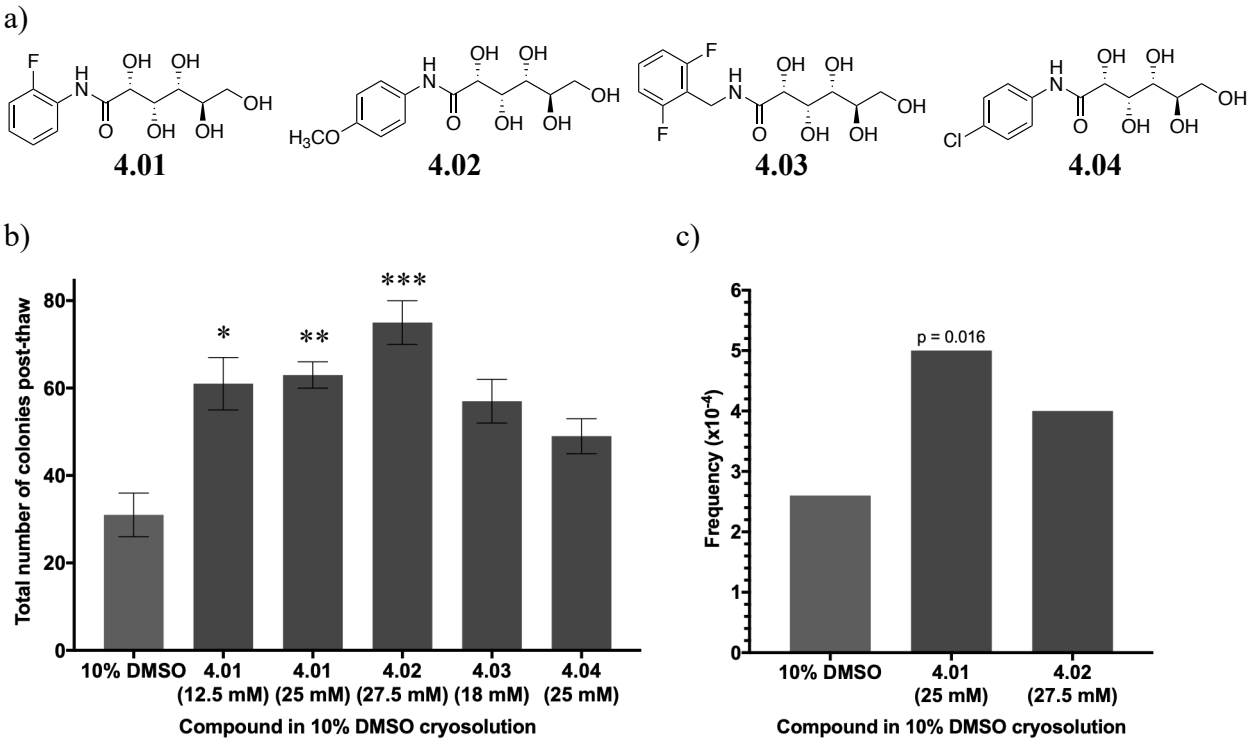

Figure 4.1.2. The improved post-thaw function of cryopreserved HSPCs from UCB through the supplementation of the cryosolution with IRIs, where **a)** depicts IRI structures, **b)** displays results of the colony-forming unit assay (average total number of colonies per 80 μL of thawed sample ± standard error of the mean, n = 2-10 adapted exactly as described in the reference) where sub-populations of total CFU include the Colony-Forming Unit-Granulocyte, Monocyte (CFU-GM) population, the Colony-Forming Unit-Granulocyte, Erythrocyte, Monocyte, and Megakaryocyte (CFU-GEMM) population, and the Burst-Forming Unit-Erythroid (BFU-E) population, and **c)** results of the long-term culture-initiating cell assay (represented as the mean frequency).[61] Asterisks indicate statistical significant from the 10% DMSO control (ANOVA with Dunnett's test with * 95%, ** 99%, or *** 99.9% confidence intervals.[61] Data adapted with permission from reference 61 (contact ACS directly for additional permissions relating to this article: https://pubs.acs.org/doi/10.1021/acsomega.6b00178).

Notably, the addition of gluconamide **4.01** to the DMSO-cryomedium (5% dextran in 0.9% saline) of these small-scale experiments significantly increased the post-thaw recovery of clonogenic progenitors determined through the use of the methylcellulose colony-forming cell assay (CFC assay),[25,62] as well as multipotent progenitors determined using the long-term culture-initiating cell assay (LTC-IC assay). A two-fold increase was also observed when the cryosolution contained 12.5 mM **4.01** (with 50% v/v plasma) or 25 mM **4.01**. When the solution contained 27.5 mM gluconamide **4.02** (with 50% v/v plasma), a greater than 2.4-time increase in colonies was observed, while there was some increase with **4.03** and no significant change with **4.04** as part of the solution. There was up to a 2-fold increase in the frequency of multipotent progenitors (as determined using the human LTC-IC assay) observed when HSPCs had been cryopreserved in the presence of gluconamides **4.01** and **4.02** (with 50% v/v plasma).[61] The results of this collaboration highlighted that supplementation with the most IRI-active gluconamides led to the highest increase of multipotent and committed progenitors compared to the addition of less IRI-active molecules.[61] In fact, Briard and co-workers noted that the addition of IRI-inactive small molecules did not significantly affect the post-thaw viability or clonogenic potential of cryopreserved HSPCs. It is also important to note that the impact of IRI cryoprotectants on the *in vivo* function of cryopreserved stem cell grafts had yet to be investigated and that the HSPC transplantation experiment is truly the best method for determining the functional capacity of HSPCs to re-establish the hematopoietic system of an organism.[63,64] Owing to the promising small-scale results of using IRIs as HSPC cryoprotectants as well as the urgent need for improved stem cell grafts for HSCTs in the clinic, further investigation into the cryoprotectant abilities of these *N*-aryl-D-gluconamides is certainly warranted.

The current chapter delves into the continued development of ice recrystallization inhibitors as cryoprotectants. Specifically, gluconamides **4.01-4.04** as well as their analogues (**4.05-4.09**) with varying aryl or carbohydrate modifications were selected as promising candidates stemming from structure-activity relationship (SAR) studies and were therefore further examined for their potential as cryoprotectants (**Figure 4.1.2.2**). 2-Fluoro-4-methoxyphenyl-D-gluconamide **4.05** contains both aryl substituents of its parent compounds 2-fluorophenyl **4.01** and 4-methoxyphenyl **4.02**. This derivative displayed weaker IRI activity than its parents, however, its increased aqueous solubility made this compound a candidate for further *in vitro* testing. *C6*-azide derivatives **4.06-4.08** were poorly soluble but from a SAR approach, we were interested in the influence of a *C6*-azide on its ability to preserve hematopoietic stem and progenitor cells *in vitro*. Finally, gluconamido derivative **4.09** was structurally intriguing and its cytotoxicity was therefore also assessed. Among the encouraging results presented herein includes the first report into the impact of an *N*-aryl-D-gluconamide cryoprotectant on the *in vivo* engraftment activities of cryopreserved cord blood grafts, which includes results from a collaboration between the Ben laboratory and the Pineault laboratory at Canadian Blood Services. An article titled "Inhibition of Ice Recrystallization during Cryopreservation of Cord Blood Grafts Improves Platelet Engraftment" highlighted this pioneering investigation published in *Transfusion*, in which we hypothesized that inhibiting ice recrystallization during the cryopreservation of cord blood would result in improved engraftment activities of HSPCs.[65]

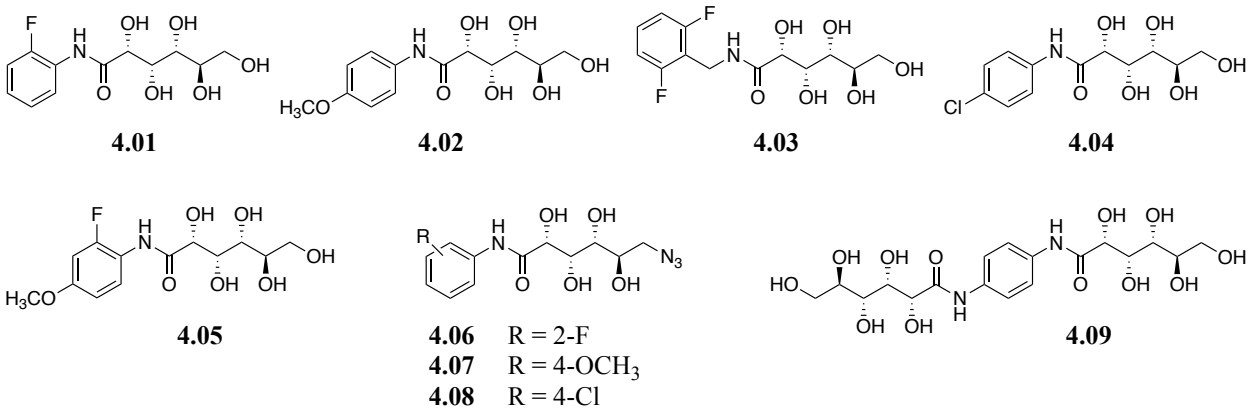

Figure 4.1.3. Structures of the gluconamide IRIs investigated for their potential as cryoprotectants.

The objectives of this chapter include:

- Determination of the cytotoxicity of promising gluconamide IRIs investigated by measuring the metabolic activity of cells *in vitro*.
- Analysis of the *in vitro* ability of promising IRIs to act as cryoprotectants for hematopoietic stem and progenitor cells (HSPCs) by determining the post-thaw viability and functional capacity of cryopreserved HSPCs.
- Investigation of the impact of a gluconamide cryoprotectant on the *in vivo* engraftment activities of cryopreserved cord blood grafts through the use of xenograft transplantation (serial transplantation assay) to determine the ability of cryopreserved HSPCs to differentiate and self-renew.

4.2 *N*-Aryl-D-gluconamides as cryoprotectants

4.2.1 Cytotoxicity of *N*-aryl-D-gluconamide ice recrystallization inhibitors

The novel molecules from **Sections 3.2** and **3.3** were assessed for their cytotoxicity to cells using a fluorescent-based assay and a model cell line. The human hepatocellular carcinoma cell line (HepG2) is a widely used adherent cell line that offers advantages for studying the cytotoxicity of small molecules owing to the cell's similarities to normal liver cells.[66] The cell viability of human hepatic cells (HepG2) in the presence or absence of the IRIs was indirectly determined using resazurin (a phenoxazine dye) as a measure of metabolic activity of the cells.[67] Resazurin is a non-toxic and cell-permeable fluorescent dye that is reduced in metabolically-active cells, where resazurin is blue in its oxidized state but if cells maintain metabolic activity, resazurin will be irreversibly reduced to resorufin, a pink-coloured compound (**Figure 4.2.1.1**). Briefly, the assay involves incubation of cultured cells with or without the molecules followed by fluorescent readings. The use of resazurin avoids issues that arise with other dyes such as poor sensitivity or the necessity for a solubilization solution due to insoluble dyes. Studies have shown that the use of the resazurin assay results in comparable information as that obtained from other assays, such as the MTT assay, which uses 3-[4,5-dimethylthiazol-2-yl]-2,5-diphenyl tetrazolium bromide (MTT) as the dye, in addition to enhancing the sensitivity of the experiments compared to the MTT assay.[68] Note that a substantial limitation to both the aforementioned assays is that they provide an overall snapshot of cell viability; however, they do not discern between the mechanisms by which the cells are undergoing cell death such as apoptosis or necrosis. Future work should utilize more powerful diagnostic tools (e.g. live/dead cell staining using flow cytometry) in order to use this information to better develop subsequent

novel non-toxic IRIs. Nevertheless, the resazurin assay is used herein as an initial probe into the cell viability of HepG2 cells in the presence of gluconamide-based IRIs. Following this, flow cytometry analysis is subsequently performed in cryopreservation experiments where IRI candidates are assessed for their ability to preserve human umbilical cord blood during cold storage (UCB is a less readily available cell line than the HepG2 cells used during preliminary cytotoxicity studies).

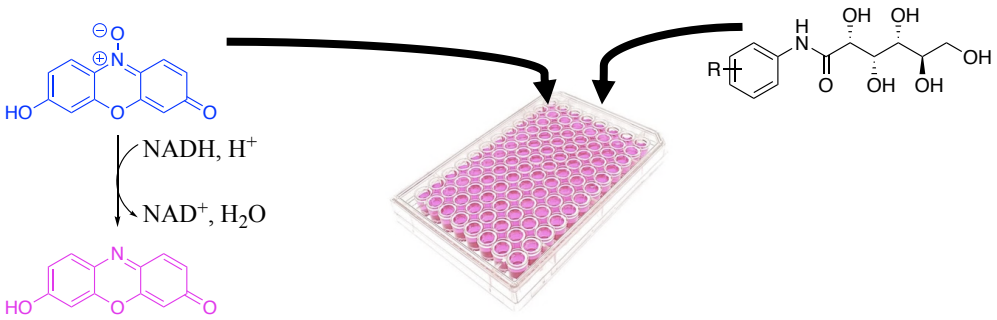

Figure 4.2.1.1. The reduction of resazurin in metabolically active cells.

Previous work on the gluconamides **4.01-4.04** by Dr. Briard determined the cytotoxicity of some of the small molecule IRIs using the MTT assay.[61,69] The results suggested a dose-response correlation whereby reduced cell viability was observed with higher concentrations of gluconamides **4.01-4.04**. The 2-fluorophenyl gluconamide **4.01** at 22 mM resulted in approximately 50% cell viability of HepG2 cells.[61] Approximately 50% cell viability was observed when HepG2 were exposed to ~44 mM of the 4-methoxyphenyl gluconamide **4.02** or the 2,6-difluorobenzyl gluconamide **4.03**.[61] Finally, the 4-chlorophenyl gluconamide **4.04** was shown to be significantly cytotoxic by concentrations of 10-15 mM where only 10% cell viability was observed when the hepatic cells were exposed to 15 mM gluconamide **4.04**.[61] However, **Figure 4.2.1.2**, displays the new results obtained using the resazurin assay.[65] Note that dose-response curves could not be generated since 0% cell viability was not achieved up to the

maximum solubilities of the gluconamides in media (e.g. sigmoidal curves could not be fit to the data and therefore additional LD_{50} values could not be determined). A table in the **Experimental Section** (**Table A1** in **Appendix III**) lists the maximum solubilities for IRIs presented throughout this thesis. Interestingly, 2-fluorophenyl gluconamide **4.01** was well tolerated by HepG2 cells up to the gluconamide's maximum solubility in media (96% hepatic cell viability at 25 mM **4.01**).[65] 4-Methoxyphenyl gluconamide **4.02** was found to be more cytotoxic than previously reported (52% hepatic cell viability when subjected to 20 mM gluconamide **4.02** and 17% viability at 40 mM **4.02**) while 2,6-difluorobenzyl gluconamide **4.03** was found to be less cytotoxic than previously observed (73% hepatic cell viability at the maximum solubility of 40 mM **4.03**). In the case of 4-chlorophenyl gluconamide **4.04**, 43% hepatic cell viability was observed when cells were subjected to 10 mM **4.04** (the maximum solubility of this gluconamide in media). The current results obtained using the resazurin assay may provide more accurate conclusions than those previously obtained using the MTT assay for two main reasons: 1) the increased sensitivity observed with the resazurin assay than that of the MTT assay,[68] and 2) the resazurin assay's fluorescent measurements were directly obtained from the spectrophotometer readings as opposed to the use of indirect measurements of absorbance for MTT samples.[70]

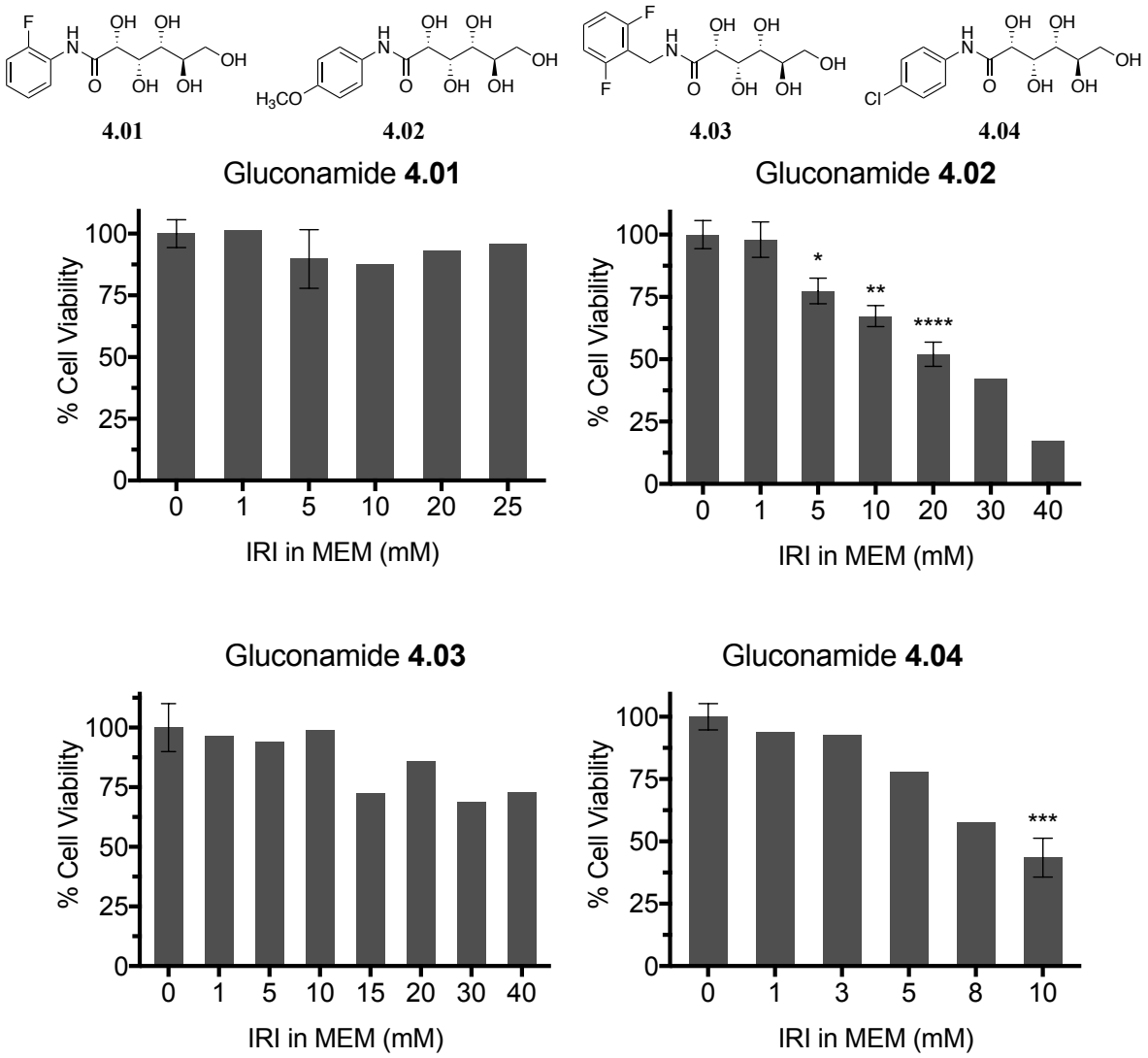

Figure 4.2.1.2. Cell viability of HepG2 cells in the presence of gluconamides **4.01-4.04** dissolved in supplemented Minimum Essential Media (MEM).[65] Using the resazurin assay, cells incubated in gluconamide-free media as well as cells incubated in the presence of surfactant, 1% Triton-X (not plotted as this is a value of 0%), were used as controls. Data are reported as the mean percent cell viability and error bars indicate % SEM for all the conditions performed at least in triplicate (n = 3 plates). All conditions without error displayed were performed in duplicate (n = 2). For the **4.01** plot, n = 4 plates performed for 0 and 5 mM **4.01**. For **4.02** plot, error bars indicate SEM of n = 3 plates performed (n = 5 for 0 mM). For **4.03** and **4.04**, 0 mM was performed on 4 plates as well as 10 mM **4.04** (n = 4). Asterisks indicate statistical significance from control conditions (0 mM) found using one-way ANOVA with Dunnett's multiple comparisons test (* $p < 0.05$, ** $p < 0.01$, ***, $p < 0.001$, **** $p < 0.0001$).

Accordingly, from the resazurin assay, gluconamide **4.01** was suggested to be well tolerated by HepG2 cells. The % cell viability was does not appear significantly altered compared to the control (compound-free condition) up to the gluconamide's maximum solubility (25 mM) in the culture media. This result in addition to previous results that the molecule preserves the functionality of HSPCs after cryopreservation suggest that IRI-active **4.01** is an excellent target for further cryopreservation studies. Gluconamides **4.02** and **4.04** show significant toxicity as their concentrations reach maximum solubilities in the culture media (one-way ANOVA with Dunnett's multiple comparisons test) but the preliminary data of **4.03** shows reduced cytotoxicity in comparison to **4.02** and **4.04**. This initial toxicity screen (and preliminary screen in the case of conditions performed in duplicate) offers insight into the cytotoxicity of gluconamides **4.01-4.04**, however, it is important to also assess the viability and functionality of the specific cell type being studied (e.g. HSPCs from UCB) since compound cytotoxicity differs based on cell line and incubation period. Additionally, it is important to acknowledge that this viability assay only provides an overview of the cell viability in the presence of the gluconamides and that future work should investigate the specific mechanisms by which HepG2 cell injury may be occurring. Nevertheless, gluconamides **4.02-4.04** will also be assessed for their impact on HSPCs during cryopreservation.

With an IC_{50} value for its IRI activity at 20 mM, gluconamide **4.05** was then assessed for its cytotoxicity (**Figure 4.2.1.3a**). Its cytotoxicity profile in the hepatic cell line HepG2 is similar to that observed with gluconamide **4.02** whereby higher concentrations of the molecules appears to lead to reduced amounts of viable cells. Since gluconamide **4.05** is less IRI-active than both **4.01** and **4.02** parent compounds, it is clear that the presence of both aryl substituents on the molecule negatively affects both the IRI activity as well as maintains the cytotoxicity of

gluconamide **4.02**. It was hypothesized that its cryoprotective ability will also be less effective than either of its parent compounds (**4.01** and **4.02**) and this will be further explored in **Section 4.2.2**.

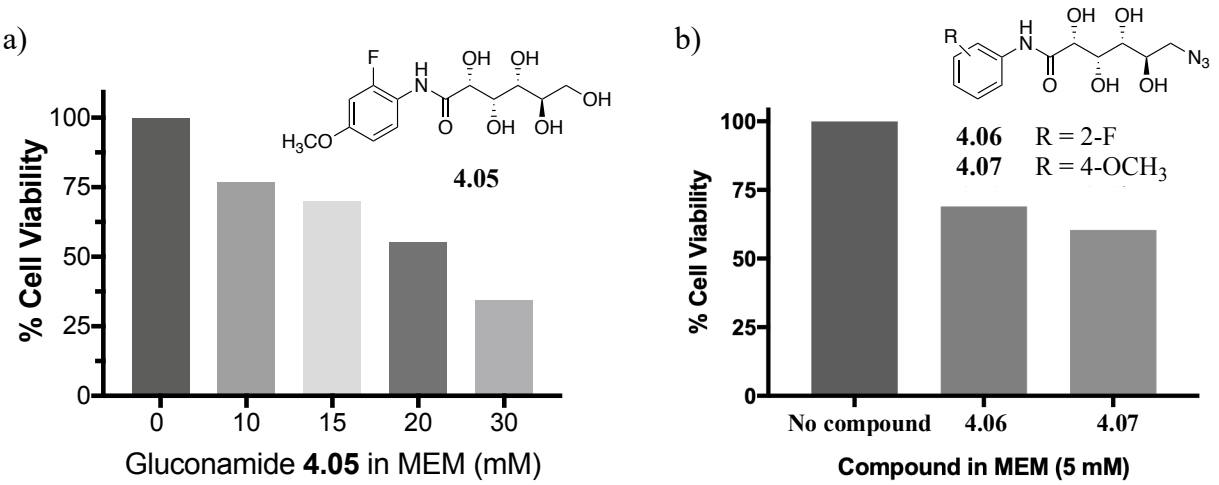

Figure 4.2.1.3. a) Cell viability of HepG2 cells in the presence of gluconamide **4.05** dissolved in appropriately supplemented Eagle's Minimum Essential Media (MEM). Data are reported as the mean percent cell viability (n = 2 plates). **b)** Percent cell viability of HepG2 cells in the presence of gluconamides 5 mM **4.06** and **4.07** dissolved in appropriately supplemented Eagle's Minimum Essential Media (MEM). Data are reported as the mean percent cell viability (n = 1 plate replicate). Using the resazurin assay, cells incubated in the absence of the gluconamide as well as cells incubated in the presence of surfactant, 1% Triton-X (not shown as these are a data point of 0%), were used as controls.

The azido-gluconamides **4.06-4.08** discussed in **Section 3.3.2** were intriguing since they represented the first-time significant modifications were made to the carbohydrate-component of the gluconamide structure. The substitution of a *C6*-hydroxyl group with a *C6*-azido group resulted in a reduction in solubility and IRI activity. As depicted in **Figure 4.2.1.3b**, this structural modification may also result in reduced cell viability of HepG2 cells in the presence of these azido compounds (note that further cytotoxicity studies must be conducted in order to

statistically determine differences in the cytotoxicity of the *C6*-azide derivatives). At a concentration of 5 mM, 2-fluorophenyl gluconamide **4.01** resulted in 90% hepatic cell viability while subjecting the hepatic cells to 5 mM **4.06** resulted in ~69% cell viability (preliminary data). Cytotoxicity appears more similar between 4-methoxyphenyl gluconamides **4.02** (77% cell viability) and its azide derivative **4.07** (~ 60% viability from preliminary data), although the addition of an azide at the terminal carbon may also increase the cytotoxicity of this molecule. Meanwhile, gluconamide **4.08** could not be assessed for its cytotoxicity owing to its significant insolubility in aqueous media (a property that is observed with its parent compound **4.04** albeit to a lesser degree). Preliminary data regarding gluconamide **4.09**, a gluconamide bearing two carbohydrate moieties with an IC_{50} value for its IRI activity at 12 mM, suggested that the compound possessed cytotoxicity even at low millimolar concentrations (data not shown in figure, < 40% cell viability when HepG2 cells were incubated with 5 mM of gluconamide **4.09**). Once again, additional cytotoxicity assessment should be conducted in order to conclude the full cytotoxicity profile of gluconamide **4.09**.

4.2.2 Cryopreservation of hematopoietic stem and progenitor cells with *N*-(2-fluorophenyl)-D-gluconamide ice recrystallization inhibitor

After determining cytotoxicity associated with the IRI-active molecules developed as described in **Chapter 3**, the next step was to assess their ability to act as protective agents during the cryopreservation of various cell types. **Section 4.2.2** details the use of *N*-(2-fluorophenyl)-D-gluconamide **4.01** as a cryoprotectant for HSPCs, while **Section 4.2.3** describes the use of gluconamides **4.02-4.07** as cryoprotectants. Importantly, these studies involved the investigation of these gluconamides to protect HSPCs in cryopreservation conditions that were more similar to

standard protocols involved with HSPC research in Canada. Previous results using small-scale experiments (0.1 mL) showed that gluconamides **4.01-4.04** were effective at preserving the function of HSPCs post-cryopreservation (and notably, with varying concentrations of plasma in the cryosolutions).[61] Conventional protocols used for HSPC research at Canadian Blood Services utilize 1 mL volume sizes for the cryopreservation of 10 x 10^6 total nucleated cells (TNC) and these were mimicked in the design of cryopreservation studies presented in **Section 4.2.2** and **Section 4.2.3**. Specifically, this involved the implementation of 1 mL solution volumes, 10 x 10^6/mL TNC concentration, approximately -1 °C/min freezing conditions for the 1 mL cryovials, cryosolutions prepared with 10% DMSO and 5% w/v dextran, and umbilical cord blood processing methods performed by Canadian Blood Services. IRI-active gluconamides were screened at multiple concentrations including up to their maximum solubilities in the cryosolutions and the cryosolutions were prepared the day of umbilical cord blood processing and cryopreservation. Further, no plasma was added to the cryosolutions during this study in order to mimic the promising small-scale results found when using gluconamide **4.01** at 25 mM (plasma-free, 10% DMSO with 5% w/v dextran in 0.9% saline).[61] It is important to note that in some cases, there are limited sample sizes due to limited availability and/or quality of the cord blood units as is the case for umbilical cord blood research (and in such cases, these results are clearly discussed as being initial probes into the potential of the gluconamides to act as cryosupplements).

4.2.2.1 The processing, cryopreservation, and thawing of human umbilical cord blood

Figure 4.2.2.1 outlines the general processing and cryopreservation steps used in the studies presented herein. Briefly, with ethics board approval, human umbilical cord blood (UCB) units were obtained through the Cord Blood for Research Program with Canadian Blood Services. The units used were obtained after informed consent by the donors and had the following cut off criteria: a hospital volume greater than 50 mL and a hospital TNC count between 0.9×10^9 and 1.5×10^9. Plasma rich in leukocytes was isolated from UCB units through Hespan (6% hetastarch in 0.9% sodium chloride) incubation. Cryopreservation conditions for the cell pellets obtained from the buffy coat layer either involved the cryopreservation of TNCs with 10% DMSO solutions or cryosolutions that also contained an IRI. 1 mL cryovials containing the experiments were first cooled to -80 °C followed by transfer to storage in liquid nitrogen vapours until use. Cryovials were thawed using a stepwise thaw-and-dilute procedure that was optimized by Canadian Blood Services.[71] This involves the rapid thawing of vials using a 37 °C water bath followed by dilution using 4% human serum albumin (HSA) in PlasmaLyte-A in a two-step manner that made use of a 15-minute incubation period for osmotic equilibration. TNCs were obtained after centrifugation and resuspended in media followed by cell count using a hematology analyzer. A FACS-Attune flow cytometer was used for TNC analysis after thawed cells were prepared using red blood cell lysis (further discussed in the **Experimental Section**). The colony-forming cell assay (CFC assay) involved the plating of TNC in MethoCult media (methylcellulose) and assessment by microscope after a 2-week culture period.

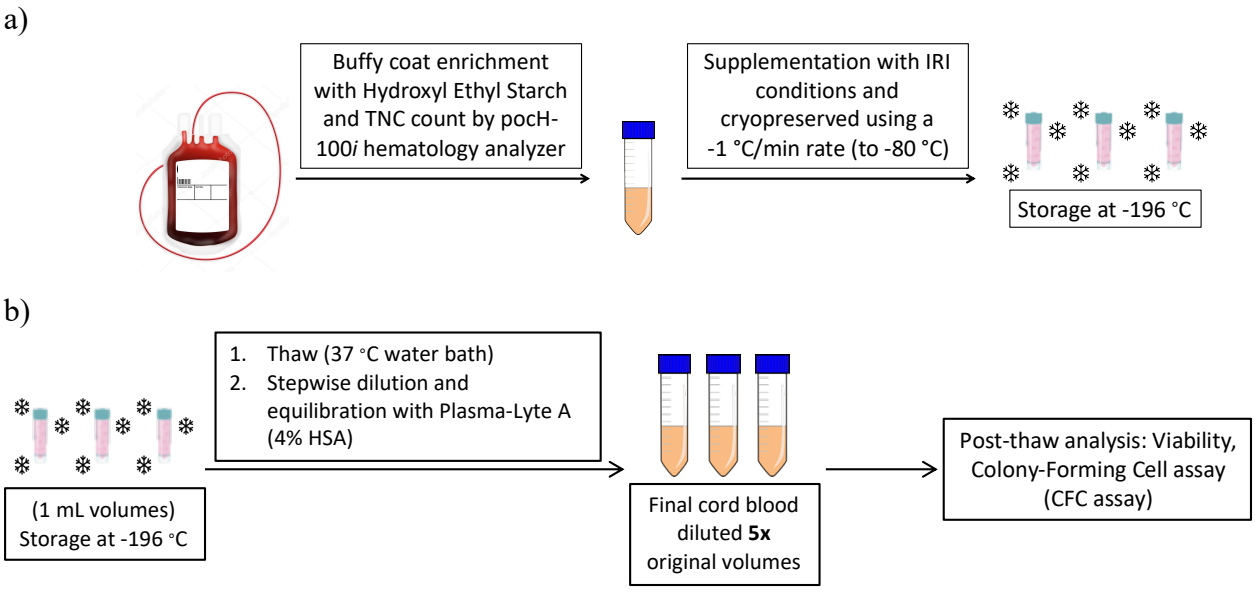

Figure 4.2.2.1. General methods used for **a)** the processing and cryopreservation of HSPCs, and **b)** the step-wise thaw-and-dilute process ahead of post-thaw analysis.[71]

4.2.2.2 The post-thaw viability of hematopoietic stem and progenitor cells cryopreserved in the presence of N-(2-fluorophenyl)-D-gluconamide

After cryopreservation of total nucleated cells (TNCs) with the appropriate concentration of IRIs dissolved in the standard cryosolution (10% DMSO with 5% w/v dextran in 0.9% saline), thawed cells were assessed for their post-thaw cell viability and recovery using flow cytometry led by Dr. Javed Manesia (postdoctoral fellow at the Canadian Blood Services), with the help of Ms. Emily Doxtator, Ms. Richa Kaushal, and myself. Since the total nucleated cell (TNC) count and the CD34+ cell count (HSPCs lineage) are important for quality assessment of banked UCB units, we were interested in these populations in our post-cryopreservation studies. Additionally, the CD45+ population (leukocytes) is also routinely assessed in the laboratory during cell viability studies. Presented in **Figure 4.2.2.2.1** is the cell viability of HSPCs cryopreserved with gluconamide **4.01** from 0 mM (10% DMSO control) up to its maximum solubility in the cryomedium (25 mM). To better detect cells undergoing apoptosis, the results are obtained by

using both Sytox-AADvanced (DNA staining) and Annexin V staining kits. Sytox-AADvanced is a stain that exhibits a high affinity for nucleic acids and therefore, the $Sytox^+$ cell population indicates those cells with compromised membranes (those allowing the penetration of the stain within the cell). Alternatively, since Annexin V binds to phosphatidylserine, Annexin V^+ cells indicate a cell population that has phosphatidylserine exposed on the external leaflets of cell membranes (a sign of early apoptosis since phosphatidylserine is normally present on the intracellular side of the membrane of healthy cells). Together, these help to discriminate between necrotic vs apoptotic cell populations. That said, the post-thaw HSPCs first underwent red cell lysis via treatment with an ammonium chloride solution followed by isolation of cells and their suspension in the Annexin V binding buffer. Cells were then stained with the appropriate antibodies (CD45-APC, CD34-PE, CD38-PECy-7), Annexin V Alexa 488, and Sytox-AADvanced™ (see **Experimental** section for further details) and were assessed within an hour. Note that post-thaw recoveries obtained (data not shown) were similar to the 10% dimethyl sulfoxide control, which were comparable to the clinical standard of approximately 80% post-thaw recovery. The amount of viable total nucleated cells (TNC), leukocytes ($CD45^+$ cell population), and HSPCs ($CD45^+CD34^+$ cell sub-population) are similar between IRI concentrations and are similar to the 10% DMSO control. Further, upon inspection of the number of apoptotic and necrotic cells within each TNC sub-population, we found these levels to be comparable to the control thereby indicating that gluconamide **4.01** (at all concentrations) exerts low cytotoxicity to cord blood cells and does not perturb the proportion of apoptotic or necrotic cells resulting from cryopreservation. It is important to note that the apoptotic cell population under discussion are those displaying signs of early apoptosis ($SYTOX^-$/Annexin V^+) while the necrotic cell population refers to the $SYTOX^+$ population. While the current method by which

we have analyzed our data adequately provides appropriate results to answer our research questions, a limitation to overcome moving forward is that cells undergoing apoptosis with compromised membranes (e.g. late stage) are not being distinguished from other populations. Future studies could address this experimental constraint to better distinguish the cellular injuries occurring as a result of our cryopreservation studies. For instance, the use of a polarity-sensitive indicator for viability and apoptosis (pSIVA^{TM} from Novus Biologicals) in conjunction with the aforementioned staining strategies could help to better distinguish early apoptosis from late apoptosis (whereby the pSIVA biosensor reversibly binds to phosphatidylserine and therefore fluoresces when bound to phosphatidylserine externally to the membrane). Alternatively, flow cytometry and the sub-G1 assay could be implemented to detect DNA fragmentation occurring during the late stages of apoptosis.

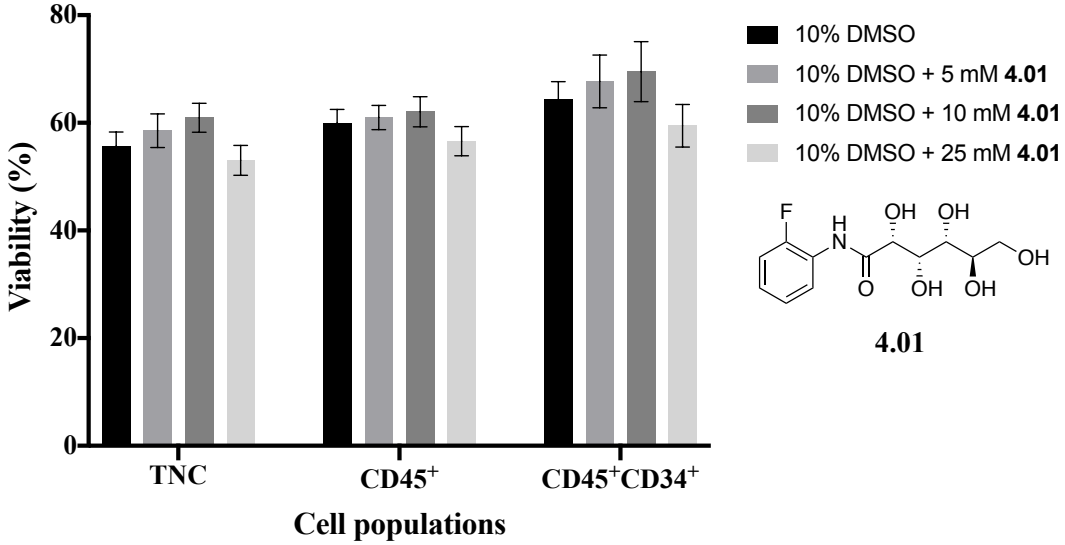

Figure 4.2.2.2.1. Cell viability of total nucleated cells (TNC), leukocytes ($CD45^+$), and HSPCs ($CD45^+CD34^+$) as a function of the concentration of gluconamide **4.01** (reprinted with permission, see reference 65).[65] UCB populations are measured using annexin V and Sytox-AAD staining where data are presented as the mean ± standard error of the mean (n = 3-7 independent UCB units: 10% DMSO performed n = 7, the 5 mM **4.01** condition assessed n = 4, the 10 mM **4.01** condition assessed n = 3, and the 25 mM **4.01** condition assessed n = 7). No statistical differences observed using two-way ANOVA with Tukey's multiple comparisons test ($p > 0.05$).

4.2.2.3 The functional capacity of hematopoietic stem and progenitor cells cryopreserved in the presence of N-(2-fluorophenyl)-D-gluconamide

The post-thaw clonogenic potential of HSPCs cryopreserved in the presence of gluconamide **4.01** was assessed using the Colony-Forming Cell (CFC) assay (**Figure 4.2.2.3.1**) in collaboration with Dr. Suria Jahan and Ph.D. candidate Ms. Richa Kaushal at the Canadian Blood Services. After thawing using the optimized diluting and equilibration conditions,[71] cells were plated in duplicate in methylcellulose and cultured for two-weeks prior to colony inspection under an inverted microscope (see the **Appendix III: Experimental Section** for further details on cell culture and CFC assay conditions). Specifically, the number of colonies observed after the incubation period in the semi-solid media is related to the proliferation and differentiation

activities of the stem cells after cryopreservation (**Figure 4.2.2.3.1a**). The types of colonies enumerated consist of the Burst Forming Unit-Erythroid (BFU-E) colony, the Colony Forming Unit-Granulocyte, Macrophage (CFU-GM) colony, and the Colony Forming Unit-Granulocyte, Erythrocyte, Macrophage, Megakaryocyte (CFU-GEMM) colony. The BFU-E colonies are primitive erythroid progenitors with high proliferation abilities that give rise to erythrocytes, while the CFU-GM progenitors lead to heterogeneous colonies comprised of both granulocytes and macrophages. Note that Colony Forming Unit-Granulocyte (CFU-G) and Colony Forming Unit-Macrophage (CFU-M) colony types are both counted within the number of CFU-GM amounts for the sake of the CFU presented in this thesis (per research at the Canadian Blood Services); however, the granulocyte progenitors give rise to homogeneous populations of eosinophils, basophils, or neutrophils (CFU-G) while the macrophage progenitors lead to homogeneous populations of macrophages. Finally, the CFU-GEMM is a colony of multi-lineage progenitors that lead to the development of granulocytes, erythrocytes, macrophages, and megakaryocytes.

a)

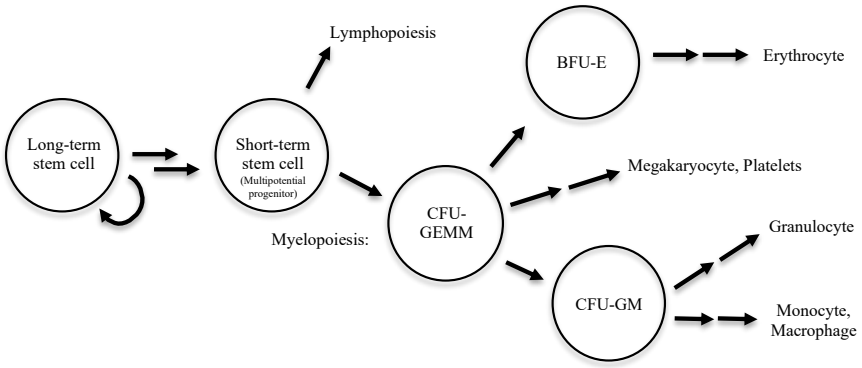

b)

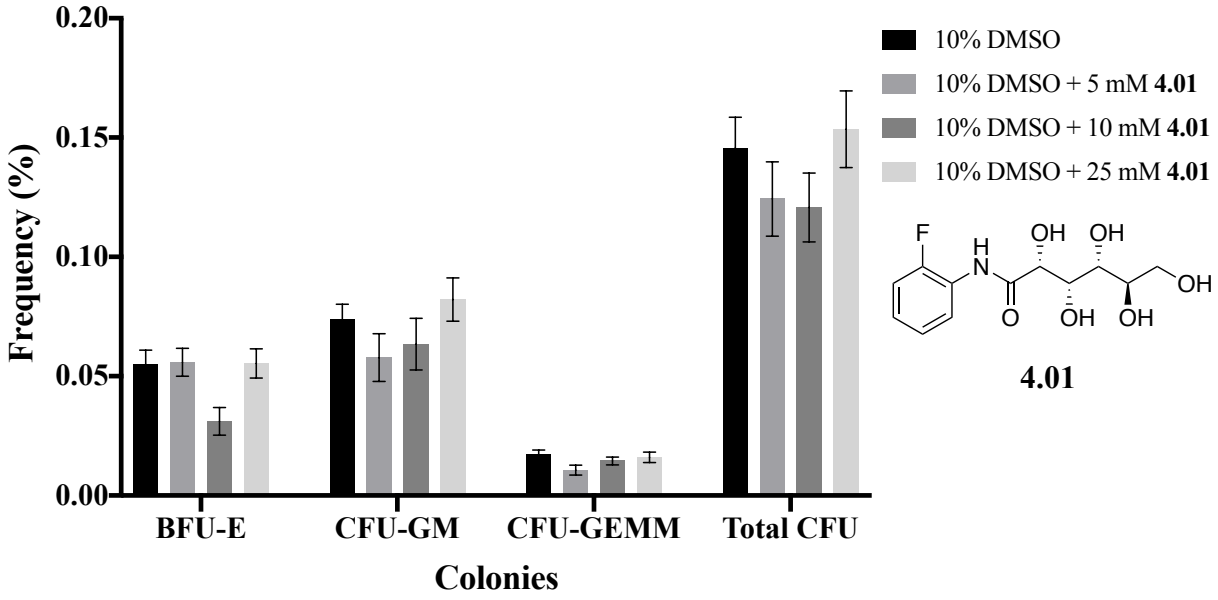

Figure 4.2.2.3.1. a) Simplified representation of the proliferation and differentiation of hematopoietic stem cells into the distinct myelo-progenitors scored in the CFC assay, and **b)** the frequency (%) of colonies from total nucleated cells cryopreserved in the presence of gluconamide **4.01** cryosolution, where the data are represented as mean ± standard error of the mean (n = 3-7 UCB units: 10% DMSO performed n = 7, the 5 mM **4.01** condition assessed n = 4, the 10 mM **4.01** condition assessed n = 4, and the 25 mM **4.01** condition assessed n = 6). No statistical differences among conditions determined using two-way ANOVA with Tukey's multiple comparisons test ($p > 0.05$). Sub-populations of total CFU include the Colony-Forming Unit-Granulocyte, Monocyte (CFU-GM) population, the Colony-Forming Unit-Granulocyte, Erythrocyte, Monocyte, and Megakaryocyte (CFU-GEMM) population, and the Burst-Forming Unit-Erythroid (BFU-E) population.

After cryopreservation with gluconamide **4.01** at varying concentrations up to the maximum solubility of the IRI in the cryomedium, the clonogenic potential of HSPCs from cord blood was found to be similar to that of the 10% DMSO control. This suggests that the IRI maintains the functionality of the HSPCs post-cryopreservation. While previous small-scale work had noted a significant improvement in the functionality of the cord blood-derived HSPCs post-cryopreservation with gluconamide **4.01**, it is possible that further cryopreservation protocols must be optimized in order to observe the same outcomes using the clinical conditions (e.g. use of plasma in the cryomedium, differing cell dose preserved per vial,[72] etc.).[61] Nevertheless, gluconamide **4.01** remains a promising cryoadditive due to its ability to maintain the functionality of the HSPCs. Further, the impact of exposing fresh cord blood cells (not cryopreserved) to 25 mM gluconamide **4.01** for one hour was also measured using the CFC assay (**Figure 4.2.2.3.2**). The results confirm that gluconamide **4.01** is not cytotoxic to human HSPCs at its maximum solubility since the functionality of cells exposed to the molecule was similar to the properties of those exposed to the 10% DMSO solution or to plasma alone.

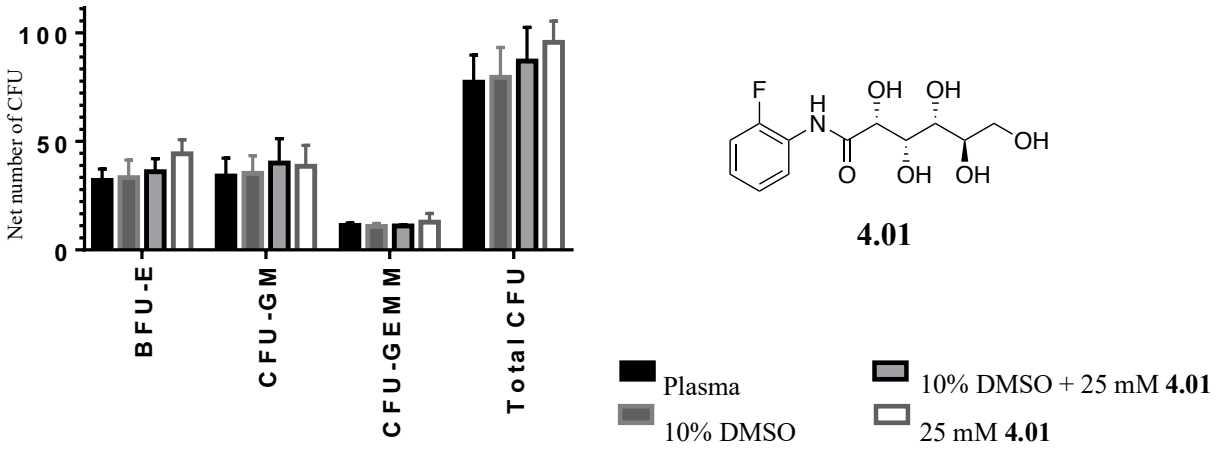

Figure 4.2.2.3.2. The net number of CFU per 40,000 total nucleated cells from fresh cord blood (not cryopreserved) exposed to 25 mM gluconamide **4.01** cryosolution for one hour (reprinted with permission, see reference 65).[65] Sub-populations of total CFU include the Colony-Forming Unit-Granulocyte, Monocyte (CFU-GM) population, the Colony-Forming Unit-Granulocyte, Erythrocyte, Monocyte, and Megakaryocyte (CFU-GEMM) population, and the Burst-Forming Unit-Erythroid (BFU-E) population. Data are represented as mean with SEM (n = 3 units). No significant difference observed among conditions.

4.2.2.4 The post-thaw viability and clonogenic potential of hematopoietic stem and progenitor cells cryopreserved in the presence of N-(2-fluorophenyl)-D-gluconamide and reduced dimethyl sulfoxide concentrations

These *in vitro* data together suggest that gluconamide **4.01** is not detrimental to the cryopreservation process of cord blood cells. Owing to the toxicity of dimethyl sulfoxide and recent literature reports highlighting that reducing the DMSO amount from 10% to 5% may be warranted in the clinic,[73] we were interested to see whether the amount of cytotoxic DMSO cryoprotectant could be minimized in the presence of gluconamide **4.01** while still observing the beneficial results obtained using 10% DMSO cryosolutions. Therefore, HSPCs were cryopreserved with varying concentrations of gluconamide **4.01** in the presence of a decreasing concentration of dimethyl sulfoxide. The post-thaw viabilities obtained through Annexin V/Sytox-AAD staining and flow cytometry are depicted in **Figure 4.2.2.4.1**. As the

concentration of DMSO is reduced in the cryomedium, so does the number of viable TNC and leukocytes with substantial reductions occurring using 5% DMSO and 10 mM or 25 mM **4.01**. Notably, however, there was no significant loss of HSPC viability observed by reducing the DMSO concentration in the presence of gluconamide **4.01**. While no significant changes were observed between the proportion of cells undergoing apoptosis (specifically those within $Sytox^-$/$AnnexinV^+$) in the 10% DMSO control compared to all conditions (two-way ANOVA with Dunnett's multiple comparisons test, $p > 0.05$), there were increased levels of necrotic cells observed in the 5% DMSO with higher gluconamide **4.01**. Specifically, increased levels of $Sytox^+$ cells were observed with 5% DMSO + 10 mM **4.01** (1.7-fold increase, $p < 0.05$) and 5% DMSO with 25 mM gluconamide **4.01** (2.2-fold increase, $p < 0.0001$). There also was a 1.7-fold increase in $Sytox^+$ leukocytes in 5% DMSO + 10 mM **4.01** compared to the 10% DMSO ($p < 0.05$) and a 2.1-fold increase with the 5% DMSO + 25 mM **4.01** condition ($p < 0.0001$). These increases may explain the loss of cell viability observed with the 5% DMSO + 10 mM or 25 mM gluconamide **4.01**.

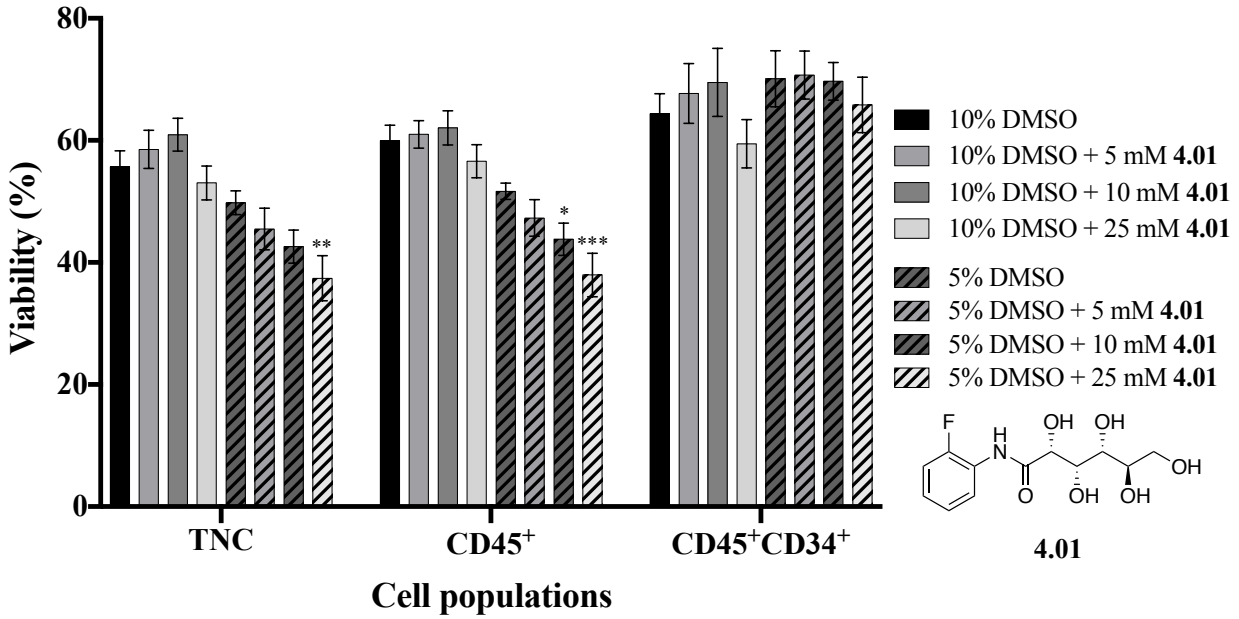

Figure 4.2.2.4.1. Post-thaw viabilities of cord blood cells cryopreserved in varying concentrations of gluconamide **4.01** and dimethyl sulfoxide. Viability of cells determined using Annexin V/Sytox-AAD staining where data are presented as the mean ± standard error of the mean (n = 3-7 UCB units: 10% DMSO performed n = 7, the 10% DMSO + 5 mM **4.01** condition assessed n = 4, the 10% DMSO + 10 mM **4.01** condition assessed n = 3, the 10% DMSO + 25 mM **4.01** condition assessed n = 7, and all 5% DMSO with/without IRI were performed n = 3). Asterisk indicates significant difference from the 10% DMSO condition determined using two-way ANOVA with Tukey's multiple comparisons with ≥ 95% confidence (* $p < 0.05$, ** $p < 0.01$, *** $p < 0.001$).

The CFC assay was then implemented to assess the clonogenic potential of cord blood cells cryopreserved with varying amounts of dimethyl sulfoxide and gluconamide **4.01** (**Figure 4.2.2.4.2**). Generally, the frequency of each colony did not differ significantly as the gluconamide concentration was increased or the dimethyl sulfoxide concentration was reduced. The only difference observed was with cord blood that had been cryopreserved with 5% DMSO + 25 mM **4.01** instead of 10% DMSO + 25 mM (where the 5% DMSO condition produced a lower frequency of colonies). The general lack of statistically significant differences among

conditions is consistent with the fact that HSPC viability was also unaffected by cryoprotectant concentration (**Figure 4.2.2.4.1**). Evidently, the reduction of dimethyl sulfoxide in the presence of gluconamide **4.01** below 10 mM is tolerated within the HSPC population as those cells remained viable and equally functional after cryopreservation. However, as discussed in **Section 4.1**, the TNC dose is used to determine the quality of a UCB unit in the clinic and lower TNC cell doses used for transplants has been associated with more adverse outcomes.[13–22] Therefore, the reduced viability of total nucleated cells and leukocytes observed after cryopreservation with 5% DMSO and higher gluconamide **4.01** concentrations would not be amenable to clinical settings. Interestingly, both the 5% DMSO condition and the 5% DMSO with 5 mM gluconamide **4.01** condition maintain the viability and functionality of HSPCs observed in the 10% DMSO conditions, and consequently, these cryosolutions should be further investigated.

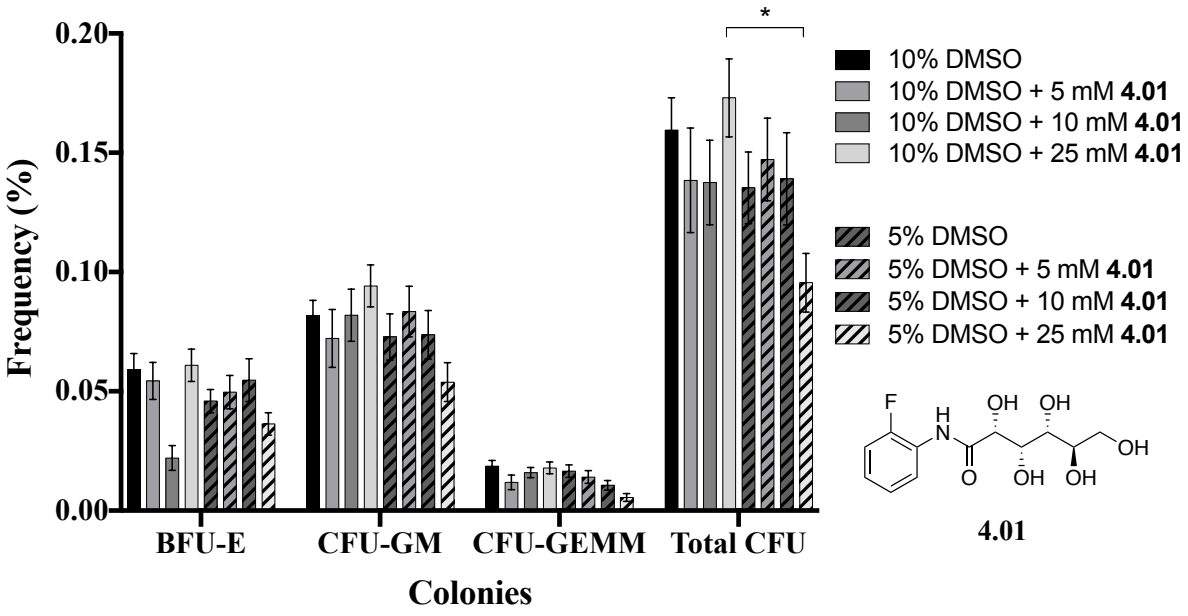

Figure 4.2.2.4.2. Frequency of CFU per 1 mL of cryopreserved total nucleated cells in the presence of gluconamide **4.01** cryosolution with varying concentrations of DMSO. Data are represented as mean frequency ± standard error of the mean (n = 3-7 units: 10% DMSO performed n = 7, the 10% DMSO + 5 mM **4.01** condition assessed n = 4, the 10% DMSO + 10 mM **4.01** condition assessed n = 4, the 10% DMSO + 25 mM **4.01** condition assessed n = 6, and all 5% DMSO with/without IRI conditions assessed n = 4 except 5% DMSO + 25 mM **4.01** which was performed in triplicate). Asterisks indicate significant difference between 25 mM **4.01** and 10% DMSO or 5% DMSO ($p < 0.05$) as determined using two-way ANOVA with Tukey's multiple comparisons test. Sub-populations of total CFU include the Colony-Forming Unit-Granulocyte, Monocyte (CFU-GM) population, the Colony-Forming Unit-Granulocyte, Erythrocyte, Monocyte, and Megakaryocyte (CFU-GEMM) population, and the Burst-Forming Unit-Erythroid (BFU-E) population.

4.2.2.5 The in vitro outcomes of using N-(2-fluorophenyl)-D-gluconamide as a cryoprotectant for hematopoietic stem and progenitor cells

After considering the data set presented in **Section 4.2.2** in addition to the preliminary data previously published,[61] it is likely that gluconamide **4.01** is well tolerated by the cells during the preservation of cord blood cells when supplemented to a 10% dimethyl sulfoxide

cryosolution containing 5% w/v dextran in 0.9% saline. This is exemplified by the maintenance of high amounts of viable and functional cells post-thaw. These results differ slightly from the previous promising results likely due to the fact that more optimization of the conditions is required for the current cryopreservation conditions (which more closely mimic the clinical standards) compared to the previous work, which studied the use of gluconamide **4.01** using a small-scale approach. It is important to note that more work to optimize the cryopreservation conditions with gluconamide **4.01** should be done in the future in order for the IRI to be the most beneficial to the cryopreservation of HSPCs and this may include investigation into incorporating plasma into the cryomedium or studying the optimal cell dose cryopreserved in the presence of varying concentrations of gluconamide **4.01**.[72,74,75] Nevertheless, recall that the true assessment of cryopreservation success is through the use of a serial transplantation assay to study the *in vivo* engraftment activities of cryopreserved cord blood grafts.[76,77] The results presented in **Section 4.2.2** highlight that gluconamide **4.01** should, therefore, be further assessed for its impact on the *in vivo* engraftment activities of cryopreserved cord blood and the study thereof is presented in **Section 4.3**.[65]

4.2.3 The post-thaw viability and clonogenic potential of hematopoietic stem and progenitor cells cryopreserved with *N*-aryl-D-gluconamides 4.02-4.07

After fully characterizing the *in vitro* impact of exposing hematopoietic stem and progenitor cells to IRI **4.01** (*N*-(2-fluorophenyl)-D-gluconamide) during the cryopreservation process (10 x 10^6 total nucleated cell/mL and frozen using 1 mL cryosolutions), the next step was to determine whether other gluconamide-IRIs possessed similar cryoprotectant abilities. Specifically, this involved investigating **4.02-4.04**, which have only been investigated using the

small-scale studies to date (0.1 mL cryosolutions with varying concentrations of plasma added during cryopreservation).[61] Novel gluconamides **4.05-4.07** described earlier in **Chapter 3** and **Section 4.2.1** were also examined. In collaboration with students at the Canadian Blood Services including Dr. Manesia and Ms. Kausal, the experimental plan was the same as described in **Section 4.2.2**. Total nucleated cells (TNC) were isolated from human umbilical cord blood and preserved in the presence of an IRI-active gluconamide added to the 10% dimethyl sulfoxide cryomedium (with 5% w/v dextran in 0.9% saline). As described with gluconamide **4.01**, samples were thawed followed by the assessment of post-thaw viabilities using Annexin V/Sytox-AAD staining and assessment of post-thaw functionalities by the CFC assay (duplicate plates for each independent unit). Note that post-thaw recoveries of samples were comparable to the clinical standard of approximately 80% post-thaw cell recoveries. After cryopreservation in the presence of gluconamide **4.02**, the post-thaw viabilities of the cord blood cells are similar to the 10% DMSO control while the clonogenic potentials were substantially reduced when the higher concentrations of **4.02** were investigated (**Figure 4.2.3.1**). The similarities of post-thaw viabilities of cells amongst all conditions suggest that the presence of gluconamide **4.02** does not perturb the cord blood cells despite the cytotoxicity of **4.02** at higher millimolar concentrations (**Section 4.2.1**). However, the detection of fewer colonies in conditions where cells had been exposed to higher levels of gluconamide **4.02** (most notably by 15 mM) suggests that the cytotoxic nature of the IRI may be impacting the ability of the HSPCs from cord blood to function optimally after cryopreservation. As observed in **Figure 4.2.3.1b**, it is important to note that lower concentrations of gluconamide **4.02** (e.g. at or below 5 mM) may not be harmful and could actually be beneficial to the functional capacity of HSPCs after cryopreservation, and therefore, this should be further investigated. The proportion of apoptotic and necrotic leukocytes

and HSPCs after cryopreservation were not significantly different between the 10% DMSO control condition and the 15 mM gluconamide **4.02** (+10% DMSO) condition. Interestingly, it wasn't until a concentration of 27 mM **4.02** that an increase in apoptotic cells within those cell populations was observed compared to lower concentrations of the gluconamide (10 mM and 25 mM). The increased level of toxicity of gluconamide **4.02** at high millimolar concentrations could account for this increase in apoptosis. Additionally, studies have shown that cell death associated with cryopreservation may take hours to days to manifest.[78,79] As such, post-thaw viability analysis may not fully capture the occurrence of delayed-onset cell death while the results of the CFC assay (obtained two weeks after cryopreservation) may be revealing the adverse impact of the cryoinjuries on the cell functionality. Further studies are certainly warranted to distinguish the mechanisms of cryoinjury incurring during cryopreservation with the gluconamide IRIs. It is also important to note that the previous small-scale experiments that highlighted a 2.4-fold increase in colonies with 27.5 mM gluconamide **4.02** also had a cryosolution containing 50% plasma while the results presented herein are from a cryosolution without any plasma in order to be consistent throughout the entire data set. Future work could investigate the inclusion of plasma along with gluconamide **4.02** in order to counteract the cytotoxic properties observed with the IRI. Overall, while gluconamide **4.02** has a similar IC_{50} for its IRI activity to that of gluconamide **4.01** (5 mM and 3 mM, respectively), the difference in their cytotoxicities may have led to substantial differences regarding the preservation of HSPCs. As a result, gluconamide **4.02** does not preserve cord blood cells as well as gluconamide **4.01** at higher millimolar concentrations.

a)

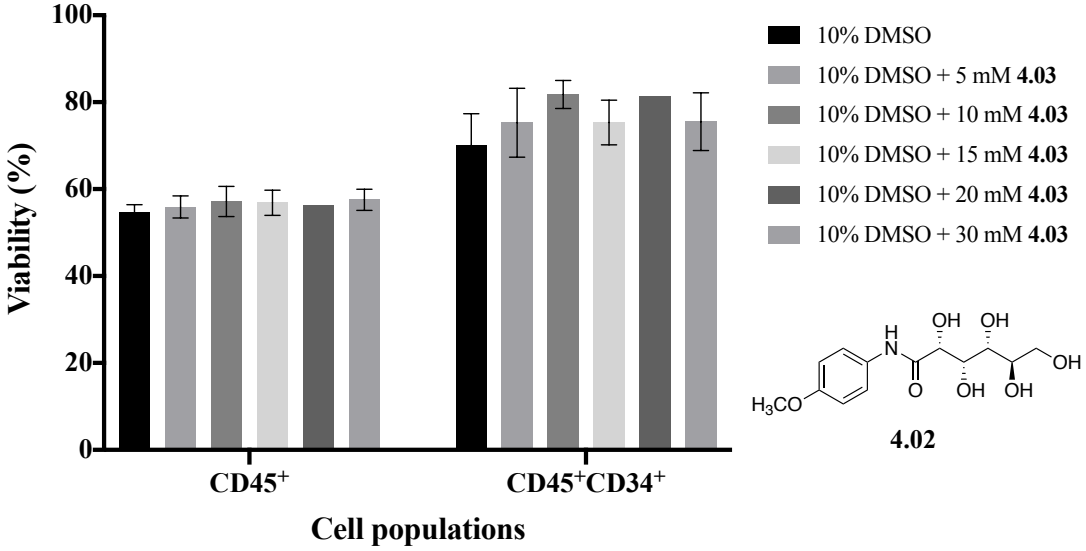

b)

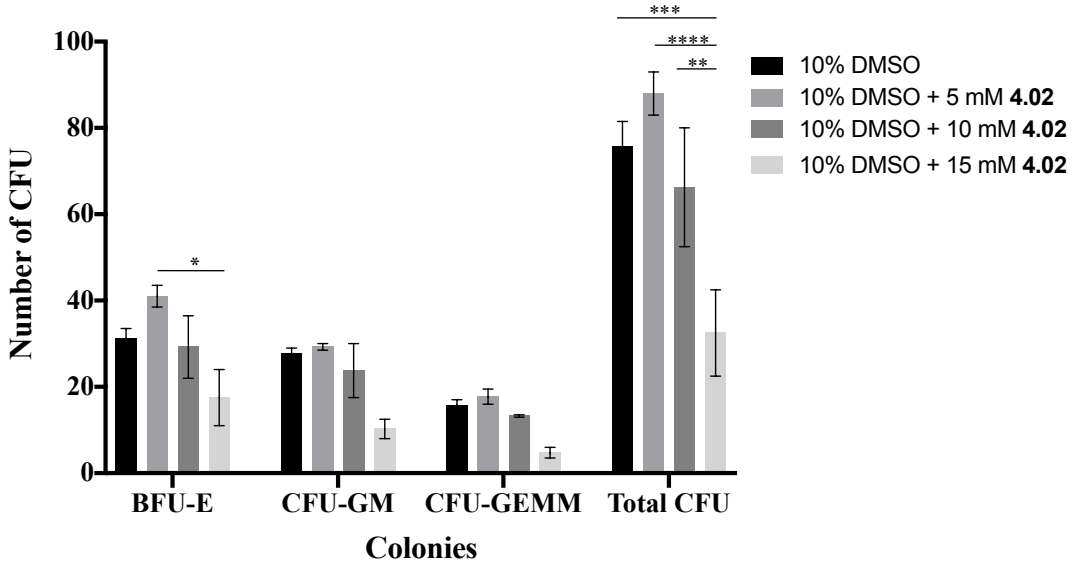

Figure 4.2.3.1. a) Post-thaw viabilities of leukocytes ($CD45^+$ cells) and HSPCs ($CD45^+CD34^+$ cells) after cryopreservation with gluconamide **4.02** determined by flow cytometry using ISHAGE-gating (mean ± SEM, n = 2-5 units: 10% DMSO assessed n = 5; 5 mM, 15 mM, and 27 mM **4.02** assessed n = 3; and 10 mM, 20 mM **4.02** assessed n = 2), and **b)** the clonogenic potential of UCB cells cryopreserved with gluconamide **4.02**, determined using the CFC assay (n = 2 units, 6 plates), where the net number of colonies per 50,000 TNC is presented as mean ± SEM. Sub-colonies of the total CFU include the CFU-GM, CFU-GEMM, and BFU-E. Asterisks indicate statistical significance found using two-way ANOVA with Tukey's multiple comparisons test (*$p < 0.05$, **$p < 0.01$, ***$p < 0.001$, ****$p < 0.0001$). No error shown if n< 3.

Prior work using small-scale experiments suggested that gluconamide **4.03** exerted a slight increase in HSPC functionality of HSPCs cryopreserved in the presence of the molecule; therefore, we were also interested about the outcome after using more clinically-relevant cryopreservation conditions (1 mL volumes with 10 x 10^6 TNC/mL). The post-thaw viability (**Figure 4.2.3.2a**) of cord blood cells in the presence of cryoadditive **4.03** is similar compared to the 10% DMSO control condition suggesting that the molecule maintains the preservation of HSPCs similarly to the 10% DMSO solution. The proportions of apoptotic and necrotic cells within each cell population were also similar among all cryosolution conditions (two-way ANOVA with Tukey's multiple comparisons test, $p > 0.05$). Meanwhile, the number of colonies observed from cells cryopreserved with IRI **4.03** is statistically increased compared to the control, and therefore, the CFC assay results indicate that the functionality of the cells is improved in the molecule's presence during cryopreservation (**Figure 4.2.3.2b**). This is especially apparent when considering the total number of colonies observed between the 10% DMSO condition and those conditions supplemented with **4.03** at 10 mM, 20 mM, 30 mM. The results obtained with gluconamide **4.03** are generally very promising (apart from cytotoxicity discussed in **Section 4.2.1**) and they are comparable to those previously observed with the small-scale experiments.[61] Further work is warranted with this cryosolution (specifically at its lower concentrations) in order to fully compare it to gluconamide **4.01**.

a)

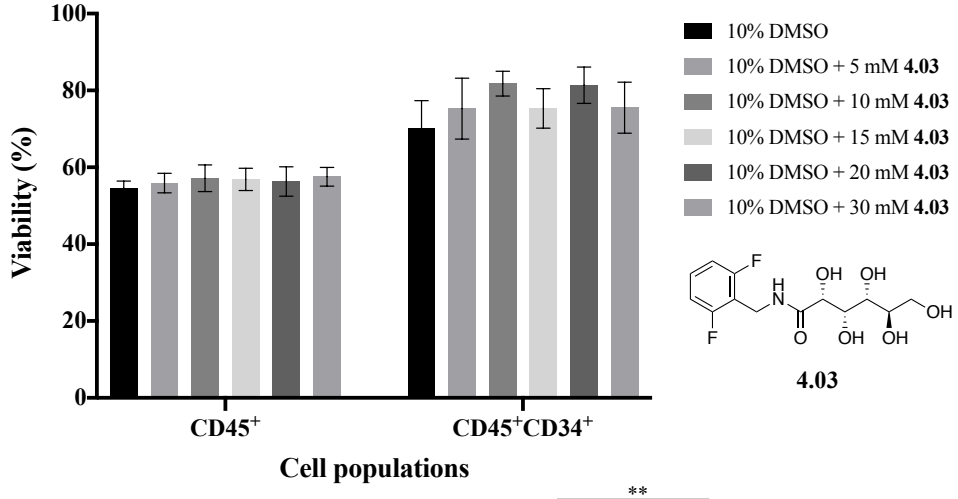

b)

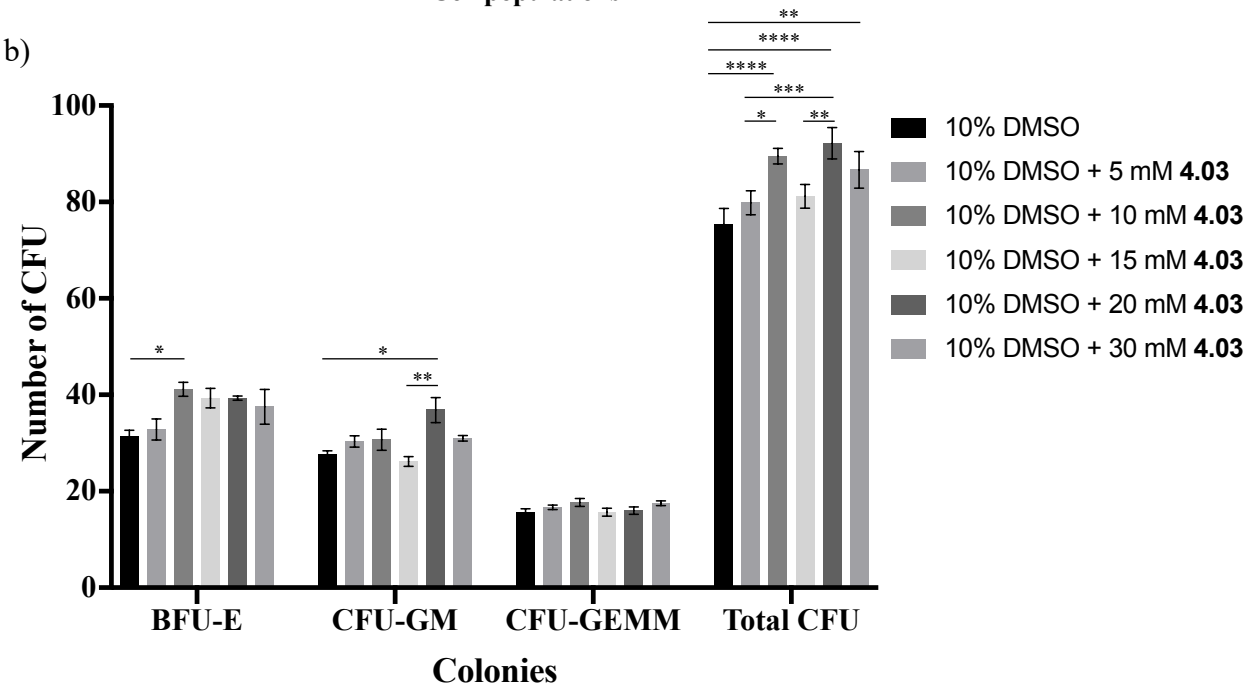

Figure 4.2.3.2. a) Post-thaw viabilities of leukocytes ($CD45^+$ cells) and HSPCs ($CD45^+CD34^+$ cells) after cryopreservation with gluconamide **4.03** determined by flow cytometry using ISHAGE-gating (presented as mean ± SEM, n = 3-4 units where 10 mM and 20 mM **4.03** conditions were assessed n = 3 and others were performed at n = 4), and **b)** the clonogenic potential of cryopreserved cells determined using the CFC assay, where the net number of colonies per 50,000 TNC is presented as the mean ± SEM (n = 3 units). Sub-colonies of the total CFU include the CFU-GM, CFU-GEMM, and BFU-E. No significant differences observed in a) using two-way ANOVA with Tukey's multiple comparisons test ($p > 0.05$); however, asterisks in b) indicate statistical significance (* $p < 0.05$, ** $p < 0.01$, *** $p < 0.001$, **** $p < 0.0001$).

The post-thaw viability of gluconamide **4.04** was re-assessed using the current protocols for cryopreservation of cord blood-derived cells. In accordance with the previous small-scale results,[61] the proportion (%) of viable cells within each (sub)population does not appear to differ substantially (results from one UCB unit) from the 10% DMSO condition (**Figure 4.2.3.3**) with the 1 mL cryopreservation volumes tested herein. Note that limited conclusions may be made based on this preliminary data (n = 1).

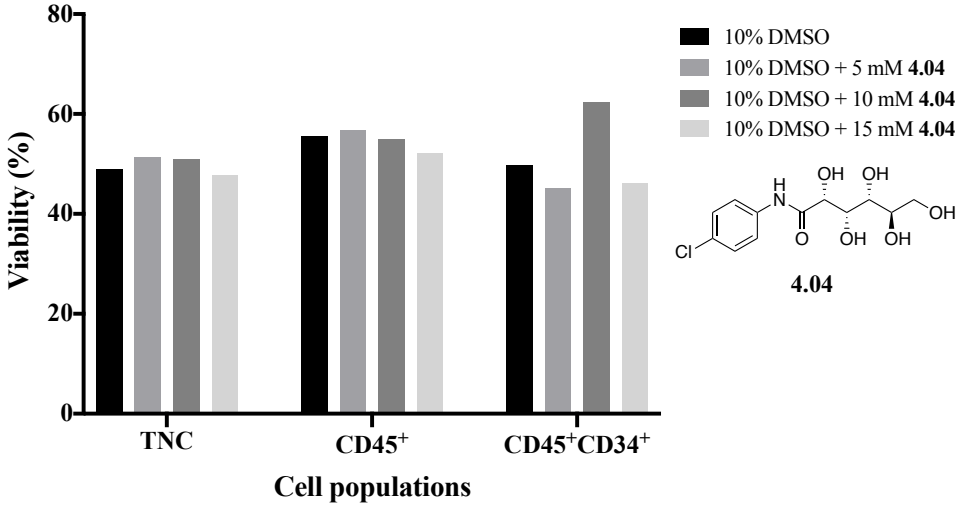

Figure 4.2.3.3. Proportion (%) of viable cells within each (sub)population after cryopreservation of cord blood cells in the presence of gluconamide **4.04**. Data presented as the mean of 1 unit.

Next, the novel gluconamides **4.05-4.07** were assessed for their ability to preserve the viability and functionality of HSPCs derived from human UCB. Using the same experimental methods as with the previous gluconamides, the proportion of viable cells within each population (TNC, leukocytes, and HSPCs) after cryopreservation with gluconamide **4.05** was determined by flow cytometry and staining using Annexin V and Sytox-AAD (**Figure 4.2.3.4a**). The proportion of viable cells within each population is similar to that obtained with the 10% DMSO control in this preliminary experiment (n = 1 independent UCB unit). Further, as the concentration of

gluconamide **4.05** is increased, a similar number of colonies were observed in the CFC assay thereby indicating that the functionality of the HSPCs may not be hindered by the higher concentrations of the cryoadditive (**Figure 4.2.3.4b**). Interestingly, these results appear similar to the results obtained for gluconamides **4.01** and **4.02** (the parent compounds for this derivative where **4.05** shares the 2-fluorophenyl functionality with **4.01** and the 4-methoxyphenyl moiety with **4.02**). Recall that gluconamides **4.02** and **4.05** exhibit similar cytotoxicity profiles while gluconamide **4.01** is not toxic up to its maximum solubilities (displayed in **Section 4.2.1**). Because of the difference in cytotoxicities, it is possible that the inclusion of the 2-fluoro component to gluconamide **4.05** results in maintaining the functionalities of HSPCs post-thaw similar to **4.01** (determined by examining the clonogenic potential of cells in the CFC assay) while cytotoxic gluconamide **4.02** is detrimental to the cell's clonogenic potentials.

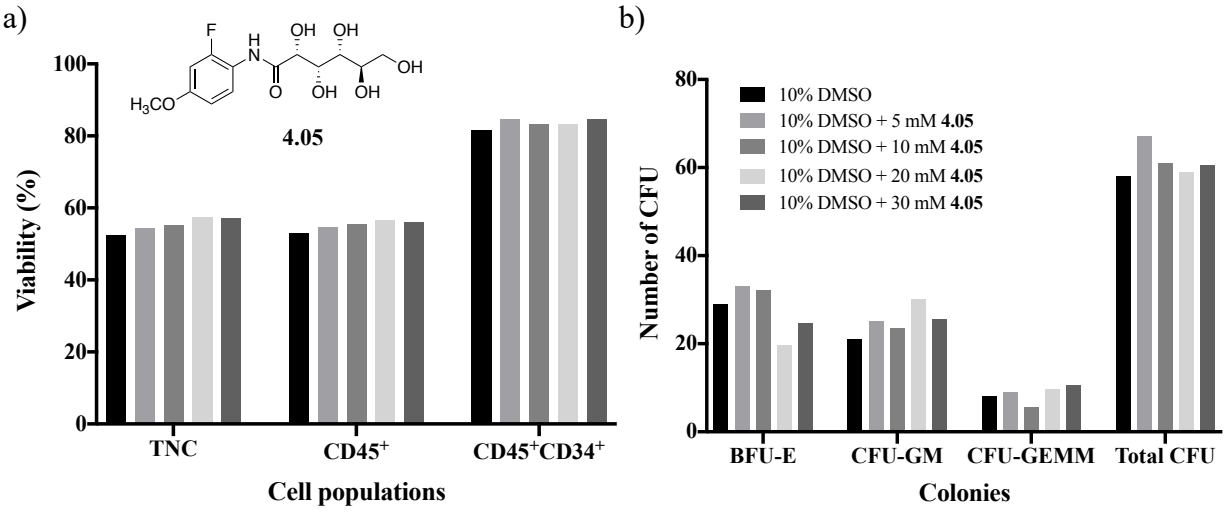

Figure 4.2.3.4. a) Post-thaw viabilities of total nucleated cells (TNC), leukocytes ($CD45^+$ cells), and HSPCs ($CD45^+CD34^+$ cells) after cryopreservation with gluconamide **4.05** determined by flow cytometry (n = 1), and **b)** the clonogenic potential of cord blood cells cryopreserved with gluconamide **4.05**, determined using the CFC assay, where the net number of colonies per 40,000 total nucleated cells is presented as the mean (n = 1 unit, 2 plates). Sub-colonies of the total CFU include the CFU-GM, CFU-GEMM, and BFU-E.

Finally, the post-thaw cell viabilities observed for the total nucleated cells (TNCs), leukocytes, and HSPCs (**Figure 4.2.3.5a**) were not found to be significantly different with or without the use of the azido-gluconamides **4.06** and **4.07**. Nor did there appear to be significant differences among the preliminary data obtained for the proportion of apoptotic or necrotic TNCs, leukocytes, or HSPCs. Interestingly, the post-thaw clonogenic potential of the cord blood-derived HSPCs appeared to increase with the use of **4.06** and **4.07** (**Figure 4.2.3.5b**). There was an approximately 1.5-fold increase in the number of Burst-Forming Unit-Erythroid (BFU-E) colonies and Colony-Forming Unit-Granulocyte, Monocyte (CFU-GM) colonies observed when cryopreserving cells with the gluconamides. These increases were noted in the total number of colonies observed with an increase in colonies with the use of gluconamide **4.07**. Moreover, improved TNC recoveries were also obtained when the conventional 10% DMSO cryosolution was supplemented with either of the IRIs (data not shown). Taken together, these initial cell viability and functionality data suggest that the azido-gluconamides may preserve the cord blood cells in a way that maintains the post-thaw cell viability whilst also improving HSPC functionality after cryopreservation. There is a notable improvement in preservation ability when comparing **4.06** and **4.07** to that of their parent compounds 2-fluorophenyl gluconamide **4.01** and 4-methoxyphenyl gluconamide **4.02** (especially when considering **4.02** to **4.07**). While **4.07** and **4.02** had similar cytotoxic properties at 5 mM (recall that this was a preliminary result obtained with the hepatic cell line), the cytotoxicity of gluconamide **4.06** at 5 mM appeared higher than its parent molecule **4.01** at that concentration. These results are very intriguing and warrant future investigation into how the azide molecules preserve the cells during the cryopreservation process.

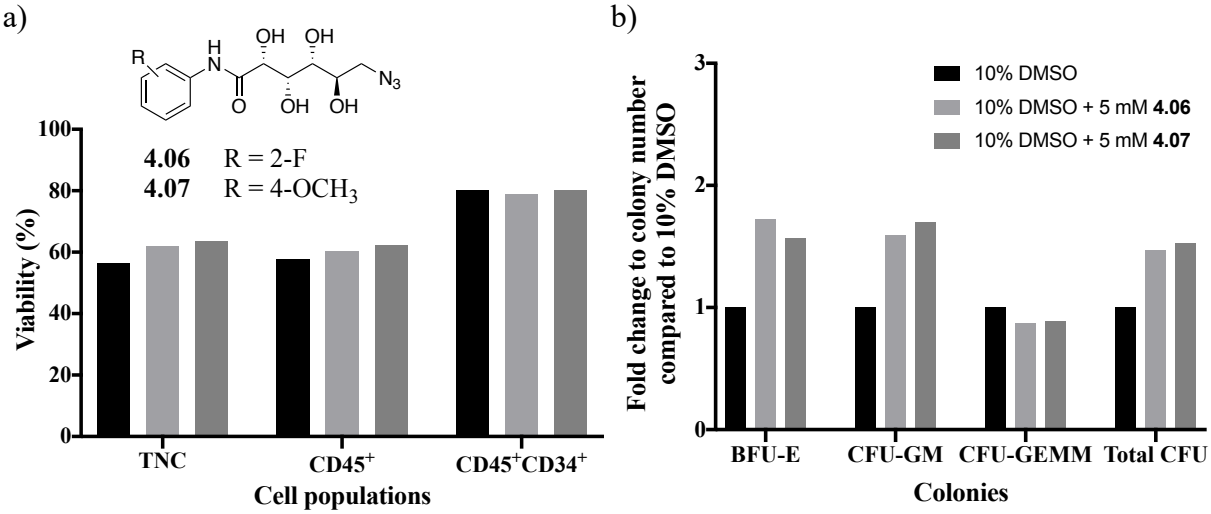

Figure 4.2.3.5. a) Post-thaw viabilities of total nucleated cells (TNC), leukocytes ($CD45^+$ cells), and HSPCs ($CD45^+CD34^+$ cells) after cryopreservation with gluconamides **4.06** and **4.07** determined by flow cytometry using the ISHAGE gating protocol, where data are presented as mean (n = 2 units), and **b)** the clonogenic potential of cord blood cells cryopreserved with gluconamides **4.06** and **4.07**, determined using the CFC assay, where data are presented as the average fold change compared to 10% DMSO (n = 2 units). Sub-colonies of the total CFU include the Colony-Forming Unit-Granulocyte, Monocyte (CFU-GM) population, the Colony-Forming Unit-Granulocyte, Erythrocyte, Monocyte, and Megakaryocyte (CFU-GEMM) population, and the Burst-Forming Unit-Erythroid (BFU-E) population.

Overall, using gluconamides **4.02** and **4.04** (the 4-methoxyphenyl and 4-chlorophenyl derivatives, respectively) as cryoadditives for the cryopreservation of cord blood cells is less successful than using *N*-(2-fluorophenyl)-D-gluconamide **4.01** (**Section 4.2.2**). Specifically, cryoadditives **4.02** and **4.04** were found to maintain the proportion of viable cells while, in the case of gluconamide **4.02**, reducing the functionalities of the HSPCs post-thaw. Gluconamide **4.03** (the 2,6-difluorobenzyl derivative), on the other hand, increased the number of colonies observed in the CFC assay post-thaw. While gluconamide **4.03** is less IRI-active than gluconamide **4.01**, the promising results obtained (regarding its use as a cryoprotectant for cord

blood cells) suggests further analysis regarding the full cryoprotecting nature of this molecule should be conducted. Preliminary data suggests that gluconamide **4.05** (the 2-fluoro-4-methoxyphenyl derivative) maintains both the cell viability and the functionality of the cells after cryopreservation similar to the 10% DMSO control. Interestingly, the use of azido-gluconamide **4.06** (2-F) and **4.07** (4-OCH_3) resulted in increased HSPC functionality after cryopreservation; an indication that further studies should be conducted on azides and their role in the cryopreservation of UCB. Notably, these future studies will have to overcome significant solubility issues. When considering the cytotoxicities (**Section 4.2.1**) that each molecule displayed and comparing this to the resulting clonogenic potential of HSPCs cryopreserved upon treatment with a gluconamide, we conclude that molecules with increased cytotoxicity (e.g. gluconamide **4.02**) resulted in significantly reduced HSPC functionality after cryopreservation while those gluconamides with minimal or no observed cytotoxicity (e.g. gluconamide **4.01**, **4.03**, **4.06**, **4.07**) led to maintained or improved levels of HSPC clonogenic potential. Within these cases, the mechanism by which cellular injuries occurred may be different and further studies are necessary to grasp the nature of each molecule's toxicity. For example, previous preliminary data (collaboration with Prof. Wolkers discussed within Dr. Jennie Briard's thesis) suggested that gluconamides may interact with cell membranes based on observing carboxyfluorescein leakage in liposomes after incubation with a gluconamide. Further investigation into this is certainly warranted since these interactions may alter post-thaw HSPC signaling among other factors. Metabonomic studies could also offer substantial insight into the physiological impact felt by HSPCs cryopreserved in the presence of a gluconamide thereby facilitating future cryoprotectant development. This would be especially impactful for UCB research where the availability and quality of a unit donated for research purposes varies and can

contribute to limited sample sizes for experiments as a result. Taken altogether, gluconamide **4.01** remains the strongest contender amongst all the gluconamides tested owing to its lack of cytotoxicity and its ability to maintain and slightly increase the viabilities and functionalities of cord blood cells after cryopreservation. With these results in mind, **Section 4.3** delves into the *in vivo* impact of using the 2-fluorphenyl gluconamide **4.01** as a cryoprotectant for human umbilical cord blood.

4.3 The impact of an *N*-aryl-D-gluconamide ice recrystallization inhibitor on engraftment activities of cryopreserved cord blood grafts

Owing to the promising results obtained *in vitro* when using IRI-active gluconamide **4.01** as a cryosupplement, we then sought to determine the molecule's *in vivo* impact on the engraftment activities of cryopreserved cord blood grafts transplanted in immunodeficient mice (NSG mice, or NOD scid gamma mice).[65] Four cord blood units were processed following standard protocols performed at the Canadian Blood Services (and as described in **Section 4.2.2.1** and the **Experimental** section). The TNCs obtained from each unit were cryopreserved in the absence or presence of IRI **4.01** (concentrations were based off the outcomes of the previous *in vitro* small-scale studies[61]) in a cryosolution consisting of 10% dimethyl sulfoxide and 5% w/v dextran in 0.9% saline. Specifically, there were three cord blood units cryopreserved with a concentration of 25 mM gluconamide **4.01** and one unit preserved with 10 mM gluconamide **4.01**, and the results of these four units were combined for statistical purposes as outlined below. After thawing the cryovials using the optimized two-step dilute protocol,[71] UCB cells were incubated with the OKT-3 antibody for 20 minutes at 4 °C in order to prevent xenogeneic GVHD.[80] With approval of the Animal Care Committee at the University of Ottawa

and by following the standards set out by the Animal for Research Act and the Canadian Council on Animal Care, the serial transplantation assay involving NOD.Cg-*Prkdc*^{scid} *Il2rg*^{tm1Wjl}*/SzJ* mice and subsequent analysis were performed by Dr. Suria Jahan. This strain of mouse was an ideal model for analyzing the hematopoietic recovery of the transplanted cord blood cells due to their deficiency in mature T cells, B cells, natural killer (NK) cells, numerous cytokine signalling pathways, and multiple deficiencies in their innate immunity.[81,82] Eight-to-ten-week-old mice were first irradiated followed by intravenous transplantation, where all conditions were sex- and age-matched. **Figure 4.3.1.1** highlights the experimental design as well as details of the transplantation experiments.

a)

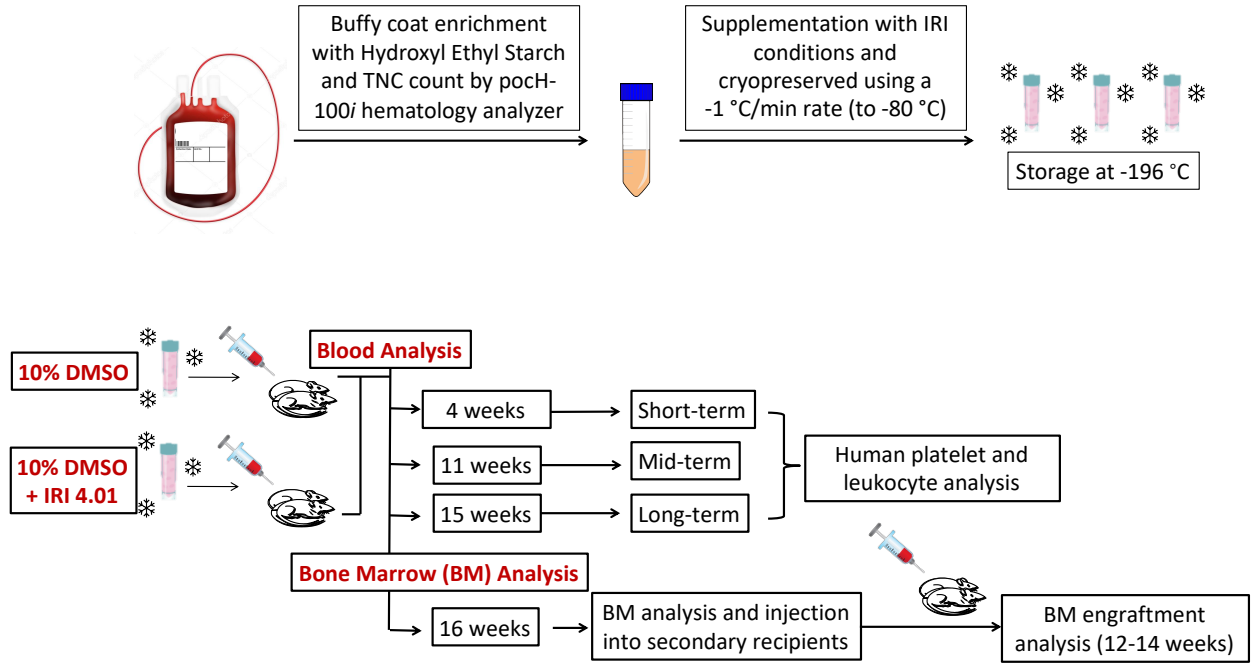

b)

Unit #	Condition	% Frequency of $CD34^+$ cells	% Viability of TNC	% Viability of $CD34^+$ cells	TNC dose transplanted ($x10^6$/mice[2])
1	DMSO IRI **4.01** (25 mM)	0.29 0.28	61.1 64.6	70.5 70.1	2.00 2.00
2	DMSO IRI **4.01** (25 mM)	0.72 0.65	50.9 47.6	65.6 67.9	1.50 1.50
3	DMSO IRI **4.01** (25 mM)	0.57 0.59	43.6 41.3	69.5 59.6	2.00 2.00
4	DMSO IRI **4.01** (10 mM)	0.20 0.23	56.6 51.8	56.4 56.7	3.00 3.00
Overall Mean (SD)	**DMSO** **IRI 4.01**	**0.45 (0.2)** **0.44 (0.2)**	**53.0 (7.6)** **51.3 (9.9)**	**65.5 (6.4)** **63.6 (6.4)**	**2.10 (0.6)** **2.10 (0.6)**

Figure 4.3.1.1. a) The experimental design for determining the impact of gluconamide **4.01** on the engraftment activities of cryopreserved cord blood grafts in immunodeficient mice, and b) details of the cord blood units cryopreserved for transplant experiments including the post-thaw viabilities of the $CD45^+$ and $CD34^+$ cell populations of the units (reprinted with permission, see reference 65).[65]

Throughout the *in vivo* experiments, the human engraftment analyses by flow cytometry or colony-forming assay were performed by researchers at the Canadian Blood Services including Dr. Suria Jahan, Dr. Javed Manesia, and Roya Pasha, and included analysis at short-term (4-weeks), mid-term (<12-weeks), and long-term (<16-weeks) time points as well as the bone marrow analysis (after 16-weeks) post-transplantation. Notably, analyses at each time point involved investigating cell populations and lineages commonly used in the literature for serial transplantation experiments. It is also important to acknowledge biostatistician Dr. Qi-Long Yi for statistical analyses performed for this study. The statistical software SAS/STAT 9.3 and GraphPad Prism (version 7) were used for statistical analysis, where the engraftment data were log-transformed prior to statistical analysis, and where p values below or equal to 0.05 were considered significant. There was a total of four cord blood units used for the hematopoietic xenotransplantation study, where three of the units were cryopreserved either with or without 25 mM *N*-(2-fluorophenyl)-D-gluconamide **4.01** and one of the units was cryopreserved either with or without 10 mM gluconamide **4.01**. Notably, there are solely two conditions considered for this study: the mice transplanted with cord blood cells cryopreserved using a cryosolution consisting of 10% dimethyl sulfoxide and 5% w/v dextran in 0.9% saline (n = 4 units) and those mice transplanted with cord blood cells cryopreserved using the 10% DMSO cryosolution supplemented with gluconamide **4.01** (n = 4, where the engraftment outcomes of the two different IRI conditions were analyzed together). A mixed model analysis was used to determine the significant differences between the two conditions and the potential for a clustering problem was controlled by also modelling for donor random effects.

4.3.1 Post-transplantation analysis of murine peripheral blood

Peripheral blood analysis at short- (4 weeks), mid- (11 weeks), and long-term (15 weeks) time points of the serial transplantation assay enabled the investigation of human platelet and leukocyte engraftment in the immunodeficient mice. Specifically, the levels of human platelets (hPLT) and human $CD45^+$ leukocytes were tracked by flow cytometry analysis of mouse peripheral blood. The two conditions, mice transplanted with cord blood cells cryopreserved with a 10% dimethyl sulfoxide cryosolution (with 5% w/v dextran in 0.9% saline) and mice transplanted with cells cryopreserved with the 10% DMSO solution supplemented with gluconamide **4.01** at 25 mM or 10 mM (**Figure 4.3.1.2** and **Figure 4.2.1.3**) were analyzed. Throughout the xenotransplantation study, the levels of hPLT were generally increased in the IRI-cohort compared to the mice transplanted with the 10% DMSO cryosolution without the presence of IRI **4.01**.[65] At the short-term time point, the increase in hPLT was not significant ($p = 0.17$). However, the enhanced levels of hPLT were more evident as time progressed, as there was a 3.7- and 2.0-fold increase of hPLTs in the IRI-cohort at the mid- ($p < 0.001$) and long-term ($p < 0.05$) time points.[65] Taking an overall snapshot of the hPLT levels by combining the entire data set supports the observed trend; there were higher levels of hPLTs in the group of mice transplanted with cells cryopreserved in the presence of **4.01** compared to the levels in the control condition ($p < 0.001$).

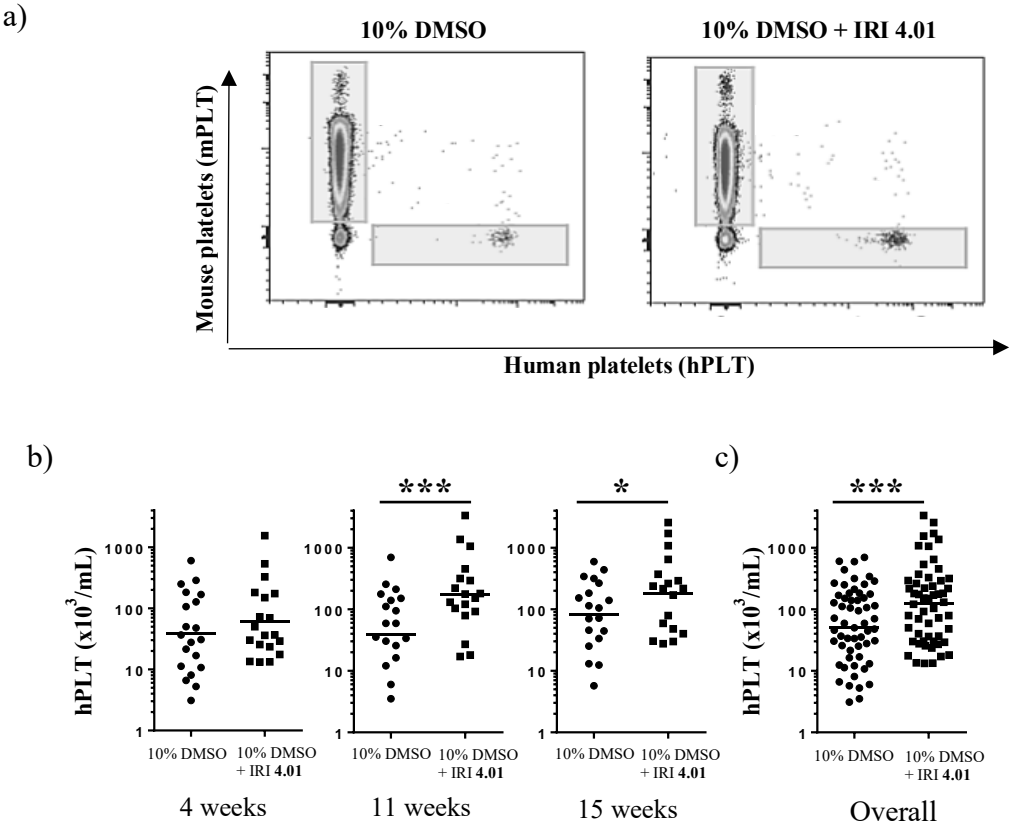

Figure 4.3.1.2. The human platelet engraftment activity of cord blood cells cryopreserved with or without IRI **4.01** supplementation (reprinted with permission, see reference 65).[65] **a)** An example of the flow cytometry analysis of periphery blood highlighting the detection of human and mouse platelets in the mice, **b)** human platelet levels as a function of time, and **c)** the overall levels of human platelets in mice. Data points indicate the mean level for each mouse and the geometric mean is represented by the line (17-19 mice per group). Data were analyzed using a time-adjusted mixed model (17-19 mice per group, n = 4). Asterisks indicate statistical significance (* $p < 0.05$, *** $p < 0.001$).

The overall leukocyte ($CD45^+$ population) levels in the peripheral blood of the humanized mice, meanwhile, were maintained regardless of the presence or absence of gluconamide **4.01** during the cryopreservation of the cord blood (**Figure 4.3.1.3**).[65] The frequency of $CD45^+$ cells were similar between the two studied conditions at the short- ($p = 0.064$), mid- ($p = 0.272$), and long-term ($p = 0.281$) time points. Combining the data set from all

the time points confirms that the frequency of human leukocytes was similar between the two cohorts ($p = 0.193$). While the flow cytometry analysis detected the presence of human myeloid ($CD45^+CD33^+$) and B-cell ($CD45^+CD19^+$) populations in all the mice, it was only at the 15-week post-transplantation time point that the frequency of myeloids in the IRI-mice group was slightly increased over the control group ($p < 0.05$). At this long-term time point, the periphery of the mice with UCB cells cryopreserved with IRI **4.01** had a mean myeloid frequency of 0.80% ± 0.78 (standard deviation) while the mice group that had transplanted cord blood cells cryopreserved with DMSO alone had a mean myeloid frequency of 0.59% ± 0.59. These results together suggest that the levels of leukocytes are maintained post-transplantation when gluconamide **4.01** is used as a supplement to the cryosolution of cord blood cells. One possible reason for why there isn't a larger difference observed between the leukocyte levels of the two cohorts like that observed for human platelet levels is due to the lifespan of those cell populations in a murine system. Specifically, phagocytosis leads to a half-life of approximately 12 hours for human platelets in mice, while leukocytes can remain present for weeks or months.[83,84]

a)

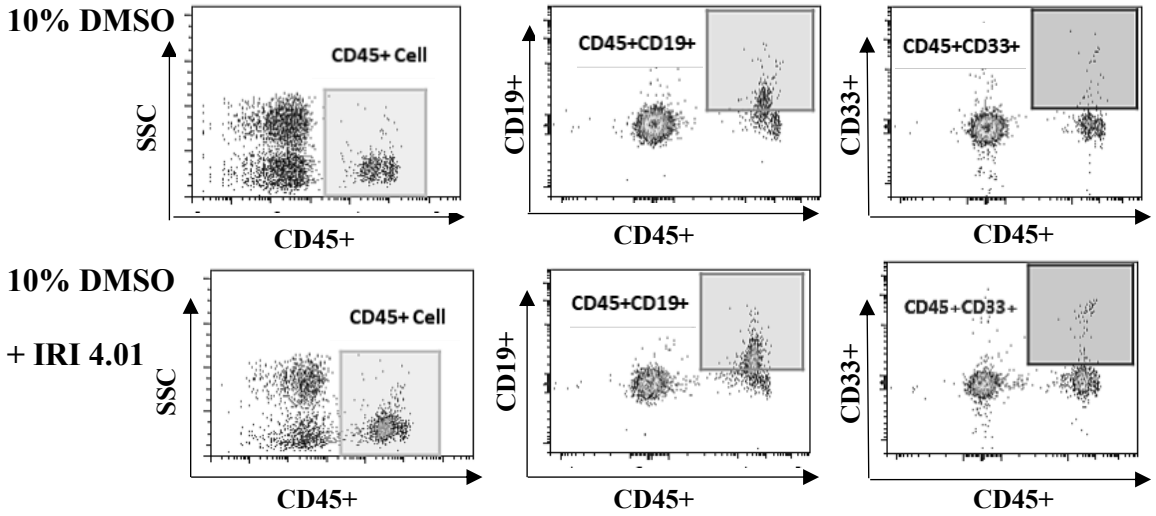

b)

Condition	4 weeks	11 weeks	15 weeks	Overall
10% DMSO	2.5 ± 0.9	9.3 ± 4.3	14.7 ± 5.5	9.2 ± 5.1
10% DMSO + IRI **4.01**	2.1 ± 0.9	12.4 ± 4.8	17.1 ± 7.0	9.5 ± 6.4

Figure 4.3.1.3. The human leukocyte ($CD45^+$) engraftment activity of cord blood cells cryopreserved with or without IRI **4.01** supplementation, where $CD45^+CD33^+$ are myeloid cells and $CD45^+CD19^+$ are B-cells (reprinted with permission, see reference 65).[65] **a)** An example of the flow cytometry analysis of periphery blood highlighting the detection of human leukocytes present in the humanized mice, and **b)** the frequency of human $CD45^+$ leukocytes at short-, mid-, and long-term time points (data presented as the mean ± SEM of 17-19 mice per group, n = 4).

Along with the levels of leukocytes being similar in both conditions (in the presence or absence of IRI **4.01**) of the hematopoietic xenotransplantation studies, the enhanced number of human platelets observed in the IRI-group (at short- and long-term time points, and overall levels throughout the assay) suggest that supplementation of the cryomedium of HSPCs with gluconamide **4.01** increases the engraftment abilities of cryopreserved umbilical cord blood.[65] This enhancement of platelet numbers is promising since the platelet recovery in recipients of cord blood transplantation in the clinic is delayed compared to the time for platelet reconstitution

in recipients receiving stem cell grafts from other sources (e.g. bone marrow or adult peripheral blood). By improving the cryopreservation methods of cord blood stem cells using an IRI, these results suggest that it is indeed possible to enhance the engraftment abilities of the stem cells after transplantation into a recipient.

4.3.2 Bone marrow analysis post-transplantation of cryopreserved cord blood grafts

With promising results observed from analysis of the peripheral blood of primary recipients, our attention was then turned to the analysis of the bone marrow of these mice in order to assess the long-term engraftment potential of the previously-cryopreserved cord blood. Therefore, after 16 weeks post-transplantation, the bone marrows of the primary recipients were analyzed followed by further transplantation of this bone marrow into secondary recipients (results detailed below). The levels of leukocytes observed in the mice bone marrow of the IRI-cohort compared to the DMSO-control group indicated that there was an enhanced level of progenitors present in the mice transplanted with IRI-preserved cord blood (**Figure 4.3.2.1**).[65] This included increased levels of total colonies in the colony-forming cell (CFC) assay as well as within various sub-populations: including the Colony-Forming Unit-Granulocyte, Monocyte (CFU-GM) population and the Colony-Forming Unit-Granulocyte, Erythrocyte, Monocyte, and Megakaryocyte (CFU-GEMM) population. The level of the Burst-Forming Unit-Erythroid (BFU-E) population was similar between both mouse cohorts. Differentiation abilities of HSPCs cryopreserved with IRI **4.01** were also maintained compared to the control HSPCs as observed by detecting similar myeloid and lymphoid lineages present in the bone marrow of the primary recipients of both cohorts. Note that the lineages assessed are routinely analyzed in similar transplantation experiments in the literature.

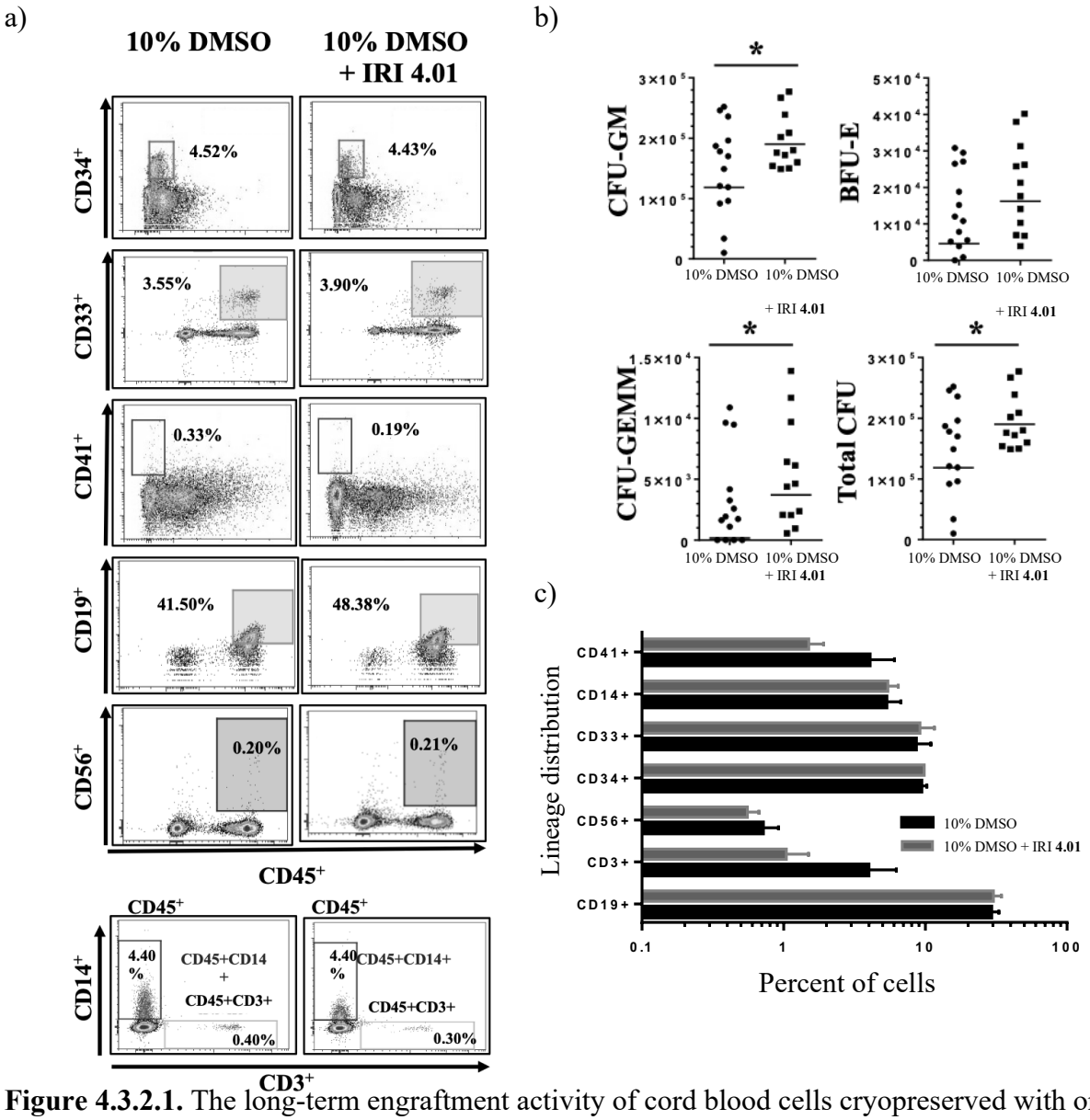

Figure 4.3.2.1. The long-term engraftment activity of cord blood cells cryopreserved with or without IRI **4.01** supplementation, where $CD45^+CD41^+$ are megakaryocytes, where $CD45^+CD14^+$ are monocytes, $CD45^+CD33^+$ are myeloids, $CD45^+CD34^+$ are progenitor stem cells, $CD45^+CD56^+$ are natural killer cells, $CD45^+CD3^+$ are T-cells, and $CD45^+CD19^+$ are B-cells (reprinted with permission, see reference 65).[65] **a)** An example of the flow cytometry analysis for the human bone marrow engraftment highlighting the detection of human lympho-myeloids present in the humanized mice, **b)** the net number of HSPCs present in the bone marrow of both mice cohorts (n = 3 with 11 mice per group) with asterisks indicating statistical significance ($p < 0.05$), and **c)** the lineage distribution detected in the bone marrow of the mice presented as the mean ± the standard error of the mean (n = 4).

The mean engraftment levels observed in mice transplanted with UCB cryopreserved with the IRI was enhanced compared to the levels observed in mice injected with UCB cryopreserved with DMSO alone (**Figure 4.3.2.2**, $p < 0.05$). This signifies that the overall human chimerism observed in the mice was increased using IRI **4.01** as a cryosupplement.

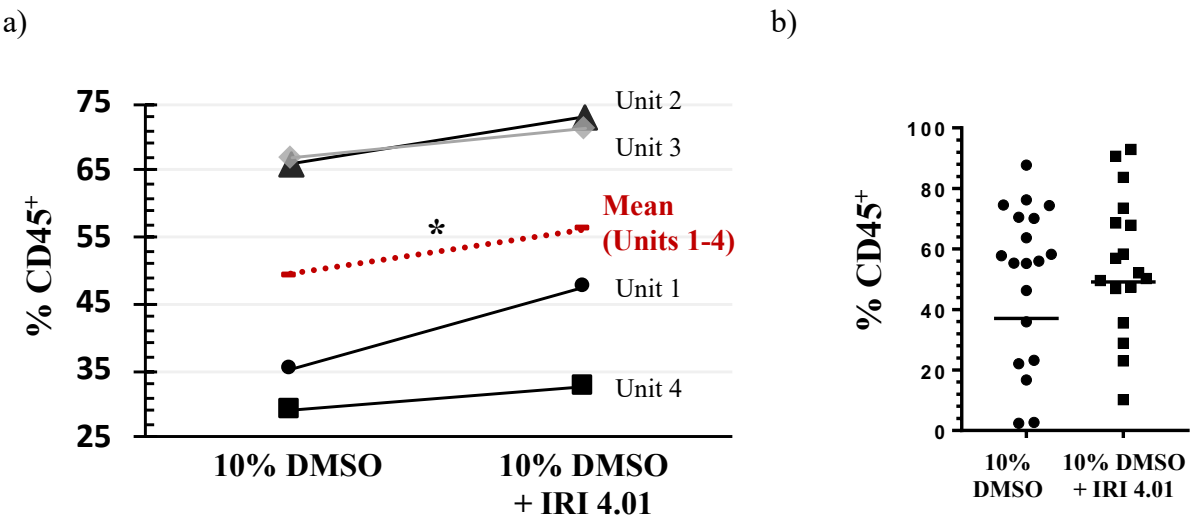

Figure 4.3.2.2. The human leukocyte ($CD45^+$) long-term engraftment activity of cord blood cells cryopreserved with or without IRI **4.01** supplementation, as detected in the bone marrow of primary recipients 16-weeks post-transplantation (reprinted with permission, see reference 65).[65] **a)** the frequency of human $CD45^+$ leukocytes for each unit tested including a dashed line representing the mean (n = 4, and statistical significance indicated by asterisk where * $p < 0.05$ from a paired t-test), and **b)** the overall levels of human $CD45^+$ leukocytes present in each mouse (geometric mean indicated by the line, 17-19 mice total per condition, n = 4).

The secondary transplantation portion of the serial transplantation assay involved transplantation of 85% of the bone marrow obtained from the primary recipients into secondary recipients followed by bone marrow analysis of the secondary recipients after 12-14 weeks (**Figure 4.3.2.3**). Importantly, the serial transplantation assay is considered a "gold standard" for

investigating the ability of cryopreserved cord blood grafts to replenish an organism's hematopoietic system through assessing the self-renewal and longevity of the HSPCs.[76,77] The results of three independent secondary transplant experiments indicated that the level of human chimerism in the bone marrow of secondary recipients comprising the IRI-mouse cohort was similar to the level observed in the DMSO only cohort ($p = 0.37$).[65] This once again confirms the conclusion obtained from the bone marrow analysis of the primary recipients: the supplementation of a cryomedium with IRI **4.01** preserves the long-term potential of cryopreserved HSPCs from umbilical cord blood.

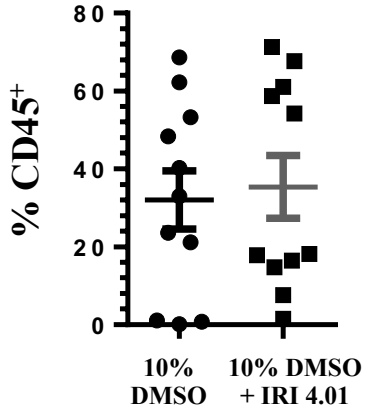

Figure 4.3.2.3. The overall frequency of human leukocytes (% $CD45^+$ cells) in the bone marrow of secondary recipients represented as the mean ± standard error of the mean for three experiments (reprinted with permission, see reference 65).[65]

The improved bone marrow engraftment observed in primary recipients along with the enhanced levels of platelets observed in the peripheral blood of the primary mice suggest a promising and first-of-its-kind result: improving the cryopreservation of cord blood grafts using an ice recrystallization inhibitor as a supplement to the conventional cryosolution can improve the engraftment activities of a stem cell graft. These *in vivo* results make it evident that reducing

the cryoinjury associated with the freezing and thawing processes of cryopreservation can lead to significant clinical improvements in the future.

4.4 Summary

Collection of hematopoietic stem and progenitor cells (HSPCs) from human umbilical cord blood (UCB) offers tremendous advantages over other sources, such as the bone marrow and adult peripheral blood collections, including that the collection of this readily available and HSPC-rich source is not invasive for the cord blood donor, there are less stringent HLA matching criteria, and lower rates of Graft-versus-Host disease are observed in recipients of UCB transplants.[6,8–11] Despite these unique advantages, UCB remains the least common source for HSCTs largely due to the reduced number of cells isolated from UCB compared to the other sources. The low cell dose obtained from a single unit is associated with delayed hematopoietic recovery, specifically that of neutrophil and platelets, which can lead to adverse outcomes.[9,23–26] Notably, with the increasing number of diseases and disorders that can be treated with hematopoietic stem cell transplants (HSCTs), there is a tremendous need for improving the number and quality of cord blood cells for transplants. One method of doing this would be to improve how cord blood is cryopreserved by improving the post-thaw viabilities and functionalities of the HSPCs after preservation. Ice recrystallization inhibitors (IRIs) can mitigate cell injuries associated with the uncontrollable growth of ice crystals during the freezing and thawing processes of cryopreservation. Based on previous work in the Ben laboratory, including work by Dr. Briard in identifying IRIs able to improve the post-thaw function of cryopreserved HSPCs,[61] we hypothesized that *N*-aryl-D-gluconamides would improve the engraftment activities of cord blood grafts *in vivo* in addition to the improvements exhibited *in vitro*. This project,

therefore, began by identifying gluconamides with low cytotoxicity profiles in HepG2 cells, and the results indicated that gluconamide **4.01** (*N*-(2-fluorophenyl)-D-gluconamide) was the least toxic out of the IRIs assessed. Gluconamides **4.02-4.05** all exhibited increasing levels of cytotoxicity as their concentrations were increased in cell culture media. *C*6-azido-gluconamides, such as the 2-fluorophenyl derivative **4.06**, resulted in reduced levels of viable HepG2 cells compared to their parent compounds such as gluconamide **4.01** in preliminary studies.

Next, the abilities of the gluconamides to preserve cord blood cells in addition to the conventional cryoprotective agents were assessed. Specifically, gluconamide **4.01** maintained high levels of post-thaw cell viabilities and cell functionalities after cryopreservation. Gluconamides **4.03, 4.06, 4.07** warrant future investigation into their full potential as cryoprotectants for cord blood owing to the increased functionalities of the HSPCs observed after cryopreservation in the presence of those molecules. Nevertheless, with the promising *in vitro* results obtained for *N*-(2-fluorophenyl)-D-gluconamide **4.01**, the molecule was chosen as the ideal candidate for the first *in vivo* studies performed with regards to IRI molecules. Using the serial xenotransplantation assay which is the 'gold-standard' method for assessing the hematopoietic stem cell engraftment activities, the activities of stem cells cryopreserved with the cryoadditive **4.01** were assessed by detecting human cell populations in the mice peripheral blood and in the bone marrow. Supplementation of the cryomedium with **4.01** was found to enhance the engraftment activities of the cord blood grafts. Increased levels of platelets were found in the periphery at mid- and long-term time points; a result that is especially noteworthy since in the clinic, delayed platelet recoveries in patients of HSCTs have been associated with UCB transplants. Further, human leukocyte chimerism was increased at 16-weeks post-transplantation as well as the levels of hematopoietic progenitors. Finally, the results also

indicated that the long-term hematopoietic stem cells were also well preserved with gluconamide **4.01** as a cryo-supplement. Overall, the use of non-toxic gluconamide **4.01** during cryopreservation maintains stem cell properties, and notably, it leads to enhanced platelet and bone marrow engraftment activities in primary murine recipients. After considering the results discussed herein, it is clear that the use of an ice recrystallization inhibitor as a supplement in the cryopreservation of hematopoietic stem and progenitor cells can offer significant potential for future clinical applications.

4.5 References

(1) Dessels, C.; Alessandrini, M.; Pepper, M. S. Factors Influencing the Umbilical Cord Blood Stem Cell Industry: An Evolving Treatment Landscape. *Stem Cells Transl. Med.* **2018**, *7* (9), 643–650. https://doi.org/10.1002/sctm.17-0244.

(2) WHO | Haematopoietic Stem Cell Transplantation HSCtx. *WHO* **2013**.

(3) Niederwieser, D.; Baldomero, H.; Szer, J.; Gratwohl, M.; Aljurf, M.; Atsuta, Y.; Bouzas, L. F.; Confer, D.; Greinix, H.; Horowitz, M.; Iida, M.; Lipton, J.; Mohty, M.; Novitzky, N.; Nunez, J.; Passweg, J.; Pasquini, M. C.; Kodera, Y.; Apperley, J.; Seber, A.; Gratwohl, A. Hematopoietic Stem Cell Transplantation Activity Worldwide in 2012 and a SWOT Analysis of the Worldwide Network for Blood and Marrow Transplantation Group Including the Global Survey. *Bone Marrow Transplant.* **2016**, *51* (6), 778–785. https://doi.org/10.1038/bmt.2016.18.

(4) D'Souza, A.; Lee, S.; Zhu, X.; Pasquini, M. Current Use and Trends in Hematopoietic Cell Transplantation in the United States. *Biology of Blood and Marrow Transplantation*. Elsevier Inc. September 1, 2017, pp 1417–1421. https://doi.org/10.1016/j.bbmt.2017.05.035.

(5) Bruno, B.; Rotta, M.; Patriarca, F.; Mordini, N.; Allione, B.; Carnevale-Schianca, F.; Giaccone, L.; Sorasio, R.; Omedè, P.; Baldi, I.; Bringhen, S.; Massaia, M.; Aglietta, M.; Levis, A.; Gallamini, A.; Fanin, R.; Palumbo, A.; Storb, R.; Ciccone, G.; Boccadoro, M. A Comparison of Allografting with Autografting for Newly Diagnosed Myeloma. *N. Engl. J. Med.* **2007**, *356* (11), 1110–1120. https://doi.org/10.1056/NEJMoa065464.

(6) Mehta, R. S.; Rezvani, K.; Olson, A.; Oran, B.; Hosing, C.; Shah, N.; Parmar, S.; Armitage, S.; Shpall, E. J. Novel Techniques for Ex Vivo Expansion of Cord Blood: Clinical Trials. *Front. Med.* **2015**, *2*, 89. https://doi.org/10.3389/fmed.2015.00089.

(7) Gluckman, E.; Broxmeyer, H. E.; Auerbach, A. D.; Friedman, H. S.; Douglas, G. W.; Devergie, A.; Esperou, H.; Thierry, D.; Socie, G.; Lehn, P.; Cooper, S.; English, D.; Kurtzberg, J.; Bard, J.; Boyse, E. A. Hematopoietic Reconstitution in a Patient with Fanconi's Anemia by Means of Umbilical-Cord Blood from an HLA-Identical Sibling. *N. Engl. J. Med.* **1989**, *321* (17), 1174–1178. https://doi.org/10.1056/NEJM198910263211707.

(8) Hordyjewska, A.; Popiołek, Ł.; Horecka, A. Characteristics of Hematopoietic Stem Cells of Umbilical Cord Blood. *Cytotechnology*. Kluwer Academic Publishers May 1, 2015, pp 387–396. https://doi.org/10.1007/s10616-014-9796-y.

(9) Keating, A. K.; Langenhorst, J.; Wagner, J. E.; Page, K. M.; Veys, P.; Wynn, R. F.; Stefanski, H.; Elfeky, R.; Giller, R.; Mitchell, R.; Milano, F.; O'Brien, T. A.; Dahlberg, A.; Delaney, C.; Kurtzberg, J.; Verneris, M. R.; Boelens, J. J. The Influence of Stem Cell Source on Transplant Outcomes for Pediatric Patients with Acute Myeloid Leukemia. *Blood Adv.* **2019**, *3* (7), 1118–1128. https://doi.org/10.1182/bloodadvances.2018025908.

(10) Bender, J. G.; Unverzagt, K.; Walker, D. E.; Lee, W.; Smith, S.; Williams, S.; Van Epps, D. E. Phenotypic Analysis and Characterization of CD34+ Cells from Normal Human Bone Marrow, Cord Blood, Peripheral Blood, and Mobilized Peripheral Blood from Patients Undergoing Autologous Stem Cell Transplantation. *Clin. Immunol. Immunopathol.* **1994**, *70* (1), 10–18. https://doi.org/10.1006/clin.1994.1003.

(11) Gluckman, E. Ten Years of Cord Blood Transplantation: From Bench to Bedside. *British Journal of Haematology*. October 2009, pp 192–199. https://doi.org/10.1111/j.1365-2141.2009.07780.x.

(12) Rocha, V.; Sanz, G.; Gluckman, E. Umbilical Cord Blood Transplantation. *Curr. Opin. Hematol.* **2004**, *11* (6), 375–385. https://doi.org/10.1097/01.moh.0000145933.36985.eb.

(13) Rocha, V.; Gluckman, E. Improving Outcomes of Cord Blood Transplantation: HLA Matching, Cell Dose and Other Graft- and Transplantation-Related Factors. *Br. J. Haematol.* **2009**, *147* (2), 262–274. https://doi.org/10.1111/j.1365-2141.2009.07883.x.

(14) Danby, R.; Rocha, V. Improving Engraftment and Immune Reconstitution in Umbilical Cord Blood Transplantation. *Frontiers in Immunology*. Frontiers Research Foundation February 24, 2014, p 68. https://doi.org/10.3389/fimmu.2014.00068.

(15) Gluckman, E.; Rocha, V.; Boyer-Chammard, A.; Locatelli, F.; Arcese, W.; Pasquini, R.; Ortega, J.; Souillet, G.; Ferreira, E.; Laporte, J. P.; Fernandez, M.; Chastang, C. Outcome of Cord-Blood Transplantation from Related and Unrelated Donors. *N. Engl. J. Med.* **1997**, *337* (6), 373–381. https://doi.org/10.1056/NEJM199708073370602.

(16) Rubinstein, P.; Carrier, C.; Scaradavou, A.; Kurtzberg, J.; Adamson, J.; Migliaccio, A. R.; Berkowitz, R. L.; Cabbad, M.; Dobrila, N. L.; Taylor, P. E.; Rosenfield, R. E.; Stevens, C. E. Outcomes among 562 Recipients of Placental-Blood Transplants from Unrelated

Donors. *N. Engl. J. Med.* **1998**, *339* (22), 1565–1577. https://doi.org/10.1056/NEJM199811263392201.

(17) Barker, J. N.; Scaradavou, A.; Stevens, C. E. Combined Effect of Total Nucleated Cell Dose and HLA Match on Transplantation Outcome in 1061 Cord Blood Recipients with Hematologic Malignancies. *Blood* **2010**, *115* (9), 1843–1849. https://doi.org/10.1182/blood-2009-07-231068.

(18) Eapen, M.; Rubinstein, P.; Zhang, M. J.; Stevens, C.; Kurtzberg, J.; Scaradavou, A.; Loberiza, F. R.; Champlin, R. E.; Klein, J. P.; Horowitz, M. M.; Wagner, J. E. Outcomes of Transplantation of Unrelated Donor Umbilical Cord Blood and Bone Marrow in Children with Acute Leukaemia: A Comparison Study. *Lancet* **2007**, *369* (9577), 1947–1954. https://doi.org/10.1016/S0140-6736(07)60915-5.

(19) Eapen, M.; Klein, J. P.; Ruggeri, A.; Spellman, S.; Lee, S. J.; Anasetti, C.; Arcese, W.; Barker, J. N.; Lee, A. B. L.; Brown, M.; Fernandez-Vina, M. A.; Freeman, J.; He, W.; Iori, A. P.; Horowitz, M. M.; Locatelli, F.; Marino, S.; Maiers, M.; Michel, G.; Sanz, G. F.; Gluckman, E.; Rocha, V. Impact of Allele-Level HLA Matching on Outcomes after Myeloablative Single Unit Umbilical Cord Blood Transplantation for Hematologic Malignancy. *Blood* **2014**, *123* (1), 133–140. https://doi.org/10.1182/blood-2013-05-506253.

(20) Wagner, J. E.; Barker, J. N.; DeFor, T. E.; Scott Baker, K.; Blazar, B. R.; Eide, C.; Goldman, A.; Kersey, J.; Krivit, W.; MacMillan, M. L.; Orchard, P. J.; Peters, C.; Weisdorf, D. J.; Ramsay, N. K. C.; Davies, S. M. Transplantation of Unrelated Donor Umbilical Cord Blood in 102 Patients with Malignant and Nonmalignant Diseases: Influence of CD34 Cell Dose and HLA Disparity on Treatment-Related Mortality and Survival. *Blood* **2002**, *100* (5), 1611–1618. https://doi.org/10.1182/blood-2002-01-0294.

(21) Rocha, V.; Cornish, J.; Sievers, E. L.; Filipovich, A.; Locatelli, F.; Peters, C.; Remberger, M.; Michel, G.; Arcese, W.; Dallorso, S.; Tiedemann, K.; Busca, A.; Chan, K. W.; Kato, S.; Ortega, J.; Vowels, M.; Zander, A.; Souillet, G.; Oakill, A.; Woolfrey, A.; Pay, A. L.; Green, A.; Gamier, F.; Ionescu, I.; Wernet, P.; Sirchia, G.; Rubinstein, P.; Chevret, S.; Gluckman, E. Comparison of Outcomes of Unrelated Bone Marrow and Umbilical Cord Blood Transplants in Children with Acute Leukemia. *Blood* **2001**, *97* (10), 2962–2971. https://doi.org/10.1182/blood.V97.10.2962.

(22) Gluckman, E.; Rocha, V.; Arcese, W.; Michel, G.; Sanz, G.; Chan, K. W.; Takahashi, T. A.; Ortega, J.; Filipovich, A.; Locatelli, F.; Asano, S.; Fagioli, F.; Vowels, M.; Sirvent, A.; Laporte, J. P.; Tiedemann, K.; Amadori, S.; Abecassis, M.; Bordigoni, P.; Diez, B.; Shaw, P. J.; Vora, A.; Caniglia, M.; Garnier, F.; Ionescu, I.; Garcia, J.; Koegler, G.; Rebulla, P.; Chevret, S. Factors Associated with Outcomes of Unrelated Cord Blood Transplant: Guidelines for Donor Choice. *Exp. Hematol.* **2004**, *32* (4), 397–407. https://doi.org/10.1016/j.exphem.2004.01.002.

(23) Allan, D. S.; Keeney, M.; Howson-Jan, K.; Popma, J.; Weir, K.; Bhatia, M.; Sutherland, D. R.; Chin-Yee, I. H. Number of Viable CD34+ Cells Reinfused Predicts Engraftment in Autologous Hematopoietic Stem Cell Transplantation. *Bone Marrow Transplant.* **2002**, *29* (12), 967–972. https://doi.org/10.1038/sj.bmt.1703575.

(24) Abrahamsen, J. F.; Rusten, L.; Bakken, A. M.; Bruserud, Ø. Better Preservation of Early Hematopoietic Progenitor Cells When Human Peripheral Blood Progenitor Cells Are Cryopreserved with 5 Percent Dimethylsulfoxide Instead of 10 Percent Dimethylsulfoxide. *Transfusion* **2004**, *44* (5), 785–789. https://doi.org/10.1111/j.1537-2995.2004.03336.x.

(25) Page, K. M.; Zhang, L.; Mendizabal, A.; Wease, S.; Carter, S.; Gentry, T.; Balber, A. E.; Kurtzberg, J. Total Colony-Forming Units Are a Strong, Independent Predictor of Neutrophil and Platelet Engraftment after Unrelated Umbilical Cord Blood Transplantation: A Single-Center Analysis of 435 Cord Blood Transplants. *Biol. Blood Marrow Transplant.* **2011**, *17* (9), 1362–1374. https://doi.org/10.1016/j.bbmt.2011.01.011.

(26) Yoder, M. C. Cord Blood Banking and Transplantation: Advances and Controversies. *Curr. Opin. Pediatr.* **2014**, *26* (2), 163–168. https://doi.org/10.1097/MOP.0000000000000065.

(27) Zaucha, J. M.; Gooley, T.; Bensinger, W. I.; Heimfeld, S.; Chauncey, T. R.; Zaucha, R.; Martin, P. J.; Flowers, M. E.; Storek, J.; Georges, G.; Storb, R.; Torok-Storb, B. CD34 Cell Dose in Granulocyte Colony-Stimulating Factor-Mobilized Peripheral Blood Mononuclear Cell Grafts Affects Engraftment Kinetics and Development of Extensive Chronic Graft-versus-Host Disease after Human Leukocyte Antigen-Identical Sibling Transpla. *Blood* **2001**, *98* (12), 3221–3227. https://doi.org/10.1182/blood.v98.12.3221.

(28) Theilgaard-Mönch, K.; Raaschou-Jensen, K.; Heilmann, C.; Andersen, H.; Bock, J.; Russel, C. A.; Vindeløv, L.; Jacobsen, N.; Dickmeiss, E. A Comparative Study of CD34+ Cells, CD34+ Subsets, Colony Forming Cells and Cobblestone Area Forming Cells in Cord Blood and Bone Marrow Allografts. *Eur. J. Haematol.* **2009**, *62* (3), 174–183. https://doi.org/10.1111/j.1600-0609.1999.tb01741.x.

(29) Sieburg, H. B.; Cho, R. H.; Müller-Sieburg, C. E. Limiting Dilution Analysis for Estimating the Frequency of Hematopoietic Stem Cells: Uncertainty and Significance. *Exp. Hematol.* **2002**, *30* (12), 1436–1443. https://doi.org/10.1016/S0301-472X(02)00963-3.

(30) Carral, A.; de la Rubia, J.; Martín, G.; Mollá, S.; Martínez, J.; Sanz, G. F.; Soler, M. A.; Jarque, I.; Jiménez, C.; Sanz, M. A. Factors Influencing the Collection of Peripheral Blood Stem Cells in Patients with Acute Myeloblastic Leukemia and Non-Myeloid Malignancies. *Leuk. Res.* **2003**, *27* (1), 5–12. https://doi.org/10.1016/s0145-2126(02)00068-1.

(31) Bourgeois, W.; Ricci, A.; Jin, Z.; Hall, M.; George, D.; Bhatia, M.; Garvin, J.; Satwani, P. Health Care Utilization and Cost among Pediatric Patients Receiving Unrelated Donor Allogeneic Hematopoietic Cell Transplantation. *Bone Marrow Transplant.* **2019**, *54* (5), 691–699. https://doi.org/10.1038/s41409-018-0308-0.

(32) Rangarajan, H. G.; Smith, L. C.; Stanek, J. R.; Hall, M.; Abu-Arja, R.; Auletta, J. J.; O'brien, S. H. Increased Health Care Utilization and Costs during Allogeneic Hematopoietic Cell Transplantation for Acute Leukemia and Myelodysplastic Syndromes in Adolescents and Young Adults Compared with Children: A Multicenter Study. *Biol. Blood Marrow Transplant.* **2019**, *25*, 1031–1038. https://doi.org/10.1016/j.bbmt.2019.01.004.

(33) Yang, H.; Zhao, H.; Acker, J. P.; Liu, J. Z.; Akabutu, J.; McGann, L. E. Effect of Dimethyl Sulfoxide on Post-Thaw Viability Assessment of CD45+ and CD34+ Cells of Umbilical Cord Blood and Mobilized Peripheral Blood. *Cryobiology* **2005**, *51* (2), 165–175. https://doi.org/10.1016/j.cryobiol.2005.06.003.

(34) Shim, J. S.; Cho, B.; Kim, M.; Park, G. S.; Shin, J. C.; Hwang, H. K.; Kim, T. G.; Oh, I. H. Early Apoptosis in CD34+ Cells as a Potential Heterogeneity in Quality of Cryopreserved Umbilical Cord Blood. *Br. J. Haematol.* **2006**, *135* (2), 210–213.

https://doi.org/10.1111/j.1365-2141.2006.06270.x.

(35) Sasnoor, L. M.; Kale, V. P.; Limaye, L. S. Supplementation of Conventional Freezing Medium with a Combination of Catalase and Trehalose Results in Better Protection of Surface Molecules and Functionality of Hematopoietic Cells. *J. Hematother. Stem Cell Res.* **2003**, *12* (5), 553–564. https://doi.org/10.1089/152581603322448268.

(36) Hunt, C. J.; Armitage, S. E.; Pegg, D. E. Cryopreservation of Umbilical Cord Blood: 1. Osmotically Inactive Volume, Hydraulic Conductivity and Permeability of CD34(+) Cells to Dimethyl Sulphoxide. *Cryobiology* **2003**, *46* (1), 61–75. https://doi.org/10.1016/s0011-2240(02)00180-3.

(37) Hunt, C. J.; Pegg, D. E.; Armitage, S. E. Optimising Cryopreservation Protocols for Haematopoietic Progenitor Cells: A Methodological Approach for Umbilical Cord Blood. *Cryo Letters 27* (2), 73–86.

(38) Duggleby, R. C.; Querol, S.; Davy, R. C.; Fry, L. J.; Gibson, D. A.; Horton, R. B. V.; Mahmood, S. N.; Gomez, S. G.; Madrigal, J. A. Flow Cytometry Assessment of Apoptotic CD34+ Cells by Annexin v Labeling May Improve Prediction of Cord Blood Potency for Engraftment. *Transfusion* **2012**, *52* (3), 549–559. https://doi.org/10.1111/j.1537-2995.2011.03305.x.

(39) Wu, L.; Al-Hejazi, A.; Filion, L.; Ben, R.; Halpenny, M.; Yang, L.; Giulivi, A.; Allan, D. S. Increased Apoptosis in Cryopreserved Autologous Hematopoietic Progenitor Cells Collected by Apheresis and Delayed Neutrophil Recovery after Transplantation: A Nested Case-Control Study. *Cytotherapy* **2012**, *14* (2), 205–214. https://doi.org/10.3109/14653249.2011.610302.

(40) Sasnoor, L. M.; Kale, V. P.; Limaye, L. S. A Combination of Catalase and Trehalose as Additives to Conventional Freezing Medium Results in Improved Cryoprotection of Human Hematopoietic Cells with Reference to in Vitro Migration and Adhesion Properties. *Transfusion* **2005**, *45* (4), 622–633. https://doi.org/10.1111/j.0041-1132.2005.04288.x.

(41) Chaytor, J. L.; Tokarew, J. M.; Wu, L. K.; Leclre, M.; Tam, R. Y.; Capicciotti, C. J.; Guolla, L.; Von Moos, E.; Findlay, C. S.; Allan, D. S.; Ben, R. N. Inhibiting Ice Recrystallization and Optimization of Cell Viability after Cryopreservation. *Glycobiology* **2012**, *22* (1), 123–133. https://doi.org/10.1093/glycob/cwr115.

(42) Deller, R. C.; Vatish, M.; Mitchell, D. A.; Gibson, M. I. Glycerol-Free Cryopreservation of Red Blood Cells Enabled by Ice-Recrystallization-Inhibiting Polymers. *ACS Biomater. Sci. Eng.* **2015**, *1* (9), 789–794. https://doi.org/10.1021/acsbiomaterials.5b00162.

(43) Bevilacqua, A. E.; Zaritzky, N. E. Ice Recrystallization in Frozen Beef. *J. Food Sci.* **1982**, *47* (5), 1410–1414. https://doi.org/10.1111/j.1365-2621.1982.tb04950.x.

(44) Berz, D.; McCormack, E. M.; Winer, E. S.; Colvin, G. A.; Quesenberry, P. J. Cryopreservation of Hematopoietic Stem Cells. *Am. J. Hematol.* **2007**, *82* (6), 463–472. https://doi.org/10.1002/ajh.20707.

(45) Rodrigues, C. A.; Sanz, G.; Brunstein, C. G.; Sanz, J.; Wagner, J. E.; Renaud, M.; de Lima, M.; Cairo, M. S.; Fürst, S.; Rio, B.; Dalley, C.; Carreras, E.; Harousseau, J.-L.; Mohty, M.; Taveira, D.; Dreger, P.; Sureda, A.; Gluckman, E.; Rocha, V. Analysis of Risk Factors for Outcomes After Unrelated Cord Blood Transplantation in Adults With Lymphoid Malignancies: A Study by the Eurocord-Netcord and Lymphoma Working Party of the European Group for Blood and Marrow Transplantation. *J. Clin. Oncol.* **2009**, *27* (2), 256–263. https://doi.org/10.1200/JCO.2007.15.8865.

(46) Rubinstein, P.; Dobrila, L.; Rosenfield, R. E.; Adamson, J. W.; Migliaccio, G.; Migliaccio, A. R.; Taylor, P. E.; Stevens, C. E. Processing and Cryopreservation of Placental/Umbilical Cord Blood for Unrelated Bone Marrow Reconstitution. *Proc. Natl. Acad. Sci. U. S. A.* **1995**, *92* (22), 10119–10122. https://doi.org/10.1073/pnas.92.22.10119.

(47) Zambelli, A.; Poggi, G.; Da Prada, G.; Pedrazzoli, P.; Cuomo, A.; Miotti, D.; Perotti, C.; Preti, P.; Robustelli della Cuna, G. Clinical Toxicity of Cryopreserved Circulating Progenitor Cells Infusion. *Anticancer Res. 18* (6B), 4705–4708.

(48) Davis, J. M.; Rowley, S. D.; Braine, H. G.; Piantadosi, S.; Santos, G. W. Clinical Toxicity of Cryopreserved Bone Marrow Graft Infusion. *Blood* **1990**, *75* (3), 781–786. https://doi.org/10.1182/blood.v75.3.781.bloodjournal753781.

(49) Davis, J.; Rowley, S. D.; Santos, G. W. Toxicity of Autologous Bone Marrow Graft Infusion. *Prog. Clin. Biol. Res.* **1990**, *333*, 531–540.

(50) Alessandrino, E. P.; Bernasconi, P.; Caldera, D.; Colombo, A.; Bonfichi, M.; Malcovati, L.; Klersy, C.; Martinelli, G.; Maiocchi, M.; Pagnucco, G.; Varettoni, M.; Perotti, C.; Bernasconi, C. Adverse Events Occurring during Bone Marrow or Peripheral Blood Progenitor Cell Infusion: Analysis of 126 Cases. *Bone Marrow Transplant.* **1999**, *23* (6),

533–537. https://doi.org/10.1038/sj.bmt.1701609.

(51) Yang, H.; Acker, J. P.; Cabuhat, M.; Letcher, B.; Larratt, L.; McGann, L. E. Association of Post-Thaw Viable CD34+ Cells and CFU-GM with Time to Hematopoietic Engraftment. *Bone Marrow Transplant.* **2005**, *35* (9), 881–887. https://doi.org/10.1038/sj.bmt.1704926.

(52) Beaujean, F.; Bourhis, J. H.; Bayle, C.; Jouault, H.; Divine, M.; Rieux, C.; Janvier, M.; Le Forestier, C.; Pico, J. L. Successful Cryopreservation of Purified Autologous CD34+ Cells: Influence of Freezing Parameters on Cell Recovery and Engraftment. *Bone Marrow Transplant.* **1998**, *22* (11), 1091–1096. https://doi.org/10.1038/sj.bmt.1701494.

(53) Halle, P.; Tournilhac, O.; Knopinska-Posluszny, W.; Kanold, J.; Gembara, P.; Boiret, N.; Rapatel, C.; Berger, M.; Travade, P.; Angielski, S.; Bonhomme, J.; Deméocq, F. Uncontrolled-Rate Freezing and Storage at-80°C, with Only 3.5-Percent DMSO in Cryoprotective Solution for 109 Autologous Peripheral Blood Progenitor Cell Transplantations. *Transfusion* **2001**, *41* (5), 667–673. https://doi.org/10.1046/j.1537-2995.2001.41050667.x.

(54) Woods, E. J.; Liu, J.; Derrow, C. W.; Smith, F. O.; Williams, D. A.; Critser, J. K. Cutting Edge Communication: Osmometric and Permeability Characteristics of Human Placental/Umbilical Cord Blood CD34T $^{+}$ Cells and Their Application to Cryopreservation. *J. Hematother. Stem Cell Res.* **2000**, *9* (2), 161–173. https://doi.org/10.1089/152581600319379.

(55) Woods, E. J.; Thirumala, S.; Badhe-Buchanan, S. S.; Clarke, D.; Mathew, A. J. Off the Shelf Cellular Therapeutics: Factors to Consider during Cryopreservation and Storage of Human Cells for Clinical Use. *Cytotherapy* **2016**, *18* (6), 697–711. https://doi.org/10.1016/J.JCYT.2016.03.295.

(56) Svalgaard, J. D.; Haastrup, E. K.; Reckzeh, K.; Holst, B.; Glovinski, P. V.; Gørløv, J. S.; Hansen, M. B.; Moench, K. T.; Clausen, C.; Fischer-Nielsen, A. Low-Molecular-Weight Carbohydrate Pentaisomaltose May Replace Dimethyl Sulfoxide as a Safer Cryoprotectant for Cryopreservation of Peripheral Blood Stem Cells. *Transfusion* **2016**, *56* (5), 1088–1095. https://doi.org/10.1111/trf.13543.

(57) Svalgaard, J. D.; Talkhoncheh, M. S.; Haastrup, E. K.; Munthe-Fog, L.; Clausen, C.; Hansen, M. B.; Andersen, P.; Gørløv, J. S.; Larsson, J.; Fischer-Nielsen, A.

Pentaisomaltose, an Alternative to DMSO. Engraftment of Cryopreserved Human CD34+ Cells in Immunodeficient NSG Mice. *Cell Transplant.* **2018**, *27* (9), 1407–1412. https://doi.org/10.1177/0963689718786226.

(58) Xian, M.; Fatima, Z.; Zhang, W.; Fang, J.; Li, H.; Pei, D.; Loo, J.; Stevenson, T.; Wang, P. Identification of α-Galactosyl Epitope Mimetics through Rapid Generation and Screening of C-Linked Glycopeptide Library. *J. Comb. Chem.* **2004**, *6* (1), 126–134. https://doi.org/10.1021/CC030042U.

(59) Motta, J. P. R.; Paraguassú-Braga, F. H.; Bouzas, L. F.; Porto, L. C. Evaluation of Intracellular and Extracellular Trehalose as a Cryoprotectant of Stem Cells Obtained from Umbilical Cord Blood. *Cryobiology* **2014**, *68* (3), 343–348. https://doi.org/10.1016/j.cryobiol.2014.04.007.

(60) Wu, L. K.; Tokarew, J. M.; Chaytor, J. L.; Von Moos, E.; Li, Y.; Palii, C.; Ben, R. N.; Allan, D. S. Carbohydrate-Mediated Inhibition of Ice Recrystallization in Cryopreserved Human Umbilical Cord Blood. *Carbohydr. Res.* **2011**, *346* (1), 86–93. https://doi.org/10.1016/j.carres.2010.10.016.

(61) Briard, J. G.; Jahan, S.; Chandran, P.; Allan, D.; Pineault, N.; Ben, R. N. Small-Molecule Ice Recrystallization Inhibitors Improve the Post-Thaw Function of Hematopoietic Stem and Progenitor Cells. *ACS Omega* **2016**, *1* (5), 1010–1018. https://doi.org/10.1021/acsomega.6b00178.

(62) Migliaccio, A. R.; Adamson, J. W.; Stevens, C. E.; Dobrila, N. L.; Carrier, C. M.; Rubinstein, P. Cell Dose and Speed of Engraftment in Placental/Umbilical Cord Blood Transplantation: Graft Progenitor Cell Content Is a Better Predictor than Nucleated Cell Quantity. *Blood* **2000**, *96* (8), 2717–2722.

(63) Purton, L. E.; Scadden, D. T. Limiting Factors in Murine Hematopoietic Stem Cell Assays. *Cell Stem Cell*. September 13, 2007, pp 263–270. https://doi.org/10.1016/j.stem.2007.08.016.

(64) Harrison, D. Competitive Repopulation: A New Assay for Long-Term Stem Cell Functional Capacity. *Blood* **1980**, *55* (1), 77–81. https://doi.org/10.1182/blood.V55.1.77.77.

(65) Jahan, S.; Adam, M. K.; Manesia, J. K.; Doxtator, E.; Ben, R. N.; Pineault, N. Inhibition of Ice Recrystallization during Cryopreservation of Cord Blood Grafts Improves Platelet

Engraftment. *Transfusion* **2020**, *60* (4), 769–778. https://doi.org/10.1111/trf.15759.

(66) Gerets, H. H. J.; Tilmant, K.; Gerin, B.; Chanteux, H.; Depelchin, B. O.; Dhalluin, S.; Atienzar, F. A. Characterization of Primary Human Hepatocytes, HepG2 Cells, and HepaRG Cells at the MRNA Level and CYP Activity in Response to Inducers and Their Predictivity for the Detection of Human Hepatotoxins. *Cell Biol. Toxicol.* **2012**, *28* (2), 69–87. https://doi.org/10.1007/s10565-011-9208-4.

(67) Anoopkumar-Dukie, S.; Carey, J. B.; Conere, T.; O'Sullivan, E.; van Pelt, F. N.; Allshire, A. Resazurin Assay of Radiation Response in Cultured Cells. *Br. J. Radiol.* **2005**, *78* (934), 945–947. https://doi.org/10.1259/bjr/54004230.

(68) Hamid, R.; Rotshteyn, Y.; Rabadi, L.; Parikh, R.; Bullock, P. Comparison of Alamar Blue and MTT Assays for High Through-Put Screening. *Toxicol. Vitr.* **2004**, *18* (5), 703–710. https://doi.org/10.1016/j.tiv.2004.03.012.

(69) Briard, J. G. The Rational Design and Use of Novel Small-Molecule Ice Recrystallization Inhibitors for the Cryopreservation of Hematopoietic Stem Cells and Red Blood Cells (Doctoral Dissertation), Université d'Ottawa/University of Ottawa, 2016.

(70) Jaasma, M. J.; Jackson, W. M.; Keaveny, T. M. The Effects of Morphology, Confluency, and Phenotype on Whole-Cell Mechanical Behavior. *Ann. Biomed. Eng.* **2006**, *34* (5), 759–768. https://doi.org/10.1007/s10439-005-9052-x.

(71) Pasha, R.; Elmoazzen, H.; Pineault, N. Development and Testing of a Stepwise Thaw and Dilute Protocol for Cryopreserved Umbilical Cord Blood Units. *Transfusion* **2017**, *57* (7), 1744–1754. https://doi.org/10.1111/trf.14136.

(72) Félix, O. M. W. de O.; Tunes, G.; Ginani, V. C.; Simões, P. C.; Barros, D. P.; Delbuono, E.; Alves, M. T. de S.; Petrilli, A. S.; Lee, M. L. de M.; Gouveia, R. V.; Zecchin, V. G.; Seber, A. The Influence of Cell Concentration at Cryopreservation on Neutrophil Engraftment after Autologous Peripheral Blood Stem Cell Transplantation. *Hematol. Transfus. Cell Ther.* **2018**, *40* (3), 233–239. https://doi.org/10.1016/j.htct.2018.01.007.

(73) Mitrus, I.; Smagur, A.; Fidyk, W.; Czech, M.; Prokop, M.; Chwieduk, A.; Glowala-Kosinska, M.; Czerw, T.; Sobczyk-Kruszelnicka, M.; Mendrek, W.; Michalak, K.; Sadus-Wojciechowska, M.; Najda, J.; Holowiecki, J.; Giebel, S. Reduction of DMSO Concentration in Cryopreservation Mixture from 10% to 7.5% and 5% Has No Impact on Engraftment after Autologous Peripheral Blood Stem Cell Transplantation: Results of a

Prospective, Randomized Study. *Bone Marrow Transplant.* **2018**, *53* (3), 274–280. https://doi.org/10.1038/s41409-017-0056-6.

(74) Hauck-Dlimi, B.; Dlimi, A.; Zimmermann, R.; Eckstein, R.; Zingsem, J. The Effect of Cell Concentrations from Different Cell Populations on the Viability of Umbilical Blood Stem Cells. *Clin. Lab.* **2014**, *60* (10), 1635–1640. https://doi.org/10.7754/clin.lab.2013.131022.

(75) Hornberger, K.; Yu, G.; McKenna, D.; Hubel, A. Cryopreservation of Hematopoietic Stem Cells: Emerging Assays, Cryoprotectant Agents, and Technology to Improve Outcomes. *Transfus. Med. Hemotherapy* **2019**, *46* (3), 188–196. https://doi.org/10.1159/000496068.

(76) Rundberg Nilsson, A.; Pronk, C. J. H.; Bryder, D. Probing Hematopoietic Stem Cell Function Using Serial Transplantation: Seeding Characteristics and the Impact of Stem Cell Purification. *Exp. Hematol.* **2015**, *43* (9), 812–817. https://doi.org/10.1016/j.exphem.2015.05.003.

(77) Doulatov, S.; Notta, F.; Laurenti, E.; Dick, J. E. Hematopoiesis: A Human Perspective. *Cell Stem Cell*. February 3, 2012, pp 120–136. https://doi.org/10.1016/j.stem.2012.01.006.

(78) Baust, J. M.; Vogel, M. J.; Buskirk, R. Van; Baust, J. G. *A Molecular Basis of Cryopreservation Failure and Its Modulation to Improve Cell Survival*; 2001; Vol. 10.

(79) Boon, C. H.; Chao, P. Y.; Liu, H.; Wei, S. T.; Rufaihah, A. J.; Yang, Z.; Boon, H. B.; Ge, Z.; Hog, W. O.; Eng, H. L.; Cao, T. Loss of Viability during Freeze-Thaw of Intact and Adherent Human Embryonic Stem Cells with Conventional Slow-Cooling Protocols Is Predominantly Due to Apoptosis Rather than Cellular Necrosis. *J. Biomed. Sci.* **2006**, *13* (3), 433–445. https://doi.org/10.1007/s11373-005-9051-9.

(80) Wunderlich, M.; Brooks, R. A.; Panchal, R.; Rhyasen, G. W.; Danet-Desnoyers, G.; Mulloy, J. C. OKT3 Prevents Xenogeneic GVHD and Allows Reliable Xenograft Initiation from Unfractionated Human Hematopoietic Tissues. *Blood* **2014**, *123* (24), e134-44. https://doi.org/10.1182/blood-2014-02-556340.

(81) Shultz, L. D.; Schweitzer, P. A.; Christianson, S. W.; Gott, B.; Schweitzer, I. B.; Tennent, B.; McKenna, S.; Mobraaten, L.; Rajan, T. V; Greiner, D. L. Multiple Defects in Innate and Adaptive Immunologic Function in NOD/LtSz-Scid Mice. *J. Immunol.* **1995**, *154* (1), 180–191.

(82) Shultz, L. D.; Lyons, B. L.; Burzenski, L. M.; Gott, B.; Chen, X.; Chaleff, S.; Kotb, M.; Gillies, S. D.; King, M.; Mangada, J.; Greiner, D. L.; Handgretinger, R. Human Lymphoid and Myeloid Cell Development in NOD/LtSz- Scid IL2R γ Null Mice Engrafted with Mobilized Human Hemopoietic Stem Cells . *J. Immunol.* **2005**, *174* (10), 6477–6489. https://doi.org/10.4049/jimmunol.174.10.6477.

(83) Schipper, L. F.; Van Hensbergen, Y.; Fibbe, W. E.; Brand, A. A Sensitive Quantitative Single-Platform Flow Cytometry Protocol to Measure Human Platelets in Mouse Peripheral Blood. *Transfusion* **2007**, *47* (12), 2305–2314. https://doi.org/10.1111/j.1537-2995.2007.01472.x.

(84) Miller, P. H.; Rabu, G.; Macaldaz, M.; Knapp, D. J. H. F.; Cheung, A. M. S.; Dhillon, K.; Nakamichi, N.; Beer, P. A.; Shultz, L. D.; Humphries, R. K.; Eaves, C. J. Analysis of Parameters That Affect Human Hematopoietic Cell Outputs in Mutant C-Kit-Immunodeficient Mice. https://doi.org/10.1016/j.exphem.2016.12.012.

5. Photocontrollable Glyco(peptide)-Functionalized Ice Recrystallization Inhibitors

5.1 Introduction

5.1.1 Lipopeptide- and glyco(peptide)-functionalized analogues of antifreeze glycoproteins

Many living organisms (a variety of plants, fish, amphibians, and insects) have adapted to the threat of ice recrystallization during cold temperatures through various strategies. Species that utilize the "freeze-tolerating" strategy produce antifreeze proteins (AFPs) and antifreeze glycoproteins (AFGPs) that allow ice formation whilst inhibiting ice growth.[1–3] These AF(G)Ps belong to the class of biological antifreezes (BAs) and they inhibit ice growth by adsorbing to various faces of hexagonal ice (I_h).[4–9] This ice recrystallization inhibition (IRI) ability has been of great interest in various fields of cryobiology including for the cryopreservation of biological samples.[10,11] Notably, however, a BA's ability to irreversibly bind to ice also leads to the presence of another ability, thermal hysteresis (TH) activity. Molecules that possess TH activity are undesirable for cryopreservation applications since TH leads to reduced post-cryopreservation cell survival.[12–15] Nevertheless, studying the key structural features required for BAs to exhibit antifreeze activity offers insight into the development of novel cryoprotectants. A number of important properties necessary for antifreeze activities have been determined from a multitude of studies including a BA's ideal balance between hydrogen bonding, van der Waals interactions, hydrophobic forces, the ordering of bulk water, as well as other contributors.[16–25] Furthermore, hydrophobic domains for binding optimization at the ice/water interface in

samples, solution-phase aggregation, and interfacial absorption of AF(G)Ps have all been shown to be important for antifreeze activity.[26–28] While the structural and conformational properties of AF(G)Ps differ based on type and species, they have several general characteristics: AFGPs contain a repeating Alanine-Alanine-Threonine sequence (Ala-Ala-Thr, n = 4-55), and this peptide unit is linked by a glycosidic bond to the disaccharide β-D-galactosyl-(1,3)-α-*N*-acetyl-D-galactosamine via Thr's secondary hydroxyl group. Further, AFGPs are classified into eight groups based on decreasing size: ranging from AFGP 1 (MW = 33.7 kDa, n = 50 Ala-Ala-Thr repeats) to AFGP 8 (MW = 2.6 kDa, n = 4 Ala-Ala-Thr repeats).[29–38] While the properties differ for the various AFGPs, these BAs typically take on a defined polyproline type II helix or an extended random coil conformation when in solution.[34,39–43]

As mentioned in **Chapter 1** (Introduction), the early development of ice recrystallization inhibitors was inspired by the glycopeptides present in the naturally occurring BAs. A library of ice recrystallization inhibitors has been developed over the years including *C*-linked analogues, as well as *C*-serine and ornithine analogues (see **Section 1.3.3** of **Chapter 1** for a detailed analysis). In an effort to continue the development of novel AFGP analogues as ice recrystallization inhibitors, a collaboration between the Ben laboratory and the group of Dr. Brendan Wilkinson (University of New England) resulted in the analysis of a series of lipopeptide-based AFGP analogues (**Figure 5.1.1.1**). **Section 5.2.1** examines the antifreeze activity of the series of lipopeptides toward the development of novel IRIs. I would like to acknowledge my previous Undergraduate Student Researcher (USRA from the Natural Sciences and Engineering Research Council of Canada, or NSERC), Mr. Emiliyan Staykov, for his assistance with the studies presented in **Section 5.2**.

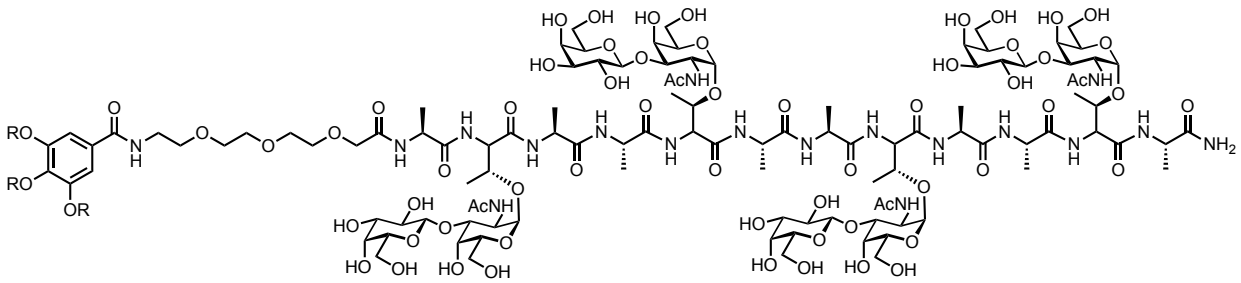

Figure 5.1.1.1. The general structure of lipopeptides studied in **Section 5.2.1**, where R denotes long alkyl chains of varying lengths.

Another strategy for the development of novel mimetics of BAs involves the design of macromolecular IRIs that contain the glycopeptide unit of AFGPs and functionality that promotes molecular self-assembly. Supramolecular self-assemblies built from low molecular-weight building blocks are of considerable interest in order to combat the practical limitations of obtaining adequate amounts and purities of the AFGPs. Efforts toward this end have included strategies like the use of aromatic dye stacks, star polymers, and metallohelices.[44–46] With this in mind, and through a collaboration between the Wilkinson and Ben laboratories, AF(G)P-functionalized perylene bisimides (AFGP-PBIs) were designed in which the IRI activity and 1D self-assembly in aqueous media could be controlled through the structure of the PBI core (a structure known to instill molecular self-assembly properties in solution, **Figure 5.1.1.2**). We hypothesized that the incorporation of PBIs, which have a strong propensity to undergo π-π stacking in media, in conjunction with the structural components of AFGPs would lead to a series of novel IRIs possessing promising supramolecular properties. Further, we believed that these AFGP-PBIs would offer further insight into the antifreeze activity (e.g. mechanism of action) and aggregation of AF(G)Ps. Therefore, **Section 5.2** details the design and investigation of novel AFGP-PBIs as IRIs, and thereby offers significant progress for the on-going development of AFGP-like IRIs as supramolecular cryoprotectants. This proof-of-concept

development of IRI-active antifreeze glycopeptide-functionalized perylene bisimides (AFGP-PBIs) was published in *Chemistry, A European Journal*.[47]

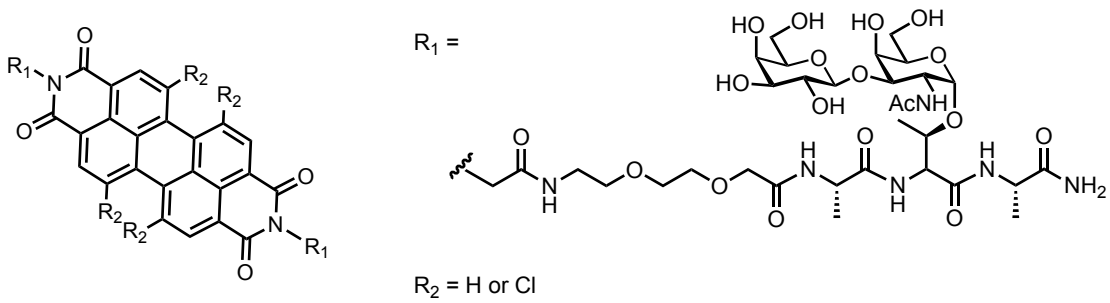

Figure 5.1.1.2. The general structure of AFGP-PBIs investigated in **Section 5.2** (adapted from reference 47 with permission).[47]

The 1D self-assembly of AFGP-substituted PBIs is achieved through π-π stacking of the planar PBI. The planar and π-conjugated PBI molecules are both photo- and chemically stable. They display strong fluorescent properties, and as a result, have been well-studied in a variety of fields. The π-π stacking propensity of PBIs in both aqueous and organic media has been of great interest for applications such as supramolecular building blocks and as biological probes.[48–57] PBI-macromolecules that bear either ionic or non-ionic groups at various positions around the PBI core have led to promising materials for biosensing, imaging, and for mimicking biological systems.[48–51,58–61] Moreover, substituting PBIs with monosaccharides or amino acids has led to the production of nanoscale structures that have controllable helicity and self-assembly properties.[62–66]

5.1.2 Azobenzene-functionalized glyco(peptides) as photoswitchable ice recrystallization inhibitors

Tuning the physicochemical properties of molecules using an external stimulus has also been of considerable interest for the development of supramolecular materials possessing macromolecular self-assembly, as well as for synthetic and catalytic applications, drug delivery potential, environmental remediation, among many other applications.[67–71] Recent studies report the use of physical and chemical properties for activating the IRI activity of proteins and biologically-inspired polymers.[72,73] The ability to activate IRI activity of compounds using an external source enables the possibility of adding molecules that offer multiple different functions based on the stage of cryopreservation a cellular product may be undergoing. The IRI-inactive state of a compound may interact with the cell membrane differently than its IRI-active state based on the hydrophobicity/hydrophilicity differences between states, among other properties. That said, designing new amphiphilic IRIs could be envisioned in which the glyco(peptide)'s physicochemical features could be tuned using an external trigger thereby controlling the IRI activity of the molecule. **Section 5.3** begins by exploring azobenzene-functionalized glycopeptides as ice recrystallization inhibitors in an effort to develop photocontrollable IRIs bearing azobenzene "switches." The work in **Section 5.3** (and **Section 5.4**) was a collaboration between the Dr. Wilkinson laboratory and colleagues and the Ben laboratory (studied in conjunction with previous Ben laboratory member, Dr. Jessica Poisson). Inspired by the initial analysis of azobenzene-functionalized glycopeptidomimetics, the investigation then focused on the use of photoisomerization to control the IRI activity of a class of carbohydrate-based surfactants bearing azobenzene moieties (**Figure 5.1.2.1**).[74]

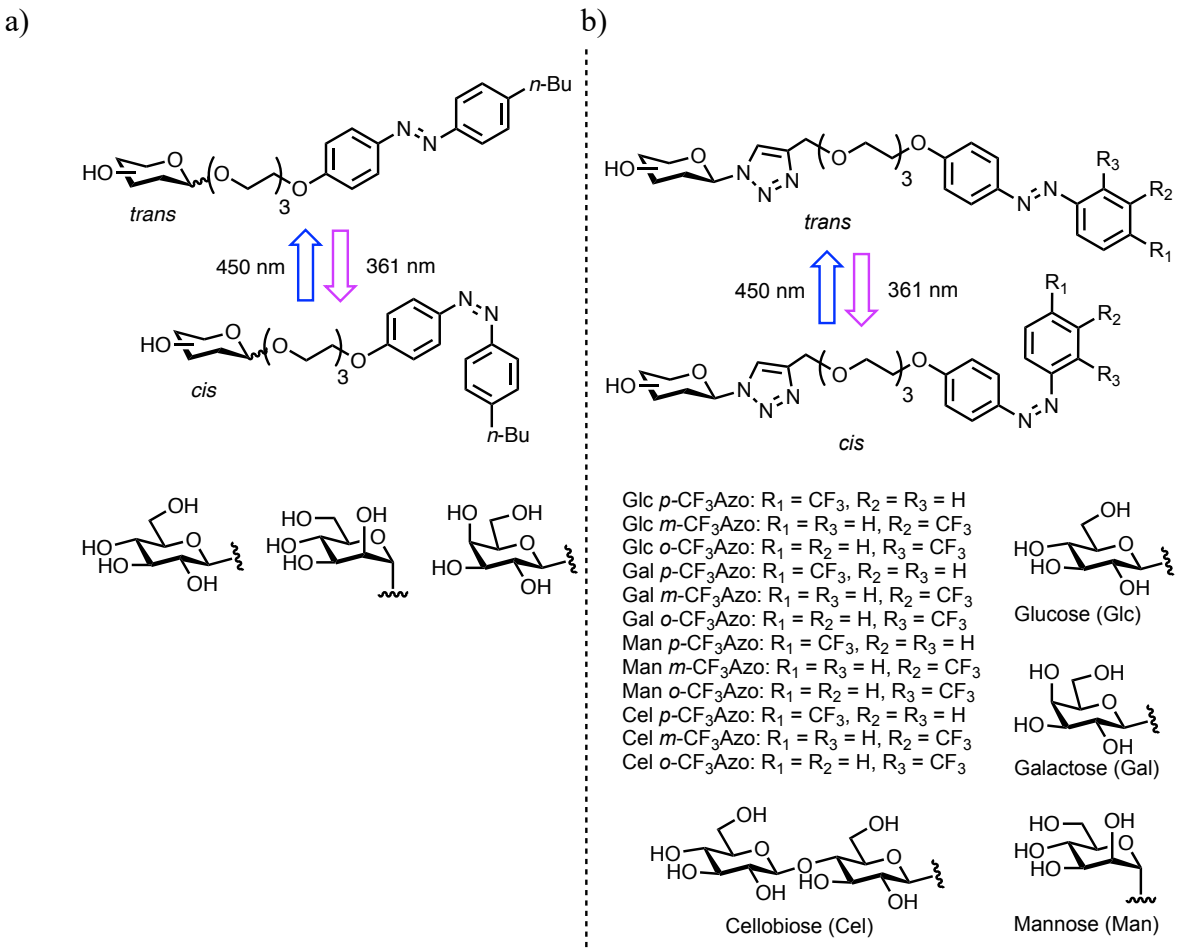

Figure 5.1.2.1. Photoisomerization of the azobenzene groups present in carbohydrate-based surfactants discussed in a) **Sections 5.3.2** and b) **5.4**.[74,75]

Briefly, a planar and hydrophobic *trans*-azobenzene molecule undergoes a rapid and reversible change to its *cis*-isomer under UV light (361 nm), resulting in a molecule that is less hydrophobic and no longer planar. Visible light (450 nm), meanwhile, reverts the *cis*-isomer back to its more hydrophobic and planar *trans*-azobenzene isomer. This exposure of diazo compounds to UV-vis light is known to instill changes to a number of properties including the critical micelle concentration (CMC), the surface tension equilibrium, and interfacial activity; and as a result, this allows for control of molecular function with high quantum yields and high reproducibility.[76–79] The aggregation and adsorption properties can also be controlled using

photoisomerization.[80] In fact, the *trans-cis* photoisomerization of an azobenzene group has been useful toward studying the supramolecular self-assembly of amphiphiles, the structural changes of biomolecules, the biological activity of a variety of drugs, activation of nanomaterials, among many other applications including various *in vivo* applicability.[81–90] Since the azobenzene functionality offers a means of tuning the molecule's amphiphilicity using a light source, we hypothesized that IRI activity could also be controlled owing to the delicate hydrophilic-lipophilic balance (HLB) required for IRI activity. Previous work from the Wilkinson laboratory has shown that the size, stereochemistry, and the polarity of carbohydrate-based surfactants had a drastic effect on the self-assembly and interfacial properties of a panel of carbohydrate-based surfactants.[78,79,91] Toward this end, **Section 5.3.2** further examines the photocontrollable nature of the carbohydrate-based surfactants' IRI activities. We hypothesized that disrupting the HLB of the surfactants would not only alter the IRI activity of the molecules but specifically if the balance was altered significantly to one extreme or the other, that the IRI activity would be greatly diminished. By carefully selecting the carbohydrate-head group based on the changes to the degree of hydration, the polarity, and the stereochemical configuration, azobenzene photoisomerization could trigger changes to the IRI activity.

The next section (**Section 5.4**) describes the investigation of the photoswitchable IRI activity for a panel of carbohydrate-based fluorosurfactants (**Figure 5.1.2.2**).[75] We hypothesized that IRI activity would depend on changes to the regiochemistry of the trifluoromethyl group positioned on the azobenzene tail and the selection of the carbohydrate head group. These modifications were expected to alter the hydrophilic-lipophilic balance required for IRI activity. As with the surfactants presented in **Section 5.3**, photoisomerization was also predicted to impact the resulting IRI activities since conversion of the azobenzene group was expected to

sufficiently alter the amphiphilicity of the fluorosurfactants. The examination of IRI activity, TH activity, and cytotoxicity of the derivatives was conducted in the Ben laboratory using the traditional splat-cooling assay[92,93] (30-minute annealing period) as a general screen for the IRI activities, followed by the use of the modified splat-cooling assay[94] for analysis of promising compounds.

5.2 Lipopeptides and glyco(peptide)-functionalized perylene bisimides as ice recrystallization inhibitors

5.2.1 Lipopeptides

A set of lipopeptides as antifreeze glycoprotein (AFGP) analogues were designed (**Figure 5.2.1.1a**) in order to continue the development of glycopeptide-based ice recrystallization inhibitors. These derivatives were comprised of a tetramer of an AFGP glycotripeptide $(Ala\text{-}Thr\text{-}Ala)_4$ tethered to a phenol ether using a triethylene glycolate spacer. The IRI activity of these derivatives was assessed both at 20 mM and 5.5 μM (**Figure 5.2.1.1b**), apart from **5.01** which was assessed at 1 mM and 5.5 μM. For reference, 5.5 μM AFGP-8, a potent ice recrystallization inhibitor, results in approximately 13% MGS of ice crystals compared to the phosphate-buffered saline (PBS) control. Compared to AFGP-8, these AFGP-lipopeptides **5.01-5.03** at 5.5 μM were significantly less IRI-active with % MGS between 85-95% (at 5.5 μM). Excitingly, at 20 mM, both lipopeptides **5.02** and **5.03** displayed potent IRI activity with % MGS of 7% and 19%, respectively. The fact that these derivatives retained potent IRI activity at these low millimolar concentrations is a promising start for the further development of lipopeptides. Finally, no TH activity or dynamic ice shaping (DIS) was observed for 10 mg/mL

of **5.03** dissolved in high purity deionized water as determined using nanoliter osmometry (see page 252 in the **Experimental** section for more assay details and image of ice crystal morphology).[95] Importantly, the lack of TH activity (and DIS) indicates that lipopeptide **5.03** does not inhibit ice recrystallization by binding interactions to ice crystals.

a)

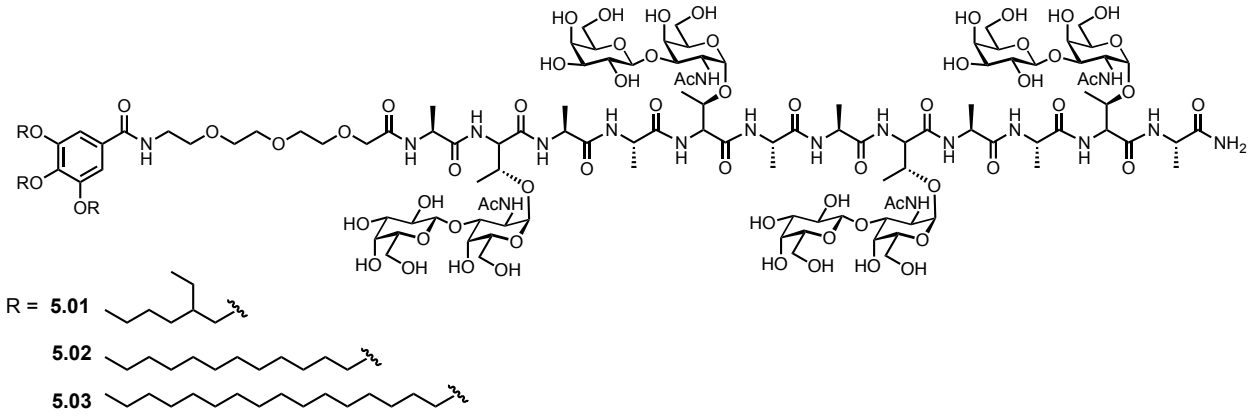

b)

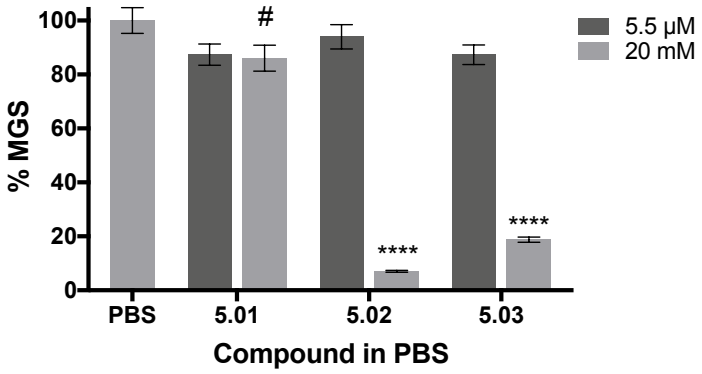

Figure 5.2.1.1. **a)** The structures of AFGP lipopeptides **5.01-5.03**, and **b)** their IRI activity represented as the percent mean grain size (% MGS) of ice crystals in the presence of test samples compared to ice crystals in the presence of PBS alone. Error bars indicate % SEM (n = 3 experiments) and statistical significance between test condition and PBS was determined using two-way ANOVA with Tukey's multiple comparisons test (**** $p < 0.0001$). Lipopeptides **5.02** and **5.03** at 20 mM were also statistically significant from **5.01**. The symbol # indicates that the compound was tested at 1 mM and not 20 mM.

The IRI activity of AFGP-lipopeptide class of derivatives **5.01-5.03** at 20 mM in addition to the lack of TH activity observed is promising for the continued development of AFGP analogues. Moreover, these results offer significant baselines for the future development of AFGP analogues that are IRI-active without displaying TH activity. To continue the development of AFGP analogues, we turned our attention to AFGP analogues where a perylene bisimide core is inserted between two AFGP glycopeptide fragments (akin to the glycopeptide units present in the lipopeptides). The use of the perylene core is hypothesized to promote the development of self-assembled IRI materials.

5.2.2 Antifreeze glyco(peptide)-functionalized perylene bisimides

Self-assembled materials are of great interest for the development of analogues of antifreeze glycoproteins (AFGPs). This sub-section furthers the development of AFGP analogues through the analysis of glyco(peptide)-functionalized perylene bisimides (AFGP-PBIs). As introduced in **Section 5.1**, the Wilkinson laboratory designed and synthesized a series of bisimides bearing variable core substitutions and glyco(peptides) at the imide position in order to mimic AFGPs (**Figure 5.2.2.1**). The structures of AFGP-PBI **5.04** and **5.05** involved a planar PBI core unit with no additional functionality. Their imide position was linked to a (glyco)peptide unit mimicking that of the naturally occurring AFGPs (Ala-Thr-Ala) using an ethylene glycolate spacer. The ethylene glycolate spacer served to enhance the solubility of analogues in aqueous media as well as the pi-pi stacking interactions of the perylene cores. The peptide was glycosylated at threonine's hydroxyl group with a β-D-galactosyl-(1,3)-*N*-acetyl-α-D-galactosaminyl disaccharide in PBI **5.05**. The PBI core unit of the remaining AFGP-PBIs was distorted owing to a tetrachloro-substitution. These derivatives had varying substitutions present

at the imide position, including glycopeptide functionalization (**5.06**) or glycosyl moieties (glucose **5.07**, galactose **5.08**, mannose **5.09**, and maltose **5.10**). The impact of a planar or distorted PBI core on antifreeze activity was assessed in the Ben laboratory, including the presence of any ice recrystallization inhibition and/or thermal hysteresis activity. Part of these results has been highlighted in the article entitled "1D Self-Assembly and Ice Recrystallization Inhibition Activity of Antifreeze Glycopeptide-Functionalized Perylene Bisimides" published in *Chemistry – A European Journal*[47] while others represent unpublished work.

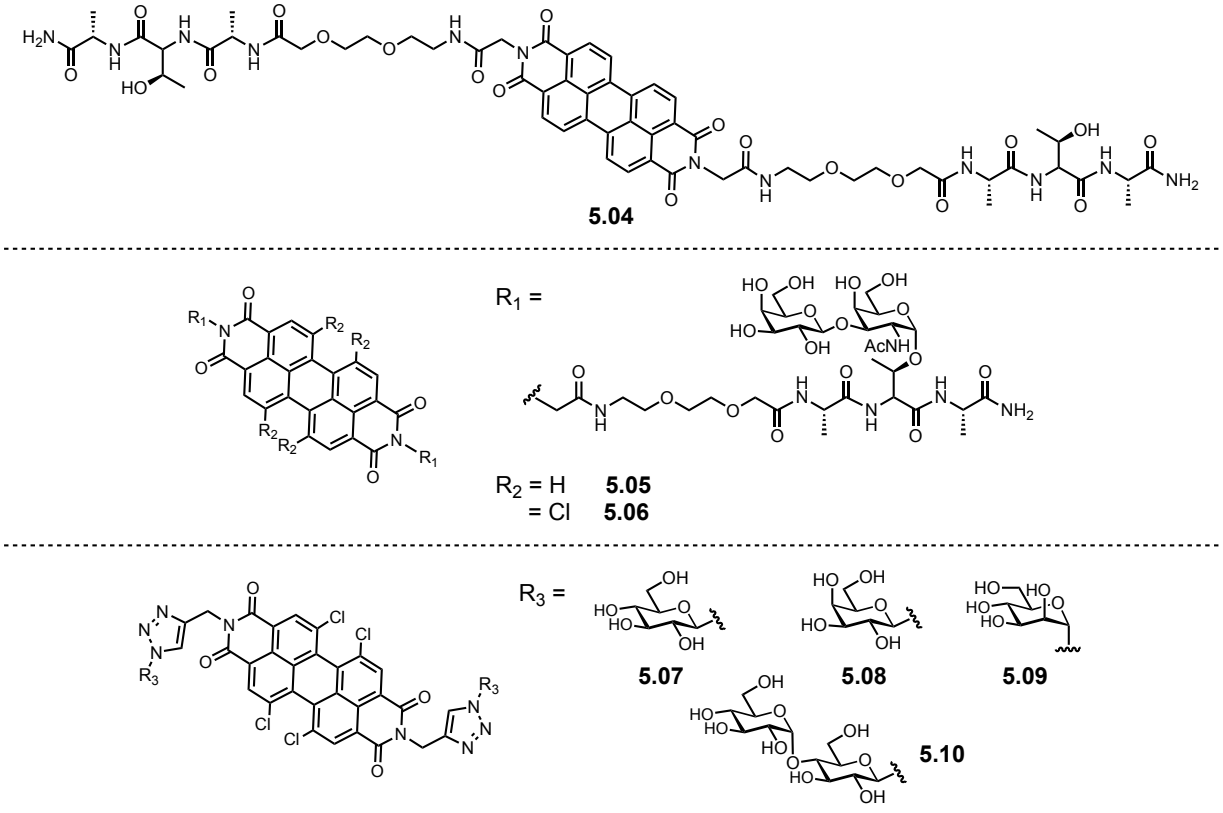

Figure 5.2.2.1. Structures of the AFGP-PBIs **5.04-5.10** assessed in **Section 5.4**.[47]

The synthesis of the target PBIs (e.g. bisimides **5.05** and **5.06**) was conducted in the Wilkinson laboratory using known literature methods (**Scheme 5.2.2.1**).[47,96–98] Briefly, bisimide **5.05** was prepared by coupling the glycopeptide **5.11** (prepared via the Fmoc-strategy in solid-

phase synthesis[40,99]) to dicarboxylic acid **5.12** (prepared using literature procedures[97]) using the HATU/HOAt peptide coupling strategy.[47] Bisimide **5.06** was also prepared using the aforementioned peptide coupling strategy involving the coupling of the dicarboxylic acid **5.13** (prepared using literature methods[98,100]) with glycopeptide **5.11**. The target PBIs were purified by reverse-phase preparative high-performance liquid chromatography (HPLC) and lyophilized prior to analysis of 1D self-assembly or antifreeze activity.[47] Other PBI analogues were approached in a synthetically similar manner.

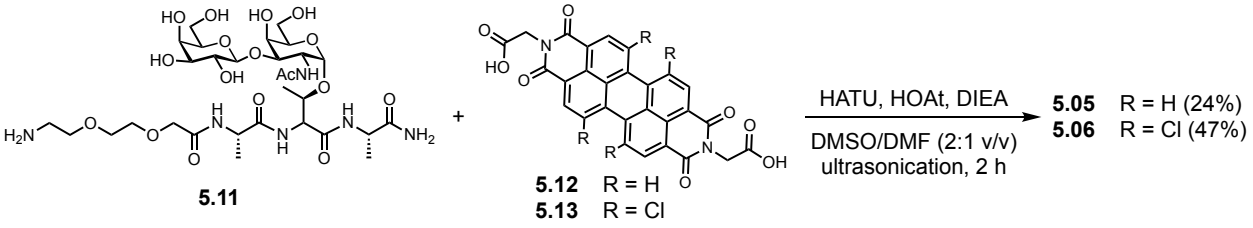

Scheme 5.2.2.1. Peptide coupling strategy employed to synthesize AFGP-PBIs **5.05** and **5.06**.[47] Yields of this final synthetic step are presented in brackets. Glycopeptide **5.11** and dicarboxylic acids **5.12** and **5.13** were prepared using literature procedures.[40,97–100]

With AFGP-PBI analogues in hand, attention was turned toward their potential antifreeze activity and self-assembly properties. The initial screen of the ice recrystallization inhibition (IRI) activities of the AFGP-PBIs was performed using the splat-cooling assay whereby sample droplets were flash-frozen and allowed to anneal for 30 minutes at -6.4 °C prior to analysis of ice crystals in each test case.[92] However, before assessment, the PBIs were heated to 90 °C for one hour and then cooled and stored at room temperature for 24 hours in order to promote aggregation and equilibration. For example, a sample of AFGP-PBI **5.05** dissolved in PBS was found to have aggregated and equilibrated after 10 minutes (up to 5 hours) by time-dependent fluorescence emission spectroscopy whereby a lack of change in fluorescence intensity of peaks

associated with the monomeric (547 nm) and aggregated (673 nm) forms of the analogue was indicative of aggregation and equilibration.[47] This result, as well as the investigation of the other self-assembly properties of the AFGP-PBIs, were performed by other collaborators of this project.[47] Interestingly, using transmission electron microscopy (TEM), atomic force microscopy (AFM) and further measurements, the planar AFGP-PBI **5.05** was found to undergo 1D self-assembly in aqueous media resulting in extended nanofibers, and near-ultraviolet circular dichroism (CD) spectroscopy suggested that this analogue may form helical aggregates.[47] The ring-distorted AFGP-PBI **5.06** analogue, meanwhile, displayed only weak aggregative behaviour in aqueous media.

With the self-assembly properties determined for AFGP-PBIs **5.05** and **5.06**, **Figure 5.2.2.2** depicts the ice recrystallization inhibition activity displayed as the percent mean grain size (% MGS) of ice crystals compared to ice crystals in the presence of the phosphate-buffered saline (PBS) control. These analogues were soluble at 22 mM and therefore initially tested at this concentration (the traditionally tested concentration for other AFGP analogues assessed by the Ben laboratory). Both PBI **5.05** and **5.06** were found to possess moderate IRI activity; which were either similar or enhanced to that of previous amphiphilic AFGP analogues developed in the Ben laboratory.[101] While it appeared that AFGP-PBI **5.05** displayed slightly more inhibitory effects at 22 mM, there was no statistical significance between the two activities (n = 3). Therefore, at this statistical power, the trend as to how a planar or ring-distorted PBI core may impact IRI activity is difficult to conclude; however, more data (e.g. modified AFGP-PBIs based on these initial compounds) may suggest the potential that a planar PBI core and AFGP-PBI aggregative behaviour enhances the IRI activity. While the perylene core alone could not be analyzed for IRI activity owing to its extremely poor solubility in phosphate-buffered saline, the

glycopeptide **5.11** was assessed and was found to have significantly reduced IRI activity compared to both AFGP-PBIs **5.05** and **5.06**. In fact, a sample of 10 mM AFGP-PBI **5.06** was still found to have a statistically enhanced ability to inhibit ice recrystallization compared to that of the glycopeptide **5.11** at 22 mM (one-way ANOVA with Tukey's multiple comparisons test, $p < 0.0001$).[47] Additionally, AFGP-PBI **5.04** which contains the peptide sequence without glycosylated threonines, did not display any IRI activity when tested at its maximum solubility of 5 μM. Since this analogue was not soluble at higher concentrations, future PBIs should be functionalized with glycopeptides for added solubilities. Taken all together, these results suggest that the presence of the hydrophobic PBI core is essential for the activity of the AFGP-PBIs. Finally, these AFGP-PBI IRIs displayed weak IRI activity compared to that of the native AFGP-8 at 5.5 μM. However, using nanoliter osmometry (see page 252 in the **Experimental** section for further details), AFGP-PBIs **5.05** and **5.06** (10 mg/mL) were found to lack thermal hysteresis (TH) or dynamic ice shaping (DIS) behaviours contrary to the antifreeze activities of AFGP-8. Therefore, while these novel IRIs are weaker inhibitors of ice recrystallization than AFGP-8, it is promising that they do not exhibit their antifreeze activity via ice binding which is correlated with detrimental properties (including that of ice spicule formation at high AFGP concentrations).[16,22]

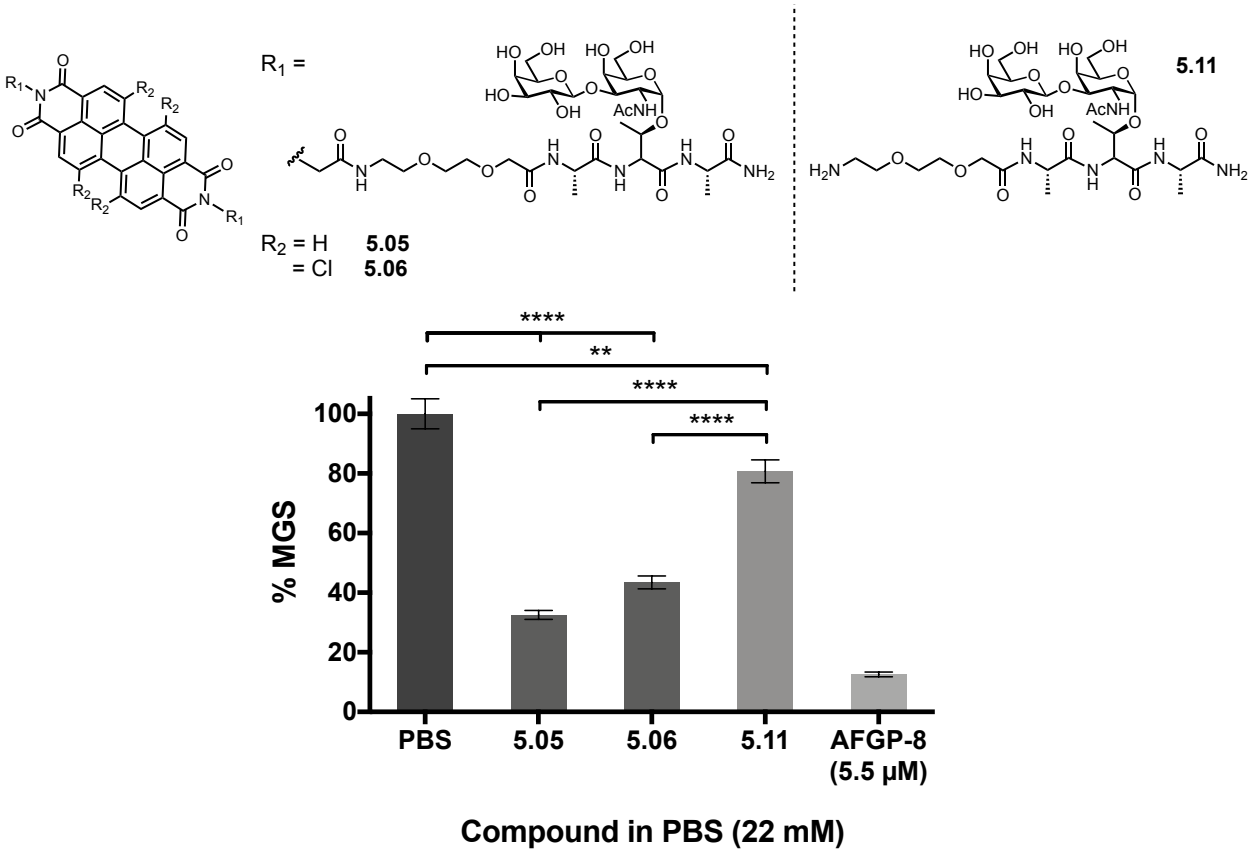

Figure 5.2.2.2. Ice recrystallization inhibition of AFGP-PBI analogues **5.05** and **5.06** compared to the glycopeptide **5.11**, AFGP-8 (5.5 μM), and the phosphate-buffered saline (PBS) control for IRI activity (adapted from reference 47 with permission).[47] Activity is presented as the percent mean grain size (% MGS) of ice crystals in the presence of an inhibitor compared to ice crystals in the presence of PBS and error bars represent the percent standard error of the mean (% SEM). Asterisks indicate statistical significance as was determined by one-way ANOVA with Tukey's multiple comparisons test (n = 3, ** $p < 0.01$, **** $p < 0.0001$). All data points are statistically significant from AFGP-8; however, this is not displayed on the figure for graphical simplicity.

Following the initial IRI screen, promising compounds are then subjected to further IRI analysis using a modified splat-cooling assay (details of the overall IRI analysis process is previously outlined in **Chapter 1**).[94] Instead of considering one single concentration as was the case of the initial IRI screen, in the modified assay, the IRI activity of AFGP-PBI **5.06** was quantified by examining the effect of multiple concentrations after the frozen samples were

annealed at -6.4 °C for 5 minutes prior to ice crystal area assessment.[94] The dose-response curve for the inhibitory activity of AFGP-PBI **5.06** and resulting IC_{50} value was generated by fitting a two-parameter sigmoidal curve to the normalized rate constants for each inhibitor concentration (**Figure 5.2.2.3a**). An IC_{50} value of 10 ± 1 mM was found for the AFGP-PBI. For comparison, this IC_{50} value falls into the range of the efficacious gluconamides studied in **Chapter 3**. Since AFGP-PBI **5.06** was found to be effective at inhibiting ice recrystallization, it was further investigated for its potential cryoprotective abilities. To that end, the preliminary cytotoxicity of AFGP-PBI was assessed using the resazurin assay (discussed further in **Chapter 4** and **Experimental** sections). **Figure 5.2.2.3b** depicts the significant cytotoxicity observed in human hepatocellular carcinoma cells (HepG2 cells) with concentrations of AFGP-PBI **5.06** that were below the IC_{50} value for IRI activity (10 ± 1 mM). For instance, the normalized initial rate of ice recrystallization in the presence of 3 mM was approximately 85% compared to the rate with no inhibitor present. The hepatic cell viability was already reduced to ~17% at this concentration. While cytotoxicity depends on the cell line, the significant cytotoxicity present at low millimolar concentrations in the absence of substantial IRI activity suggests that this AFGP-PBI would not be a beneficial cryoprotectant. Despite AFGP-PBI **5.06** not being amenable to cryopreservation purposes, future investigation into the full cytotoxicity profile and the mechanism by which these compounds induce cellular injury would be beneficial for the development of IRI-active PBIs that could be used in cellular systems.

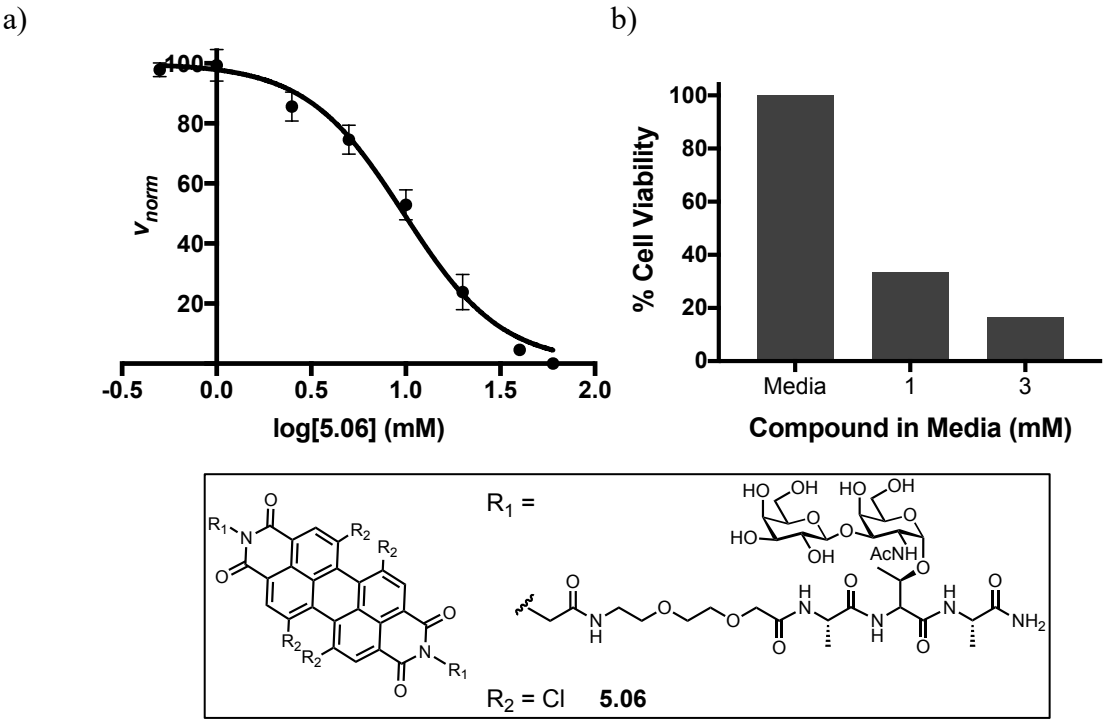

Figure 5.2.2.3 a) The dose-response curve generated for the IRI activity of AFGP-PBI **5.06** (IC_{50} = 10 ± 1 mM, R^2 = 0.99) (adapted from reference 47 with permission).[47] Rate constants normalized to those of the PBS control for each inhibitor concentration are reported with error bars indicating the standard error of the mean (SEM). **b)** The cell viability of HepG2 cells in the absence or presence of AFGP-PBI **5.06** using the resazurin assay (1 plate, n = 3 wells).

A series of carbohydrate-based PBIs were also prepared (PBIs **5.07-5.10**). These analogues did not possess the peptide portion present in the AFGP-PBIs previously investigated, and therefore, had a simplified synthesis. Using the splat-cooling assay where a series of compounds are initially screened for IRI activity at a single concentration, these PBIs were investigated at their maximum solubilities of 5 μM or 1 mM in PBS and these results are depicted in **Figure 5.2.2.4**. Note that a table in the **Experimental Section** (**Table A1** in **Appendix III**) provides a list of the maximum solubilities for select ice recrystallization inhibitors presented throughout this thesis. At these low millimolar and micromolar concentrations, PBIs **5.07-5.10** displayed weak to negligible IRI activity. It is difficult to

conclude how these analogues would inhibit ice recrystallization at higher concentrations; however, in any case, it is clear that these PBIs are not as effective inhibitors as the native AFGP-8 at these concentrations. Given the poor solubility and lack of IRI activity, these PBIs were not further assessed for their potential cytotoxicity.

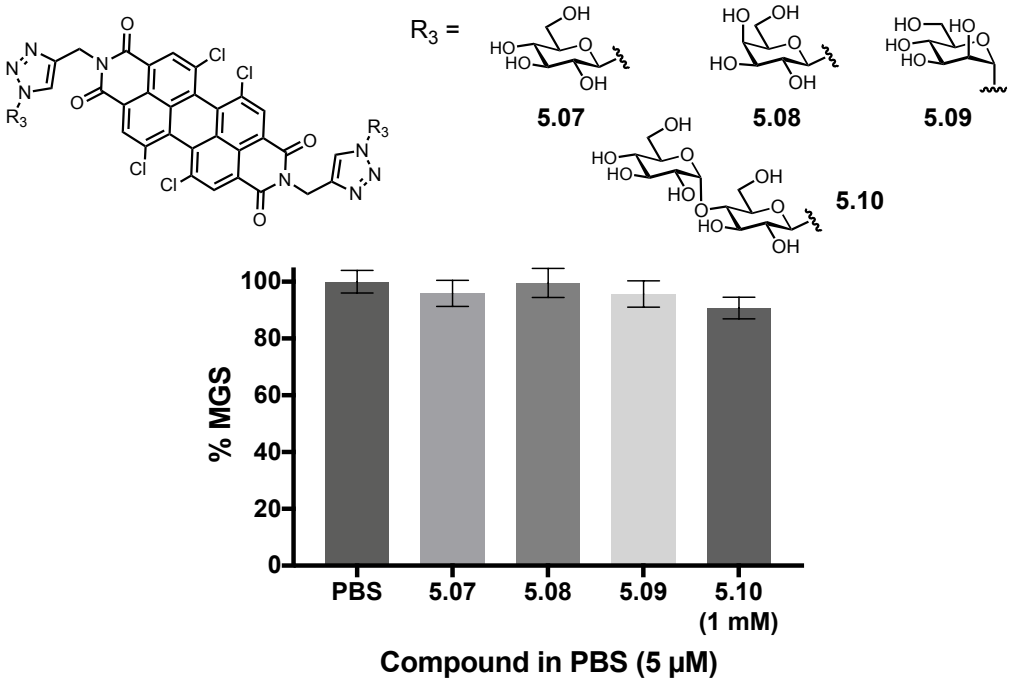

Figure 5.2.2.4. IRI activity of AFGP-PBI **5.04** and PBIs **5.07-5.10**. The percent mean grain size (% MGS) for each condition is compared to the PBS control, and error bars represent the percent standard error of the mean (% SEM, n = 3). No statistical differences observed based on one-way ANOVA with Tukey's multiple comparisons test ($p > 0.05$).

Overall, a series of AFGP-PBIs and PBIs were developed to assess the self-assembly and antifreeze activities of these biomimetics. AFGP-PBI **5.05** was found to exhibit 1D self-assembly with nanofiber extensions in aqueous media leading to helical aggregates. Meanwhile **5.06**, the ring-distorted AFGP-PBI, displayed only weak aggregative properties in aqueous media. Both analogues were found to possess moderate IRI activity at 22 mM while their glycopeptide

precursor **5.11** displayed only weak IRI activity. It was therefore concluded that the presence of the PBI core was required for inhibition of ice recrystallization. Further, these AFGP-PBIs did not display thermal hysteresis or dynamic ice shaping properties thereby suggesting that their antifreeze activity is not due to ice binding properties (images of the ice crystal habits are presented in the **Experimental** section, page 252). AFGP-PBI **5.06** possessed an IC_{50} value of 10 ± 1 mM for IRI activity, while unfortunately, preliminary cytotoxicity results suggest that the PBI is toxic to hepatocellular cells. Further, PBIs **5.07-5.10** did not display IRI activity at their maximum solubilities in phosphate-buffered saline.

5.3 Photoswitchable glycopeptides and carbohydrate-based *n*-butylazobenzene surfactants as ice recrystallization inhibitors

5.3.1 Azobenzene-functionalized glycopeptides as ice recrystallization inhibitors

A series of glycopeptides were envisioned based on the hypothesis that we could control their ability to inhibit ice recrystallization by altering their physicochemical properties. Specifically, tuning the physicochemical properties would be possible by utilizing the photoswitchable nature of azobenzene functionality tethered to a glycopeptide moiety (as a mimetic of those in the naturally occurring AFGPs). While AFGPs possess intriguing and potent antifreeze activities, they are generally not amenable to cryoprotective applications owing to the presence of thermal hysteresis activity; a property that has shown to be detrimental to cell survival after cryopreservation.[12–15] On top of this, the applicability of AFGPs for commercial purposes is also limited by the difficulty in attaining large quantities of AFGPs in high purities. One approach aimed at mitigating these limitations is to incorporate the key structural features of

AFGPs into more easily produced ice recrystallization inhibitors whilst avoiding the undesirable TH activity. As a result of this notion, a series of azobenzene-functionalized glycopeptides incorporating the glycopeptide portion of AFGPs attached to an azobenzene tail was designed (**Figure 5.3.1.1**). Specifically, glycopeptides bearing one repeat of the AFGP tripeptide (Ala-(glyco)Thr-Ala)$_{n=1}$ were developed with either a *n*-hexyl group (**5.14**) or a *n*-decyl group (**5.15**) attached to the azobenzene moiety in order to determine the impact of differing alkyl chain length. Compounds **5.16-5.19** were analogues where (Ala-(glyco)Thr-Ala)$_{n=2}$ were designed to compare to analogues **5.14** and **5.15**, and thus, the impact of a monomer or dimer of the (Ala-(glyco)Thr-Ala) unit. Different alkyl chain lengths on the azobenzene group of glycopeptides **5.16-5.19** included *n*-butyl (**5.16**), *n*-hexyl (**5.17**), *n*-octyl (**5.18**), and *n*-decyl (**5.19**) groups.

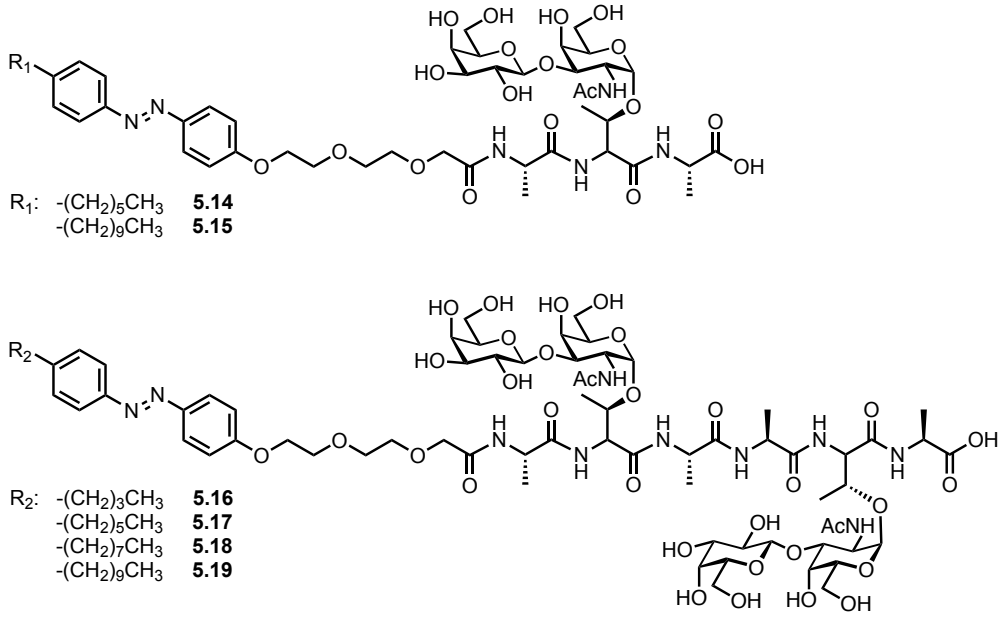

Figure 5.3.1.1. The structure of azobenzene-functionalized glycopeptides **5.14-5.19**.

The IRI activity of the azobenzene-functionalized glycopeptides was assessed using the splat-cooling assay whereby a droplet of sample dissolved in phosphate-buffered saline (PBS) was frozen and annealed at -6.4 °C for 30 minutes prior to the assessment of ice crystal area (the % MGS of ice crystals in the presence of inhibitors are compared % MGS of crystals in the presence of PBS). As depicted in **Figure 5.3.1.2**, these azobenzene-functionalized glycopeptides exhibited weak-to-negligible inhibitory activity at a concentration of ≤ 11 mM. Note that the tested concentrations were the maximum solubilities of the glycopeptides in PBS. Compared to PBS, no significant changes were observed with the glycopeptides bearing one peptide unit (Ala-(glyco)Thr-Ala)$_{n=1}$ (glycopeptides **5.14** and **5.15**). Interestingly, within the panel of glycopeptides bearing two peptide units, the glycopeptides that were soluble at 11 mM in PBS (**5.16** and **5.19**) showed statistically increased levels of IRI activity compared to the control, albeit still resulting in weak IRI activity. By considering glycopeptides **5.16** (possessing an *n*-butyl group) and **5.19** (with an *n*-decyl group), we can conclude that varying the alkyl chain length positioned on the azobenzene moiety does not significantly influence the IRI activity (data were not statistically significant determined using one-way ANOVA with multiple comparisons test and $p > 0.05$; the comparison between **5.16** and **5.19** is not shown in **Figure 5.3.1.2**). Altogether, these results suggest that an increase in IRI activity is observed with increasing repeats of the glycopeptide unit while alkyl chain length on the azobenzene moiety does not impart significant changes to the activity.

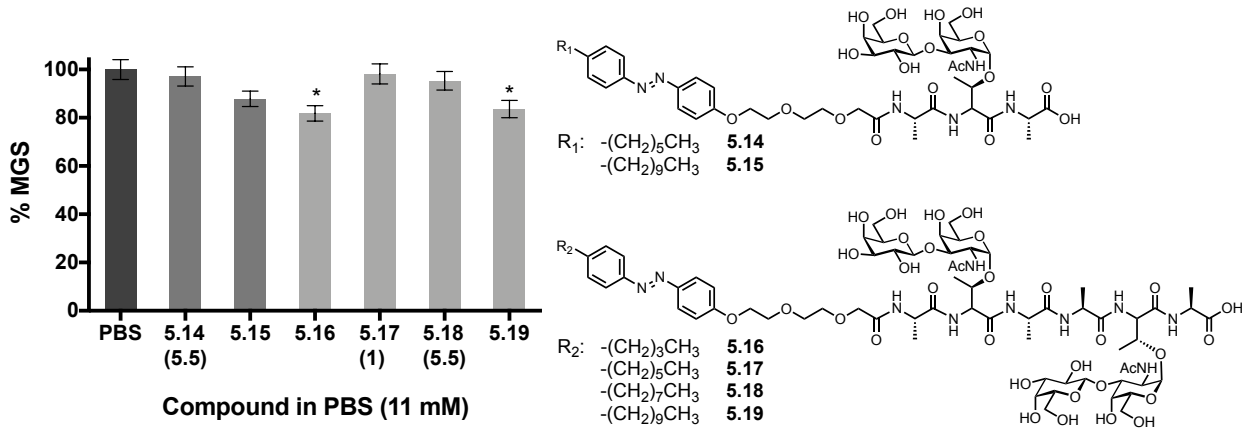

Figure 5.3.1.2. The percent mean grain size (% MGS) of ice crystals in the presence of azobenzene-functionalized glycopeptides **5.14-5.19** dissolved in PBS (at 11 mM unless indicated by a different mM concentration in brackets) compared to ice crystals in the presence of the PBS control alone. Error bars represent the % SEM, with statistical significance between the control and a sample indicated using an asterisk as determined using a one-way ANOVA with Dunnett's multiple comparisons test (* $p < 0.05$, $n = 3$).

After determining the IRI activity, our attention was focused on the potential for these azobenzene-functionalized glycopeptides to possess TH activity. As mentioned previously, TH activity has been shown to be detrimental to cell survival in cryopreservation applications. These derivatives were found to lack TH activity and dynamic ice shaping (DIS) using nanoliter osmometry (see page 252 in the **Experimental Section** for assay details and images of ice crystals). Specifically, the ice crystals formed in the presence of **5.14** and **5.17** (10 mg/mL) grew uniformly upon gradual temperature change thereby indicating an absence of thermal hysteresis. Importantly for the continued development of azobenzene-based glycopeptides toward cryoprotectant purposes, a lack of TH activity (and DIS) is attributed to a lack of binding interactions between the azobenzene-functionalized glycopeptides and the ice crystal lattice. Unfortunately, with the low solubility and weak-to-negligible IRI activity observed, these derivatives were not ideal candidates for further experiments in developing photoswitchable

IRIs. Our attention was therefore turned toward azobenzene derivatives that we hypothesized would have increased solubilities and IRI activity. As detailed in **Section 5.3.2**, the glycopeptide portions of the azobenzene compounds were replaced with monosaccharides. Further, since increasing the length of the alkyl chain on the azobenzene group did not alter IRI activity, the carbohydrate-based azobenzene derivatives were designed with an *n*-butyl group.

5.3.2 Photocontrollable carbohydrate-based *n*-butylazobenzene surfactants as ice recrystallization inhibitors

In an effort to design azobenzene-functionalized derivatives with photocontrollable IRI activity, a series of carbohydrate-based surfactants were envisioned based on the hypothesis that the compounds would have better solubility than the azobenzene-functionalized glycopeptides. Specifically, tuning the physicochemical properties of carbohydrate-based surfactants would be possible by utilizing the photoswitchable nature of *n*-butylazobenzenes while the selection of the carbohydrate head group would also balance the hydrophobicity thereby offering additional control through the carbohydrate's variable polarity, stereochemical configuration, and their degree of hydration.[102] Recall that IRI activity was found to increase among mono- and disaccharides with increasing hydration indexes (e.g. IRI activity of D-galactose > D-glucose > D-mannose > D-talose and IRI activity of D-melibiose > D-lactose > D-trehalose > D-maltose > D-sucrose), and this trend prompted the use of the three most active monosaccharides into the design of carbohydrate-based surfactants. The parallel synthesis of the carbohydrate-based surfactants was conducted by the Wilkinson laboratory and involved tethering a D-galactose, D-glucose, or D-mannose head group to a *n*-butylazobenzene tail group (**Scheme 5.3.2.1**).[78] Briefly, the appropriate acetylated trichloroacetimidate-glycosides were produced from the corresponding

glycosyl pentaacetates while the *n*-butylazobenzene alcohol was synthesized starting with 4-butylaniline, phenol, and tosylated-PEG3 precursors.[78,103] Since these surfactants had to be soluble in aqueous media for IRI testing as well as for future applications, increased solubility was achieved through the incorporation of a triethylene glycolate spacer (originating in the PEG3 precursor) between the head and tail groups. A lewis acid-promoted glycosidation between the trichloroacetimidate-glycosyl donor with the *n*-butylazobenzene alcohol acceptor as well as deacetylation of the crude products led to the desired carbohydrate-based surfactants (**5.20-5.22**).[74]

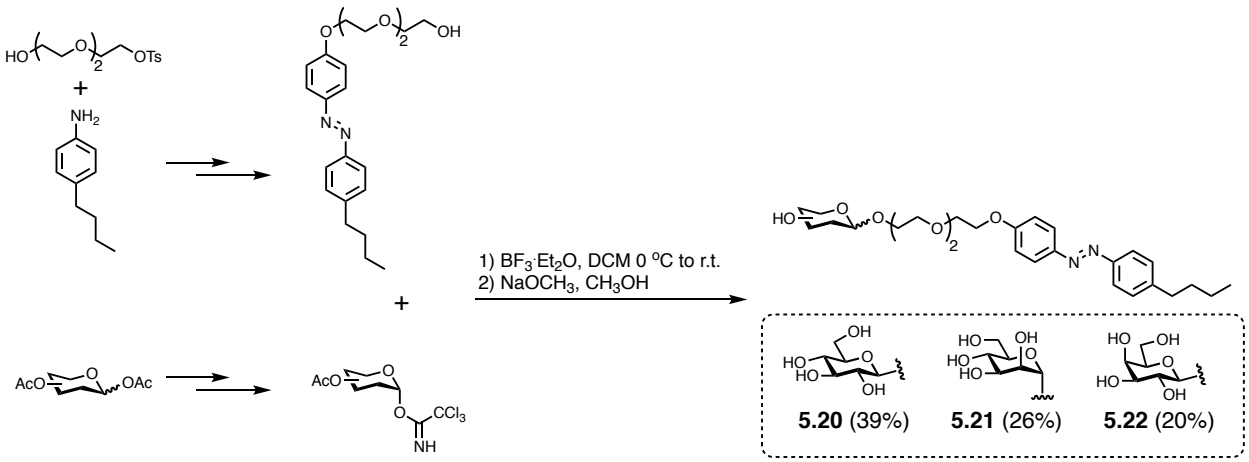

Scheme 5.3.2.1. General synthesis of the carbohydrate-based surfactants **5.20-5.22**.[74,78,103] Yields for the final two steps for each surfactant are presented in brackets.

With surfactants **5.20-5.22** in hand, attention was focused on their potential IRI and TH activity. The ability of the surfactants to inhibit ice recrystallization (**Figure 5.3.2.1**) was determined using the splat-cooling assay with a 30-minute annealing period at -6.4 °C.[92] The *trans*-isomers of the surfactants, which were the resting photostationary states as estimated by integration of a proton signal in the ^{1}H NMR spectra, were dissolved at 22 mM (**5.20** and **5.21**)

or 5 mM (**5.22**, due to poor solubility) in phosphate-buffered saline (PBS) before being assessed for their IRI activity. See the NMR spectra in the **Appendix IV** for further details. In order to assess the IRI activity of the *cis*-photoisomers, samples were irradiated with UV light (361 nm) for 10 minutes just before performing the splat-cooling assay and kept in the dark until assessment. It is important to note that the *cis*-dominated photostationary state (after sample irradiation with UV light) was comprised of approximately 70% *cis*-isomers based off ^{1}H NMR spectral integrations while the *trans*-dominated state was comprised of less than 10% of *cis*-photoisomers.[77,104,105] Further, UV-vis spectroscopy was used to observe azobenzene photoisomerization by monitoring the reduction of the intensity of the π-π* transition peak (350 nm) and the increase of intensity of the n-π transition peak (440 nm) as well as two isobestic points (320 nm and 420 nm).[104,105] Studies suggested that minimal thermal *cis*-*trans* relaxation was observed for 24 hours at 20 °C; signifying that negligible relaxation occurs during the time it took to complete the splat-cooling assay for IRI activity.[74] As depicted in **Figure 5.3.2.1**, the glucose-based surfactant **5.20** displayed weak IRI activity at 22 mM that was similar to the PBS control in both its *trans* and *cis*-photostationary states. Similarly, the galactose-based surfactant **5.22** also exhibited negligible IRI activity at 5 mM (its maximum solubility in PBS) and no photomodulation was observed for its IRI activity. Interestingly, however, the *trans*-isomer of the mannose-based surfactant **5.21** displayed significant IRI activity at 22 mM. Furthermore, photoirradiation of surfactant **5.21** to its *cis*-dominated photostationary state resulted in a significant reduction of IRI activity. This reduction in IRI activity can be attributed to the diminished hydrophobicity of the *n*-butylazobenzene tail group present in the *cis*-photoisomers. This lowered hydrophobicity of *cis*-photoisomers was supported when evaluating the interfacial activity of the surfactants using pendant drop tensiometry as well as in evaluating the 1-octanol

partition coefficient (log *P*) of the surfactants.[74] Specifically, an increase in the critical micelle concentration (CMC) after photoirradiation, as observed from the surface tension data for the surfactants, can be attributed to the reduced hydrophobicity and non-planar geometry of the *cis*-photoisomers compared to the *trans*-isomers.[77] The CMC value was increased from 0.21 mM to 0.45 mM upon photoisomerization of glucose-based surfactant **5.20** while the CMC value was increased from 0.23 mM to 0.49 mM upon photoisomerization of mannose-surfactant **5.21**. Both **5.20** and **5.21** displayed similar CMC values in both their *trans*- and *cis*- states thereby suggesting that they possess comparable hydrophilic-lipophilic balances (HLBs), while the CMC of **5.22** could not be determined due to its poor aqueous solubility. Unfortunately, the *cis*-isomers of **5.20** and **5.21** could not be assessed for their log *P* values due to considerable hydrophilicity; however, in the case of **5.22**, the log *P* value decreased upon photoirradiation (-0.35 to -0.85) which also confirms the notion that *cis*-isomers possess enhanced hydrophilicity.[74] Finally, a lactose-based analogue and a cellobiose-based analogue were also assessed for their ability to inhibit ice recrystallization. At 1 mM in its *trans*-dominated state, the lactose analogue did not possess any IRI activity (100% MGS) while the cellobiose analogue displayed moderate activity with a % MGS of 56% (data not shown in **Figure 5.3.2.1**).

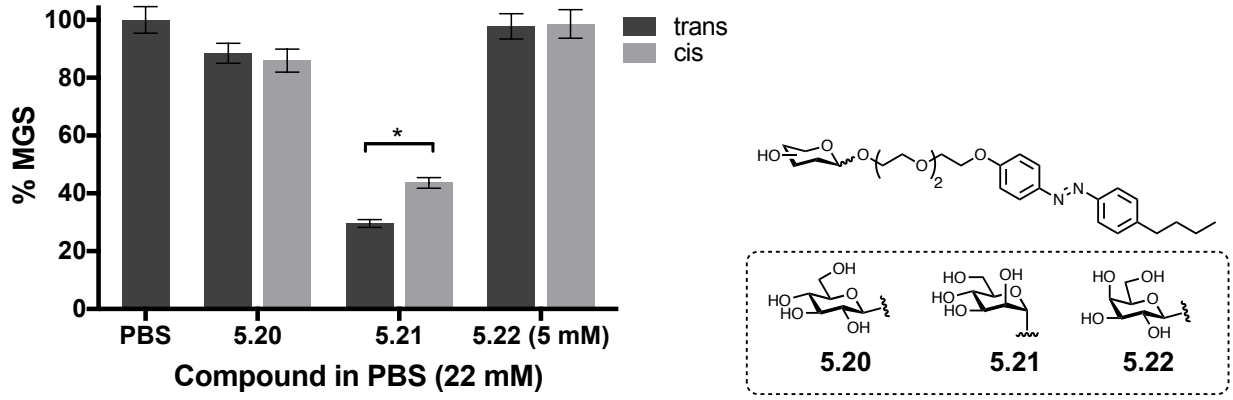

Figure 5.3.2.1. The IRI activity of the *trans*- and *cis*-dominated photostationary states of carbohydrate-based surfactants **5.20-5.22** dissolved in phosphate-buffered saline (PBS) at 22 mM (unless otherwise indicated).[74] Activity is represented as the percent mean grain size (% MGS) of ice crystals compared to the PBS control and error bars indicated percent standard error of the mean (% SEM, n = 3). Statistical significance is denoted using an asterisk (unpaired Student's T test, $p < 0.05$). **5.21** is statistically significant from all other data points.

Another noteworthy result (observed in **Figure 5.3.2.1)** was that the mannose-surfactant **5.21** displayed more IRI activity than its glucose analogue **5.20**. This result was surprising since D-glucose and D-mannose have similar hydration indexes and that up to this project, glucosyl analogues were found to be more IRI-active than their mannose counterparts.[106] With this opposite trend observed for surfactants **5.20** and **5.21**, this project has further emanated that IRI activity is strongly affected by changes to carbohydrate polarity and stereochemical configuration in relation to the rest of the molecule's hydrophobicity. To further accentuate the difference between the *trans*-isomers of the glucose- and mannose-derivatives (**5.20** and **5.21**, respectively), a dose-response curve for their IRI activity was determined using the modified splat-cooling assay (**Figure 5.3.2.2** for surfactant **5.21**).[94] Briefly, this assay involved determining the rates of ice recrystallization for multiple sample concentrations after 5-minute

annealing periods at -6.4 °C. This kinetic analysis revealed an IC_{50} value of 7 ± 3 mM for **5.21** while no such data could be obtained for **5.20** due to its lack of activity even at increasing concentrations up to its maximum solubility.

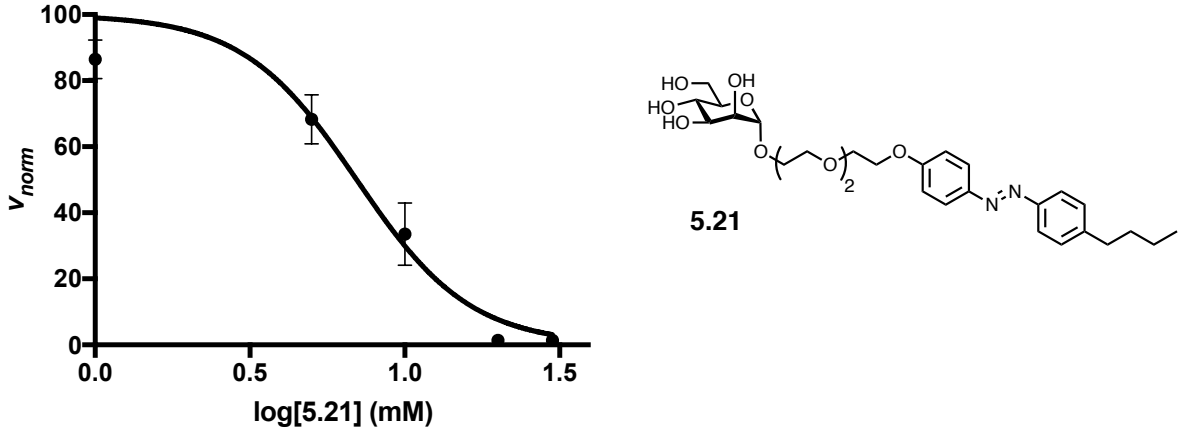

Figure 5.3.2.2. The dose-response curved generated for surfactant **5.21** (IC_{50} = 7 ± 3 mM, R^2 = 0.96).[74] The IC_{50} value was obtained by fitting a two-parameter sigmoidal curve to the normalized rate constants obtained from three experiments (± SEM).

Owing to the potent IRI activity observed for the mannose-surfactant **5.21**, the surfactant's potential thermal hysteresis (TH) activity was assessed using nanoliter osmometry (see page 252 in the **Experimental Section** for protocol and ice crystal image).[74] Briefly, a thermoelectrically-controlled microscope stage was used to freeze and slowly thaw an aqueous sample droplet enclosed in oil until only one single ice crystal remains. TH activity is noted as the depression of the freezing point of a sample in relation to its melting point, with non-uniform ice growth being indicative of a compound interacting with the ice crystal lattice. Therefore, the morphology of the single ice crystal was observed while the temperature was incrementally decreased. Notably, since **5.21** was not soluble at 10 mg/mL (a concentration that has been previously used to assess previous surfactants and hydrogelators in the laboratory[102,107]), it was

tested at 0.5 mg/mL. The ice crystal grew uniformly as the temperature was gradually decreased thereby indicating that no TH activity was observed at this concentration and that the compound does not interact with the ice crystal lattice in order to instill its ice recrystallization inhibitory activity.

With the significant IRI activity of surfactant **5.21** at low millimolar concentrations as well as its lack of TH activity, this mannose-surfactant was the ideal candidate for analysis into the potential cryoprotective ability *in vitro* (**Figure 5.3.2.3**). As a preliminary model of cryoprotection studies that is relatively easy to use (whereby promising candidates would be further assessed in more precious cell lines like human umbilical cord blood), cultured human bone marrow erythroblasts (TF-1α cells) were cryopreserved with 30 mM of **5.21** with varying concentrations of dimethyl sulfoxide (0%, 2%, 5%, and 10 % DMSO).[74] 30 mM was used as the preliminary concentration of **5.21** as this was its maximum solubility in aqueous media (in this case, RPMI-1640 media; see **Experimental** section for further details). TF-1α cells were frozen at 2 x 10^6 cells/mL in the presence or absence of surfactant in DMSO solutions and frozen to -80 °C using an *iso*-propyl freezing container ("Mr. Frosty"). After 18 hours, cells were transferred to -196 °C and analysis was performed after a minimum of 12 hours. Samples were thawed under fast-thaw conditions using a 37 °C water bath, and cell viability and recovery were assessed using flow cytometry. These preliminary results suggest that the mannose-surfactant does not possess cryoprotective abilities at the high concentration of 30 mM. Incubation of TF-1α cells with or without surfactant for 30 minutes followed by cell viability assessment (**Figure 5.3.2.3b**) led to results that were consistent with the notion that high concentrations of surfactants can solubilize cell membranes thereby leading to increased cell death.[108] The loss of cell viability during cryopreservation with surfactant **5.21** (**Figure 5.3.2.3a**) was also due to this

toxicity. While dimethyl sulfoxide appeared to preserve cells in the absence of the test compound, the inability of dimethyl sulfoxide to protect cells while in the presence of surfactant **5.21** can be explained by the surfactant's ability to solubilize the membrane. Additionally, the significant damage to membrane integrity may occur prior to the cells' ability to initiate apoptosis (as observed by the lack of apoptotic cells in the test conditions). It is worth noting that there are contradicting reports in the literature regarding the toxicity of azobenzene analogues.[82,90,109]

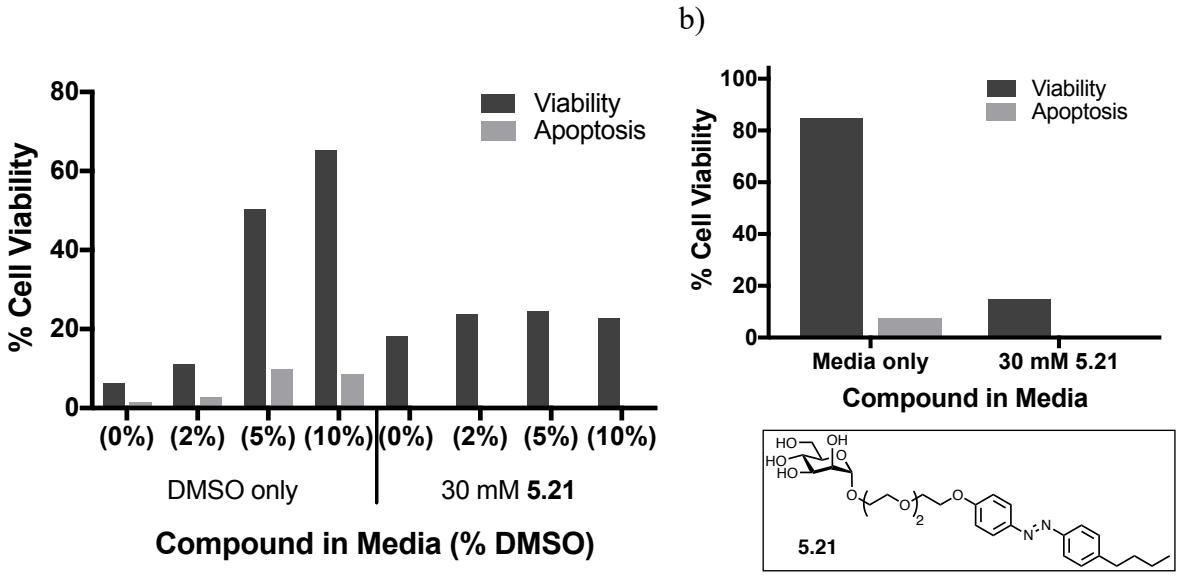

Figure 5.3.2.3. **(a)** Post-thaw percent cell viability TF-1α cells cryopreserved with 30 mM surfactant **5.21** in varying concentrations of DMSO, and (b) Percent cell viability of TF-1α cells incubated in the absence or presence of mannose-surfactant **5.21** (1 plate with n = 2-3 replicates).

Overall, the IRI analysis of a panel of carbohydrate-based surfactants (**5.20-5.22**) revealed that a mannose derivative was more IRI-active than its glucose and galactose counterparts and that the derivative did not enact this ice recrystallization inhibition through direct interaction with the ice crystal lattice (e.g. no TH activity). This was the first time that a mannose derivative

displayed more activity than a glucose analogue. Moreover, upon photoirradiation to the *cis*-dominated photostationary state, surfactant **5.21** displayed significantly weaker activity than as the *trans*-photoisomer, thereby suggesting that the increase in hydrophilicity following *trans*-*cis* photoisomerization was detrimental to IRI activity. While initial cryopreservation studies revealed that high concentrations of surfactant **5.21** resulted in significant loss of cell viability and recovery, these surfactants mark the first investigation into the IRI activity of carbohydrate-based surfactants bearing an azobenzene moiety. This study is an important benchmark for the development of future novel photoresponsive IRIs. The next panel of photocontrollable IRIs developed as a result of this initial investigation is detailed in **Section 5.4** and involves the use of carbohydrate-based fluorosurfactants as photoresponsive ice recrystallization inhibitors.

5.4 Photocontrollable carbohydrate-based fluorosurfactants as inhibitors of ice recrystallization

Next, the synthesis and IRI analysis were investigated for a panel of fluorosurfactants involving a variable head group (e.g. various mono- and disaccharides) attached to a trifluoromethyl-substituted azobenzene tail group. We hypothesized that IRI activity could be modulated through modifications to a surfactant's hydrophilic-lipophilic balance (HLB) via variations in the carbohydrate head group, the regiochemistry of the trifluoromethyl group on the azobenzene aromatic ring, and finally, via the isomeric state of the azobenzene tail. Non-ionic fluorosurfactants were the ideal candidates for the development of novel photocontrollable IRIs since they have a number of promising physicochemical properties and they have been shown to result in low hemolytic activity of rabbit red blood cells.[110–112] The synthesis of these surfactants included a Copper(I)-catalyzed Azide-Alkyne Cycloaddition (CuAAC) between a glycosyl azide

and the appropriate azobenzene-functionalized alkyne (**Scheme 5.4.1**).[75] The azobenzene alkyne was synthesized starting with the appropriately substituted (trifluoromethyl)aniline, phenol, and tosylated-PEG3 precursors while the glycosyl azide was also prepared using literature procedures.[78,103] The targets were obtained in adequate yields after deacetylation of the carbohydrate-head group under Zemplén conditions followed by purification of the crude products by reverse-phase preparation high-performance liquid chromatography (HPLC).[113–116] Fluorosurfactants incorporated either a D-glucose (Glc, **5.23-5.25**), D-galactose (Gal, **5.26-5.28**), D-mannose (Man, **5.29-5.31**), or D-cellobiose (Cel, **5.32-5.34**) carbohydrate group. Further, surfactants either bore a *para*-substituted azobenzene with respect to the trifluoromethyl group relative to the N=N bond (*p*-CF_3, **5.23**, **5.26**, **5.29**, and **5.32**), a *meta*-substituted azobenzene (*m*-CF_3, **5.24**, **5.27**, **5.30**, and **5.33**), or an *ortho*-substituted tail group (*o*-CF_3, **5.25**, **5.28**, **5.31**, **5.34**). In an effort to impart sufficient aqueous solubility for these surfactants, a triethylene glycolate spacer (originating from the PEG3 precursor) was incorporated between the head and tail groups; a strategy that was also utilized for the previously discussed *n*-butylazobenzene surfactants (**Section 5.3**).

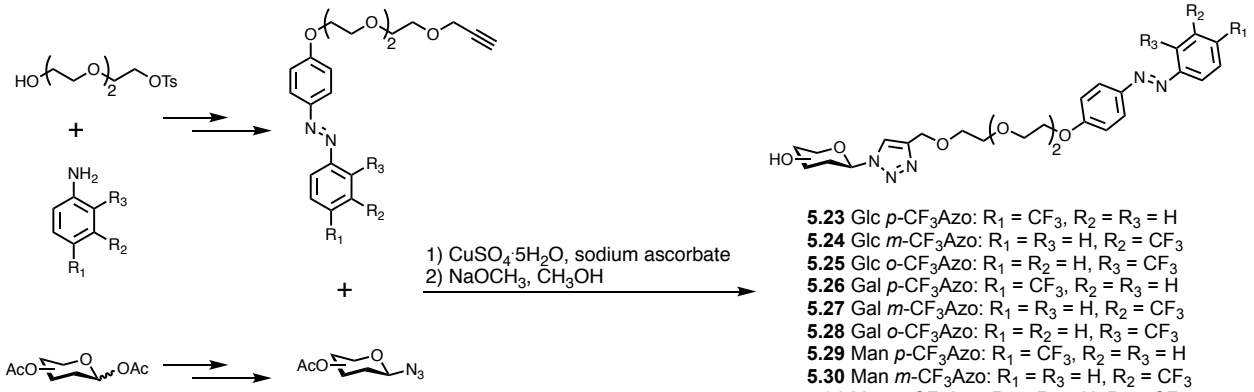

5.23 Glc *p*-CF_3Azo: R_1 = CF_3, R_2 = R_3 = H
5.24 Glc *m*-CF_3Azo: R_1 = R_3 = H, R_2 = CF_3
5.25 Glc *o*-CF_3Azo: R_1 = R_2 = H, R_3 = CF_3
5.26 Gal *p*-CF_3Azo: R_1 = CF_3, R_2 = R_3 = H
5.27 Gal *m*-CF_3Azo: R_1 = R_3 = H, R_2 = CF_3
5.28 Gal *o*-CF_3Azo: R_1 = R_2 = H, R_3 = CF_3
5.29 Man *p*-CF_3Azo: R_1 = CF_3, R_2 = R_3 = H
5.30 Man *m*-CF_3Azo: R_1 = R_3 = H, R_2 = CF_3
5.31 Man *o*-CF_3Azo: R_1 = R_2 = H, R_3 = CF_3
5.32 Cel *p*-CF_3Azo: R_1 = CF_3, R_2 = R_3 = H
5.33 Cel *m*-CF_3Azo: R_1 = R_3 = H, R_2 = CF_3
5.34 Cel *o*-CF_3Azo: R_1 = R_2 = H, R_3 = CF_3

Scheme 5.4.1. The general synthesis of the fluorosurfactants **5.23-5.34**.[75,115]

With the targets in hand, we determined the interfacial activity of the fluorosurfactants using the previous methods implemented for the photocontrollable IRIs presented in **Section 5.3**.[75] The composition of both the *trans*-dominated and *cis*-dominated photostationary states was estimated by integration of the triazole proton present in the ^{1}H NMR spectra of surfactants **5.26-5.28**. See the NMR spectra in the **Appendix IV** for further details. Using this method, the *trans*-dominated state was comprised of approximately 90% of the *trans* photoisomer. After UV irradiation (361 nm) of the resting state for 10 minutes, the *cis*-dominated state was made up of approximately 70% *cis*-photoisomer, and negligible thermal relaxation of this photoexcited state was observed after 24 hours at 20 °C in the dark. Similar to that observed with the *n*-butylazobenzene surfactants **5.20-5.22**, an increase in the critical micelle concentration (CMC) occurred after surfactants were irradiated to their photoexcited states as determined using pendant drop tensiometry.[78,115] The changes in CMC values upon photoisomerization of the glucose-based fluorosurfactants were from 0.24 mM to 0.25 mM for the *p*-CF_3 **5.23**, from 0.26 mM to 0.91 mM for the *m*-CF_3 **5.24**, and from 1.52 mM to 2.81 mM for the *o*-CF_3 **5.25**. The changes in CMC values upon photoisomerization of the galactose-based fluorosurfactants were from 0.23 mM to 0.53 mM for the *p*-CF_3 **5.26**, from 1.41 mM to 1.71 mM for the *m*-CF_3 **5.27**, and from 1.94 mM to 2.03 mM for the *o*-CF_3 **5.28**. The changes in CMC values upon photoisomerization of the mannose-based fluorosurfactants were from 0.26 mM to 0.36 mM for the *p*-CF_3 **5.29**, from 0.17 mM to 0.54 mM for the *m*-CF_3 **5.30**, and from 0.13 mM to 0.51 mM for the *o*-CF_3 **5.31**. Finally, the changes in CMC values upon photoisomerization of the cellobiose-based fluorosurfactants were from 0.48 mM to 0.49 mM for the *p*-CF_3 **5.32**, from 0.81 mM to 1.28 mM for the *m*-CF_3 **5.33**, and from 0.59 mM to 2.29 mM for the *o*-CF_3 **5.34**. The increases observed upon photoirradiation could be explained by the reduction of planarity and

hydrophobicity of the *cis*-isomer compared to its *trans*-counterpart.[117] Interestingly, the magnitude of the change in CMC observed upon photoirradiation was most apparent with the *ortho*-substituted derivatives (**5.25**, **5.28**, **5.31**, **5.34**), less so between *meta*-substituted surfactants (**5.24**, **5.27**, **5.30**, and **5.33**), and finally, even less with *para*-derivatives (**5.23**, **5.26**, **5.29**, and **5.32**). Further, while the *trans*-isomers of the *p*-CF_3 surfactants had a slightly larger dipole than their *cis*-counterparts, the difference in the dipole moment between the respective photostationary states of the *p*-CF_3 surfactants was small; a conclusion obtained upon observing that the respective changes in CMC values were negligible.[118,119] The overall trend observed with the CMC values highlighted the delicate HLB achieved in designing fluorosurfactants with varying trifluoromethyl-substituted azobenzene groups.

Log *P* values obtained for the surfactants once again depended on the carbohydrate head group and the substitution of the azobenzene tail. The changes in log *P* values upon photoisomerization of the glucose-based fluorosurfactants were from -0.32 to -0.20 for the *p*-CF_3 **5.23**, from -0.25 to -0.26 for the *m*-CF_3 **5.24**, and from -0.65 to -0.47 for the *o*-CF_3 **5.25**. The changes in log *P* values upon photoisomerization of the galactose-based fluorosurfactants were from -0.08 to 0.03 for the *p*-CF_3 **5.26**, from -0.14 to -0.03 for the *m*-CF_3 **5.27**, and from -0.02 to -0.01 for the *o*-CF_3 **5.28**. The changes in log *P* values upon photoisomerization of the mannose-based fluorosurfactants were from -0.32 to 0.07 for the *p*-CF_3 **5.29**, from -0.25 to -0.37 for the *m*-CF_3 **5.30**, and then from -0.31 to 0.14 for the *o*-CF_3 **5.31**. Finally, the changes in log *P* values upon photoisomerization of the cellobiose-based fluorosurfactants were from -1.22 to -0.10 for the *p*-CF_3 **5.32**, from -1.27 to -1.41 for the *m*-CF_3 **5.33**, and from -2.18 to -1.01 for the *o*-CF_3 **5.34**. Generally, the *ortho*-CF_3 surfactants (**5.25**, **5.28**, **5.31**, **5.34**) showed the most affinity for the hydrophilic aqueous phase out of all the regioisomers. Contrary to the results obtained for the

CMC values as well as those obtained for the log *P* values of the non-fluorinated surfactants **5.20-5.22**, an increase in hydrophobicity (increase in log *P* values) was observed upon photoirradiation of the *trans*-photoisomeric fluorosurfactants.[119] This result was surprising, yet still highlights the control that can be achieved with these photoswitchable fluorosurfactants.

The ability of these fluorosurfactants to inhibit ice recrystallization was assessed using the splat-cooling assay where a droplet of surfactant dissolved in phosphate-buffered saline (PBS) was frozen and allowed to anneal at -6.4 °C for 30 minutes prior to assessment (**Figure 5.4.1**).[92] In order to assess the IRI activity of the *cis*-dominated photostationary states, the samples were irradiated with UV light prior to performing the splat-cooling assay as usual. The areas of ice crystals in the presence of the surfactants were compared to the areas of ice crystals in the presence of PBS alone, which is represented by the percent mean grain size (% MGS) of ice crystals. Interestingly, not all *p*-CF_3 surfactants (**5.23**, **5.26**, **5.29**, and **5.32**) were soluble at the testing concentration of 22 mM (standard concentration used for IRIs assessed by the splat-cooling assay), and therefore, these select analogues were assessed at 5 μM. The *p*-CF_3 surfactants (**5.23**, **5.26**, **5.29**, and **5.32**) exhibited weak-to-negligible IRI activity compared to the PBS control. The *m*-CF_3 surfactants (**5.24**, **5.27**, **5.30**, and **5.33**) generally exhibited more IRI activity than their *p*-CF_3 counterparts, and notably, the *o*-CF_3 surfactants (**5.25**, **5.28**, **5.31**, **5.34**) displayed the most inhibitory activity compared to their *p*-CF_3 analogues. Therefore, the IRI activity of the fluorosurfactants is dependent on the regiochemistry of the azobenzene tail group.

a) IRI activity of glucose- and galactose-based fluorosurfactants:

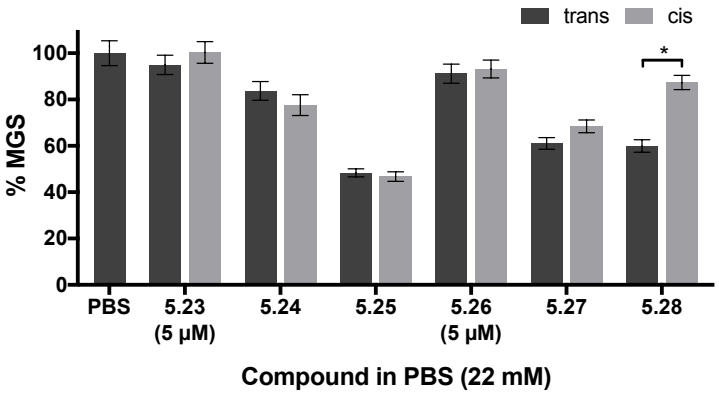

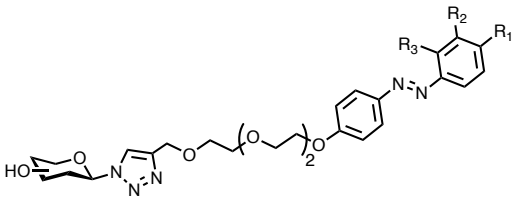

5.23 Glc *p*-CF_3Azo: $R_1 = CF_3$, $R_2 = R_3 = H$
5.24 Glc *m*-CF_3Azo: $R_1 = R_3 = H$, $R_2 = CF_3$
5.25 Glc *o*-CF_3Azo: $R_1 = R_2 = H$, $R_3 = CF_3$
5.26 Gal *p*-CF_3Azo: $R_1 = CF_3$, $R_2 = R_3 = H$
5.27 Gal *m*-CF_3Azo: $R_1 = R_3 = H$, $R_2 = CF_3$
5.28 Gal *o*-CF_3Azo: $R_1 = R_2 = H$, $R_3 = CF_3$

b) IRI activity of mannose- and cellobiose-based fluorosurfactants:

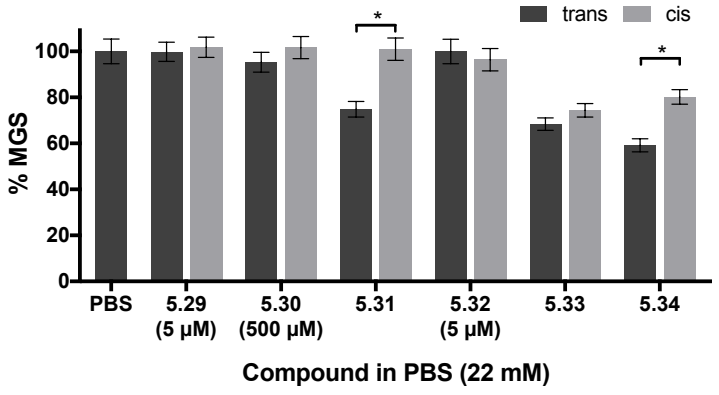

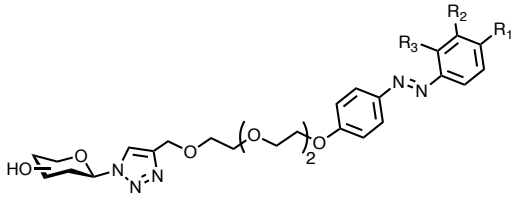

5.29 Man *p*-CF_3Azo: $R_1 = CF_3$, $R_2 = R_3 = H$
5.30 Man *m*-CF_3Azo: $R_1 = R_3 = H$, $R_2 = CF_3$
5.31 Man *o*-CF_3Azo: $R_1 = R_2 = H$, $R_3 = CF_3$
5.32 Cel *p*-CF_3Azo: $R_1 = CF_3$, $R_2 = R_3 = H$
5.33 Cel *m*-CF_3Azo: $R_1 = R_3 = H$, $R_2 = CF_3$
5.34 Cel *o*-CF_3Azo: $R_1 = R_2 = H$, $R_3 = CF_3$

Figure 5.4.1. The percent mean grain size (% MGS) of ice crystals in the presence of fluorosurfactants a) glucose- and galactose-based **5.23-5.28** and b) mannose- and cellobiose-based **5.29-5.34** at 22 mM unless otherwise indicated.[75] The IRI activity is reported as the mean of three experiments ± % SEM. Asterisks indicated statistical significance between photostationary states as determined using student's T test ($p < 0.05$).

More conclusions can be made upon further inspection of the IRI activity of the fluorosurfactants. For one, in comparing the *o*-CF_3 surfactants (**5.25**, **5.28**, **5.31**, **5.34**), the glucose-based surfactant **5.25** exhibited moderate activity with a % MGS of 48% while the other *ortho*-derivatives displayed activity with a % MGS above 60%. Notably, this is the opposite of that observed with the *n*-butyl azobenzene surfactants presented in **Section 5.2** whereby a

mannose-surfactant was more IRI-active than the glucose-analogue.[74] This is also contrary to what has been previously observed between glucose and galactose analogues; the galactose amphiphiles have previously been more active which has been attributed to the higher hydration index (HI) of galactose compared to glucose.[102,107] Interestingly, in considering the *m*-CF_3 fluorosurfactants (**5.24**, **5.27**, **5.30**, and **5.33**), the galactose derivative **5.27** was more active than the glucose analogue (**5.24**) thereby following the previously reported trend observed between a carbohydrate's HI and the resulting IRI activity. Taken together, these results emphasize the sensitivity of IRI activity to the regiochemistry of the azobenzene tail group. When considering the changes in IRI activity between the two photostationary states of each surfactant, the regiochemistry of the CF_3-substituted azobenzene tail once again affected the resulting inhibitory activity observed. Specifically, IRI activity was significantly reduced upon exciting the *o*-CF_3 surfactants (**5.28**, **5.31**, and **5.34**) with UV light into their *cis*-dominated states.[75] This result was not observed for any of the *p*-CF_3 or *m*-CF_3 derivatives nor was it observed for the glucose-based *o*-CF_3 surfactant **5.25**. The reduction in IRI activity observed for the *o*-CF_3 surfactants could have been due to the large differences observed in the hydrophobicity and interfacial activity between the two isomeric states of each surfactant (e.g. differences in CMC values). Overall, the IRI activity of the fluorosurfactants only appeared to be tuneable when the trifluoromethyl group was positioned *ortho* to the N=N bond present in the azobenzene tail (apart from **5.25**). Additionally, IRI activity was dependent on both the carbohydrate head group and CF_3-substitution of the tail.

Owing to the interesting activity of the *o*-CF_3 fluorosurfactants (**5.25**, **5.28**, and **5.34**), their cytotoxicity was assessed using the colorimetric MTT assay; an assay that was commonly utilized in the Ben laboratory prior to development of the resazurin assay (**Figure 5.4.2**). Briefly,

metabolically active cells are represented as those with enzymes capable of reducing 3-(4,5-dimethylthiazol-2-yl)-2,5-diphenyltetrazolium bromide (the MTT tetrazolium dye) to its insoluble formazan.[120] Unfortunately, incubation of human hepatocellular carcinoma cells (HepG2) with low millimolar concentrations of the fluorosurfactants resulted in substantial loss of viable cells. Concentrations assessed in the splat-cooling assay were not investigated for toxicity since significant cell loss was already observed in the low millimolar concentration screen of surfactant (up to 10 mM or 20 mM of surfactant). In fact, no viable cells were observed after incubation with galactose-based surfactant **5.28** while a significantly reduced number of viable cells were observed at low millimolar concentrations of glucose analogue **5.25** and cellobiose analogue **5.34**. The extent of these results was only somewhat surprising given the well-documented ability of surfactants to solubilize cell membranes as well as the results obtained for the *n*-butylazobenzene derivatives from **Section 5.3**.

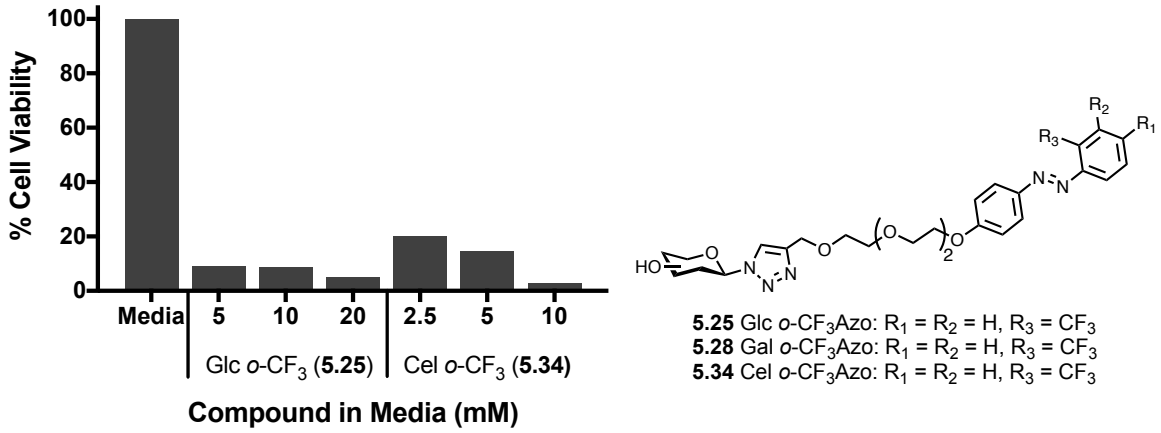

Figure 5.4.2. The percent cell viability (% cell viability) of HepG2 cells treated with *o*-CF_3 fluorosurfactants **5.25** and **5.34** compared to the control (cells in Minimum Essential Media, MEM) Performed on one plate with n = 3-12/condition, MTT assay.[75]

Overall, the IRI activity of a panel of photoswitchable carbohydrate-based fluorosurfactants was determined in addition to the modular synthesis and interfacial activity of the surfactant family.[75] IRI activity was found to be dependent on the regiochemistry of the trifluoromethyl group substitution on the azobenzene tail as well as the carbohydrate selected for the surfactant head group. The inhibition of ice recrystallization was increased when moving the *p*-CF_3 group to the *meta* position, and even more enhanced when the trifluoromethyl group was positioned *ortho* to the N=N bond of the azobenzene group. The most inhibition was observed with the moderately IRI-active glucose-based *ortho*-CF_3 surfactant; a result that is in contrast to previous reports highlighting galactose derivatives being more active than their glucose analogues as well as the result obtained in **Section 5.3** where a mannose surfactant was more active than its glucose counterpart. Interestingly, upon photoisomerization of the *trans*-dominated states of the *ortho*-CF_3 surfactants to their corresponding *cis*-dominated photoexcited states resulted in a decrease in IRI activity (with the exception from the glucose analogue). These *ortho*-CF_3 surfactants were, unfortunately, cytotoxic to human hepatocellular carcinoma cells. Nevertheless, the analysis of these azobenzene derivatives continue to highlight the dependency of IRI activity on the HLB of surfactants as well as the presence of tuneable IRI activity, and these results can certainly be used for the development of future novel IRI molecules.

5.5 Summary

The results herein represent significant advancements in the development of novel photoresponsive ice recrystallization inhibitors as well as biomimetic IRIs. **Section 5.2** highlighted the development of lipopeptides and glyco(peptide)-functionalized perylene bisimides (AFGP-PBIs) as biomimetic ice recrystallization inhibitors. AFGP-PBIs that displayed

1D self-assembly (or weakly exhibited) were also found to exhibit moderate IRI activity. The perylene core was found to be imperative for the presence of ice recrystallization inhibition. While these AFGP derivatives were less potent antifreezes than their counterparts found in nature (e.g. AFGP-8), the AFGP-PBIs did not display the undesirable TH activity. Additionally, since there PBIs would be found externally to cells (e.g. not cell permeable), we are not concerned with the PBI core's potential to disrupt cellular DNA. Taken together, this offers great advancement in the development of novel IRIs for their use in numerous biological and industrial applications. Next, in **Section 5.3**, a panel of glycopeptides and carbohydrate-based azobenzene surfactants were assessed for IRI activity. Among the carbohydrate-based surfactants, mannose *n*-butylazobenzene derivative was found to be the most IRI active compared to its glucose and galactose analogues. This antifreeze activity was not the result of ice-binding activities and this represented the first time that a mannose derivative exhibited more IRI activity than its glucose counterpart. Notably, photoisomerization of the *trans*-dominated photostationary states of azobenzenes to their *cis*-dominated states resulted in a reduction of inhibitor activity; possibly due to the increase in hydrophilicity. Altogether, these results represent the first report of a series of photoresponsive ice recrystallization inhibitors.[74] From these surfactants came a series of photoswitchable fluorosurfactants (**Section 5.4**). The regiochemistry of the trifluoromethyl group present on the azobenzene tail affected the resulting IRI activity as well as the carbohydrate selection for the surfactant head group. An *ortho*-substituted glucose fluorosurfactant was the most IRI-active analogue of this class of IRI. Generally, photoisomerization of the *ortho*-CF_3 surfactants to their *cis*-dominated photostationary states resulted in a reduction of IRI activity; a result consistent with that obtained for the carbohydrate-based surfactants presented in **Section 5.3**.

5.6 References

(1) Zachariassen, K. E.; Kristiansen, E. Ice Nucleation and Antinucleation in Nature. *Cryobiology* **2000**, *41* (4), 257–279. https://doi.org/10.1006/cryo.2000.2289.

(2) Franks, F.; Mathias, S. F.; Hatley, R. H. M.; Baust, J. G.; Hvidt, A.; Chapman, D.; Jaenicke, R. Water, Temperature and Life. *Philos. Trans. R. Soc. B Biol. Sci.* **1990**, *326* (1237), 517–533. https://doi.org/10.1098/rstb.1990.0029.

(3) Smallwood, M.; Bowles, D. J. Plants in a Cold Climate. *Philos. Trans. R. Soc. London. Ser. B Biol. Sci.* **2002**, *357* (1423), 831–847. https://doi.org/10.1098/rstb.2002.1073.

(4) Devries, A. L.; Lin, Y. Structure of a Peptide Antifreeze and Mechanism of Adsorption to Ice. *Biochim. Biophys. Acta - Protein Struct.* **1977**, *495* (2), 388–392. https://doi.org/10.1016/0005-2795(77)90395-6.

(5) Harding, M. M.; Ward, L. G.; Haymet, A. D. J. Type I "antifreeze" Proteins. Structure-Activity Studies and Mechanisms of Ice Growth Inhibition. *Eur. J. Biochem.* **1999**, *264* (3), 653–665. https://doi.org/10.1046/j.1432-1327.1999.00617.x.

(6) Hayward, J. A.; Haymet, A. D. J. The Ice/Water Interface: Molecular Dynamics Simulations of the Basal, Prism, {20$\bar{2}$1}, and {21$\bar{1}$0} Interfaces of Ice Ih. *J. Chem. Phys.* **2001**, *114* (8), 3713–3726. https://doi.org/10.1063/1.1333680.

(7) Knight, C. A.; De Vries, A. L.; Oolman, L. D. Fish Antifreeze Protein and the Freezing and Recrystallization of Ice. *Nature* **1984**, *308* (5956), 295–296. https://doi.org/10.1038/308295a0.

(8) Yeh, Y.; Feeney, R. E. Antifreeze Proteins: Structures and Mechanisms of Function. *Chem. Rev.* **1996**, *96* (2), 601–618. https://doi.org/10.1021/cr950260c.

(9) Davies, P. L.; Baardsnes, J.; Kuiper, M. J.; Walker, V. K. Structure and Function of Antifreeze Proteins. *Philos. Trans. R. Soc. London. Ser. B Biol. Sci.* **2002**, *357* (1423), 927–935. https://doi.org/10.1098/rstb.2002.1081.

(10) Feeney, R. E.; Yeh, Y. Antifreeze Proteins: Current Status and Possible Food Uses. *Trends Food Sci. Technol.* **1998**, *9* (3), 102–106. https://doi.org/10.1016/S0924-2244(98)00025-9.

(11) Wang, J.-H. A Comprehensive Evaluation of the Effects and Mechanisms of Antifreeze Proteins during Low-Temperature Preservation. *Cryobiology* **2000**, *41*, 1–9.

https://doi.org/10.1006/cryo.2000.2265.

(12) Carpenter, J. F.; Hansen, T. N. Antifreeze Protein Modulates Cell Survival during Cryopreservation: Mediation through Influence on Ice Crystal Growth. *Proc. Natl. Acad. Sci. U. S. A.* **1992**, *89* (19), 8953–8957. https://doi.org/10.1073/pnas.89.19.8953.

(13) Chao, H.; Davies, P. L.; Carpenter, J. F. Effects of Antifreeze Proteins on Red Blood Cell Survival during Cryopreservation. *J. Exp. Biol.* **1996**, *199* (Pt 9), 2071–2076.

(14) Wang, T.; Zhu, Q.; Yang, X.; Layne, J. R.; Devries, A. L. Antifreeze Glycoproteins from Antarctic Notothenioid Fishes Fail to Protect the Rat Cardiac Explant during Hypothermic and Freezing Preservation. *Cryobiology* **1994**, *31* (2), 185–192. https://doi.org/10.1006/cryo.1994.1022.

(15) Rubinsky, B.; Arav, A.; Devries, A. L. The Cryoprotective Effect of Antifreeze Glycopeptides from Antarctic Fishes. *Cryobiology* **1992**, *29* (1), 69–79. https://doi.org/10.1016/0011-2240(92)90006-n.

(16) Knight, C. A.; Cheng, C. C.; DeVries, A. L. Adsorption of Alpha-Helical Antifreeze Peptides on Specific Ice Crystal Surface Planes. *Biophys. J.* **1991**, *59* (2), 409–418. https://doi.org/10.1016/S0006-3495(91)82234-2.

(17) Sun, T.; Lin, F.-H.; Campbell, R. L.; Allingham, J. S.; Davies, P. L. An Antifreeze Protein Folds with an Interior Network of More than 400 Semi-Clathrate Waters. *Science* **2014**, *343* (6172), 795–798. https://doi.org/10.1126/science.1247407.

(18) Meister, K.; Strazdaite, S.; DeVries, A. L.; Lotze, S.; Olijve, L. L. C.; Voets, I. K.; Bakker, H. J. Observation of Ice-like Water Layers at an Aqueous Protein Surface. *Proc. Natl. Acad. Sci. U. S. A.* **2014**, *111* (50), 17732–17736. https://doi.org/10.1073/pnas.1414188111.

(19) Garnham, C. P.; Campbell, R. L.; Davies, P. L. Anchored Clathrate Waters Bind Antifreeze Proteins to Ice. *Proc. Natl. Acad. Sci. U. S. A.* **2011**, *108* (18), 7363–7367. https://doi.org/10.1073/pnas.1100429108.

(20) Howard, E. I.; Blakeley, M. P.; Haertlein, M.; Petit-Haertlein, I.; Mitschler, A.; Fisher, S. J.; Cousido-Siah, A.; Salvay, A. G.; Popov, A.; Muller-Dieckmann, C.; Petrova, T.; Podjarny, A. Neutron Structure of Type-III Antifreeze Protein Allows the Reconstruction of AFP-Ice Interface. *J. Mol. Recognit.* **2011**, *24* (4), 724–732. https://doi.org/10.1002/jmr.1130.

(21) Fairley, K.; Westman, B. J.; Pham, L. H.; Haymet, A. D. J.; Harding, M. M.; Mackay, J. P. Type I Shorthorn Sculpin Antifreeze Protein: Recombinant Synthesis, Solution Conformation, and Ice Growth Inhibition Studies. *J. Biol. Chem.* **2002**, *277* (27), 24073–24080. https://doi.org/10.1074/jbc.M200307200.

(22) Haymet, A. D. J.; Ward, L. G.; Harding, M. M. Winter Flounder "Antifreeze" Proteins: Synthesis and Ice Growth Inhibition of Analogues That Probe the Relative Importance of Hydrophobic and Hydrogen-Bonding Interactions. *J. Am. Chem. Soc.* **1999**, *121* (5), 941–948. https://doi.org/10.1021/JA9801341.

(23) Davies, P. L. Ice-Binding Proteins: A Remarkable Diversity of Structures for Stopping and Starting Ice Growth. *Trends Biochem. Sci.* **2014**, *39* (11), 548–555. https://doi.org/10.1016/j.tibs.2014.09.005.

(24) Gwak, Y.; Jung, W.; Lee, Y.; Kim, J. S.; Kim, C. G.; Ju, J.-H.; Song, C.; Hyun, J.-K.; Jin, E. An Intracellular Antifreeze Protein from an Antarctic Microalga That Responds to Various Environmental Stresses. *FASEB J.* **2014**, *28* (11), 4924–4935. https://doi.org/10.1096/fj.14-256388.

(25) Yang, D. S. C.; Hon, W. C.; Bubanko, S.; Xue, Y.; Seetharaman, J.; Hew, C. L.; Sicheri, F. Identification of the Ice-Binding Surface on a Type III Antifreeze Protein with a "flatness Function" Algorithm. *Biophys. J.* **1998**, *74* (5), 2142–2151. https://doi.org/10.1016/S0006-3495(98)77923-8.

(26) Bouvet, V. R.; Lorello, G. R.; Ben, R. N. Aggregation of Antifreeze Glycoprotein Fraction 8 and Its Effect on Antifreeze Activity. *Biomacromolecules* **2006**, *7* (2), 565–571. https://doi.org/10.1021/bm050605t.

(27) Sarno, D. M.; Murphy, A. V.; DiVirgilio, E. S.; Jones, W. E.; Ben, R. N. Direct Observation of Antifreeze Glycoprotein-Fraction 8 on Hydrophobic and Hydrophilic Interfaces Using Atomic Force Microscopy. *Langmuir* **2003**, *19* (11), 4740–4744. https://doi.org/10.1021/la027046l.

(28) Wierzbicki, A.; Dalal, P.; Cheatham, T. E.; Knickelbein, J. E.; Haymet, A. D. J.; Madura, J. D. Antifreeze Proteins at the Ice/Water Interface: Three Calculated Discriminating Properties for Orientation of Type I Proteins. *Biophys. J.* **2007**, *93* (5), 1442–1451. https://doi.org/10.1529/biophysj.107.105189.

(29) Harding, M. M.; Anderberg, P. I.; Haymet, A. D. J. "Antifreeze" Glycoproteins from

Polar Fish. *Eur. J. Biochem.* **2003**, *270* (7), 1381–1392. https://doi.org/10.1046/j.1432-1033.2003.03488.x.

(30) DeVries, A. L.; Komatsu, S. K.; Feeney, R. E. Chemical and Physical Properties of Freezing Point-Depressing Glycoproteins from Antarctic Fishes. *J. Biol. Chem.* **1970**, *245* (11), 2901–2908.

(31) Garner, J.; Harding, M. M. Design and Synthesis of Antifreeze Glycoproteins and Mimics. *Chembiochem* **2010**, *11* (18), 2489–2498. https://doi.org/10.1002/cbic.201000509.

(32) Peltier, R.; Brimble, M. A.; Wojnar, J. M.; Williams, D. E.; Evans, C. W.; DeVries, A. L. Synthesis and Antifreeze Activity of Fish Antifreeze Glycoproteins and Their Analogues. *Chem. Sci.* **2010**, *1* (5), 538. https://doi.org/10.1039/c0sc00194e.

(33) DeVries, A. L.; Vandenheede, J.; Feeney, R. E. Primary Structure of Freezing Point-Depressing Glycoproteins. *J. Biol. Chem.* **1971**, *246* (2), 305–308.

(34) Bouvet, V.; Ben, R. N. Antifreeze Glycoproteins: Structure, Conformation, and Biological Applications. *Cell Biochem. Biophys.* **2003**, *39* (2), 133–144. https://doi.org/10.1385/CBB:39:2:133.

(35) Gibson, M. I. Slowing the Growth of Ice with Synthetic Macromolecules: Beyond Antifreeze(Glyco) Proteins. *Polym. Chem.* **2010**, *1* (8), 1141. https://doi.org/10.1039/c0py00089b.

(36) Feeney, R. E.; Burcham, T. S.; Yeh, Y. Antifreeze Glycoproteins from Polar Fish Blood. *Annu. Rev. Biophys. Biophys. Chem.* **1986**, *15* (1), 59–78. https://doi.org/10.1146/annurev.bb.15.060186.000423.

(37) Giubertoni, G.; Meister, K.; DeVries, A. L.; Bakker, H. J. Determination of the Solution Structure of Antifreeze Glycoproteins Using Two-Dimensional Infrared Spectroscopy. *J. Phys. Chem. Lett.* **2019**, *10* (3), 352–357. https://doi.org/10.1021/acs.jpclett.8b03468.

(38) Kim, H.; Lee, J.; Hur, Y.; Lee, C.; Park, S.-H.; Koo, B.-W. Marine Antifreeze Proteins: Structure, Function, and Application to Cryopreservation as a Potential Cryoprotectant. *Mar. Drugs* **2017**, *15* (2), 27. https://doi.org/10.3390/md15020027.

(39) Tachibana, Y.; Fletcher, G. L.; Fujitani, N.; Tsuda, S.; Monde, K.; Nishimura, S.-I. Antifreeze Glycoproteins: Elucidation of the Structural Motifs That Are Essential for Antifreeze Activity. *Angew. Chemie* **2004**, *116* (7), 874–880. https://doi.org/10.1002/ange.200353110.

(40) Wilkinson, B. L.; Stone, R. S.; Capicciotti, C. J.; Thaysen-Andersen, M.; Matthews, J. M.; Packer, N. H.; Ben, R. N.; Payne, R. J. Total Synthesis of Homogeneous Antifreeze Glycopeptides and Glycoproteins. *Angew. Chemie - Int. Ed.* **2012**, *51* (15), 3606–3610. https://doi.org/10.1002/anie.201108682.

(41) Lane, A. N.; Hays, L. M.; Feeney, R. E.; Crowe, L. M.; Crowe, J. H. Conformational and Dynamic Properties of a 14 Residue Antifreeze Glycopeptide from Antarctic Cod. *Protein Sci.* **1998**, *7* (7), 1555–1563. https://doi.org/10.1002/pro.5560070709.

(42) Lane, A. N.; Hays, L. M.; Tsvetkova, N.; Feeney, R. E.; Crowe, L. M.; Crowe, J. H. Comparison of the Solution Conformation and Dynamics of Antifreeze Glycoproteins from Antarctic Fish. *Biophys. J.* **2000**, *78* (6), 3195–3207. https://doi.org/10.1016/S0006-3495(00)76856-1.

(43) Urbańczyk, M.; Góra, J.; Latajka, R.; Sewald, N. Antifreeze Glycopeptides: From Structure and Activity Studies to Current Approaches in Chemical Synthesis. *Amino Acids*. Springer-Verlag Wien February 1, 2017, pp 209–222. https://doi.org/10.1007/s00726-016-2368-z.

(44) Phillips, D. J.; Congdon, T. R.; Gibson, M. I. Activation of Ice Recrystallization Inhibition Activity of Poly(Vinyl Alcohol) Using a Supramolecular Trigger. *Polym. Chem.* **2016**, *7* (9), 1701–1704. https://doi.org/10.1039/C5PY01948F.

(45) Mitchell, D. E.; Clarkson, G.; Fox, D. J.; Vipond, R. A.; Scott, P.; Gibson, M. I. Antifreeze Protein Mimetic Metallohelices with Potent Ice Recrystallization Inhibition Activity. *J. Am. Chem. Soc.* **2017**, *139* (29), 9835–9838. https://doi.org/10.1021/jacs.7b05822.

(46) Drori, R.; Li, C.; Hu, C.; Raiteri, P.; Rohl, A. L.; Ward, M. D.; Kahr, B. A Supramolecular Ice Growth Inhibitor. *J. Am. Chem. Soc.* **2016**, *138* (40), 13396–13401. https://doi.org/10.1021/jacs.6b08267.

(47) Adam, M. K.; Jarrett-Wilkins, C.; Beards, M.; Staykov, E.; MacFarlane, L. R.; Bell, T. D. M.; Matthews, J. M.; Manners, I.; Faul, C. F. J.; Moens, P. D. J.; Ben, R. N.; Wilkinson, B. L. 1D Self-Assembly and Ice Recrystallization Inhibition Activity of Antifreeze Glycopeptide-Functionalized Perylene Bisimides. *Chem. - A Eur. J.* **2018**, *24* (31), 7834–7839. https://doi.org/10.1002/chem.201800857.

(48) Sun, M.; Müllen, K.; Yin, M. Water-Soluble Perylenediimides: Design Concepts and

Biological Applications. *Chemical Society Reviews*. Royal Society of Chemistry March 21, 2016, pp 1513–1528. https://doi.org/10.1039/c5cs00754b.

(49) Weil, T.; Abdalla, M. A.; Jatzke, C.; Hengstler, J.; Müllen, K. Water-Soluble Rylene Dyes as High-Performance Colorants for the Staining of Cells. *Biomacromolecules* **2005**, *6* (1), 68–79. https://doi.org/10.1021/bm049674i.

(50) Qu, J.; Kohl, C.; Pottek, M.; Müllen, K. Ionic Perylenetetracarboxdiimides: Highly Fluorescent and Water-Soluble Dyes for Biolabeling. *Angew. Chemie - Int. Ed.* **2004**, *43* (12), 1528–1531. https://doi.org/10.1002/anie.200353208.

(51) Yang, S. K.; Shi, X.; Park, S.; Doganay, S.; Ha, T.; Zimmerman, S. C. Monovalent, Clickable, Uncharged, Water-Soluble Perylenediimide-Cored Dendrimers for Target-Specific Fluorescent Biolabeling. *J. Am. Chem. Soc.* **2011**, *133* (26), 9964–9967. https://doi.org/10.1021/ja2009136.

(52) Wang, K. R.; An, H. W.; Rong, R. X.; Cao, Z. R.; Li, X. L. Synthesis of Biocompatible Glycodendrimer Based on Fluorescent Perylene Bisimides and Its Bioimaging. *Macromol. Rapid Commun.* **2014**, *35* (7), 727–734. https://doi.org/10.1002/marc.201300916.

(53) Zhao, Q.; Li, K.; Chen, S.; Qin, A.; Ding, D.; Zhang, S.; Liu, Y.; Liu, B.; Sun, J. Z.; Tang, B. Z. Aggregation-Induced Red-NIR Emission Organic Nanoparticles as Effective and Photostable Fluorescent Probes for Bioimaging. *J. Mater. Chem.* **2012**, *22* (30), 15128–15135. https://doi.org/10.1039/c2jm31368e.

(54) Würthner, F.; Saha-Möller, C. R.; Fimmel, B.; Ogi, S.; Leowanawat, P.; Schmidt, D. Perylene Bisimide Dye Assemblies as Archetype Functional Supramolecular Materials. *Chemical Reviews*. American Chemical Society February 10, 2016, pp 962–1052. https://doi.org/10.1021/acs.chemrev.5b00188.

(55) Chen, S.; Slattum, P.; Wang, C.; Zang, L. Self-Assembly of Perylene Imide Molecules into 1D Nanostructures: Methods, Morphologies, and Applications. *Chemical Reviews*. American Chemical Society November 11, 2015, pp 11967–11998. https://doi.org/10.1021/acs.chemrev.5b00312.

(56) Kim, F. S.; Ren, G.; Jenekhe, S. A. One-Dimensional Nanostructures of π-Conjugated Molecular Systems: Assembly, Properties, and Applications from Photovoltaics, Sensors, and Nanophotonics to Nanoelectronics. *Chem. Mater.* **2011**, *23* (3), 682–732. https://doi.org/10.1021/cm102772x.

(57) Huang, C.; Barlow, S.; Marder, S. R. Perylene-3,4,9,10-Tetracarboxylic Acid Diimides: Synthesis, Physical Properties, and Use in Organic Electronics. *Journal of Organic Chemistry*. April 15, 2011, pp 2386–2407. https://doi.org/10.1021/jo2001963.

(58) Görl, D.; Zhang, X.; Würthner, F. Molecular Assemblies of Perylene Bisimide Dyes in Water. *Angewandte Chemie - International Edition*. June 25, 2012, pp 6328–6348. https://doi.org/10.1002/anie.201108690.

(59) Zhang, X.; Rehm, S.; Safont-Sempere, M. M.; Würthner, F. Vesicular Perylene Dye Nanocapsules as Supramolecular Fluorescent PH Sensor Systems. *Nat. Chem.* **2009**, *1* (8), 623–629. https://doi.org/10.1038/nchem.368.

(60) Sorrenti, A.; Leira-Iglesias, J.; Sato, A.; Hermans, T. M. Non-Equilibrium Steady States in Supramolecular Polymerization. *Nat. Commun.* **2017**, *8*, 15899. https://doi.org/10.1038/ncomms15899.

(61) Tidhar, Y.; Weissman, H.; Wolf, S. G.; Gulino, A.; Rybtchinski, B. Pathway-Dependent Self-Assembly of Perylene Diimide/Peptide Conjugates in Aqueous Medium. *Chem. - A Eur. J.* **2011**, *17* (22), 6068–6075. https://doi.org/10.1002/chem.201003419.

(62) Hu, J.; Kuang, W.; Deng, K.; Zou, W.; Huang, Y.; Wei, Z.; Faul, C. F. J. Self-Assembled Sugar-Substituted Perylene Diimide Nanostructures with Homochirality and High Gas Sensitivity. *Adv. Funct. Mater.* **2012**, *22* (19), 4149–4158. https://doi.org/10.1002/adfm.201200973.

(63) Liu, X.; Huang, Z.; Huang, Y.; Zhu, L.; Fu, J. Tunable Supramolecular Helical Aggregate and Optoelectrical Properties of Perylene Diimides by Stereoisomerism of Sugar. *J. Phys. Chem. C* **2017**, *121* (13), 7558–7563. https://doi.org/10.1021/acs.jpcc.7b02014.

(64) Bai, S.; Debnath, S.; Javid, N.; Frederix, P. W. J. M.; Fleming, S.; Pappas, C.; Ulijn, R. V. Differential Self-Assembly and Tunable Emission of Aromatic Peptide Bola -Amphiphiles Containing Perylene Bisimide in Polar Solvents Including Water. *Langmuir* **2014**, *30* (25), 7576–7584. https://doi.org/10.1021/la501335e.

(65) Echue, G.; Lloyd-Jones, G. C.; Faul, C. F. J. Chiral Perylene Diimides: Building Blocks for Ionic Self-Assembly. *Chem. - A Eur. J.* **2015**, *21* (13), 5118–5128. https://doi.org/10.1002/chem.201406094.

(66) Sun, K.; Xiao, C.; Liu, C.; Fu, W.; Wang, Z.; Li, Z. Thermally Sensitive Self-Assembly of Glucose-Functionalized Tetrachloro-Perylene Bisimides: From Twisted Ribbons to

Microplates. *Langmuir* **2014**, *30* (37), 11040–11045. https://doi.org/10.1021/la502532g.

(67) Drillaud, N.; Banaszak-Léonard, E.; Pezron, I.; Len, C. Synthesis and Evaluation of a Photochromic Surfactant for Organic Reactions in Aqueous Media. *J. Org. Chem.* **2012**, *77* (21), 9553–9561. https://doi.org/10.1021/jo301466w.

(68) Rajaganesh, R.; Gopal, A.; Mohan Das, T.; Ajayaghosh, A. Synthesis and Properties of Amphiphilic Photoresponsive Gelators for Aromatic Solvents. *Org. Lett.* **2012**, *14* (3), 748–751. https://doi.org/10.1021/ol203294v.

(69) Matsumoto, S.; Yamaguchi, S.; Ueno, S.; Komatsu, H.; Ikeda, M.; Ishizuka, K.; Iko, Y.; Tabata, K. V; Aoki, H.; Ito, S.; Noji, H.; Hamachi, I. Photo Gel-Sol/Sol-Gel Transition and Its Patterning of a Supramolecular Hydrogel as Stimuli-Responsive Biomaterials. *Chemistry* **2008**, *14* (13), 3977–3986. https://doi.org/10.1002/chem.200701904.

(70) Ogawa, Y.; Yoshiyama, C.; Kitaoka, T. Helical Assembly of Azobenzene-Conjugated Carbohydrate Hydrogelators with Specific Affinity for Lectins. *Langmuir* **2012**, *28* (9), 4404–4412. https://doi.org/10.1021/la300098q.

(71) Li, J.; Huo, M.; Wang, J.; Zhou, J.; Mohammad, J. M.; Zhang, Y.; Zhu, Q.; Waddad, A. Y.; Zhang, Q. Redox-Sensitive Micelles Self-Assembled from Amphiphilic Hyaluronic Acid-Deoxycholic Acid Conjugates for Targeted Intracellular Delivery of Paclitaxel. *Biomaterials* **2012**, *33* (7), 2310–2320. https://doi.org/10.1016/j.biomaterials.2011.11.022.

(72) Phillips, D. J.; Congdon, T. R.; Gibson, M. I. Activation of Ice Recrystallization Inhibition Activity of Poly(Vinyl Alcohol) Using a Supramolecular Trigger. *Polym. Chem.* **2016**, *7* (9), 1701–1704. https://doi.org/10.1039/c5py01948f.

(73) Mitchell, D. E.; Gibson, M. I. Latent Ice Recrystallization Inhibition Activity in Nonantifreeze Proteins: Ca2+-Activated Plant Lectins and Cation-Activated Antimicrobial Peptides. *Biomacromolecules* **2015**, *16* (10), 3411–3416. https://doi.org/10.1021/acs.biomac.5b01118.

(74) Adam, M. K.; Poisson, J. S.; Hu, Y.; Prasannakumar, G.; Pottage, M. J.; Ben, R. N.; Wilkinson, B. L. Carbohydrate-Based Surfactants as Photocontrollable Inhibitors of Ice Recrystallization. *RSC Adv.* **2016**, *6* (45), 39240–39244. https://doi.org/10.1039/c6ra07030b. - Reproduced by permission of The Royal Society of Chemistry

(75) Adam, M. K.; Hu, Y.; Poisson, J. S.; Pottage, M. J.; Ben, R. N.; Wilkinson, B. L.

Photoswitchable Carbohydrate-Based Fluorosurfactants as Tuneable Ice Recrystallization Inhibitors. *Carbohydr. Res.* **2017**, *439*, 1–8. https://doi.org/10.1016/j.carres.2016.12.004.

(76) Chevallier, E.; Monteux, C.; Lequeux, F.; Tribet, C. Photofoams: Remote Control of Foam Destabilization by Exposure to Light Using an Azobenzene Surfactant. *Langmuir* **2012**, *28* (5), 2308–2312. https://doi.org/10.1021/la204200z.

(77) Fliegl, H.; Köhn, A.; Hättig, C.; Ahlrichs, R. Ab Initio Calculation of the Vibrational and Electronic Spectra of Trans- and Cis-Azobenzene. *J. Am. Chem. Soc.* **2003**, *125* (32), 9821–9827. https://doi.org/10.1021/ja034433o.

(78) Tabor, R. F.; Tan, D. D.; Han, S. S.; Young, S. A.; Seeger, Z. L. E.; Pottage, M. J.; Garvey, C. J.; Wilkinson, B. L. Reversible PH- and Photocontrollable Carbohydrate-Based Surfactants. *Chem. - A Eur. J.* **2014**, *20* (43), 13881–13884. https://doi.org/10.1002/chem.201404945.

(79) Tabor, R. F.; Pottage, M. J.; Garvey, C. J.; Wilkinson, B. L. Light-Induced Structural Evolution of Photoswitchable Carbohydrate-Based Surfactant Micelles. *Chem. Commun.* **2015**, *51* (25), 5509–5512. https://doi.org/10.1039/c4cc07657e.

(80) Brown, P.; Butts, C. P.; Eastoe, J. Stimuli-Responsive Surfactants. *Soft Matter*. The Royal Society of Chemistry February 28, 2013, pp 2365–2374. https://doi.org/10.1039/c3sm27716j.

(81) Eastoe, J.; Vesperinas, A. Self-Assembly of Light-Sensitive Surfactants. *Soft Matter*. The Royal Society of Chemistry November 14, 2005, pp 338–347. https://doi.org/10.1039/b510877m.

(82) Beharry, A. A.; Woolley, G. A. Azobenzene Photoswitches for Biomolecules. *Chemical Society Reviews*. The Royal Society of Chemistry August 14, 2011, pp 4422–4437. https://doi.org/10.1039/c1cs15023e.

(83) Velema, W. A.; van der Berg, J. P.; Hansen, M. J.; Szymanski, W.; Driessen, A. J. M.; Feringa, B. L. Optical Control of Antibacterial Activity Supporting Information. *Nat. Chem.* **2013**, *5* (11), 924–928. https://doi.org/10.1038/nchem.1750.

(84) Li, L.; Yang, Y.; Dong, J.; Li, X. Azobenzene Dye Induced Micelle to Vesicle Transition in Cationic Surfactant Aqueous Solutions. *J. Colloid Interface Sci.* **2010**, *343* (2), 504–509. https://doi.org/10.1016/j.jcis.2009.11.056.

(85) Song, B.; Hu, Y.; Zhao, J. A Single-Component Photo-Responsive Fluid Based on a

Gemini Surfactant with an Azobenzene Spacer. *J. Colloid Interface Sci.* **2009**, *333* (2), 820–822. https://doi.org/10.1016/j.jcis.2009.02.030.

(86) Sortino, S. Photoactivated Nanomaterials for Biomedical Release Applications. *Journal of Materials Chemistry*. The Royal Society of Chemistry January 14, 2012, pp 301–318. https://doi.org/10.1039/c1jm13288a.

(87) Fujita, H.; Shrestha, N. K.; Ogihara, H.; Saji, T. Effect of Hydrophilic Group on Thin Film Formation Using Redox-Active Surfactants with an Azobenzene Group. *Electrochim. Acta* **2008**, *53* (28), 8161–8165. https://doi.org/10.1016/j.electacta.2008.03.024.

(88) Laurent, N.; Lafont, D.; Dumoulin, F.; Boullanger, P.; Mackenzie, G.; Kouwer, P. H. J.; Goodby, J. W. Synthesis of Amphiphilic Phenylazophenyl Glycosides and a Study of Their Liquid Crystal Properties. *J. Am. Chem. Soc.* **2003**, *125* (50), 15499–15506. https://doi.org/10.1021/ja037347x.

(89) Bricout, H.; Banaszak, E.; Len, C.; Hapiot, F.; Monflier, E. Amphiphilic Photo-Isomerisable Phosphanes for Aqueous Organometallic Catalysis. *Chem. Commun.* **2010**, *46* (41), 7813–7815. https://doi.org/10.1039/c0cc02458a.

(90) Dong, M.; Babalhavaeji, A.; Samanta, S.; Beharry, A. A.; Woolley, G. A. Red-Shifting Azobenzene Photoswitches for in Vivo Use. *Acc. Chem. Res.* **2015**, *48* (10), 2662–2670. https://doi.org/10.1021/acs.accounts.5b00270.

(91) Hu, Y.; Tabor, R. F.; Wilkinson, B. L. Sweetness and Light: Design and Applications of Photo-Responsive Glycoconjugates. *Org. Biomol. Chem.* **2015**, *13* (8), 2216–2225. https://doi.org/10.1039/c4ob02296c.

(92) Knight, C. A.; Hallett, J.; DeVries, A. L. Solute Effects on Ice Recrystallization: An Assessment Technique. *Cryobiology* **1988**, *25* (1), 55–60. https://doi.org/10.1016/0011-2240(88)90020-X.

(93) Jackman, J.; Noestheden, M.; Moffat, D.; Pezacki, J. P.; Findlay, S.; Ben, R. N. Assessing Antifreeze Activity of AFGP 8 Using Domain Recognition Software. *Biochem. Biophys. Res. Commun.* **2007**, *354* (2), 340–344. https://doi.org/10.1016/j.bbrc.2006.12.225.

(94) Abraham, S.; Keillor, K.; Capicciotti, C. J.; Perley-Robertson, G. E.; Keillor, J. W.; Ben, R. N. Quantitative Analysis of the Efficacy and Potency of Novel Small Molecule Ice Recrystallization Inhibitors. *Cryst. Growth Des.* **2015**, *15* (10), 5034–5039. https://doi.org/10.1021/acs.cgd.5b00995.

(95) Chakrabartty, A.; Hew, C. L. The Effect of Enhanced A-Helicity on the Activity of a Winter Flounder Antifreeze Polypeptide. *Eur. J. Biochem.* **1991**, *202*, 1057–1063.

(96) Zhao, J. S.; Wang, J. H.; He, W. Bin; Ruan, Y. Bin; Jiang, Y. B. Isolable Chiral Aggregates of Achiral π-Conjugated Carboxylic Acids. *Chem. - A Eur. J.* **2012**, *18* (12), 3631–3636. https://doi.org/10.1002/chem.201103651.

(97) Xu, Y.; Leng, S.; Xue, C.; Sun, R.; Pan, J.; Ford, J.; Jin, S. A Room-Temperature Liquid-Crystalline Phase with Crystalline π Stacks. *Angew. Chemie - Int. Ed.* **2007**, *46* (21), 3896–3899. https://doi.org/10.1002/anie.200604607.

(98) Lemouchi, C.; Simonov, S.; Zorina, L.; Gautier, C.; Hudhomme, P.; Batail, P. Amino Acid Derivatives of Perylenediimide and Their N-H...O Peptide Bond Dipoles-Templated Solid State Assembly into Stacks. *Org. Biomol. Chem.* **2011**, *9* (23), 8096–8101. https://doi.org/10.1039/c1ob06213a.

(99) Wilkinson, B. L.; Day, S.; Malins, L. R.; Apostolopoulos, V.; Payne, R. J. Self-Adjuvanting Multicomponent Cancer Vaccine Candidates Combining Per-Glycosylated MUC1 Glycopeptides and the Toll-like Receptor 2 Agonist Pam3CysSer. *Angew. Chemie Int. Ed.* **2011**, *50* (7), 1635–1639. https://doi.org/10.1002/anie.201006115.

(100) Partridge, B. E.; Leowanawat, P.; Aqad, E.; Imam, M. R.; Sun, H. J.; Peterca, M.; Heiney, P. A.; Graf, R.; Spiess, H. W.; Zeng, X.; Ungar, G.; Percec, V. Increasing 3D Supramolecular Order by Decreasing Molecular Order. A Comparative Study of Helical Assemblies of Dendronized Nonchlorinated and Tetrachlorinated Perylene Bisimides. *J. Am. Chem. Soc.* **2015**, *137* (15), 5210–5224. https://doi.org/10.1021/jacs.5b02147.

(101) Trant, J. F.; Biggs, R. A.; Capicciotti, C. J.; Ben, R. N. Developing Highly Active Small Molecule Ice Recrystallization Inhibitors Based upon C-Linked Antifreeze Glycoprotein Analogues. *RSC Adv.* **2013**, *3* (48), 26005–26009. https://doi.org/10.1039/c3ra43835j.

(102) Tam, R. Y.; Ferreira, S. S.; Czechura, P.; Chaytor, J. L.; Ben, R. N. Hydration Index - A Better Parameter for Explaining Small Molecule Hydration in Inhibition of Ice Recrystallization. *J. Am. Chem. Soc.* **2008**, *130* (8), 17494–17501.

(103) Billamboz, M.; Mangin, F.; Drillaud, N.; Chevrin-Villette, C.; Banaszak-Leónard, E.; Len, C. Micellar Catalysis Using a Photochromic Surfactant: Application to the Pd-Catalyzed Tsuji−Trost Reaction in Water. *J. Org. Chem.* **2014**, *79* (2), 493–500. https://doi.org/10.1021/jo401737t.

(104) Le Ny, A.-L. M.; Lee, C. T. Photoreversible DNA Condensation Using Light-Responsive Surfactants. *J. Am. Chem. Soc.* **2006**, *128* (19), 6400–6408. https://doi.org/10.1021/ja0576738.

(105) Lee, C. T.; Smith, K. A.; Alan Hatton, T. Small-Angle Neutron Scattering Study of the Micellization of Photosensitive Surfactants in Solution and in the Presence of a Hydrophobically Modified Polyelectrolyte. *Langmuir* **2009**, *25* (24), 13784–13794. https://doi.org/10.1021/la9016239.

(106) Czechura, P.; Tam, R. Y.; Dimitrijevic, E.; Murphy, A. V.; Ben, R. N. The Importance of Hydration for Inhibiting Ice Recrystallization with C-Linked Antifreeze Glycoproteins. *J. Am. Chem. Soc.* **2008**, *130* (10), 2928–2929. https://doi.org/10.1021/ja7103262.

(107) Capicciotti, C. J.; Leclère, M.; Perras, F. A.; Bryce, D. L.; Paulin, H.; Harden, J.; Liu, Y.; Ben, R. N. Potent Inhibition of Ice Recrystallization by Low Molecular Weight Carbohydrate-Based Surfactants and Hydrogelators. *Chem. Sci.* **2012**, *3* (5), 1408–1416. https://doi.org/10.1039/c2sc00885h.

(108) Manaargadoo-Catin, M.; Ali-Cherif, A.; Pougnas, J.-L.; Perrin, C. Hemolysis by Surfactants--A Review. *Adv. Colloid Interface Sci.* **2016**, *228*, 1–16. https://doi.org/10.1016/j.cis.2015.10.011.

(109) Samanta, S.; Beharry, A. A.; Sadovski, O.; McCormick, T. M.; Babalhavaeji, A.; Tropepe, V.; Woolley, G. A. Photoswitching Azo Compounds in Vivo with Red Light. *J. Am. Chem. Soc.* **2013**, *135* (26), 9777–9784. https://doi.org/10.1021/ja402220t.

(110) Krafft, M. P.; Riess, J. G. Chemistry, Physical Chemistry, and Uses of Molecular Fluorocarbon- Hydrocarbon Diblocks, Triblocks, and Related Compounds-Unique "Apolar" Components for Self-Assembled Colloid and Interface Engineering. *Chem. Rev.* **2009**, *109* (5), 1714–1792. https://doi.org/10.1021/cr800260k.

(111) Chiu, Y. L.; Chan, H. F.; Phua, K. K. L.; Zhang, Y.; Juul, S.; Knudsen, B. R.; Ho, Y. P.; Leong, K. W. Synthesis of Fluorosurfactants for Emulsion-Based Biological Applications. *ACS Nano* **2014**, *8* (4), 3913–3920. https://doi.org/10.1021/nn500810n.

(112) Li, X.; Turánek, J.; Knötigová, P.; Kudláčková, H.; Mašek, J.; Parkin, S.; Rankin, S. E.; Knutson, B. L.; Lehmler, H. J. Hydrophobic Tail Length, Degree of Fluorination and Headgroup Stereochemistry Are Determinants of the Biocompatibility of (Fluorinated) Carbohydrate Surfactants. *Colloids Surfaces B Biointerfaces* **2009**, *73* (1), 65–74.

https://doi.org/10.1016/j.colsurfb.2009.04.023.

(113) Rostovtsev, V. V.; Green, L. G.; Fokin, V. V.; Sharpless, K. B. A Stepwise Huisgen Cycloaddition Process: Copper(I)-Catalyzed Regioselective "Ligation" of Azides and Terminal Alkynes. *Angew. Chemie - Int. Ed.* **2002**, *41* (14), 2596–2599. https://doi.org/10.1002/1521-3773(20020715)41:14<2596::AID-ANIE2596>3.0.CO;2-4.

(114) Wilkinson, B. L.; Bornaghi, L. F.; Poulsen, S. A.; Houston, T. A. Synthetic Utility of Glycosyl Triazoles in Carbohydrate Chemistry. *Tetrahedron* **2006**, *62* (34), 8115–8125. https://doi.org/10.1016/j.tet.2006.06.001.

(115) Hu, Y.; Marlow, J. B.; Ramanathan, R.; Zou, W.; Tiew, H. G.; Pottage, M. J.; Bansal, V.; Tabor, R. F.; Wilkinson, B. L. Synthesis and Properties of Photoswitchable Carbohydrate Fluorosurfactants. *Aust. J. Chem.* **2015**, *68* (12), 1880–1884. https://doi.org/10.1071/CH15434.

(116) Zemplén, G.; Kunz, A. Über Die Natriumverbindungen Der Glucose Und Die Verseifung Der Acylierten Zucker. *Berichte der Dtsch. Chem. Gesellschaft* **1923**, *56B*, 1705–1710.

(117) Shang, T.; Smith, K. A.; Hatton, T. A. Photoresponsive Surfactants Exhibiting Unusually Large, Reversible Surface Tension Changes under Varying Illumination Conditions. *Langmuir* **2003**, *19* (26), 10764–10773. https://doi.org/10.1021/la0350958.

(118) Yoon, J. H.; Yoon, S. Photoisomerization of Azobenzene Derivatives Confined in Gold Nanoparticle Aggregates. *Phys. Chem. Chem. Phys.* **2011**, *13* (28), 12900–12905. https://doi.org/10.1039/c0cp02588g.

(119) Han, M. R.; Hirayama, Y.; Hara, M. Fluorescence Enhancement from Self-Assembled Aggregates: Substituent Effects on Self-Assembly of Azobenzenes. *Chem. Mater.* **2006**, *18* (12), 2784–2786. https://doi.org/10.1021/cm060543t.

(120) Stockert, J. C.; Horobin, R. W.; Colombo, L. L.; Blázquez-Castro, A. Tetrazolium Salts and Formazan Products in Cell Biology: Viability Assessment, Fluorescence Imaging, and Labeling Perspectives. *Acta Histochem.* **2018**, *120* (3), 159–167. https://doi.org/10.1016/j.acthis.2018.02.005.

6. Thesis Conclusions and Future Work

Conclusions

The overall goal of this thesis was to develop novel ice recrystallization inhibitors (IRIs) for the improvement of the cryopreservation of cellular products. This involved the synthesis of *N*-aryl-D-gluconamide derivatives bearing structural modifications to the aryl and carbohydrate components in order to assess the structural features required for effective IRI activity. Promising candidates were subjected to further IRI characterization and cytotoxicity analysis. The ability of the novel *N*-aryl-D-gluconamides to protect hematopoietic stem and progenitor cells (HSPCs) isolated from human umbilical cord blood (UCB) during cryopreservation was determined through analyzing both the *in vitro* and *in vivo* activities of cells post-thaw. Finally, glyco(peptide)s were designed in order to further elucidate the structural features required for IRI activity for the macromolecular class of antifreeze glycoprotein (AFGP) analogues. This involved the novel development of IRIs with tuneable activity using an external probe.

The first objective of studying the structural features required for the development of IRI-active *N*-aryl-D-gluconamides involved the design and synthesis of a series of gluconamide analogues. The series of derivatives with aryl component modifications included one possessing both a 2-fluoro and 4-methoxy aryl substituent. This derivative was found to be less active than its parent compounds (e.g. *N*-(2-fluorophenyl)-D-gluconamide and *N*-(4-methoxyphenyl)-D-gluconamide). A series of aminophenyl-D-gluconamides were then developed to further probe the effects of having electron-donating groups on the aryl ring. Generally, the aminophenyl gluconamides were found to exhibit similar-to-somewhat reduced IRI activity to *N*-(4-methoxyphenyl)-D-gluconamide. Next, attention was turned toward modifications to the

carbohydrate tail component. Upon altering the stereochemistry of *N*-(4-methoxyphenyl)-D-gluconamide, IRI activity was impacted, thereby further confirming that stereochemical changes can have drastic influences on the IRI activity of the aldonamides. Following this, the functionality linked to the *C6*-position of the carbohydrate was modified to a carboxylate, resulting in reduced solubility and IRI activity, and was also modified to an azide group, also resulting in reduced solubility and IRI activity. These results suggested that the *C6*-hydroxyl group is an integral component required for the IRI activity of the *N*-aryl-D-gluconamides. Taken altogether, the results obtained with the gluconamide analogues highlighted the delicate balance required between the hydrophilicity and hydrophobicity in the IRI-active small molecules.

Following the development of novel gluconamides, these small-molecules' abilities to act as cryoprotectants for HSPCs were next assessed. The cytotoxicity of the derivatives was assessed *in vitro* and select gluconamides were found to be non-toxic (or minimally toxic). *N*-(2-fluorophenyl)-D-gluconamide (**4.01**), for example, was consistently found to be non-toxic to various cell types (human hepatic cells as well as total nucleated cells from UCB). The *in vitro* properties of total nucleated cells (TNCs) from UCB cryopreserved in the presence of dimethyl sulfoxide and an IRI was assessed. The post-thaw viability and function of TNCs were largely preserved when supplementing the cryomedium with IRIs; results that in addition to the previous small-scale experiments suggest that these gluconamide-based cryosupplements are well tolerated for UCB cryopreservation. Since a serial xenotransplantation assay is considered the 'gold-standard' method for determining the function of HSPCs, this *in vivo* assay was implemented in order to assess the impact of using *N*-(2-fluorophenyl)-D-gluconamide **4.01** as a supplement to the cryopreservation of HSPCs from UCB. The engraftment activities of the stem cells transplanted into mice were found to be enhanced when gluconamide **4.01** was used as a

cryosupplement. This included increased levels of platelets found in mice periphery blood as well as increased levels of human leukocyte chimerism and hematopoietic progenitors at the "long-term" time point after transplantation. Finally, long-term HSPCs were also preserved with the use of gluconamide **4.01**. Taken together, these results clearly show the promise of using an IRI for clinical applications. This work is significant as it marks the first time an IRI's potential has been investigated using *in vivo* methods, and this research, therefore, offers substantial insight to the relevance of these IRIs at improving cryopreservation methods in general.

Finally, the last objective involved the design and analysis of photocontrollable glyco(peptide)-functionalized IRIs through a collaboration with Dr. Wilkinson and colleagues. This objective first involved the design of lipopeptides bearing peptide functionality similar to that of the AFGPs. Macromolecules able to self-assemble in solution were then assessed. These "AFGP-PBIs" were comprised of a perylene bisimide (PBI) core tethered to two AFGP-glyco(peptides). Interestingly, the AFGP-PBIs were found to be IRI-active. Finally, the ability to control a compound's IRI activity using an external stimulus was investigated through the design of photocontrollable glyco(peptide)-based surfactants. An azobenzene structure was used to "switch" the physicochemical properties of the surfactants. Changing the properties of the surfactants using UV-vis light resulted in altering the balance between the hydrophobicity and hydrophilicity of IRIs, and thereby modulating the corresponding IRI activity. This novel proof-of-concept approach to controllable IRI activity offers substantial ground for future IRI applications.

Taken together, these results can lead to improved cryopreservation techniques for cellular products for several reasons. First, the exploration of the structural features required for IRI-active gluconamides presented herein offers new insight for the development of future IRIs.

Second, the *in vitro* and *in vivo* properties of HSPCs from UCB were preserved and/or enhanced using IRIs thereby confirming the clinical applicability of the IRI technology. And finally, the development of novel glyco(peptide)-based macromolecules offers new approaches in the design of AFGP analogues. Particularly, the IRI materials able to self-assemble in solution as well as the photocontrollable IRI activity of the surfactants developed are truly innovative. These discoveries will lead to novel uses for IRIs in clinical and industrial settings.

Future Work

The outcomes of the structure function studies presented in this thesis continue to highlight that there is a need for both a hydrophobic and hydrophilic region in order for gluconamides to be active inhibitors of ice recrystallization. Unfortunately, without knowing the exact structural features required for activity of these small molecules, the ongoing development of novel inhibitors remains laborious and often subject to trial-and-error. As shown throughout **Chapter 3** and **Chapter 4**, there is a clear need for the continued exploration of the chemical space of gluconamide IRIs. Accordingly, further modifications to both the aryl and carbohydrate regions should be examined with consideration into ways to improve the solubilities of the small molecules in aqueous solutions. While some derivatives bearing charged species were considered in **Chapter 3** (the carboxylate analogues), other charged groups should be investigated. Next, since a mannonamide derivative of *N*-(4-methoxyphenyl)-D-gluconamide was found to possess enhanced IRI activity, further studies into other mannonamide IRIs (and other stereochemical alterations) are warranted. Finally, studies that reveal additional mechanistic insights into the way IRI-active aldonamides inhibit ice recrystallization would also be beneficial. For example, investigation into the hill slopes of the IRIs may offer important insights.

Further studies on the features of IRI-active aldonamides required for promising *in vitro* properties would also be beneficial for the development of novel cryoprotectants. In addition to the functional assays described in **Chapter 4**, metabolomic and/or metabonomic studies would progress the understanding of cell physiology after incubation with an IRI as well as after cryopreservation with the use of an IRI. Assessment of whether aldonamide-IRIs are being internalized into cells during cryopreservation in conjunction with using cryomicroscopy to visualize the potential IRI activity within cells would also offer insight into the mechanism by which these small molecules may act as cryoprotectants. Furthermore, there were a number of compounds presented in this thesis that warrant additional *in vitro* and potentially *in vivo* studies. For instance, gluconamide **4.03** (the 2,6-difluorobenzyl derivative) showed promising *in vitro* results despite the cryopreservation conditions not being fully optimized. Studying the incorporation of plasma and investigating the ideal cell dose per 1 mL cryovolumes (when an IRI is being utilized) are among the numerous optimization studies that would facilitate future work with IRIs. Notably, UCB research is dependent on the availability and quality of units being donated, and these factors resulted in limited sample sizes for some experiments. Therefore, increasing the sample sizes (e.g. n = 3 and greater) for some of the cryoprotectant studies discussed herein would be beneficial. Importantly, the *in vivo* study reported herein on the outcomes of using an IRI as a cryosupplement marks the first time this has been investigated and thereby offers a great baseline for future work. Subsequent IRI candidates that display promising results *in vitro* and subsequently from the *in vivo* serial transplantation model can now be compared back to this initial murine study with *N*-(2-fluorophenyl)-D-gluconamide (gluconamide **4.01**). Pharmacokinetic studies on the use of gluconamide **4.01** in animal models

would also offer substantial insight into the outcome of using a gluconamide IRI for the storage of cell products.

Chapter 5 reported the development of glyco(peptide)-based ice recrystallization inhibitors with unique properties. With continued structure function work, the IRI-active AFGP-PBIs could be envisioned as self-assembled IRIs that mitigate cryoinjury extracellularly (and consequently avoid interaction of the aryl PBIs with DNA within the cell). Next, additional investigation into the photocontrollable activity of azobenzene-functionalized IRIs offers novel applications for ice recrystallization inhibitors. Under the right conditions, IRI photomodulation could be used to provide thermal radiation during the warming phase of cryopreservation. This would first involve investigation into the ability of azobenzene-based IRIs to undergo photoisomerization at sub-zero temperatures (e.g. by subjecting cold samples to UV light followed by analysis using the splat-cooling assay) in addition to overcoming the cytotoxicity of the molecules. Investigation into how these IRIs may interact with the extracellular membrane of cells and how photoisomerization may mitigate this activity is also of considerable interest.

Altogether, the results presented in this thesis as well as the corresponding subsequent work will facilitate the future development of ice recrystallization inhibitors. Producing IRIs with efficacy similar to the AFGPs (without the detrimental thermal hysteresis activity observed with the AF(G)P class of biological antifreezes) can lead to reduced concentrations required for the cryopreservation of umbilical cord blood thereby leading to more efficient procedures post-thaw. This improvement of the post-thaw outcomes of cryopreserved stem cell grafts is essential to improving the treatment of diseases using hematopoietic stem cell transplants. That said, IRI technologies not only have tremendous value in improving the long-term storage of cellular products but also in improving patient care of HSCT recipients.

APPENDICES

Appendix I: Contributions to Original Research

1. Synthesis and IRI analysis of *N*-aryl-D-gluconamide derivatives presented in **Chapter 3**: This includes full IRI characterization of *N*-(4-methoxyphenyl)-D-gluconamide **3.01** and *N*-(2-fluorophenyl)-D-gluconamide **3.02**. This also consists of the synthesis and IRI analysis of *N*-(2-fluoro-4-methoxyphenyl)-D-gluconamide **3.38**, *N*-(aminophenyl)-D-gluconamides **3.39-3.41** and their derivatives **3.42-3.47**, aldonamides **3.63-3.64**, *C6*-carboxylate derivatives **3.65-3.67** and the aldonamide mimics **3.68-3.74**, and finally, the *C6*-azido gluconamides **3.80-3.82**. Studies of amino derivatives **3.39-3.47** were conducted with honour's student, Ms. Odile Pressoir. Summer student, Mr. Emiliyan Staykov, assisted with azide derivatives **3.80-3.81**.
2. The cytotoxicity of *N*-aryl-D-gluconamides **4.01-4.09** presented in **Chapter 4**.
3. The *in vitro* assessment of gluconamides **4.01-4.07** as cryoprotectants for UCB presented in **Chapter 4**: This work was performed together with Dr. Jahan, Dr. Manesia, Ms. Kausal, and Ms. Doxtator at the Canadian Blood Services. Specifically, most cryopreservation studies were conducted by me while some were done together with Dr. Jahan or Ms. Kausal. The CFC assays were conducted similarly. Dr. Manesia performed most of the flow cytometry methodology and analysis with help from myself, Ms. Kausal, and Ms. Doxtator.
4. The *in vivo* assessment of gluconamide **4.01** using a serial transplantation assay in a murine model (**Chapter 4**): The cryopreservation and determination of *in vitro* properties of units used for the *in vivo* analysis was conducted by myself, Dr. Jahan, and Dr. Manesia; however, the *in vivo* work (and analysis) was performed by Dr. Jahan.
5. The IRI analysis, TH activity, cytotoxicity, and cryoprotectant studies on the glyco(peptides) presented in **Chapter 5** were mainly performed by me. The synthesis was performed by the Wilkinson laboratory, while some of the IRI and TH assessment of select analogues was performed by Dr. Jessica Poisson and Mr. Staykov.

Appendix II: Thesis and Non-Thesis Related Publications and Presentations

Publications and Presentations Relating to Thesis

Publications

1. Jahan, S.; **Adam, M. K.;** Manesia, J. K.; Doxtator, E.; Ben, R. B.; Pineault, N. Inhibition of Ice Recrystallization During Cryopreservation of Cord Blood Grafts Improves Platelet Engraftment. *Transfusion*. **2020**, 60, 769-778.
2. **Adam, M. K.**; Jarrett-Wilkins, C.; Beards, M.; Staykov, E.; MacFarlane, L. R.; Bell, T. D. M.; Matthews, J. M.; Manners, I.; Faul, C. F. J.; Moens, P. D. J.; Ben, R. N.; Wilkinson, B. L. 1D Self-Assembly and Ice Recrystallization Inhibition Activity of Antifreeze Glycopeptide-Functionalized Perylene Bisimides. *Chem. Eur. J.* **2018**, 24(*31*), 7834-7839.
3. **Adam, M. K.**; Hu, Y.; Poisson, J.; Pottage, M.; Ben, R.; Wilkinson, B. L. Photoswitchable Carbohydrate-Based Fluorosurfactants as Tuneable Ice Recrystallization Inhibitors. *Carbohydr. Res.* **2017**, 439, 1-8.
4. **Adam, M. K.**; Poisson, J. S.; Hu, Y.; Prasannakumar, G.; Pottage, M. J.; Ben, R. N.; Wilkinson, B. L. Carbohydrate-Based Surfactants as Photocontrollable Inhibitors of Ice Recrystallization. *RSC Adv.* **2016**, 6, 39240.

Presentations

1. **Adam, M. K.**; Jahan, S.; Charlton, T. A.; Manesia, J.; Pineault, N.; Ben, R. N. Impact of N-Aryl-D-Gluconamide Cryoprotectants on Engraftment of Cryopreserved Hematopoietic Stem and Progenitor Cells from Human Umbilical Cord Blood. Poster, 35th International Congress for the International Society of Blood Transfusion, Toronto, ON, June 2018.
2. **Adam, M. K.**; Jahan, S.; Manesia, J.; Charlton, T. A.; Poisson, J. S.; Pineault, N.; Ben, R. N. Ice Recrystallization Inhibitors to Facilitate Engraftment with Hematopoietic Stem and Progenitor Cells from Human Umbilical Cord Blood. Poster, 3rd Annual GlycoNet meeting, Banff, AB, May 2018.

3. **Adam, M. K.**; Jahan, S.; Charlton, T. A.; Staykov, E.; Briard, J. G.; Pineault, N.; Ben, R. N. Development of a Probe to Elucidate the Role of N-Aryl Aldonamides in the Cryopreservation of Hematopoietic Stem and Progenitor Cells. Poster, 100th Canadian Chemistry Conference and Exhibition, Toronto, ON, May 2017.
4. **Adam, M. K.**; Jahan, S.; Charlton, T. A.; Manesia, J.; Meyer, J. E.; Poisson, J. S.; Briard, J. G.; Pineault, N.; Ben, R. N. Ice Recrystallization Inhibitors to Facilitate Engraftment with Hematopoietic Stem and Progenitor Cells from Human Umbilical Cord Blood. Poster, 2nd Annual GlycoNet meeting, Banff, AB, May 2017.
5. **Adam, M. K.**; Poisson, J. S.; Hu, Y.; Wilkinson, B. L.; Ben, R. N. Carbohydrate-Based Surfactants as Photoswitchable Inhibitors of Ice Recrystallization. Poster presentation at the 42nd Symposium in Organic Synthesis, University of Ottawa, Ottawa, ON, June 2016 and at CRYO2016, Ottawa, ON, July 2016.

Non-Thesis Related Publications

1. Diaz-Dussan, D.; Peng, Y.-Y.; Sengupta, J.; Zabludowski, R.; **Adam, M. K.**; Acker, J. P.; Ben, R. N.; Kumar, P.; Narain, R. Trehalose-Based Polyethers for Cryopreservation and Three-Dimensional Cell Scaffolds. *Biomacromolecules*. **2020**, 21(*3*), 1264-1273.
2. Raju, R.; Merl, T.; **Adam, M.**; Staykov, E.; Ben, R.; Bryant, G.; Wilkinson, B. n-Octyl (Thio)glycosides as Potential Cryoprotectants: Glass Transition Behaviour, Membrane Permeability and Ice Recrystallization Inhibition Studies. *Aust. J. Chem*. **2019**, 72, 637-643.
3. Tri, D. L.; Childers, C. L.; **Adam, M. K.**; Ben, R. N.; Storey, K. B.; Biggar, K. K. Characterization of Ice Recrystallization Inhibition Activity in the Novel Freeze-Responsive Protein Fr10 From Freeze-Tolerant Wood Frogs, Rana sylvatica. *J. Therm. Biol.* **2019**, 84, 426-430.
4. Nagao, M.; Sengupta, J.; Diaz-Dussan, D.; **Adam, M.**; Wu, M.; Acker, J.; Ben, R.; Ishihara, K.; Zeng, H.; Miura, Y.; Narain, R. Synthesis of Highly Biocompatible and Temperature-Responsive Physical Gels for Cryopreservation and 3D Cell Culture. *ACS Appl. Bio Mater.* **2018**, 1(*2*), 356-366.

Appendix III: Experimental Section

Data plotting and statistical analysis

Data figures were prepared using GraphPad Prism 7 software (La Jolla, California, USA; www.graphpad.com). IC_{50} values (e.g. for IRI activity) were determined by applying non-linear regression to the data inputted in GraphPad. Statistical analysis of IRI data and *in vitro* cellular studies was also performed using GraphPad Prism 7 software where ANOVA (and multiple comparisons tests) was implemented (e.g. 95% confidence intervals). p values below 0.05 were considered significant. Calculations regarding the dispersion of data (e.g. SEM or SD) were performed in accordance with protocols routinely used in the Ben laboratory. Where applicable, the standard error of the mean was utilized to quantify the precision of the mean obtained from experiments.

Biostatistician Dr. Qi-Long Yi performed the statistical analyses for the *in vivo* engraftment data presented in **Chapter 4**. This included the use of SAS/STAT 9.3 statistical software (SAS Institute, Cary, North Carolina, USA; www.sas.com) and GraphPad Prism 7 software. The data were log-transformed ahead of analysis and p values equal to or less than 0.05 were considered significant. A mixed-model analysis was performed for comparing the dimethyl sulfoxide control condition and the IRI condition. Donor random effects were modelled in order to control for a possible clustering problem.[1]

Experimental protocols for ice recrystallization inhibition determination and thermal hysteresis analysis

Ice recrystallization inhibition (IRI) activity investigation by splat-cooling assay

The splat-cooling assay was used to assess ice recrystallization inhibition (IRI) activity after a 30-minute annealing period (or 5-minute annealing) as previously described.[2,3] Briefly, 10 μL of the analyte dissolved in phosphate-buffered saline (PBS) was dropped onto a polished aluminum block cooled to -80 °C. By dropping the sample from a height of 2 metres, the droplet was immediately frozen. With pre-cooled tools, the wafer was transferred to a coverslip (Fisherbrand, 12-545-80) which was then placed in a cryostage kept at -6.4 °C using a programmable Peltier unit (S3 Series 800 temperature controller, Alpha Omega Instruments). The wafer was annealed for 30 minutes and then photographed between crossed polarizing filters using a digital camera (Nikon CoolPix 5000) fitted to a microscope. Three images were chosen from each wafer for further analysis. To compare the IRI activity between compounds, the difference in the dynamics of ice crystal size distribution was examined using a novel domain recognition software (DRS)22. The cross-sectional areas of randomly-selected ice crystals in each of the three images analyzed per sample were calculated and the resulting mean grain size (MGS) could then be determined. IRI activities of the samples are reported in this thesis as percent mean grain size (% MGS) and compared to the % MGS of the positive control, PBS. Error bars represent percent standard error of the mean (% SEM) as testing for was compound was performed in triplicate. Samples were prepared on the day of testing unless otherwise indicated.

For samples annealed for five minutes (instead of the 30-minute period), one image is chosen from each ice wafer and the full image is analyzed in ImageJ (Image Processing and Analysis in Java, version 1.51s). Using ImageJ, ice crystals with well-defined boundaries within the image were circled, and the area of each circled ice crystal was calculated. From there, the mean grain size can be calculated and compared to the MGS of the positive control, PBS. The rest of the protocol is the same as that for the 30-minute annealing assay.

Ice recrystallization inhibition (IRI) activity investigation by modified splat-cooling assay

To quantify ice recrystallization inhibition (IRI) activity (and thereby obtaining an IC_{50} curve), a modified splat-cooling assay was employed.[4] A minimum of five concentrations are investigated for each compound. The ice wafer was annealed for 5 minutes at -6.4 °C as previously described for the splat-cooling assay. One image was selected from each wafer for further analysis using ImageJ software. Ice crystals with well-defined boundaries within the selected image were circled in the software and the area of each circled ice crystal was calculated. A binning approach based on ice crystal size was implemented in order to obtain an initial rate (v) of ice recrystallization. Using Excel, the ice crystal areas were then sorted into discrete bins based on size (bin size increases in increments of 0.001 mm^2). As ice crystals grew due to recrystallization, their resulting areas moved from bin 1 to higher bins. The proportionate area of each bin was then calculated for each wafer by dividing the sum of areas within a bin by the sum of the areas of all crystals in the image. Rates were determined for each test concentration and normalized based on the rate determined for the PBS control (zero inhibitor concentration). The generated dose-response curve was plotted in GraphPad using the normalized rate constants, v_{norm}, for each inhibitor concentration and the corresponding log

values of the concentration. A value for the half-maximal inhibition concentration (IC_{50}) was obtained from the two-parameter sigmoidal curve fit to the data. Error bars represent SEM.

Thermal hysteresis (TH) and dynamic ice shaping ability determined using nanoliter osmometry

The thermal hysteresis (TH) activity and dynamic ice shaping (DIS) of compounds investigated in this thesis were determined by nanoliter osmometry using a Clifton nanoliter osmometer (Clifton Technical Physics, Hartford, NY) as described by Chakrabartty and Hew.[5] A droplet of analyte dissolved in high purity deionized water was enclosed within an oil-filled well. The sample was frozen and slowly thawed until a single ice crystal remained using a thermoelectrically-controlled microscope stage. The morphology of the ice crystal was monitored using a Leitz compound microscope equipped with an Olympus 20X (infinity-corrected) objective, a Leitz Periplan 32X photo eyepiece, and a Hitachi KPM2U CCD camera connected to a Toshiba MV13K1 TV/VCR system.

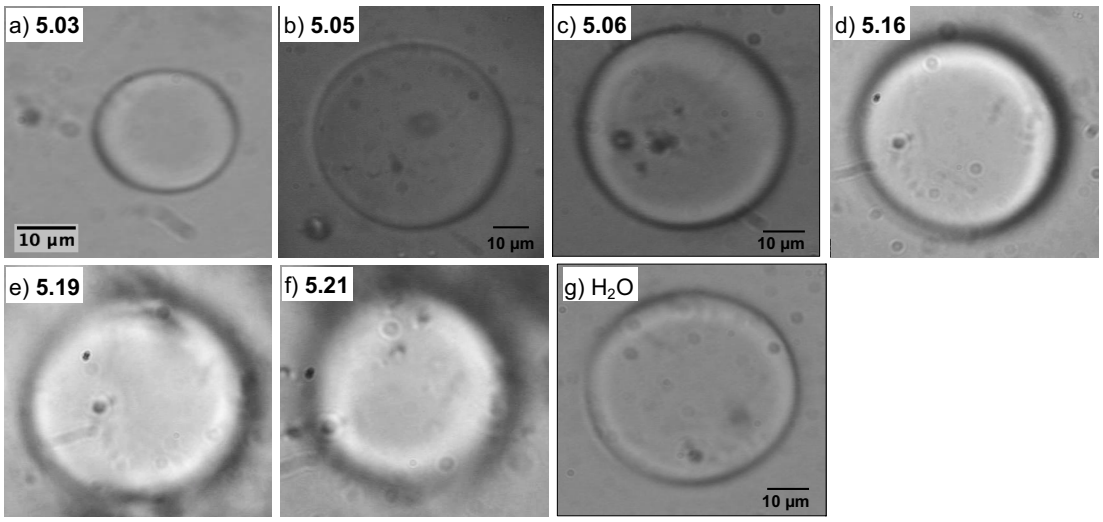

Figure A1. Ice crystal habits for IRIs discussed in **Chapter 5**. The IRIs were dissolved in water where a) 10 mg/mL **5.03**, b) 10 mg/mL **5.05**, c) 10 mg/mL **5.06**, d) 10 mg/mL **5.16**, e) 10 mg/mL **5.19**, f) 0.5 mg/mL **5.21**, g) H_2O (reproduced with permission from reference 8).[6–8]

Table A1. Maximum solubilities of select ice recrystallization inhibitors

Compound	Solubility		
	Phosphate-buffered saline (PBS)	**10% DMSO (5% dextran + 0.9% saline)**	**Minimum Essential Media (MEM)**
3.01 (**4.02**)			40 mM
3.02 (**4.01**)		25 mM	25 mM
3.03 (**4.04**)		15 mM	10 mM
3.04 (**4.03**)		30 mM	40 mM
3.39	10 mM		
3.40	12 mM		
3.65	5 mM		
3.66	20 mM		
3.67	< 1 mM		
3.68	20 mM		
3.69	20 mM		
3.71	10 mM		
3.73	10 mM		
3.74	50 mM		
3.80 (**4.07**)	15 mM		
3.81	20 mM		
3.82	1 mM		
4.05		30 mM	30 mM
5.01	1 mM		
5.04	5 μM		
5.07	5 μM		
5.08	5 μM		
5.09	5 μM		
5.10	1 mM		
5.14	5.5 mM		
5.15	11 mM		
5.16	11 mM		
5.17	1 mM		
5.18	5.5 mM		
5.19	11 mM		
5.21			30 mM (RPMI-1640 media)
5.22	5 mM		
5.23 (trans)	5 μM		
5.26 (trans)	5 μM		
5.29 (trans)	5 μM		
5.30 (trans)	500 μM		
5.32 (trans)	5 μM		

Experimental protocols for Biochemical Assays

Tf-1α cell culture, cryopreservation, and post-thaw analysis

Tf-1α cell culture

TF-1α cells (human bone marrow erythroblasts, ATCC CRL-2451) were cultured in RPMI-1640 (ATCC, 30-2001) media supplemented with 1% penicillin-streptomycin (Fisher, HyClone 100X solution, SV30010) and 10% fetal bovine serum (FBS, heat-inactivated) in 150 mm culture dishes (Corning, Falcon dish, 353025). Cells were incubated at 37 °C with 5% CO_2 and the media was changed every two days. Briefly, suspended cells were transferred to a 50 mL falcon tube and centrifuged at 1000 rpm for 5 minutes at room temperature. Following this, the supernatant was removed, the pellet was re-suspended in media, and this was transferred to a new culture dish with the addition of 20 mL of media. Cells were split if the cell count exceeded 5 x 10^6 cells per plate. Using a hemocytometer, the cell count was obtained by preparing a 1/8 dilution of the cell solution and using the dye, trypan blue (Sigma, T8154).

Tf-1α cryopreservation and post-cryopreservation flow cytometry analysis

The cultured cells were transferred to 50 mL falcon tubes and centrifuged at 1000 rpm for 5 minutes at room temperature. After supernatant removal, the pellets were re-suspended in media, combined, and a cell count was obtained as described above. 2 x 10^6 cells were aliquoted into each cryovial (Fisher, 12-567-501) and these were centrifuged at 1000 rpm for 5 minutes at rt. Following this, the supernatants were removed, and 100 µL of the appropriate cryosolution was added to each vial which was subsequently transferred to a “Mr. Frosty” freezing container. The container was placed in a -80 °C freezer (-1 °C/min freezing rate) for 18 hours followed by the transfer of the vials to a -196 °C storage dewar for a minimum of 12 hours prior to analysis.

Cryovials were thawed under fast-thaw conditions (37 °C water bath) followed by the addition of 900 µL 1X Annexin V binding buffer (BD Biosciences, 556454) to each cryovial. The contents were mixed and 400 µL of each vial was transferred to microcentrifuge tubes. 10 µL 7-AAD (BD Biosciences, 559925) and 10 µL Annexin V FITC (BD Biosciences Annexin V FITC 556419) were added, and the tubes were incubated in the dark for 15 minutes at room temperature. 20 µL counting beads (Invitrogen Countbright, C36950) were added followed by the addition of 1X Annexin V binding buffer to a total volume of 1 mL. The solutions were filtered into flow tubes prior to flow cytometry. Flow cytometry was performed on a Beckman Coulter Gallios Flow Cytometer using Kaluza for Gallios as software (version 1.3 and/or 1.5). Annexin V-FITC was measured with a 518 nm optical filter (FL-1), while 7-AAD was measured with a 570 nm optical filter (FL-4). Viability was determined as the amount of 7-AAD- cells detected and apoptosis was determined as the amount of 7-AAD- cells that were also Annexin V FITC+. Bead counts and total post-thaw cell counts were obtained for each sample. Cell recovery was calculated as the concentration of cells post-thaw divided by the pre-freeze cell concentration. The time between thawing and flow cytometry analysis was under 1 hour.

HepG2 cell culture and corresponding cytotoxicity protocols

HepG2 cell culture

HepG2 cells (human hepatocellular carcinoma cells, ATCC, HB-8065) were cultured in 75cm^2 U-shaped flasks (Fisher, 07-202-000) with Minimum Essential Medium (Fisher, Gibco MEM, 11095080 or Sigma, Eagle MEM, M4655) supplemented with 10% Fetal Bovine Serum (FBS, heat-inactivated), 1% penicillin-streptomycin (Fisher, HyClone 100X solution, SV30010), 1% non-essential amino acids (Sigma, M7145), and 0.1% 1M sodium pyruvate and incubated at

37 °C and 5% CO_2. The media was changed every two days. Once culture reached 80-85% confluency, cells were washed with Gibco DPBS (without Ca and Mg, Fisher 14190136) and Accutase (Sigma, A6964) was used to detach the cells. A cell count was obtained by hemocytometer using Trypan Blue dye (Sigma, T8154).

MTT Assay with HepG2 cells

The protocol was performed as previously described.[9,10,11] Wells of a 96-well plate (Costar, Fisher 0720090) were inoculated with 40,000 cultured HepG2 cells in MEM. The plate was incubated overnight at 37 °C and 5% CO_2 and then centrifuged at 1000 rpm for 5 minutes, the media aspirated, followed by the addition of 100 µL MEM supplemented with a test compound to each well. Wells supplemented with MEM alone served as the positive control while those supplemented with 1% Triton X-100 (Sigma, X100) in MEM served as the negative controls. The plate was incubated overnight followed by centrifugation and supernatant aspiration as described above. 200 µL MEM and 50 µL 5 mg/mL 3-(4,5-dimethylthiazol-2-yl)-2,5-diphenyltetrazolium bromide (MTT, Invitrogen, M6494) in Hanks' Balanced Salt Solution (HBSS) were added. The plate was incubated for four hours at 37 °C and 5% CO_2 followed by centrifugation for 3 minutes at 700 x g and supernatant aspiration. 200 µL of MTT solubilization solution (0.1 N HCl and 10% Triton X-100 in isopropanol) was added and the plate was incubated in the dark at room temperature until crystals had dissolved (1-3 hours). The absorbance at 570 nm was recorded by a multi-well plate reader. (AD 340C Absorbance Detector, Beckman Coulter, Inc., Mississauga, ON). Samples were performed in at least triplicate. Percent cell viability of the test conditions are the absorbances reported relative to the control absorbance readings.

Resazurin assay with HepG2 cells

Wells of a 96-well plate (Costar, Fisher 0720090) were inoculated with 10,000 cultured HepG2 cells in MEM. The plate was incubated at 37 °C and 5% CO_2 overnight and then centrifuged at 1000 rpm for 5 minutes. The media was aspirated followed by the addition of 100 µL MEM supplemented with/without test compound to appropriate wells. Wells containing no cells and inoculated with MEM only served as blanks. Wells supplemented with cells and MEM served as the positive control while those supplemented with 1% Triton X-100 (Sigma, X100) in MEM served as the negative controls. In the dark, 30 µL 0.01% resazurin (Sigma, R7017) in ddH_2O was added to each well. The plate was incubated as described above until the fluorescence was recorded 20-24 hours later by a SpectraMax Absorbance microplate reader, using 570 nm as excitation and 585 nm as emission. Blank readings were subtracted from readings. The metabolic activity present in the test conditions was reported relative to that of the controls.

Experimental protocols relating to human umbilical cord blood processing, cryopreservation, and post-thaw analysis

Cryosolution preparation for hematopoietic stem and progenitor cell (HSPC) cryopreservation

Cryosolutions were prepared with dimethyl sulfoxide (Bioreagent for molecular biology, Sigma, D8418, Oakville, Ontario, Canada) diluted to the appropriate concentration with autoclaved distilled water containing 0.9% saline and 5% w/v dextran (from Leuconostoc spp M_r ~40,000, Sigma, 31389, Oakville, Ontario, Canada). Ice recrystallization inhibitors were lyophilized prior to use using a Labconco FreeZone lyophilizer and dissolved in the appropriate DMSO solutions. Cryosolutions were prepared on the day of umbilical cord blood processing and cryopreservation. See **Table A1** for a list of the known maximum solubilities of IRIs in the cryosolution.

Umbilical cord blood (UCB) processing and HSPC cryopreservation

The processing of human umbilical cord blood (UCB) units to yield hematopoietic stem and progenitor cells (HSPCs) was performed based on common practices at Canadian Blood Services. All donors gave informed consent for the UCB donation used for research and development. Cord blood was stored at room temperature and processed within 48 hours of collection. The units had a total nucleated cell (TNC) count between 0.9 x 10^9 and 1.5 x 10^9 TNC (with a minimum volume of 50 mL). To obtain the leukorich plasma, the whole UCB was divided into 2-3 equal portions in conical tubes and mixed with Hespan (6% Hetastarch in 0.9%

sodium chloride, B. Braun Medical Inc., Irvine, CA, USA) at a proportion of 167 µL/mL UCB. The mixture was gently agitated and incubated at room temperature for 90 minutes. The resulting buffy coat was collected and centrifuged at 1390 rpm (450 x g) for 10 minutes at 10 °C. The resulting pellets were resuspended in 10 mL plasma and kept at 4 °C while a total nucleated cell (TNC) count was performed using a pocH-100i hematology analyzer (Sysmex Corporation, Ontario, Canada). Cells were divided into conical tubes for each cryo-condition based on the TNC count followed by centrifugation at 1390 rpm (450 x g) at 10 °C for 5 minutes. The resulting pellets were resuspended in the appropriate cryosolution and transferred to cryovials (VWR 2.0 mL cryotubes, 89092-262). Cryovials were transferred to a pre-cooled Mr. Frosty freezing container (isopropanol-based device, Thermo Fisher Scientific) and placed in a -80 °C freezer in order to achieve a freezing rate of -1 °C/min. The vials were transferred to the vapour-phase of -196 °C storage the following day for long-term preservation. Cryovials contained a cell concentration of 10 x 10^6 or 20 x 10^6 TNC in 1 mL of the appropriate cryosolution.

Post-thaw analysis of HSPCs

Thawing protocol for cryopreserved HSPCs

Thawing of cryovials containing 10 x 10^6 TNC/mL or 20 x 10^6 TNC/mL was performed based on a stepwise thaw-and-dilute protocol optimized by Canadian Blood Services.[12] The cryovials were thawed in a 37 °C water bath followed by a five-fold dilution of the aliquot with a solution consisting of 4% human albumin (Grifols Ltd, Barcelona, Spain) in PlasmaLyte-A (Baxter, Deerfield, IL, USA). This involved a two-step process with a 15-minute equilibration period at room temperature. These diluted samples were then centrifuged at 300 x g for 10 minutes at room temperature and the resulting pellets were resuspended in 2 mL of Iscove's

Modified Dulbecco's Medium (Life Technologies) supplemented with 2% Fetal Bovine Serum (HyClone, Thermo Fisher Scientific). A total nucleated cell (TNC) count was performed by a hematology analyzer and this TNC count was used for further post-thaw analysis.

Post-thaw viability by flow cytometry analysis of HSPCs

A FACS-Attune flow cytometer (Thermo Fisher Scientific) was used to determine the post-thaw viability (as well as the analysis of UCB cells, platelets, white blood cells, and bone marrow preparations; see *in vivo* experimental section), where fluorescent-labelled microbeads (Molecular Probes, Thermo Fisher Scientific) were utilized to carry out compensation.[1] Specifically, a FMO control was generated by staining the appropriate sample with all fluorochromes except the one best tested by that control sample. The analysis was performed by Dr. Javed Manesia at the Canadian Blood Services (with experimental procedures often conducted together with myself, Ms. Kausal, and/or Ms. Doxtator). Quadrants and gates were set using fluorescent intensity minus one (FMO) stained samples as well as conducting analysis on an unstained sample. Dead cells and debris were either gated out using a SYTOX AADvanced Dead Cell Stain Kit (Life Technologies, Thermo Fisher S10274) and/or by forward and side scatter. Based on the cell count after the thawing process, samples containing 1.25 x 10^6 cells were placed in 15 mL tubes. Red blood cells present in samples were lysed using an ammonium chloride solution (BD Biosciences; e.g. 2 mL for 1 x 10^6 TNC). The resulting samples were centrifuged at 250 x g for 8 minutes before aspiration of the supernatant and subsequent resuspension in 1X Annexin Binding Buffer (5X, Thermo Fisher Scientific V13246 diluted using deionized water to 1X prior to use). Staining was performed with the appropriate antibodies: CD34-PE (BD Biosciences PE mouse anti-human CD34, 555822), CD38-PECy-&, and CD45-

allophycocyanine (APC) antibodies (BD Biosciences). The Annexin V Alexa 488 conjugate was added to the samples as well as the diluted SYTOX AADvanced stain (diluted 10X with PBS + 2% FBS) following the manufacturer's protocols. Samples were mixed and incubated in the dark for 20 minutes (room temperature) prior to the addition of 1X annexin binding buffer. Samples for were kept on ice until data acquisition (performed within the hour).

The gating, region placement, and plotting strategy for the cell viability analysis of cells from UCB after cryopreservation is outlined below through analysis of an *in vitro* sample (e.g. TNC, CD45, CD38, CD34+ based on guidelines set out by the International Society of Hematotherapy and Graft Engineering, ISHAGE, unless indicated. Refer to: Sutherland, D. R.; Anderson, L.; Keeney, M.; Nayar, R.; Chin-Yee, I. The ISHAGE Guidelines for CD34+ Cell Determination by Flow Cytometry. *J. Hematother.* **1996**, *5* (3), 213-226.). Apoptotic cells were determined as $SYTOX^{-}$/Annexin V^{+} while necrotic were designated as $SYTOX^{+}$.

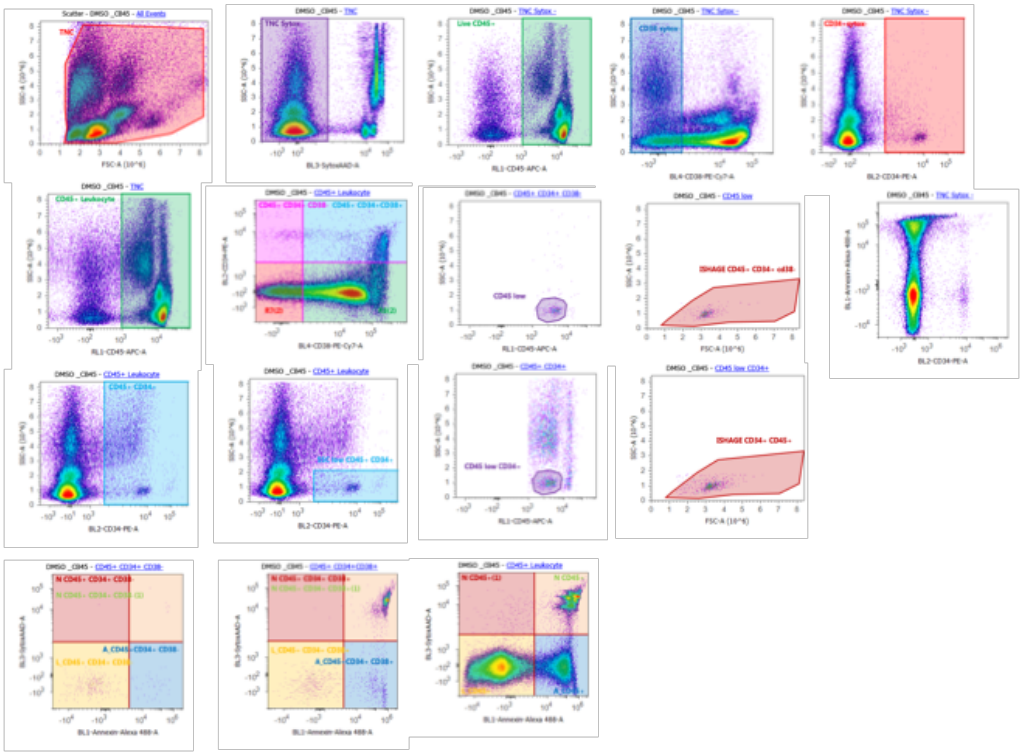

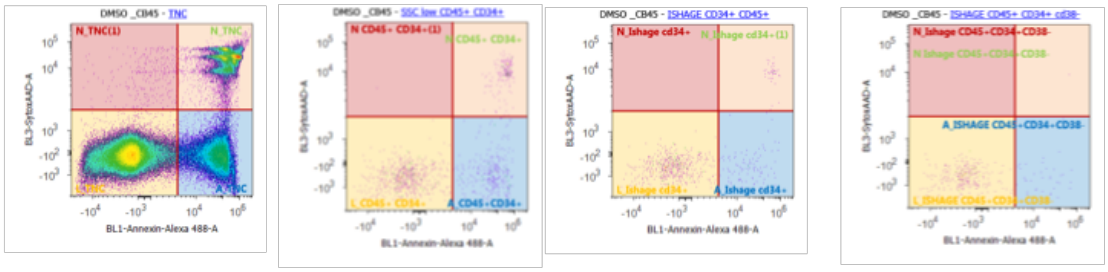

Post-thaw colony-forming cell (CFC) assay

The assay was performed following instructions by Stem Cell Technologies, Inc.[13] No RBC lysis was required before plating of CFU due to the cryopreserved nature of the cells. Using the post-thaw TNC count, a 10X cell stock solution (e.g. 400,000 TNC/mL for 40,000 TNC/plating dose) for each condition was prepared in supplemented media (as described in HSPC thawing protocol). 0.3 mL of the stock solution was added to pre-aliquoted 3 mL methylcellulose medium (MethoCult, H4434 Classic, Stem Cell Technologies) for each testing condition. The MethoCult cell mixture was vigorously mixed and let stand for 15 minutes prior to plating in dishes. A sterile 16-gauge blunt-end needle (28110, Stem Cell Technologies) attached to a sterile 3 mL luer lock syringe to draw up approximately 2.6 mL of the MethoCult-cell mixture while ensuring the absence of bubbles. 1.1 mL of the mixture was then expelled into 35 mm culture dishes (27150, Stem Cell Technologies) and this was repeated for a total of two culture dishes per condition. The dishes were tilted to evenly distribute the media. The two culture dishes per condition were placed in a larger culture dish along with a 35 mm culture dish without a lid containing sterile water. The lid was placed on the culture dish and all the dishes were placed in the incubator for 14 days (37 °C, 5% CO_2 with 97% humidity) prior to colony visualization. Colony counting was performed on an Olympus CKX41-inverted phase-contrast microscope (Olympus America) including the scoring of the following colonies: burst-forming

unit-erythroid (BFU-E), granulocyte-macrophage (CFU-G, CFU-M, CFU-GM), and the granulocyte, erythroid, macrophage, and megakaryocyte (CFU-GEMM) colonies. The CFC assay was performed in duplicate for the post-thaw analysis of UCB TNCs as well as murine BM samples (40,000 – 50,000 cells per plate).

Experimental protocols for investigating the *in vivo* activity of cord blood grafts: UCB transplantation in NSG mice and human engraftment analysis

Experiments (approved by the Animal Care Committee, University of Ottawa) were performed following the standards set out by the Animal for Research Act and the Canadian Council on Animal Care. Before transplantation, TNCs were thawed following the protocol described above and were then incubated with the OKT-3 antibody at 4 °C for 20 minutes (1 x 10^6 TNC with 1 µL of 1 mg/mL OKT-3 solution from BioXCell). The serial transplantation assay using NOD.Cg-*Prkdc*^{scid} *Il2rg*^{tm1Wjl}/SzJ mice (NSG mice, Jackson Laboratory) was performed by collaborator, Dr. Suria Jahan.[1] A Gammacell 40 Exactor irradiator (300 cGy ^{137}Cs, Best Thetratonics) was used to irradiate eight-to-ten-week old mice before intravenous transplantation of TNCs. Transplant groups (dimethyl sulfoxide condition vs dimethyl sulfoxide + gluconamide **4.01** condition) were both age- and sex-matched. There were five primary mouse recipients for both experimental groups and this was performed for each UCB unit (n = 4 units). Human engraftment analysis was performed by flow cytometry and colony-forming assay at 4 weeks post-transplant (short-term), < 12 weeks, and < 16 weeks post-transplant (long-term). Bone marrow analysis was performed after 16-weeks post-transplant, at which point a set of secondary mouse recipients were intravenously transplanted with 85% of the bone marrow collected from mice from the primary transplant. The secondary transplantation experiment was

performed in triplicate with 3-4 mice for each experimental group (and all groups were age- and sex-matched).

Human engraftment analysis involved a two-step protocol.[1,14] First, the murine platelet concentration at a time point was determined by staining diluted blood with rat anti-mCD41-fluorescein isothiocyanate (FITC). Secondly, the human platelet concentration and the murine platelet concentration was determined by staining plasma (platelet-rich with 400,000 total platelet events acquired) with antibodies specific to each species (e.g. hCD41-APC or mCD41-FITC, Becton Dickinson Pharmingen). Human white blood cell populations (myeloid using CD450APC/CD33-PE and lymphoid using CD45-APC-CD19-PE) were determined using the plasma-poor fraction. To analyze the bone marrow engraftment, bone marrow cells were obtained from the hind legs of the mice and analyzed by flow cytometry as described above (e.g. with ammonium chloride red blood cell lysis and subsequent staining protocol). As stated in the experimental section of the corresponding publication, the following antibodies were used for analysis: CD19-phycoerythrin (PE), CD14-PE, CD45-APC, CD33-PE, CD34-PE, CD3-APC human CD41a (GPIIb)-FITC, CD56-PE, CD45-FITC (Becton Dickinson Pharmingen).[1]

General Experimental for Chemical Synthesis

General experimental protocols

The synthesis and characterization data presented herein are for compounds in **Chapter 3-4**; compounds in **Chapter 5** were developed in the Wilkinson laboratory and the synthetic details can be found in the relevant publications.[6–8] Chemical reagents were purchased from commercial sources and used without further purification unless indicated. Reactions were monitored by analytical thin-layer chromatography (TLC) on 0.2 mm pre-coated silica gel aluminum sheets cut to size (60 F_{254}, E. Merck), and visualized using ultra-violet light (254 nm) along with the indicated staining methods. Flash chromatography was performed using SiliCycle (QC) or E. Merck silica gel 60 (230-400 mesh). Anhydrous conditions (under inert atmosphere, argon at 1 atm) involved the use of oven-dried syringes/cannulae for the transfer of air-sensitive materials, and solvents dispensed from a benchtop solvent purifier (SPBT-1, LC Technology Solutions Inc, Salisbury, MA) or purchased and stored over activated 4Å molecular sieves.

Nuclear magnetic resonance (NMR) spectroscopy was performed on Bruker Avance 300 and 400 MHz (Bruker, Madison, WI) instruments at ambient temperature. NMR solvents used for analysis included deuterated water (D_2O), chloroform ($CDCl_3$), methanol (MeOD), and dimethyl sulfoxide (DMSO-d_6). Spectral data were reported in chemical shifts (ppm) and referenced using residual solvent peaks. Splitting patterns observed include: singlet (s), doublet (d), triplet (t), quartet (q), multiplet (m), broad (br), doublet of doublets, (dd), doublet of doublet of doublets (ddd), doublet of doublet of doublet of doublets (dddd), and triplet of triplets (tt). Low resolution mass spectrometry (LRMS) was performed on a Micromass Q-TOF mass spectrometer (Waters Corporation, Milford, MA) in positive electrospray ionization mode (ESI+) at the John L. Holmes Mass Spectrometry Facility (University of Ottawa).

Synthesis and characterization data for chemical compounds

Synthesis of compounds 3.01-3.04 and 3.38:

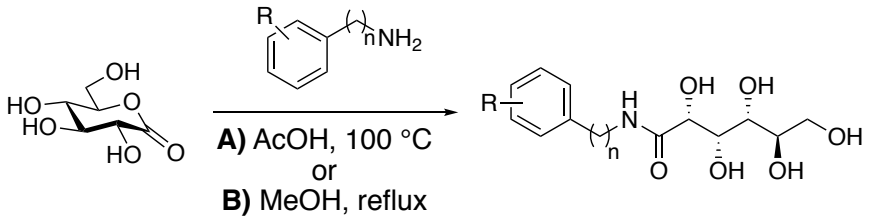

Scheme A1. The general one-step synthesis of compounds **3.01-3.04** and **3.38**.

Compound 3.01 (≡ 4.02) – *N*-(4-methoxyphenyl)-D-gluconamide

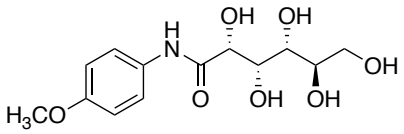

The synthesis of *N*-(4-methoxyphenyl)-D-gluconamide was adapted from that previously described.[15,16] *p*-Anisidine was purified prior to the reaction by recrystallization in dH_2O.[17] *p*-Anisidine (1.532 g, 12.44 mmol) was added to a stirring suspension of D-(+)-gluconic acid δ-lactone (2.001 g, 11.23 mmol) in methanol (112 mL). The mixture was refluxed overnight before being cooled to RT and the solvent removed *in vacuo*. The crude product was recrystallized twice from boiling 99% ethanol to yield a white solid (1.997 g, 59 %). **^{1}H NMR** (400 MHz, DMSO-d_6): δ 9.39 (s, 1H), 7.61 (ddd, J = 10.3, 3.4, 3.4 Hz, 2H), 6.87 (ddd, J = 10.3, 3.4, 3.4 Hz, 2H), 5.63 (d, J = 5.2 Hz, 1H), 4.57 (d, J = 5.3 Hz, 1H), 4.53 (d, J = 5.7 Hz, 1H), 4.51 (d, J = 7.1 Hz, 1H), 4.35 (dd, J = 5.7, 5.7 Hz, 1H), 4.14 (dd, J = 5.2, 3.8 Hz, 1H), 4.00 (ddd, J = 7.1, 3.7, 2.1 Hz, 1H), 3.72 (s, 3H), 3.59 (ddd, J = 10.9, 5.7, 2.6 Hz, 1H), 3.54-3.48 (m, 2H), 3.39 (ddd, J = 10.9, 5.5, 5.5 Hz, 1H) ppm. **^{13}C NMR** (101 MHz, DMSO-d_6) : δ 171.0, 155.3, 131.7, 121.1, 113.7, 74.1, 72.3, 71.5, 70.3, 63.3, 55.1 ppm. **LRMS (ESI)**: *m/z* calculated for $C_{13}H_{19}NO_7$ $[M+Na]^+$: 324.1; found: 324.0.

Compound 3.02 (≡ 4.01) – *N*-(2-fluorophenyl)-D-gluconamide

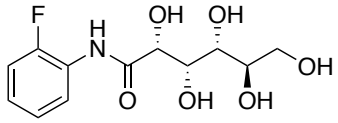

The synthesis of *N*-(2-fluorophenyl)-D-gluconamide was adapted from that previously described.[15,16] 2-Fluoroaniline (3.2 mL, 33 mmol) was added to a stirring suspension of D-(+)-gluconic acid δ-lactone (2.00 g, 11.2 mmol) in glacial acetic acid (20 mL). The mixture was stirred at 100 °C for 2.5 hours before being cooled to room temperature (TLC analysis: 8:2 ethyl acetate:methanol as solvent system with product R_f of 0.25). After solvent removal, the resulting brown crude product was recrystallized twice from minimal boiling 99% ethanol to yield white crystalline solid (1.51 g, 47%). **^{1}H NMR** (400 MHz, DMSO-d_6): δ 9.20 (d, J = 2.2 Hz, 1H), 8.13 (ddd, J = 7.9, 7.9, 2.0 Hz, 1H), 7.28 (ddd, J = 11.3, 7.7, 1.8 Hz, 1H), 7.17 (dddd, J = 7.6, 7.6, 7.6, 1.7 Hz, 1H), 7.13 (dddd, J = 7.7, 7.7, 5.0, 1.9 Hz, 1H), 5.94 (d, J = 4.8 Hz, 1H), 4.66 (d, J = 7.4 Hz, 1H), 4.62 (d, J = 5.4 Hz, 1H), 4.60 (d, J = 5.8 Hz, 1H), 4.37 (dd, J = 5.7, 5.7 Hz, 1H), 4.24 (dd, J = 5.0, 3.3 Hz, 1H), 4.03 (ddd, J = 7.3, 3.0, 3.0 Hz, 1H), 3.62 – 3.48 (m, 3H), 3.40 (ddd, J = 11.1, 5.7, 5.7 Hz, 1H) ppm. **^{13}C NMR** (101 MHz, DMSO-d_6): δ 171.5, 152.7 (d, $J_{C\text{-}F}$ = 243.2 Hz), 125.9 (d, $J_{C\text{-}F}$ = 10.7 Hz), 124.7 (d, $J_{C\text{-}F}$ = 7.6 Hz), 124.5 (d, $J_{C\text{-}F}$ = 3.4 Hz), 122.0, 115.2 (d, $J_{C\text{-}F}$ = 19.2 Hz), 73.9, 72.2, 71.6, 70.2, 63.3 ppm. **LRMS (ESI)**: *m/z* calculated for $C_{12}H_{16}FNO_6$ $[M+Na]^+$: 312.1; found: 311.9.

Compound 3.03 (≡ 4.04) – *N*-(4-chlorophenyl)-D-gluconamide

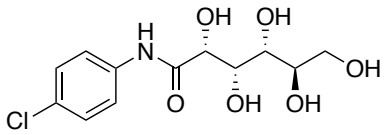

The synthesis of *N*-(4-chlorophenyl)-D-gluconamide was adapted from that previously described.[15,16] 4-Chloroaniline (3.596 g, 28.19 mmol) was added to a stirring suspension of D-(+)-gluconic acid δ-lactone (5.004 g, 28.09 mmol) in glacial acetic acid (125 mL). The mixture was stirred at 100 °C for 2 hours before being cooled to room temperature. After solvent removal, the crude product was recrystallized from minimal boiling 99% ethanol to yield white crystalline solid (4.305 g, 50%). **^{1}H NMR** (400 MHz, DMSO-d_6): δ 9.70 (s, 1H), 7.77 (ddd, J = 9.9, 3.1, 3.1 Hz, 2H), 7.35 (ddd, J = 10.0, 3.1, 3.1 Hz, 2H), 5.70 (d, J = 5.2 Hz, 1H), 4.58 (d, J = 5.2 Hz, 1H), 4.54 (d, J = 5.6 Hz, 1H), 4.54 (d, J = 7.1 Hz, 1H), 4.35 (dd, J = 5.7, 5.7 Hz, 1H), 4.18 (dd, J = 5.2, 3.7 Hz, 1H), 4.01 (ddd, J = 7.1, 3.7, 2.2 Hz, 1H), 3.59 (ddd, J = 10.9, 5.7, 2.7 Hz, 1H), 3.54 – 3.47 (m, 2H), 3.39 (ddd, J = 10.9, 5.6, 5.6 Hz, 1H) ppm. **^{13}C NMR** (101 MHz, DMSO-d6): δ 171.8, 137.6, 128.4, 126.9, 121.2, 74.2, 72.2, 71.5, 70.3, 63.3 ppm. **LRMS (ESI)**: *m/z* calculated for $C_{12}H_{16}ClNO_6$ $[M+Na]^+$: 328.1; found: 328.0.

Compound 3.04 (≡ 4.03) – *N*-(2,6-difluorobenzyl)-D-gluconamide

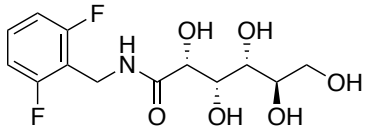

Gluconamide **3.04** was synthesized as previously reported.[15,16] **^{1}H NMR** (400 MHz, DMSO-d_6): δ 7.86 (t, J = 5.7 Hz, 1H), 7.38 (tt, J = 8.5, 6.7 Hz, 1H), 7.11 – 7.03 (m, 2H), 5.35 (d, J = 5.4 Hz, 1H), 4.52 (d, J = 5.1 Hz, 1H), 4.47 – 4.42 (m, 1H), 4.44 (d, J = 5.5 Hz, 1H), 4.39 (d, J = 7.2 Hz, 1H), 4.36 – 4.26 (m, 2H), 4.00 (dd, J = 5.4, 3.8 Hz, 1H), 3.89 (ddd, J = 7.1, 3.7, 2.2 Hz, 1H),

3.56 (ddd, J = 11.1, 5.7, 2.8 Hz, 1H), 3.49 – 3.42 (m, 2H), 3.35 (ddd, J = 11.1, 5.7, 5.7 Hz, 1H) ppm. **^{13}C NMR** (101 MHz, DMSO-d_6): δ 172.2, 161.0 (dd, $J_{C\text{-}F}$ = 247.4, 8.2 Hz), 129.8 (t, $J_{C\text{-}F}$ = 10.6 Hz), 114.2 (t, $J_{C\text{-}F}$ = 19.2 Hz), 111.5 (dd, $J_{C\text{-}F}$ = 18.7, 6.5 Hz), 73.5, 72.3, 71.5, 70.1, 63.4, 30.4 (t, $J_{C\text{-}F}$ = 3.7 Hz) ppm. **LRMS (ESI)**: *m/z* calculated for $C_{13}H_{17}F_2NO_6$ $[M+Na]^+$: 344.1; found: 343.9.

Compound 3.38 (≡ 4.05) – *N*-(2-fluoro-4-methoxyphenyl)-D-gluconamide

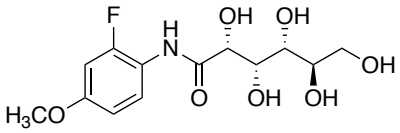

D-(+)-gluconic acid δ-lactone (2.85 g, 16.0 mmol) and 2-fluoro-4-methoxyaniline (4.26 g, 30.2 mmol) were suspended in glacial acetic acid (56 mL). The mixture was stirred at 100 °C for 1.5 hours before being cooled to room temperature. Hexanes was added and the mixture was placed in the freezer to promote precipitation. The crude product was filtered and the resulting solid was recrystallized first from minimum boiling 99% ethanol and a second recrystallization from minimum boiling dH_2O to yield a white solid (2.30 g, 45% yield). **^{1}H NMR** (400 MHz, DMSO-d_6): δ 9.07 (s, 1H), 7.84 (dd, J = 9.1, 9.1 Hz, 1H), 6.92 (dd, J = 12.7, 2.7 Hz, 1H), 6.77 (dd, J = 8.8, 1.7 Hz, 1H), 5.84 (d, J = 4.2 Hz, 1H), 4.61 (d, J = 6.1 Hz, 2H), 4.58 (d, J = 4.9 Hz, 1H), 4.38 (dd, J = 5.7, 5.7 Hz, 1H), 4.20 (dd, J = 3.6, 3.6 Hz, 1H), 4.01 (ddd, J = 6.4, 3.4, 3.4 Hz, 1H), 3.75 (s, 3H), 3.62 – 3.57 (m, 1H), 3.55 – 3.49 (m, 2H), 3.39 (ddd, J = 10.6, 5.1, 5.1 Hz, 1H) ppm. **^{13}C NMR** (101 MHz, DMSO-d_6): δ 171.3, 156.6 (d, $J_{C\text{-}F}$ = 9.6 Hz), 154.0 (d, $J_{C\text{-}F}$ = 242.9 Hz), 124.0 (d, $J_{C\text{-}F}$ = 2.9 Hz), 118.6 (d, $J_{C\text{-}F}$ = 11.7 Hz), 109.7 (d, $J_{C\text{-}F}$ = 3.1 Hz), 101.7 (d, $J_{C\text{-}F}$ = 23.1 Hz), 73.9, 72.3, 71.6, 70.2, 63.3, 55.7 ppm. **LRMS (ESI)**: *m/z* calculated for $C_{13}H_{18}FNO_7$ $[M+Na]^+$: 342.1; found: 342.2.

Synthesis of compounds 3.39-3.44 through intermediates 3.50-3.59:

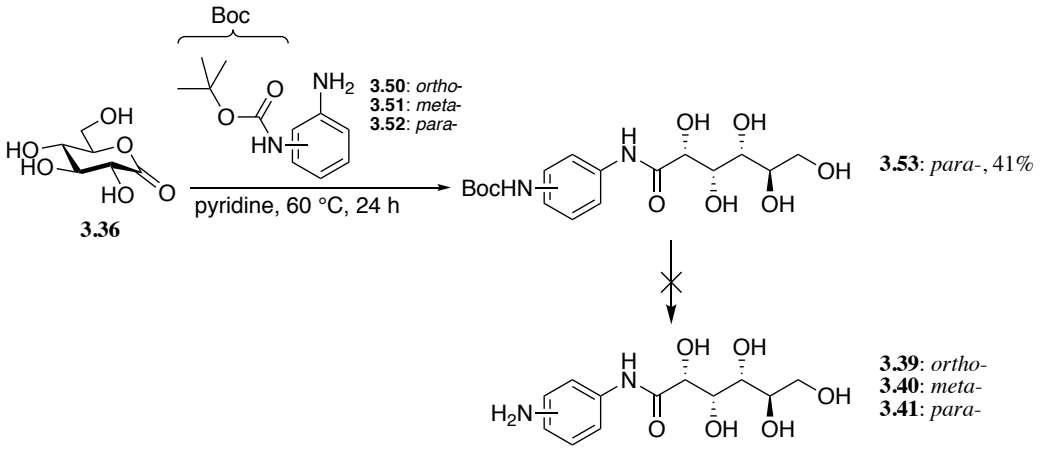

Scheme A2. Attempted synthesis of compounds **3.39-3.41** using Boc protecting groups.

Compounds 3.50-3.52

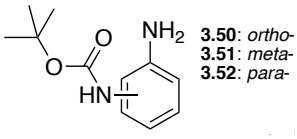

ortho- derivative **3.50**: To a flame-dried flask under argon, was added 1,2-phenylenediamine (7.996 g, 73.94 mmol) and dioxane (144 mL) to dissolve.[18] The solution was cooled to 0 °C in an ice-water bath followed by the slow addition of Boc_2O (3.283 g, 15.04 mmol) pre-dissolved in dioxane (16 mL). The mixture was allowed to warm to room temperature and stir for 22 hours. The solvent was removed and the crude solid was dissolved in 9:1 DCM:MeOH and washed with saturated aqueous $NaHCO_3$, H_2O, and brine. The organic layer was dried over Na_2SO_4, filtered, and concentrated. The resulting crude solid was purified by flash chromatography in 8:2 pet. ether:EtOAc to yield a white product (2.976 g, 96%). **^{1}H NMR** (400 MHz, DMSO-d_6): δ 8.28 (br s, 1H), 7.18 (d, J = 7.6 Hz, 1H), 6.83 (ddd, J = 8.0, 7.6, 1.6 Hz, 1H), 6.68 (dd, J = 8.0, 1.6 Hz, 1H), 6.52 (ddd, J = 8.0, 8.0, 1.6 Hz, 1H), 4.81 (s, 2H), 1.46 (s, 9H) ppm. **^{13}C NMR** (101 MHz, DMSO-d_6): δ 153.6, 141.2, 124.9, 124.5, 123.7, 116.2, 115.7, 78.6, 28.2 ppm. **LRMS (ESI)**: *m/z* calculated for $C_{11}H_{16}N_2O_2$ $[M+Na]^+$: 231.1; found: 231.1.

meta- derivative **3.51:** To a flame-dried flask under argon, was added 1,2-phenylenediamine (7.997 g, 73.95 mmol) and dioxane (144 mL) to dissolve.[18] The solution was cooled to 0 °C in an ice-water bath followed by the slow addition of Boc_2O (3.300 g, 15.12 mmol) pre-dissolved in dioxane (16 mL). The mixture was allowed to warm to room temperature and stir for 22 hours. The solvent was removed and the crude solid was dissolved in 9:1 DCM:MeOH and washed with saturated aqueous $NaHCO_3$, H_2O, and brine. The organic layer was dried over Na_2SO_4, filtered, and concentrated. The resulting crude solid was purified by flash chromatography in 8:2 pet. ether:EtOAc to yield a white product (2.640 g, 86%). **^{1}H NMR** (400 MHz, DMSO-d_6): δ 8.98 (s, 1H), 6.84 (dd, *J* = 8.0, 8.0 Hz, 1H), 6.81 (dd, *J* = 2.0, 2.0 Hz, 1H), 6.53 (ddd, *J* = 8.0, 2.0, 0.8 Hz, 1H), 6.16 (ddd, *J* = 8.0, 2.0, 0.8 Hz, 1H), 4.95 (s, 2H), 1.45 (s, 9H) ppm. **^{13}C NMR** (101 MHz, DMSO-d_6): δ 152.7, 148.9, 140.0, 128.7, 108.2, 106.3, 103.9, 78.5, 28.2 ppm. **LRMS (ESI)**: *m/z* calculated for $C_{11}H_{16}N_2O_2$ $[M+Na]^+$: 231.1; found: 231.1.

para- derivative **3.52:** To a flame-dried flask under argon, was added 1,4-phenylenediamine (10.015 g, 92.61 mmol) and dioxane (180 mL) to dissolve.[18] The solution was cooled to 0 °C in an ice-water bath followed by the slow addition of Boc_2O (4.083 g, 18.71 mmol) pre-dissolved in dioxane (20 mL). The mixture was allowed to warm to room temperature and stir for 24 hours. The solvent was removed and the crude solid was dissolved in 9:1 DCM:MeOH and washed with saturated aqueous $NaHCO_3$, H_2O, and brine. The organic layer was dried over Na_2SO_4, filtered, and concentrated. The resulting crude solid was purified by flash chromatography in 6:4 pet. ether:EtOAc to yield an off-white product (3.316 g, 86%). **^{1}H NMR** (400 MHz, MeOD): δ 7.10 (d, *J* = 8.0 Hz, 2H (Ar)), 6.69-6.66 (m, 2H (Ar)), 1.49 (s, 9H, Boc group). **^{13}C NMR** (101 MHz, DMSO-d_6): δ 153.1, 143.9, 128.5, 120.2, 113.9, 78.1, 28.2 ppm. **LRMS (ESI)**: *m/z* calculated for $C_{11}H_{16}N_2O_2$ $[M+Na]^+$: 231.1; found: 231.0.

Compound 3.53

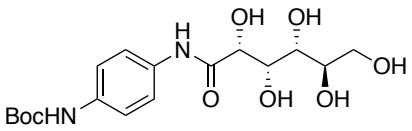

In a flame-dried flask under argon, the aryl amine (boc protected) (0.505 g, 2.42 mmol) was dissolved in pyridine (19 mL). Gluconic acid δ-lactone (0.332 g, 1.86 mmol) was then added and the reaction was stirred for 24 hours at 60 °C (TLC system: 8:2 EtOAc:MeOH, UV and pA stain for visualization). The solvent was then removed and the resulting crude product was recrystallized from 99% ethanol to yield white product (0.299 g, 41%). **^{1}H NMR** (400 MHz, DMSO-d_6): δ 9.38 (s, 1H), 9.23 (br s, 1H), 7.57 (ddd, *J* = 8.8, 1.6, 1.6 Hz, 2H), 7.35 (d, *J* = 8.8 Hz, 2H), 5.64 (d, *J* = 5.6 Hz, 1H), 4.57 (d, *J* = 5.2 Hz, 1H), 4.53 (d, *J* = 5.2 Hz, 1H), 4.51 (d, *J* = 6.8 Hz, 1H), 4.34 (dd, *J* = 5.6, 5.6 Hz, 1H), 4.14 (dd, *J* = 5.2, 3.6 Hz, 1H), 4.01-3.98 (m, 1H), 3.63-3.56 (m, 1H), 3.53-3.49 (m, 2H), 3.45-3.36 (m, 1H), 1.47 (s, 9H) ppm. **^{13}C NMR** (101 MHz, DMSO-d_6): δ 171.0, 152.8, 135.1, 133.0, 119.9, 118.3, 78.8, 74.1, 72.3, 71.5, 70.3, 63.3, 28.1 ppm. **LRMS (ESI)**: *m/z* calculated for $C_{17}H_{26}N_2O_8$ $[M+Na]^+$: 409.2; found: 409.1.

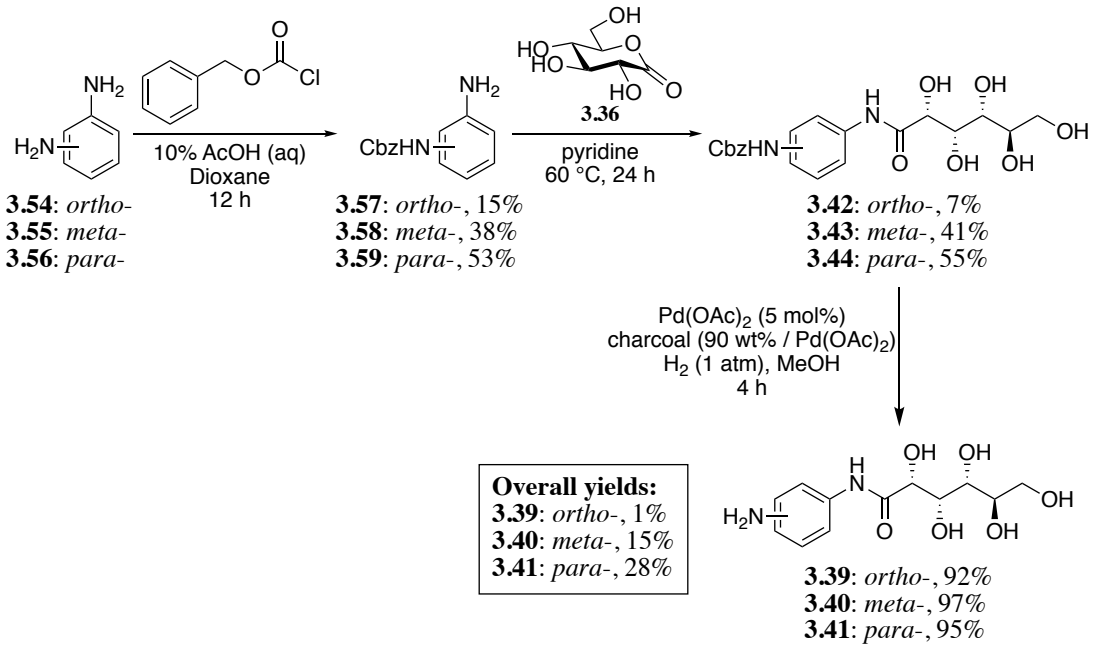

Scheme A3: Synthesis of compounds **3.39-3.44**.[19]

Compounds 3.57-3.59

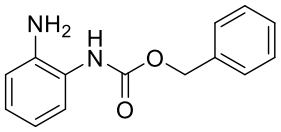

<u>*ortho*- intermediate **3.57**</u>**:**

To a solution of benzyl chloroformate (0.70 mL, 4.9 mmol) dissolved in 1,4-dioxane (40.7 mL) was added a solution of *o*-phenylenediamine (2.686 g, 24.83 mmol) in 10% aqueous acetic acid (214 mL).[19,20] The reaction mixture was allowed to stir at room temperature overnight before washing the solution with Et_2O (3x). A solution of 2N NaOH was added until pH 14 was achieved. After extracting the mixture with Et_2O (3x), the solution was concentrated *in vacuo*. The crude product was purified by flash chromatography (20%, then 30% EtOAc:Hexane) to yield a light orange solid (0.19 g, 15%). **^{1}H NMR** (400 MHz, $CDCl_3$): δ 9.72 (s, 1H), 7.78 (dd, J = 7.60 Hz, 1.56 Hz, 1H), 7.53 (dd, J = 6.60 Hz, 1.56 Hz, 2H), 7.42 to 7.34 (m, 3H), 7.16 (ddd, J = 7.60 Hz, 7.60 Hz, 1.12 Hz, 1H), 7.10 (ddd, J = 7.80 Hz, 7.80 Hz, 1.2 Hz, 2H), 5.51 (s, 2H) ppm. **^{13}C NMR** (101 MHz, $CDCl_3$): δ 150.30, 134.75, 128.73, 128.69, 128.40, 127.69, 126.81,

124.50, 122.48, 114.72, 109.72, 69.00, 30.93, 29.70 ppm. **LRMS (ESI)**: *m/z* calculated for $C_{14}H_{14}N_2O_2$ $[M+Na]^+$: 265.1; found: 265.0.

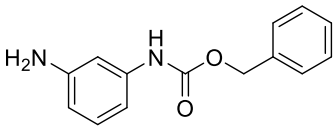

meta- intermediate **3.58:**

The synthesis was adapted from previously reported (see compound **3.57**).[19,20] To benzyl chloroformate (0.70 mL, 4.97 mmol) dissolved in 1,4-dioxane (40.5 mL) was added *m*-phenylenediamine (2.689 g, 24.86 mmol) in 10% aq. acetic acid (213 mL). The crude product was purified by flash chromatography (25% then 30% EtOAc:Hexane) to obtain a white solid (0.45 g, 38%). **^{1}H NMR** (400 MHz, MeOD): δ 7.42 to 7.28 (m, 5H), 7.00 (t, J = 8.00 Hz, 1H), 6.94 (t, J = 2.16 Hz, 1H), 6.73 (dddd, J = 2.76 Hz, 1.88 Hz, 0.72 Hz, 1H), 6.44 (dddd, J = 3.08 Hz, 2.16 Hz, 0.96 Hz, 1H), 5.15 (s, 2H) ppm. **^{13}C NMR** (101 MHz, MeOD): δ 154.37, 147.48, 139.47, 136.80, 128.96, 128.09, 127.65, 127.52, 110.38, 108.90, 105.93, 65.99 ppm. **LRMS (ESI)**: *m/z* calculated for $C_{14}H_{14}N_2O_2$ $[M+Na]^+$: 265.1; found: 265.1.

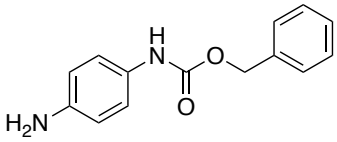

para- intermediate **3.59:**

The synthesis was adapted from previously reported (see compound **3.57**).[19,20] To benzyl chloroformate (1.30 mL, 9.22 mmol) dissolved in 1,4-dioxane (75.58 mL) and *p*-phenylenediamine (4.986 g, 46.09 mmol) in 10% aq. acetic acid (398 mL). The crude product was purified by flash chromatography (50% EtOAc:Hexane) to obtain a brown solid (1.1797 g, 53%). **^{1}H NMR** (400 MHz, MeOD): δ 7.39 to 7.26 (m, 5H), 7.14 (d, J = 7.80 Hz, 2H), 6.68 (dddd, J = 9.72 Hz, 3.04 Hz, 3.04 Hz, 2H), 5.13 (s, 2H) ppm. **^{13}C NMR** (101 MHz, MeOD): δ 155.02, 143.18, 136.88, 129.71, 128.08, 127.61, 127.48, 120.71, 115.61, 65.98 ppm. **LRMS (ESI)**: *m/z* calculated for $C_{14}H_{14}N_2O_2$ $[M+Na]^+$: 265.1; found: 265.0.

Compounds 3.42-3.44

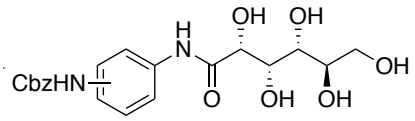

3.42: *ortho-*, 7%
3.43: *meta-*, 41%
3.44: *para-*, 55%

ortho- intermediate **3.42**: In a flame-dried flask under argon, D-gluconolactone (0.484 g, 2.70 mmol) was added to a solution of compound **3.57** (0.722 g, 2.98 mmol) dissolved in dry pyridine (27 mL).[19] The reaction mixture was stirred at 60 °C for 24h before solvent was removed *in vacuo*. The product was recrystallized in ethanol 99% to yield a beige solid (75.7 mg, 7%). **^{1}H NMR** (400 MHz, DMSO-d_6): δ 9.37 (s, 1H), 9.12 (s, 1H), 7.77 (d, J = 6.56 Hz, 1H), 7.44 to 7.38 (m, 5H), 7.36 to 7.32 (m, 1H), 7.15 (dddd, 2H), 5.83 (d, J = 4.76 Hz, 1H), 5.15 (s, 2H), 4.63 (d, J = 2.08 Hz, 2H), 4.63 (s, 1H), 4.39 (t, J = 5.60 Hz, 1H), 4.21 (t, J = 3.88 Hz, 1H), 4.05 (ddd, J = 6.52 Hz, 2.96 Hz, 2.96 Hz, 1H), 3.63 to 3.56 (m 2H), 3.54 to 3.55 (m, 1H), 3.41 (ddd, J = 10.96 Hz, 5.56 Hz, 5.56 Hz, 1H) ppm. **^{13}C NMR** (101 MHz, DMSO-d_6): δ 172.25, 154.80, 137.01, 128.91, 128.44, 128.39, 125.47, 125.22, 124.37, 74.25, 72.58, 72.01, 70.78, 66.56, 63.82 ppm. **LRMS (ESI)**: *m/z* calculated for $C_{20}H_{24}N_2O_8$ $[M+Na]^+$: 443.1; found: 443.3.

meta- intermediate **3.43:** The protocol followed that of compound **3.42**. Compound **3.58** (0.397 g, 1.64 mmol) dissolved in dry pyridine (15 mL) to yield crude product recrystallized as previously described (0.265 g, 41%).[19] **^{1}H NMR** (400 MHz, DMSO-d_6): δ 9.76 (s, 1H), 9.44 (s, 1H), 7.86 (dd, J = 2.00 Hz, 2.00 Hz, 1H), 7.43 to 7.37 (m, 4H), 7.35 to 7.30 (m, 2H), 7.17 (dd, J = 8.04 Hz, 8.04 Hz, 1H), 7.13 (ddd, J = 12.24 Hz, 4.12 Hz, 4.12 Hz, 1H), 5.64 (d, J = 5.44 Hz, 1H), 5.13 (s, 2H), 4.58 (d, J = 5.00 Hz, 1H), 4.54 (s, 1H), 4.52 (d, J = 4.48 Hz, 1H), 4.35 (dd, J = 5.68 Hz, 5.68 Hz, 1H), 4.16 (dd, J = 5.32 Hz, 3.84 Hz, 1H), 4.00 to 3.97 (m, 1H), 3.58 (ddd, J = 10.84 Hz, 5.72 Hz, 2.24 Hz, 1H), 3.50 (dd, J = 2.52 Hz, 2.52 Hz, 2H), 3.39 (dd, J = 10.88 Hz,

5.52 Hz, 1H) ppm. **^{13}C NMR** (101 MHz, DMSO-d_6): δ 171.79, 153.78, 139.76, 139.30, 137.14, 129.24, 128.90, 128.50, 128.47, 114.41, 114.06, 110.18, 74.69, 72.76, 72.00, 70.77, 66.11, 63.77 ppm. **LRMS (ESI)**: *m/z* calculated for $C_{20}H_{24}N_2O_8$ $[M+Na]^+$: 443.1; found: 443.2.

para- intermediate **3.44**: The protocol was that used for compound **3.42**. D-gluconolactone (0.669 g, 3.75 mmol) was added to a solution of compound **3.59** (0.999 g, 4.13 mmol) dissolved in dry pyridine (38 mL) .[19] Purified as previously described yielded a white solid (0.875 g, 55%). **^{1}H NMR** (400 MHz, DMSO-d_6): δ 9.68 (s, 1H), 9.42 (s, 1H), 7.60 (d, J = 8.92 Hz, 2H), 7.44 to 7.32 (m, 7H), 5.65 (d, J = 5.20 Hz, 1H), 5.13 (s, 2H), 4.58 (d, J = 4.92 Hz, 1H), 4.53 (d, J = 4.00 Hz, 1H), 4.51 (s, 1H), 4.35 (dd, J = 5.64 Hz, 5.64 Hz, 1H), 4.15 (dd, J = 5.00 Hz, 3.84 Hz, 1H), 4.01 to 3.99 (m, 1H), 3.59 (ddd, J = 10.36 Hz, 5.12 Hz, 1.96 Hz, 1H), 3.51 (ddd, J = 9.8 Hz, 7.48 Hz, 7.48 Hz, 2H), 3.40 (dd, J = 10.8 Hz, 5.44 Hz, 1H) ppm. **^{13}C NMR** (101 MHz, DMSO-d_6): δ 171.58, 153.86, 137.15, 133.91, 128.90, 128.54, 128.48, 74.60, 72.76, 72.01, 70.74, 66.12, 63.77 ppm. **LRMS (ESI)**: *m/z* calculated for $C_{20}H_{24}N_2O_8$ $[M+Na]^+$: 443.1; found: 442.2.

Compounds 3.39-3.41

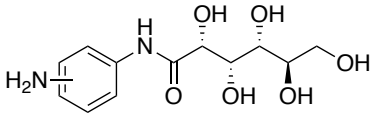

3.39: *ortho-*, 92%
3.40: *meta-*, 97%
3.41: *para-*, 95%

ortho- compound **3.39**: The protocol was adapted from the literature.[21] Cbz-protected intermediate **3.42** (0.07 g, 0.17 mmol) was dissolved in a minimal amount of methanol followed by the addition of $Pd(OAc)_2$ (1.9 mg, 0.01 mmol) and charcoal (17 mg).[19] The flask was cycled (4x) under vacuum to introduce a hydrogen atmosphere and the reaction was allowed to stir at room temperature for 4 hours. Water was added to the reaction to dissolve the precipitated

product and the reaction mixture was filtered through celite. A pure brown solid was obtained after solvent removal (0.044 g, 92%). **^{1}H NMR** (400 MHz, DMSO-d_6): δ 8.98 (s, 1H), 7.26 (dd, J = 7.76 Hz, 1.04, 1H), 6.89 (ddd, J = 7.44 Hz, 7.44 Hz, 1.28 Hz, 1H), 6.71 (dd, J = 7.88 Hz, 1.00 Hz, 1H), 6.54 (ddd, J = 7.84 Hz, 7.84 Hz, 1.16 Hz, 1H), 4.90 (s, 2H), 4.18 (d, J = 2.96 Hz, 1H), 4.01 (dd, J = 2.68 Hz, 2.68 Hz, 1H), 3.60 to 3.48 (m, 5H), 3.16 (s, 2H) ppm. **^{13}C NMR** (101 MHz, DMSO-d_6): δ 172.15, 142.49, 126.22, 125.55, 123.72, 116.61, 116.16, 74.79, 72.89, 71.97, 70.71, 63.86 ppm. **LRMS (ESI)**: *m/z* calculated for $C_{12}H_{18}N_2O_6$ $[M+Na]^+$: 309.1; found: 309.0.

meta- compound **3.40**: The protocol was adapted from that used for compound **3.39**.[19,21] Cbz-protected intermediate (84 mg, 0.20 mmol) dissolved in MeOH followed by the addition of $Pd(OAc)_2$ (2.3 mg, 0.01 mmol) and charcoal (21 mg). The light beige solid product was yielded without additional purification (58 mg, 97%). **^{1}H NMR** (400 MHz, DMSO-d_6): δ 9.14 (s, 1H), 7.00 (s, 1H), 6.91 (dd, J = 7.64 Hz, 7.64 Hz, 1H), 6.72 (d, J = 7.28 Hz, 1H), 6.26 (d, J = 6.68 Hz, 1H), 5.04 (s, 2H), 4.65 (br, 3H), 4.12 (s, 1H), 3.98 (s, 1H), 3.58 (d, J = 10.04 Hz, 1H), 3.50 (s, 2H) ppm. **^{13}C NMR** (101 MHz, DMSO-d_6): δ 171.48, 149.42, 139.45, 129.32, 109.93, 107.77, 105.43, 74.71, 72.87, 71.98, 70.68, 63.79 ppm. **LRMS (ESI)**: *m/z* calculated for $C_{12}H_{18}N_2O_6$ $[M+Na]^+$: 309.1; found: 309.2.

para- compound **3.41:** The protocol was adapted from that used for compound **3.39**.[19,21] Cbz-protected intermediate (0.397 g, 0.94 mmol) dissolved in MeOH followed by the addition of $Pd(OAc)_2$ (11 mg, 0.05 mmol) and charcoal (96 mg). The light beige solid product was yielded without additional purification (0.257 g, 95%). **^{1}H NMR** (400 MHz, DMSO-d_6): δ 9.08 (s, 1H), 7.30 (ddd, J = 4.92 Hz, 2.96 Hz, 2.96 Hz, 2H), 6.49 (ddd, J = 4.96 Hz, 2.92 Hz, 2.92 Hz, 2H),

4.85 (s, 2H), 4.57 (br, 3H), 4.10 (d, J = 3.72 Hz, 1H), 3.98 (d, J = 2.64 Hz, 1H), 3.58 (d, J = 11.28 Hz, 1H), 3.50 (s, 1H), 3.50 (s, 2H), 3.40 (dd, J = 3.12 Hz, 2.16 Hz, 1H) ppm. **^{13}C NMR** (101 MHz, DMSO-d_6): δ 170.80, 145.34, 128.19, 121.54, 114.15, 74.52, 72.83, 71.99, 70.69, 63.81 ppm. **LRMS (ESI)**: *m/z* calculated for $C_{12}H_{18}N_2O_6$ $[M+Na]^+$: 309.1; found: 309.1.

Synthesis of compounds 3.45-3.47 through intermediates 3.60-3.62:

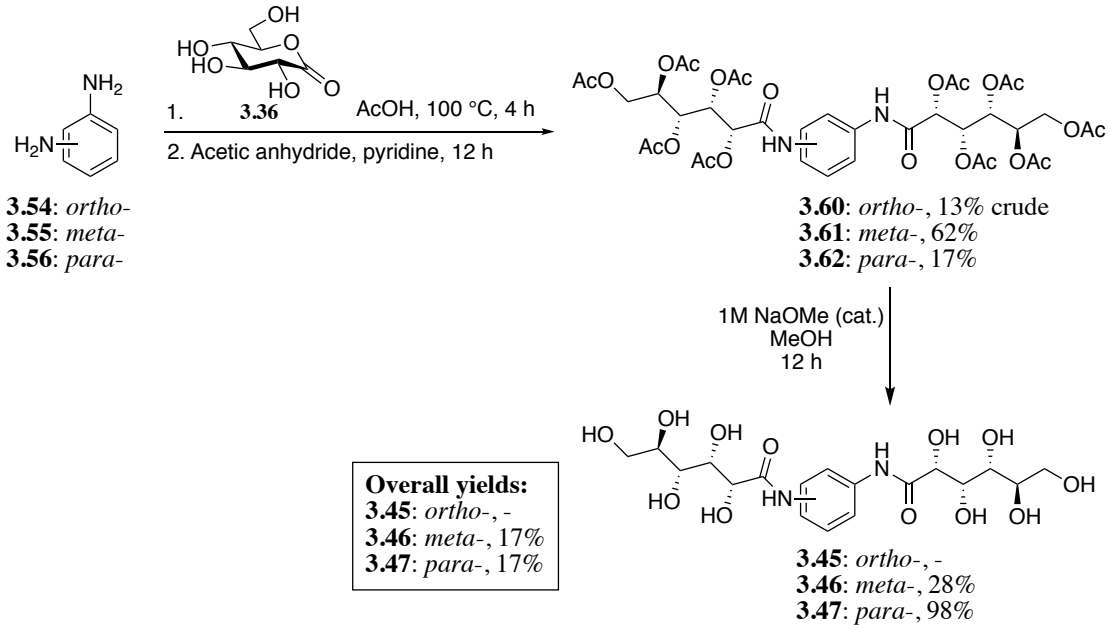

3.54: *ortho-*
3.55: *meta-*
3.56: *para-*

3.60: *ortho-*, 13% crude
3.61: *meta-*, 62%
3.62: *para-*, 17%

3.45: *ortho-*, -
3.46: *meta-*, 28%
3.47: *para-*, 98%

Scheme A4: Synthesis of compounds **3.45-3.47** through intermediates **3.60-3.62**.[19]

Compound 3.60

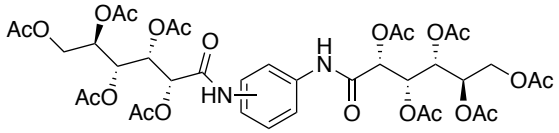

3.60: *ortho-*, 13% crude

In a flame-dried flask under argon, D-gluconolactone (4.287 g, 24.2 mmol) was dissolved in AcOH (106 mL) followed by the addition of *o*-phenylenediamine (0.65 g, 6.0 mmol).[19] The mixture was heated to 100 °C and stirred for 4 hours before the solvent was removed under

vacuum. Once the resulting light brown crude oil was obtained, it was dissolved in anhydrous pyridine (30 mL) and cooled to 0 °C. After 5 minutes, acetic anhydride (11.5 mL) was added dropwise, and the resulting reaction was allowed to warm to room temperature overnight. The reaction was quenched using saturated $NaHCO_3$ (aq) followed by the addition of EtOAc (3x the volume of pyridine). The solution was washed with 10% HCl (aq), saturated $NaHCO_3$, and brine. The solvent was removed from the organic layer to yield a yellow solid as the crude product which could not be purified (0.673 g; 13% crude).

Compound 3.61

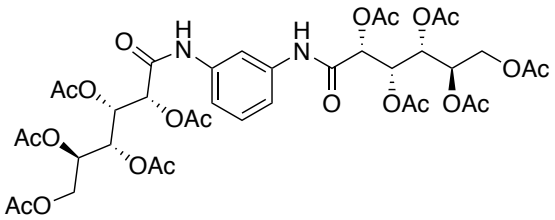

The protocol was similar to that used for compound **3.50**.[19] Under inert atmosphere, D-gluconolactone (1.647 g, 9.25 mmol) was dissolved in AcOH (41 mL) followed by the addition of *m*-phenylenediamine (0.250 g, 2.31 mmol). The mixture was heated to 100 °C and stirred for 4 hours before the solvent was removed under vacuum. Once the resulting light brown crude oil was obtained, it was dissolved in anhydrous pyridine (12 mL) and cooled to 0 °C. After 5 minutes, acetic anhydride (4.4 mL) was added dropwise, and the resulting reaction was allowed to warm to room temperature overnight. The reaction was quenched using saturated $NaHCO_3$ (aq) followed by the addition of EtOAc (3x the volume of pyridine). The solution was washed with 10% HCl (aq), saturated $NaHCO_3$, and brine. The solvent was removed from the organic layer and the crude product was purified by flash chromatography (78% EtOAc:Hexane) to yield a yellow oil (1.23 g, 62%). **^{1}H NMR** (400 MHz, DMSO-d_6): δ 10.23 (s, 2H), 7.74 (dd, J = 1.92 Hz, 1.92 Hz, 1H), 7.24 to 7.16 (m, 3H), 5.55 (dd, J = 3.88 Hz, 3.88 Hz, 2H), 5.34 (q, J = 7.00 Hz,

4.08 Hz, 2H), 5.16 (d, J = 3.76 Hz, 2H), 4.99 (ddd, J = 8.88 Hz, 5.76 Hz, 3.04 Hz, 2H), 4.21 (dd, J = 12.36 Hz, 3.16 Hz, 2H), 4.11 (dd, J = 12. 36 Hz, 5.92, 2H), 2.08 (s, 6H), 2.03 (s, 6H), 1.96 (s, 6H), 1.96 (s, 6H), 1.95 (s, 6H) ppm. **^{13}C NMR** (101 MHz, DMSO-d_6): δ 170.86, 170.48, 170.05, 169.98, 169.89, 169.64, 164.69, 138.85, 115.81, 111.72, 72.69, 69.21, 68.65, 61.65, 21.05, 21.01, 20.93, 20.84, 20.79 ppm. **LRMS (ESI)**: *m/z* calculated for $C_{38}H_{48}N_2O_{22}$ $[M+Na]^+$: 907.3; found: 907.1.

Compound 3.62

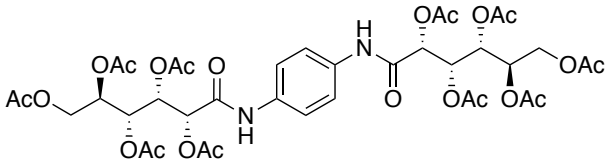

The protocol was similar to that used for compound **3.50**.[19] Under inert atmosphere, D-gluconolactone (4.283 g, 24.15 mmol) was dissolved in AcOH (107 mL) followed by the addition of *p*-phenylenediamine (0.650 g, 6.04 mmol). The mixture was heated to 100 °C and stirred for 4 hours before the solvent was removed under vacuum. The resulting crude intermediate was dissolved in anhydrous pyridine (30 mL) and cooled to 0 °C. After 5 minutes, acetic anhydride (11.5 mL) was added dropwise, and the resulting reaction was allowed to warm to room temperature overnight. The solvent was removed from the organic layer after work up, and the crude product was purified by flash chromatography (75% EtOAc:Hexane) to yield a beige solid (0.93 g, 17%). **^{1}H NMR** (400 MHz, DMSO-d_6): δ 10.18 (s, 2H), 7.41 (s, 4H), 5.57 (dd, J = 3.96 Hz, 3.96 Hz, 2H), 5.36 (dd, J = 6.96 Hz, 4.08 Hz, 2H), 5.18 (d, J= 3.88 Hz, 2H), 5.01 (ddd, J = 5.88 Hz, 3.04 Hz, 2H), 4.23 (dd, J = 12.32 Hz, 3.12 Hz, 2H), 4.13 (dd, J = 12.40 Hz, 5.80 Hz, 2H), 2.11 (s, 6H), 2.06 (s, 6H), 1.99 (s, 6H), 1.99 (s, 6H), 1.98 (s, 6H) ppm. **^{13}C NMR** (101 MHz, DMSO-d_6): δ 170.47, 170.06, 169.97, 169.89, 169.64, 164.49, 134.49, 120.81,

72.72, 69.22, 68.77, 68.62, 61.65, 21.05, 21.02, 20.93, 20.86, 20.79 ppm. **LRMS (ESI)**: *m/z* calculated for $C_{38}H_{48}N_2O_{22}$ $[M+Na]^+$: 907.3; found: 907.4.

Compound 3.46

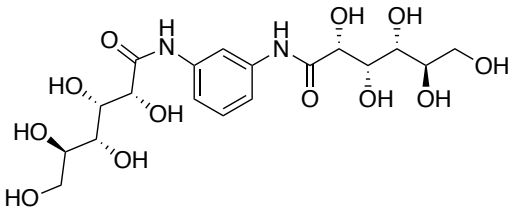

1M NaOMe (1 mL) was added to a solution of compound **3.61** (0.601 g, 1.11 mmol) dissolved in methanol (22.3 mL).[19] The resulting reaction was stirred for 3 hours at which point amberlite (IR120 hydrogen form resin) was added until an acidic reaction mixture was achieved. The amberlite IR120 resin was filtered and the solvent was removed. After recrystallization with 99% EtOH, a light orange product was obtained (0.087 g, 28%). **^{1}H NMR** (400 MHz, DMSO-d_6): δ 9.46 (s, 2H), 8.06 (dd, J = 2.00 Hz, 2.00 Hz, 1H), 7.38 (dd, J = 8.04 Hz, 1.64 Hz, 2H), 7.22 (dd, J = 7.92 Hz, 7.92 Hz, 1H), 5.66 (d, J = 5.44 Hz, 2H), 4.58 (d, J = 4.8 Hz, 2H), 4.56 (s, 2H), 4.53 (d, J = 5.64 Hz, 2H), 4.36 (dd, J = 5.64 Hz, 5.64 Hz, 2H), 4.18 (dd, J = 5.44 Hz, 3.72 Hz, 2H), 4.02 to 3.99 (m, 2H), 3.59 (ddd, J = 11.28 Hz, 5.44 Hz, 2.12 Hz, 2H), 3.51 (dd, 4H), 3.40 (dd, J = 10.84 Hz, 5.40 Hz, 2H) ppm. **^{13}C NMR** (101 MHz, DMSO-d_6): δ 171.84, 139.12, 129.14, 115.30, 111.36, 74.65, 72.74, 72.01, 70.81, 63.78, 55.37 ppm. **LRMS (ESI)**: *m/z* calculated for $C_{18}H_{28}N_2O_{12}$ $[M+Na]^+$: 487.2; found: 487.2.

Compound 3.47 (≡ 4.09)

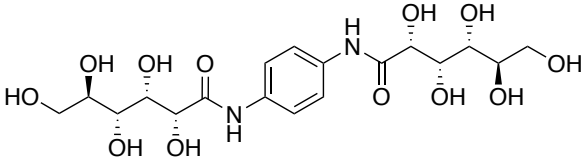

The protocol was similar to that used for compound **3.45**.[19] 1M NaOMe was added to a solution of compound **3.62** (0.93 g, 1.1 mmol) dissolved in methanol (21 mL) The resulting reaction was

stirred overnight at which point amberlite (IR120 hydrogen form resin) was added until an acidic reaction mixture was achieved. The amberlite resin was filtered and the solvent was removed. A light-yellow solid was obtained (0.478 g, 98%). **^{1}H NMR** (400 MHz, DMSO-d_6): δ 9.46 (s, 2H), 7.63 (s, 4H), 5.67 (br, 2H), 4.53 (br, 7H), 4.17 (d, J = 3.56 Hz, 2H), 4.01 (s, 2H), 3.59 (dd, J = 2.40 Hz, 2H), 3.51 (dd, 4H), 3.39 (dd, J = 10.72 Hz, 5.2 Hz, 2H) ppm. **^{13}C NMR** (101 MHz, DMSO-d_6): δ 171.64, 134.60, 120.20, 74.62, 72.77, 72.02, 70.75, 63.78 ppm. **LRMS (ESI)**: *m/z* calculated for $C_{18}H_{28}N_2O_{12}$ $[M+Na]^+$: 487.2; found: 487.1.

Synthesis of aldonamides 3.63-3.64:

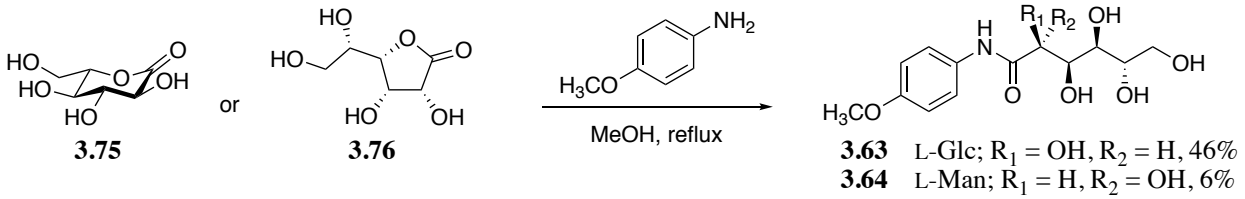

3.75 **3.76**

3.63 L-Glc; R_1 = OH, R_2 = H, 46%
3.64 L-Man; R_1 = H, R_2 = OH, 6%

Scheme A5. General synthesis of aldonamides **3.63-3.64**.

Compound 3.63

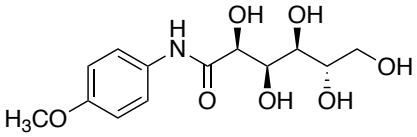

p-Anisidine was purified prior to the reaction by recrystallization in dH_2O.[17] L-Glucono-1,5-lactone (0.199 g, 1.12 mmol) and *p*-anisidine (0.178 g, 1.44 mmol) were suspended in methanol (11 mL). The reaction was refluxed for 24 hours before the mixture was cooled to RT and the solvent removed *in vacuo*. The crude off-white mixture was recrystallized from 99% EtOH followed by 95% EtOH to yield white crystals (0.156 g, 46%). **^{1}H NMR** (400 MHz, DMSO-d_6): δ 9.39 (s, 1H, NH), 7.61 (ddd, *J* = 10.2, 3.3, 3.3 Hz, 2H, ArH), 6.87 (ddd, *J* = 10.2, 3.3, 3.3 Hz, 2H, ArH), 5.63 (d, *J* = 5.2 Hz, 1H, HO-C^2), 4.57 (d, *J* = 4.3 Hz, 1H, -OH), 4.53 (d, *J* = 5.3 Hz, 1H,

-OH), 4.51 (d, *J* = 7.2 Hz, 1H, HO-C^3), 4.35 (dd, *J* = 5.6 Hz, 1H, HO-C^6), 4.14 (dd, *J* = 5.2, 3.8 Hz, 1H, H-C^2), 4.02-3.99 (m, 1H, H-C^3), 3.72 (s, 3H, -OCH_3), 3.59 (ddd, *J* = 10.8, 5.5, 2.5 Hz, 1H, H-C^6), 3.54-3.50 (m, 2H, H-C^4 and H-C^5), 3.39 (ddd, *J* = 11.0, 5.6, 5.6 Hz, 1H, H-C^6) ppm. **^{13}C NMR** (101 MHz, DMSO-d_6): δ 171.0 (C=O), 155.3 (Ar), 131.7 (Ar), 121.1 (Ar), 113.7 (Ar), 74.1 (C^2), 72.3 (C^4 or C^5), 71.5 (C^4 or C^5), 70.3 (C^3), 63.3 (C^6), 55.1 (-OCH_3) ppm. **LRMS (ESI)**: *m/z* calculated for $C_{13}H_{19}NO_7$ $[M+Na]^+$: 324.1; found: 324.0.

Compound 3.64

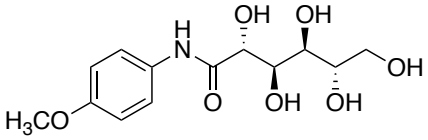

p-Anisidine was purified prior to the reaction by recrystallization in dH_2O.[17] L-Mannono-1,4-lactone (1.00 g, 5.62 mmol) was suspended in MeOH (30 mL) followed by the addition of *p*-anisidine (0.701 g, 5.69 mmol). The reaction was refluxed for 2.5 days at which point the TLC of the orange and clear solution still indicated presence of starting material (could stop reaction after 1 day). The solvent was removed and the crude product was recrystallized from MeOH (washed x3 with minimal MeOH) followed by recrystallization from dH_2O (washed x3 with dH_2O) to yield white crystals (0.102 g, 6 %). **^{1}H NMR** (400 MHz, DMSO-d_6): δ 9.67 (s, 1H, -NH), 7.60 (ddd, *J* = 10.3, 3.4, 3.4 Hz, 2H, ArH), 6.87 (ddd, *J* = 10.3, 3.4, 3.4 Hz, 2H, ArH), 5.48 (d, *J* = 6.2 Hz, 1H, HO-C^2/C^3), 4.46 (d, *J* = 5.3 Hz, 1H, HO-C^5), 4.43 (d, *J* = 6.9 Hz, 1H, HO-C^4), 4.37 (d, *J* = 7.7 Hz, 1H, HO-C^2/C^3), 4.34 (dd, *J* = 5.6, 5.6 Hz, 1H, HO-C^6), 4.02 (dd, *J* = 7.4, 6.4 Hz, 1H, H-C^2/C^3), 3.87 (dd, *J* = 7.2, 7.2 Hz, 1H, H-C^2/C^3), 3.72 (s, 3H, -OCH_3), 3.62 (ddd, *J* = 10.9, 5.5, 3.2 Hz, 1H, H-C^6), 3.54 (dd, *J* = 8.0, 7.0 Hz, 1H, H-C^4), 3.47 (dddd, *J* = 8.3, 5.5, 5.5, 3.1 Hz, 1H, H-C^5), 3.39 (ddd, *J* = 11.0, 5.6, 5.6 Hz, 1H, H-C^6) ppm. **^{13}C NMR** (101 MHz, DMSO-d_6): δ 172.0 (C=O), 155.2 (Ar), 132.1 (Ar), 120.9 (Ar), 113.7 (Ar), 72.7 (C^2 or C^3), 71.0

(C^5), 70.4 (C^2 or C^3), 69.9 (C^4), 63.7 (C^6), 55.1 (-OCH_3) ppm. **LRMS (ESI)**: *m/z* calculated for $C_{13}H_{19}NO_7$ $[M+Na]^+$: 324.1; found: 324.2.

Synthesis of compounds 3.65-3.67:

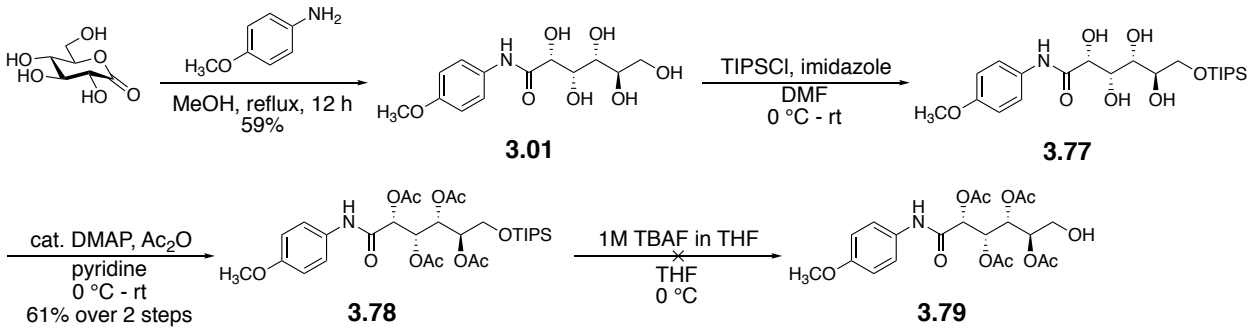

Scheme A6. Attempted synthesis toward compounds **3.65-3.67**.

Intermediate 3.78

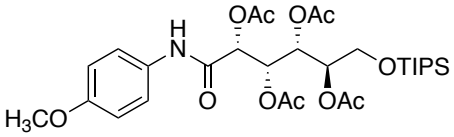

To a flame-dried flask under argon was added *p*-methoxyphenyl-D-gluconamide (2.01 g, 6.67 mmol) and anhydrous DMF (66 mL). After the gluconamide was fully dissolved, the solution was cooled to 0 °C in an ice-water bath. After 10 minutes, imidazole (0.92 g, 13 mmol) was added and the reaction was stirred for 5 minutes before the dropwise addition of triisopropylsilyl chloride (1.9 mL, 8.9 mmol). The solution was allowed to warm to room temperature and was stirred for 21 hours. Once TLC (8:2 EtOAc, UV and *p*A stain, product $R_f = 0.8$) indicated starting material consumption, the reaction was diluted with saturated $NaHCO_3$ (aq), taken up in EtOAc and extracted (x3). The combined organic layer was washed with brine, dried over Na_2SO_4, filtered, and concentrated. The pale orange crude product was used directly in the next step without further purification.

Crude silylated gluconamide was dissolved in anhydrous pyridine (24 mL). The solution was cooled to 0 °C in an ice-water bath and acetic anhydride (12.5 mL, mmol) was added dropwise followed by the addition of DMAP (0.0825 g, mmol). The solution was allowed to warm to room temperature and stir for 24 hours. Once TLC indicated starting reaction completion, the reaction was quenched with $NaHCO_3$ and concentrated to afford a pale yellow solid. The residue was taken up in EtOAc and 10% HCl (aq), and extracted. The organic layer was washed with saturated $NaHCO_3$ (aq) followed by brine. The organic layer was then dried over Na_2SO_4, filtered, and concentrated to afford crude pale yellow solid. The crude product was purified by recrystallization using minimal EtOAc and pet. ether to yield a white powder (2.564 g, 61% over two steps). **^{1}H NMR** (400 MHz, $CDCl_3$): δ 7.94 (br, 1H, NH), 7.41 (dt, *J* = 10.4, 3.6, 3.6 Hz, 2H, 2 x ArH), 6.84 (dt, *J* = 10.4, 3.6, 3.6 Hz, 2H, 2 x ArH), 5.76 (dd, *J* = 6.4, 4.0 Hz, 1H, H-C3), 5.55 (dd, *J* = 7.0, 4.0 Hz, 1H, H-C4), 5.35 (d, *J* = 6.4 Hz, 1H, H-C2), 4.94 (ddd, *J* = 7.0, 4.6, 4.4 Hz, 1H, H-C5), 3.91 (dd, *J* = 11.2, 4.4 Hz, 1H, H-C6), 3.78 (s, 3H, -OCH_3), 3.76 (dd, *J* = 11.2, 4.6 Hz, 1H, H-C6), 2.23 (s, 3H, -$OCOCH_3$), 2.11 (s, 3H, -$OCOCH_3$), 2.06 (s, 3H, -$OCOCH_3$), 2.04 (s, 3H, -$OCOCH_3$), 1.03 (sept, *J* = 5.0 Hz, 3H, -Si(C<u>H</u>$(CH_3)_2)_3$), 1.01 (d, *J* = 5.0 Hz, 18H, -Si(CH(C<u>H</u>$_3)_2)_3$) ppm. **^{13}C NMR** (101 MHz, $CDCl_3$): δ 170.6 (O<u>C</u>OCH_3), 170.1 (O<u>C</u>OCH_3), 169.9 (O<u>C</u>OCH_3), 169.5 (O<u>C</u>OCH_3), 164.0 (C=O), 156.9 (Ar-C), 130.1 (Ar-C), 122.0 (Ar, 2xCH), 114.3 (Ar, 2xCH), 72.3 ($C^{(2)}H$), 71.2 ($C^{(5)}H$), 69.4 ($C^{(4)}H$), 69.1 ($C^{(3)}H$), 61.6 ($C^{(6)}H_2$), 55.6 (O<u>C</u>H_3), 21.0 (OCO<u>C</u>H_3), 21.0 (OCO<u>C</u>H_3), 20.9 (OCO<u>C</u>H_3), 20.6 (OCO<u>C</u>H_3), 18.0 (Si(<u>C</u>H$(CH_3)_2)_3$), 12.0 (Si(CH(<u>C</u>$H_3)_2)_3$) ppm. **LRMS (ESI)**: *m/z* calculated for $C_{30}H_{47}NO_{11}Si$ $[M+Na]^+$: 648.3; found: 648.4.

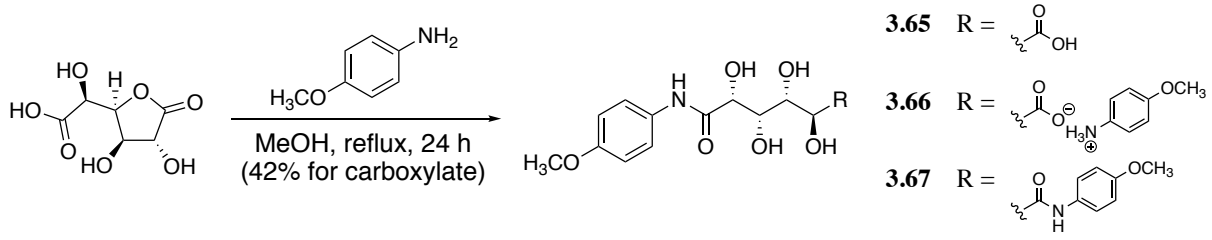

Scheme A7. Synthesis of compounds **3.65-3.67**.

Compounds 3.65-3.67:

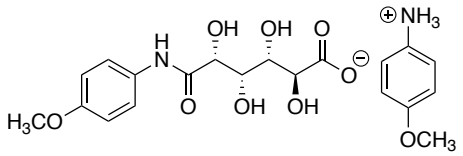

Compound **3.66**:

p-Anisidine was purified prior to the reaction by recrystallization in dH_2O.[17] D-Saccharic acid-1,4-lactone monohydrate (0.251 g, 1.19 mmol) was dissolved in methanol (12.0 mL) followed by the addition of *p*-anisidine (0.256 g, 2.40 mmol). The homogeneous reaction mixture was refluxed for 24 hours prior to being cooled to room temperature. The resulting precipitate was filtered to yield the pure carboxylate **3.66** (0.221 g of carboxylate, 42%). The carboxylate precipitated as a salt with *p*-anisidine as observed by NMR spectroscopy. **^{1}H NMR** (400 MHz, DMSO-d_6): δ 9.40 (s, 1H), 7.61 (ddd, *J* = 10.3, 3.4, 3.4 Hz, 2H), 6.87 (ddd, *J* = 10.3, 3.4, 3.4 Hz, 2H), 6.64 (ddd, *J* = 10.0, 3.4, 3.4 Hz, 2H), 6.52 (ddd, *J* = 10.0, 3.4, 3.4 Hz, 2H), 6.45-5.05 (br s, 4H), 4.15 (d, *J* = 3.7 Hz, 1H), 3.97 (dd, *J* = 4.0, 4.0 Hz, 1H), 3.96 (d, *J* = 7.3 Hz, 1H), 3.73 (dd, *J* = 7.1, 3.5 Hz, 1H), 3.72 (s, 3H), 3.61 (s, 3H) ppm. **^{13}C NMR** (101 MHz, DMSO-d_6): δ 174.4, 170.8, 155.3, 150.8, 141.9, 131.7, 121.1, 115.1, 114.5, 113.7, 73.5, 73.0, 71.5, 70.3, 55.3, 55.1 ppm. **LRMS (ESI)**: *m/z* calculated for $C_{13}H_{16}NO_8Na$ $[M+Na]^+$: 360.1; found: 360.1.

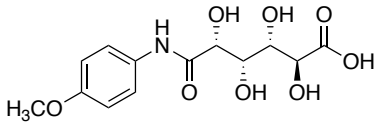

Compound **3.65**:

To produce the carboxylic acid (**3.65**) from carboxylate **3.66**, the carboxylate (0.156 g, 0.356 mmol) was taken up in 1% HCl (to dissolve, 6 mL) and stirred until pH 1. The product was extracted by using EtOAc (6 mL, x4), combining the organic layers, followed by removal of solvent *in vacuo*. The resulting white product was pure (0.022 g, 20% isolation from carboxylate). **^{1}H NMR** (400 MHz, DMSO-d_6): δ 11.70 (br s, 1H), 9.41 (s, 1H), 7.61 (ddd, *J* = 10.3, 3.4, 3.4 Hz, 2H), 6.87 (ddd, *J* = 10.3, 3.3, 3.3 Hz, 2H), 5.66 (br s, 1H), 5.42 (br s, 1H), 4.69 (br s, 2H), 4.15 (d, *J* = 3.7 Hz, 1H), 3.98-3.96 (m, 2H), 3.74 (dd, *J* = 7.1, 3.5 Hz, 1H), 3.72 (s, 3H) ppm. **^{13}C NMR** (101 MHz, DMSO-d_6): δ 174.3, 170.8, 155.3, 131.7, 121.1, 113.7, 73.5, 73.0, 71.5, 70.3, 55.1 ppm. **LRMS (ESI)**: *m/z* calculated for $C_{13}H_{16}NO_8Na$ $[M+Na]^+$: 360.1; found: 360.2.

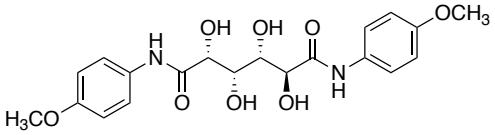

Compound **3.67**:

p-Anisidine was purified prior to the reaction by recrystallization in dH_2O.[17] To prepare the diamide, D-saccharic acid-1,4-lactone monohydrate (0.250 g, 1.19 mmol) was dissolved in methanol (12.0 mL) followed by the addition of *p*-anisidine (0.296 g, 2.40 mmol). The homogeneous mixture was refluxed for 24 hours before being cooled to room temperature and the precipitate filtered. The carboxylate precipitate was taken up in 10% HCl and stirred until pH 1. The diamide was obtained by extraction with EtOAc (x2). The combined organic layers were washed with 10% HCl and the solvent removed to yield pure white solid (0.022 g, 4%). **^{1}H NMR** (400 MHz, DMSO-d_6): δ 9.62 (s, 1H), 9.40 (s, 1H), 7.62 (ddd, *J* = 8.6, 3.3, 3.3 Hz, 2H), 7.59 (ddd, *J* = 8.6, 3.3, 3.3 Hz, 2H), 6.87 (ddd, *J* = 8.9, 3.1, 3.1 Hz, 4H), 5.67 (d, *J* = 5.7 Hz, 1H),

5.64 (d, *J* = 6.5 Hz, 1H), 4.71 (d, *J* = 2.7 Hz, 1H), 4.69 (d, *J* = 3.9 Hz, 1H), 4.19 (dd, *J* = 5.7, 3.9 Hz, 1H), 4.08 (dd, *J* = 6.7, 6.7 Hz, 1H), 4.03 (ddd, *J* = 7.1, 3.7, 3.7 Hz, 1H), 3.82 (ddd, *J* = 6.5, 6.5, 3.2 Hz, 1H), 3.72 (s, 6H) ppm. **^{13}C NMR** (101 MHz, DMSO-d_6): δ 171.2, 170.8, 155.3, 155.2, 132.0, 131.7, 121.1, 120.9, 113.7, 73.7, 73.0, 72.5, 70.4, 55.1 ppm. **LRMS (ESI)**: *m/z* calcd. for $C_{20}H_{24}N_2O_8$ $[M+Na]^+$: 443.1; found: 443.2.

Synthesis of compounds 3.68-3.74:

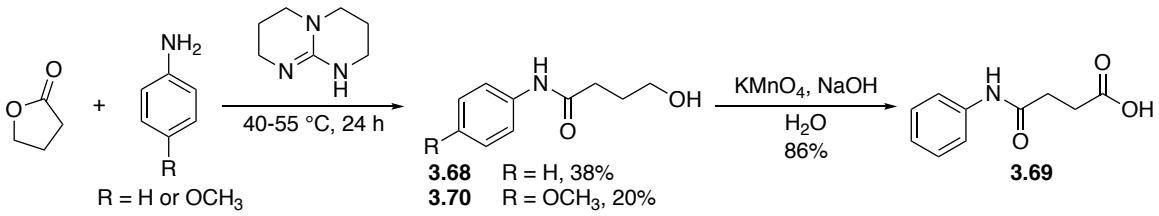

Scheme A8. Synthesis of compounds **3.68-3.70**.

Compound 3.68

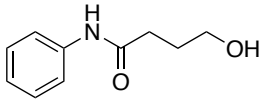

The preparation of desired compound was performed using an adapted literature procedure.[22] γ-butyrolactone (0.323 g, 3.75 mmol), *p*-anisidine (0.423 g, 4.54 mmol), and 1,5,7-triazabicyclo[4.4.0]dec-5-ene (0.330 g, 2.37 mmol) were added to a flask and the mixture was stirred at 40 °C for 24 hours before allowing to cool to room temperature. The product was purified by flash chromatography (EtOAc as eluent, R_f = 0.33) to yield an off-white solid (0.273 g, 38%). **^{1}H NMR** (400 MHz, DMSO-d_6): δ 9.86 (br s, 1H), 7.59 (dd, *J* = 8.6, 1.2 Hz, 2H), 7.27 (dddd, *J* = 8.4, 7.6, 2.0, 2.0 Hz, 2H), 7.01 (tt, *J* = 7.4, 1.2 Hz, 1H), 4.51 (br s, 1H), 3.44 (t, *J* = 6.4 Hz, 2H), 2.35 (t, *J* = 7.8 Hz, 2H), 1.74 (tt, *J* = 7.7, 6.6 Hz, 2H) ppm. **^{13}C NMR** (101 MHz, DMSO-d_6): δ 171.3, 139.4, 128.6, 122.9, 119.0, 60.2, 33.1, 28.4 ppm. **LRMS (ESI)**: *m/z* calculated for $C_{10}H_{13}NO_2$ $[M+Na]^+$: 202.1; found: 202.1.

Compound 3.69

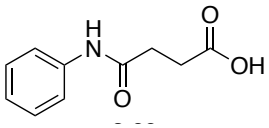

The desired compound was prepared using a literature procedure by Guo *et al*.[22] Hydroxy *N*-aryl amide (0.088 g, 0.489 mmol) was dissolved in H_2O (0.05 M, 8.0 mL) prior to the addition of ground NaOH (0.014 g, 0.35 mmol) and $KMnO_4$ (0.190 g, 1.20 mmol). The reaction mixture was stirred at room temperature for two hours until TLC (EtOAc as eluent) indicated starting material consumption. A saturated solution of $NaHSO_3$ was added to the purple mixture until the solution turned clear and colourless. EtOAc was then added and the mixture was extracted and later washed with 10% aqueous HCl solution. The solvent was removed to yield a pure white solid (0.081 g, 86%). **^{1}H NMR** (400 MHz, DMSO-d_6): δ 12.12 (br s, 1H), 9.94 (s, 1H), 7.57 (dd, *J* = 8.7, 1.2 Hz, 2H), 7.28 (dd, *J* = 8.5, 7.6 Hz, 2H), 7.01 (t, *J* = 7.4 Hz, 1H), 2.58-2.51 (m, 4H) ppm. **^{13}C NMR** (101 MHz, DMSO-d_6): δ 173.8, 170.0, 139.3, 128.6, 122.9, 118.9, 31.0, 28.8 ppm. **LRMS (ESI)**: *m/z* calculated for $C_{10}H_{11}NO_3$ $[M+K]^+$: 232.0; found: 232.1.

Compound 3.70

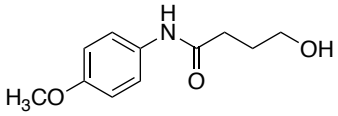

The desired compound was prepared by adapting a literature procedure.[22] *p*-Anisidine was purified prior to the reaction by recrystallization in dH_2O.[17] γ-butyrolactone (0.441 g, 5.12 mmol), *p*-anisidine (0.776 g, 6.30 mmol), and 1,5,7-triazabicyclo[4.4.0]dec-5-ene (0.438 g, 3.15 mmol) were added to a flask and the mixture was stirred at 55 °C for 25 hours before allowing to cool to room temperature. The product was purified by flash chromatography (98:2 EtOAc:MeOH as eluent, R_f = 0.29) to yield an pink solid which was further recrystallized (MeOH:Ether) to yield off-white crystals (0.232 g, 20%). **^{1}H NMR** (400 MHz, DMSO-d_6): δ

9.72 (br s, 1H), 7.49 (ddd, *J* = 10.3, 3.5, 3.5 Hz, 2H), 6.85 (ddd, *J* = 10.3, 3.4, 3.4 Hz, 2H), 4.50 (t, *J* = 5.1 Hz, 1H), 3.70 (s, 3H), 3.42 (td, *J* = 6.5, 5.1 Hz, 2H), 2.30 (t, *J* = 7.7 Hz, 2H), 1.72 (tt, *J* = 7.7, 6.5 Hz, 2H) ppm. **^{13}C NMR** (101 MHz, DMSO-d_6): δ 170.7, 154.9, 132.6, 120.5, 113.7, 60.2, 55.1, 33.0, 28.5 ppm. **LRMS (ESI)**: *m/z* calculated for $C_{12}H_{17}NO_3$ $[M+Na]^+$: 232.1; found: 232.0.

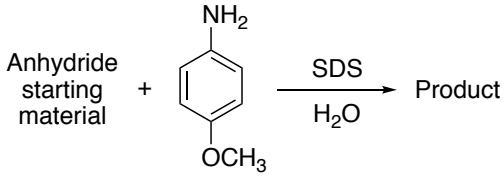

Scheme A9. General synthesis of compounds **3.71-3.74**.

Compounds 3.71

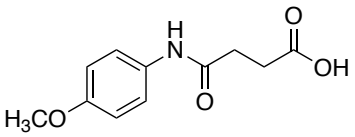

The preparation of the desired compound was adapted from the literature procedure by Naik *et al*.[23] *p*-Anisidine was purified prior to the reaction by recrystallization in dH_2O.[17] *p*-Anisidine (0.206 g, 1.67 mmol) was suspended in dH_2O (6.5 mL) followed by the addition of SDS (0.007 g, 4 mg/mmol aniline). The heterogeneous mixture was stirred and heated until the mixture became a homogeneous solution. Once the reaction mixture cooled to room temperature, succinic anhydride (0.192 g, 1.92 mmol) was added portion-wise over 5 minutes. The pale yellow clear solution turned cloudy once the anhydride was added. The mixture was stirred for 1 hour with the appearance of white precipitate and then was cooled in an ice-water bath. The precipitate was filtered and washed with cool dH_2O to afford pure white solid (0.159 g, 43%). **^{1}H NMR** (400 MHz, DMSO-d_6): δ 12.09 (br s, 1H), 9.79 (s, 1H), 7.48 (ddd, *J* = 10.3, 3.5, 3.5 Hz, 2H), 6.85 (ddd, *J* = 10.4, 3.5, 3.5 Hz, 2H), 3.70 (s, 3H), 2.53-2.50 (m, 4H) ppm. **^{13}C NMR** (101

MHz, DMSO-d_6): δ 173.8, 169.5, 154.9, 132.5, 120.4, 113.8, 55.1, 30.9, 28.9 ppm. **LRMS (ESI)**: *m/z* calculated for $C_{11}H_{13}NO_4$ $[M+Na]^+$: 246.1; found: 245.9.

Compound 3.72

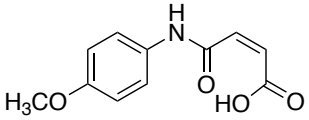

The preparation of the desired compound was adapted from the literature procedure by Naik *et al*.[23] *p*-Anisidine was purified prior to the reaction by recrystallization in dH_2O and maleic anhydride was purified by crystallization in CH_2Cl_2.[17] *p*-Anisidine (0.302 g, 2.45 mmol) was suspended in dH_2O (9.7 mL) followed by the addition of SDS (0.010 g, 4 mg/mmol aniline). The heterogeneous mixture was stirred and heated until the mixture became a homogeneous solution. Once the reaction mixture cooled to room temperature, maleic anhydride (0.287 g, 2.93 mmol) was added portion-wise over 10 minutes. As maleic anhydride was added, bright yellow precipitate immediately formed. The mixture was stirred for another 30 minutes before being cooled in an ice-water bath. The precipitate was filtered and washed with cool dH_2O to afford pure yellow solid (0.426 g, 79%). **^{1}H NMR** (300 MHz, DMSO-d_6): δ 13.40 (br s, 1H), 10.39 (s, 1H), 7.54 (ddd, *J* = 10.3, 3.4, 3.4 Hz, 2H), 6.91 (ddd, *J* = 10.3, 3.4, 3.4 Hz, 2H), 6.46 (d, *J* = 12.1 Hz, 1H), 6.30 (d, *J* = 12.2 Hz, 1H), 3.73 (s, 3H) ppm. **^{13}C NMR** (101 MHz, DMSO-d_6): δ 166.6, 162.8, 155.8, 131.6, 131.4, 130.9, 121.2, 114.0, 55.2 ppm. **LRMS (ESI)**: *m/z* calculated for $C_{11}H_{11}NO_4$ $[M+Na]^+$: 244.1; found: 244.1.

Compound 3.73

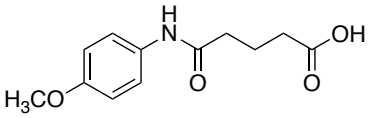

The preparation of the desired compound was adapted from the literature procedure by Naik *et al*.[23] *p*-Anisidine was purified prior to the reaction by recrystallization in dH_2O.[17] *p*-Anisidine (0.099 g, 0.80 mmol) was suspended in dH_2O (3.2 mL) followed by the addition of SDS (0.003 g, 4 mg/mmol aniline). The heterogeneous mixture was stirred and heated until the mixture became a homogeneous solution. Once the reaction mixture cooled to room temperature, glutaric anhydride (0.108 g, 0.945 mmol) was added portion-wise over 15 minutes. As anhydride was added, the mixture turned cloudy and white. The mixture was stirred for another 20 minutes before being cooled in an ice-water bath. The precipitate was filtered and washed with cool dH_2O to afford pure white solid (0.103 g, 54%). **^{1}H NMR** (400 MHz, DMSO-d_6): δ 12.06 (br s, 1H), 9.73 (s, 1H), 7.48 (ddd, *J* = 10.3, 3.5, 3.5 Hz, 2H), 6.85 (ddd, *J* = 10.3, 3.4, 3.4 Hz, 2H), 3.71 (s, 3H), 2.30 (t, *J* = 7.3 Hz, 2H), 2.26 (t, *J* = 7.3 Hz, 2H), 1.79 (tt, *J* = 7.3, 7.3 Hz, 2H) ppm. **^{13}C NMR** (101 MHz, DMSO-d_6): δ 174.2, 170.1, 155.0, 132.5, 120.6, 113.8, 55.1, 35.3, 33.0, 20.5 ppm. **LRMS (ESI)**: *m/z* calculated for $C_{12}H_{15}NO_4$ $[M+Na]^+$: 260.1; found: 260.0.

Compound 3.74

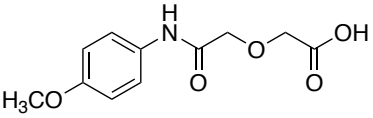

The preparation of the desired compound was adapted from the literature procedure by Naik *et al*.[23] *p*-Anisidine was purified prior to the reaction by recrystallization in dH_2O.[17] *p*-Anisidine (0.204 g, 1.66 mmol) was suspended in dH_2O (6.5 mL) followed by the addition of SDS (0.007 g, 4 mg/mmol aniline). The heterogeneous mixture was stirred and heated until the mixture became a homogeneous solution. Once the reaction mixture cooled to room temperature, 2,3-

diglycolic anhydride (0.163 g, 1.40 mmol) was added portion-wise over 10 minutes. As anhydride was added, the mixture turned cloudy. The mixture was stirred for another 1.5 hours before being extracted with EtOAc (x2). The combined organic layer was dried over Na_2SO_4, filtered, and the solvent removed. The crude product was recrystallized from EtOAc:pet ether to produce purple crystals (0.123 g, 31%). **^{1}H NMR** (400 MHz, DMSO-d_6): δ 12.88 (br s, 1H), 9.73 (s, 1H), 7.54 (ddd, *J* = 10.3, 3.5, 3.5 Hz, 2H), 6.89 (ddd, *J* = 10.3, 3.5, 3.5 Hz, 2H), 4.20 (s, 2H), 4.14 (s, 2H), 3.72 (s, 3H) ppm. **^{13}C NMR** (101 MHz, DMSO-d_6): δ 171.7, 167.3, 155.5, 131.4, 121.2, 113.8, 70.5, 68.1, 55.2 ppm. **LRMS (ESI)**: *m/z* calculated for $C_{11}H_{13}NO_5$ $[M+Na]^+$: 262.1; found: 261.9.

Synthesis of compounds 3.80-3.82 through intermediates 3.83-3.88:

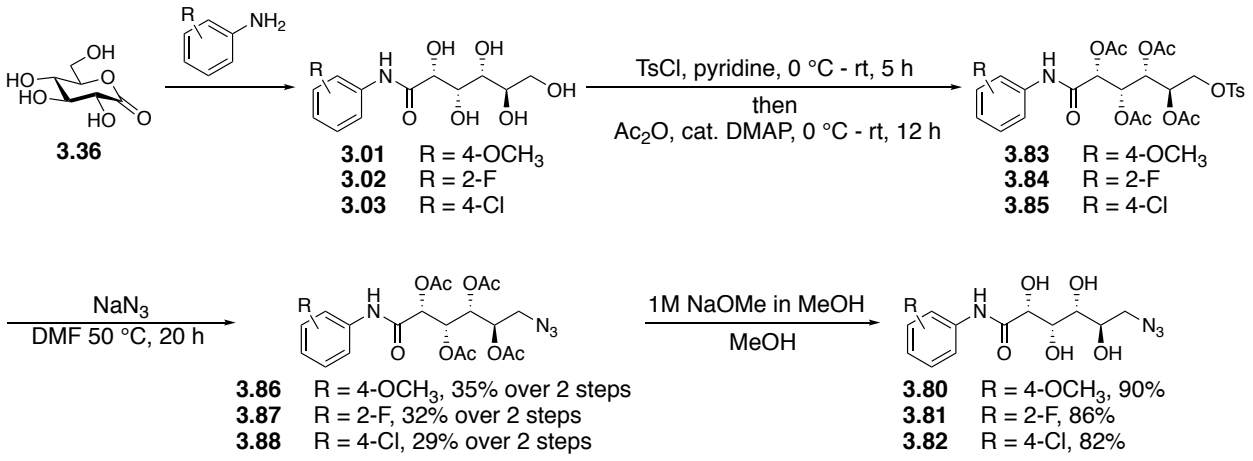

Scheme A10. Synthesis of compounds **3.80-3.82** through intermediates **3.83-3.88**.

Compounds 3.83 and 3.86

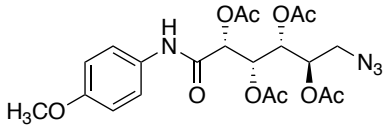

Preparation of the acetylated tosylate was adapted from literature protocol.[24] Gluconamide **3.01** (1.316 g, 4.368 mmol) was added to a flame-dried flask under argon. Anhydrous pyridine (62 mL) was added and the solution was stirred at 0 °C for 20 minutes at which point *p*-toluenesulfonyl chloride (0.993 g, 5.21 mmol, recrystallized from pet. ether[17]) was added slowly over a period of 5 minutes. The mixture was stirred at 0 °C for one hour and then warmed to RT for 4 hours. The reaction mixture was then stirred at 0 °C for the dropwise addition of acetic anhydride (9.5 mL, 101 mmol) and addition of a catalytic amount of 4-dimethylaminopyridine (0.053 g, 0.55 mmol). The acetylation was allowed to warm to RT and stir overnight. The mixture was quenched using saturated $NaHCO_3$ (aq) and poured over an ice-sat. $NaHCO_3$ (aq) mixture. The resulting crude product was filtered and taken up in EtOAc. The organic layer was washed with 10% HCl, sat. $NaHCO_3$ (aq), and then brine. The layer was then dried over Na_2SO_4, filtered, and concentrated to afford a crude product that was used directly in the next step.

The crude tosylate **3.83** was dried under high vacuum before use. Tosylate **3.83** was added to a flame-dried flask and dissolved in anhydrous DMF (43 mL). Sodium azide (0.981 g, 15.1 mmol) was added slowly. The flask was fitted with a condenser, heated to 50 °C, and stirred overnight. The mixture was then cooled to RT and diluted with EtOAc and sat. $NaHCO_3$ (aq). The mixture was extracted with EtOAc (x3). The combined organic layer was washed with sat. $NaHCO_3$ (aq), dH_2O, and then brine before being dried over Na_2SO_4, filtered, and concentrated to yield a crude product. The product was purified by flash chromatography (4:6 EtOAc:pet. ether as eluent, UV light and *p*A stain for visualization) to yield a white solid (0.751 g, 35% over two steps).

^{1}H NMR (400 MHz, DMSO-d_6): δ 10.06 (s, 1H, NH), 7.37 (ddd, *J* = 10.1, 3.3, 3.3 Hz, 2H, ArH), 6.89 (ddd, *J* = 10.3, 3.4, 3.4 Hz, 2H, ArH), 5.54 (dd, *J* = 4.5, 4.0 Hz, 1H, H-C^3), 5.36 (dd, *J* = 6.5, 4.5 Hz, 1H, H-C^4), 5.18 (d, *J* = 4.0 Hz, 1H, H-C^2), 4.95 (ddd, *J* = 6.7, 6.7, 3.1 Hz, 1H, H-C^5), 3.72 (s, 3H, -OCH_3), 3.70 (dd, *J* = 13.6, 3.1 Hz, 1H, H-C^6), 3.53 (dd, *J* = 13.6, 6.8 Hz, 1H, H-C^6), 2.12 (s, 3H, -OAc), 2.08 (s, 3H, -OAc), 2.01 (s, 3H, -OAc), 1.99 (s, 3H, -OAc) ppm. **^{13}C NMR** (101 MHz, DMSO-d_6): δ 169.6, 169.5, 169.4, 169.2, 163.7, 155.8, 131.0, 121.5, 113.9, 72.0, 69.2, 69.2, 68.4, 55.2, 49.3, 20.6, 20.6, 20.4, 20.3 ppm. **LRMS (ESI)**: *m/z* calculated for $C_{21}H_{26}N_4O_{10}$ $[M+Na]^+$: 517.2; found: 517.2.

Compound 3.80 (≡ 4.07)

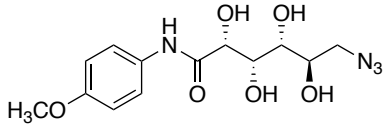

Azide **3.86** (0.490 g, 0.991 mmol) was dissolved in MeOH (20 mL) and a catalytic amount of 1 M NaOMe was added by pipette. The reaction was stirred at RT for 1 hour at which point TLC indicated starting material consumption (1:1 pet ether:EtOAc system, UV light for visualization). Upon reaction completion, Amberlite IR120 (H^+ resin, washed with MeOH prior to use) was added to the stirring solution until pH < 5. The mixture was filtered, and the filtrate was collected and concentrated *in vacuo*. The white solid was recrystallized from dH_2O to yield white solid (0.291 g, 90%). **^{1}H NMR** (400 MHz, DMSO-d_6): δ 9.44 (s, 1H), 7.60 (ddd, *J* = 10.2, 3.4, 3.4 Hz, 2H), 6.87 (ddd, *J* = 10.2, 3.4, 3.4 Hz, 2H), 5.69 (d, *J* = 5.5 Hz, 1H), 5.23 (d, *J* = 6.0 Hz, 1H), 4.65 (d, *J* = 6.3 Hz, 1H), 4.59 (d, *J* = 7.4 Hz, 1H), 4.15 (dd, *J* = 5.5, 4.1 Hz, 1H), 4.00 (ddd, *J* = 7.4, 4.1, 2.3 Hz, 1H), 3.75-3.69 (m, 1H), 3.72 (s, 3H), 3.51 (ddd, *J* = 8.6, 6.3, 2.4 Hz, 1H), 3.40 (dd, *J* = 12.7, 2.7 Hz, 1H), 3.27 (dd, *J* = 12.7, 6.7 Hz, 1H) ppm. **^{13}C NMR** (101 MHz, DMSO-d_6): δ

170.9, 155.3, 131.7, 121.1, 113.7, 73.8, 72.4, 70.2, 70.0, 55.1, 53.9 ppm. **LRMS (ESI)**: *m/z* calculated for $C_{13}H_{18}N_4O_6$ $[M+Na]^+$: 349.1; found: 349.2.

Compounds 3.84 and 3.87

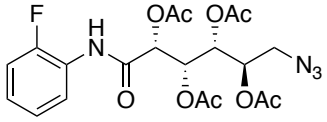

Preparation of the acetylated tosylate was adapted from literature protocol.[24] Gluconamide **3.02** (2.021 g, 6.988 mmol) was added to a flame-dried flask under argon. Anhydrous pyridine (69 mL) was added and the solution was stirred at 0 °C for 20 minutes at which point *p*-toluenesulfonyl chloride (1.611 g, 8.450 mmol, recrystallized from pet. ether[17]) was added slowly over a period of 5 minutes. The mixture was allowed to stir at 0 °C for one hour and warmed to RT for 5 hr. The reaction mixture was then stirred at 0 °C for the dropwise addition of acetic anhydride (13 mL, 140 mmol) and addition of a catalytic amount of 4-dimethylaminopyridine (0.086 g, 0.71 mmol). The acetylation was allowed to warm to room temperature and stir overnight. The mixture was quenched using saturated aqueous $NaHCO_3$ and poured over ice-sat. $NaHCO_3$ (aq) mixture. The resulting crude product was filtered and taken up in EtOAc. The organic layer was washed with 10% HCl, followed by sat. $NaHCO_3$ (aq), and brine. The layer was then dried over Na_2SO_4, filtered, and concentrated to afford a crude product that was used directly in the next step without further purification.

The crude tosylate **3.84** was dried under high vacuum before use. Tosylate **3.84** was added to a flame-dried flask and dissolved in anhydrous DMF (37 mL). Sodium azide (0.885 g, 13.6 mmol) was added slowly. The flask was fitted with a condenser, heated to 50 °C, and stirred overnight (20 hours). The mixture was then cooled to RT and diluted with EtOAc and saturated $NaHCO_3$

(aq). The mixture was extracted with EtOAc (x2). The combined organic layer was washed with saturated $NaHCO_3$ (aq), followed by dH_2O, and brine before being dried over Na_2SO_4, filtered, and concentrated to yield a crude product. The crude product was purified by flash chromatography with 96:4 DCM:EtOAc as eluent to yield white product (1.09 g, 32% over two steps). **^{1}H NMR** (400 MHz, DMSO-d_6): δ 10.11 (s, 1H), 7.70 (ddd, *J* = 7.7, 7.7, 2.3 Hz, 1H), 7.30-7.25 (m, 1H), 7.21-7.13 (m, 2H), 5.58 (dd, *J* = 4.9, 3.0 Hz, 1H), 5.43 (dd, *J* = 6.5, 4.9 Hz, 1H), 5.37 (d, *J* = 2.9 Hz, 1H), 4.95 (ddd, *J* = 6.6, 6.6, 3.0 Hz, 1H), 3.73 (dd, *J* = 13.7 Hz, 3.0 Hz, 1H), 3.56 (dd, *J* = 13.7, 6.8 Hz, 1H), 2.13 (s, 3H), 2.08 (s, 3H), 2.00 (s, 3H), 1.99 (s, 3H) ppm. **^{13}C NMR** (101 MHz, DMSO-d_6): δ 169.6, 169.6, 169.4, 169.2, 164.7, 153.7 (d, $J_{C\text{-}F}$ = 245.4 Hz), 125.8 (d, $J_{C\text{-}F}$ = 7.4 Hz), 125.2 (d, $J_{C\text{-}F}$ = 11.6 Hz), 124.4 (d, $J_{C\text{-}F}$ = 3.4 Hz), 124.2 (d, $J_{C\text{-}F}$ = 1.0 Hz), 115.6 (d, $J_{C\text{-}F}$ = 19.4 Hz), 71.9, 69.4, 69.3, 68.2, 49.3, 20.5 (x2), 20.3, 20.3 ppm. **LRMS (ESI)**: *m/z* calculated for $C_{20}H_{23}N_4O_9F$ $[M+Na]^+$: 505.1; found: 505.2.

Compound 3.81 (≡ 4.06)

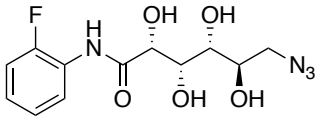

Azide **3.87** (1.09 g, 2.26 mmol) was dissolved in MeOH (32.5 mL) and a catalytic amount of 1 M NaOMe was added by pipette. The reaction was stirred at RT for 1 hour at which point TLC indicated starting material consumption (1:1 pet ether:EtOAc system, UV light for visualization). Upon reaction completion, Amberlite IR120 (H^+ resin, washed with MeOH prior to use) was added to the stirring solution until pH < 5. The mixture was filtered and the filtrate was collected and concentrated *in vacuo*. The crude white solid was recrystallized from dH_2O to yield white solid (0.61 g, 86%). **^{1}H NMR** (400 MHz, DMSO-d_6): δ 9.24 (d, *J* = 2.4 Hz, 1H, NH), 8.10 (ddd, *J* = 8.0, 8.0, 2.3 Hz, 1H, ArH), 7.28 (ddd, *J* = 11.3, 8.0, 2.0 Hz, 1H, ArH), 7.17 (ddd, *J* = 15.2,

7.6, 1.8 Hz, 1H, ArH), 7.16-7.11 (m, 1H, ArH), 5.99 (d, J = 5.2 Hz, 1H, HO-C^2), 5.26 (d, J = 5.9 Hz, 1H, HO-C^5), 4.74 (d, J = 7.6 Hz, 1H, HO-C^3), 4.71 (d, J = 6.6 Hz, 1H, HO-C^4), 4.25 (dd, J = 5.2, 3.7 Hz, 1H, H-C^2), 4.02 (ddd, J = 7.6, 3.8, 2.6 Hz, 1H, H-C^3), 3.72 (dddd, J = 11.1, 6.3, 6.3, 2.6 Hz, 1H, H-C^5), 3.55 (ddd, J = 8.8, 6.8, 2.5 Hz, 1H, H-C^4), 3.40 (dd, J = 12.4, 2.5 Hz, 1H, H-C^6), 3.27 (dd, J = 12.8, 6.6 Hz, 1H, H-C^6) ppm. **^{13}C NMR** (101 MHz, DMSO-d_6): δ 171.5 (C=O), 152.8 (d, $J_{C\text{-}F}$ = 242.6 Hz, Ar-C), 125.9 (d, $J_{C\text{-}F}$ = 10.5 Hz, Ar-C), 124.8 (d, $J_{C\text{-}F}$ = 7.6 Hz, Ar-C), 124.5 (d, $J_{C\text{-}F}$ = 34 Hz, Ar-C), 122.2 (d, $J_{C\text{-}F}$ = 0.5 Hz), 115.2 (d, $J_{C\text{-}F}$ = 19.0 Hz, Ar-C), 73.7 ($C^{(2)}$-H), 72.3 ($C^{(4)}$-H), 70.3 ($C^{(5)}$-H), 69.9 ($C^{(3)}$-H), 53.9 ($C^{(6)}$-H_2) ppm. **LRMS (ESI)**: *m/z* calculated for $C_{12}H_{15}FN_4O_5$ $[M+Na]^+$: 337.1; found: 337.2.

Compounds 3.85 and 3.88

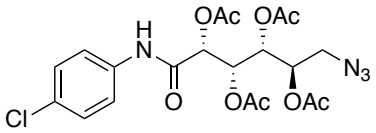

Preparation of the acetylated tosylate was adapted from literature protocol.[24] Gluconamide **3.03** (0.500 g, 1.64 mmol) was added to a flame-dried flask under argon. Anhydrous pyridine (23 mL) was added and the solution was stirred at 0 °C for 20 minutes at which point *p*-toluenesulfonyl chloride (0.380 g, 1.99 mmol, recrystallized from pet. ether[17]) was added slowly over a period of 5 minutes. The mixture was allowed to stir at 0 °C for one hour and warmed to RT for 4 hr until TLC indicated starting material consumption (4:1 EtOAc:MeOH as eluent, UV light and *p*A stain for visualization). The reaction mixture was stirred at 0 °C for the dropwise addition of acetic anhydride (1.5 mL, 16 mmol) and addition of a catalytic amount of 4-dimethylaminopyridine (0.020 g, 0.16 mmol). The acetylation was allowed to warm to room temperature and stir overnight (17.5 h) until TLC indicated starting material consumption. The mixture was quenched using saturated aqueous $NaHCO_3$ and poured over ice-sat. $NaHCO_3$ (aq)

mixture. The resulting crude product was filtered and taken up in EtOAc. The organic layer was washed with 10% HCl, followed by sat. $NaHCO_3$ (aq), and brine. The layer was then dried over Na_2SO_4, filtered, and concentrated to afford a crude product that was used directly in the next step without further purification.

The crude tosylate **3.85** was dried under high vacuum before use. Tosylate **3.85** was added to a flame-dried flask and dissolved in anhydrous DMF (16 mL). Sodium azide (0.372 g, 5.98 mmol) was added slowly. The flask was fitted with a condenser, heated to 50 °C, and stirred overnight. TLC (1:1 pet ether:EtOAc) indicated minimal starting material ($R_f \sim 0.3$) and therefore mixture was cooled to RT and diluted with EtOAc and saturated $NaHCO_3$ (aq). The mixture was extracted with EtOAc (x3). The combined organic layer was washed with saturated $NaHCO_3$ (aq), followd by dH_2O, and brine before being dried over Na_2SO_4, filtered, and concentrated to yield a crude product. The crude product was purified by recrystallization in 99% EtOH to yield white solid (0.222 g, 29% over two steps). **^{1}H NMR** (400 MHz, DMSO-d_6): δ 10.36 (s, 1H), 7.51 (ddd, *J* = 8.9, 2.1, 2.1 Hz, 2H), 7.38 (ddd, *J* = 8.9, 2.2, 2.2 Hz, 2H), 5.53 (dd, *J* = 4.0, 4.0 Hz, 1H), 5.37 (dd, *J* = 6.7, 4.3 Hz, 1H), 5.18 (d, *J* = 3.8 Hz, 1H), 4.96 (ddd, *J* = 6.7, 6.7, 3.1 Hz, 1H), 3.69 (dd, *J* = 13.7, 3.1 Hz, 1H), 3.52 (dd, *J* = 13.7, 6.7 Hz, 1H), 2.12 (s, 3H), 2.08 (s, 3H), 2.00 (s, 3H), 1.99 (s, 3H) ppm. **^{13}C NMR** (101 MHz, DMSO-d_6): δ 169.6, 169.5, 169.3, 169.2, 164.3, 136.9, 128.7, 127.6, 121.4, 72.1, 69.1 (x2 based on HMQC), 68.1, 49.4, 20.6, 20.5, 20.3, 20.3 ppm. **LRMS (ESI)**: *m/z* calculated for $C_{20}H_{23}N_4O_9Cl$ $[M+Na]^+$: 521.1; found: 521.2.

Compound 3.82 (≡ 4.08)

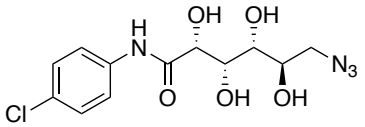

The azide **3.88** (0.064 g, 0.13 mmol) was dissolved in MeOH (2.6 mL) and a catalytic amount of 1 M NaOMe (0.8 mL) was added by pipette. The reaction was stirred at RT until starting material consumption (TLC eluent: 1:1 pet ether:EtOAc, UV light for visualization). Upon reaction completion, Amberlite IR120 (H^+ resin) was added to the stirring solution until pH < 5. The mixture was filtered, and the filtrate was collected and concentrated *in vacuo* to obtain a pure white solid (0.035 g, 82%). **^{1}H NMR** (400 MHz, DMSO-d_6): δ 9.74 (s, 1H), 7.76 (ddd, *J* = 8.9, 2.2, 2.2 Hz, 2H), 7.35 (ddd, *J* = 8.9, 2.2, 2.2 Hz, 2H), 5.76 (d, *J* = 5.5 Hz, 1H), 5.23 (d, *J* = 6.1 Hz, 1H), 4.67 (d, *J* = 6.4 Hz, 1H), 4.62 (d, *J* = 7.3 Hz, 1H), 4.18 (dd, *J* = 5.4, 4.0 Hz, 1H), 4.00 (ddd, *J* = 6.8, 4.1, 2.4 Hz, 1H), 3.71 (dddd, *J* = 8.5, 6.5, 6.5, 2.7 Hz, 1H), 3.50 (ddd, *J* = 8.5, 6.2, 2.3 Hz, 1H), 3.40 (dd, *J* = 12.6, 2.7 Hz, 1H), 3.26 (dd, *J* = 12.7, 6.7 Hz, 1H) ppm. **^{13}C NMR** (101 MHz, DMSO-d_6): δ 171.7, 137.5, 128.4, 127.0, 121.2, 74.0, 72.3, 70.2, 70.0, 53.9 ppm. **LRMS (ESI)**: *m/z* calculated for $C_{12}H_{15}ClN_4O_5$ $[M+Na]^+$: 353.1; found: 353.2.

References

(1) Jahan, S.; Adam, M. K.; Manesia, J. K.; Doxtator, E.; Ben, R. N.; Pineault, N. Inhibition of Ice Recrystallization during Cryopreservation of Cord Blood Grafts Improves Platelet Engraftment. *Transfusion* **2020**, *60* (4), 769–778. https://doi.org/10.1111/trf.15759.

(2) Knight, C. A.; Hallett, J.; DeVries, A. L. Solute Effects on Ice Recrystallization: An Assessment Technique. *Cryobiology* **1988**, *25* (1), 55–60. https://doi.org/10.1016/0011-2240(88)90020-X.

(3) Jackman, J.; Noestheden, M.; Moffat, D.; Pezacki, J. P.; Findlay, S.; Ben, R. N. Assessing Antifreeze Activity of AFGP 8 Using Domain Recognition Software. *Biochem. Biophys. Res. Commun.* **2007**, *354* (2), 340–344. https://doi.org/10.1016/j.bbrc.2006.12.225.

(4) Abraham, S.; Keillor, K.; Capicciotti, C. J.; Perley-Robertson, G. E.; Keillor, J. W.; Ben, R. N. Quantitative Analysis of the Efficacy and Potency of Novel Small Molecule Ice Recrystallization Inhibitors. *Cryst. Growth Des.* **2015**, *15* (10), 5034–5039. https://doi.org/10.1021/acs.cgd.5b00995.

(5) Chakrabartty, A.; Hew, C. L. The Effect of Enhanced A-Helicity on the Activity of a Winter Flounder Antifreeze Polypeptide. *Eur. J. Biochem.* **1991**, *202*, 1057–1063.

(6) Adam, M. K.; Poisson, J. S.; Hu, Y.; Prasannakumar, G.; Pottage, M. J.; Ben, R. N.; Wilkinson, B. L. Carbohydrate-Based Surfactants as Photocontrollable Inhibitors of Ice Recrystallization. *RSC Adv.* **2016**, *6* (45), 39240–39244. https://doi.org/10.1039/c6ra07030b. - Reproduced by permission of The Royal Society of Chemistry

(7) Adam, M. K.; Hu, Y.; Poisson, J. S.; Pottage, M. J.; Ben, R. N.; Wilkinson, B. L. Photoswitchable Carbohydrate-Based Fluorosurfactants as Tuneable Ice Recrystallization Inhibitors. *Carbohydr. Res.* **2017**, *439*, 1–8. https://doi.org/10.1016/j.carres.2016.12.004.

(8) Adam, M. K.; Jarrett-Wilkins, C.; Beards, M.; Staykov, E.; MacFarlane, L. R.; Bell, T. D. M.; Matthews, J. M.; Manners, I.; Faul, C. F. J.; Moens, P. D. J.; Ben, R. N.; Wilkinson, B. L. 1D Self-Assembly and Ice Recrystallization Inhibition Activity of Antifreeze Glycopeptide-Functionalized Perylene Bisimides. *Chem. - A Eur. J.* **2018**, *24* (31), 7834–7839. https://doi.org/10.1002/chem.201800857.

(9) Chaytor, J. L.; Tokarew, J. M.; Wu, L. K.; Leclre, M.; Tam, R. Y.; Capicciotti, C. J.;

Guolla, L.; Von Moos, E.; Findlay, C. S.; Allan, D. S.; Ben, R. N. Inhibiting Ice Recrystallization and Optimization of Cell Viability after Cryopreservation. *Glycobiology* **2012**, *22* (1), 123–133. https://doi.org/10.1093/glycob/cwr115.

(10) Lui, S.; Wang, W.; von Moos, E.; Jackman, J.; Mealing, G.; Monette, R.; Ben, R. N. In Vitro Studies of Antifreeze Glycoprotein (AFGP) and a C-Linked AFGP Analogue. *Biomacromolecules* **2007**, *8* (5), 1456–1462. https://doi.org/10.1021/bm061044o.

(11) Mosmann, T. Rapid Colorimetric Assay for Cellular Growth and Survival: Application to Proliferation and Cytotoxicity Assays. *J. Immunol. Methods* **1983**, *65*, 55–63.

(12) Pasha, R.; Elmoazzen, H.; Pineault, N. Development and Testing of a Stepwise Thaw and Dilute Protocol for Cryopreserved Umbilical Cord Blood Units. *Transfusion* **2017**, *57* (7), 1744–1754. https://doi.org/10.1111/trf.14136.

(13) Stem Cell Tecnologies. *Human Colony-Forming Unit (CFU) Assays Using MethoCult™*; 2019.

(14) Dumont, N.; Boyer, L.; Émond, H.; Çelebi-Saltik, B.; Pasha, R.; Bazin, R.; Mantovani, D.; Roy, D. C.; Pineault, N. Medium Conditioned with Mesenchymal Stromal Cell-Derived Osteoblasts Improves the Expansion and Engraftment Properties of Cord Blood Progenitors. *Exp. Hematol.* **2014**, *42* (9), 741-752.e1. https://doi.org/10.1016/j.exphem.2014.04.009.

(15) Briard, J. G.; Jahan, S.; Chandran, P.; Allan, D.; Pineault, N.; Ben, R. N. Small-Molecule Ice Recrystallization Inhibitors Improve the Post-Thaw Function of Hematopoietic Stem and Progenitor Cells. *ACS Omega* **2016**, *1* (5), 1010–1018. https://doi.org/10.1021/acsomega.6b00178.

(16) Briard, J. G.; Fernandez, M.; De Luna, P.; Woo, T. K.; Ben, R. N. QSAR Accelerated Discovery of Potent Ice Recrystallization Inhibitors. *Sci. Rep.* **2016**, *6* (October 2015), 1–8. https://doi.org/10.1038/srep26403.

(17) Armarego, Wilfred L. F., Chai, C. L. L. *Purification of Laboratory Chemicals*, 6th ed.; Elsevier Inc., 2009. https://doi.org/https://doi.org/10.1016/C2009-0-26589-5.

(18) Bonger, K. M.; Hoogendoorn, S.; Van Koppen, C. J.; Timmers, C. M.; Overkleeft, H. S.; Van Der Marel, G. A. Synthesis and Pharmacological Evaluation of Dimeric Follicle-Stimulating Hormone Receptor Antagonists. *ChemMedChem* **2009**, *4* (12), 2098–2102. https://doi.org/10.1002/cmdc.200900344.

(19) Pressoir, O. Amino-Aryl-Gluconamides and Their Derivatives: Potential Ice Recrystallization Inhibitors, University of Ottawa (Honours thesis), 2019.

(20) Perron, V.; Abbott, S.; Moreau, N.; Lee, D.; Penney, C.; Zacharie, B. A Method for the Selective Protection of Aromatic Amines in the Presence of Aliphatic Amines. *Synthesis (Stuttg).* **2009**, No. 2, 283–289. https://doi.org/10.1055/s-0028-1083290.

(21) Felpin, F. X.; Fouquet, E. A Useful, Reliable and Safer Protocol for Hydrogenation and the Hydrogenolysis of o-Benzyl Groups: The in Situ Preparation of an Active Pd 0/C Catalyst with Well-Defined Properties. *Chem. - A Eur. J.* **2010**, *16* (41), 12440–12445. https://doi.org/10.1002/chem.201001377.

(22) Guo, W.; Gómez, J. E.; Martínez-Rodríguez, L.; Bandeira, N. A. G.; Bo, C.; Kleij, A. W. Metal-Free Synthesis of N-Aryl Amides Using Organocatalytic Ring-Opening Aminolysis of Lactones. *ChemSusChem* **2017**, *10* (9), 1969–1975. https://doi.org/10.1002/cssc.201700415.

(23) Naik, S.; Bhattacharjya, G.; Talukdar, B.; Patel, B. K. Chemoselective Acylation of Amines in Aqueous Media. *European J. Org. Chem.* **2004**, No. 6, 1254–1260. https://doi.org/10.1002/ejoc.200300620.

(24) Rudi J. H. Hafkamp; Martinus C. Feiters, A.; Nolte, R. J. M. Organogels from Carbohydrate Amphiphiles. *J. Org. Chem.* **1999**, *64* (2), 412–426. https://doi.org/10.1021/JO981158T.

Appendix IV: Nuclear Magnetic Resonance Spectra

^{1}H and ^{13}C nuclear magnetic resonance (NMR) spectra are included for compounds without previously published data, intermediates leading to the final target compounds, as well as the final compounds themselves presented in **Chapter 3**. The corresponding synthetic details and characterization data can be found in the **Experimental Section** under "Experimental protocols and characterization data for chemical compounds." NMR spectroscopy was performed on Bruker Avance 300 and 400 MHz (Bruker, Madison, WI) instruments at ambient temperature. Spectra data were analyzed using MestreNova software or Bruker Topspin software. An example of how the proportion of photostationary states of surfactants presented in **Sections 5.3** and **5.4** were estimated by the integration of signals in ^{1}H spectra is also included. See references 6 and 7 of Appendix III for further analysis.

Compound 3.01 (≡ 4.02)

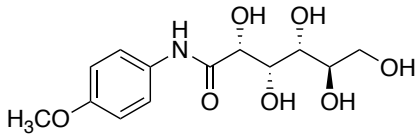

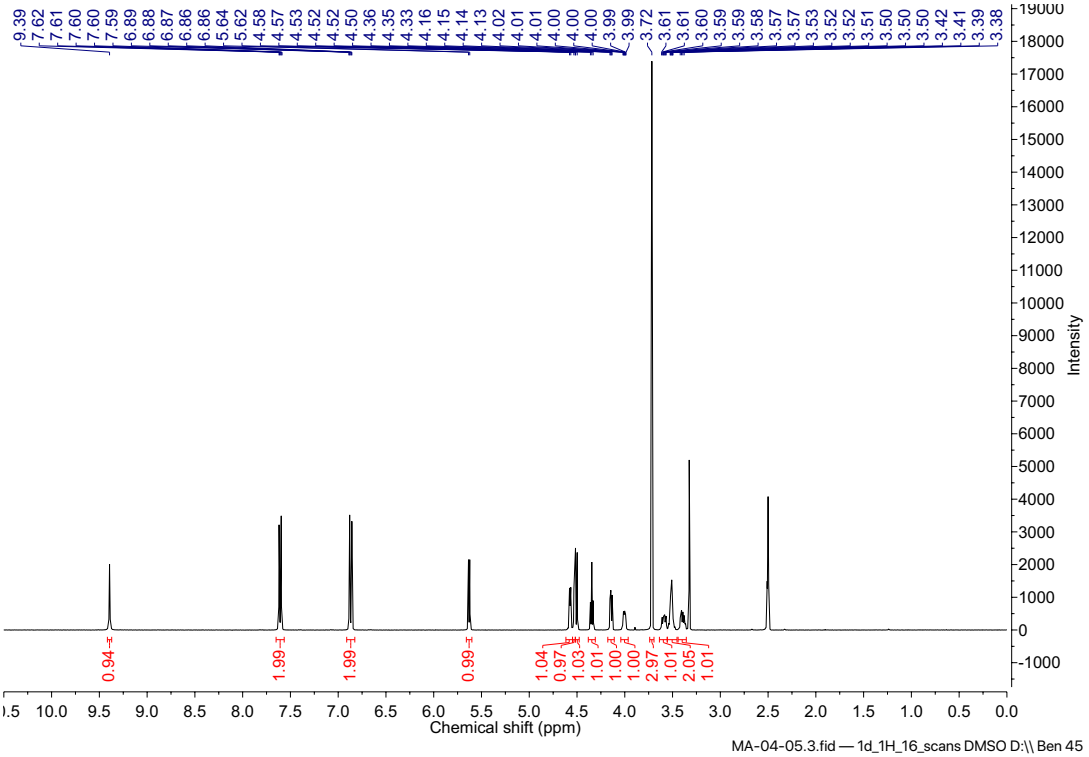

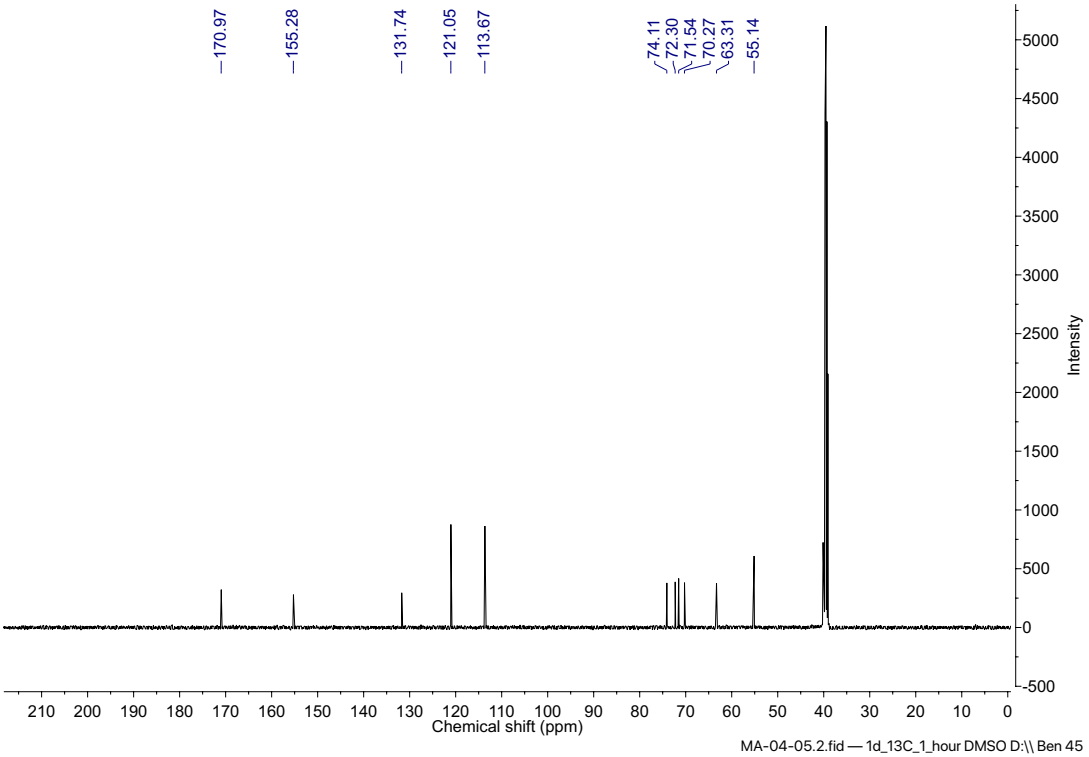

Compound 3.02 (≡ 4.01)

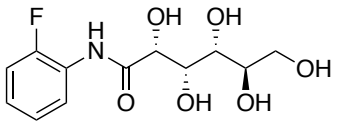

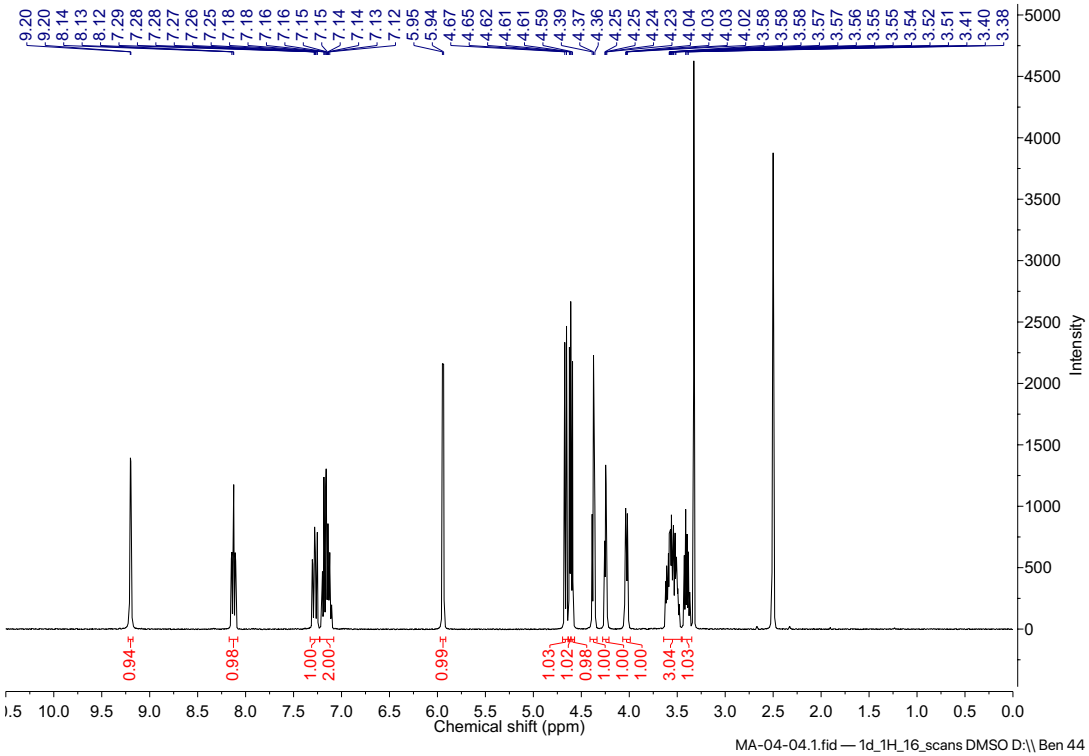

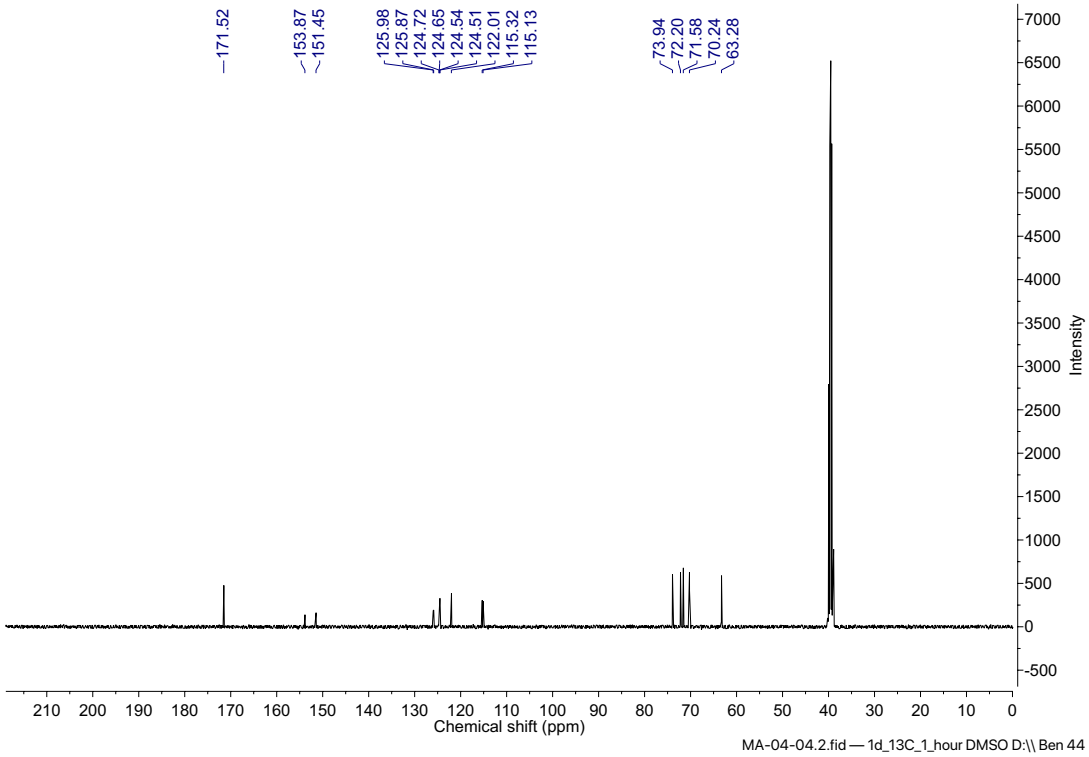

Compound 3.03 (≡ 4.04)

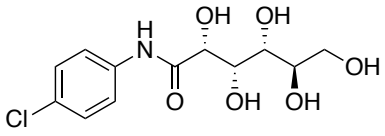

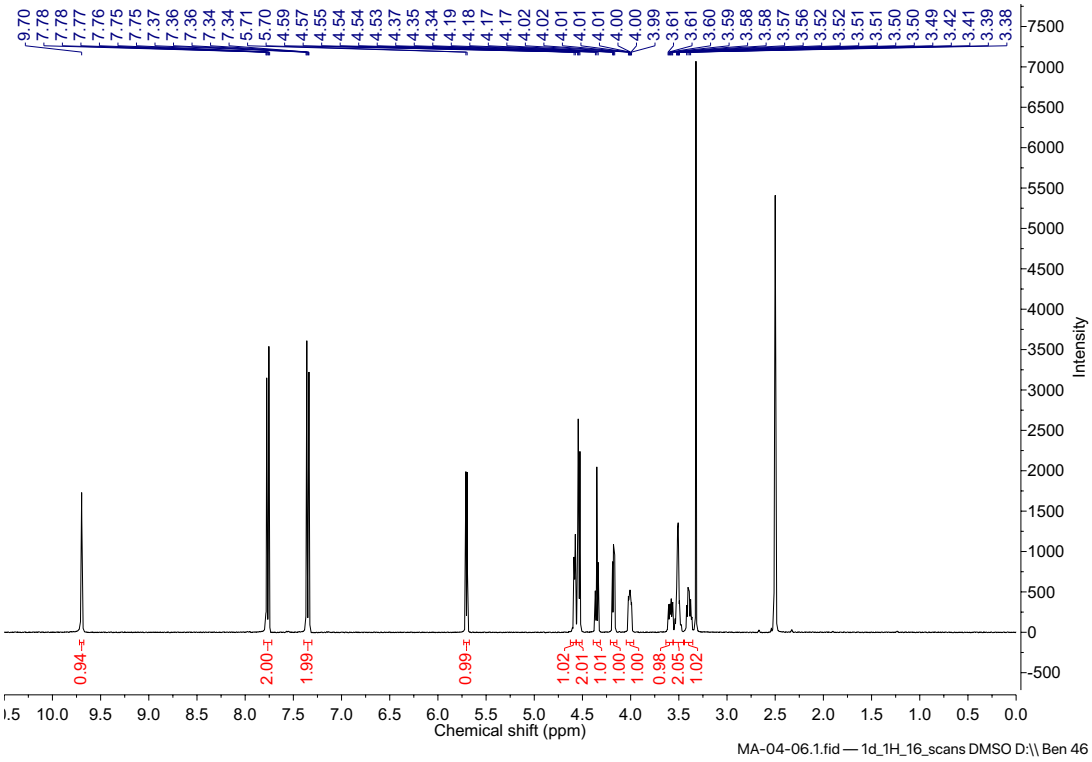

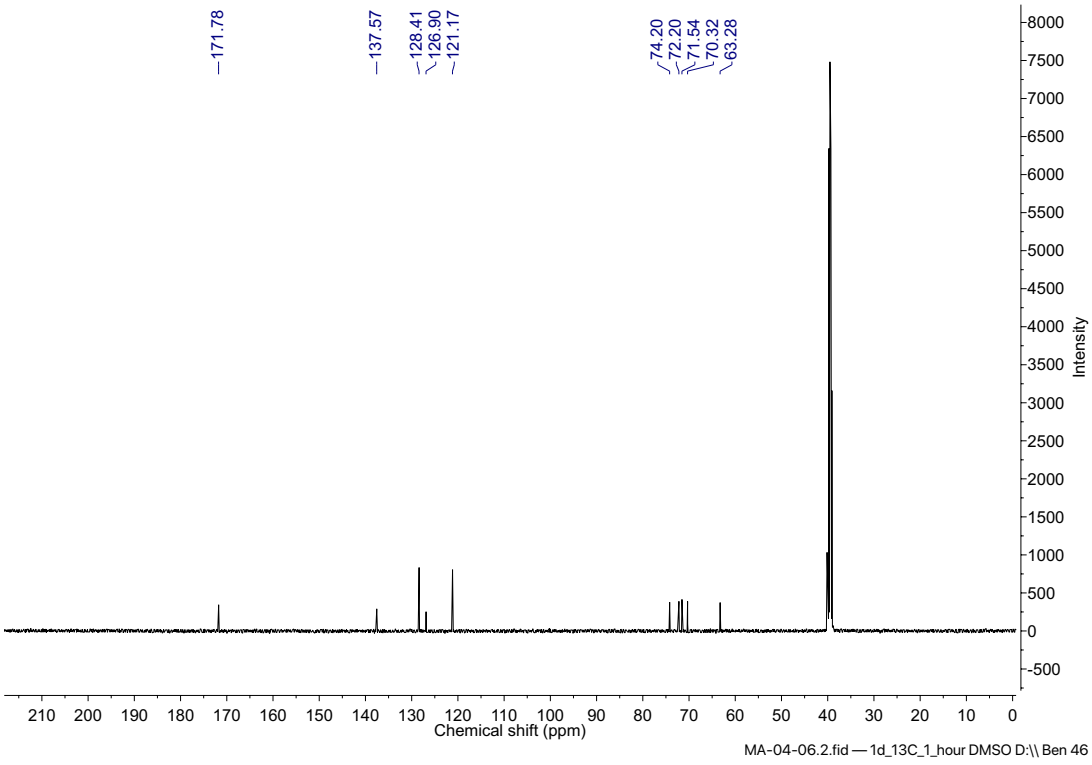

Compound 3.04 (≡ 4.03)

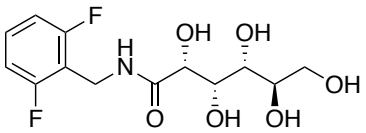

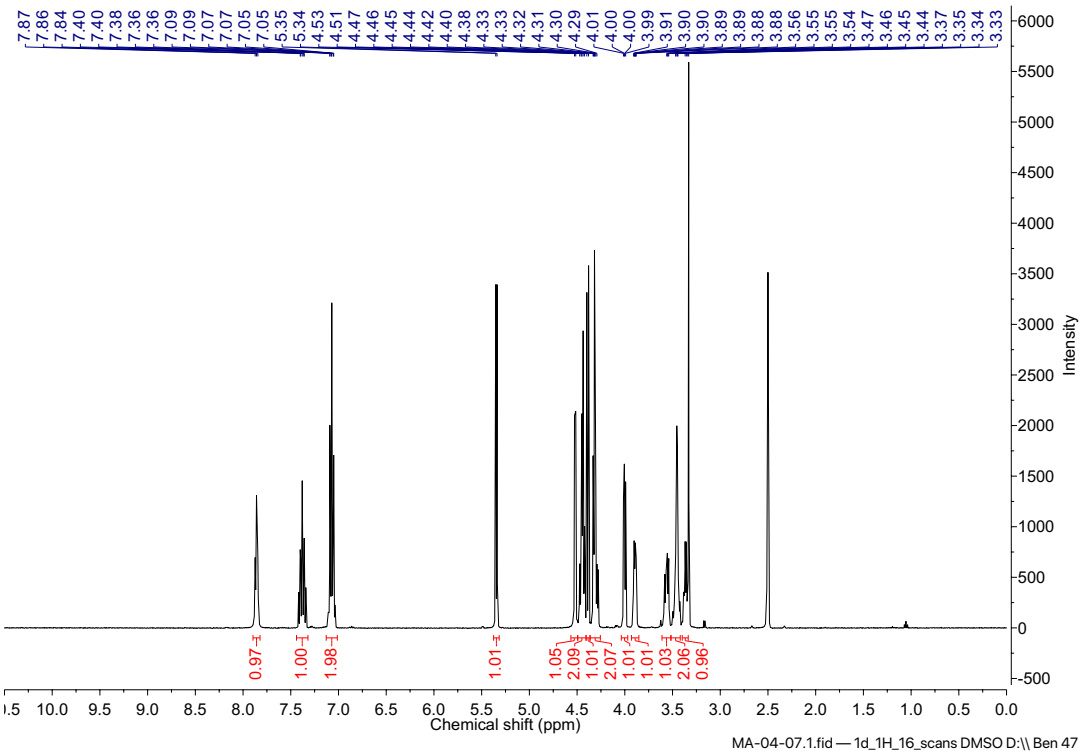

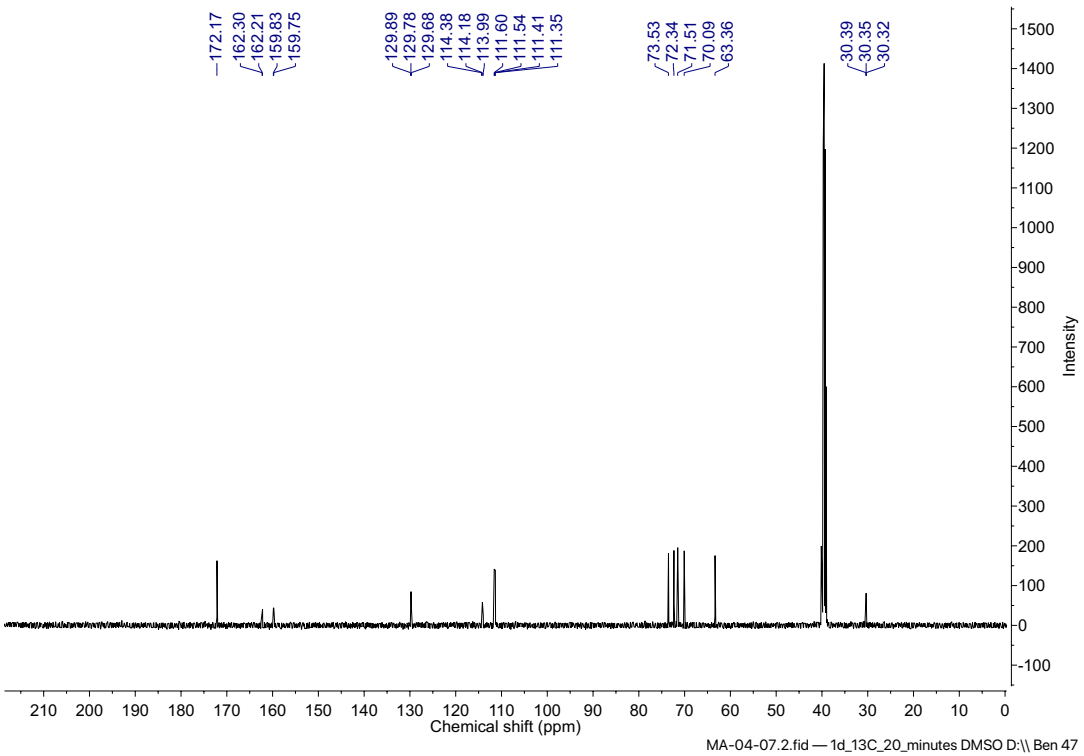

Compound **3.38 (≡ 4.05)**

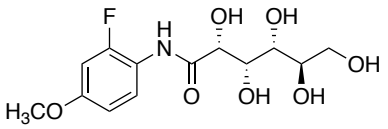

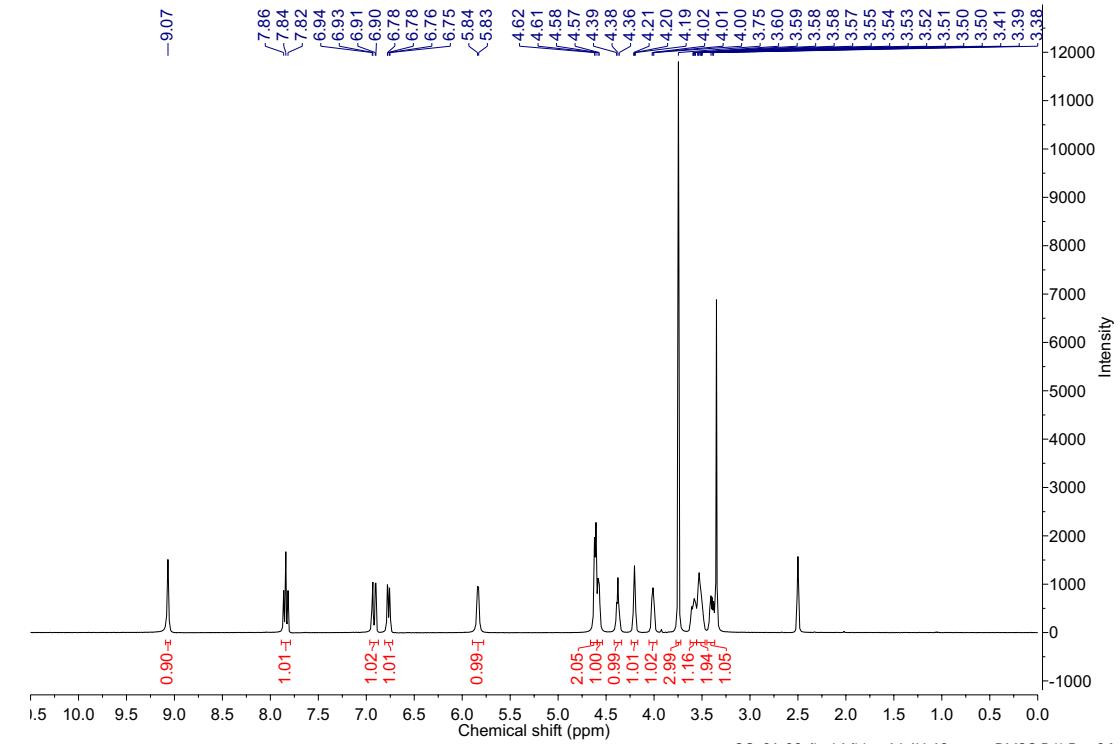

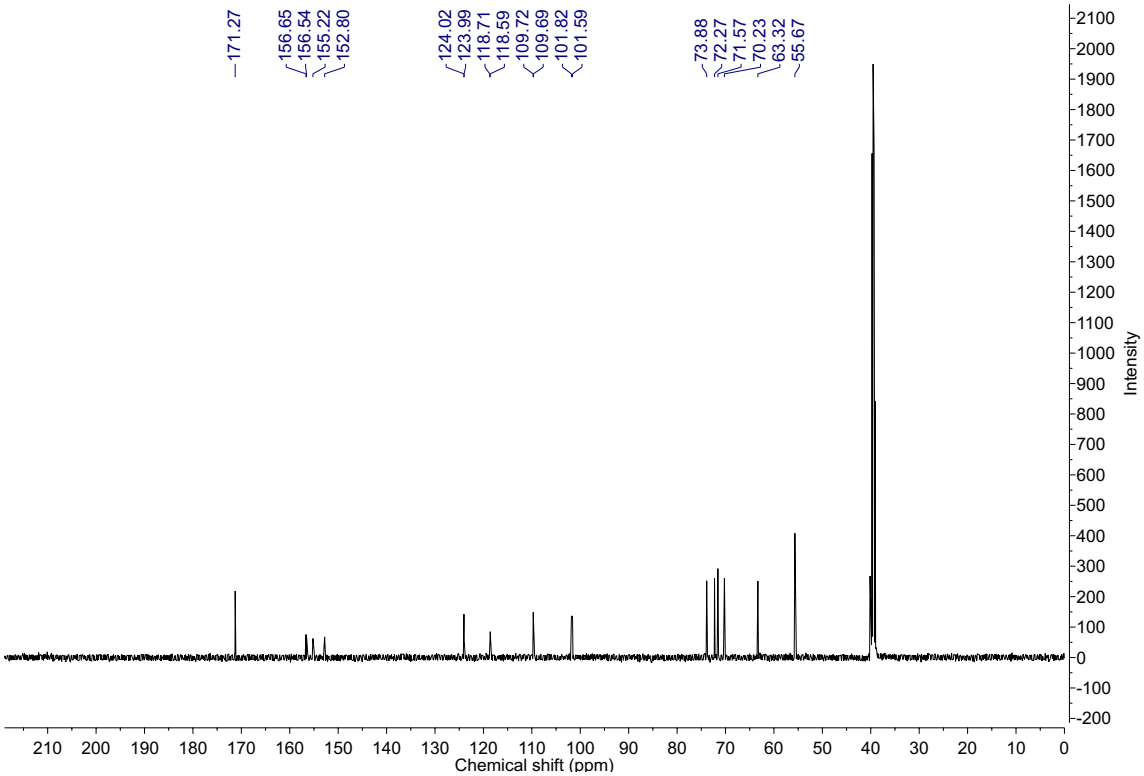

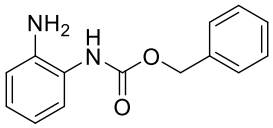

Compound 3.57

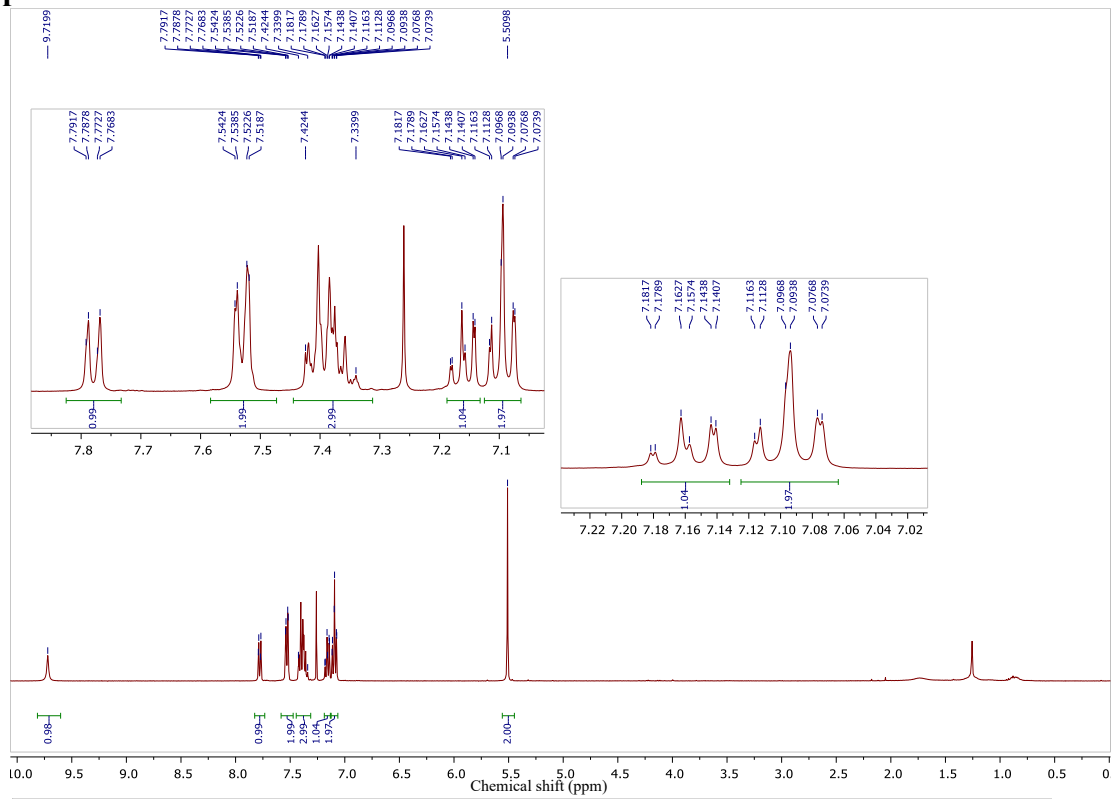

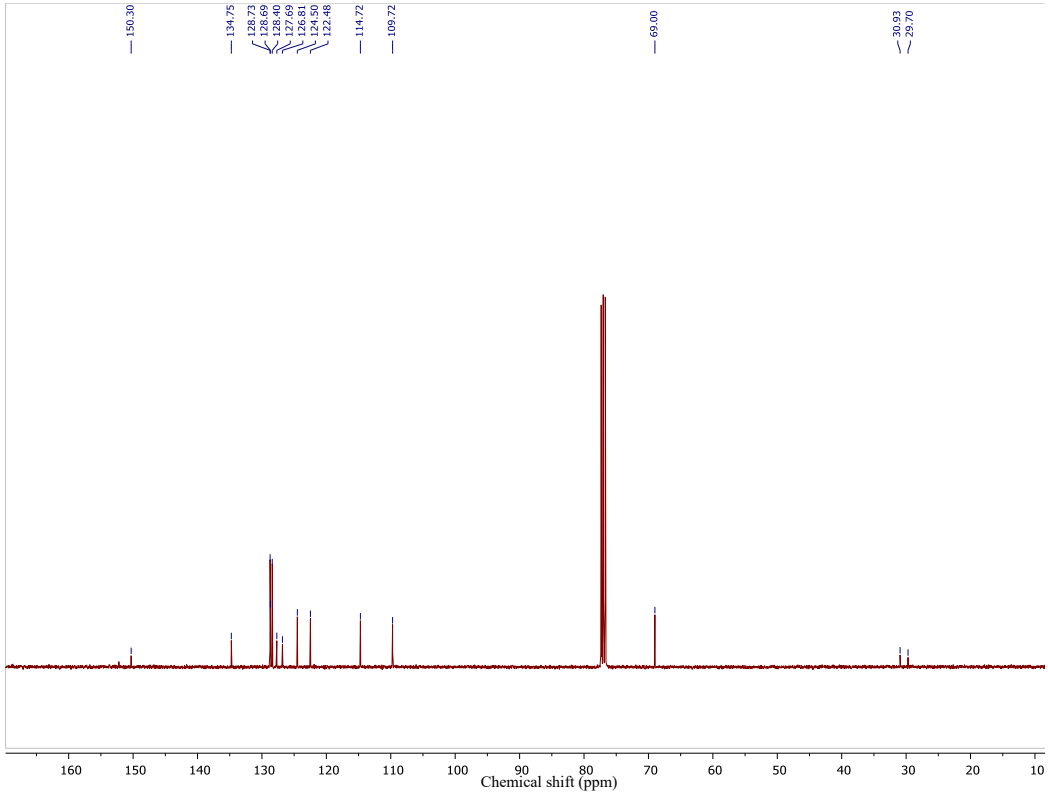

Compound 3.58

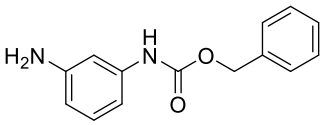

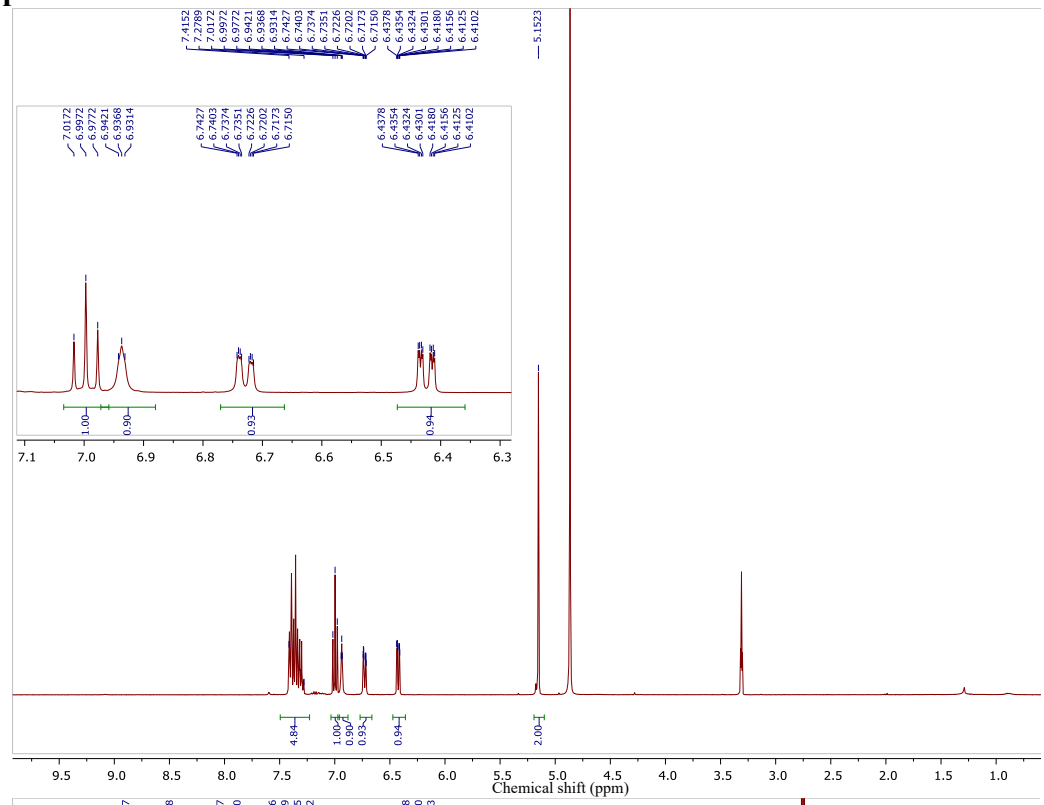

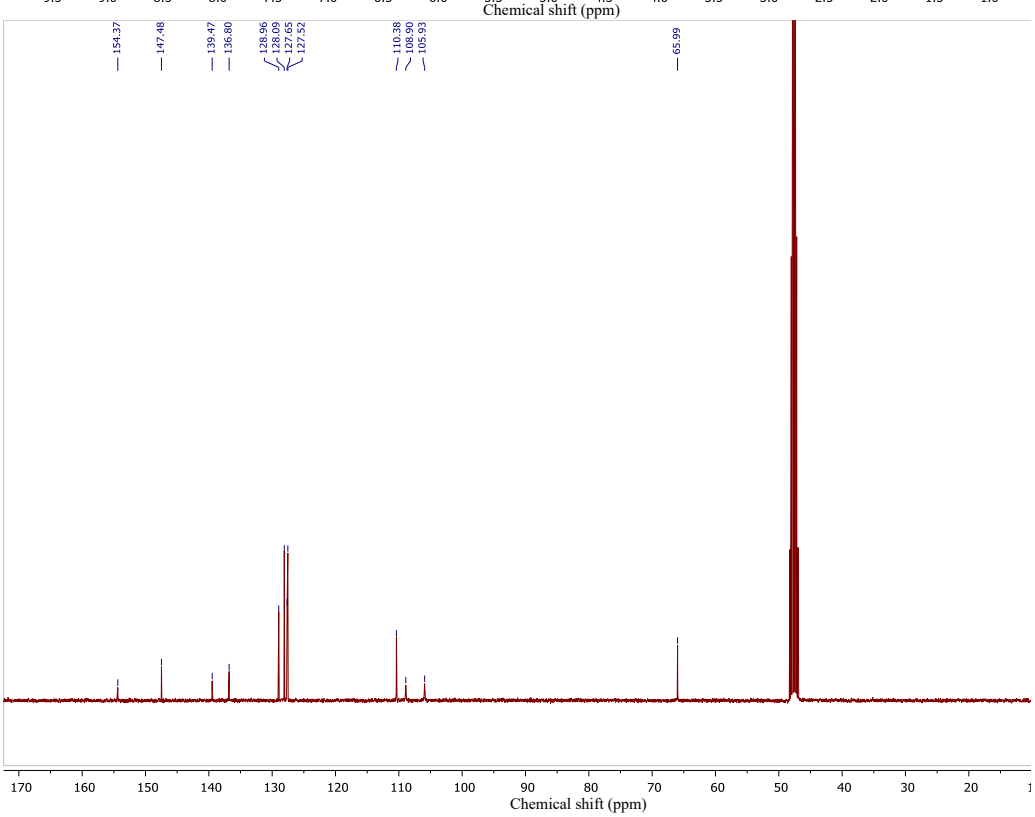

Compound 3.59

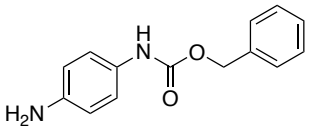

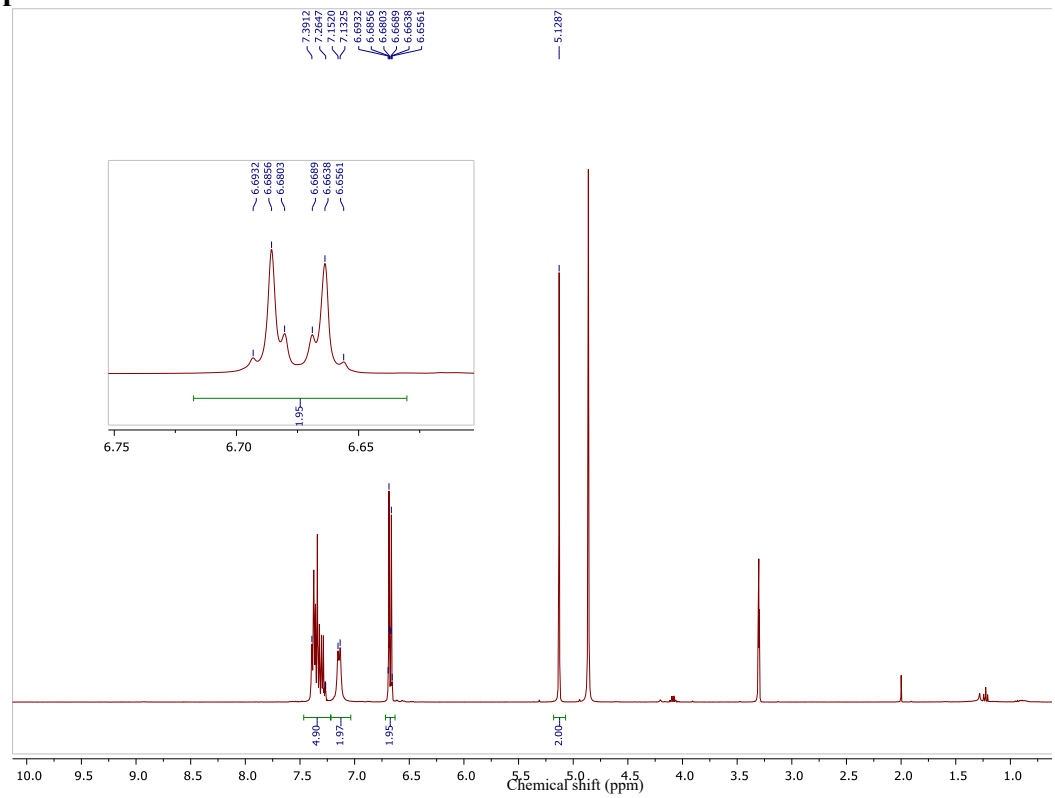

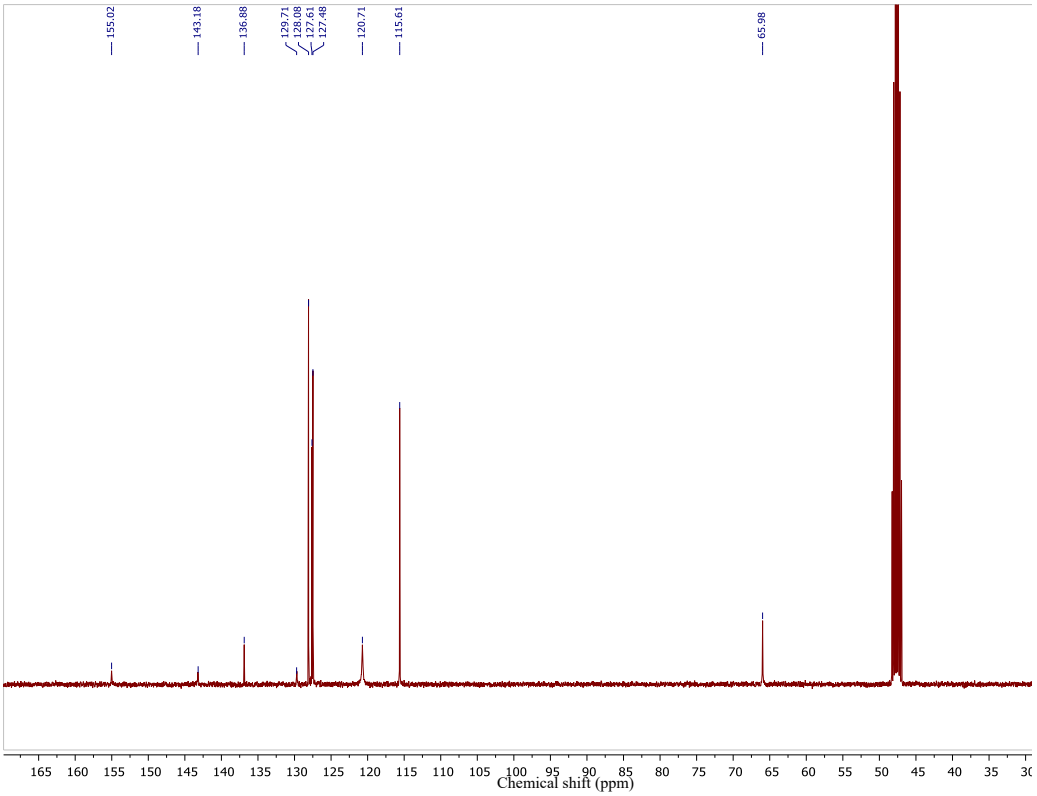

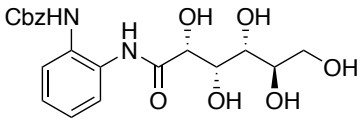

Compound 3.42

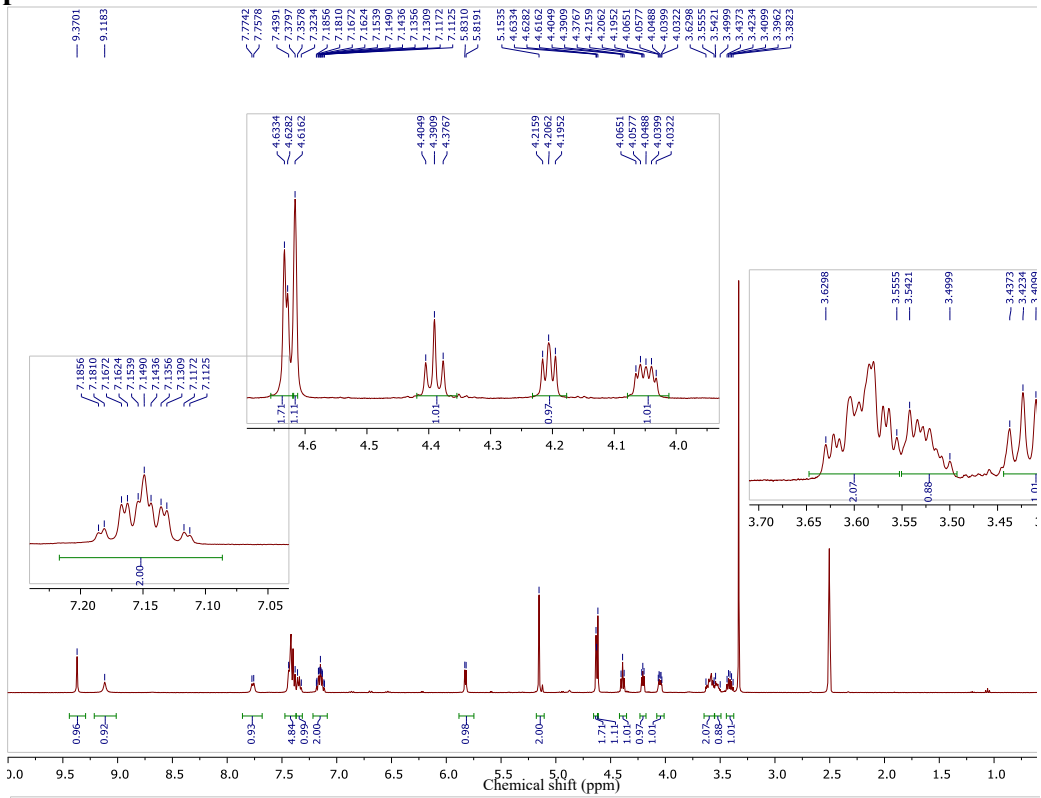

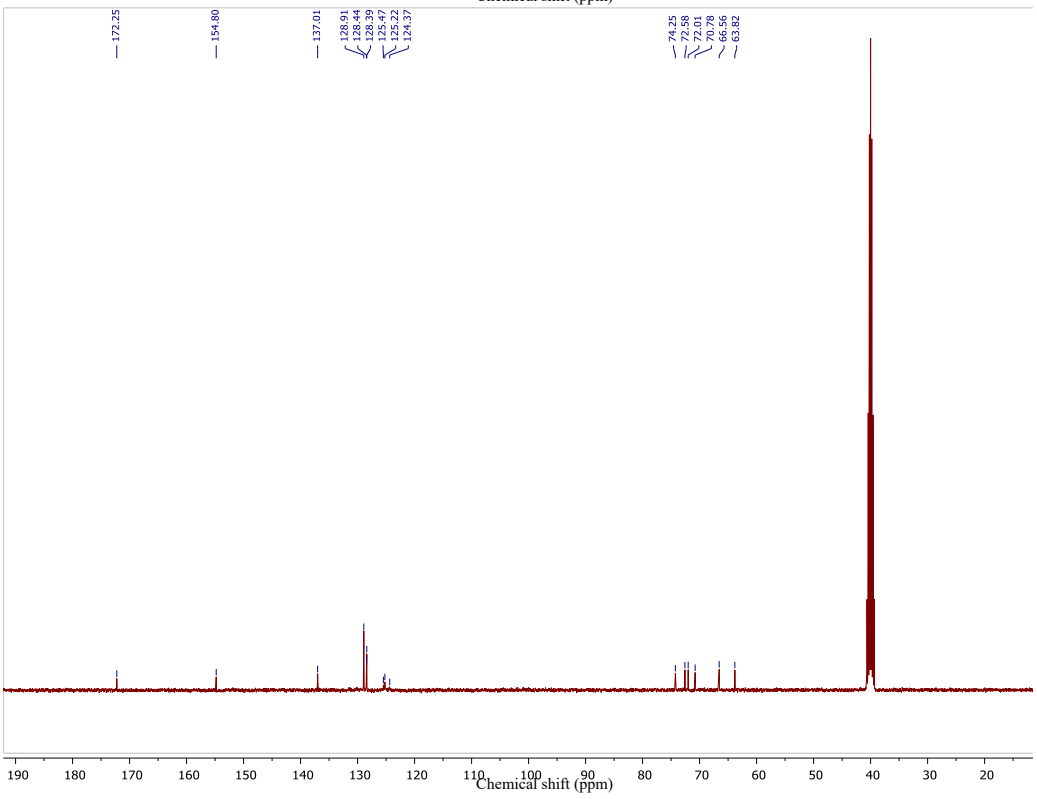

Compound 3.43

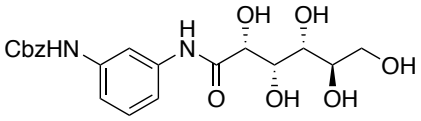

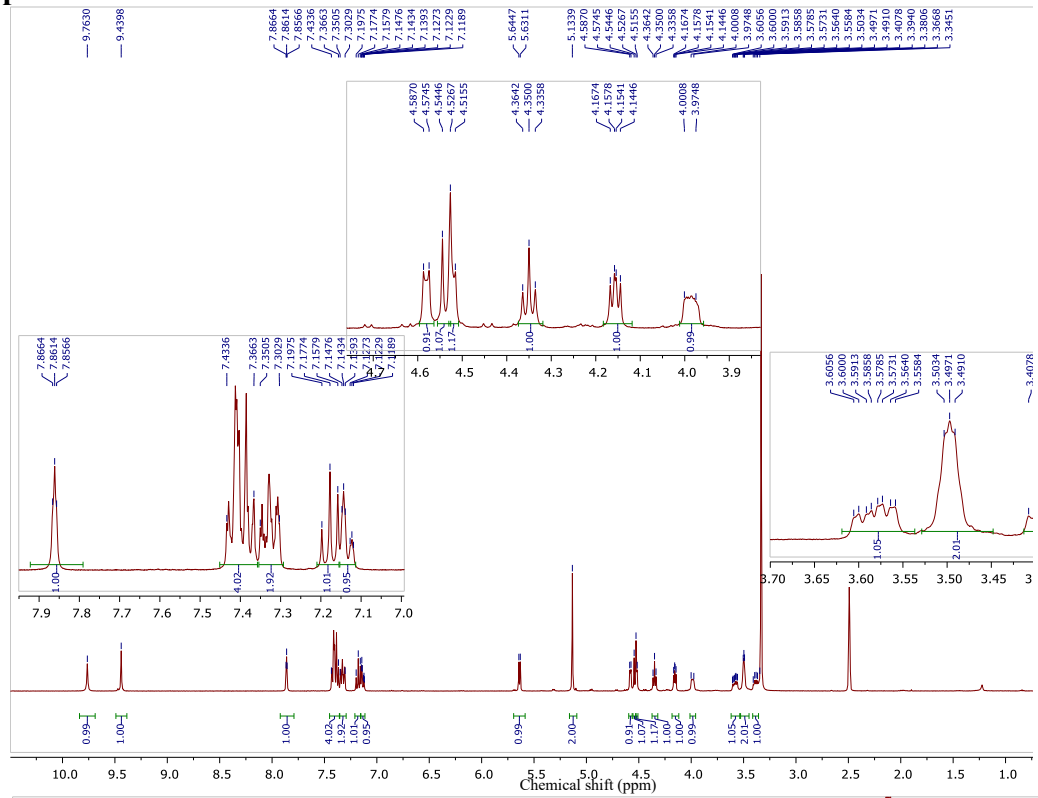

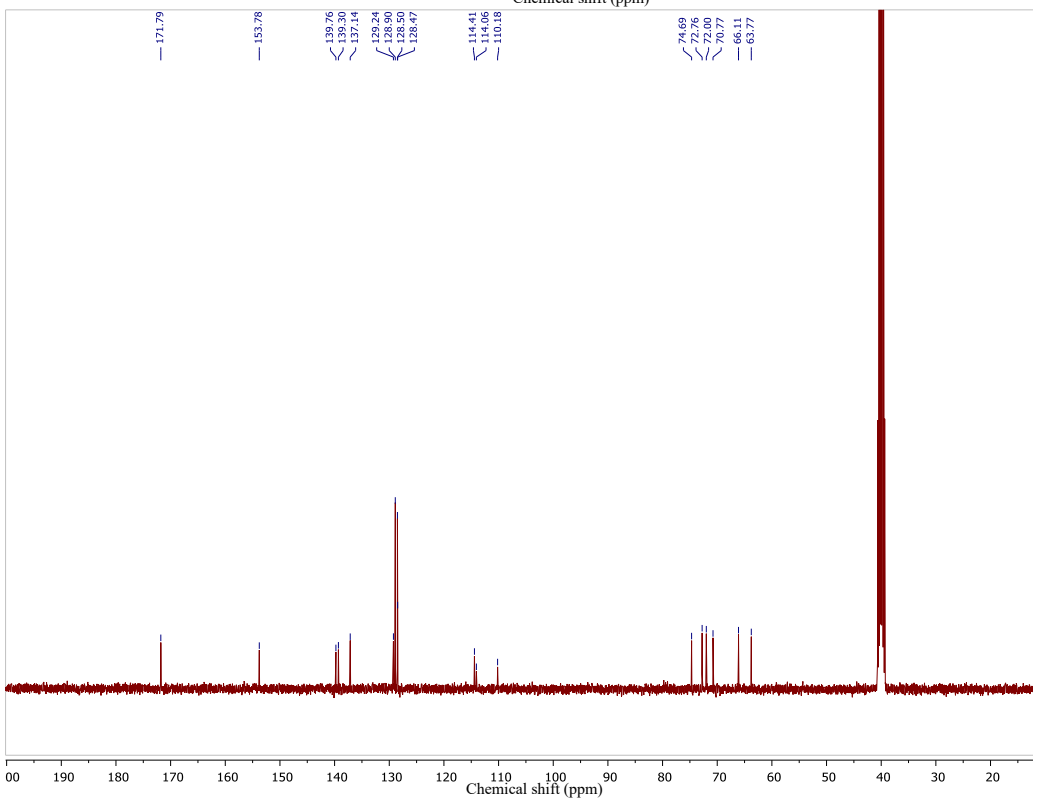

Compound 3.44

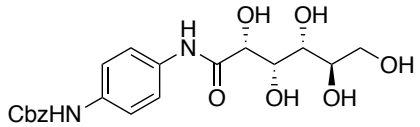

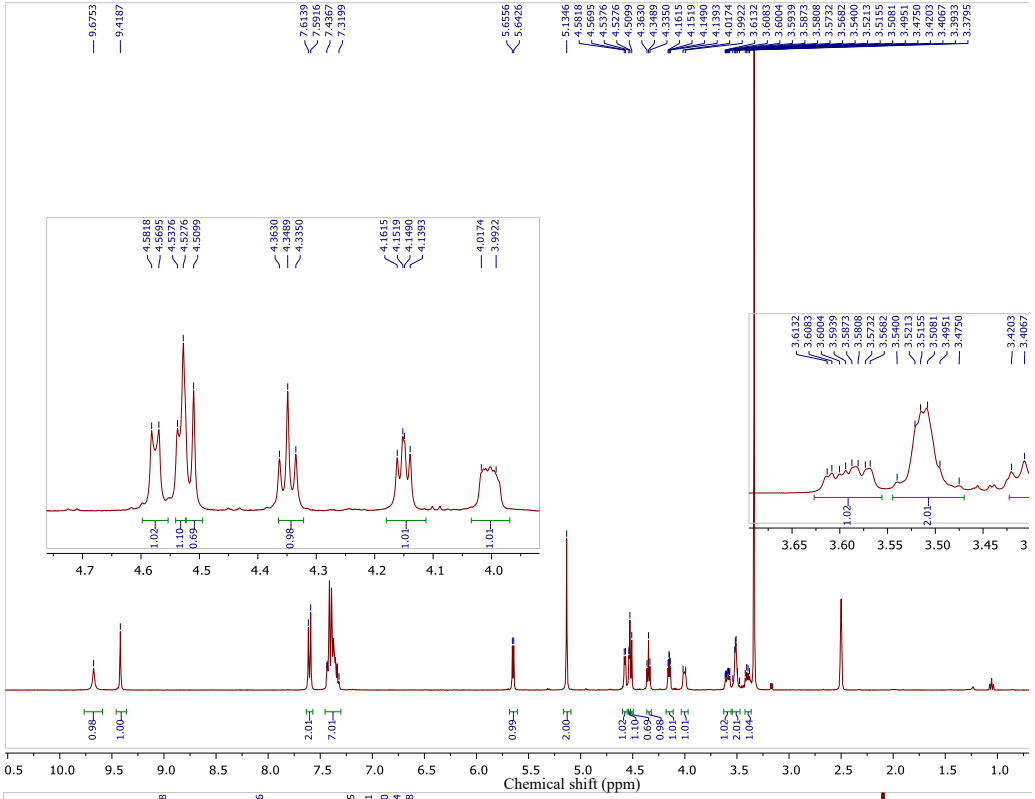

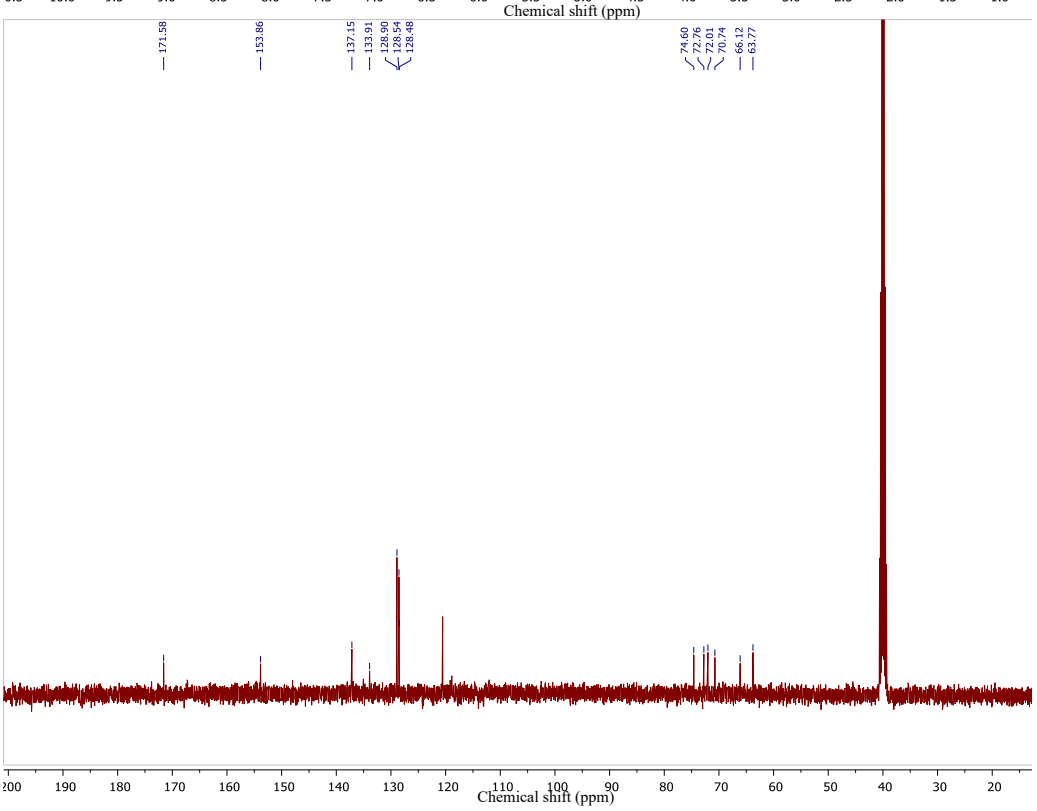

Compound 3.39

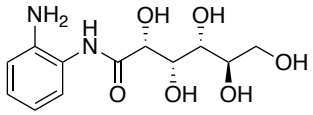

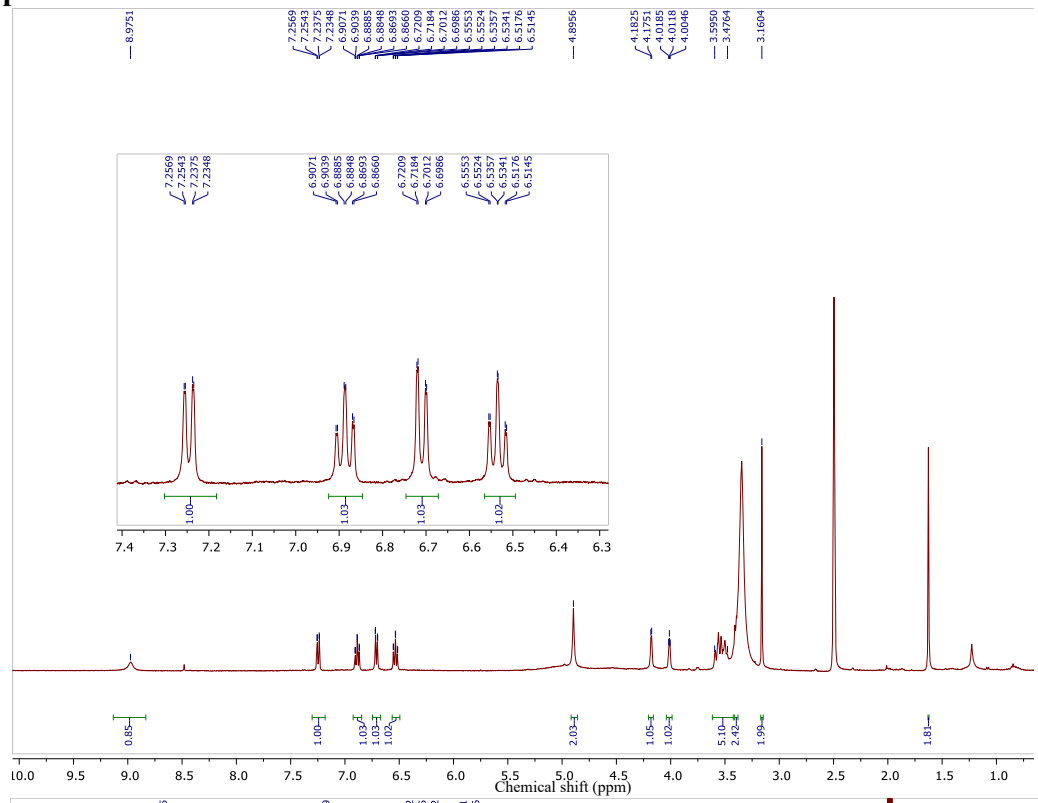

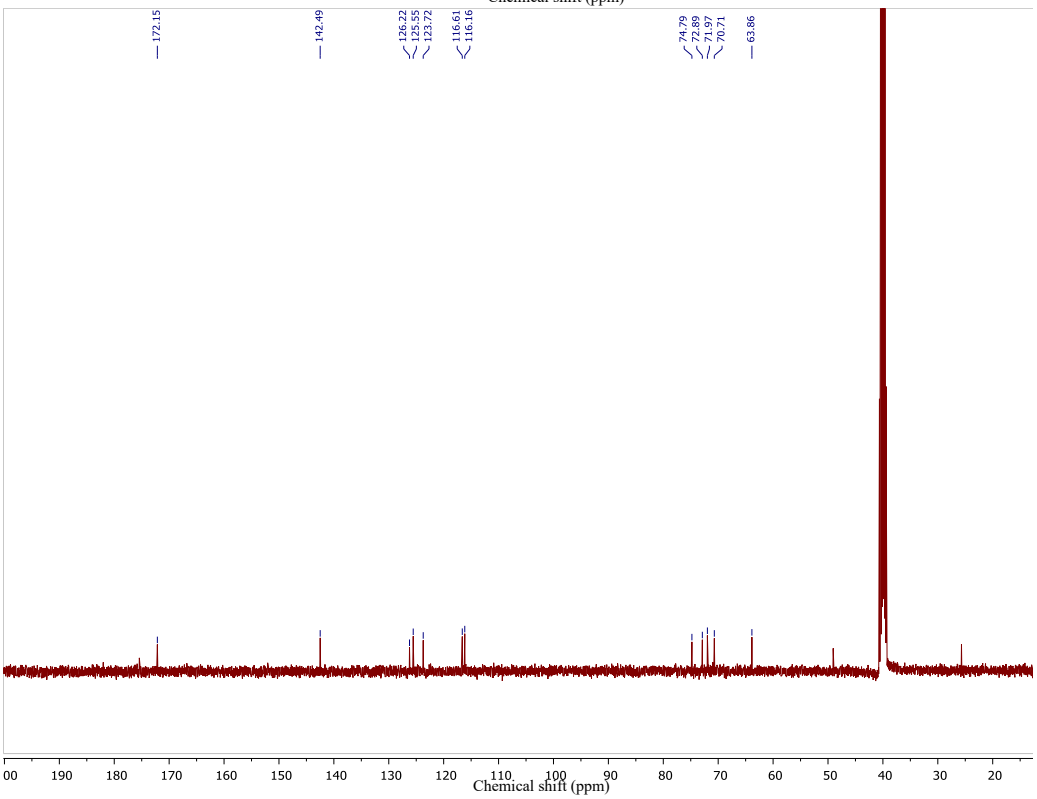

Compound 3.40

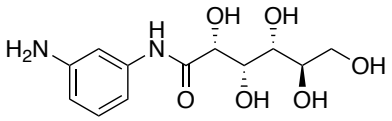

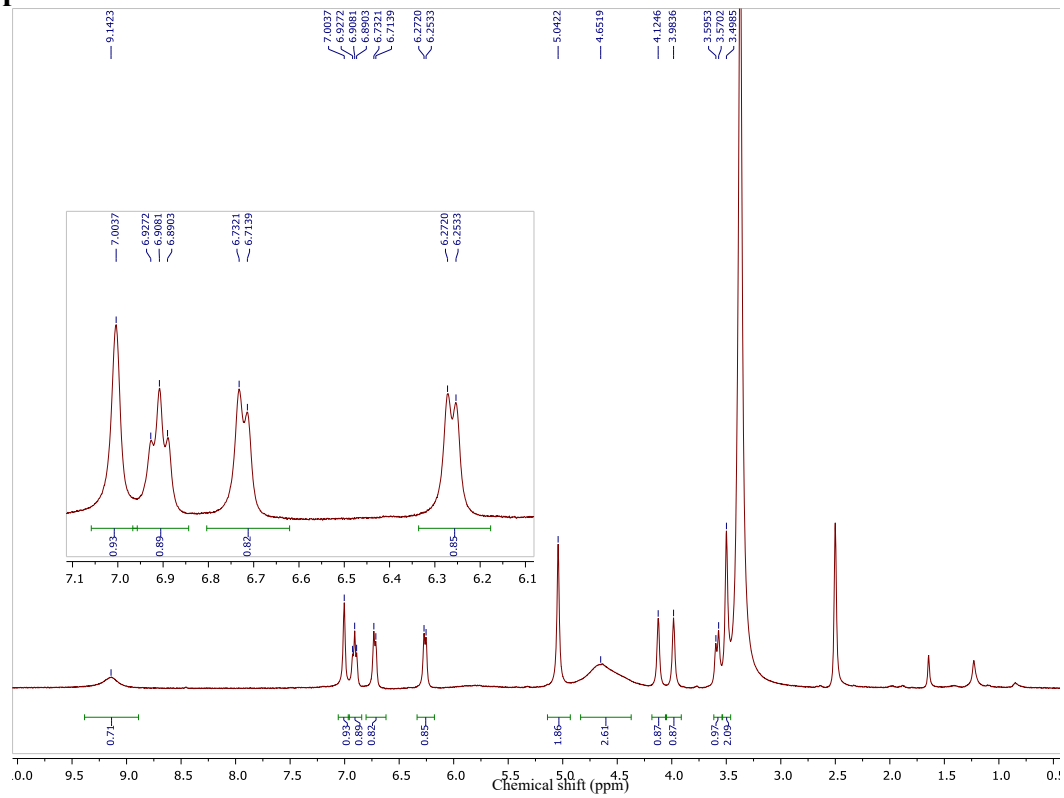

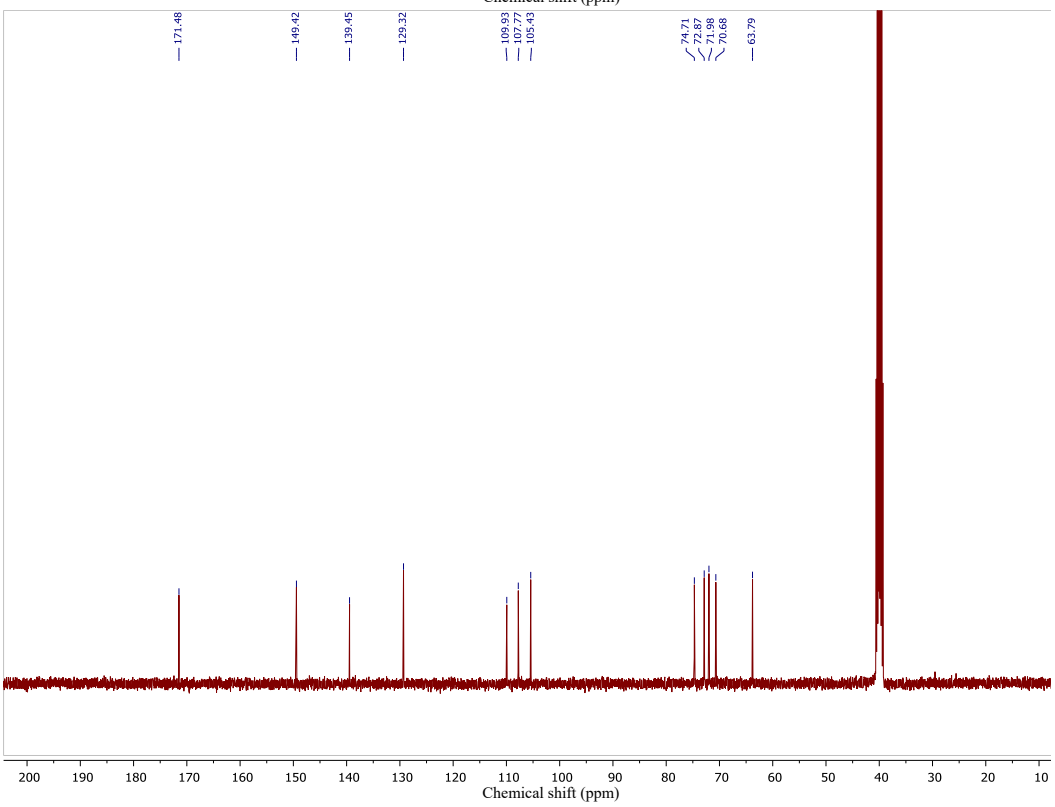

Compound 3.41

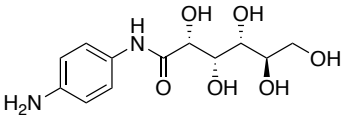

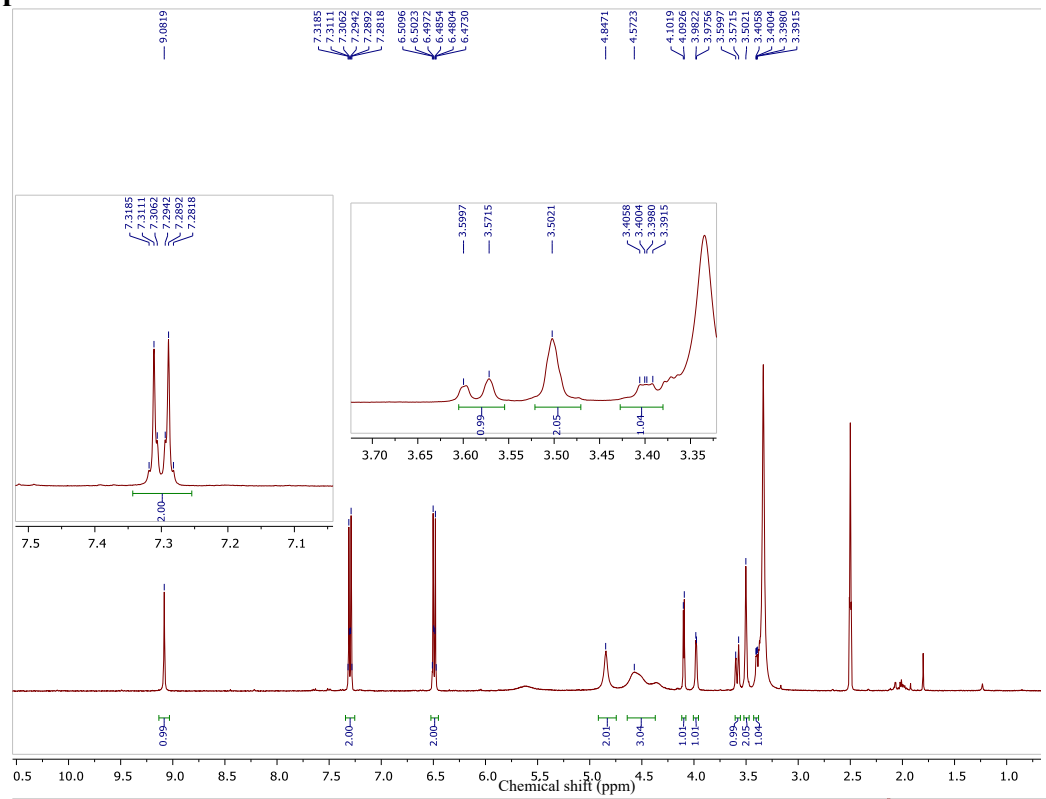

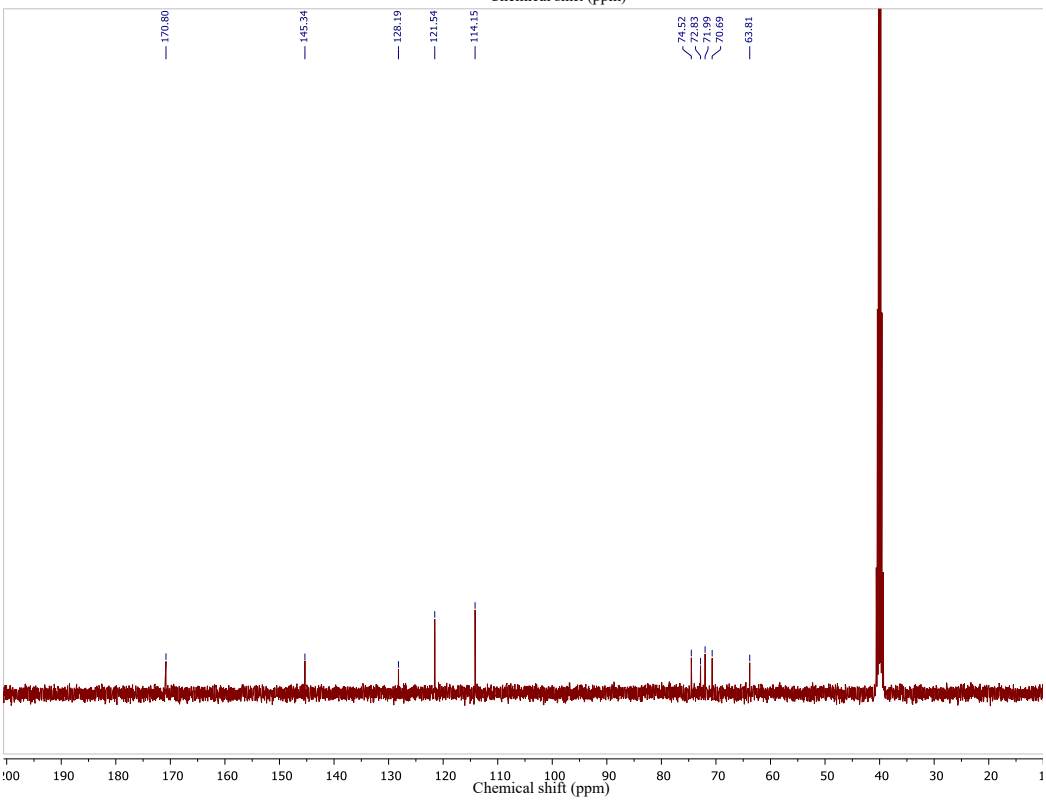

Compound 3.61

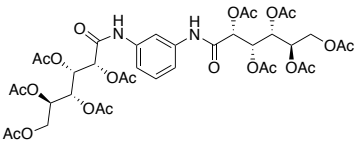

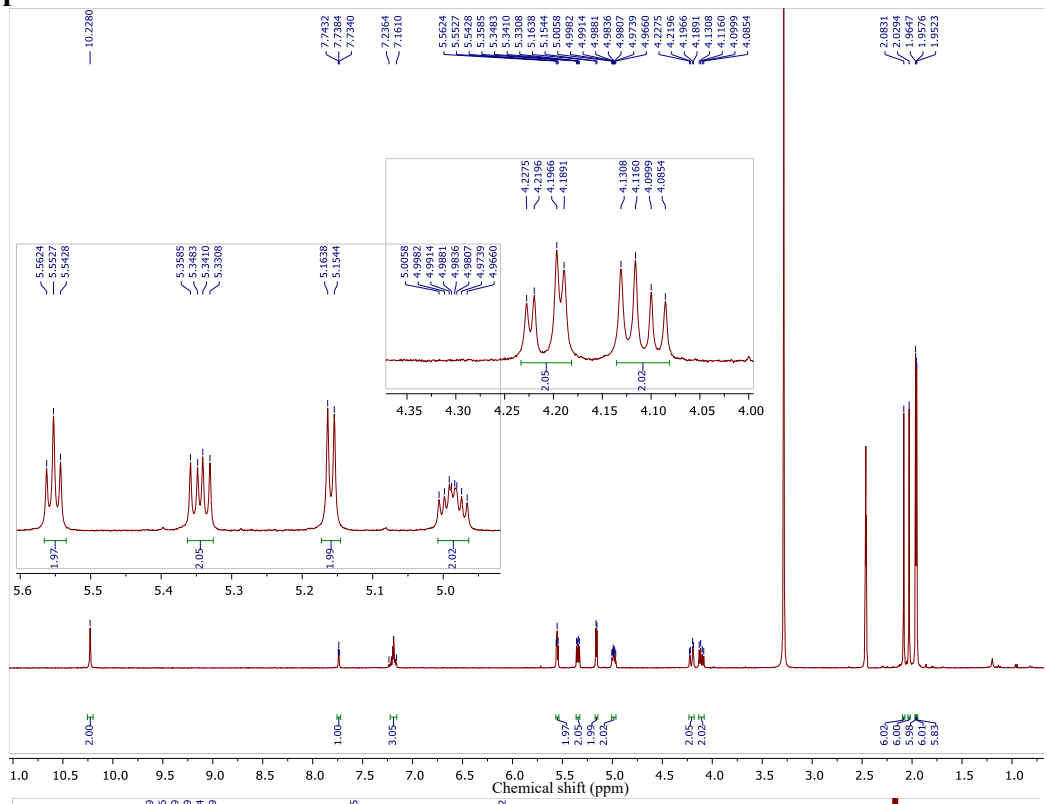

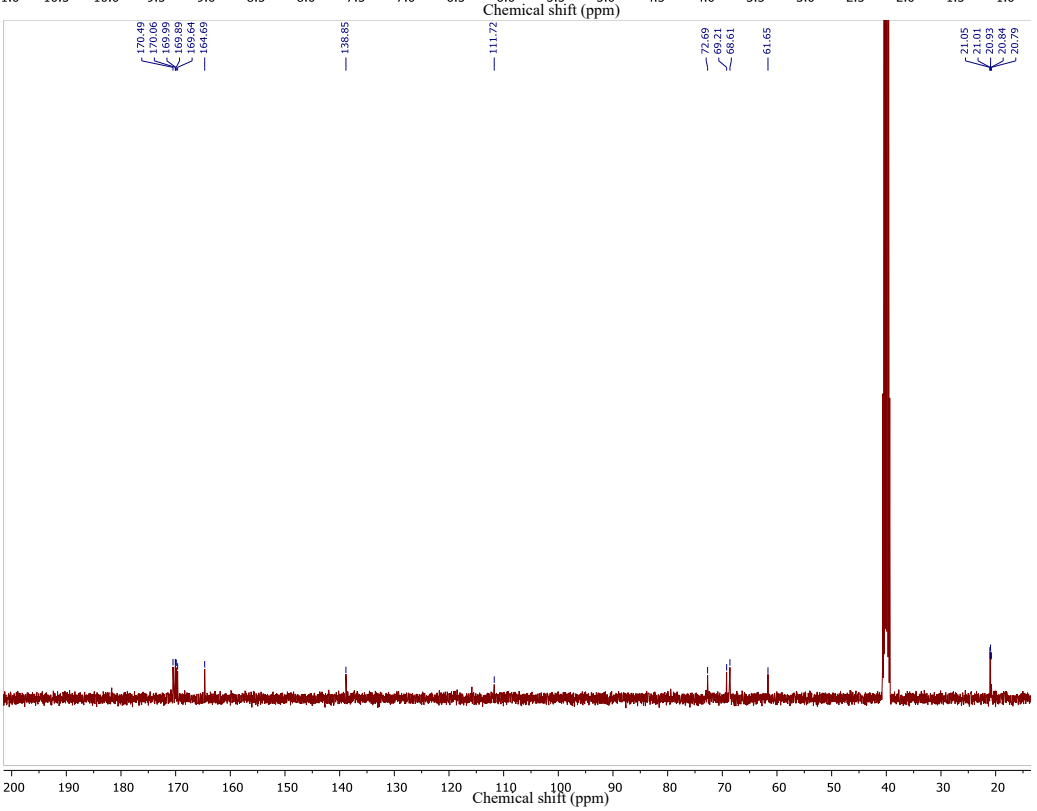

Compound 3.62

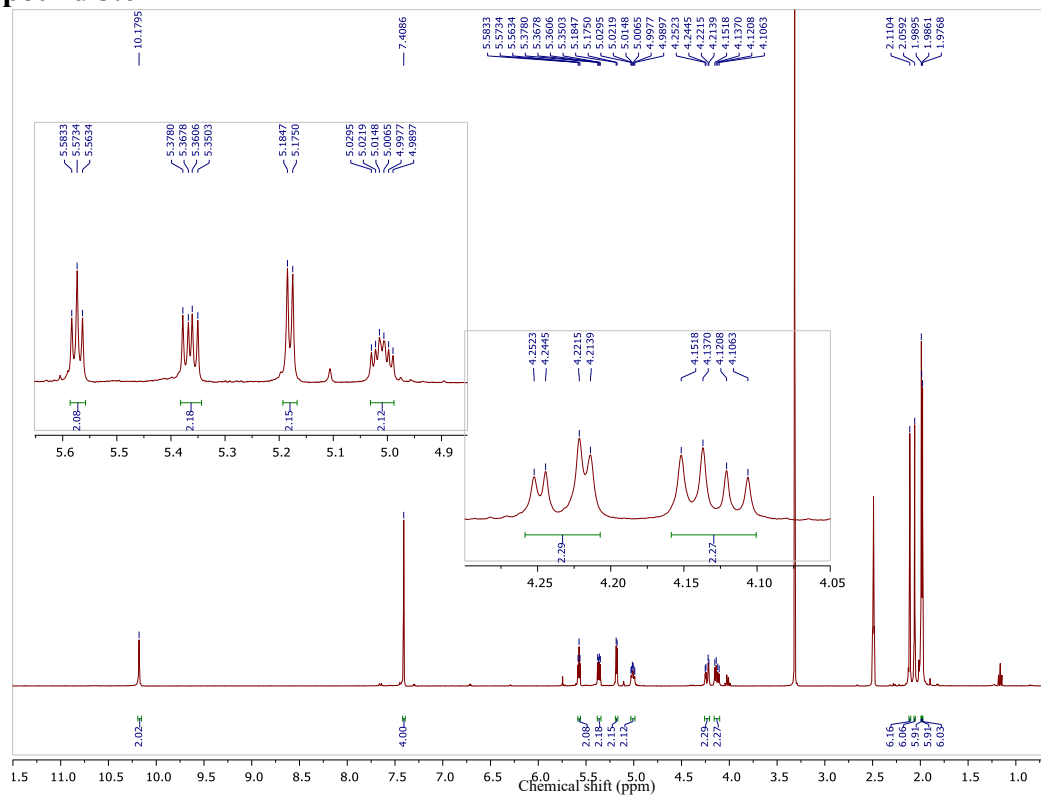

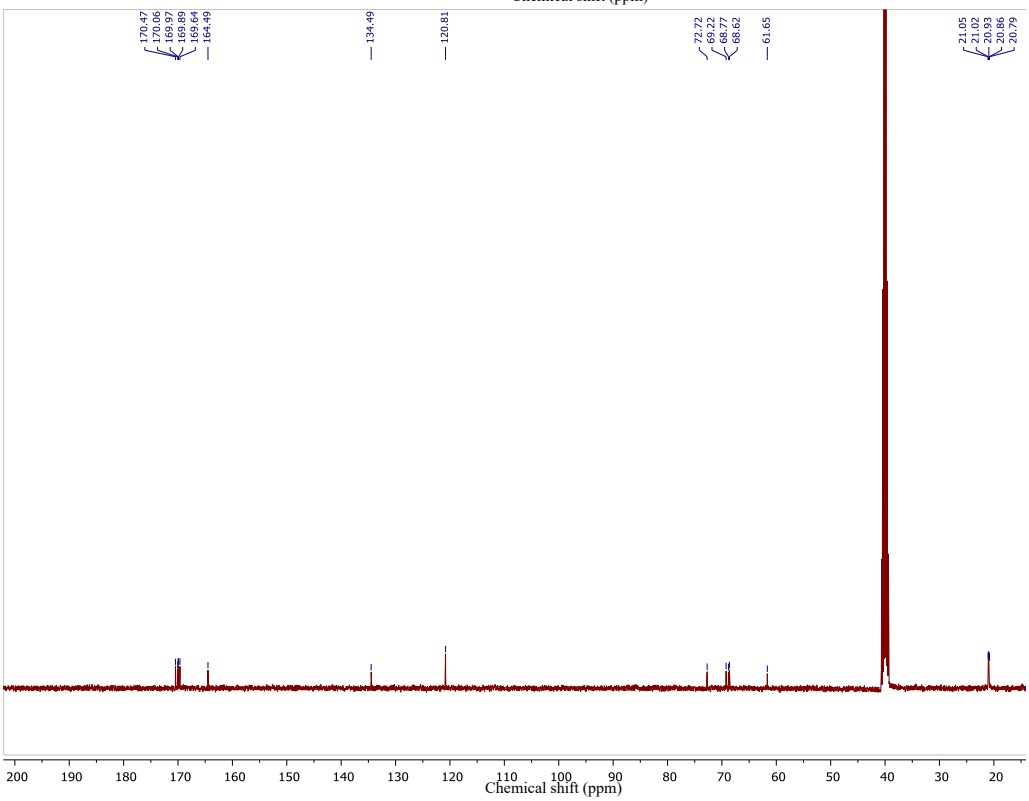

Compound 3.46

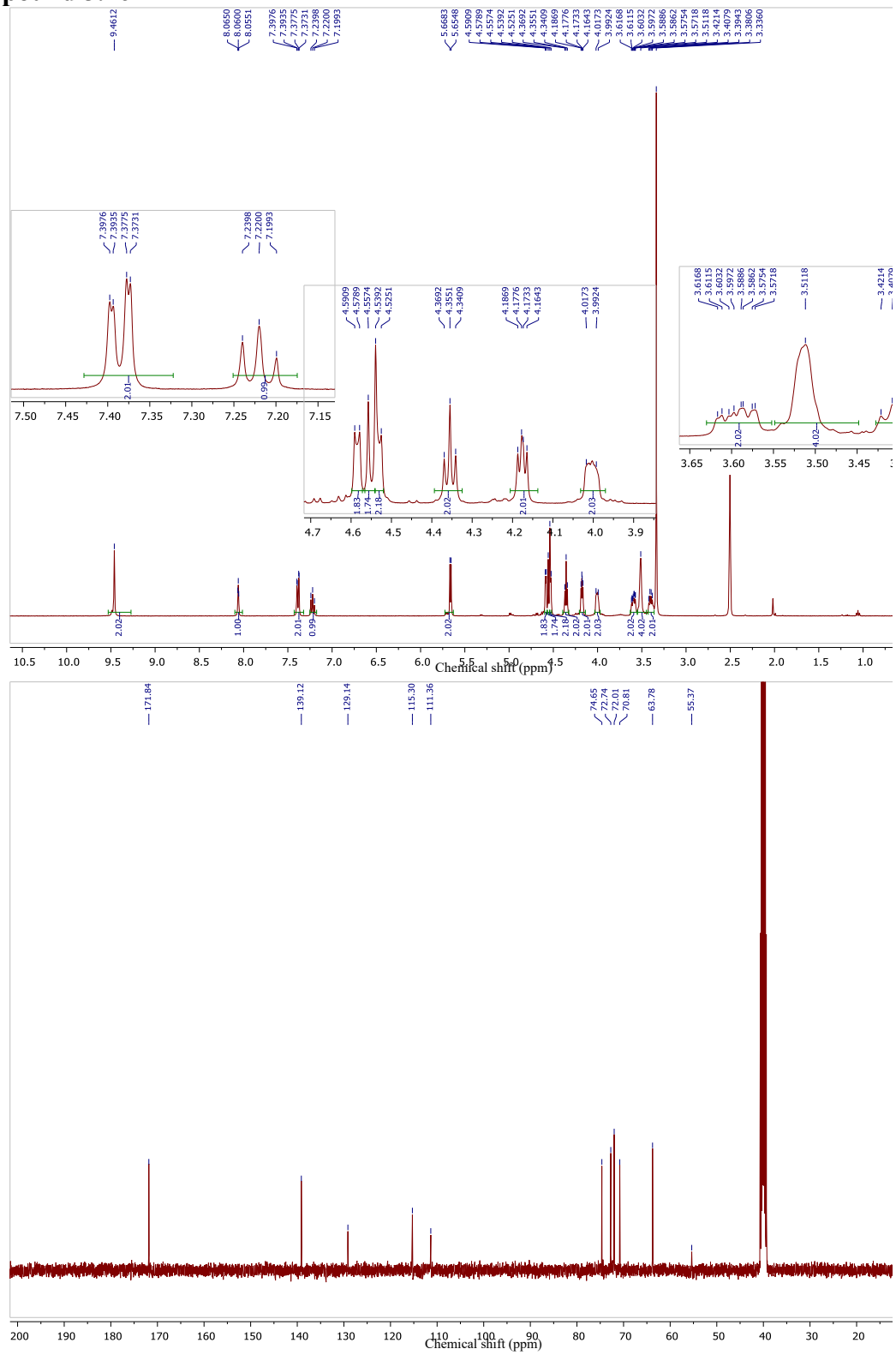

Compound 3.47

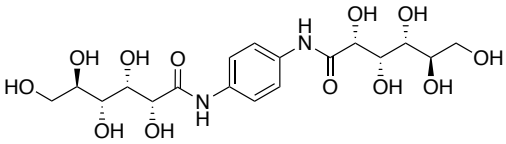

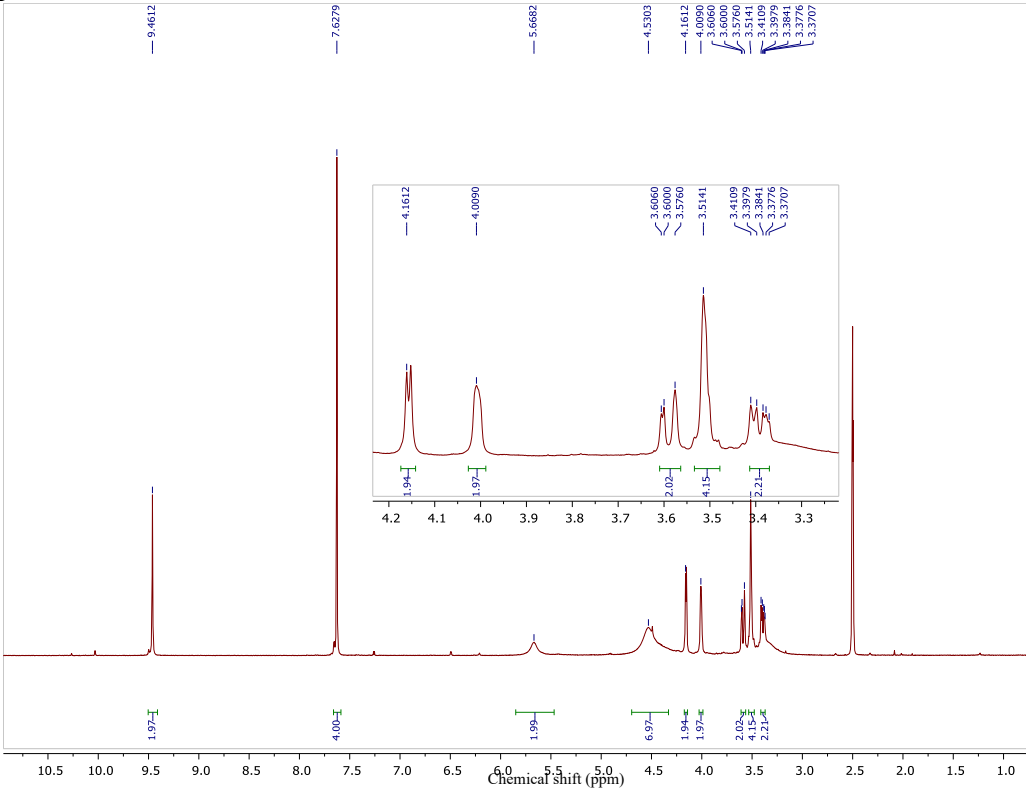

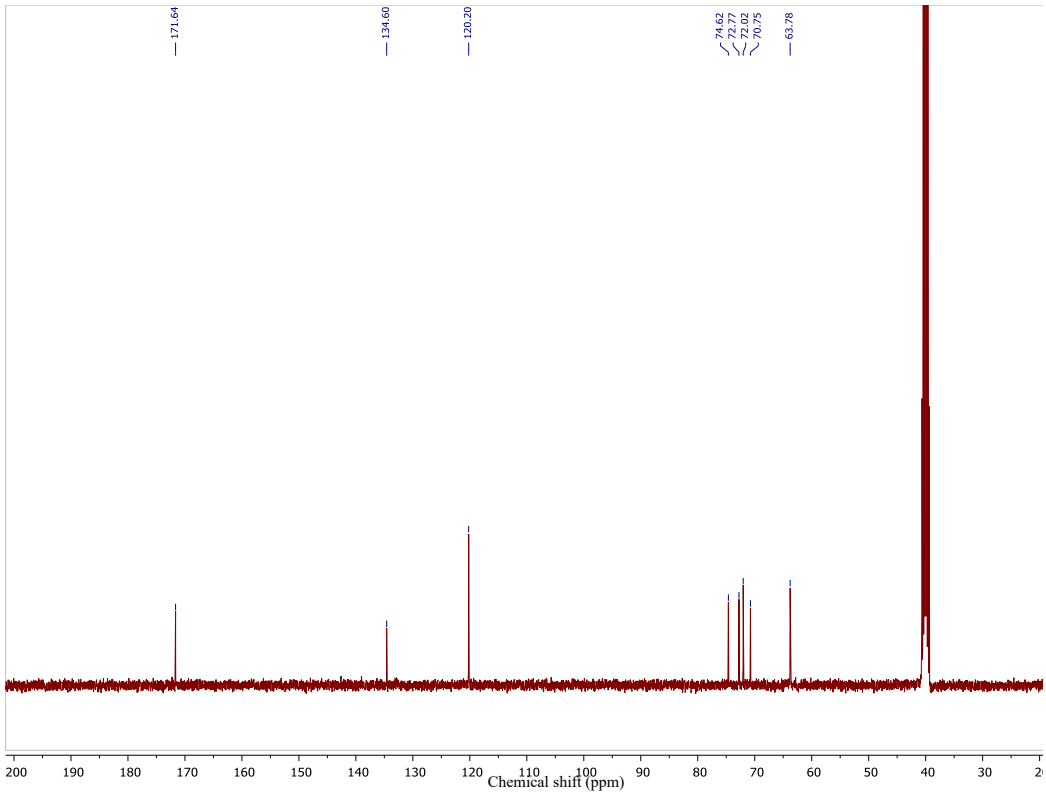

Compound 3.63

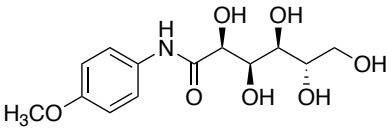

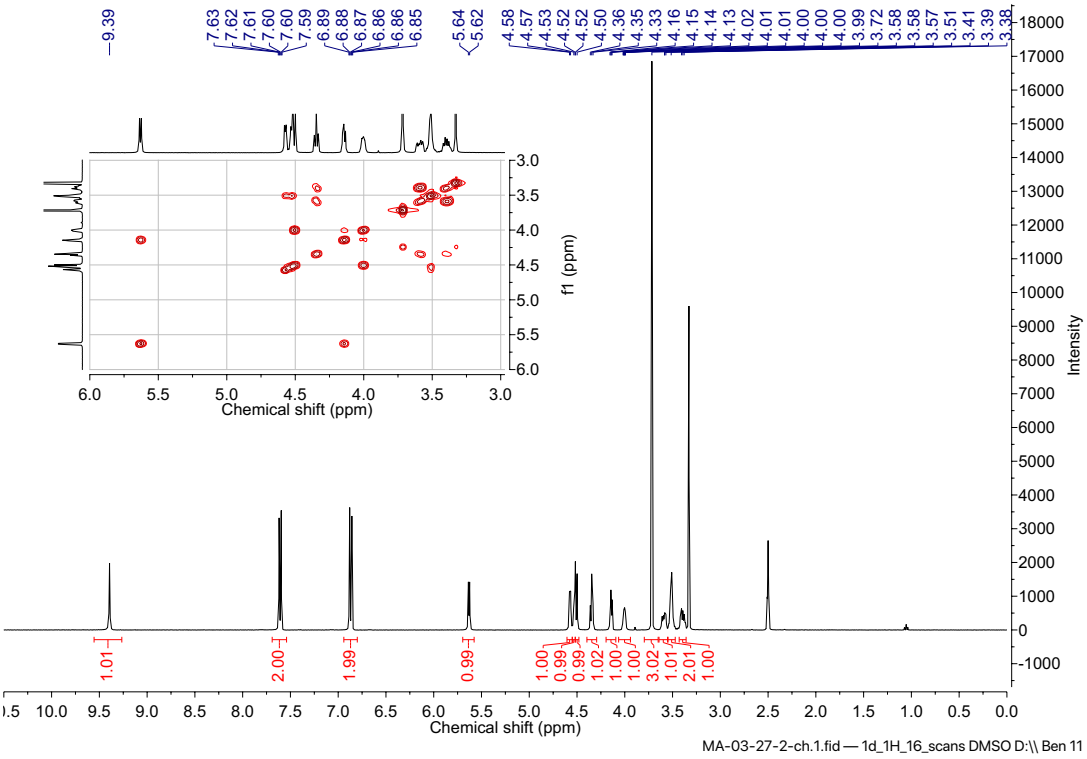

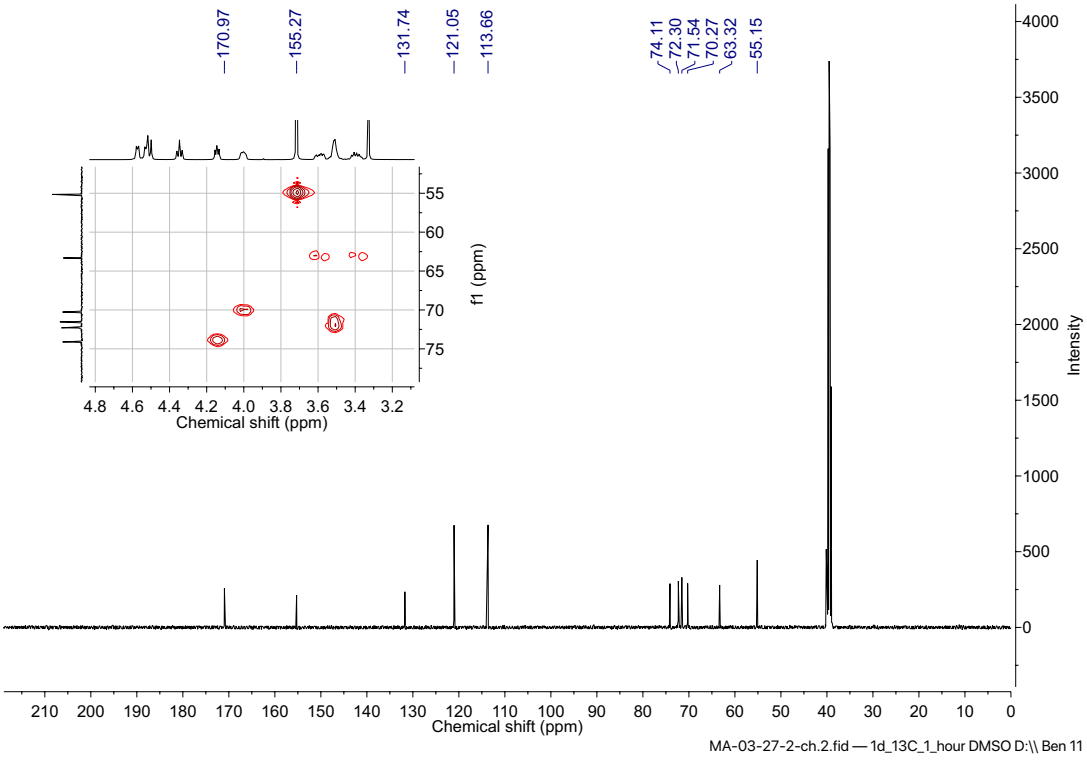

Compound 3.64

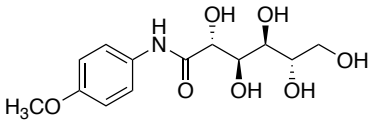

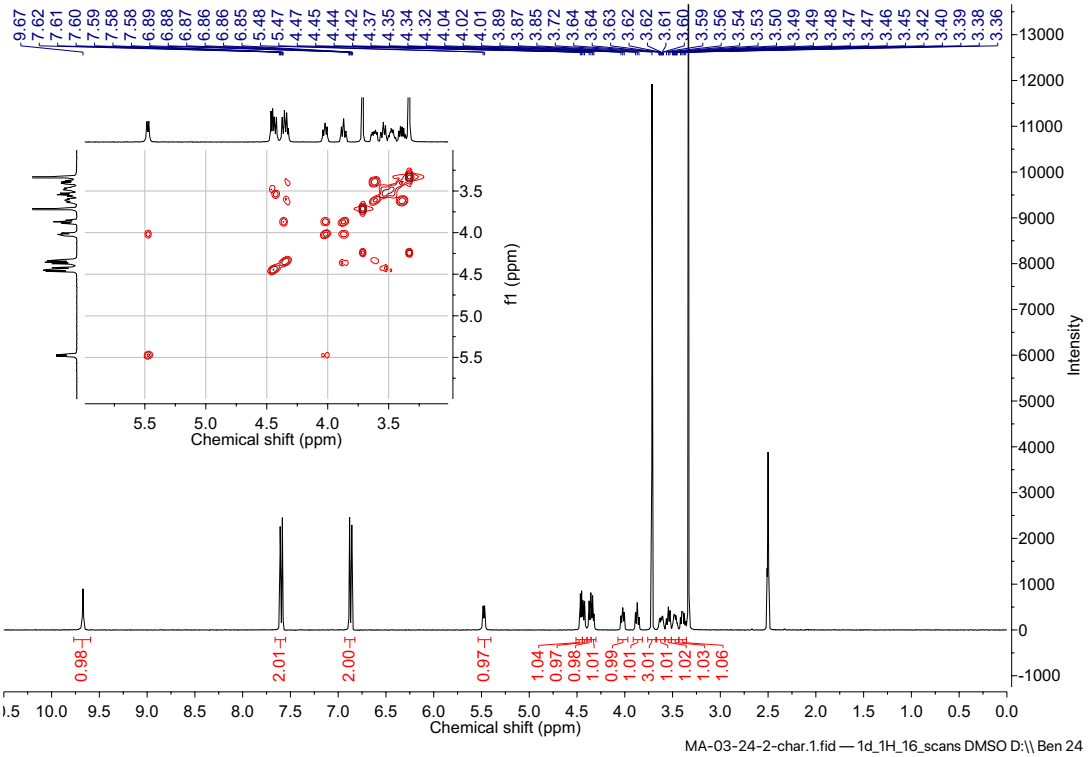

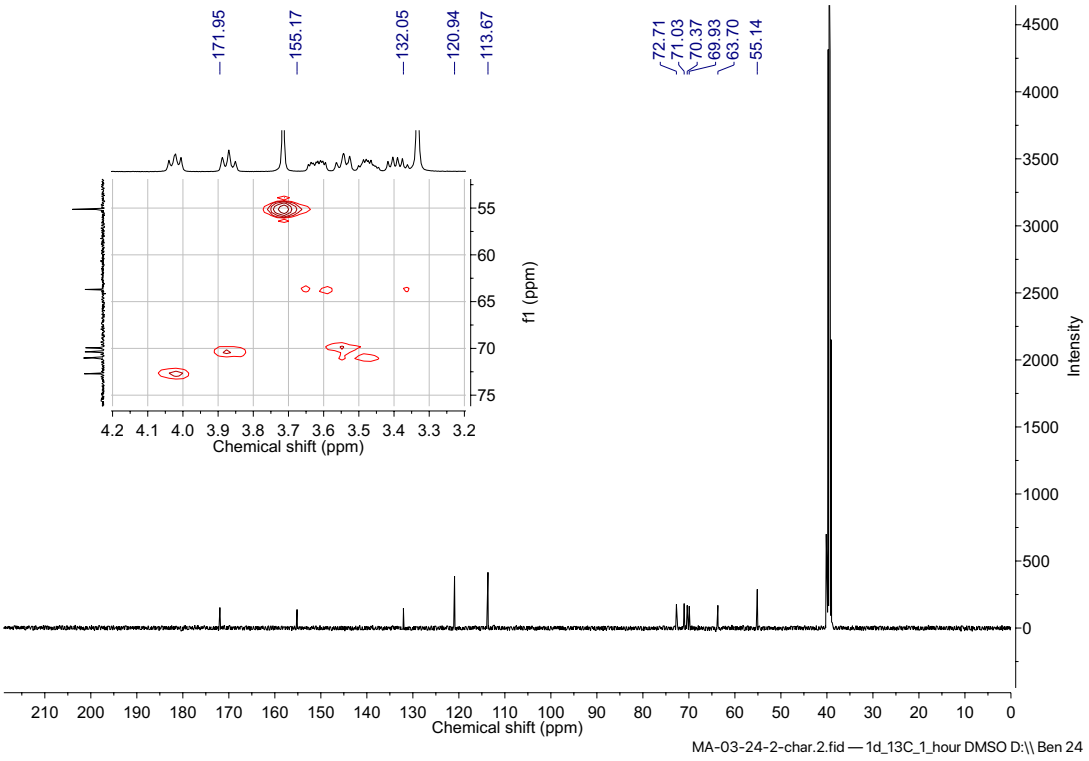

Compound 3.78

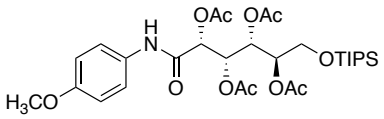

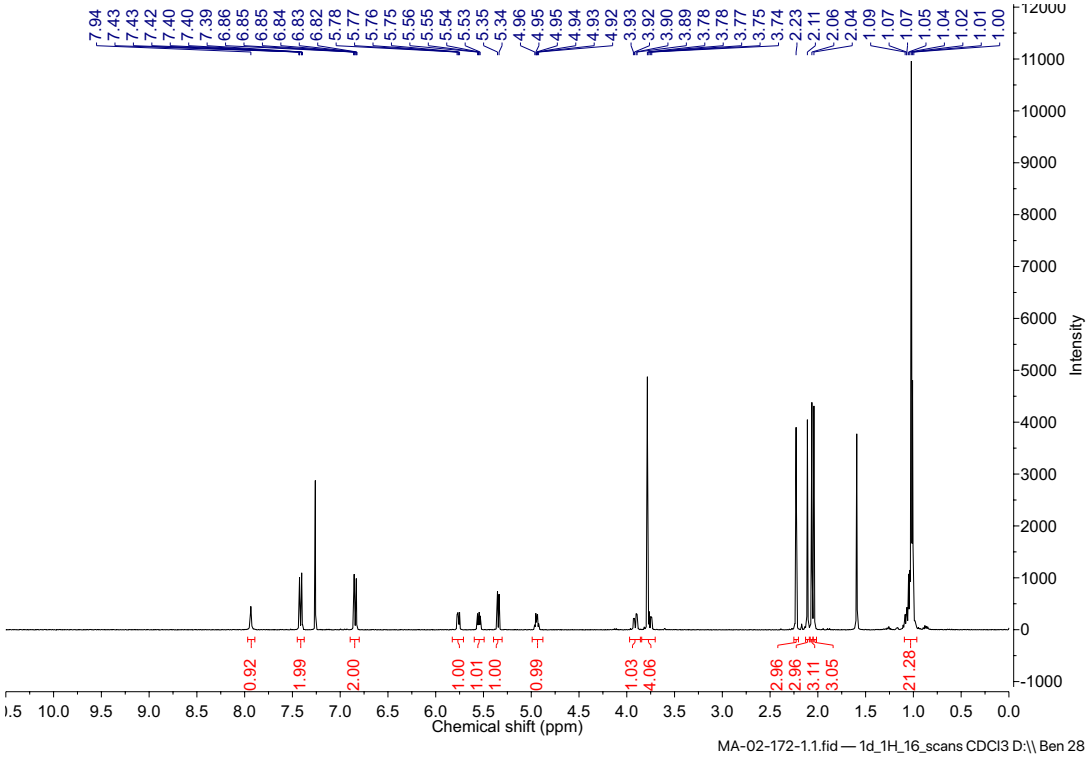

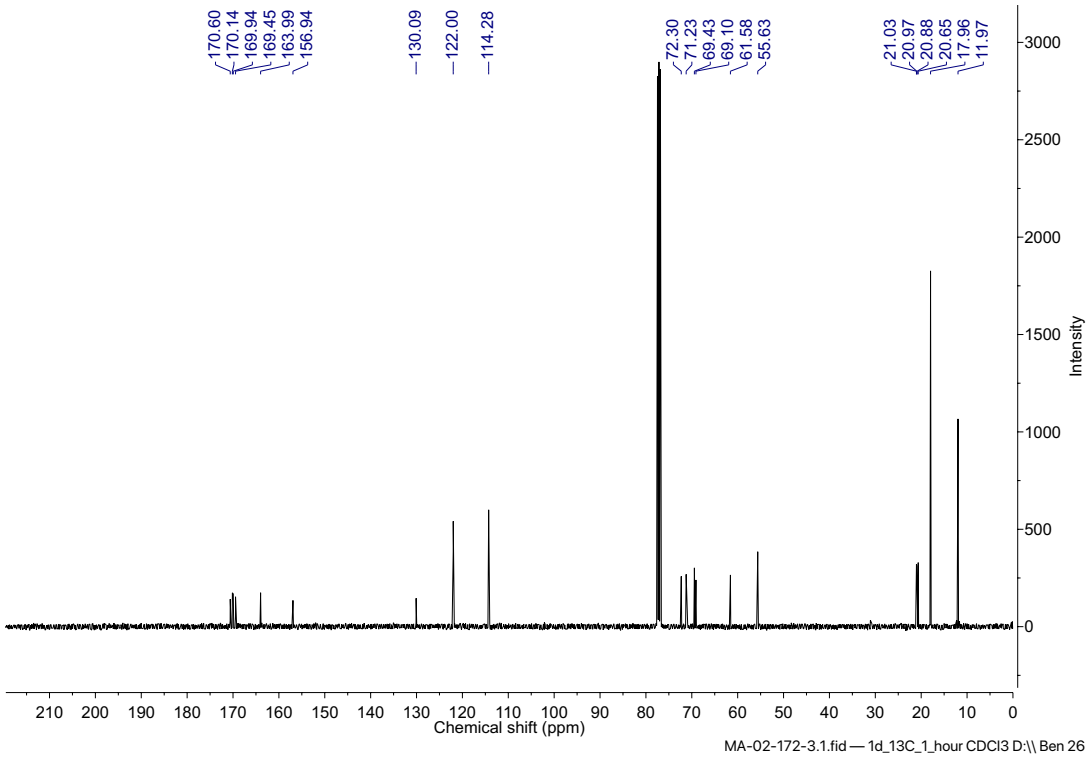

Compound 3.65

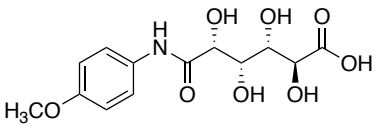

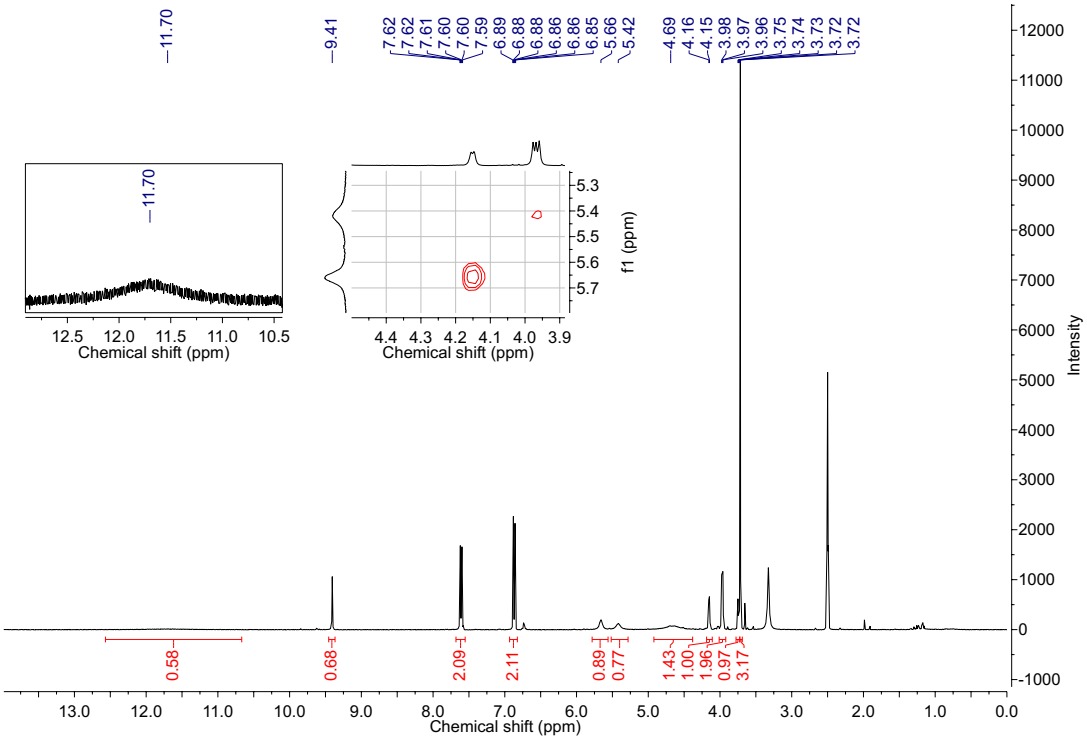

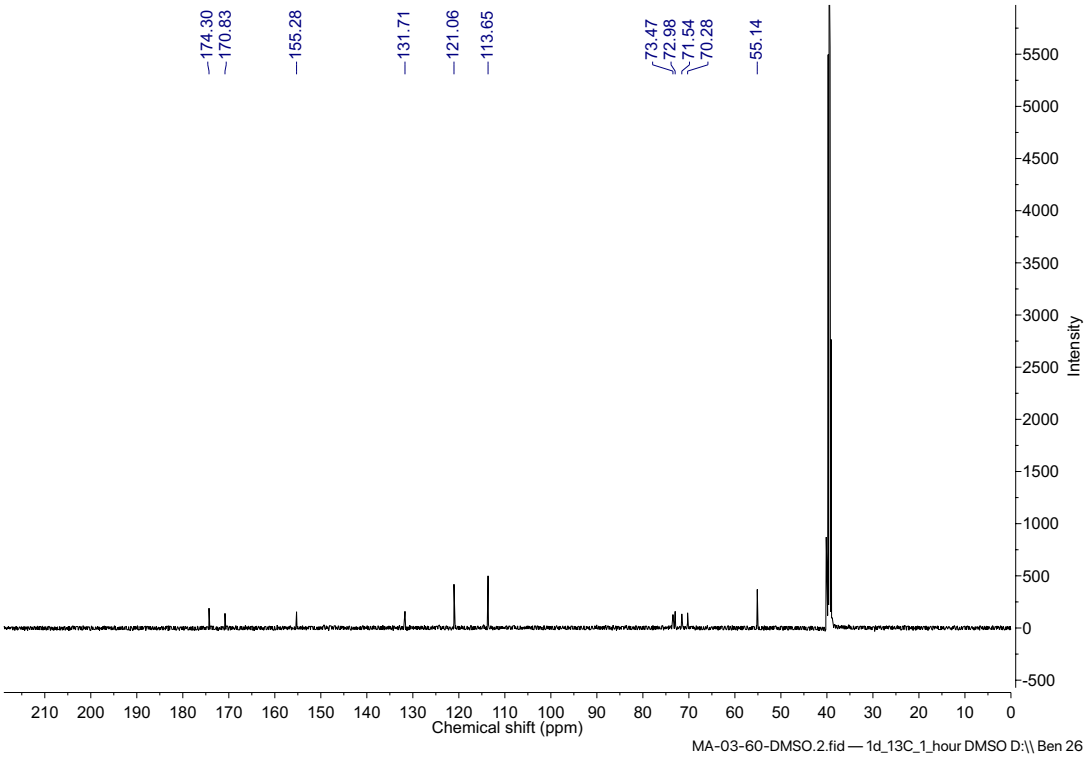

Compound 3.66

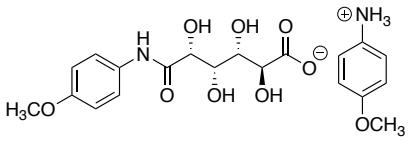

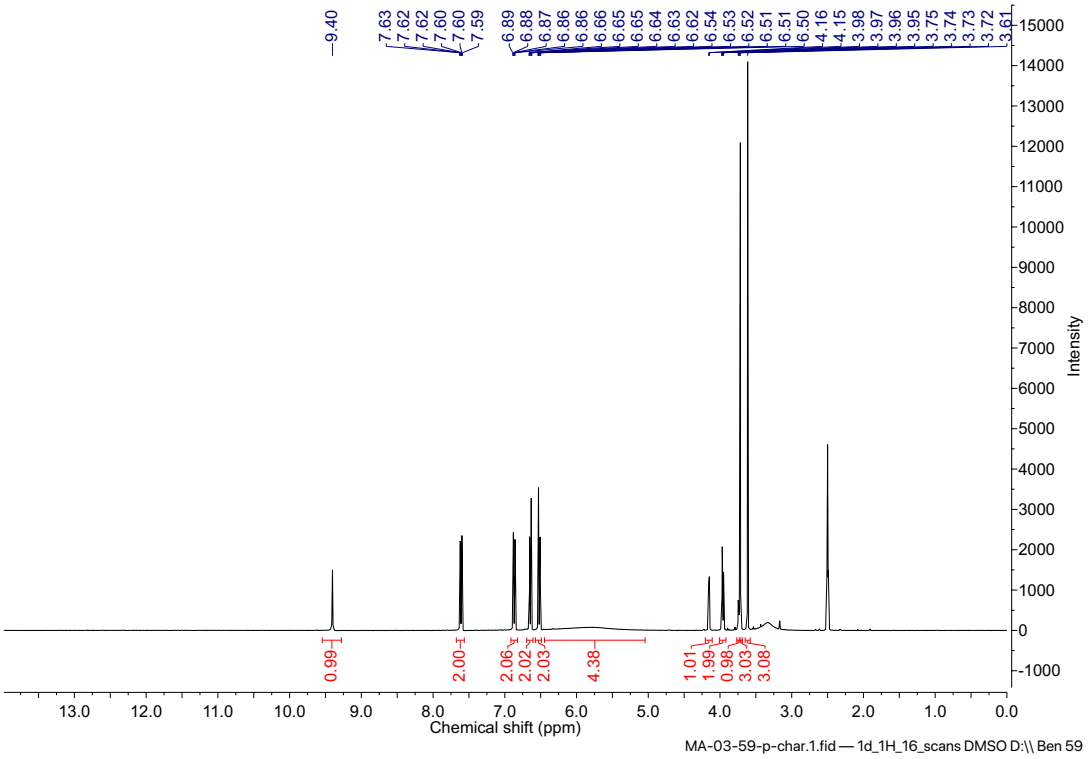

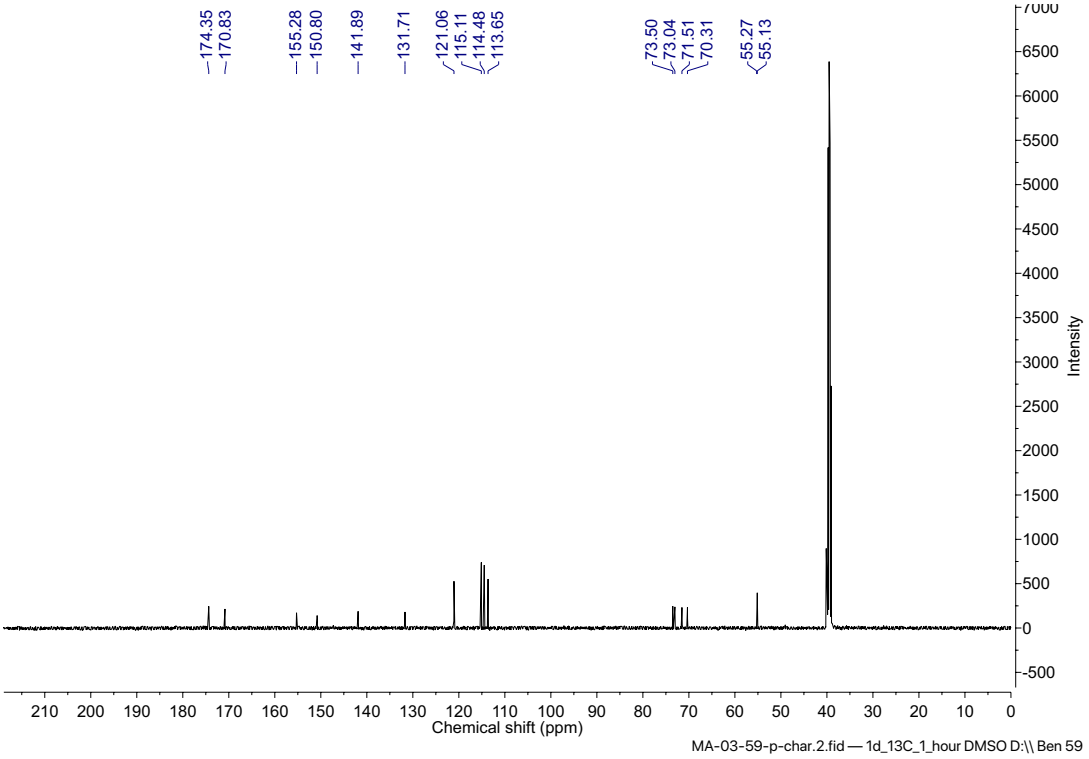

Compound 3.67

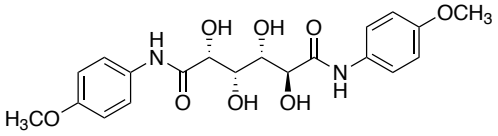

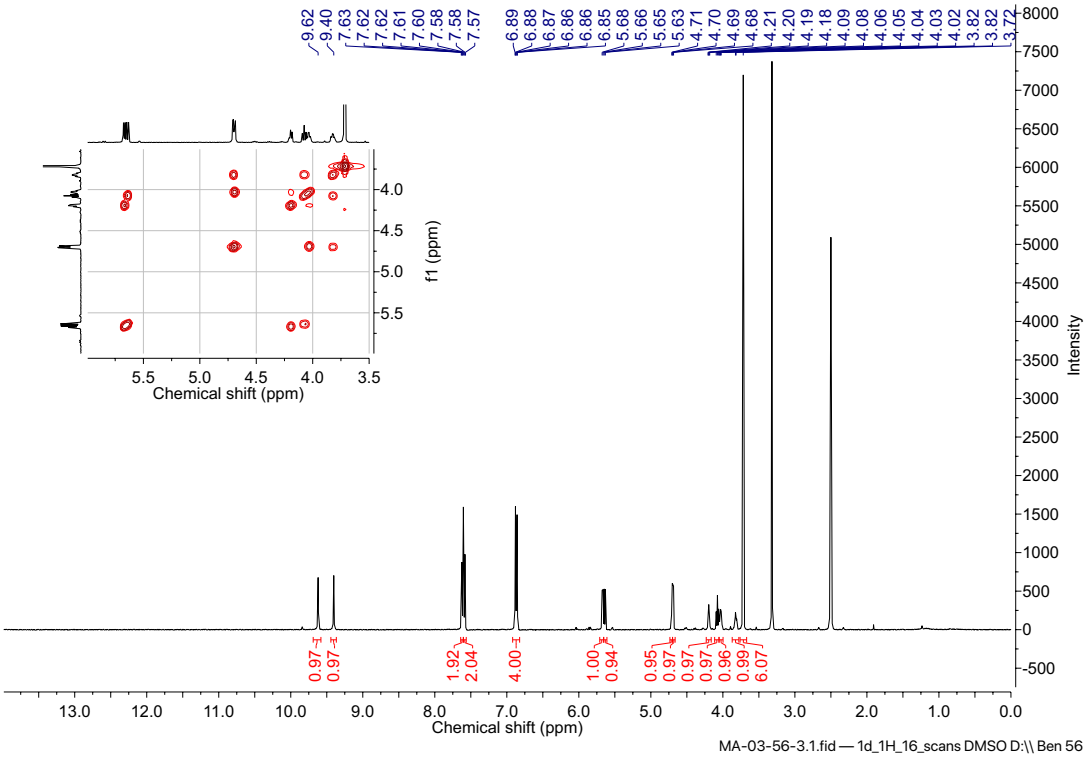

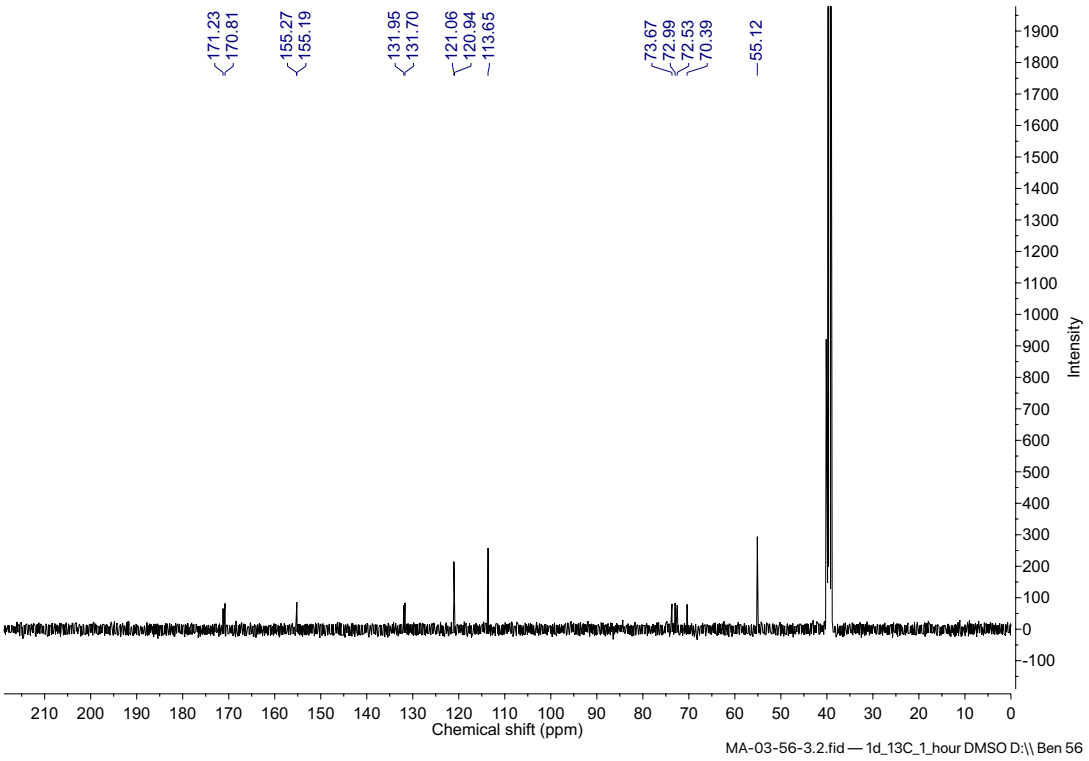

Compound 3.68

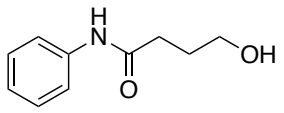

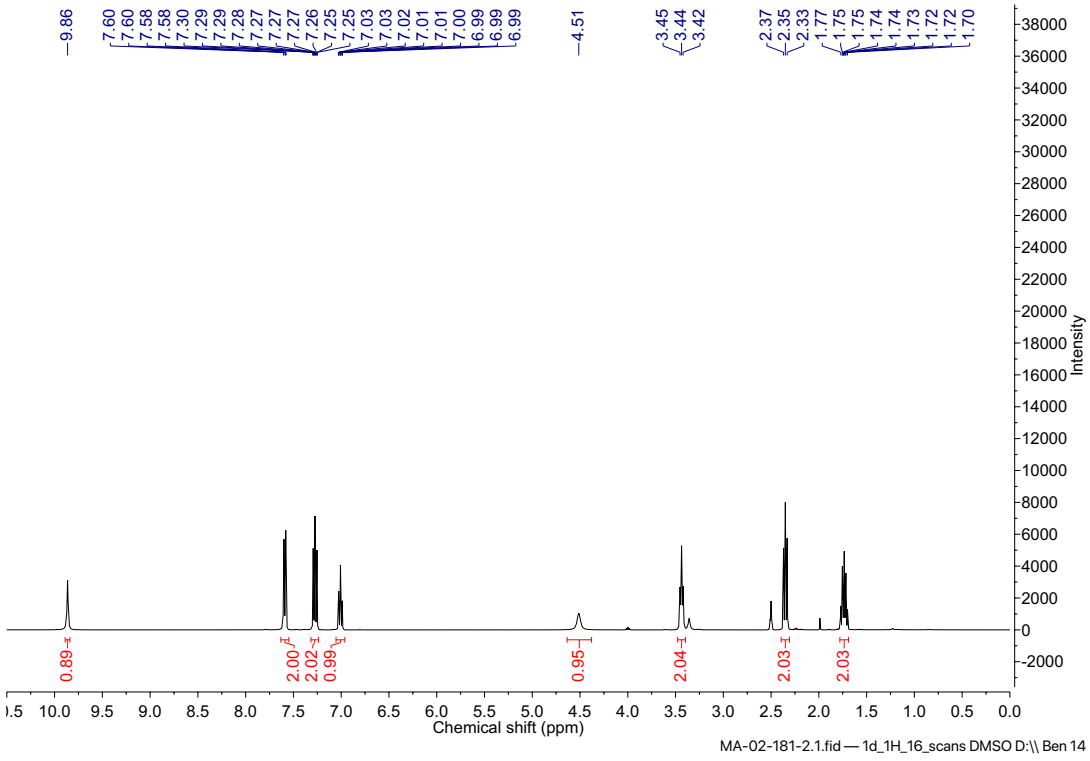

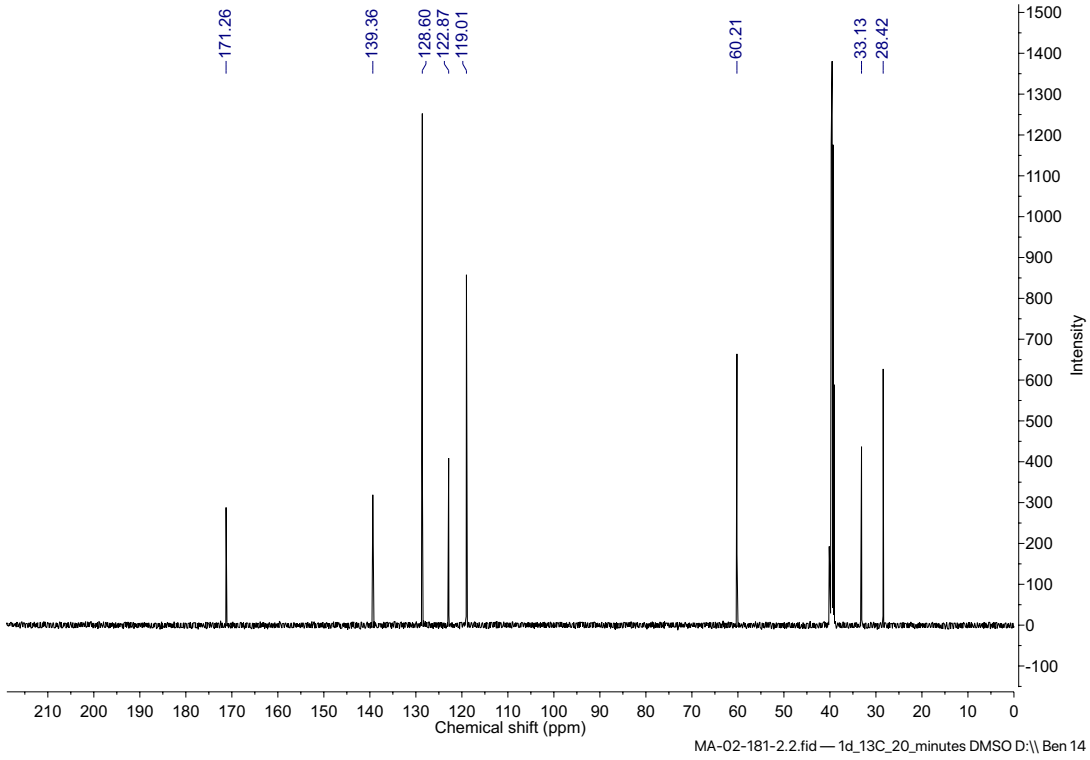

Compound 3.69

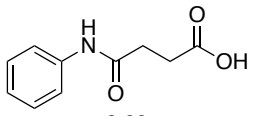

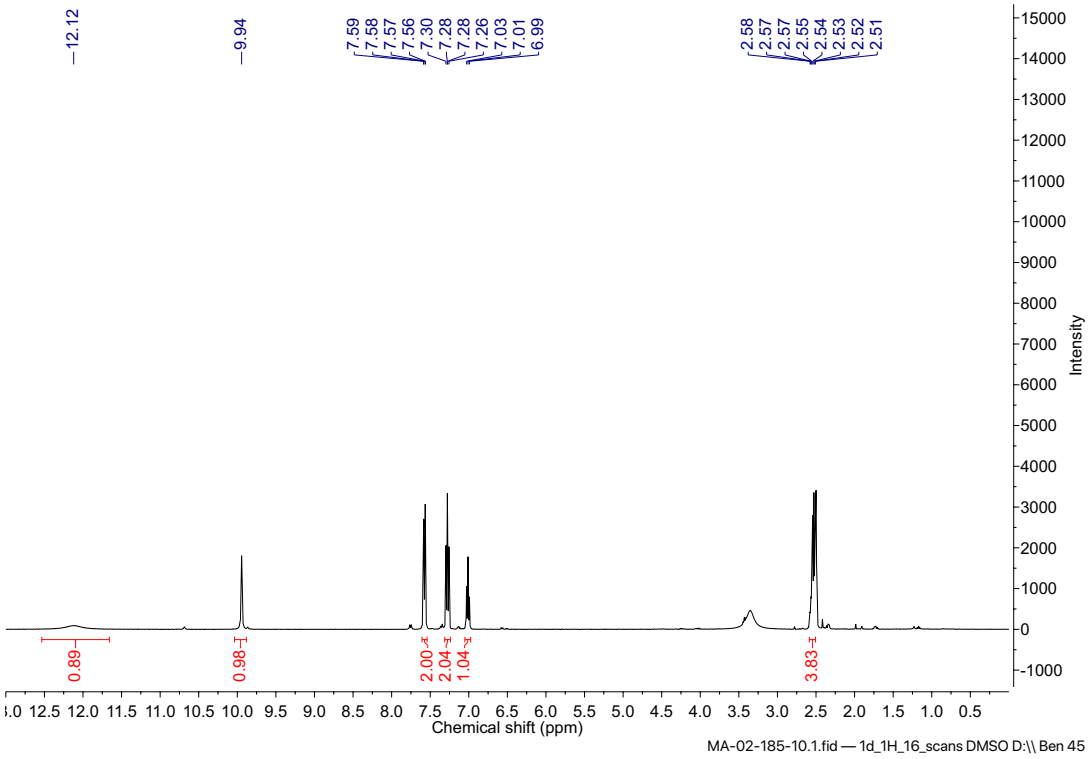

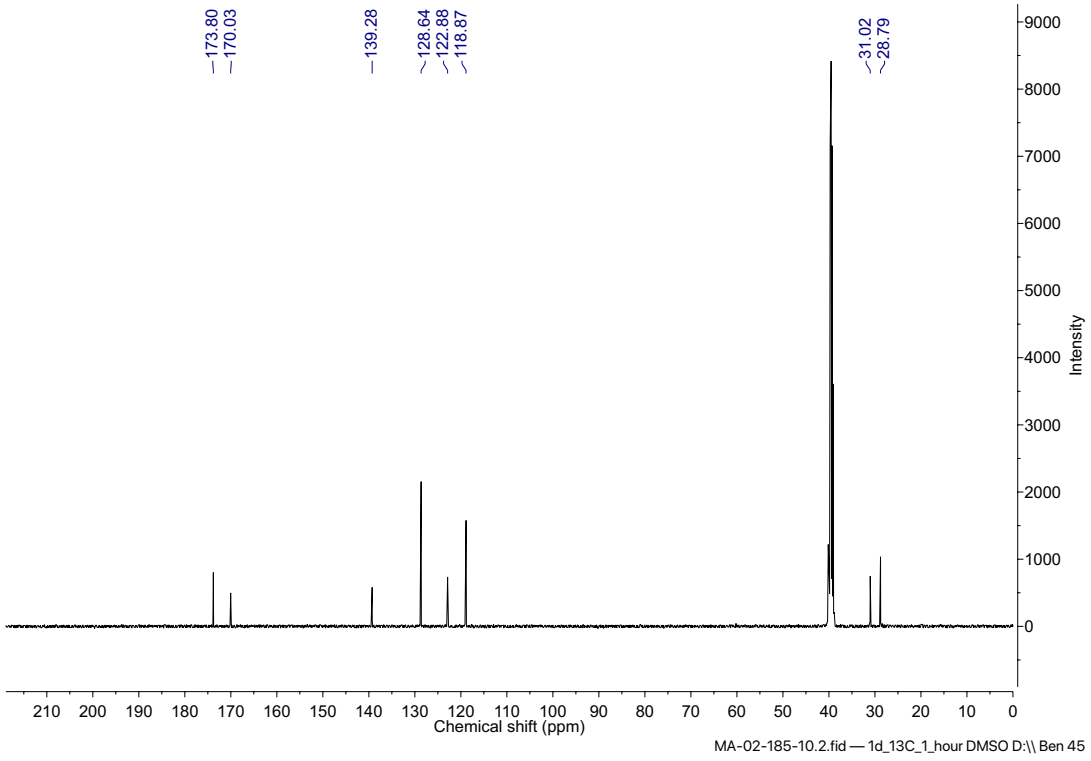

Compound 3.70

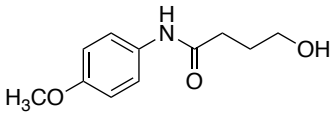

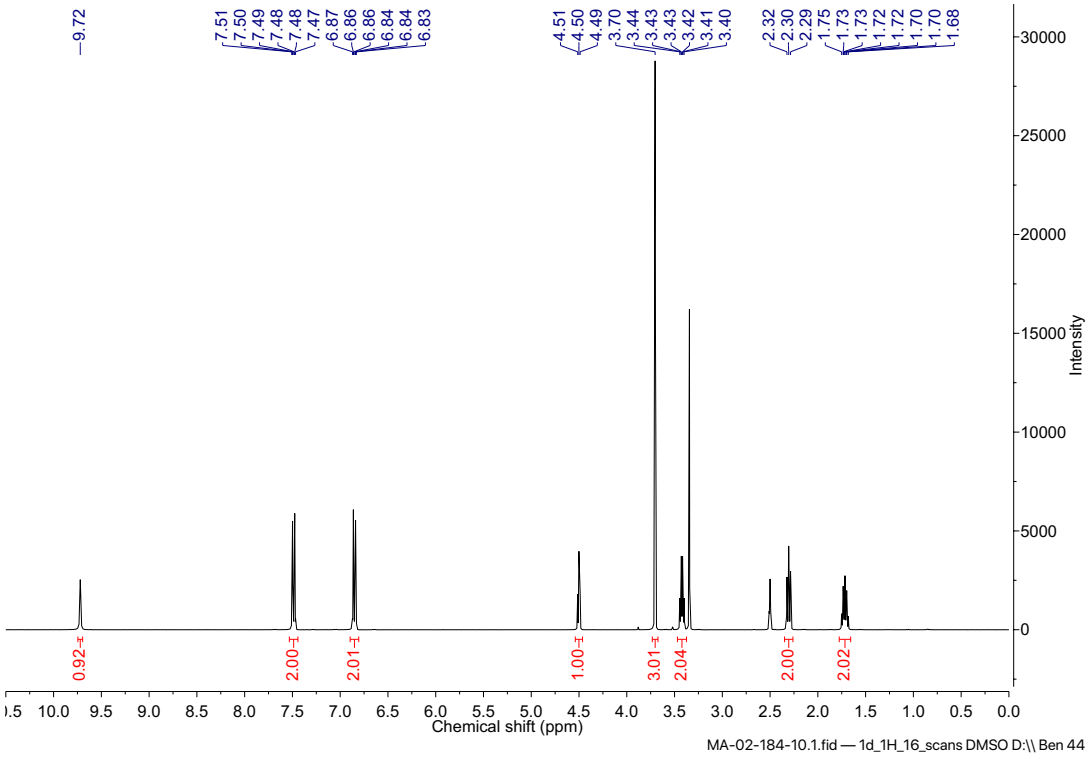

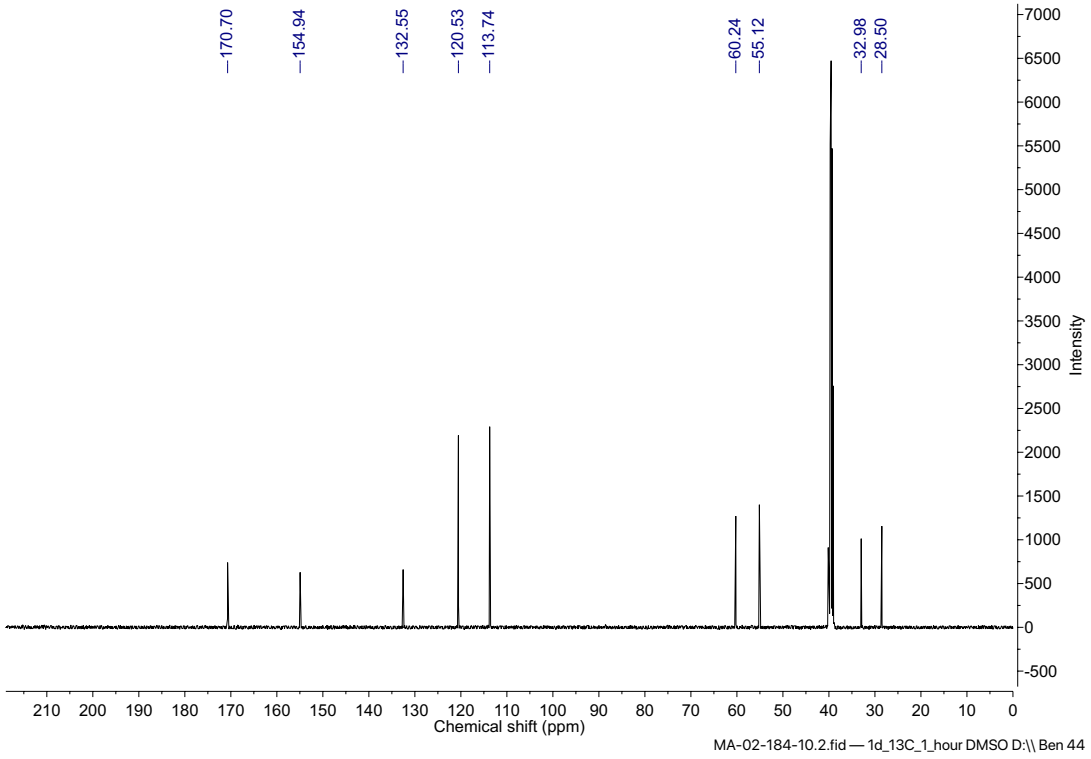

Compound 3.71

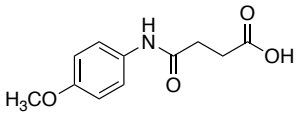

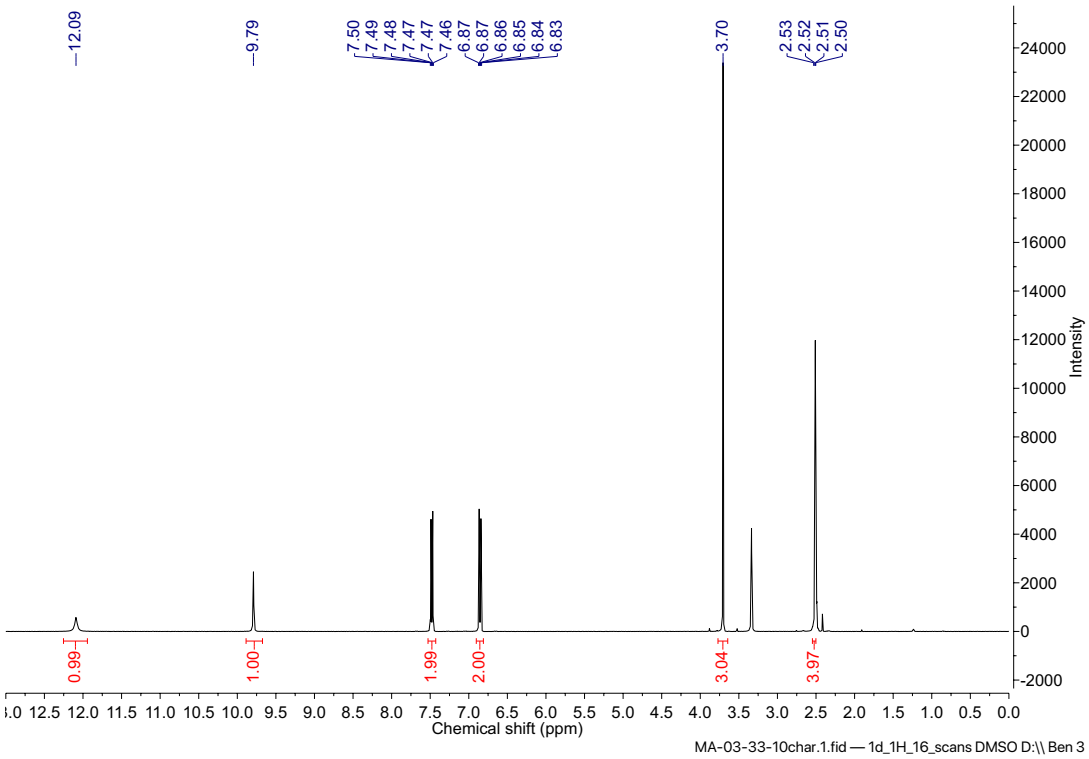

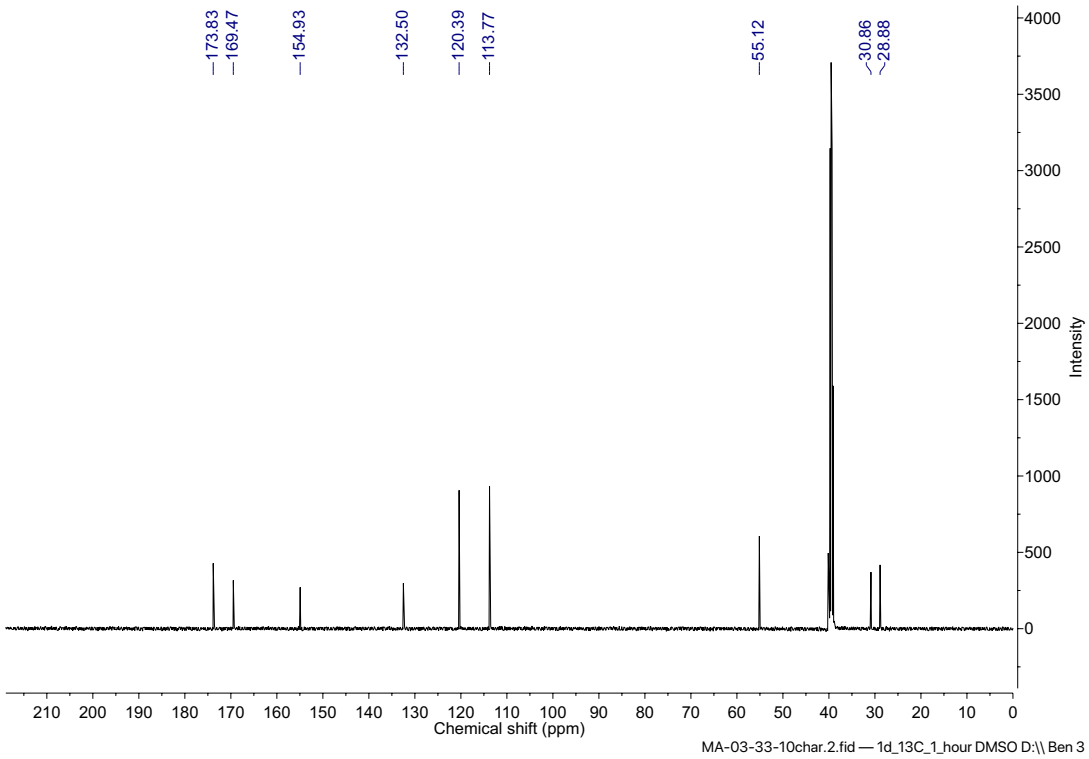

Compound 3.72

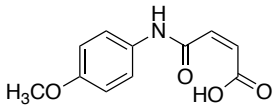

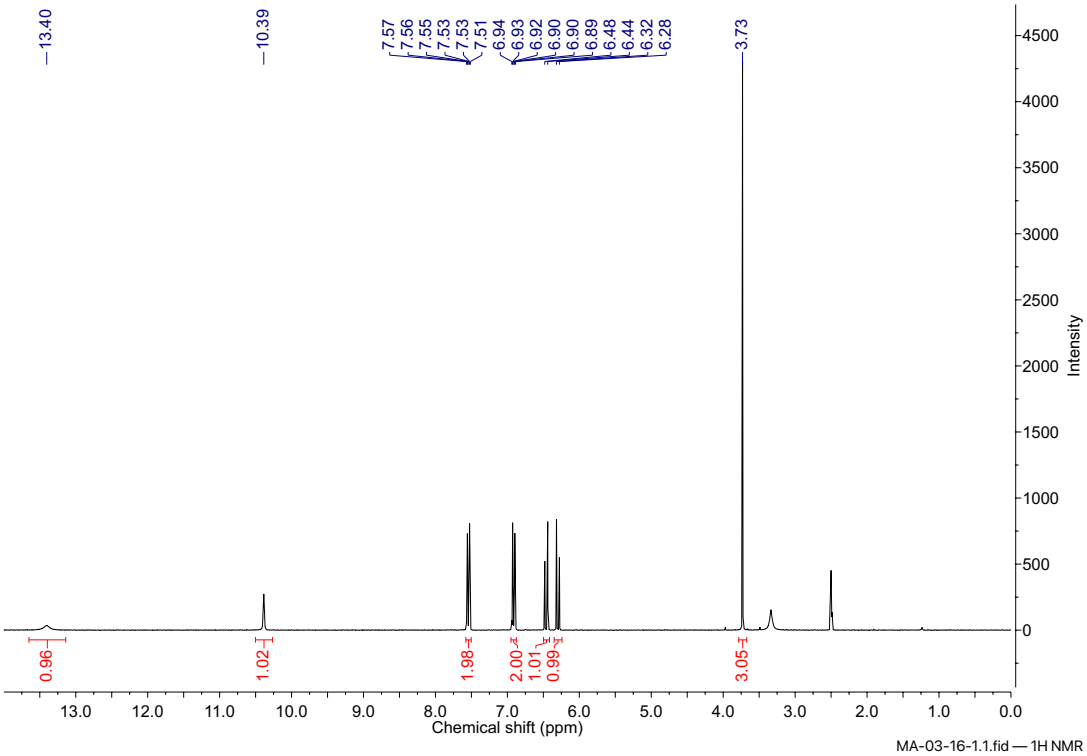

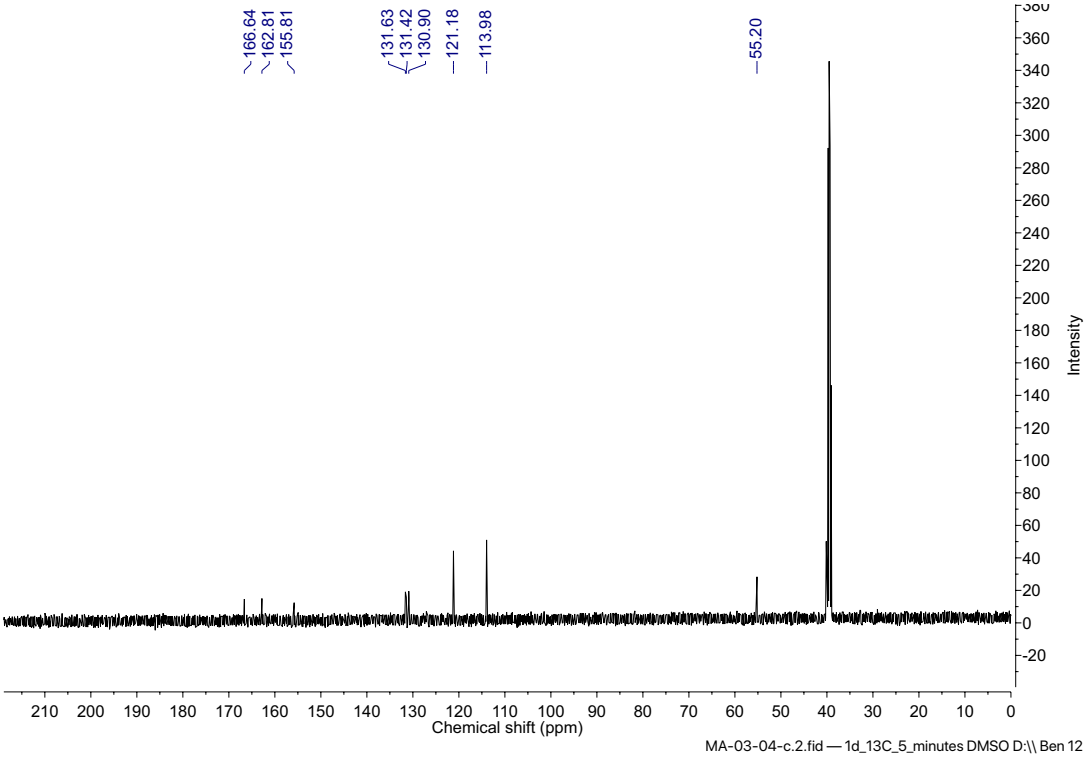

Compound 3.73

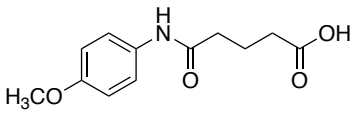

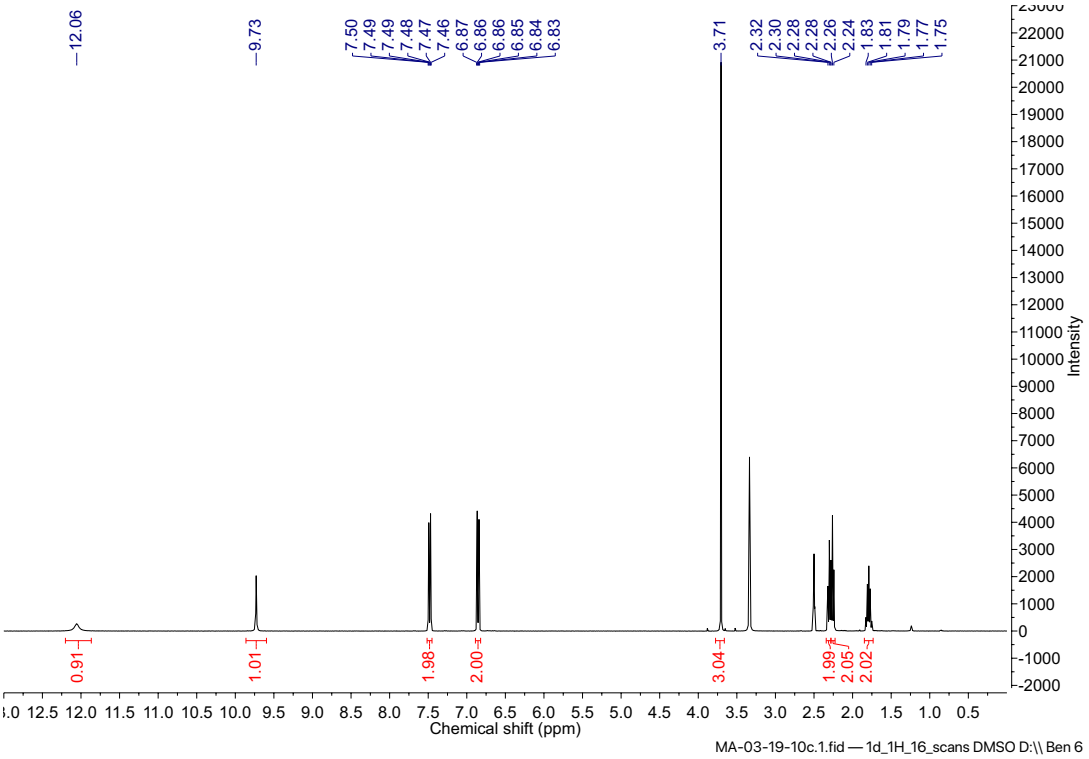

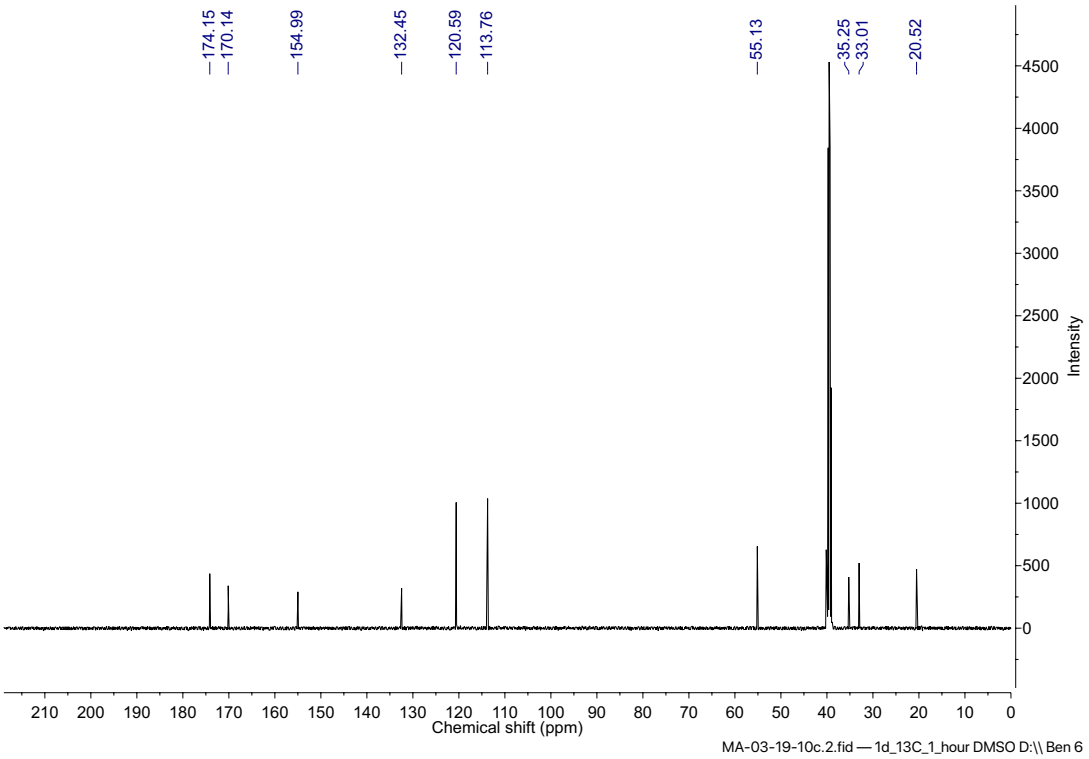

Compound 3.74

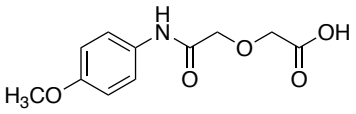

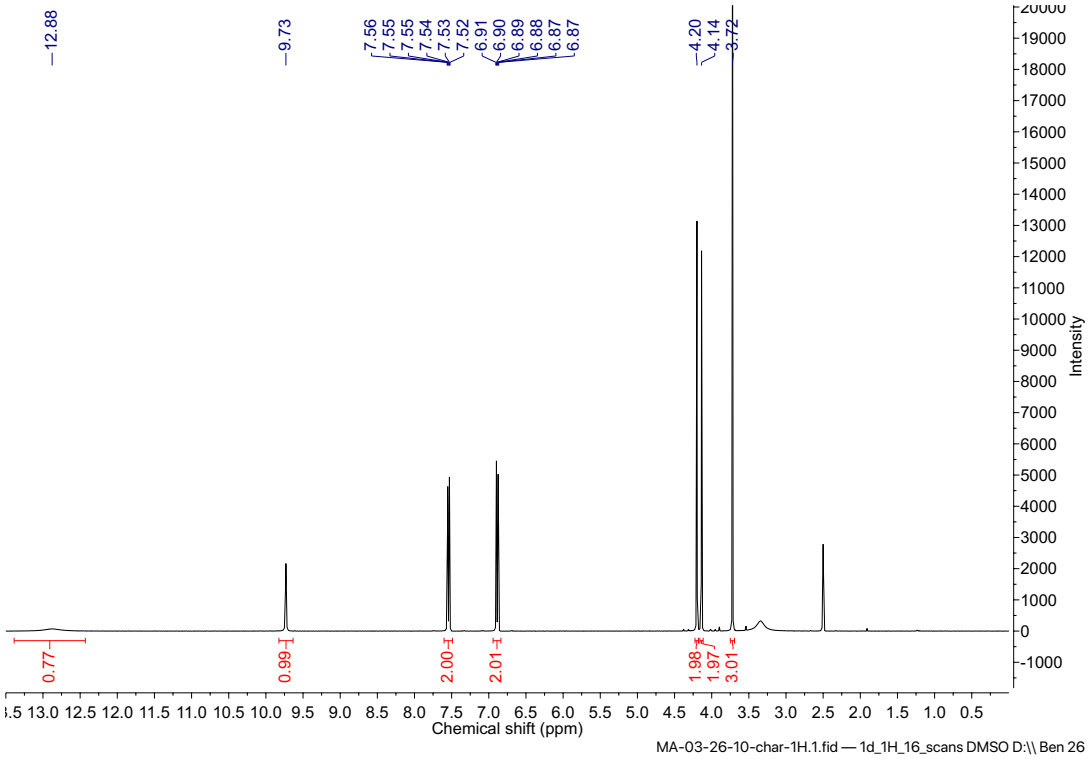

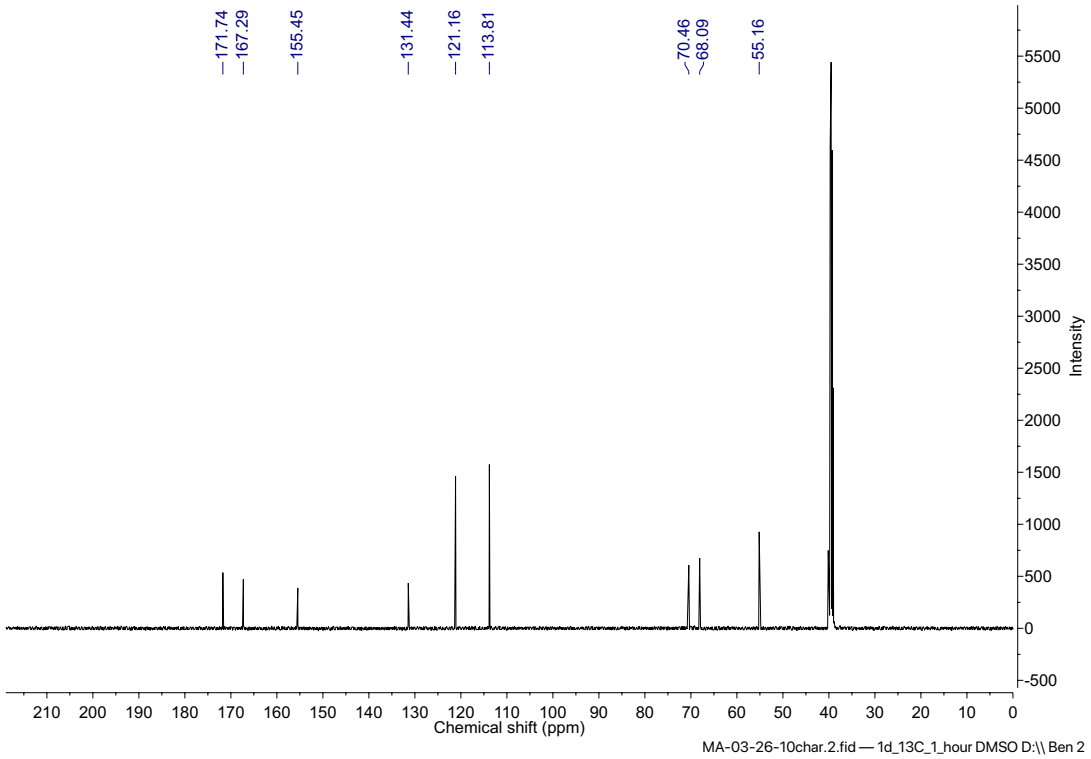

Compound 3.86

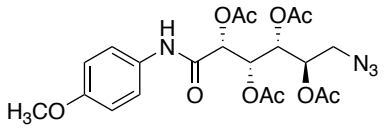

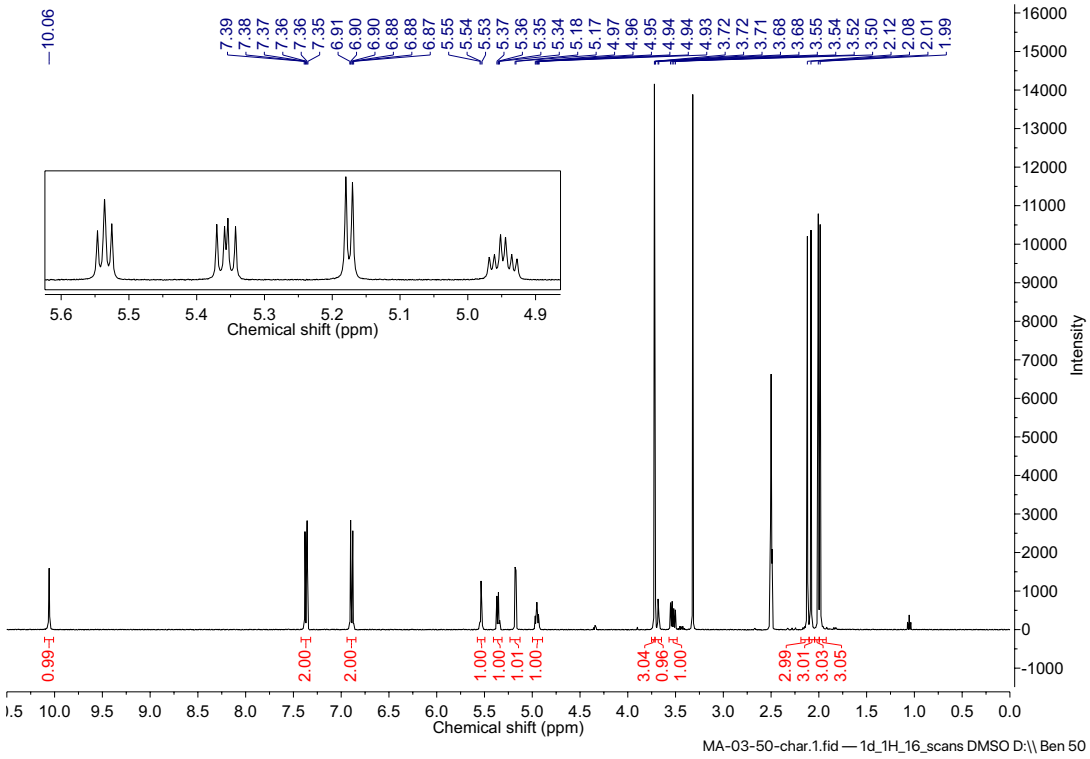

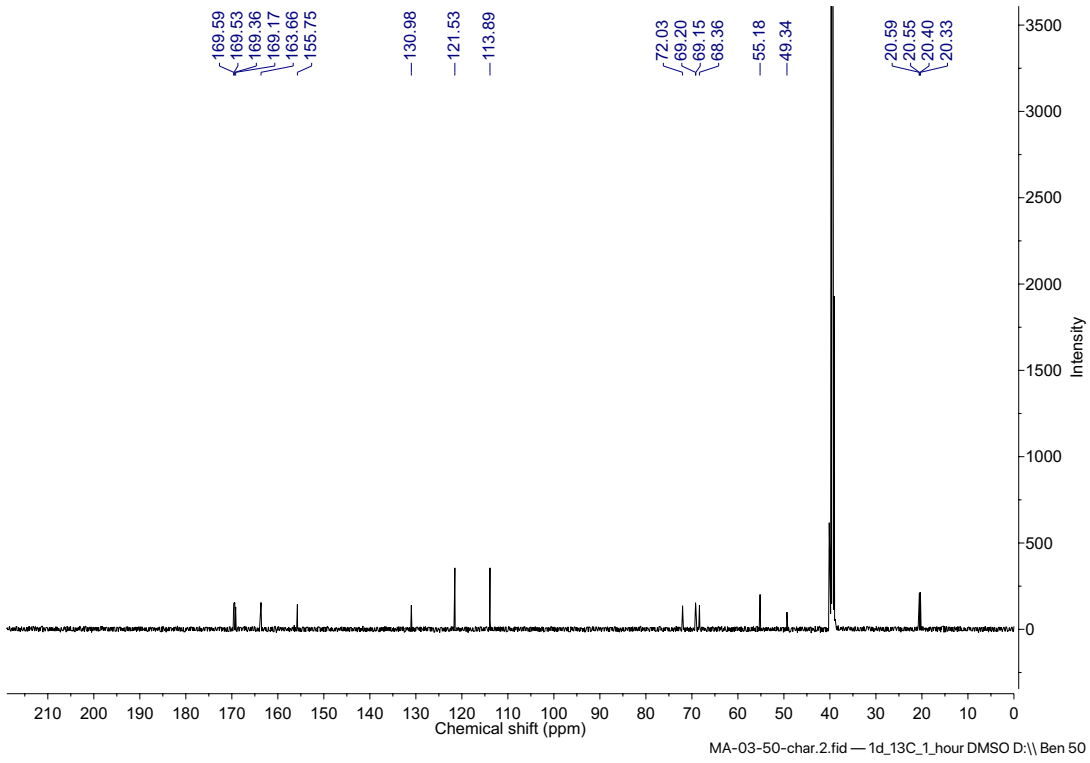

Compound 3.80

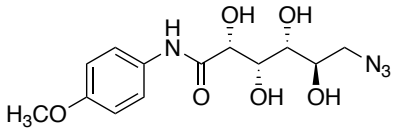

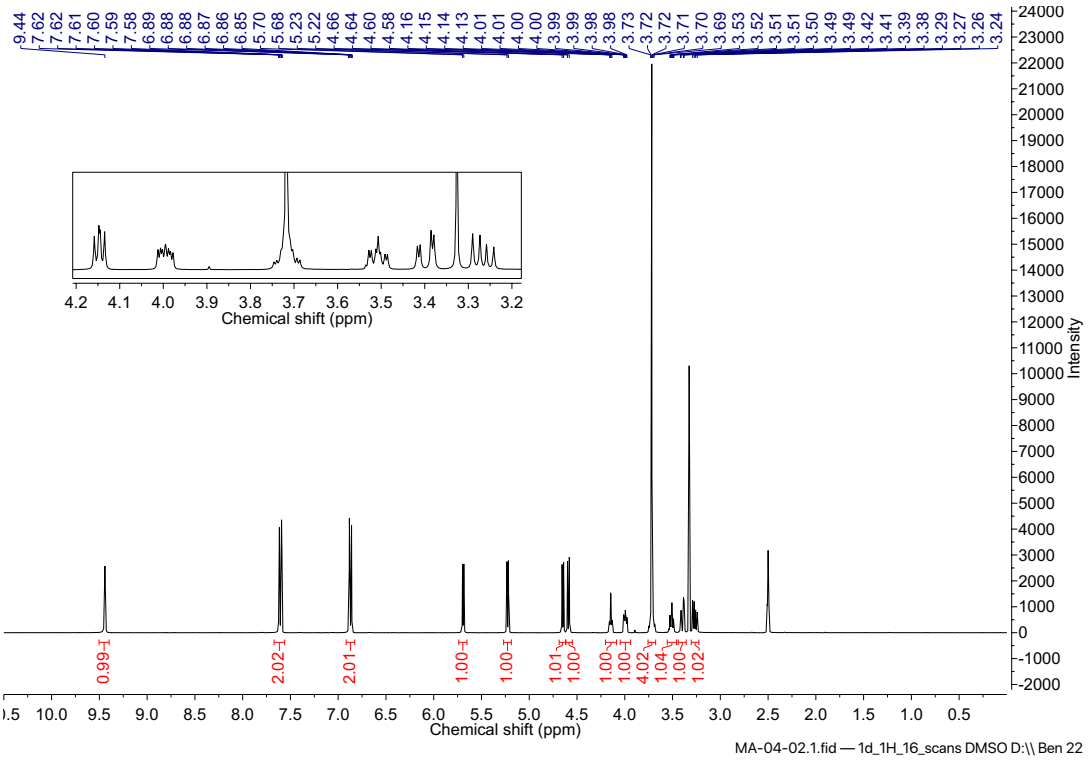

MA-04-02.1.fid — 1d_1H_16_scans DMSO D:\\ Ben 22

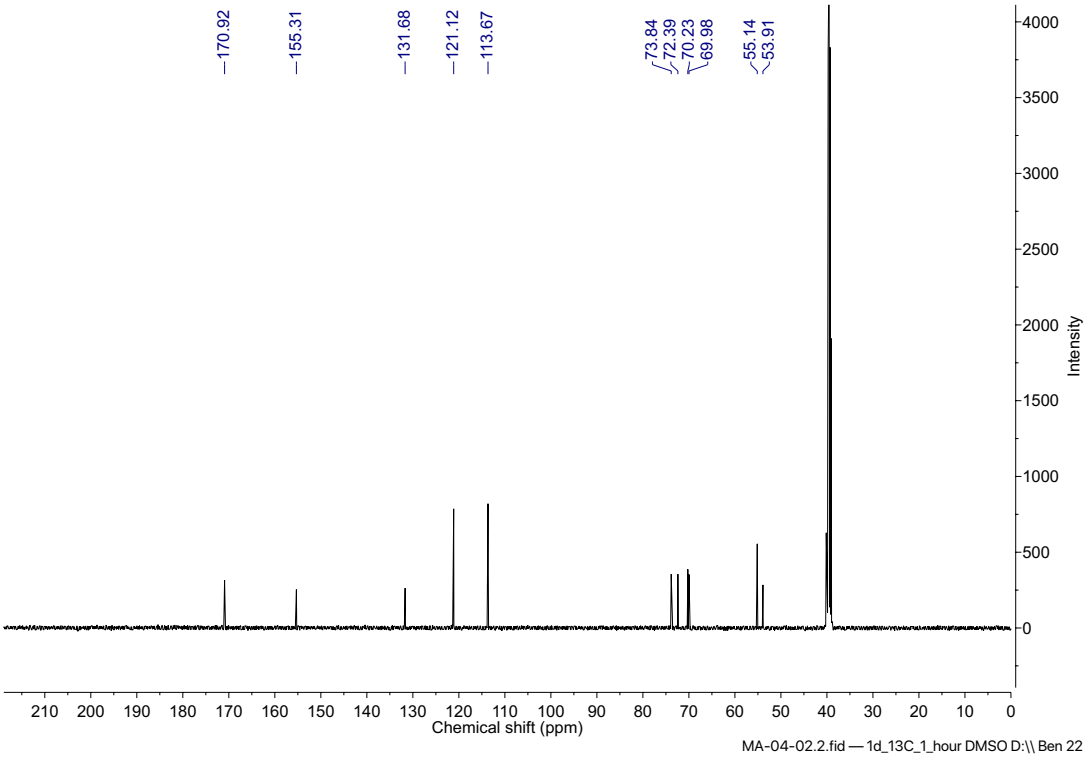

MA-04-02.2.fid — 1d_13C_1_hour DMSO D:\\ Ben 22

Compound 3.87

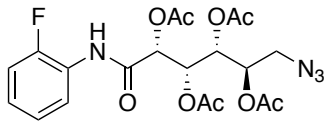

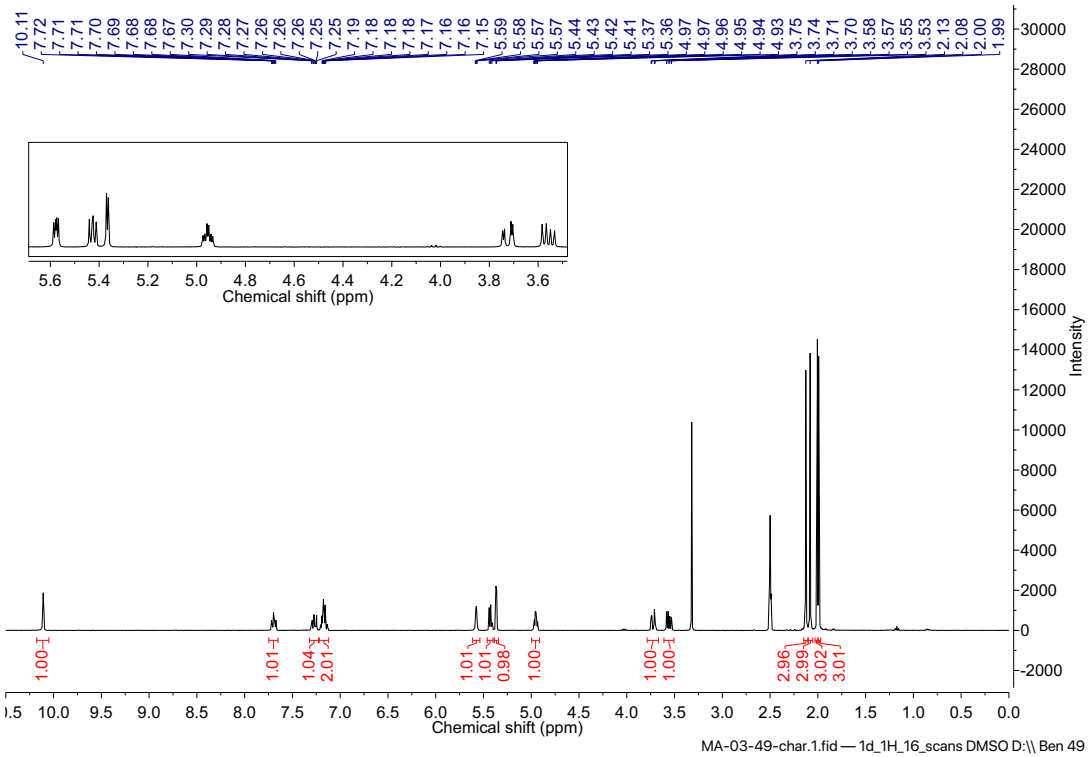

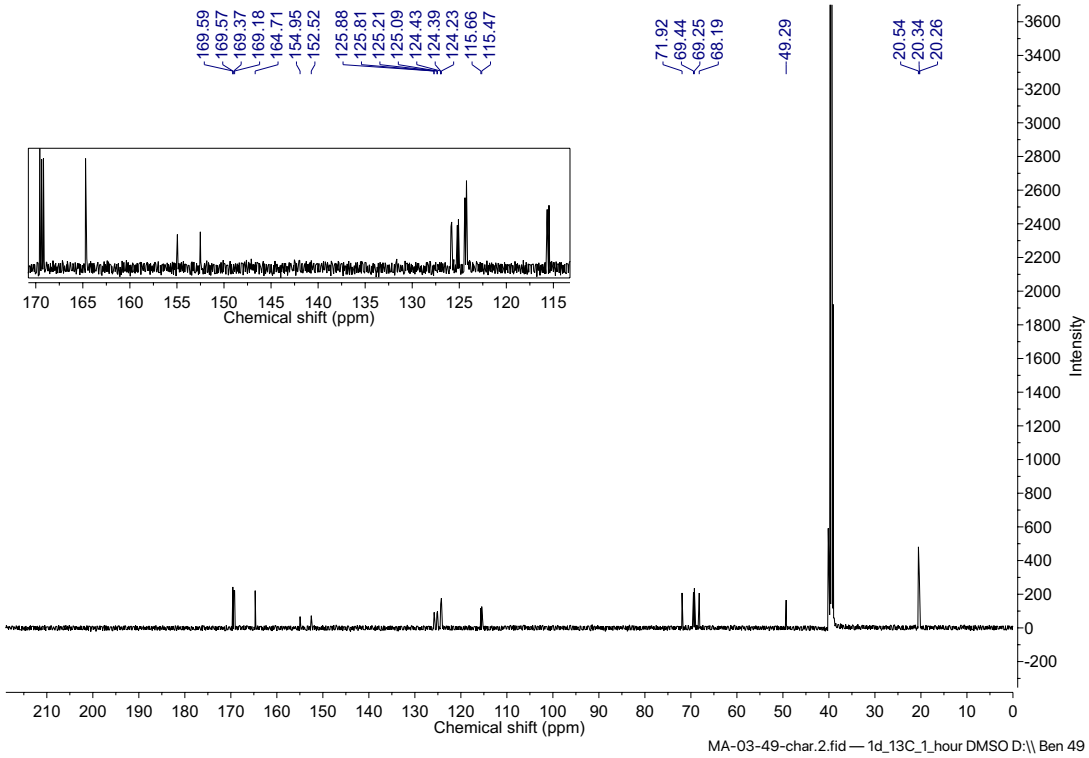

Compound 3.81

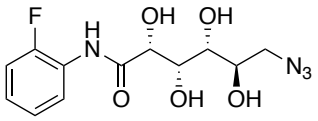

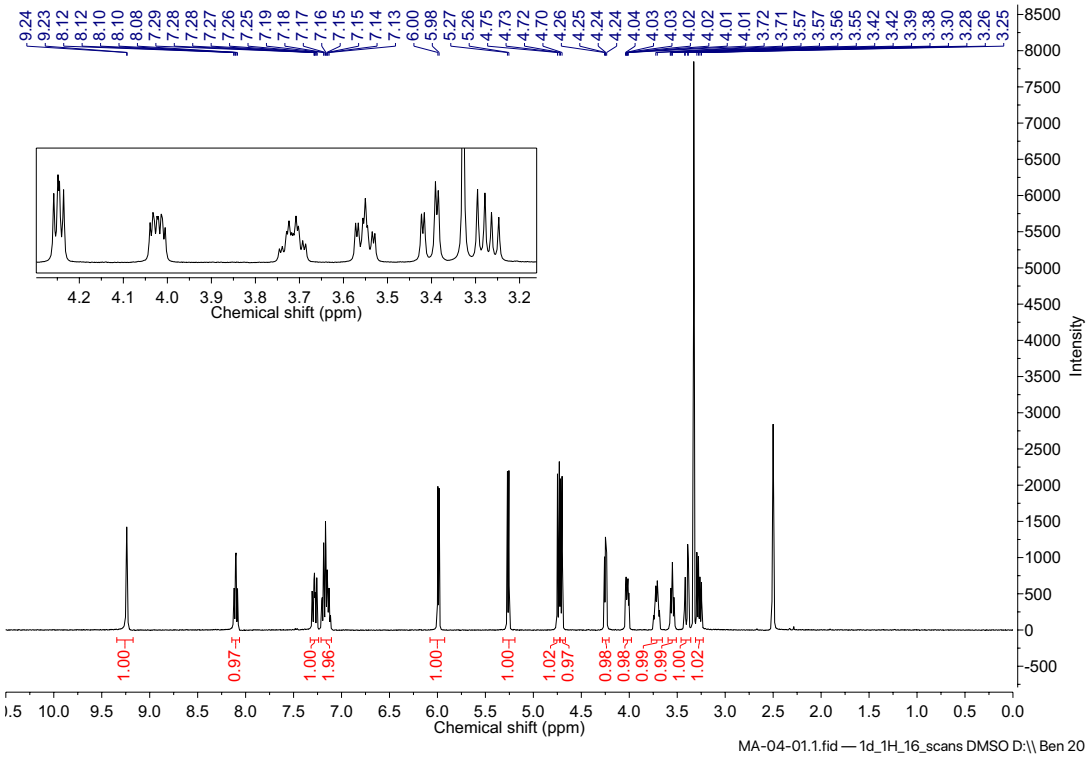

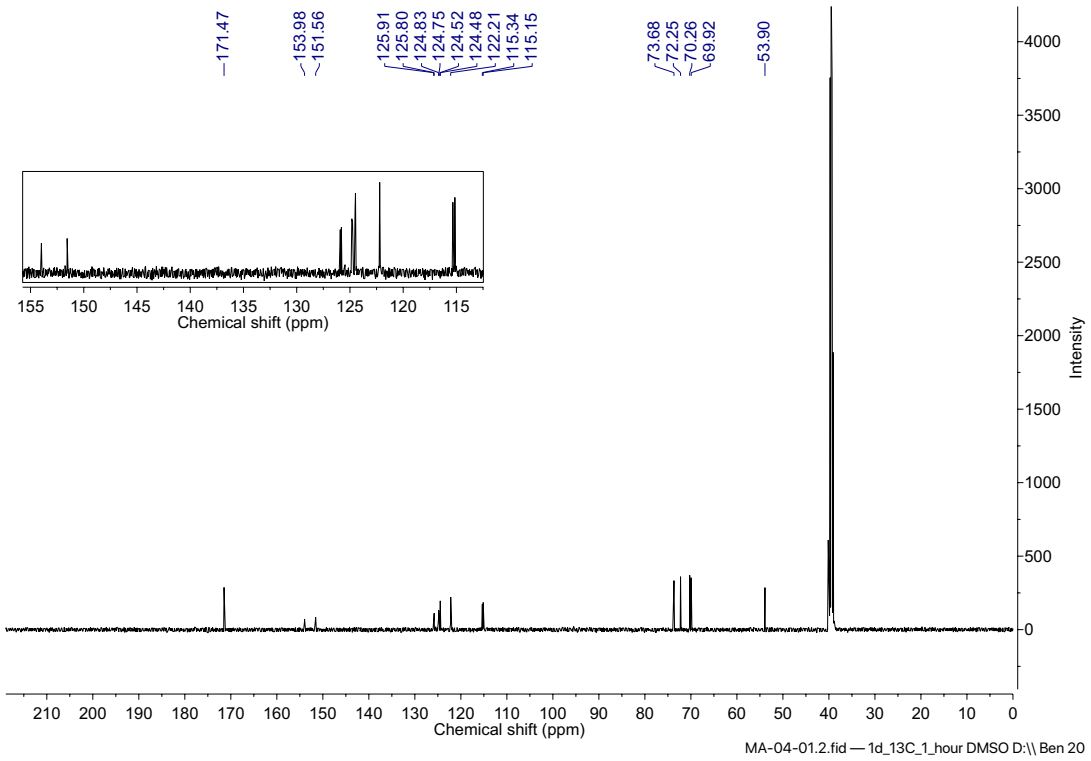

Compound 3.88

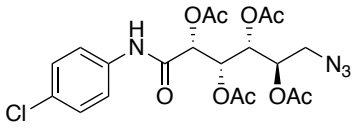

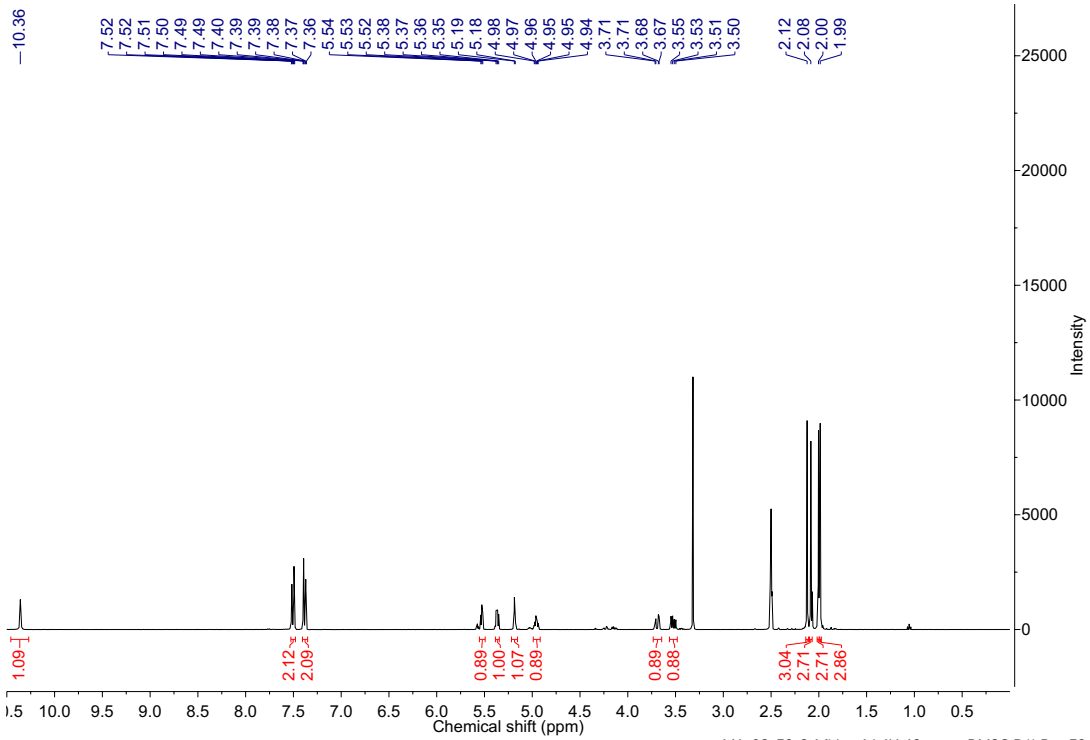

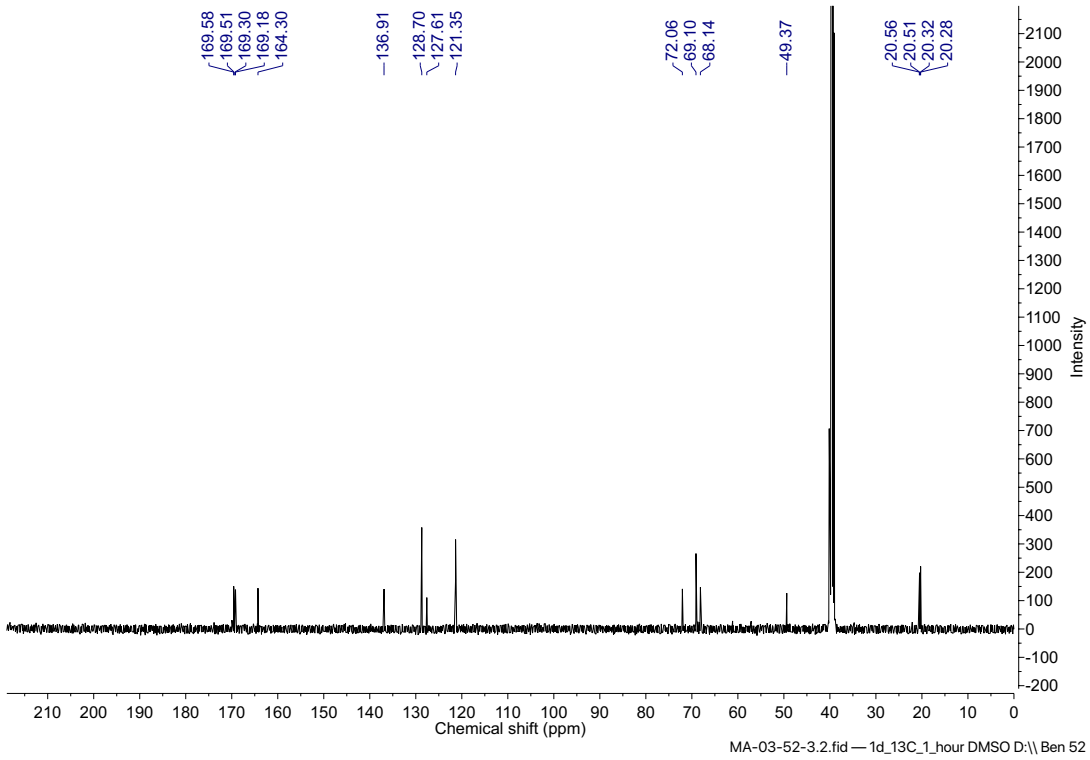

Compound 3.82

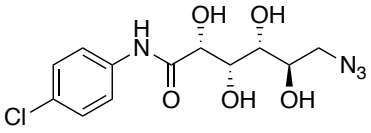

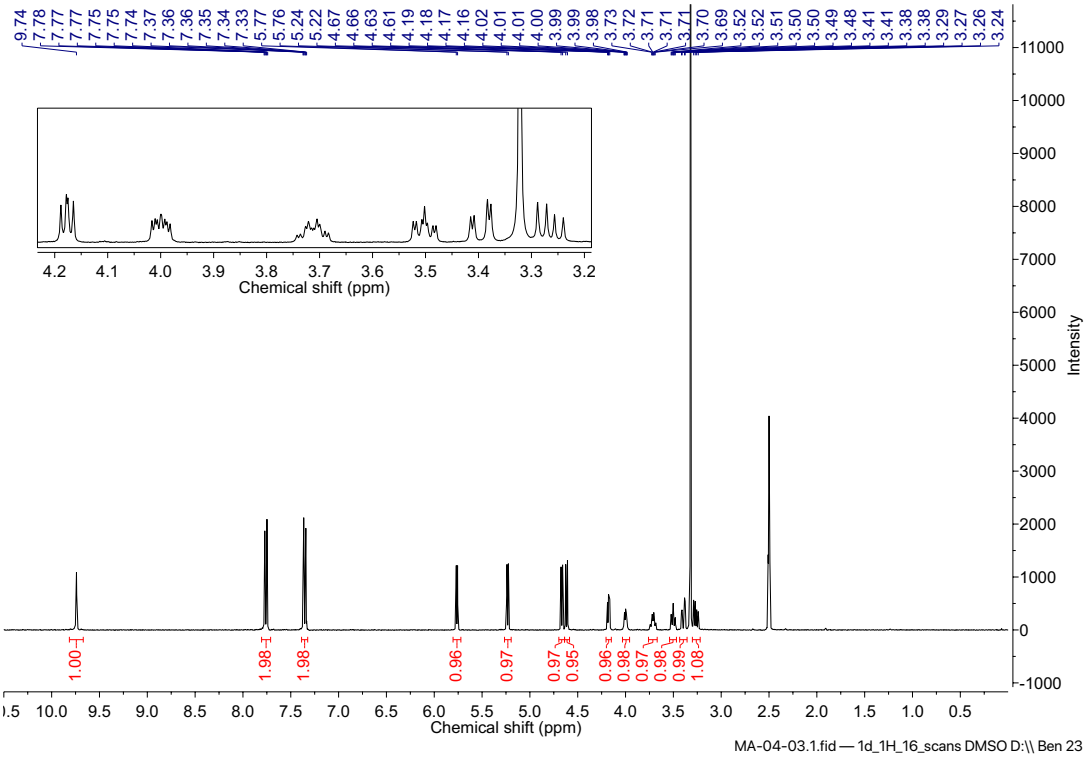

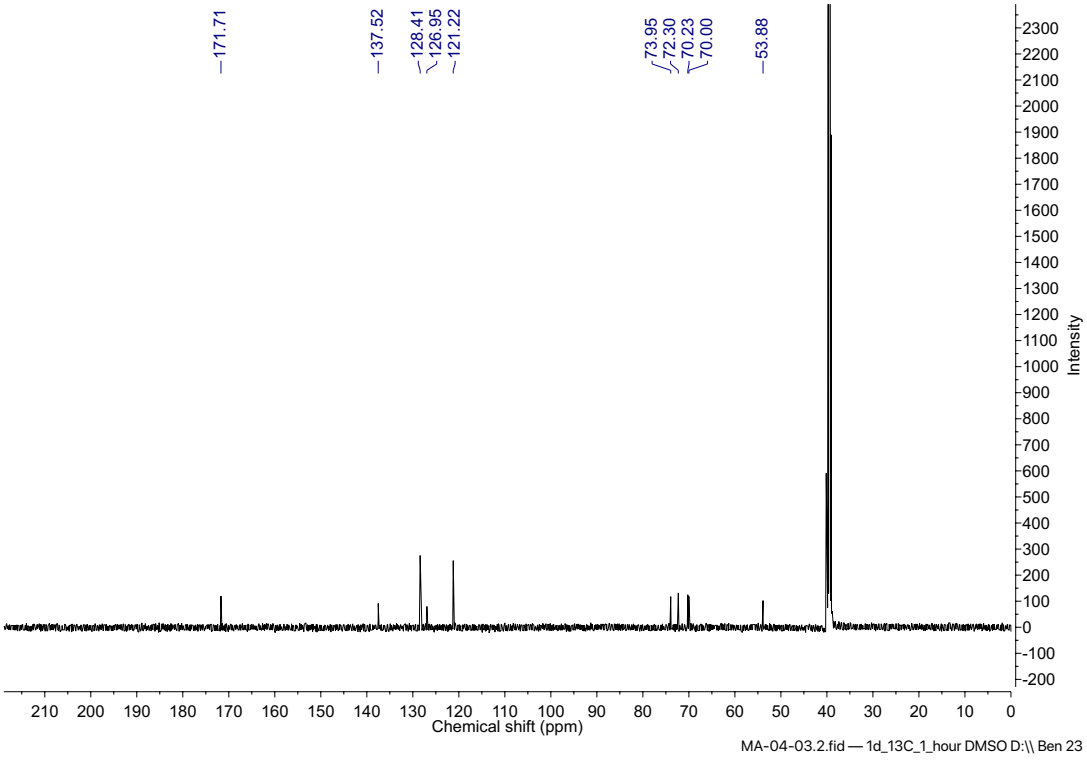

Compound 5.26

Example use of a triazole proton signal (e.g. in the ^{1}H NMR spectrum of fluorosurfactant **5.26** dissolved at 20 mM in deuterated methanol) to estimate the ratio of molecules in the *trans*- (top spectrum) or *cis*- (bottom) photostationary states.[1] For further details, refer to: (1) Adam, M. K.; Hu, Y.; Poisson, J. S.; Pottage, M. J.; Ben, R. N.; Wilkinson, B. L. Photoswitchable Carbohydrate-Based Fluorosurfactants as Tuneable Ice Recrystallization Inhibitors. *Carbohydr. Res.* **2017**, *439*, 1–8.